Universitat Autònoma de Barcelona

Study of the disassembling of the nucleus induced by gossypol in apoptotic nuclear fragmentation-deficient human glioblastoma cells

Laura Martínez Escardó

Universitat Autònoma de Barcelona

Departament de Bioquímica i de Biologia Molecular
Unitat de Medicina

INc Institut de Neurociències

Study of the disassembling of the nucleus induced by gossypol in apoptotic nuclear fragmentation-deficient human glioblastoma cells

Laura Martínez Escardó

Doctoral thesis

2020

Universitat Autònoma de Barcelona

Departament de Bioquímica i de Biologia Molecular
Unitat de Medicina

INc Institut de Neurociències

Study of the disassembling of the nucleus induced by gossypol in apoptotic nuclear fragmentation-deficient human glioblastoma cells

Doctoral thesis submitted by **Laura Martínez Escardó** in candidacy for the **degree of Ph.D. in Biochemistry, Molecular Biology and Biomedicine** from the Universitat Autònoma de Barcelona.

Thesis performed at the Departament de Bioquímica i de Biologia Molecular (Unitat de Medicina) and Institut de Neurociències from Universitat Autònoma de Barcelona, under the supervision of Dr. Víctor J. Yuste Mateos.

With the financial support from the trainee research (PIF) fellowship from the Universitat Autònoma de Barcelona; and Fondos PGE-FEDER (Presupuestos Generales del Estado-Fondo Europeo de Desarrollo Regional) assigned through the Plan Estatal de Investigación Científica y Técnica y de Innovación, grant reference SAF2012-31485 (PGE-FEDER) and SAF2017-83206-R (PGE).

Barcelona, July 2020

Ph.D. candidate,	Thesis director,
Laura Martínez Escardó	Dr. Víctor J. Yuste Mateos

INDEX

ABBREVIATIONS

3-D	3-dimensionality
3-MA	3-Methyladenine

A

aa	Amino acids
ACD	Accidental cell death
ADCD	Autophagy-dependent cell death
ADP	Adenosine diphosphate
AIF	Apoptosis inducing factor
AKT	RAC-alpha serine/threonine-protein kinase
ALDH	Aldehyde dehydrogenases
AM	Acetoxymethyl
AMBRA1	Activating molecule in BECN1 regulated autophagy protein 1
AMP	Adenosine monophosphate
AMPK	AMP-activated protein kinase
APAF1	Apoptotic protease activating factor 1
ApoG	Apogossypol
ApoG2	Apogossypolone
Asn	Aspargine (also indicated with the letter N)
Asp	Aspartic acid (also indicated with the letter D)
ATCC	American type culture collection
ATG	Autophagy-related
ATP	Adenosine triphosphate
ATR	Ataxia-telangiectasia and Rad3-related
ATRX	Alpha thalassemia/mental retardation syndrome X-linked
A.U.F.	Arbitrary units of fluorescence
AV	Autophagic vacuoles

B

BAD	BCL2 associated death promoter
BAF	Barrier-to-autointegration factor
Baf A_1	Bafilomycin A_1
BAK	BCL2-antagonist/killer (also referred to as BAK1)
BAX	BCL2-associated X
BCL- X_L	BCL-extra large (also known as BCL2L1)
BCL2	B-cell lymphoma 2
BCL2A1	BCL2-related protein A1 (also known as BFL-1 in humans)
BCL2L1	BCL2 like 1 (also known as BCL-X_L)
BCL2L2	BCL2 like protein 2 (also known as BCL-W)
BECLIN-1	BCL2-interacting myosin/moesin-like coiled-coil protein
BH	BCL2 homology domains
BID	BH3-interacting domain death agonist
BIK	BCL2-interacting killer
BIM	BCL2-interacting mediator of cell death
BIR	Baculoviral IAP repeat
BMF	BCL2 modifying factor
BOK	BCL2-related ovarian killer
Bp	Base pair

BSA	Bovine serum albumin

C

Ca^{2+}	Calcium ion
CAD	Caspase-activated DNAse
CaMKKβ	Ca^{2+}/calmodulin-dependent kinase kinaseβ
CARD	Caspase recruitment domain
Caspase	Cysteine-dependent aspartate-specific proteases
CDK	Cyclin-dependent kinase
cDNA	Complementary DNA
CHOP	C/EBP homologous protein
CIDE	Cell death-inducing DFF45-like effector
CLL	Chronic lymphocytic leukemia
CNS	Central nervous system
Co	Cobalt
CO_2	Carbon dioxide
CPAN	Caspase-activated nuclease
CrmA	Cytokine response modifier A
CT	Computed tomography
Cu	Copper
Cu^{1+}	Cuprous ion (also referred to as Cu(I))
Cu^{2+}	Cupric ion (also referred to as Cu(II))
CYLD	Carboxyl-terminal hydrolase/Cylindromatosis
CypA	Cyclophilin A
CypD	Cyclophilin D
Cys	Cysteine

D

DAMP	Damage-associated molecular pattern
DD	Death domain
DDR	DNA damage response
DED	Death effector domain
DEPTOR	DEP domain containing mTOR interacting protein
DFF40 / 45 / 35	DNA fragmentation factor, 40 / 45 / 35 kDa subunit
DFNA5	Deafness, autosomal dominant 5
DIABLO	Direct IAP-binding protein with low pI
DISC	Death-inducing signaling complex
DKO	Double-knockout
DMEM	Dulbecco's modified Eagle's medium
DMSO	Dimethyl sulfoxide
DNA	Deoxyribonucleic acid
DR	Death receptors
DRP1	Dynamin-related protein 1
DSB	dsDNA break
dsDNA	Double-stranded DNA
DTT	Dithiothreitol

E

E2F	E2 transcription factor
ECACC	European collection of authenticated cell cultures

EDTA	Ethylenediaminetetraacetic acid
EGF	Epidermal growth factor
EGFRvIII	Epidermal growth factor receptor variant 3
EGTA	Ethylene glycol-bis(β-aminoethyl ether)-N,N,N′,N′-tetraacetic acid
eIF2α	Eukaryotic inititation factor 2α
ER	Endoplasmic reticulum

F

FADD	Fas associated via death domain
FAIM	Fas apoptotic inhibitory molecule
FBS	Fetal bovine serum
FDA	Food and Drug Administration
Fe^{2+}	Ferrous ion (also referred to as Fe(II))
Fe^{3+}	Ferric ion (also referred to as Fe(III))
FIP200	Focal adhesion kinase family kinase-interacting protein 200 kDa
FLAIR	Fluid-attenuated inversion recovery
FLICE	FADD-like interleuin-1β-converting enzyme
FLIP	FLICE-like inhibitory protein
FoxO	Forkhead Box O

G

GA	Golgi apparatus
GABARAP	Gamma-aminobutyric acid receptor-associated protein
GB	Glioblastoma
GFP	Green fluorescent protein
GLB1	Galactosidase beta 1
GLI1	Glioma-associated oncogene homolog 1
Glu	Glutamic acid (also indicated with the letter E)
Gly	Glycine (also indicated with the letter G)
GPX	Glutathione peroxidase 4
GSK3	Glycogen synthase kinase 3
GSP	Gossypol
Gy	Grays

H

H2AX	H2A histone family member X
HCMV	Human *Cytomegalovirus*
HEPES	(4-(2-hydroxyethyl)-1-piperazineethanesulfonic acid
HIF	Hypoxic inducible factor
His	Histidine (also indicated with the letter H)
HMG	High mobility group
HMW	High molecular weight
HP1	Heterochromatin protein 1
HRK	Harakiri
HSP70	Heat shock protein 70
HtrA	High temperature requirement A
HTRA2	HtrA serine peptidase 2

I

IAP	Inhibitor of apoptosis

$ICAD_{(L/S)}$	Inhibitor of CAD ($_L$ or $_S$ means long or short isoform, respectively)
ICE	Interleukin-1β-converting enzyme
ICO	Institut Català d'Oncologia
Id1	Inhibitor of DNA binding 1
IDH	Isocitrate dehydrogenase 1
IF	Immunofluorescence
IFN	Interferon
IKK	IκB kinase
IMS	Intermembrane space
INM	Inner nuclear membrane
IR	Irradiation

K

Kb	Kilobase
kDa	Kilodalton
KH	Krebs-Henseleit
KO	Knockout
KPNA2	Karyopherin Subunit Alpha 2
$KPN\beta_1$	Karyopherin Subunit Beta 1

L

LAMP2A	Lysosomal-associated membrane protein A2
LAP	LC3-associated phagocytosis
LAP2	Lamina-associated polypeptide-2
LC3	Microtubule-associated protein light chain 3
LEM	LAP2-emerin-MAN1
LINC	Linker of nucleoskeleton and cytoskeleton
LMP	Lysosomal membrane permeabilization
LMW	Low molecular weight
LOH	Loss of heterozygosity
LPS	Lipopolysaccharides
LST8	Lethal with SEC13 protein 8
LTα	Lymphotoxin α
LUBAC	Linear ubiquitin chain assembly complex

M

MAPK	Mitogen-activated protein kinase
MAR	Matrix attachment regions
MCL1	Myeloid cell leukemia 1
MDM2	Mouse double minute 2
MEF	Mouse embryonic fibroblasts
MGMT	O^6-methylguanine DNA methyltransferase
MLC	Myosin light chain
MLKL	Mixed lineage kinase domain like pseudokinase
MLL	Mixed lineage leukemia
MOMP	Mitochondrial outer membrane permeabilization
MPT	Mitochondrial permeability transition
MRI	Magnetic resonance imaging
M.Sc.	Master of Science
MST1	Mammalian sterile-20 kinase

mTORC	Mammalian target of rapamycin complex
MTT	3-(4,5-dimethylthiazol-2-yl)-2,5-diphenyltetrazolium bromide

N

NBD	Nucleotide binding domain
NCCD	Nomenclature Committee on Cell Death
NDGA	Nordihydroguaiaretic acid
NE	Nuclear envelope
NET	Neutrophil extracellular traps
NETs	Nuclear envelope transmembrane proteins
NF-κB	Nuclear factor kappa-light-chain-enhancer of activated B cells
NF1	neurofibromatosis type I
NLS	Nuclear localization sequence
NMR	Nuclear magnetic resonance
NOS	Not otherwise specified
NOXA	Phorbol-12-myristate-13-acetate-induced protein 1
NPC	Nuclear pore complex
NR	non-relevant
NSA	Necrosulfonamide
NuMA	Nuclear mitotic apparatus protein

O

OCT	Optimal cutting temperature
OMM	Outer mitochondrial membrane
ONM	Outer nuclear membrane
ORF	Open reading frame
OS	Overall survival

P

PARP	Poly(ADP-ribose) polymerases
PBS	Phosphate-buffered saline
PCD	Programmed cell death
pcDNA	Plasmid cloning DNA
PDGF	Platelet-derived growth factor
PDH	Pyruvate dehydrogenase
PE	Phosphatidilethanolamine
PERK	PKR-like ER kinase
PFA	Paraformaldehyde
PFS	Progression free survival
Ph.D.	Doctor of Philosophy
PI	Propidium iodide
PI3K	Phosphoinositide 3-kinase
PI3P	Phosphatidylinositol 3-phosphate
PIF	*Personal Investigador en formació*
PIN1	Prolyl isomerase peptidylprolyl cis/trans isomerase NIMA-interacting 1
PKB	Protein kinase B
PLA2	Phospholipase A2
PP2A	Protein phosphatase 2A
PRAS40	Prolin-rich Akt substrate of 40 kDa
PRR	Pathogen recognition receptors

PS	Phosphatidylserine
PtdINs3K	Phosphatidylinositol 3-kinase
PTEN	Phosphatase and tensin homolog
PTM	Post-translational modifications
PTPC	Permeability transition pore complex
PUMA	p53-upregulated modulator of apoptosis

Q

q-VD-OPh	Quinoline-Val-Asp-Difluorophenoxymethyl ketone

R

RAPTOR	Regulatory associated protein of mTOR
RB	Retinoblastoma
RCD	Regulated cell death
RFP	Red fluorescent protein
RGB	Red, green, and blue
RHIM	RIP homotypic interaction motif
RING	Really Interesting New Gene domain
RIPK	Receptor-interacting protein kinase
RNA	Ribonucleic acid
ROCK	Rho-associated protein kinase
RT	Room temperature
RTK	Receptor tyrosine kinase

S

SAHB	Stabilized Alpha-Helices of BCL-2 domains
SAHF	Senescence-associated heterochromatic foci
SAR	Scaffold attachment region
SD	Standard deviation
SDS	Sodium dodecyl sulfate
SEM	Standard error of the mean
SEM	Scanning electron microscopy
Ser	Serine (also indicated with the letter S)
siRNA	Small interfering RNA
SMAC	Second mitochondrial activator of caspases
SNARE	Soluble N-ethylmaleimide-sensitive factor activating protein receptor
ssDNA	Single-stranded DNA
STP	Staurosporine
SV40	Simian vacuolating virus 40

T

TBS	Tris-buffered saline
TBS-T	TBS-Tween
TEM	Transmission electron microscopy
TERT	Telomerase reverse transcriptase
TEVP	Tobacco etch virus protease
TfR	Transferrin receptor protein
Thr	Threonine (also indicated with the letter T)
TIR	Toll/interleukin-1 receptor
TKR	Tyrosine kinase receptor

TLR	Toll-like receptor
TMZ	Temozolomide
TNF	Tumor necrosis factor
TNFRSF	TNF receptor superfamily
TRADD	TNFRSF1A associated via DD
TRAF	TNF receptor-associated factor
TRAIL	TNF-related apoptosis-inducing ligand
TRIF	TIR-domain-containing adapter-inducing interferon-β
Trp	Tryptophan (also indicated with the letter W)
TSC2	Tuberous Sclerosis Complex 2
TTF	Tumor treating fields
TUNEL	Terminal deoxynucleotidyl transferase dUTP nick end labeling

U

Ub	Ubiquitin
UBA	Ubiquitin-associated domain
ULK	Unc-51-like kinase
UPR	Unfolded protein response
UT	Untreated
UTP	Uridine triphosphate
UVA	Ultraviolet A
UVRAG	UV radiation resistance-associated gene

V

v/v	Volume per volume
Val	Valine (also indicated with the letter V)
VEGF	Vascular endothelial growth factor
VPS34	Vacuolar protein sorting 34

W

w/v	Weight per volume
WB	Western blot
WIPI	WD repeat domain phosphoinositide-interacting
WHO	World Health Organization
Wt	Wild-type

X

XBP1	X-box binding protein-1
XIAP	X-linked inhibitor of apoptosis

Z

ZBP1	Z-DNA binding protein 1

SUMMARY

Apoptosis, a tightly regulated form of cell death, involves a caspase-triggered cascade of biochemical and morphological events. The activation of the DNA Fragmentation Factor, 40-kDa Subunit, or Caspase-activated Deoxyribonuclease (DFF40/CAD) is considered a key event allowing dying cells to show classical apoptotic nuclear changes. The apoptotic nuclear morphology is depicted by chromatin condensation into highly-packaged round masses and fragmentation of the nucleus.

Glioblastoma, a particularly aggressive solid brain tumor, is characterized by extreme resistance to apoptosis. Among the possibilities that could explain glioblastoma resistance to most of the drugs used in the clinic, our group pointed out the impossibility of glioblastoma cells to undergo complete apoptotic cell death (Sanchez-Osuna *et al.*, 2014) and reported an intrinsic DFF40/CAD endonuclease deficiency as a common trait in human glioblastoma cells (Sanchez-Osuna *et al.*, 2016). When faced to different cytotoxic compounds, the predominant behavior of glioblastoma cells is to show a DFF40/CAD-independent nuclear morphology characterized by a unique mass of compacted chromatin in the absence of nuclear fragmentation.

This Doctoral Thesis evidence that, despite the deficient expression of DFF40/CAD, human glioblastoma cells can switch its predominant nuclear aspect to a DFF40/CAD-dependent apoptotic nuclear morphology when challenged with an adequate stimulus. Gossypol is here reported as an adequate insult able to trigger a proper activation of caspases and DFF40/CAD in human glioblastoma cells. However, a limited number of cells show this nuclear morphology after gossypol treatment. In this sense, our results evidence an unfavorable intracellular context in human glioblastoma cells impeding the proper function of DFF40/CAD as an endonuclease regardless of its levels. Here, we point to intracellular metal ions, such as iron or copper, as intracellular candidates that may contribute to glioblastoma cells' refractoriness to display apoptotic nuclear morphology after different cytotoxic insults. Moreover, besides metal ions, an accurate modulation of autophagy is here suggested to be critical to allow apoptotic nuclear morphology in glioblastoma cells.

The comprehension of this nuclear outcome is of particular interest since an accurate fragmentation and packaging of the genomic content constitute a fundamental process to prevent the spreading of harmful genes and to facilitate the elimination of apoptotic cells. Reduced efficiency in the removal of apoptotic cells with DNA damage may contribute to tumorigenesis. Since different effects may derive from different modes of cell death, the knowledge of the specific intracellular mechanisms that become activated when facing tumor cells to chemotherapeutic treatments is essential to understand better the biological consequences that may derive from this therapeutic approach.

RESUMEN

La apoptosis, una forma de muerte celular regulada, se caracteriza por una cadena de eventos bioquímicos y morfológicos orquestados por una familia de proteasas denominada caspasas. La puesta en marcha de las caspasas desencadena la activación de la endonucleasa CAD (*Caspase-Activated DNase*, también llamada DFF40, del inglés *Death Fragmentation Factor*, *40 kDa subunit*), un acontecimiento clave que permite a las células mostrar cambios nucleares apoptóticos clásicos, que incluyen la condensación de la cromatina y la fragmentación del núcleo.

El glioblastoma, un tumor cerebral primario especialmente agresivo, presenta una resistencia extrema a la apoptosis. Entre las posibilidades que podrían explicar la resistencia de este tumor a la mayoría de fármacos pro-apoptóticos que se utilizan en la clínica, nuestro grupo señaló la imposibilidad de las células derivadas de glioblastoma de presentar una muerte apoptótica completa (Sanchez-Osuna *et al.*, 2014), y describió una deficiencia intrínseca en la expresión de la endonucleasa DFF40/CAD como rasgo común en las células humanas de glioblastoma (Sanchez-Osuna *et al.*, 2016). Cuando se tratan con diferentes compuestos citotóxicos, estas células muestran como comportamiento predominante una morfología nuclear independiente de la activación de la endonucleasa DFF40/CAD, representada por una masa única de cromatina compactada en ausencia de fragmentación nuclear.

Esta Tesis Doctoral manifiesta que, a pesar de la expresión deficiente de DFF40/CAD, las células humanas de glioblastoma pueden mostrar una morfología nuclear apoptótica (dependiente de DFF40/CAD) cuando se tratan con el estímulo adecuado. El gossypol es presentado en este trabajo como un estímulo capaz de desencadenar una correcta activación de las caspasas y de DFF40/CAD en células humanas derivadas de glioblastoma. Sin embargo, solo un número limitado de células muestran esta morfología nuclear tras el tratamiento con gossypol. En este sentido, nuestros resultados señalan un contexto intracelular desfavorable en las células de glioblastoma humano que impide la correcta función de DFF40/CAD como endonucleasa, independientemente de sus niveles. Los iones metálicos, como el hierro o el cobre, son presentados en esta tesis como posibles responsables de la refractariedad de las células de glioblastoma para mostrar una morfología nuclear apoptótica tras diferentes estímulos citotóxicos. Además, se sugiere que una modulación precisa de la autofagia puede ser determinante para permitir la morfología nuclear apoptótica en células de glioblastoma.

Cabe destacar que el estudio preciso de esta morfología nuclear es de especial interés, ya que una fragmentación y un empaquetamiento adecuado del contenido genómico constituyen un proceso fundamental para evitar la propagación de genes nocivos y facilitar la eliminación de las células apoptóticas, que, por el contrario, podrían contribuir a la aparición de fenotipos agresivos.

En este sentido, el conocimiento de los mecanismos intracelulares específicos que se activan cuando se enfrentan las células tumorales a tratamientos quimioterapéuticos es esencial para comprender mejor los efectos biológicos que se derivarán de este planteamiento terapéutico.

RESUM

L'apoptosi, una forma de mort cel·lular regulada, es caracteritza per una cadena d'esdeveniments bioquímics i morfològics orquestrats per una família de proteases anomenades caspases. La posada en marxa de les caspases desencadena l'activació de l'endonucleasa CAD (*Caspase-Activated DNase*, també anomenada DFF40, de l'anglès *Death Fragmentation Factor, 40 kDa subunit*), un esdeveniment clau que permet a les cèl·lules mostrar canvis nuclears apoptòtics clàssics, que inclouen la condensació de la cromatina i la fragmentació del nucli.

El glioblastoma, un tumor cerebral primari especialment agressiu, mostra una resistència extrema a l'apoptosi. Entre les possibilitats que podrien explicar la resistència d'aquest tumor a la majoria dels fàrmacs pro-apoptòtics que s'utilitzen a la clínica, el nostre grup va assenyalar la impossibilitat de les cèl·lules de glioblastoma de presentar una mort apoptòtica completa (Sanchez-Osuna *et al.*, 2014), i va descriure una deficiència intrínseca en l'expressió de l'endonucleasa DFF40/CAD com a tret comú en les cèl·lules de glioblastoma (Sanchez-Osuna *et al.*, 2016). Quan es tracten amb diferents compostos citotòxics, aquestes cèl·lules mostren com a comportament predominant una morfologia nuclear independent de l'activació de l'endonucleasa DFF40/CAD, representada per una massa única de cromatina compactada en absència de fragmentació nuclear.

Aquesta Tesi Doctoral evidencia que, malgrat l'expressió deficient de DFF40/CAD, les cèl·lules humanes de glioblastoma poden mostrar una morfologia nuclear apoptòtica (depenent de DFF40/CAD) quan es tracten amb l'estímul adequat. El gossypol és presentat en aquest treball com un estímul capaç de provocar una correcta activació de les caspases i de DFF40/CAD en les cèl·lules humanes derivades de glioblastoma. Tot i això, només un nombre limitat de cèl·lules mostra aquesta morfologia nuclear després del tractament amb gossypol. En aquest sentit, els nostres resultats assenyalen un context intracel·lular desfavorable en les cèl·lules de glioblastoma que impedeix la correcta funció de DFF40/CAD com a endonucleasa, independentment dels seus nivells. Els ions metàl·lics, com el ferro o el coure, són presentats en aquesta tesi com a possibles responsables de la refractarietat de les cèl·lules de glioblastoma per mostrar una morfologia nuclear apoptòtica després de diferents estímuls citotòxics. A més, es suggereix que una modulació precisa de l'autofàgia pot ser determinant per permetre la morfologia nuclear apoptòtica en cèl·lules humanes de glioblastoma.

Cal destacar que l'estudi precís d'aquesta morfologia nuclear és d'especial interès, ja que una fragmentació i un empaquetament adequat del contingut genòmic constitueixen un procés fonamental per evitar la propagació de gens nocius i facilitar l'eliminació de les cèl·lules apoptòtiques, que, per contra, podrien contribuir a l'aparició de fenotips agressius.

En aquest sentit, el coneixement dels mecanismes intracel·lulars específics que s'activen quan s'enfronten les cèl·lules tumorals a tractaments quimioterapèutics és essencial per comprendre millor els efectes biològics que es derivaran d'aquest plantejament terapèutic.

INTRODUCTION

1. The cell: to live or to die

Cell theory, originally formulated in 1839 by Matthias Schleiden and Theodor Schwann, and later by other scientists like Rudolf Virchow, states that: all living organisms are composed of one or more cells; the cell is the basic unit of structure and organization in organisms; and that cells arise from pre-existing cells. The modern version of this theory adds some other tenets: the cell has hereditary information (DNA) that is passed on from cell to cell during reproduction; all cells have virtually the same basic chemical composition and metabolic activities; all the cell's basic chemical and physiological functions are carried out inside the cell itself; and cellular activity is dependent on the activities of structures within the cell, such as the organelles, or nucleus (Ribatti, 2018).

While unicellular organisms (made up of only one cell) depend upon just one cell for all of its functions, multicellular organisms (composed of more than one cell) require different specialized cells performing different functions to support the integrity of the overall organism. However, in both cases, a variety of functions, including the absorption of nutrients, the production of energy, or the synthesis of proteins, are orchestrated inside the cell by specialized structures and organelles to sustain the life of the organism. In this sense, the environment to which the organism is exposed strongly dictates most of these intracellular reactions and pushes cells into a continuous adaptation to sustain life, the most basic precept of biology.

However, what happens if the cell dies? In the case of a multicellular organism, selective elimination of some cell types has the potential to improve the survival of the overall organism. On the contrary, cell death in a unicellular organism means the death of the entire organism. Hence, why should a unicellular organism contain machinery involved in cell death? In this sense, it has been hypothesized that programmed cell death (PCD) machinery may evolve in unicellular organisms due solely to kin selection (Vostinar *et al.*, 2019). Nevertheless, it seems cost-inefficient for one cell to restrain death-centric proteins and only activate them when a series of coordinated alterations in the internal and external environment occurs. Following this assumption, Dick and Megeney proposed that constituent proteins of PCD evolved from a non-death role as by-products of adaptation or co-option in single-celled organisms (Dick and Megeney, 2013).

Hence, although researchers have tried to categorize different intracellular machinery into different intracellular pathways and functions, increasing evidences suggests that the same machinery triggering cell death is also the machinery of life (Fernando and Megeney, 2007).

2. The concept of cell death: from origin to nowadays

Defining "cell death" has always been a challenge from the scientific point of view. Indeed, the misguide parallelism, unconscious in many cases, with the cultural and religious beliefs surrounding the notion of death, has made it even more complicated. From a non-scientific concept of cell death, it seems counterintuitive that some cells (erythrocytes and keratinocytes) exert essential functions when they are "dead". Consequently, it is difficult to conceive that death is a necessary process in development.

One of the first reported scientific observations of cell death historically occurred in 1842, when Karl Vogt observed the disappearance of cells in toads (Vogt, 1842). Previously, other authors such as Dugès had observed other examples of structural regression like the loss of tadpole gills and tails in the transition to adult toads (Dugès, 1835). However, Vogt was the first to refer to this specific loss of structures in development as a "destruction", "disappearance" or "resorption" of cells (now referred to as dying cells). A few years later, in 1858, Virchow coined the term *necrosis* to describe a tissue destruction process . However, due to technical limitations, it was not until 1885, when Walther Flemming, who introduced the terms *chromatin* and *mitosis*, observed fragmented nuclei surrounding ovarian follicles in regression (Flemming, 1885) (**Figure I1**). This nuclear fragmentation, followed by the disappearance of the nuclei, was referred to as *chromatolysis* and was the first term that received the process that we now know as *apoptosis*. Concerning this observation, Ludwing Gräper established in 1914 that the process of chromatolysis is present in all organs that need to eliminate cells with the purpose of cellular replacement (Graper, 1914). Indeed, he found that cells suffering from chromatolysis have to be phagocytized by neighboring cells. These historical events are reviewed in depth in the following reference (Clarke and Clarke, 1996).

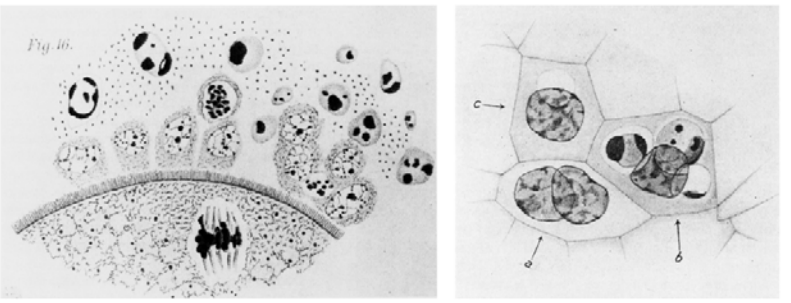

FIGURE I1. **Representative illustrations of chromatolysis.** On the left, chromatolysis observed in epithelial cells from rabbit ovarian follicle in involution (Flemming, 1885). On the right, chromatolysis observed in the yolk sac in the course of involution (Graper, 1914). Epithelial cells are illustrated by taking up the fragmented nucleus of a neighboring cell that died during the involution process.

Other relevant terminologies such as *karyolysis* (complete dissolution of the chromatin of a dying cell, mainly due to the action of endonucleases) or *karyorrhexis* (nuclear fragmentation and irregular distribution of the chromatin throughout the cytoplasm) were introduced in 1879 by Edwing Klebs. *Pyknosis*, condensation of the chromatin in the nucleus, was introduced in 1890. In 1900, the term *autolysis* consolidated to define the spontaneous destruction or lysis of the cells by its proteases. All these concepts have been conserved until now and are used to describe different morphologies displayed during the cell death process.

Moving on with the historical introduction, Lockshin and Williams introduced the concept of "Programmed Cell Death" (PCD) in 1964. They observed the demise of intersegmental muscles in developing silk moths and described that cells follow a sequential controlled program, genetically codified, that governs the development of the organisms to its death (Lockshin and Williams, 1965). The term PCD, as discussed below, has been subjected to controversy and continuous conceptual changing.

Another central historical contribution comes from 1972 when John F Kerr and collaborators, Andrew H Wyllie and Alastair R Currie, introduced the term apoptosis to describe a morphological stereotype form of cellular demise, morphologically differing from necrosis (Kerr *et al.*, 1972) (**Figure I2**).

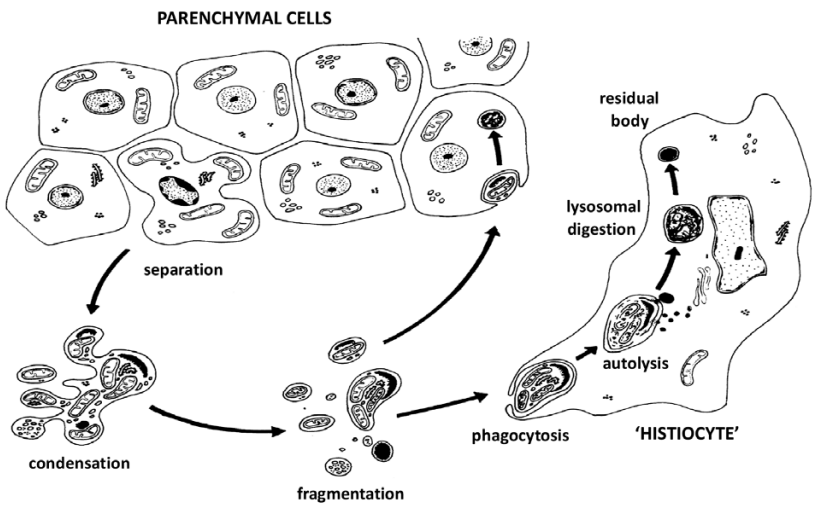

FIGURE I2. **Diagram to illustrate the morphological features of apoptosis.** Modified from Kerr *et al.*, 1972.

As indicated in a footnote in Kerr *et al.*, 1972, the use of the word *apoptosis* (from Ancient Greek ἀπόπτωσις) was a suggestion from Professor James Cormack. Interestingly, this term that in Greek describes the "dropping off" or "falling off" of petals from flowers, or leaves

from trees, was previously used in the medical writings of classical authors. Hippocrates of Cos used this word to refer to the "falling off of the bones" and subsequently, Galen to refer to the "dropping of the scabs" (reviewed in (Esposti, 1998)). Kerr *et al.*, apparently unaware of this detail, coined the term apoptosis as a synonym of programmed cell death (PCD), a concept previously termed *shrinkage necrosis* in 1971 (Kerr, 1971).

In 1973, Schweichel and Merker reported the presence of three distinct cell death morphologies in rat embryos after exposure to toxins (Schweichel and Merker, 1973). This first classification referring to type 1, 2, and 3 was later renamed by Clarke in 1990, settling the concepts of apoptosis, autophagic cell death, and vesicular non-lysosomal degradation, respectively (Clarke, 1990). Moreover, distinguishing two different sub-groups in the type 3 cell death (**Figure I3**) (**Table I1**).

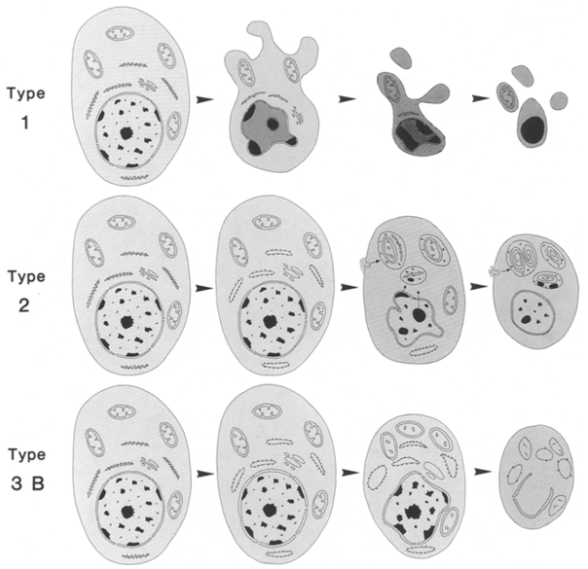

FIGURE I3. Illustrations of different types of cell death. Types 1, 2, and 3 B described by Clarke are represented, showing constant features observed in each type (see text *2.1. Cell death classification* and **Table I1**) (Clarke, 1990).

2.1. Cell death classification

Historically, morphological and structural features of cells have been employed to classify cell death. As mentioned above, the first formal classification of cell death, presented by Schweichel and Merker in 1973, introduced a morphological hallmark system for classifying cell death and differentiated it in three different categories; type 1, 2, and 3 observed in prenatal tissues treated with various embryotoxic agent (Schweichel and Merker, 1973).

Type 1 cell death or apoptosis was first associated with heterophagy ("eating of another"). As reviewed in (Galluzzi *et al.*, 2018), type 1 cell death has been historically characterized by "cytoplasmic shrinkage, chromatin condensation (pyknosis), nuclear fragmentation (karyorrhexis), and plasma membrane blebbing, culminating with the formation of apparently intact small vesicles (commonly referred to as apoptotic bodies) that are efficiently taken up by neighboring cells with phagocytic activity and degraded within lysosomes".

Type 2 cell death or autophagy was associated with autophagy ('eating of itself'), and is often referred to as autophagy-dependent cell death, featuring cytoplasmic vacuolization and also culminating with phagocytic uptake and lysosomal degradation.

Type 3 cell death or necrosis was not associated with any type of cell digestion, exhibiting neither apoptotic nor autophagic characteristics. This third category of cell death displays no distinctive features of type 1 or 2 cell death. It terminates with the clearance of cell corpses in the absence of obvious phagocytic and lysosomal contribution. More specifically, it often takes place with a loss of membrane integrity and swelling of subcellular organelles (oncosis). In 1990, Clarke divided this type 3 cell death into two subgroups; type 3A o non-lysosomal disintegration and late vacuolization followed by nuclear disintegration, and type 3B o cytoplasmic degeneration displaying karyolysis with a late increase of chromatin granularity (Clarke, 1990) (**Figure I3**) (**Table I1**).

	Various designations	Nucleus	Cell membrane	Cytoplasm	Heterophagic elimination
Type 1	Apoptosis; shrinkage necrosis; precocious pycnosis; nuclear type of cell death	Nuclear condensation, clumping of chromatin leading to *pronounced pyknosis*	Convoluted, forming blebs	Loss of ribosomes from RER and from polysomes; cytoplasm reduced in volume becoming electron-dense	Prominent and important
Type 2	Autophagic cell death	Pyknosis in some cases. Parts of nucleus may bleb or segregate	Endocytosis at least in some cases; blebbing can occur	*Abundant autophagic vacuoles*; ER and mitochondria sometimes dilated; Golgi often enlarged	Occasional and late
Type 3A	Non-lysosomal disintegration	Late vacuolization, then disintegration	Breaks	*General disintegration*; dilation of organelles, forming "empty" spaces that fuse with each other and with the extracellular space	No
Type 3B	Cytoplasmic type	Late increase in granularity of chromatin	Rounding up of cell	*Dilation of ER, nuclear envelope, Golgi and sometimes mitochondria, forming "empty" spaces*	Yes

TABLE I1. Summary of the different types of cell death described by Clarke (Clarke, 1990).

Since the introduction of Clarke's classification, the concept of PCD was inherently associated with to the concept of apoptosis. However, in 2001, Jaättela and co-workers redefined this

classification. Based on the nuclear changes, cell death was classified into classical apoptosis, apoptosis-like PCD, necrosis-like PCD, and accidental necrosis (Leist and Jaattela, 2001). As shown in **Figure I4**, different names have been introduced to describe different types of cell death.

From 2005, the Nomenclature Committee on Cell Death (NCCD) started to formulate recommendations to define and interpret cell death in a unified way. To answer what define "dead cells", NCCD proposed three different criteria (Kroemer *et al.*, 2005):

- Permanent loss of the barrier function of the plasma membrane.
- Breakdown of cells into discrete fragments, which are commonly referred to as apoptotic bodies.
- Engulfment of cells by professional phagocytes or other cells endowed with phagocytic activity.

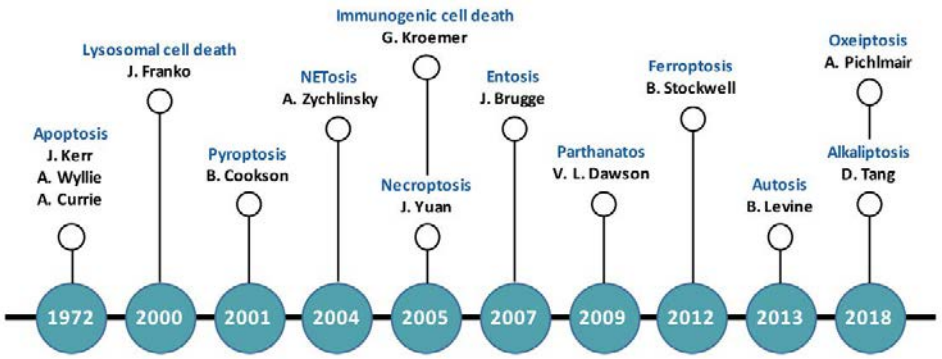

FIGURE I4. Timeline of the terms used in cell death research. Modified from Tang *et al.*, 2019.

The NCCD has been periodically formulating guidelines for the definition and interpretation of all cell death aspects, and revising the terminology and classification employed in cell death. As a result, five papers have been published in Cell Death and Differentiation journal. The first and the second round of recommendations (2005 and 2009) were focused on the classification of cell death: the first was based only on morphological criteria; and the second, in both morphological and biochemical yardsticks. In 2012, the NCCD proposed to abandon the morphological classification in favor of new criteria based on molecular definitions and quantifiable biochemical features of cell death subroutines. Thus, encouraging genetic and/or pharmacologic approaches to discriminate between various instances of cell death *in vitro* and *in vivo* (Galluzzi *et al.*, 2012b). In 2015, the report was focused on "essential" versus "accessory" aspects of cell death; traits that etiologically mediate cell death occurrence and features that change cell death kinetics or morphological and biochemical manifestations. In

the latest report (2018), the aim of the NCCD was to address the molecular mechanisms of cell death (Galluzzi *et al.*, 2018).

The different modes of cell death included in this report are schematically represented in **Figure I5** (each cell death subroutine is described in *6.Other types of cell death and non-lethal processes*). Moreover, in line with the aim of better defining "cell death", NCCD recommends to abandon expressions like "percent apoptosis" and to replace them by more precise descriptions of the parameters that are measured.

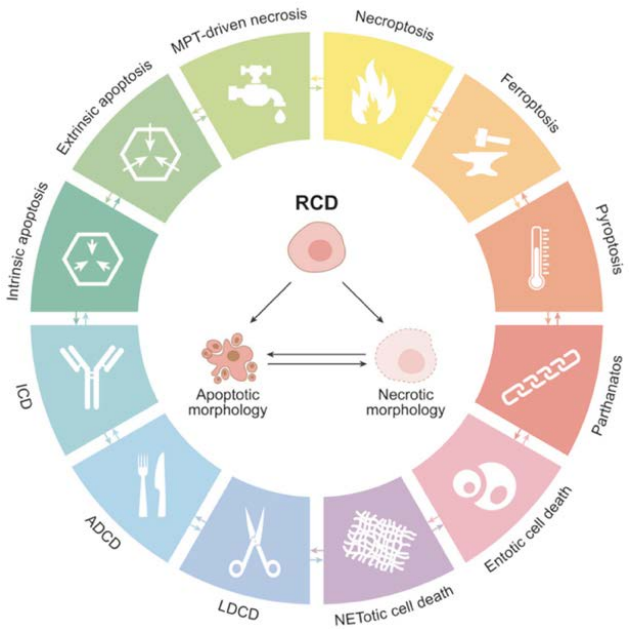

FIGURE I5. Schematic representation of the major cell death subroutines included in the last NCCD report. From Galluzzi *et al.*, 2018. NCCD, Nomenclature Committee on Cell Death ADCD: autophagy-dependent cell death, ICD: immunogenic cell death, LDCD: lysosome-dependent cell death, MPT: mitochondrial permeability transition (see *6.Other types of cell death and non-lethal processes*).

BOX 1. 'Accidental', 'regulated' and 'programmed' cell death

'Accidental', 'Regulated' and 'Programmed' cell death concepts are often misused or as synonyms in many articles. Consequently, the Nomenclature Committee on Cell Death (NCCD) proposed three different definitions for these three different concepts.

The expression '**accidental**' should be employed to indicate cell death triggered by extremely harsh physical conditions (usually an unexpected attack or injury such as freeze–thawing cycles or high concentrations of pro-oxidants), which overwhelms any possible control mechanism and cannot be inhibited by genetic and/or pharmacological strategies. Frequently accidental cell death (ACD) exhibits morphological features of necrosis.

The term '**regulated**' or 'regulated cell death' (RCD) is defined by the NCCD as the "form of cell death that results from the activation of one or more signal transduction modules, and hence can be pharmacologically or genetically modulated (at least kinetically and to some extent)" *(Galluzzi et al., 2018)*. The RCD is executed by a set of defined effector molecules and has biochemical, functional, and immunological consequences. It can be classified into multiple subroutines based on its molecular features. Among them necroptosis, pyroptosis, ferroptosis, entotic cell death, netotic cell death, parthanatos, lysosome-dependent cell death or autophagy-dependent cell death. Some of them are poor well-studied and might actually be limited to cellular responses to specific toxins. RCD can occur as a consequence of microenvironmental perturbations but also in the context of post-embryonic development, tissue homeostasis, and immune response (Galluzzi *et al.*, 2015a). The possibility to pharmacologically manipulate cell death has introduced alternative terms such as therapeutic cell death or chemically-induced cell death(Green and Kroemer, 2005); all included under the term of RCD.

The concept of '**programmed** cell death' (PCD) was coined in 1964 and it has been extensively used in the field. According to the NCCD, this term should be preserved and included as a form of RCD. NCCD defines PCD as the "form of RCD that occurs in strictly physiological scenarios, *i.e.*, it does not relate to perturbations of homeostasis and hence does not occur in the context of failing adaptation to stress" (Galluzzi *et al.*, 2018).

According to the recommendations of the NCCD, cell death instances can be functionally classified into two broad and mutually exclusive categories: 'accidental' and 'regulated'.

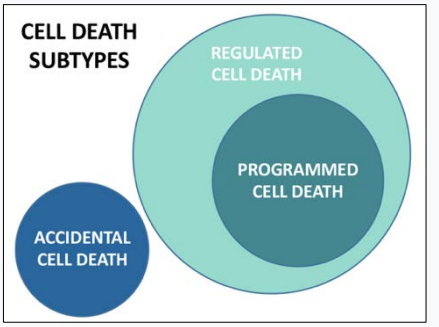

FIGURE I6. Schematic representation of the different types of cell death. Modified from Galluzzi *et al.*, 2015a.

3. Apoptosis

Apoptosis has been traditionally described by its morphological features. It is characterized by cytoplasmic shrinkage; chromatin condensation (initiating at the nuclear membrane with marginalization and then involving the whole nucleus showing pyknosis); nuclear fragmentation (karyorrhexis); minimal alterations of other organelles; and, a peculiar 'boiling-like' process (known as blebbing) culminating in the formation of a few discrete corpses that initially retain plasma membrane integrity (referred to as apoptotic bodies) (Kerr *et al.*, 1972) (Kroemer *et al.*, 2009).

Although historically this RCD program has been defined from a morphological point of view, many studies have shed light on the biochemical pathways that govern this process of death and determine the morphological apoptotic features. In this line, special recognition has to be given to the work of Ellis and Horvitz, who identified the genes implicated in the cellular suicide in *Caenorhabditis elegans*. The authors observed that precisely 131 of the 1090 cells generated in the development of an adult hermaphrodite worm die in a predictable and repeatable way, thus, offering a genetic control orchestrating a programmed cell death in the nematode worm (Ellis and Horvitz, 1986) (Conradt *et al.*, 2016). Four genes *(egl-1*, *ced-3*, *ced-4* and *ced-9*) were identified as key regulators altering the cell death phenotype prior to engulfment by neighboring cells. In 1992, two groups reported the identity of interleukin-1β-converting enzyme (ICE), the human protease responsible for activating the precursor of interleukin-1β (Cerretti *et al.*, 1992) (Thornberry *et al.*, 1992). Months later, the ICE was demonstrated to show identity with CED-3 (Yuan *et al.*, 1993).

These genetic evidence inaugurated the field of apoptosis research at the molecular level and encouraged succeeding studies detecting different mammalian homologs governing cell death (**Figure I7**). Most of these regulators are known to be members of the most relevant proteolytic family of enzymes, the cysteinyl aspartate-specific proteinases best known as caspases. Studies in *C. elegans* (nematode), *Drosophila melanogaster* (fruit fly), and mammals coincide that apoptosis is an evolutionary-conserved process tightly regulated and essential for the proper development and homeostasis of multicellular organisms (Munoz *et al.*, 2012) (Bell and Megeney, 2017).

The biochemical knowledge increased, and with it, a tendency to dichotomize cell death events into two mutually exclusive groups: a caspase-dependent, tolerogenic, programmed and physiological cell death; and, a caspase-independent, immunogenic, accidental and pathological cell death.

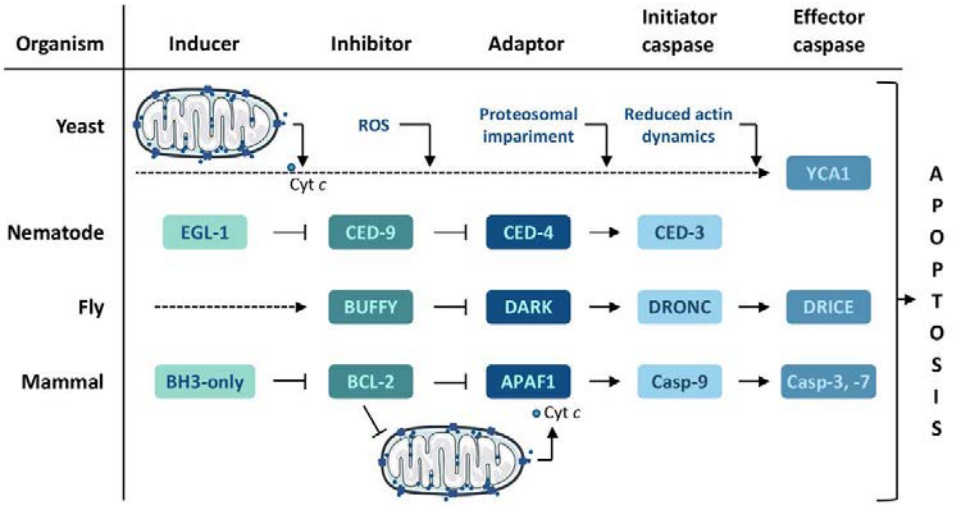

FIGURE I7. **Illustration of the core apoptotic machinery conserved in different organisms.** In the case of yeast, a detailed mechanism remains to be elucidated; however, a metacaspase-dependent pathway leading towards the YCA1 activation is shown here. Although not indicated, note that BCL-2 anti-apoptotic proteins can inhibit BH3-only proteins (see **Figure I15**). Adapted from Riedl and Shi, 2004; Muñoz *et al.*, 2012 and Bell and Megeney, 2017.

However, recent publications suggest that apoptosis and consequent efferocytosis (clearance by macrophages or other cells with phagocytic activity of apoptotic cells) are not always immunologically silent (Zitvogel *et al.*, 2004) (Boada-Romero *et al.*, 2020). Generally, cells that have undergone an apoptotic process end up displaying a necrotic morphology (a process known as secondary necrosis) in which the plasma membrane breaks down, and in which gasdermin E (or best known DFNA5) participates (Rogers *et al.*, 2017). Certainly, it should be noted that although morphologically similar, cells referred to as apoptotic cells may have been triggered through different biochemical routes. Thus the expression "apoptosis" hides a major degree of biochemical and functional heterogeneity. From a functional perspective, and as mentioned above, apoptotic cell death may occur in a non-immunogenic manner or can lead to the exposure and secretion of proteins provoking the stimulation of a specific immune response through an efficient antigen presentation by dendritic cells with engulfed apoptotic material (Zitvogel *et al.*, 2008) (Boada-Romero *et al.*, 2020).

From a biochemical standpoint, apoptosis can be initiated by extracellular (extrinsic) or intracellular (intrinsic) stimuli, and may be supported or not with the contribution of mitochondria (Danial and Korsmeyer, 2004) (Kroemer *et al.*, 2007). According to the NCCD (Galluzzi *et al.*, 2018), extrinsic apoptosis is the "specific variant of RCD initiated by perturbations of the extracellular microenvironment detected by plasma membrane receptors, propagated by CASP8 and precipitated by executioner caspases, mainly CASP3"; and intrinsic apoptosis is the "type of RCD initiated by perturbations of the extracellular or intracellular

microenvironment, demarcated by MOMP, and precipitated by executioner caspases, mainly CASP3".

3.1. Extrinsic apoptosis

As an RCD modality, extrinsic apoptosis is initiated by extracellular microenvironment perturbations and is orchestrated by specific biochemical machinery mostly driven by two types of plasma membrane receptors: death receptors and dependence receptors (Ashkenazi and Dixit, 1998) (Gibert and Mehlen, 2015).

Death receptors

Death receptors (DR) are transmembrane proteins that become activated upon binding with its related ligand(s). **Table I2** include examples of DRs and its cognate ligands (Wajant, 2002) (von Karstedt *et al.*, 2017) (Fleten *et al.*, 2016).

Death receptor	Ligand
Fas cell surface death receptor (FAS), CD95 or APO-1	FAS ligand (FASLG), CD95L or APO-1L
TNF receptor superfamily member 1A (TNFRSF1A) or TNFR1	TNFα or LTα
TNF receptor superfamily member 10a (TNFRSF10A), TRAILR1 or DR4	TNFSF10 or TRAIL
TNF receptor superfamily member 10b (TNFRSF10B), TRAILR2 or DR5	TRAIL

TABLE I2. Death receptors and its cognate ligands.

Structurally, death receptors share similar cysteine-rich extracellular domains responsible for ligand binding and a cytoplasmic domain of about 80 amino acids referred to as death domain (DD) (Ashkenazi and Dixit, 1998) (Bodmer *et al.*, 2002) (Stohr *et al.*, 2020). After death receptor ligation, a dynamic multiprotein complex will assembly at the intracellular tail of the receptor. This complex include examples such as the "death-inducing signaling complex" (DISC) (**Figure I8**), "complex I", or "complex II" (**Figure I9**). All of them functioning as molecular platforms regulating the function and activation of initiator caspases such as caspase-8 or caspase-10 (Dickens *et al.*, 2012b) (Tummers and Green, 2017).

In the case of FAS and TRAILRs, the related ligands FASLG and TRAIL (organized as homologous trimeric ligands) stabilize preformed receptor homotrimers (a cluster of three DRs) to induce a conformational change at the intracellular tails of DRs; thus, allowing the

association of the death domains (DD) with the adapter FADD (Fas associated via death domain) (Boldin *et al.*, 1995) (Chinnaiyan *et al.*, 1995) (Kischkel *et al.*, 2000). Within this complex, FADD drives DISC assembly by promoting the recruitment of caspase-8 (or caspase-10) through its death effector domain (DED), and the assembly of multiple isoforms of c-FLIP (FLICE-like inhibitory protein). This transmembrane complex contains the adapter protein FADD at the cytosolic face functioning as a bridge between the c-terminal of the death receptor and apical caspases. The binding of caspase-8 to FADD at the DISC allows the assembly of linear filaments of caspase-8 molecules and facilitates homodimerization. Homodimerization of caspase-8 promotes autoproteolytic cleavage which is crucial for its activation (Dickens *et al.*, 2012a) (Oberst *et al.*, 2010) (Kallenberger *et al.*, 2014) (see *3.3. Caspases*).

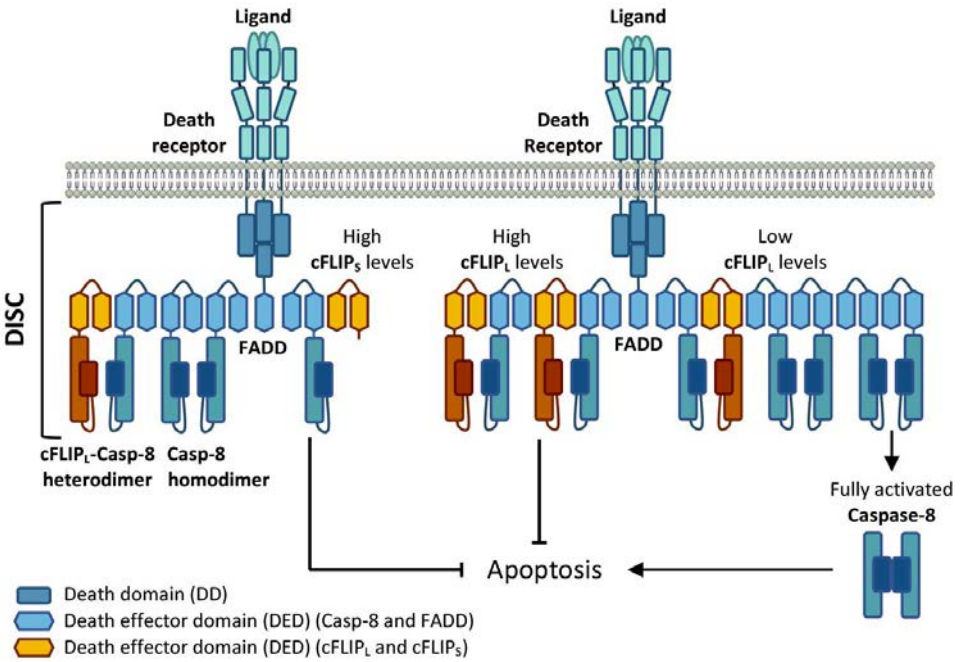

FIGURE I8. Regulation of death receptor-mediated apoptosis by cFLIP. Ligated death receptors recruits FADD via homotypic death domain (DD) interactions. FADD then recruits caspase-8 via death effector domain (DED) interactions and leads to the formation of the DISC. The levels of cFLIP regulates the activation of caspase-8 and, consequently, apoptosis. Low levels of c-FLIPL activates caspase-8 heterodimerization, whereas high expression levels of this isoform or $cFLIP_S$ inhibit apoptosis. Modified from Tummers and Green, 2017.

Caspase-8 oligomerization has been described to be regulated by c-FLIP. This catalytically inactive close relative of caspase-8 (Yeh *et al.*, 2000) (Scaffidi *et al.*, 1999) can be detected in two isoforms: c-$FLIP_S$ and c-$FLIP_L$. The short variant (c-$FLIP_S$), due to a stop codon following the DEDs, encodes no catalytic domain homology unit and seems to inhibit caspase-8 oligomerization by disrupting DED-mediated procaspase-8 oligomer assembly. The long counterpart (c-$FLIP_L$) –when present at physiological concentrations– stabilizes the

catalytic domain of the caspase and activates caspase-8 (Micheau *et al.*, 2002). Nevertheless, high expression levels of c-FLIP$_L$ can inhibit, rather than activate, extrinsic apoptosis (Fricker *et al.*, 2010) (Hughes *et al.*, 2016). c-FLIP$_L$ is an NF-κB-regulated gene and its concentration in cells is variable. Its variable expression, together with transcript splicing events generating differential amounts of c-FLIP$_L$ or c-FLIP$_S$, impacts on its role activating initiator caspases (Schleich *et al.*, 2016). Thus, the presence of cFLIP isoforms in the FADD-caspase-8-cFLIP complex and their expression levels determines if and how cells die (**Figure I8**).

Another potential regulator protein of DR-mediated apoptosis is FAIM (Fas apoptotic inhibitory molecule), which can block Fas-induced apoptosis via inhibition of caspase-8 processing. FAIM can also be detected in two isoforms, FAIM$_L$ and FAIM$_S$. The overexpression of FAIM$_L$ has been described to confer resistance to apoptotic cell death induced by DRs (Fas or R1 TNF). More specifically, FAIM$_L$ protection from Fas-induced apoptosis in type II cells is associated with its function inhibiting XIAP (X-linked inhibitor of apoptosis) ubiquitinylation (Moubarak *et al.*, 2013). FAIM$_S$ does not seems to exert anti-apoptotic functions, but does promote neuronal differentiation (Sole *et al.*, 2004) (Segura *et al.*, 2007).

In the case of TNFR1 (or TNFRSF1A), its activation to induce apoptosis is more complex. This is because ligation of TNFR1 can induce cell death, survival and differentiation. Once the ligand TNFα binds to its receptor, it can either induce caspase-8-mediated apoptosis or can block apoptosis via the activation of the transcription factor nuclear factor-kappa B (NF-κB) which induces the expression of cFLIP. In more detail, this process takes place through the formation of sequential complexes ("Complex I" and "Complex II"). The activation of NF-κB, following DR stimulation, is responsible for transcriptional activation of pro-survival genes such as the cellular inhibitor of apoptosis protein (cIAP)1/2, B-cell lymphoma (BCL)-2, BCL-X$_L$ or FLIP (Karin and Lin, 2002). In more detail, upon ligation, TNFR1 associates with the adapter TRADD (TNFRSF1A associated via DD) which functions as an adaptor for the assembly of "Complex I" that generally includes TNF receptor associated factor 2 (TRAF2), TRAF5, c-IAP1, c-IAP2, RIPK1, and the linear ubiquitin chain assembly complex (LUBAC). RIPK1 ubiquitylation by cIAP1/2 mediates activation of NF-κB and the production of pro-inflammatory and pro-survival gene expression. The release of "Complex I" from the membrane into the cytosol by receptor internalization and endosomal trafficking leads to "Complex II" formation (Schneider-Brachert *et al.*, 2004) (Schutze *et al.*, 2008). Deubiquitylated RIPK1 (by deubiquitylases such as A20 or CYLD) leaves complex I and recruits FADD (via homotypic DD interactions) and RIPK3 (through RHIM (RIP homotypic

interaction motif) homotypic interactions). This recruitment leads to the formation of the ripoptosome or "Complex IIa". Homodimerization and activation of caspase-8 on FADD induce apoptosis. As mentioned above, caspase-8 can heterodimerize with $cFLIP_L$. Indeed, $cFLIP_L$ can translocate to complex II to prevent caspase-8 activation and apoptosis upon NF-κB activation. Thus, TNFα induces apoptotic cell death when NF-κB activation is impaired or when de novo protein synthesis is blocked (Beg and Baltimore, 1996) (Marques-Fernandez *et al.*, 2013) (Wang *et al.*, 1996). In the case of RIPK3, its ameloid formation and MLKL activation engage necroptosis through the formation of "Complex IIb" or necrosome (Sun and Wang, 2014) (see *4.1. Necroptosis*) (**Figure I9**).

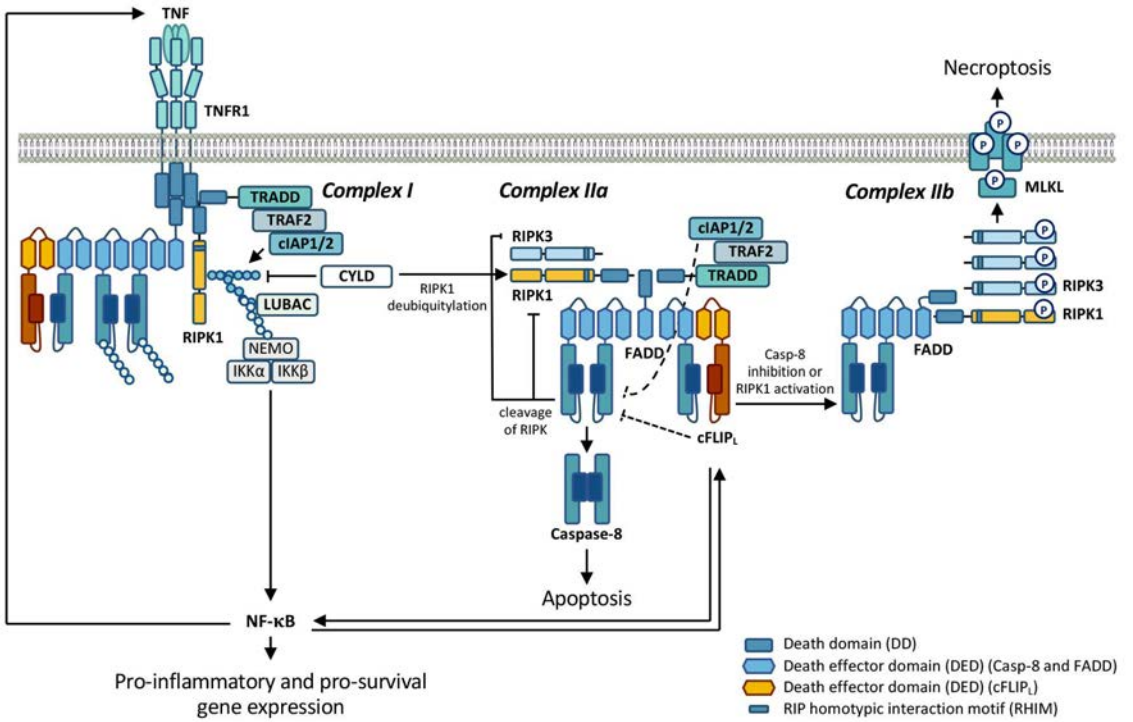

FIGURE I9. Regulation of TNFR1-mediated cell death. Death receptors recruits TRADD, TRAF2, cIAP1/2 and RIPK1 (complex I). In a pro-survival state, cIAPs inhibit RIPK1 through polyubiquitination. Additionally, LUBAC can be recruited in a cIAP dependent manner and in turn linearly ubiquitinates RIPK1 and caspase-8 to inhibit apoptosis. This complex recruit the IκB kinase complex and lead to the activation of NF-κB and the production of pro-inflammatory and pro-survival gene expression. Alternatively, in the presence of cell death stimuli (including TNF-α or TRAIL), RIPK1 can be deubiquitinated by CYLD to form the "complex IIa" or ripoptosome. The inhibition of cIAPs also lead to this complex that is composed of FADD, caspase-8, cFLIP, RIPK1 and RIPK3. Caspase-8 can cleaves RIPK1 or RIPK3 to prevent necroptosis and promote apoptosis. RIPK1, RIPK3 and FADD provides a scaffold for the activation of caspase-8. However, if caspase-8 remains inactive by cFLIP or RIPK3 is phosphorylated the complex IIb or necrosome will form to execute necroptosis. Phosphorylated RIPK1, phosphorylate RIPK3 that will phosphorylate and activate MLKL, which will form oligomers to create pores in the plasma membrane leading to necroptotic cell death. Adapted from Tummers and Green, 2017; Miller et al., 2020; and Stohr *et al.*, 2020.

Regardless of the death receptor, two distinct pathways can be followed from the execution of extrinsic apoptosis. So-called 'type I cells', which includes mature lymphocytes or thymocytes, directly activate executioner caspases by caspase-8 in a mitochondrion-independent manner. By contrast, in 'type II cells', which refers to the majority of cancer cells, once caspase-8 is activated, it cleaves the BCL-2 family protein BID leading to a truncated form of BID, referred to as tBID, that translocates to the outer mitochondrial membrane (OMM) (Luo *et al.*, 1998) (Li *et al.*, 1998). At the OMM, tBID functions as a BH3-only activator protein engaging BAX/BAK-dependent mitochondrial outer membrane permeabilization (MOMP) and, consequently, caspase-9-driven RCD to activate executioner caspases (Barnhart *et al.*, 2003) (**Figure I10**).

Besides cell death, death receptor ligation signals different cellular fates. NF-κB activation, generally resulting in cell survival associated with inflammatory response is the classic example. The association of RIPK1 in a polyubiquitinated state (triggered by c-IAP1, c-IAP2, and LUBAC) and in a TRADD-independent manner promotes cell survival and inflammation through MAPK (mitogen-activated protein kinase) signaling or IκB kinase (IKK)-dependent NF-κB activation (Varfolomeev *et al.*, 2008) (Li *et al.*, 2006) (**Figure I9**). Additionally, the preferential location of TRAILR2 outside of lipid rafts has been postulated as an influencing factor inducing pro-survival rather than pro-apoptotic signals (Shlyakhtina *et al.*, 2017). Cell death-independent activities of death receptors are extensively reviewed in (Siegmund *et al.*, 2017).

Dependence receptors

The family of dependence receptors is formed by approximately 20 members and includes examples such as the netrin 1 (NTN1) receptors, the neutotrophin receptor neurotrophic receptor tyrosin kinase 3 (NTRK3), and the sonic hedgehog (SHH) receptor patched 1 (PTCH1). Dependence receptors promote different pathways, including proliferation, cell survival, or differentiation in physiological conditions with available cognate ligands. Once the availability of these ligands falls below a specific threshold level, those receptors activate lethal signaling cascades. The role of dependence receptor-driven RCD as an oncosupressive factor has been observed through the upregulation of the cognate ligands, inactivation, downregulation, or losing of gene(s) encoding dependence receptors, and/or signaling signal transducers operating downstream of dependence receptors (Gibert and Mehlen, 2015) (Goldschneider and Mehlen, 2010).

BOX 2. Mitochondria: master regulators of life and death

The mitochondrion is a double membrane-bound organelle present in a variable number in the cytoplasm of almost all eukaryotic cells. Its size ranges from 0.5 to 10 μm and its shape is generally round or oval. Structurally, it is composed by the outer mitochondrial membrane (OMM), freely permeable to small molecules and with special channels capable of transporting large molecules; the inner mitochondrial membrane (IMM), less permeable than the OMM, allowing only very small molecules to cross into the gel-like matrix; the intermembrane space (IMS); the cristae, that contains the protein components of the electron transport chain; and, the matrix, which contains the mitochondrial genome and different enzymes including those of the tricarboxylic acid (TCA) cycle (also referred to as Krebs cycle) (**Figure I11**).

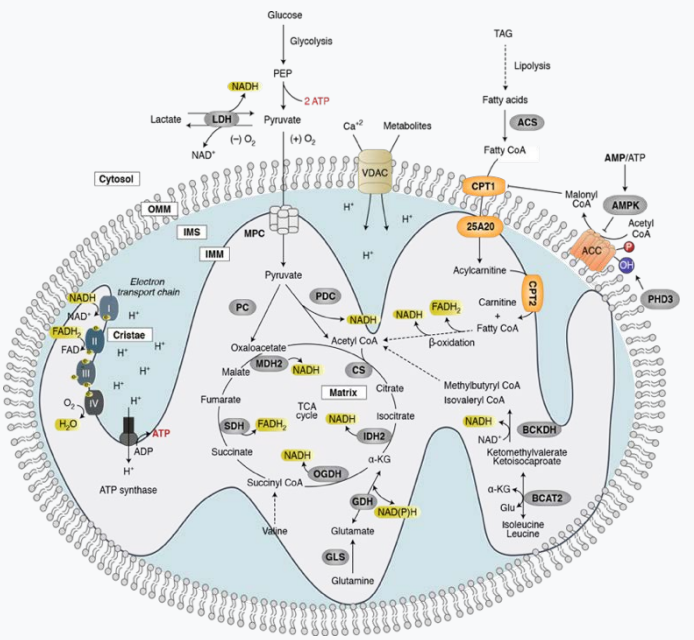

FIGURE I11. The powerhouse of the cell. Mitochondria integrate fuel metabolism to generate energy in the form of ATP. Mitochondria oxidize pyruvate (derived from glucose or lactate), fatty acids, and amino acids to harness electrons onto the carriers NADH and $FADH_2$. NADH and $FADH_2$ transport these electrons to the electron transport chain, in which an electrochemical gradient is formed to facilitate ATP production through oxidative phosphorylation. Electrons and reducing equivalents are shown in yellow. White squares indicate the different parts of the mitochondrion. Modified from Spinelli and Haigis, 2018.

Since 1970 mitochondria have been considered essential organelles for life involved in the synthesis of metabolites for macromolecule synthesis and in adenosine triphosphate (ATP) generation (Boyer *et al.*, 1977). However, thanks to the contributions of Dr. Xiaodong Wang and colleagues, *c*, since then functionally involved in oxidative phosphorylation, was described to be released from the IMS into the cytosol and to play an essential role in apoptosis (Liu *et al.*, 1996). Further research has evidenced that besides the role of mitochondria in apoptosis, this organelle is a central nexus between different cell death modalities including necroptosis, ferroptosis or pyroptosis (Bock and Tait, 2020) (**Figure I12**). Currently, it is accepted that plenty of cellular functions involve mitochondria. Not only as a cell supplier and in cell death but also in signaling, cellular differentiation, and cell cycle and growth (Tait and Green, 2012).

Particularly in cellular metabolism, mitochondria catabolize nutrients for energy, generate biosynthetic precursors for macromolecules, compartmentalize metabolites for the maintenance of redox homeostasis, and function as hubs for metabolic waste management ((Spinelli and Haigis, 2018) for an extensive review). Moreover, through fusion-fission dynamics (to dilute and segregate damaged mitochondria), as well as via motility and inter-organellar interactions (such as with the endoplasmic reticulum) mitochondria sense and respond to many stressors. In this sense, mitochondria are key regulators of the cellular adaptation to stress and prevent the transition from physiological to pathological outcomes due to maladaptive states (Eisner *et al.*, 2018).

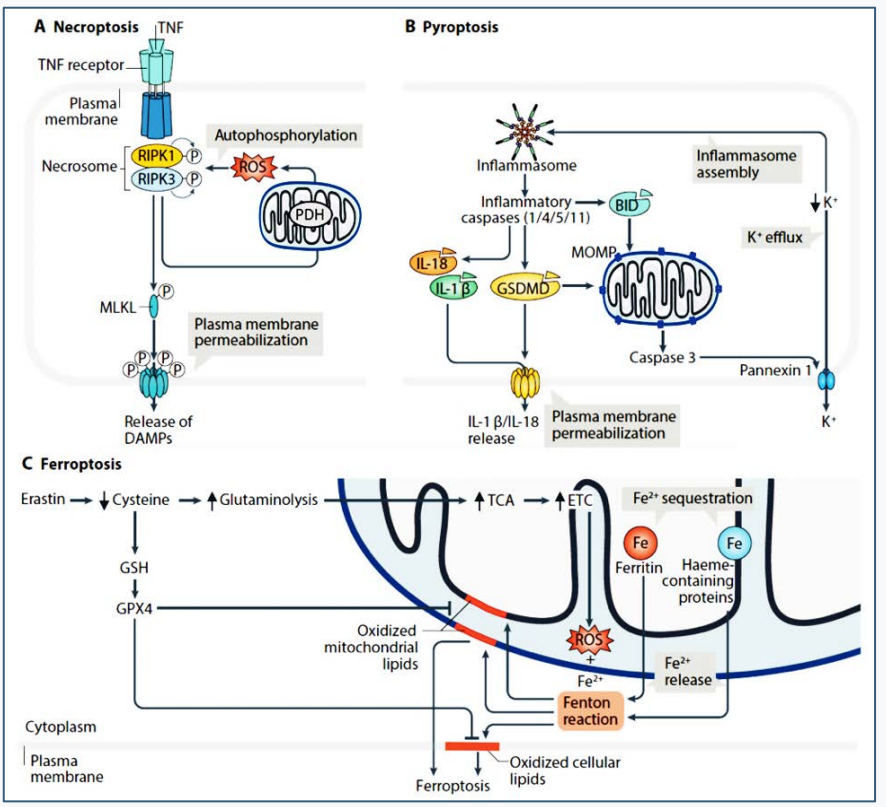

FIGURE I12. The role of mitochondria in different modes of cell death. A, necroptosis: RIPK3 activation of the mitochondrial pyruvate dehydrogenase (PDH) complex causes enhanced aerobic respiration and increased generation of ROS. Mitochondria-derived ROS can feedforward to enhance necrosome assembly and RIPK3 activity. **B**, **pyroptosis**: active gasdermin D (GSDMD) or cleaved BID lead to MOMP. Downstream of MOMP, activation of caspase 3 leads to cleavage-dependent activation of the potassium channel-forming glycoprotein pannexin 1, and this causes potassium efflux from the cell and promotes inflammasome assembly. **C**, **ferroptosis**: increased glutaminolysis induced by erastin treatment, feeds the mitochondrial tricarboxylic acid (TCA) cycle, thereby increasing mitochondrial respiration and, in consequence, augmenting levels of mitochondrial ROS. Mitochondria contribute to iron storage in various iron-binding proteins, including ferritin and haeme-containing proteins. These iron-storing proteins are degraded under certain cell death-inducing conditions, leading to iron release. The proximity of mitochondrial membranes to such sources of free iron and ROS makes them an important target for lipid oxidation associated with ferroptosis. Modified figure from Bock and Tait, 2020.

3.2. Intrinsic apoptosis

The NCCD describes intrinsic apoptosis as the "form of RCD initiated by a variety of microenvironmental perturbations including (but not limited to) growth factor withdrawal, DNA damage, endoplasmic reticulum (ER) stress, reactive oxygen species (ROS) overload, replication stress, microtubular alterations or mitotic defects" (Brumatti *et al.*, 2010) (Czabotar *et al.*, 2014) (Roos *et al.*, 2016) (Pihan *et al.*, 2017).

Mitochondria are key organelles deciding cell fate (**BOX 2**). In the case of intrinsic apoptosis, it holds, together with the apoptosis regulator B cell lymphoma 2 (BCL-2) protein family, a crucial role in cell death regulation (**Figure I10**). Structure, interactions, regulation, and functions of BCL-2 protein members are here reviewed to understand better its role in the intrinsic apoptosis and, particularly, its implication in the generation of MOMP, a crucial step for this subroutine of cell death. BCL-2 protein-mediated regulation of cell death has recently been reviewed (Kale *et al.*, 2018) (Singh *et al.*, 2019).

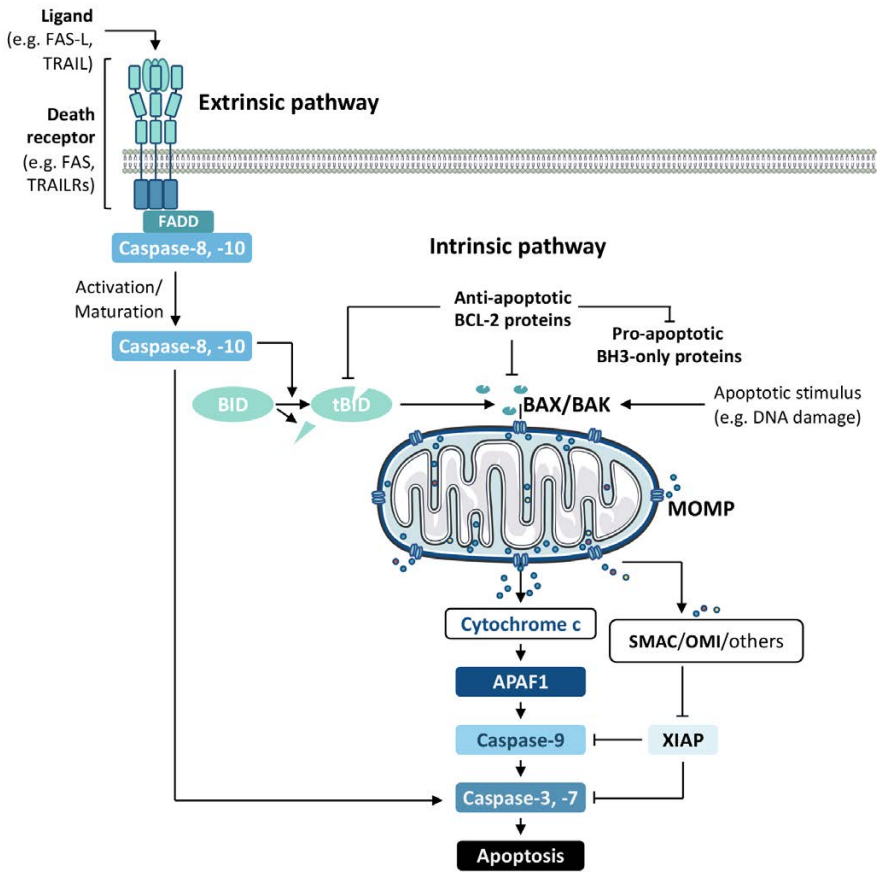

FIGURE I10. **Apoptotic signaling pathway.** Two alternative pathways, the extrinsic and the intrinsic pathway, can lead to apoptosis. Ligated death receptors recruit FADD that binds to and induces dimerization of caspase-

8, leading to its activation. Active caspase-8 can activate executioner caspases (such as -3 and -7) directly or through by cleaving BID, generating tBID, and activating the mitochondrial pathway. This pathway can be activated by different stimuli, including DNA damage or growth factor withdrawal, and lead to mitochondrial outer membrane permeabilization (MOMP) through the activation and inhibition of different BCL-2 proteins. MOMP allows the release of different mitochondrial proteins, including cytochrome *c*, which binds to APAF1 and leads to the formation of the apoptosome to recruit and activate caspase-9, which then activates executioner caspases; and SMAC and OMI that blocks the caspase inhibitor XIAP, facilitating apoptosis. Modified from Bock and Tait, 2020.

3.2.1. BCL-2 family proteins

The BCL-2 family of proteins is considered a clue member in life or death decisions because of its function integrating pro-apoptotic and anti-apoptotic signals in healthy and stressed cells. The name of this family comes from the discovery of a gene called B-cell lymphoma 2 (BCL-2), and was initially described as a partner in a reciprocal chromosomal translocation in follicular lymphomas involving chromosome 14 and 18 (Pegoraro *et al.*, 1984) (Tsujimoto *et al.*, 1985). This translocation turns out this gene to function not as a classic oncogene by driving cell division, but rather by preventing apoptosis. Indeed, the mammalian BCL-2 was then described as a potential substitute for *ced-9*, the *C. elegans* gene that inhibits cell death (Hengartner and Horvitz, 1994). The identification of this homology and the generality of the process encouraged until now thousands of studies concerning the mechanisms of action of BCL-2, now known, quite different from CED-9. While CED-9 sequesters the activator of the caspases, that is the ultimate effector of apoptosis in *C. elegans*, BCL-2 binds to other related proteins that regulate MOMP (Strasser and Vaux, 2018) (Shamas-Din *et al.*, 2013).

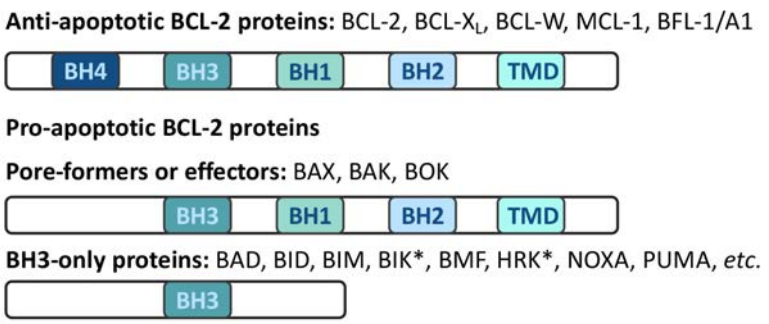

FIGURE I13. Classification and structure of BCL-2 family proteins. BH, BCL-2 homology domains; TMD, transmembrane domain; * indicates BH3-only proteins that contain TMD. Modified from Bock and Tait, 2020.

Based on their primary function, BCL-2 family proteins is divided into three groups: anti-apoptotic proteins, pro-apoptotic pore-formers and pro-apoptotic BH3-only proteins (**Figure I13**). Pro-apoptotic BH3-only proteins can be subdivided into activator and/or

'sensitizer' proteins. 'Activator' proteins (*e.g.*, BID and BIM) share the ability to physically, but transiently, bind to the mitochondrial pool of pore-former proteins (Ren *et al.*, 2010). By contrast, 'sensitizer' proteins bind to anti-apoptotic proteins and limit their ability to sequester pore-former or BH3-only 'activators' (Letai *et al.*, 2002) (O'Neill *et al.*, 2016). BH3-only proteins, essential initiators of intrinsic apoptosis, are considered the main upstream sentinels of the mitochondrial apoptotic pathway. This group of proteins function as cellular transducers of stress signaling and transmit both intrinsic and extrinsic death signals to different BCL-2 family proteins at the mitochondrial outer membrane.

Based on its structure, this evolutionarily-conserved family constitutes a group of proteins that share one to four BCL-2 homology (BH) domains (**Figure I13**). Indeed, all members contain a BH3 domain involved in the protein interactions of the family. The anti-apoptotic and pore-formers proteins are also referred to as multi-BH domain proteins and contain all four BH domains (BH1, BH2, BH3, and BH4) (Moldoveanu *et al.*, 2014) (Shamas-Din *et al.*, 2013). By contrast, and as suggested by its name, BH3-only proteins contain only the BH3 domain. Multi-BH domain proteins adopt a highly conserved tertiary structure forming a hydrophobic BH3 domain-binding groove that acts as a receptor for BH3 domains of other family members (Li *et al.*, 2017). BH3-only proteins (with the exception of BID) are mostly intrinsically unstructured in solution, undergo localized conformational changes in the BH3 region upon binding with anti-apoptotic proteins and can be activated transcriptionally or post-translationally (Hinds *et al.*, 2007). As an example, PUMA, BIM or NOXA are activated by transcriptional upregulation while others such as BID mostly undergo post-translational activation. BID, sometimes considered an outlier in the BH3-only family, shares structural-functional and phylogenetic characteristics closer to BAX (Billen *et al.*, 2008).

The BCL-2 family of proteins dictates cell death primarily by direct binding interactions between anti-apoptotic and pro-apoptotic BCL-2 family proteins. One of the last revisions addressing BCL-2 family proteins highlights how the interactions between the BCL-2 family proteins, the affinities, its relative abundance, the post-translational modifications, and the different intracellular location affects the mechanisms by which BCL-2 family proteins regulate MOMP, leading to the release of intermembrane space proteins, subsequent caspase activation, and apoptosis (Kale *et al.*, 2018). Making use of a metaphor, the authors organize a dance floor and refer to this family of proteins as 'dancers' throughout the review (**Figure I14**). In this metaphor, 'dancers' will dance with different partners along the 'dance of death', and who 'dances' with whom will dictate cell fate. Trying to avoid you feeling dizzy after so much dancing, several relevant concepts from this revision are mentioned below.

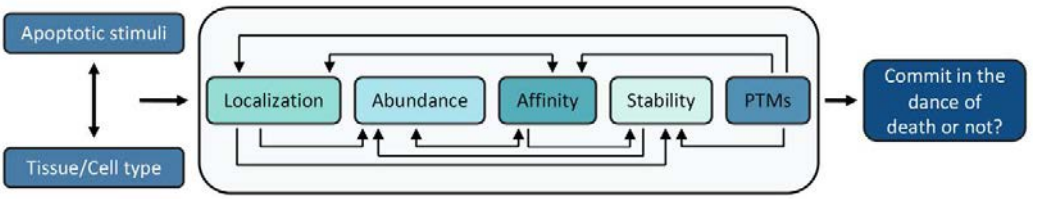

Figure I14. Cellular factors regulating commitment to the apoptotic dance of death by the BCL-2 family proteins. Differences in apoptotic stimuli and cell types lead to different responses due to the integration of the effects of localization, abundance, affinity, stability, and post-translational modifications (PTMs). Arrows connect related interactions. Figure from Kale *et al.*, 2018.

3.2.1.1. The interaction between BCL-2 family protein members

The specific interactions between the members of the three subgroups of the BCL-2 family proteins have been the object of different proposed models (Shamas-Din *et al.*, 2011) (Shamas-Din *et al.*, 2013) (**Figure I15**).

Among the different models, the embedded together model seems to be the most accepted model. According to this model, the affinity and the relative abundance of the proteins are the main factors governing BCL-2 family protein interactions. This affinity will greatly depend on protein conformation changes (most of them in the intracellular membranes) and will determine which binding interactions dominate and whether or not the cell undergoes MOMP (Kale *et al.*, 2018) (Singh *et al.*, 2019). Proteasomal degradation, phosphorylation, and subcellular (re)localization are some of the modifications that regulate BCL-2 proteins interactions, abundance and affinities (Low *et al.*, 2014) (Dumitru *et al.*, 2012) (Puthalakath *et al.*, 1999) (Gardai *et al.*, 2004). Moreover, the BH3 peptide length has been correlated with increased affinity for the binding partner; however, residues outside of the BH3 domain may facilitate proper interactions among BCL-2 family proteins (Czabotar *et al.*, 2011) (Kale *et al.*, 2018).

Given that the consequences of differing affinities determine if MOMP occurs, it is fundamental to establish the affinities between binding partners, and also their interactions with membranes to comprehend better the interactions between BCL-2 family proteins and its regulation of the cell death process. BCL-2 family protein interactions will be the result of distinct conformational changes governing their affinity for their potential partners and the relative local concentration of those binding partners (Leber *et al.*, 2007) (Bogner *et al.*, 2010). The different intracellular locations are clue factors governing the mechanisms of action of BCL-2 family proteins. In this sense, diverse localization, stated by their different affinities for various intracellular membranes and binding partners have been described within cells. Apart

from mitochondria localization, the most widely recognized location for BCL-2 family proteins is the endoplasmic reticulum (ER) where they regulate ER stress, redox and calcium homeostasis, bioenergetic metabolism, autophagy and apoptosis (Leber *et al.*, 2010). Different localization at mitochondria or at ER will result in different functions.

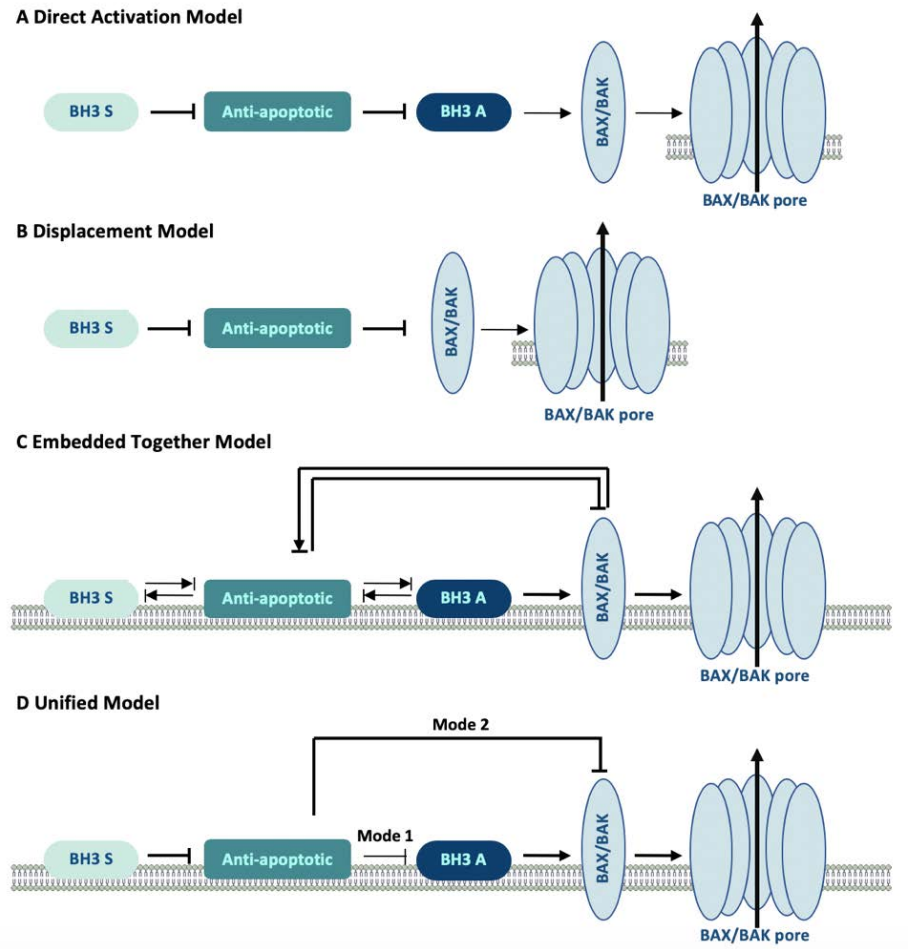

FIGURE I15. Schematic representation of different models of regulation of MOMP by BCL-2 proteins. A, direct activation model: 'sensitizer' BH3-only proteins (BH3 S) bind only to anti-apoptotic proteins, thereby liberating activator BH3 only proteins (BH3 A), which directly interact with and activate BAX and BAK to promote MOMP. Anti-apoptotic proteins can interact with both activator and 'sensitizer' BH3-only proteins, but cannot bind to BAX and BAK. **B**, **displacement model**: pore-former proteins are constitutively active and therefore have to be inhibited by anti-apoptotic proteins to impede cell death. BH3 proteins do not directly bind to BAX and BAK hence, they are not recognized as 'activators'. To undergo MOMP, the correct combination of BH3 proteins must compete based on their affinities for binding and displacing anti-apoptotic proteins from the pro-former proteins. **C**, **embedded together model**: this model combines aspects of the previous models and propose an active role for the membrane, being it the "locus of action" for different BCL-2 family proteins. 'Sensitizer' proteins bind only to anti-apoptotic proteins. Activator proteins can recruit and sequester anti-apoptotic proteins in the membrane, or directly activate BAX and BAK at membranes, which will then oligomerize and induce MOMP. This is inhibited by anti-apoptotic proteins either by sequestering BH3-only and pore-former proteins in the membrane or by preventing their binding to membranes. **D**, **unified model**:

builds on the embedded together model and propose that the anti-apoptotic proteins sequester the activator BH3 proteins (mode 1) and sequester active forms of BAX and BAK (mode 2). The unified model differs in that the inhibition of apoptosis through mode 1 is less efficient (smaller arrow in panel D) and, therefore, easier to overcome by BH3 'sensitizers'. By contrast, in the embedded together model either mode 1 or mode 2 can be dominant depending on circumstances such as the particular form of stress and cell type, the abundance of the protein, the competing equilibria or post-translational modifications. (↑) Activation; (⊥) inhibition; (⊥↑) mutual recruitment/sequestration. S and A indicate 'sensitizer' and 'activator' BH3-only protein, respectively. Modified from Shamas-Din *et al.*, 2011 and 2013.

The increasing knowledge of the mechanisms and functions of BCL-2 family proteins has led to the development of small molecules modulators of BCL-2 family proteins. In the context of a tumor, cancer cells became addicted to the expression of anti-apoptotic BCL-2 family proteins. This is because, in their absence, cancer cells would die faster than they grow. It is easy to think that the increase of BH3-only proteins inactivating anti-apoptotic proteins will push cancer cells or cells 'primed for death' to die (Singh *et al.*, 2019). This observation has attracted the attention of pharmaceutical companies encouraging the investment of a great deal of money to develop small molecules mimicking BH3 proteins. The base for this approach is to mimic the binding of BH3 peptides to the hydrophobic BH3 domain-binding groove of anti-apoptotic proteins. This lead to displace anti-apoptotic proteins from BH3-only proteins and actives BAX/BAK proteins (Tse *et al.*, 2008) (Souers *et al.*, 2013)).

Among these compounds, referred to as BH3 mimetic drugs, we find ABT-263 (Navitoclax), which inhibits BCL-2, BCL-X_L, and BCL-W (Oltersdorf *et al.*, 2005); and ABT-199 (Venetoclax), which only inhibits BCL-2 and is already approved by the FDA for its use in chronic lymphocytic leukemia (CLL) (Green, 2016). Other BH3-only-like or BH3 mimetics compounds include: chelerythrine, a BCL-X_L inhibitor (Chan *et al.*, 2003); AT-101 or gossypol, a BCL-2, BCL-X_L and MCL-1 inhibitor (Zhang *et al.*, 2003) (Kitada *et al.*, 2003); HA14-1, a BCL-2, BCL-X_L inhibitor (Wang *et al.*, 2000), EM20-25, a BCL-2 inhibitor (Milanesi *et al.*, 2006); obatoclax, an inhibitor of BCL-2, BCL-X_L, BCL-W and MCL-1 (Perez-Galan *et al.*, 2007) (Trudel *et al.*, 2007) (Nguyen *et al.*, 2007); and TW37, a BCL-2, BCL-X_L and MCL-1 inhibitor (Zeitlin *et al.*, 2006). Additionally, other molecules with a similar mechanism of action, such as S63845, an MCL-1 inhibitor, are currently under study (Kotschy *et al.*, 2016) (Roberts *et al.*, 2016). Although different clinical trials have demonstrated the therapeutic potential of these small molecules in cancer treatment, especially in those of hematopoietic origin, not all cancer cell types are sensitive to BH3-mimetic compounds, particularly those of solid origin frequently demonstrate resistance. Moreover, a mechanism of resistance to BH3 mimetics ascribed to the tight association between BH3-only 'activators' and anti-apoptotic proteins such as BCL-X_L has been recently reported. The impact of this resistance

mechanism regarding the effect of venetoclax treatment in CLL patients remains to be elucidated (Aranovich *et al.*, 2012) (Pecot *et al.*, 2016).

3.2.2. Mitochondrial outer membrane permeabilization (MOMP)

Taking up the beginning of that section (*3.2. Intrinsic apoptosis*), the permeabilization of the mitochondrial outer membrane, a process best known as MOMP, is a critical step for intrinsic apoptosis. Once the intrinsic or mitochondrial pathway is triggered, MOMP leads to the release of various intermembrane space (IMS) proteins that promote caspase activation (**Figure I10**). It is well established that MOMP causes apoptotic cell death through the activation of caspases. However, MOMP can also lead to cell death by altering mitochondrial functions irrespective of caspase activity. Moreover, although MOMP is sometimes referred to as the point of no return for cell survival, some cells can recover after MOMP and may lead to pathophysiological consequences. Indeed, pro-inflammatory signaling functions are among the non-lethal consequences engaged upon MOMP. Additional mitochondrial roles have been linked to other regulated cell death modalities such as necroptosis, ferroptosis, and pyroptosis (**Figure I12**). Hence, meaning that MOMP cannot be used as synonymous with apoptosis (Bock and Tait, 2020).

Due to the role of mitochondria not only in different forms of regulated cell death but also in non-lethal functions, anti-apoptotic and pro-apoptotic members of the BCL-2 family (*3.2.1. BCL-2 family proteins*) tightly control MOMP. In physiological conditions, the pro-apoptotic pore-former proteins cycle from the OMM to the cytosol. Traditionally, this retrotranslocation has been assigned to BAX. However, some degree of BAK retrotranslocation has also been reported (Todt *et al.*, 2015). This retrotranslocation, which exerts a protective role by limiting the mitochondrial pool of BAX and BAK, is, in part, promoted by anti-apoptotic proteins such as BCL-X_L (Edlich *et al.*, 2011) (Todt *et al.*, 2015) (Bleicken *et al.*, 2017).

The inactive form of BAX and BAK consists of a globular structure. Like different BCL-2, BAK is inserted within the membranes via its hydrophobic C-terminal transmembrane α9 helix. In the case of BAK, this membrane is generally the lipid bilayer of the outer mitochondrial membrane (OMM). By contrast, the helix α9 of BAX is sequestered to the protein core within the hydrophobic BH3 domain-binding groove and, consequently, it makes BAK generally reside at the cytoplasm (Nechushtan *et al.*, 1999). In response to a stimulus, quiescent monomeric or inactive dimeric conformation of BAX and/or BAK undergo direct

or indirect activation by pro-apoptotic BH3-only proteins (Kuwana *et al.*, 2005). Activator BH3-only proteins bind to the BH3 domain-binding groove and displace α9 helix (especially from BAX). This α9 helix is then inserted into the bilayer in a similar manner like inactive BAK does (Nechushtan *et al.*, 1999) (Dai *et al.*, 2011) (Robin *et al.*, 2015). Upon different conformational changes, activator BH3-only proteins leave the BH3 domain-binding groove, allowing BAX/BAK to proceed with its oligomerization. BAX and BAK will form homodimers with other active BAX/BAK monomers or less frequent heterodimers (**Figure I16**). At steady state, activator BH3-only proteins such as BID have been detected forming heterodimers with BAX even after pore formation (Lovell *et al.*, 2008) (Gahl *et al.*, 2016).

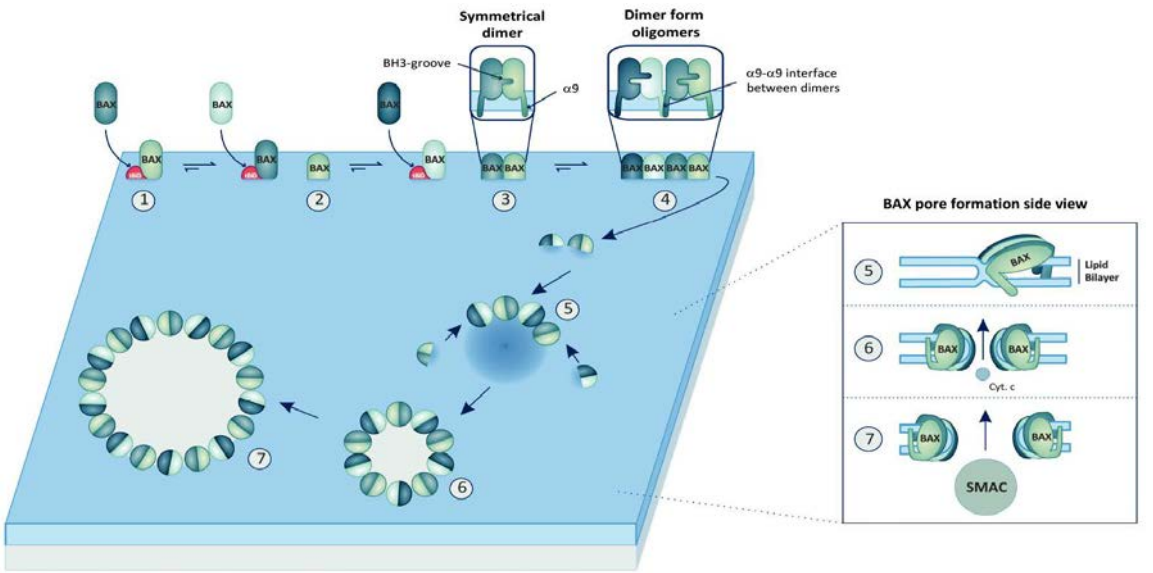

FIGURE I16. Multi-step process for BAX activation, membrane permeabilization, and release of intermembrane space (IMS) proteins. Modified from Kale *et al.*, 2018.

It seems like the most accepted hypothesis that BH3 'activators' switch inactive monomers of BAX/BAK into active membrane-embedded monomers. Once at lipid bilayer, active pore-former monomers undergo structural rearrangement that might reduce its affinity with BH3-only proteins, thus favoring BH3-only proteins displacement and BAX/BAK homodimerization. Higher affinity homotypic interactions than heterotypic interactions between pore-former proteins and BH3 'activators' could explain the transition from the BAX/BAK and BH3-only protein heterodimer to BAX/BAK homodimers. Indeed, the recruitment of multiple activated BAX/BAK monomers in close proximity leads to BAX/BAK dimerization via high-affinity symmetric interactions between BH3 domain-binding grooves. The high local concentration of BAX/BAK dimers assemble into higher-order oligomers forming lines, arcs, or rings formed pores (Subburaj *et al.*, 2015). The

formation of oligomers by weak affinity-interacting dimers explain the enlargement of pores over time. Those oligomers trigger, through those pores, membrane permeabilization and the consequent leakage of different proteins (**Figure I10** and **I16**).

As stated before, most anti-apoptotic BCL-2 family proteins will try to prevent BAX and BAK oligomerization either upon physical sequestration at the OMM or indirectly, following the sequestration of BH3-only 'activators' (Czabotar *et al.*, 2014) (Chen *et al.*, 2015) (Llambi *et al.*, 2011). However, in the absence of anti-apoptotic BCL-2 family members and pro-apoptotic BH3-only proteins, BAX and BAK can self-activate according to a relative slow kinetics (Chen *et al.*, 2015)(O'Neill *et al.*, 2016) and through the concerted action of several proteins containing BH-like motifs including p53 (Chipuk *et al.*, 2004) (Vaseva and Moll, 2009) and ATR serine/threonine kinase (ATR) (Hilton *et al.*, 2015). Additional noncanonical BAX and BAK activators like detergents, pH changes, heat, or specific monoclonal antibodies have also been described and remain to be formally established (Chen *et al.*, 2015)(O'Neill *et al.*, 2016).

Regardless of the mechanism of BAX/BAK activation, MOMP promotes the cytosolic release of factors that generally reside in the IMS (Tait and Green, 2013). Cytochrome *c* and the second mitochondrial activator of caspases (SMAC) –also known as diablo IAP-binding mitochondrial protein (DIABLO)– are the main apoptogenic factors released from the mitochondria (Du *et al.*, 2000) (Chai *et al.*, 2000) (Verhagen *et al.*, 2000). Other proteins such as the serine protease HTRA2, also known as OMI; the apoptosis-inducing factor (AIF); or the endonuclease G (EndoG) (Li *et al.*, 2001) are additional pro-apoptogenic factors released from the mitochondria upon mitochondria permeabilization.

Once at the cytosol, cytochrome *c*, which usually functions as an electron shuttle in the mitochondrial respiratory chain, binds to apoptotic peptidase activating factor 1 (APAF1) and pro-caspase 9 in a deoxyATP-dependent manner (Li *et al.*, 2000b) (Liu *et al.*, 1996) (Li *et al.*, 1997). This supramolecular complex is best known as the apoptosome and is responsible for caspase-9 activation (Li *et al.*, 1997), which in turn is responsible for caspase-3 and caspase-7 proteolytic activation. Those enzymes, commonly known as executioner caspases, are widely recognized as the enzymes responsible for the final cellular demise after activation of the intrinsic or extrinsic apoptosis in mammalian cells (Julien and Wells, 2017) (Shalini *et al.*, 2015). Moreover, the loss of cytochrome *c* from mitochondria also triggers respiratory impairment that correlates with the dissipation of the mitochondrial transmembrane potential ($\Delta\psi m$) upon MOMP and, hence, to the interruption of ($\Delta\psi m$)-dependent functions (Zamzami *et al.*, 1995a) (Zamzami *et al.*, 1995b).

Released SMAC/DIABLO binds to the inhibitor of apoptosis (IAP) protein family, including X-linked inhibitor of apoptosis (XIAP) (Verhagen *et al.*, 2000) (Du *et al.*, 2000) (Salvesen and Duckett, 2002). Due to the physical blockage of caspases through XIAP binding (Eckelman and Salvesen, 2006) (Eckelman *et al.*, 2006), the cytosolic pool of SMAC interacting with XIAP precipitates apoptosis. Likewise, HTRA2/OMI also facilitates caspase activation by blocking IAPs and, together with SMAC/DIABLO, can also trigger caspase-independent cytotoxicity (Salvesen and Duckett, 2002) (Fuentes-Prior and Salvesen, 2004) (**Figure I10**).

3.3. Caspases

Traditionally, apoptosis has been described from a morphological point of view. However, the observation of apoptotic morphological features can be a difficult issue *in vivo*. Studies in *Caenorhabditis elegans* permitted to visualize the entire process of cell death and seeded the biochemical bases of apoptosis with the discovery of *ced-3* (Ellis and Horvitz, 1986). Besides *C. elegans*, the research in many other species was crucial to determine the existence of a family of cysteine proteases called caspases, a term introduced in 1996 and coined from the contraction of cysteine-dependent aspartate specific proteases (Alnemri *et al.*, 1996). Studies in different animals has contributed to the elucidation of how this family of proteins functions, and has evidenced that the proteolytic cleavage of downstream substrates of caspases is one of the main responsible biochemical events governing the final morphological aspect of a cell that has undergone an apoptotic process (Martin and Green, 1995) (Fuentes-Prior and Salvesen, 2004) (Ramirez and Salvesen, 2018).

Until now, 18 mammalian caspases have been described but not all are equally expressed among different species. The human caspase-5 is not present in mice and caspase-11 and -13 are the murine and bovine orthologues of the human caspase-4, respectively (Eckhart *et al.*, 2008) (McIlwain *et al.*, 2013). The recently identified caspases (caspases-15, -16, -17 and -18) are absent in placental mammals except caspase-16 (Eckhart *et al.*, 2008). Caspase-12 exists in both truncated and full-length alleles in humans and as a full-length caspase in rodents (Fischer *et al.*, 2002). Except for caspase-1, which is enriched in monocytes and macrophages, and caspase-14, which is expressed in keratinocytes and has a primary role in keratinization of the skin (Hoste *et al.*, 2011) (Denecker *et al.*, 2007), caspases are widely expressed (Shalini *et al.*, 2015).

3.3.1. Structural organization of caspases

The first structures of caspases were published in 1994 (Walker *et al.*, 1994) (Wilson *et al.*, 1994). At that time, the term caspase was not yet introduced and they were described as novel proteases fold family.

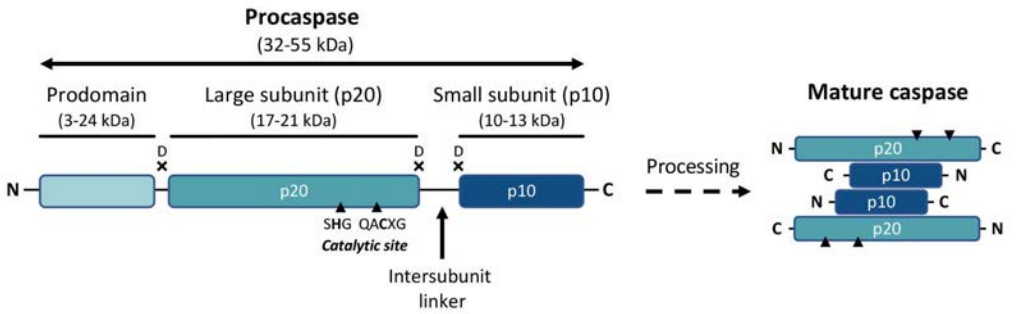

FIGURE I17. **Scheme of the procaspase structure and of the active caspase.** Cleavage of the procaspase at the aspartate (D)-X bonds and release of the prodomain leading to the formation of the mature caspase (heterotetramer $p20_2$-$p10_2$) These subunits are also referred as α and β subunits, respectively. N and C indicate the NH_2 and COOH terminus. Arrows indicate the catalytic dyad residues (histidine and cysteine) in the p20 domain involved in the formation of the catalytic site. Modified from (Chowdhury *et al.*, 2008) and Lavrik *et al.*, 2005.

Structurally, caspases are synthesized as single-chain zymogens with an N-terminal domain followed by a conserved C-terminal protease catalytic domain (**Figure I17**). Its length varies from 32 to 55 kDa and can await activation either as inactive monomers or dimers. The N-terminal domain, also referred to as the pro-domain, is variable (3 - 24 kDa). It can encode recruitment and activation signals and determines the type of activation mechanism that caspases use (Ramirez and Salvesen, 2018). The pro-domain of initiator or inflammatory caspases (see *3.3.2. Classification of caspases*), contains either death effector domains (DEDs) or caspase recruitment domains (CARDs) that vary in number among caspases and are crucial for their activation (**Table I3**). The C-terminal catalytic domain is a single domain that often splits into two chains upon proteolytic cleavage: the large subunit (17-21 kDa, generally referred to as the p20 subunit) that contains the catalytic dyad residues –cysteine (C) and histidine (H)–; and the small subunit (10-13 kDa, also known as the p10 subunit), which includes residues that primarily form the substrate recognition groove. Unstructured regions exist linking the two subunits and also linking the pro-domain and catalytic domains (**Figure I17**). Those regions are often the subject of (auto)proteolysis during maturation.

Moreover, all caspases contain a conserved pentapeptide active site motif QACXG – glutamine (Q), alanine (A), cysteine (C), X, glycine (G)– (**Figure I17**), where X is a glutamine

(Q) for caspase-8 and -10, is a glycine (G) for caspase-9, and is an arginine (R) for the rest of caspases (Cohen, 1997).

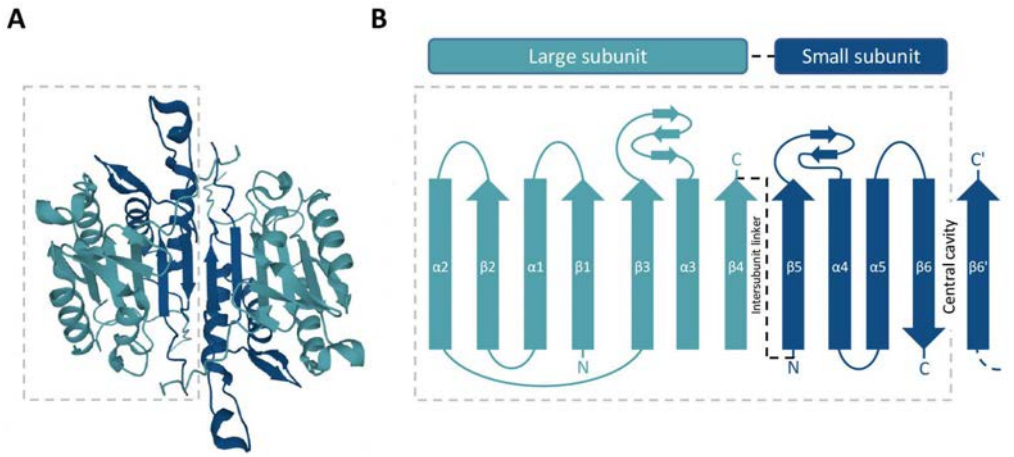

FIGURE I18. Structure of caspases. A, crystal structure of caspase-3 heterotetramer (modified from PDB code 2H51). Two heterodimers –each one formed by one large subunit (light blue) and one small subunit (dark blue)– fit together with formation of a twelve-stranded β-sheet that is sandwiched by α-helices. **B**, simplified topological diagram of the secondary structure of caspase-3 heterodimer formed of six antiparallel β-strands. Note that the C-terminal strand β6 of the small subunit is aligned in an antiparallel manner with the C-terminal strand β6' of the small subunit to form the heterotetramer. Modified from Fuentes-Prior and Salvesen, 2004.

Crystallographic studies demonstrated structural similarity among caspase recruitment domains suggesting a common evolutive origin (Hofmann, 1999) (Fesik, 2000) (Shi, 2002). Alignment of large and small subunits of different caspases evidenced around twenty-nine similar residues in at least ten members of the family (Earnshaw *et al.*, 1999). Among them, seven amino acids play a crucial role in the substrate recognition and catalytic process. Moreover, crystal structures revealed that active caspases are formed by heterotetramer complexes containing two catalytic domains (two small and two large subunits). In more detail, each catalytic domain or heterodimer, originated from a single pro-caspase molecule, is formed by hydrophobic interactions and results in the formation of a twisted, mostly parallel β-sheet inserted between two layers of α-helices. Large and small subunits, tightly packed into a compact ellipsoid fit with another catalytic domain by the alignment of the C-terminal strands β6 in an antiparallel manner (β6↓ - ↑β6'). The result of this structure is a continuous twelve-stranded β-sheet sandwiched between two layers of α-helices (Fuentes-Prior and Salvesen, 2004) (Lavrik *et al.*, 2005) (**Figure I18**).

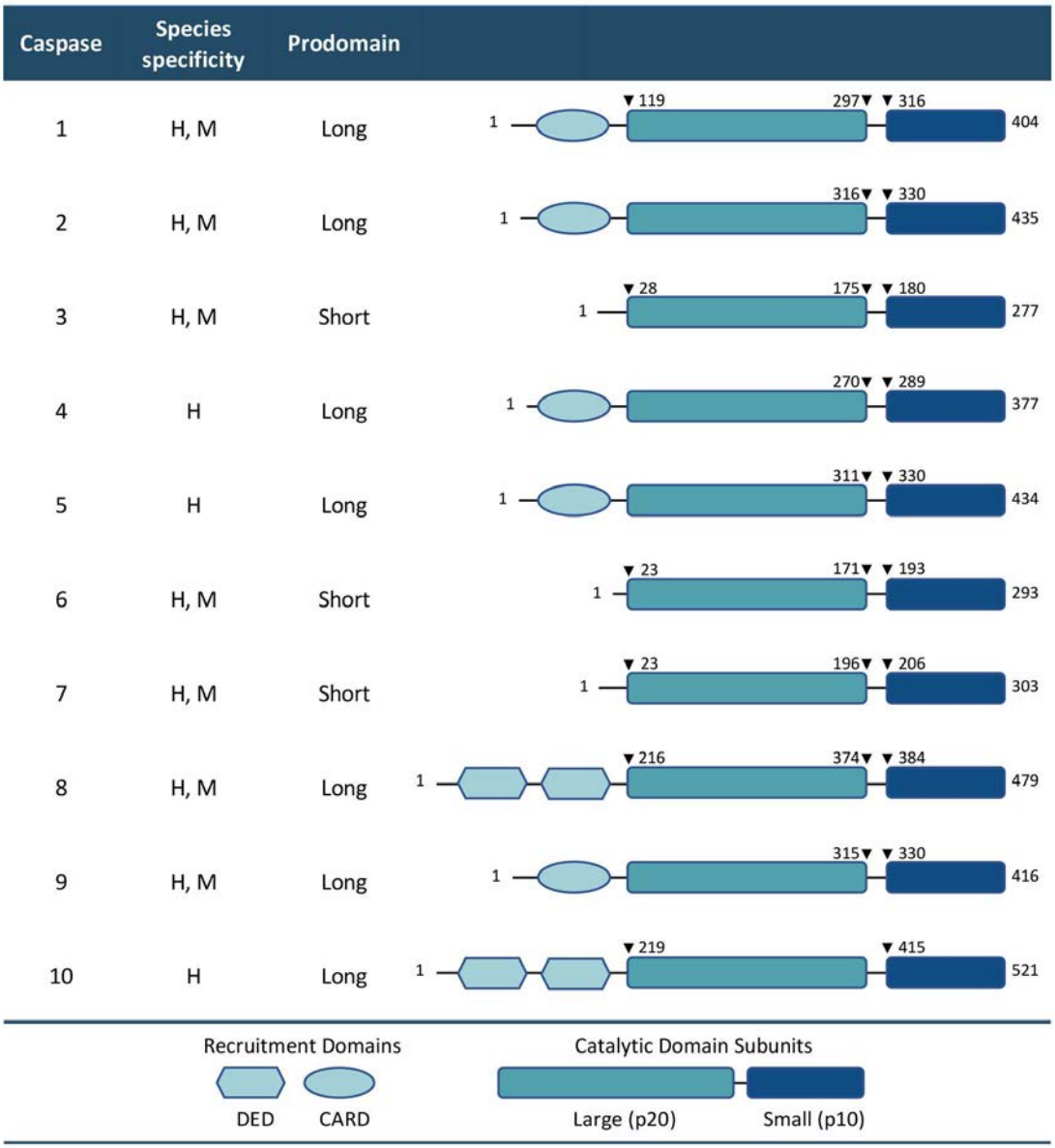

TABLE I3. Structure of caspases and sites of cleavage. H, human; M, mouse. Arrowhead indicate the site of cleavage to generate the large and the small subunits. DED, death effector domain; CARD, caspase recruitment domain. Modified from (Taylor *et al.*, 2008) (Salvesen and Ashkenazi, 2011).

3.3.2. Classification of caspases

According to their apoptotic activity, caspases have been broadly classified into 'initiator' or 'apical' (caspase-8, -9 and -10) and 'effector' or 'downstream' (caspase-3, -6, -7) caspases. This classification differentiates caspases between its presumptive function initiating or executing apoptosis, respectively (Riedl and Shi, 2004). Initiator caspases are further divided into

caspases participating in the extrinsic or death receptor-triggered pathway (caspase-8 and -10) or intrinsic or mitochondrial signaling pathway (caspase-9).

As one can notice, this classification does not include caspases such as caspase-1, -4, or -5. This is in line with the simple division between "apoptotic" and "pro-inflammatory" caspases that has been employed for several years. The inflammatory subset in humans is mainly characterized by caspase-1, -4, -5, and -12. In mice, this role is prominently performed by caspase-1, -11, and -12 (McIlwain *et al.*, 2013). Activation of caspase-1, -4, -5 or -11, but also other caspases including caspase-3 contribute to modulation of activity of cytokines and lead to maturation of proinflammatory cytokines such as IL-1β and IL-18 (Jimenez Fernandez and Lamkanfi, 2015) (He *et al.*, 2015) (Miller *et al.*, 2020). Indeed, although this classification between apoptotic and inflammatory caspases can be useful to some extent, recent studies have revealed that most apoptotic candidates (caspase-2, -3, -6, -7, -8, -9, and -10) have at least one non-apoptotic role attributed to them (Bredesen, 2008) (Nakajima and Kuranaga, 2017) (Mukherjee and Williams, 2017). The only truly remaining non-apoptotic human candidate may be caspase-14, a mediator in keratinocyte differentiation (Denecker *et al.*, 2007). Furthermore, the complexity of classifying this family of cysteine proteases is evidenced by caspase-2, which has been reported to display combined features from initiator and effector caspases, and to participate in other cellular processes such as cell cycle regulation (Bouchier-Hayes and Green, 2012). Caspase-2 and -8, under certain conditions, can trigger either cell death or the NF-κB survival pathway (Tinel *et al.*, 2007) (Wang *et al.*, 2008a) (**Figure I9**).

Apart from the classification based on the presumptive function of caspases, other criteria such as the pro-domain length, the phylogenetic relationships, and substrate preference have also been proposed. Classification of caspases according to the pro-domain length, which often concords with the mechanisms of action, divides into long pro-domain (around 100 residues) and short pro-domain caspases. The first group is composed of caspases activated by dimerization such as initiator caspases, inflammatory caspases, and caspase-2. The second group includes those caspases activated by cleavage of the catalytic domain, including caspase-3, -6, and -7. Regarding the classification based on the synthetic substrate preference, it may not be accurate to discriminate between caspases and may lead to inaccurate information since it does not mirror the real caspase substrate preference *in vivo* (Pop and Salvesen, 2009) (Ramirez and Salvesen, 2018). Despite being aware of the limitations, due to simplification and the lack of a new classification accepted, the classification between initiator and effector caspases is employed in the following sections.

3.3.3. Activation mechanisms of caspases

The synthesis of an enzyme as zymogen means that it has to await activation to exert its function. In the case of caspases, while zymogens and active conformation forms are quite similar, the mechanisms of activation of initiator and effector caspases are remarkably different (**Figure I19**).

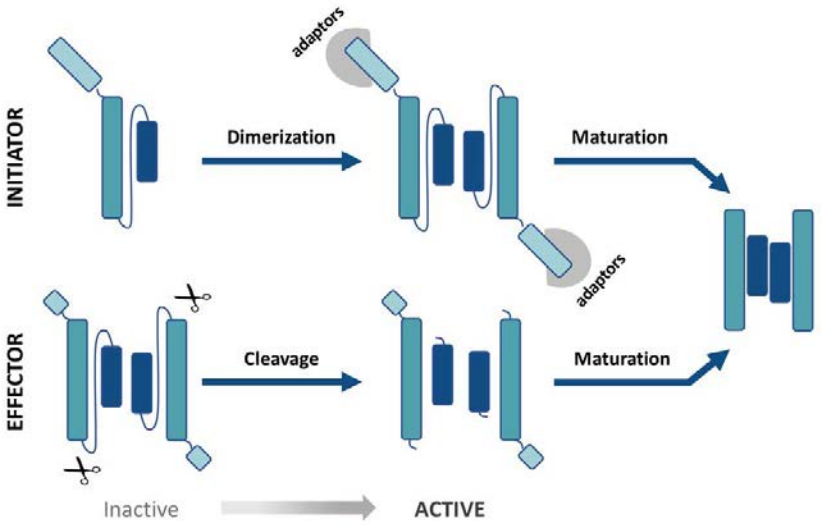

FIGURE I19. Schematic representation of the activation mechanism of initiator and effector caspases. Initiator caspases become activated by dimerization and effector caspases by cleavage of intersubunit linker. Following activation, additional proteolytic events maturate the caspases to more stable forms. Modified from Pop and Salvesen, 2009.

Activation mechanisms of initiator caspases

The most accepted model for the activation of initiator caspases is referred to as the induced proximity model (Salvesen and Dixit, 1999). This consists of a coordinated clustering mechanism leading to the dimerization of the inert monomers (off-state or zymogens initiator caspases) and, finally, to its activation. Different activation platforms have been described to interact with DED and CARD domains of initiator caspases and to facilitate their dimerization. The DISC (death-inducing signaling complex) recruits and activates caspase-8 and -10 through its DED (**Figure I8**); the apoptosome activates caspase-9 through its CARD (Cheng *et al.*, 2016) (**Figure I20**), and the PIDDosome is involved in the activation of caspase-2, which also poses a CARD. Alternatively, the endoplasmic reticulum-Golgi intermediate compartment or autophagosomal membranes can serve as activation platforms where initiator caspases such as caspase-8 can be recruited and activated to initiate the caspase-8/-3 cascade (Lam *et al.*, 2020) (Young *et al.*, 2012).

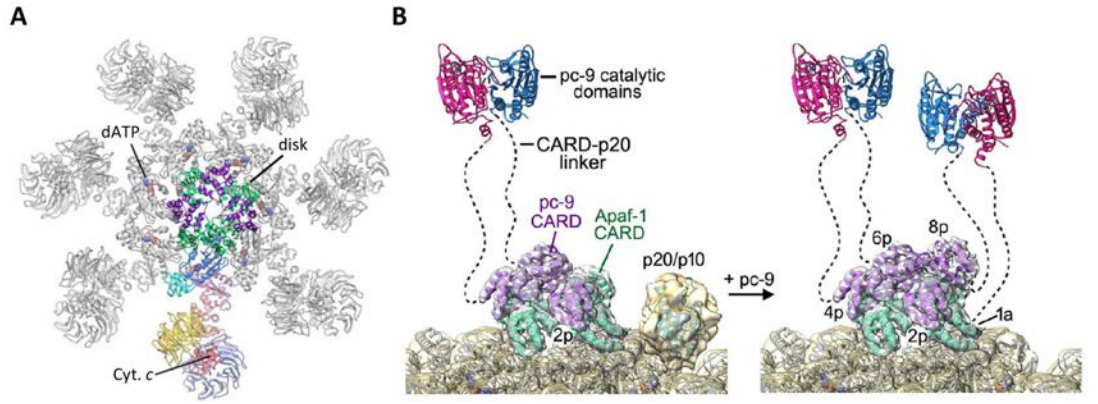

FIGURE I20. The apoptosome. A, top view of the complete model of the active apoptosome that consists of a large wheel-like complex that contains seven copies each of APAF-1 and cytochrome *c* (cyt. *c*). Cytochrome *c* interacts with APAF-1, together with a nucleotide triphosphate molecule. The central hub of the wheel recruits and activates the procaspase-9 (pc-9) through CARD domain interactions. According to Cheng *et al.* a disk-like structure made from the parts of four APAF-1 proteins and pc-9 sites atop the central hub of the wheel-like apoptosome. Domains in a single APAF-1 and the acentric CARD disk are colored, relative to the remaining APAF-1 subunits, which are shown in grey (**A**). **B**, models of the active apoptosome. Procaspase-9 dimers are flexibly-tethered to the CARD disk and may represent the activated enzyme. The number of possible pc-9 dimers in the active apoptosome may vary as a function of the number of pc-9 molecules tethered to the disk. On average, APAF-1 CARDs recruit 3 to 5 pc-9 molecules. A stoichiometry of one or at most, two pc-9 dimers per active apoptosome is suggested by Cheng *et al.*. Left panel show apoptosome with 3 bound pc-9 molecules and a right panel show an active complex with 4 bound pc-9 molecules. Modified from Cheng *et al.*, 2016.

The main apoptotic function of initiator caspases is to activate downstream effector caspases. To do so, apical caspases need to integrate a cellular death signal and convert it to proteolytic activity. After receiving an apoptotic signal, initiator caspases recruited by adaptor molecules oligomerize to different activation platforms, thus facilitating the dimerization. The close proximity and induced recruitment promote a local increase in caspase concentration (Riedl and Salvesen, 2007). Together with the proximity-induced dimerization and conformational changes, this physiological strategy results in the formation of active sites and, therefore, the activation of initiator caspases, which are now ready to engage downstream signaling pathways as the activation of effector caspases. Although not in all cases, subsequent autocleavage of initiator caspases is necessary to stabilize the mature active enzyme (Pop *et al.*, 2007) (Oberst *et al.*, 2010) (see *3.3.4. Maturation*). However, while cleavage of an executioner caspase is indicative of its activation, that of initiator caspases does not necessarily indicate activation (McStay *et al.*, 2008).

Much of the biochemical and structural work on activation of apical caspases has focused on caspases-8 and 9. Still, the same concept is thought to hold true for the activation of pro-inflammatory caspases, which are probably activated by a similar induced dimerization

mechanism. The multiprotein activation platforms for these groups of caspases are called inflammasomes and present affinity for the CARD pro-domains of caspase-1, -4, and -5 (Martinon and Tschopp, 2007). However, it is not clear whether the activation mechanism of inflammatory caspases occurs by enforced homodimerization or is the result of heterodimerization with other components of the inflammasome.

Activation mechanism of effector caspases

Contrary to initiator caspases, effector caspases are synthesized and, shortly after, they dimerize in absence of protein-interaction domains. The activation of these inactive dimers relies on the proteolytic cleavage within their β4-β5 intersubunit linker that separates large and small subunits of the catalytic domain (**Figure I18**) and the conformational rearrangement of mobile loops (Fuentes-Prior and Salvesen, 2004). This cleavage of the zymogen results in the catalytic cysteine-histidine dimer required for protease activity (**Figure I19**). *In vivo*, the proteolytic processing of the linker is due to the participation of upstream processors, including initiator caspases (caspase-8, -9, and -10) and other proteases such as the lymphocyte-specific serine protease granzyme B.

3.3.4. Maturation of caspases

Maturation events refer to the (auto)proteolytic cleavage of caspases that frequently follows its activation. It is essential not to confuse caspase maturation events with activation. The activation is needed to generate enzymatic activity, whereas the maturation process is often an optional and chronologically distinct event (Fuentes-Prior and Salvesen, 2004). As an example, the trimming of the pro-domain is considered a maturation event of caspases and, in contrast with many other proteases, does not constitute an activation mechanism. Removal of the N-terminal pro-domain or cleavage of the inter-chain linker may occur both after activation and through auto-proteolysis. As an example, the processing of procaspase-3 results in the generation of the small p12 and large p20 active subunits. The p20 fragment is further processed to the p19 and then to the p17 fragment by rapid and slow autocatalytic steps. The cleavage of the linker enhances the stability of the dimer and may contribute to other downstream regulatory events (Fuentes-Prior and Salvesen, 2004) (Ramirez and Salvesen, 2018). Likewise, one of the most appealing aspects of caspase maturation is its influence on cell processes such as proliferation or cell death. As an example, caspase-8 autocleavage stabilizes its catalytic domain enabling its activity and its permanence in the cytosol once released from the DISC. By contrast, dimerization of caspase-8 in the absence of maturation produces a form of active caspase-8 not competent for cell death but, signaling T cell

proliferation and activation (Kang *et al.*, 2008). In the case of caspase-9, the intersubunit linker cleavage has been attributed to caspase-3. This maturation event exposes new epitopes that are necessary for the endogenous inhibitor XIAP to bind and regulate caspase-9 (Srinivasula *et al.*, 2001). Thus, although additional studies are necessary to elucidate the role of maturation events in the cell context, it seems clear that maturation exerts a function generating caspase stability or signaling downstream regulatory events.

3.3.5. Specificity and substrates of caspases

As mentioned before, the name of caspases (Alnemri *et al.*, 1996) –cysteine-dependent aspartate-specific proteases– derives from the common use of a cysteine (Cys, C) side chain acting as a nucleophile during peptide bond hydrolysis and a primary specificity for aspartic (Asp, D). This last particularity is shared with the serine protease granzyme B but is less common among other proteases.

The dominant specificity for protein substrates containing Asp (D) govern the enzymatic properties of caspases; they generate a proteolytic cleavage on the C-terminal side of Asp and N-terminal to the scissile bond. Indeed, primary specificity basic pockets of caspases have a perfect shape to accommodate an Asp side chain (Fuentes-Prior and Salvesen, 2004). However, it is necessary to stress that different recent reports suggest that caspases may cleave their targets almost as efficiently on motifs containing glutamate or phosphoserine in place of aspartate (Seaman *et al.*, 2016).

Caspases	P_5	P_4	P_3	P_2	P_1	P_1'
Caspase-1, -4, -5, -14		W/Y	E	X	D	ϕ
Caspase-8, -9, -10		I/L	E	X	D	ϕ
Caspase-3, -7		D	E	X	D	ϕ
Caspase-6		V	E	X	D	ϕ
Caspase-2	V/L	D	E	X	D	ϕ

TABLE I4. Inherent substrate specificity. All caspases show selectivity for aspartic (D) in the P_1 position, a preference for a glutamic acid (E), and preference for different uncharged residues at P_1' (denoted by the ϕ symbol) (Poreba *et al.*, 2013).

In addition to Asp (D) residue requirement, many other requirements help to define proper caspase substrates. In most of the cases, caspase substrates share a peptide of sequence P_4-P_3-

P_2-P_1-P_1' in which the P_1 residue is an aspartic (D); the P_1' residue is small and uncharged - glycine (Gly, G), serine (Ser, S), alanine (Ala, A), threonine (Thr, T), asparagine (Asn, N); the P_3 is preferentially a glutamic acid (Glu, E); and P_4-P_3-P_2 residues are complementary for interactions with the catalytic groove and define the adequacy of substrates for the different caspases (**Table I4**). As an example, executioner caspases cleave DEV(D/G) peptides very efficiently, while WEH(D/G) peptides are more efficiently cleaved by inflammatory caspases (V corresponds to valine (Val), W to tryptophan (Trp) and H to histidine (His)). As a consensus, the preference of caspases for individual peptide sequences is referred to as "inherent subsite preference" (Poreba *et al.*, 2013). Moreover, although it may be obvious, the colocalization of caspases and substrate is another requirement.

Furthermore, substrate residues P_4-P_1' contribute to binding through association with S_4 through S_1' pockets in the protease active site (**Figure I21**). Indeed, the cleavage site of natural protein substrates (P_4-P_1') is exposed to the aqueous environment, and the majority of cuts occur in "loops" or "turns" regions. This observation indicates that caspase cleavage requires transient structural rearrangement of substrates to a cleavable extended conformation (Fontana *et al.*, 2004).

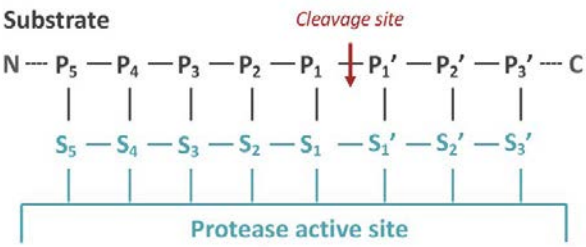

FIGURE I21. Schematic representation of the Schechter & Berger protease active site notion (Schechter and Berger, 1967). According to this convention, P1 is the substrate residue to the amino terminal of the scissile bond (arrow), and P1' the one to the carboxy-terminal side. Other substrate residues are numbered consecutively from these origins. Many of these residues occupy specific pockets on the enzyme, numbered with the matching S designation. Modified from Crawford and Wells, 2011.

Among caspase substrates are here highlighted the following: lamins A/C, which are components of the nuclear lamina and are specifically cleaved by caspase-6 (Orth *et al.*, 1996); the chaperone p23, which is a specific substrate for caspase-7 (Walsh *et al.*, 2008); and α-fodrin, which is a cytoskeletal protein specifically processed by caspase-3 (Janicke *et al.*, 1998a). Once activated, caspase-3 also cleaves the Inhibitor of Caspase-Activated DNase (ICAD), and this cleavage allows Caspase-Activated DNase (CAD) release and activation. Thanks to proteomic approaches, several hundred proteins have been reported as caspase substrates (Dix *et al.*, 2008) (Mahrus *et al.*, 2008). The occurrence of these proteolytic events will define

the final cellular morphology of a cell that has undergone an apoptotic process (Salvesen and Dixit, 1997) (Crawford and Wells, 2011). The cleavage of caspase substrates may lead to a gain-of-function, such as the cleavage of executioner caspases triggered by initiator caspases to achieve activation; loss-of-function, as it happens for PARP or DFF45/ICAD –both cleaved by caspase-3–; change of function; or change of localization. By contrast, many other substrates may be simply bystanders of the processes (Julien and Wells, 2017). CASBAH (Luthi and Martin, 2007) (http://www.casbah.ie/) and MEROPS (Rawlings *et al.*, 2010) (http://merops.sanger.ac.uk/) are two different literature-curated databases that may be useful to check for additional reported substrates.

3.3.6. Regulation of caspases

Apart from the synthesis of caspases as zymogens to prevent its activity, additional mechanisms have been identified to prevent unregulated caspase activity. Because caspase proteolysis is irreversible, tight regulatory mechanisms are needed to control the activation of caspases and to avoid lethal consequences for the cell. Caspase inhibition, caspase degradation, and decoy inhibitors are the three main strategies developed to prevent unwanted physiological responses (LeBlanc, 2003).

The first strategy is mainly under the role of inhibitors of apoptosis (IAP) proteins, a family of eight anti-apoptotic proteins highly conserved throughout evolution. All IAP proteins –including examples such as the X-linked inhibitor of apoptosis (XIAP), cellular IAP (cIAP)1, cIAP2 or survivin– possess at the N-terminus at least one baculoviral IAP repeat (BIR) domain containing among 70-80 amino acids and mediating the interaction between IAP proteins and other proteins such as caspases. Moreover, some IAP proteins also contain in the C-terminus a Really Interesting New Gene domain (RING), which functions as an E3 ubiquitin ligase and, therefore, allows IAPs to target proteins for proteasomal degradation. Among the IAP proteins, XIAP is particularly relevant as an inhibitor of caspases by stably binding to and physically blocking the catalytic activity of caspases. XIAP efficiently and selectively inhibits caspase-9, -3, and -7 (**Figure I10**). The inhibition of caspase-9 takes place through its BIR3 domain and prevents the dimerization required for initiator caspase activation. XIAP inhibition of caspase-3 and -7 occurs via its BIR2 domain and implies the insertion of an aspartic acid residue (from the region flanking BIR2) into the active site of the executioner caspases. Moreover, the insertion of the peptide in the catalytic site occurs in the reverse orientation adopted by caspase substrates (Sun *et al.*, 1999). Although it was generally assumed that direct caspase inhibition was a conserved function among IAP proteins,

biochemical and structural analysis points at XIAP as the only IAP protein that has gained the ability to directly inhibit caspase activity (Eckelman *et al.*, 2006) (Eckelman and Salvesen, 2006). In this line, IAPs such as cIAP1 and cIAP2 promote caspase inactivation via its E3 ubiquitin ligase activity and, consequently, lead to its degradation (Gyrd-Hansen and Meier, 2010) (**Figure I22**). Moreover, they can ensure the survival by promoting NF-κB activation (Varfolomeev *et al.*, 2008) via RIPK1 ubiquitination or drive the upregulation of c-FLIP (Silke and Meier, 2013) as an anti-apoptotic mechanism.

Caspase degradation is a well-described mechanism of caspase regulation. As mentioned above, the presence of the RING domain in XIAP, cIAP1, and cIAP2 contribute to the anti-apoptotic function of IAP by targeting proteins to proteasomal degradation and ensuring a dynamic turnover of activated caspases (Suzuki *et al.*, 2001) (MacFarlane *et al.*, 2002) (Hu and Yang, 2003). IAP RING domain can target proteins such as caspases (caspase-3) or SMAC/DIABLO. Indeed, XIAP E3 ligase can trigger mitochondrial membrane permeabilization that results in an intramitochondrial degradation of its inhibitor SMAC through a BCL-2 protein family-dependent mechanism (Hamacher-Brady and Brady, 2015). At the same time, RING domain can also target the IAPs themselves, triggering autoubiquitination and degradation (Yang *et al.*, 2000). Therapeutically, IAP proteins can be inhibited by using SMAC mimetics which mimic the binding of the endogenous mitochondrial protein SMAC to IAP proteins.

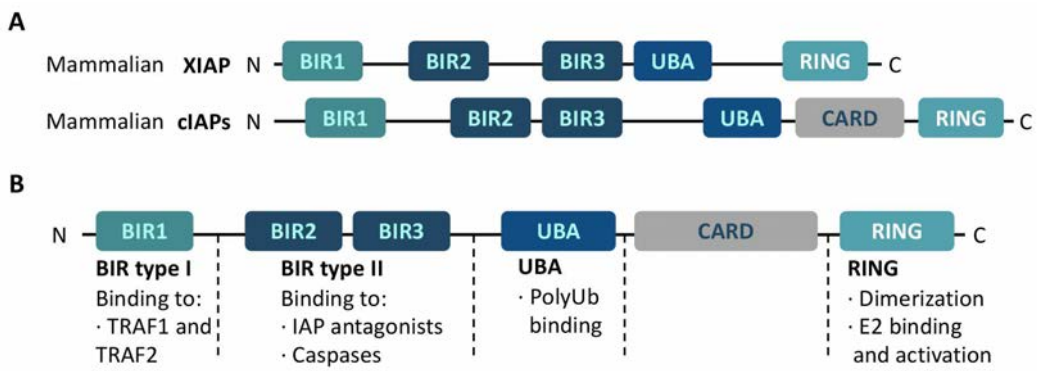

FIGURE I22. Inhibitor of apoptosis (IAP) proteins. A, schematic representation of mammalian IAPs. **B**, Bacuolovirus IAP repeat (BIR) domains enable interactions with proteins. IAPs interact with caspases or IAP antagonist such as SMAC through type II BIR domains, and with TRAF1 and TRAF2 through type I BIR domains. The ubiquitin (Ub)-binding UBA domain binds polyubiquitin (polyUb), The carboxy-terminal RING domain is required for Ub ligase activity, and is a dimerization interface and docking site for ubiquitin conjugating enzymes (E2s). Modified from Gyrd-Hansen and Meier, 2010.

An alternative strategy is based on decoy proteins. FLIP is one of the best examples of this type of protein since it is structurally related to caspase prodomains and competes for the

same adaptors within activation platforms. More specifically, FLIP, as a pseudo-caspase-8 with nonfunctional catalytic domain, impedes caspase-8 recruitment to the DISC (Kataoka, 2005) (Hughes *et al.*, 2016) (**Figure I8**).

Moreover, in nature, viral caspase inhibitors have been described as nonspecific strategies to control infections. Cytokine response modifier A (CrmA) (from the cowpox virus) and p35/p49 proteins (from baculoviruses) are two of the viral proteins described to participate in the viral mechanism activated to evade apoptotic responses to infection and to prolong host cell viability (Zhou and Salvesen, 2000). Indeed, caspase inhibitors, such as CrmA, also hamper the immune response of host cells by blocking the generation of inflammatory cytokines due to caspase-1 inhibition (Zhou *et al.*, 1997).

3.3.6.1. Synthetic caspase inhibitors

As cysteine-dependent proteases, any agent able to react with the catalytic cysteine of caspases (*e.g.*, iodoacetamide) will function as a caspase inhibitor. Thanks to the knowledge of intracellular regulatory mechanisms and caspases specificity, a broad-spectrum of peptide caspase inhibitors have been developed. The principal mechanism of these inhibitors is to act as pseudosubstrates for active caspases and therefore to function as competitive inhibitors.

With the aim of obtaining peptides with improved cell permeability, stability, and efficacy, different chemical groups can be linked to peptides. Linked groups, including aldehydes (-CHO), nitriles (-CN), or ketones (-COR), correspond to reversible inhibitors that bind to the catalytic site without chemically altering the enzyme.

In general terms, we find two types of inhibitors: reversible inhibitors and irreversible inhibitors. Reversible inhibitors interact with caspases through a covalent binding with the catalytic cysteine of caspases and can be easily hydrolyzed. By contrast, peptides linked to halomethylketones (chloro (-Cl) or fluoro (-F)), acylomethyl ketones (-OCOR) and methyl ketones bind via a thioester linkage to a transition state oxyanion and the carbonyl oxygen occupies an oxyanion hole in the caspases transition state. This second group of inhibitors correspond to irreversible inhibitors. The length of these peptides varies from single O-methyl-aspastate residue (benzyloxycarbonyl-aspartyl (OMe)-fluoromethylketone; Boc-Asp-FMK), to dipeptides (Q-Val-Asp-OPh), tripeptides (Boc-Val-Ala-Asp-FMK), tetrapeptides (Z-Tyr-Val-Ala-Asp-FMK) or pentapeptides (Z-Val-Asp-Val-Ala-Asp-FMK).

Most synthetic caspases inhibitors are hydrophobic, have low permeability, and cause nonspecific toxic effects at the concentration needed to exert their function as caspase inhibitors. The range of specificity and potency oscillate from picomolar to low micromolar concentrations. In line with solving this problem, improved efficacy was obtained by adding a carboxy-terminal O-phenoxygroup and an amino-terminal quinolyl group. The improved leaving properties of the carboxy-terminal O-phenoxy group makes, for instance, quinolyl-valyl-O-methylaspartyl-[2,6-difluorophenoxy]-methylketone (Q-VD-OPh) more reactive with the active cysteine in caspases and explains the increased effectiveness of this inhibitor compared with other inhibitors linked to fluoromethylketones (Caserta *et al.*, 2003). The amino terminal quinolyl group alone increase cell permeability and therefore decreases the peptide dose required to inhibit caspases.

Moreover, most of the synthetic caspase inhibitors have been developed with research purposes. In this line, derivatives of caspase inhibitors consisting of aspartic acid residue of a peptidic caspase substrate (such as DEVD) linked to reporter groups are frequently used to assay caspase activity. Reporter groups include fluorophores (AMC, AFC, ACC,…), chromophores (pNA), or luminophores (aminoluciferin). As an example of fluorophores, we find DEVD-AFC where AFC (7-amino-4-trifluoromethyl coumarin) occupies the P_1' position and after caspase cleavage will be released and will emit fluorescence when excited by its appropriate wavelength (Poreba *et al.*, 2013). Note that although less extended, some synthetic caspase inhibitors have been generated and tested for clinical use (Callus and Vaux, 2007) (Kudelova *et al.*, 2015).

The "inherent subsite preference" of caspases has led to the development of different peptide-based and genetically encoded probes. However, it is necessary to mention that as the consensus sequences of caspases are overlapping and, therefore, caspase substrate specificity overlaps, to define 'specific' inhibitors for each caspase is nearly impossible. Thus, cross-reactivity among caspases can easily occur when working with complex biological samples such as lysates of apoptotic cells.

3.4. DNA degradation and nuclear morphology upon cell death

Among the different apoptotic alterations that a cell can display, the DNA degradation and the morphology of the nuclei have been the object of study since many years ago.

In 1938, Spear and Glücksmann reported the fragmentation of lymphocyte nuclei exposed to irradiation (Spear and Glücksmann, 1938) (**Figure I28**). Years later, three independent groups

(Skalka *et al.*, 1976) (Yamada *et al.*, 1981) (Zhivotovsky *et al.*, 1981) analyzed the chromatin of irradiated tissues by running electrophoresis and observed chromatin fragments of different sizes organized as a ladder and corresponding to multiples of nucleosomes. In 1980, Wyllie and collaborators, related this cleavage of chromatin into nucleosome fragments with cells undergoing apoptosis (Wyllie, 1980) (**Figure I23**). This association led to the introduction of a new biochemical hallmark of apoptosis. Since then, several groups went to much effort to elucidate candidates responsible for the dismantling of DNA upon apoptosis, but none of the proposed candidates –DNase I, DNase II, cyclophilins, or DNase-γ (Peitsch *et al.*, 1993) (Barry and Eastman, 1993) (Shiokawa *et al.*, 1997a)– fulfilled the criteria to be the apoptotic DNase.

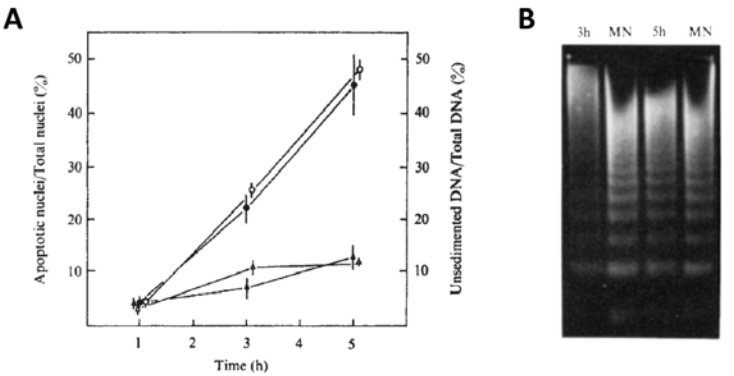

FIGURE I23. DNA degradation into nucleosomal fragments in apoptotic cells. Wyllie *et at.* reported that in methylprednisolone-treated thymocytes the proportion of chromatin cleaved endogenously to small fragments is closely similar to the proportion of nuclei whose morphology shows chromatin condensation of apoptosis. **A**, the graphs shows the percentage of total chromatin unsedimented by centrifugation in lysate prepared from thymocytes incubated *in vitro* for the times shown, in the presence (black dots) or absence (black triangles) of methylprednisolone succinate. Plotted on the same axis is the proportion of nuclei in matched cultures showing the morphology of apoptosis after incubation with (white dots) or without (white triangles) methylprednisolone. **B**, the image shows a 1,8% agarose gel stained with ethidium bromide and viewed in UV light. 3 and 5h correspond to the time of incubation of lysates with methylprednisolone succinate and MN corresponds to micrococcal nuclease digest of fresh thymocyte nuclei. Wyllie *et al.* concluded that the low molecular weight chromatin recovered from steroid-treated thymocytes consists of nucleosome chains with a normal repeat length (Wyllie, 1980).

3.4.1. The apoptotic nuclease: DFF40/CAD

The discovery of the apoptotic nuclease was thanks to *in vitro* biochemical approaches and genetic screenings performed mainly in three different laboratories.

In 1997, the group of Dr. Xiaodong Wang identified and purified the DNA fragmentation factor (DFF) from HeLa cytosol, a heterodimer of 40 kDa and 45 kDa subunit (Liu *et al.*, 1997). At the sequences DETD (aa 117) and DAVD (aa 224) of DFF, the authors identified two cleavage sites for caspase-3. The observation of these cleavage sits in cells undergoing apoptosis, together with the observation of the generation of an active factor responsible for DNA fragmentation upon caspase-3 cleavage, led to defining a direct signal transduction pathway from caspase-3 to DFF and DNA fragmentation. The authors observed DNA fragmentation after incubating active recombinant caspase-3 with HeLa cell S-100 cytosol (Liu *et al.*, 1996) and normal nuclei from hamster liver. However, a DNase activity was not detectable after incubating DFF plus caspase-3 with naked DNA. This nondetectable DNase activity led the group of X. Wang to conclude that "DFF might interact with a specific protein(s) to trigger a signal transduction pathway that activates a nuclease". Consequently, DFF was not described as a nuclease directly cleaving chromatin DNA.

The laboratory of Dr. Shigekazu Nagata, using a similar *in vitro* biochemical approach, was who reported a caspase-activated deoxyribonuclease (CAD) and its inhibitor (ICAD) in the cytoplasmic fraction of mouse lymphoma cells, and who postulated CAD as the DNase implicated in the DNA degradation in apoptotic cells (Enari *et al.*, 1998). Moreover, CAD was described to be produced as a complex with ICAD and was suggested not only as an inhibitor but also as a chaperon for CAD during its synthesis. Additionally, ICAD processing by caspases was described to allow CAD to enter in the nucleus and to degrade chromosomal DNA. Under the name of ICAD, Nagada and co-authors reported the mouse homolog of the 45 kDa subunit (DFF45) previously identified by the group of X. Wang. However, at that time, as DFF itself had not shown any DNase activity (Liu *et al.*, 1997), was not stated as the human homolog of CAD. In this line, a third laboratory contributed to the discovery of the apoptotic endonuclease.

The group of Dr. Lewis T. Williams reported the purification and cDNA cloning of a 40 kDa endonuclease from Jurkat cells (Halenbeck *et al.*, 1998). This endonuclease, activated by caspases, was designed as Caspase-Activated Nuclease (CPAN) and was suggested to be the 40 kDa subunit of the DFF (DFF40) identified by the group of X. Wang.

That same year, 1998, X. Wang reported that DFF40 exhibits an intrinsic DNase activity markedly stimulated by chromatin-associated proteins such as histone H1 and high mobility group (HMG) proteins (Liu *et al.*, 1998). The reason that the authors stated to explain the absence of DNase activity in their first publication (Liu *et al.*, 1997) was that "DFF is a poor DNase when directly incubated with naked DNA, so that a much higher concentration of

DFF was needed to cleave naked DNA than chromatin DNA in nuclei" (Liu *et al.*, 1998). The group of Williams also suggested a magnesium and sodium chloride requirement, and the implication of a carrier protein such as BSA (bovine serum albumin) for the nuclease activity of CPAN (now known to be equivalent to DFF40) (Halenbeck *et al.*, 1998). Furthermore, the conditions used to test DFF for nuclease activity involved low levels of magnesium and salt. Thus, this could additionally explain the nuclease activity of DFF to less than detectable levels in its first publication (Liu *et al.*, 1997).

3.4.1.1. Structure and regulation of DFF40/CAD and DFF45/ICAD

Structurally, DFF40/CAD contains an N-terminal regulatory domain called C1 or CIDE-N, a C2 or homodimerization domain, and a C3 or C-terminal catalytic domain (Lugovskoy *et al.*, 1999) (Sakahira *et al.*, 2001) (**Figure I24A**).

The CIDE-N domain is a conserved domain that refers to cell death-inducing DFF45-like effector domain and mediates the dimerization of DFF40/CAD monomers. The dimerization of DFF40/CAD monomers is required for its nuclease activity (Woo *et al.*, 2004). Different histidine (H) residues together with other lysine (K) and tyrosine (Y) residues are determinant for the catalytic activity of DFF40/CAD (Meiss *et al.*, 2001) (Korn *et al.*, 2002), though are irrelevant for its ability to form oligomers and to bind to DNA. Indeed, the activation of the endonuclease can occur in a DNA-bound state as the catalytic activity of DFF40/CAD is not necessary for its binding to DNA (Korn *et al.*, 2005). In this sense, the role of the CIDE domain is to facilitate the assembly of a scissor-like structure, which is an ideal shape that allows the accommodation of double-stranded DNA (dsDNA) (**Figure I24B**) and that distinguishes internucleosomal from nucleosomal DNA. More specifically, the DNA binds to a positively charged surface of DFF40/CAD with two functionally distinct parts: an active site facing the DNA minor groove and a distal helix α4 that binds to the major groove of DNA together with other close residues (Reh *et al.*, 2005). The two active sites of the homodimer coordinate the nucleophilic attack and break the phosphodiester backbone. It generates a blunt double-strand DNA break (DSB) with 5'-PO and 3'-OH. Although DFF40/CAD activity has been assumed relatively sequence non-selective, a slight sequence preference for purines (Rs) and pyrimidines (Ys) that show rotational symmetry (5'-R-R-R-Y/R-Y-Y-Y-3') has been described (Widlak *et al.*, 2000).

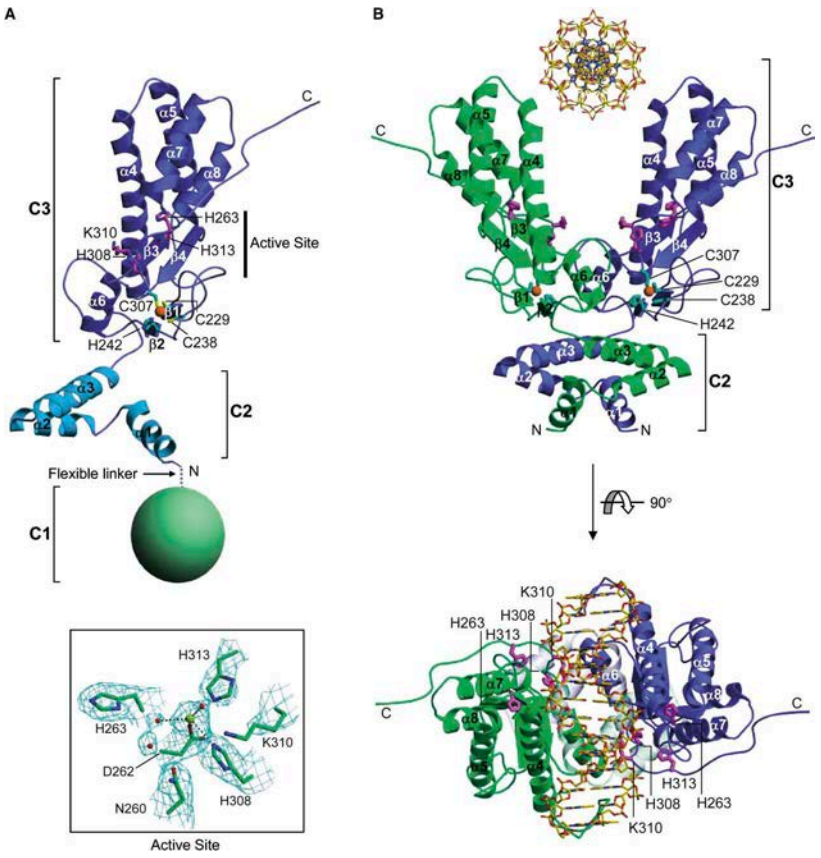

FIGURE I24. Scissors-like structure of DFF40/CAD. A, monomeric structure with C1 (represented as a sphere), C2 and C3 domains. In yellow is shown the cysteinyl sulfur, in orange the Zn^{2+} binding site –critical for the formation of the DFF40/CAD dimer–. The inset shows the detailed interactions of the catalytic residues together with the final electron density map. **B**, dimeric structure. In the side view (top), the monomeric or subunit in blue is oriented as in A. The top view (bottom) is looking down along the molecular 2-fold axis and shows the catalytic residues (H263, H308, K310, and H313). The crevice between the C3 domains spans 14 base pairs of the modeled DNA. Of note, the longest helix α4 fits into the major groove of the DNA (Woo *et al.*, 2004).

The impairment of DFF40/CAD homodimerization constitutes a regulatory mechanism to inhibit the nuclease activity of the endonuclease. This key mechanism is mainly triggered by its inhibitor, ICAD, which is synthesized in stoichiometric excess (Widlak and Garrard, 2005). From a structural view, ICAD can be divided into three different domains: an N-terminal domain called D1 or CIDE domain (Inohara *et al.*, 1998), which is structurally similar to the DFF40/CAD CIDE domain (Lugovskoy *et al.*, 1999); a central D2 domain; and a D3 or C-terminal domain. ICAD is encoded by two alternatively spliced mRNAs that generate the long (DFF45/$ICAD_L$) and the short (DFF35/$ICAD_S$) isoforms (Sakahira *et al.*, 1999). While the different introns (including intron 5) are removed from $ICAD_L$ mRNA leading to a 331-residue isoform, intron 5 is retained in the $ICAD_S$ mRNA and encodes a 268-residue isoform using a stop codon placed in at intron 5. Consequently, the $ICAD_S$ mRNA translation results

in a truncated protein with a different C-terminus (Kawane *et al.*, 1999) (**Figure I25**). For simplification purposes, ICAD can refer to both isoforms.

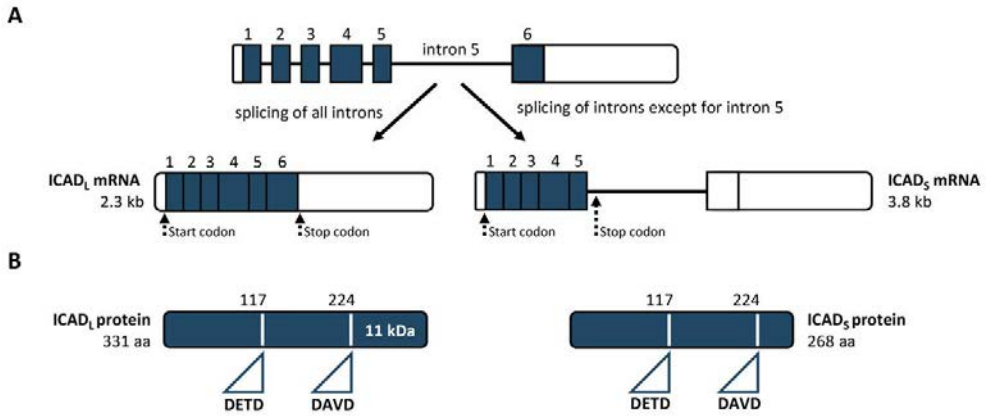

FIGURE I25. ICAD isoforms. A, schematic representation of the long (L) and short (S) mRNAs variants of ICAD. **B,** illustration of the protein isoforms of ICAD including the caspase-3 cleavage sites at the aa 117 and 224. The 11 kDa corresponding to the C-terminal fragment of ICAD$_L$ is also indicated. Modified from Kawane *et al.*, 1999 and Iglesias-Guimarais *et al.*, 2013.

The analysis of the CIDE domain complexes of DFF40/CAD·DFF45/ICAD by nuclear magnetic resonance (NMR) revealed asymmetric heterodimers with charge complementarity (Otomo *et al.*, 2000). More recent studies have identified that CIDE domains can form helical oligomers to execute their functions (Choi *et al.*, 2017). This higher-order, that assemblies through open-ended helical oligomerization serving as scaffolding components, is critically for DNA fragmentation and other biological functions such as lipid droplet metabolism. In the absence of DFF45, DFF40 CIDE domain oligomerizes (Zhou *et al.*, 2001). The examination of the surface charges of DFF40 CIDE domain revealed complementarity between the two opposing surfaces, not observed for DFF45. In the case of DFF40 those results supported the concept that the CIDE domain of DFF40 forms helical structures by head-to-tail polymerization (Choi *et al.*, 2017) (**Figure I26**).

The mechanism of inhibition of the endonuclease activity consists of the heterodimerization of DFF45/ICAD with DFF40/CAD. DFF45/ICAD$_L$ impedes the homodimerization of the endonuclease since its translation from RNA until its release. Like DFF45/ICAD$_L$, DFF35/ICADs can also function as an inhibitor of the nuclease activity of DFF40/CAD. Indeed, DFF35 can bind to DFF40 even more strongly than DFF45 (Gu *et al.*, 1999). McCarty *et al.* described that the fragments resulting from the cleavage of DFF45/ICAD are capable of inhibiting the endonuclease (McCarty *et al.*, 1999a) (McCarty *et al.*, 1999b). However, the more effective inhibition of the DFF40/CAD nuclease activity is by the full-length binding

of DFF45/ICAD (McCarty *et al.*, 1999b). The cleavage of ICAD at two aspartic acid residues (D117 and D224) (**Figure I25B and I27**) destabilizes the complex and allows DFF40/CAD to dimerize and to execute its function as a nuclease (Sakahira *et al.*, 1998). Besides caspases – mainly caspase-3 and -7 (Liu *et al.*, 1999b) (McIlroy *et al.*, 1999)– ICAD can also be cleaved by granzyme B (Sharif-Askari *et al.*, 2001) and granzyme M (Lu *et al.*, 2006b). In this complex regulation of the endonuclease activity, DFF45/ICAD$_L$ carries out an additional function; DFF45/ICAD$_L$ not only sequesters the non-functional DFF40/CAD monomer, but it also disrupts the functional homodimer of DFF40/CAD (Woo *et al.*, 2004).

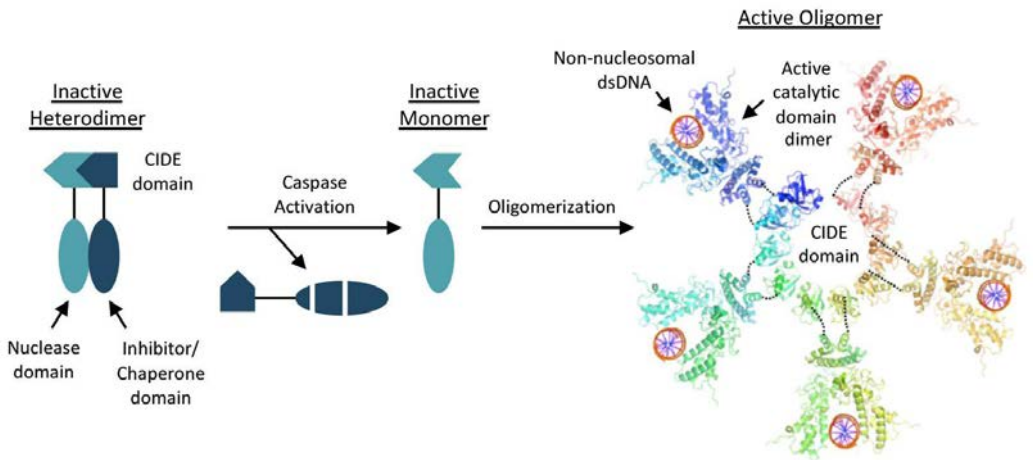

FIGURE I26. A model of CIDE domain oligomerization in activation of apoptotic nucleases in DNA fragmentation. Modified from Choi *et al.*, 2017.

In addition to the inhibitory role of ICAD, the long isoform, DFF45/ICAD$_L$, also acts as a mandatory chaperon protein of DFF40/CAD (**Figure I27**). In the absence of ICAD$_L$, DFF40/CAD is produced but folds incorrectly and remains inactive. The specific interaction of ICAD$_L$ with DFF40/CAD takes place through the binding of D1 or CIDE domain from ICAD$_L$ to the partially folded C1 or CIDE domain from DFF40/CAD (Sakahira *et al.*, 2000) (Kutscher *et al.*, 2012). Moreover, Fukushima *et al.* reported the importance of the C-terminal domain in the chaperon-like activity of DFF45/ICAD (Fukushima *et al.*, 2002). The structure of this domain consists of four α-helices, arranged in a novel helix, generating a large cluster of negatively charged residues. The ability of this negative C-terminal cluster of residues to interact, through complementary charge, with the positively charged catalytic domain of DFF40/CAD is key for the chaperon activity of DFF45/ICAD$_L$. According to this model, DFF35/ICAD$_S$ losses the chaperon activity because the amino acid sequence is truncated in the middle of the second α-helix and, consequently, the cluster of negative charges becomes disrupted. Together with DFF45/ICAD, heat shock protein 70 (HSP70) and HSP40 also participate in the folding of the endonuclease during translation (Sakahira and Nagata, 2002).

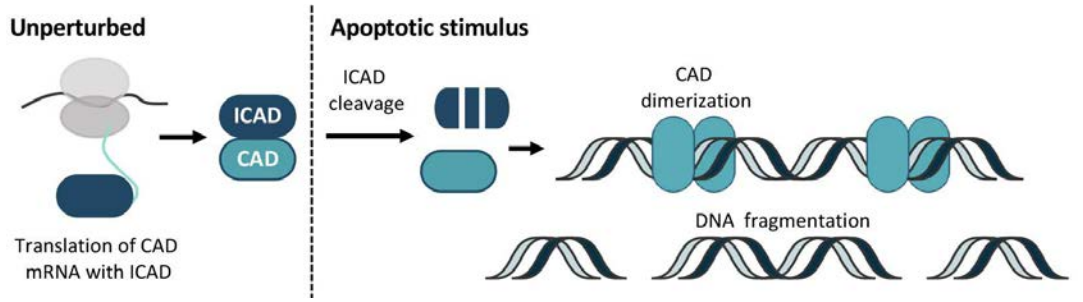

FIGURE I27. Schematic representation of the regulation and activation of Caspase activated DNAse (CAD). The association of CAD with its inhibitor ICAD begins with the translation of CAD mRNA. ICAD functions as a chaperon protein to ensure CAD is properly folded. In the presence of an apoptotic stimulus, activated caspases (mainly caspase-3) cleave ICAD,s and CAD is released from its inhibitor. Upon this release, CAD homodimerize and the scissor-like CAD-CAD dimer creates DNA breaks across the genome resulting in DNA fragmentation. For simplification, CAD and ICAD are here used as synonymous of DFF40 and DFF45, respectively. Modified from Larsen and Sorensen, 2017.

Additional regulatory elements of DFF40/CAD activity include: Mg^{2+} but not Ca^{2+}, ionic forces (K^+ range from 50 to 125 mM is detected in apoptotic cells and increase DFF40/CAD activity 100-folds from nonapoptotic cells) or pH (the optimum pH is 7.5 but DFF40/CAD is highly active from 7.0 to 8.5) (Widlak *et al.*, 2000) (Widlak and Garrard, 2001). Moreover, different proteins including histone H1, HMG proteins, topoisomerase II (Durrieu *et al.*, 2000) and phosphorylated H2AX are described to function as stimulators of DFF40/CAD activity (Lu *et al.*, 2006a) (Widlak and Garrard, 2005). Regarding the negative regulation of DFF40/CAD, besides ICAD, which is the principal factor, the endonuclease activity can also be inhibited by Cu^{2+} or Zn^{2+}, RNA, heparin and other polyanions (Widlak and Garrard, 2001) (Widlak and Garrard, 2006), by caspase-activated DNase (CAD) inhibitor that interacts with ASK1 (CIIA) (Cho *et al.*, 2003), by the nucleolar protein B23 (Ahn *et al.*, 2005) or by other regulators such as CIDE-A and -B (Inohara *et al.*, 1998).

3.4.1.2. Subcellular localization of DFF40/CAD and DFF45/ICAD

The subcellular localization of the endonuclease and its inhibitor have been subjected to continuous contradictions between publications. Initially, DFF was described as a cytoplasmic protein (Liu *et al.*, 1997). However, assessed by immunocytochemistry, X. Wang reports a nuclear localization of DFF40 and DFF45 in a latter publication (Liu *et al.*, 1998). In this case, most of the staining for the DFF heterodimeric complex was detected in the nuclei of nonapoptotic cells (Liu *et al.*, 1998). To explain the presence of DFF in the cytosolic fraction, the authors pointed to leakage from nuclei during homogenization after the biochemical fraction. Other publications influenced the controversy regarding subcellular localization of

the complex. As ICAD revealed no nuclear localization sequence (NLS) in its first identification, the group of S. Nagata stated that "ICAD remains complexed with CAD to mask its nuclear-localization signal to keep CAD in the cytoplasm" (Enari *et al.*, 1998). However, other authors suggested that ICAD function in the nucleus and could be co-transported to the nucleus with other proteins that do contain NLS such as CAD, CIDE-A and/or CIDE-B (Samejima and Earnshaw, 1998). A few years later, the same authors reported a sequence rich in basic amino acids at the C-terminal of $ICAD_L$ that could function as an independent nuclear localization sequence. This particularity and the nuclear localization were only assigned to the long isoform of ICAD, not to the short isoform, which was observed diffusely all over the cell (Samejima and Earnshaw, 2000). Although it is described as a cytosolic protein, the short isoform of ICAD can also be detected at the nuclei when complexed with CAD (Chen *et al.*, 2000).

Further studies concerning DFF45/ICAD·DFF40/CAD complex location suggested an implication of the importin system in the translocation of the complex to the nucleus. The importin α/β-heterodimer interacts with the complex through the C-terminal regions of both DFF40/CAD and DFF45/ICAD subunits. These interactions are essential for nuclear accumulation of the complex (Neimanis *et al.*, 2007). Thus, according to this observation, two different nuclear localization sequences are contained in the C-terminal of DFF40/CAD: a classical NLS for its accumulation in the nucleus and a nonclassical NLS sequence recognized by importin proteins.

The DFF45/ICAD·DFF40/CAD complex can be found at the cytosol (Enari *et al.*, 1998) (Sabol *et al.*, 1998), the nucleus (Liu *et al.*, 1998) (Samejima and Earnshaw, 1998) (Lechardeur *et al.*, 2000) (Nagata *et al.*, 2002) or at both subcellular compartments (Nagata *et al.*, 2002) in healthy cells. Certainly, our group has described that the levels of DFF40/CAD protein in each subcellular compartment are indeed a cell-specific feature regulating DNA degradation upon cell death. In this sense, we detected that in cells displaying oligonucleosomal DNA degradation upon staurosporine treatment (like SH-SY5Y cells), DFF40/CAD is located in both cytosol and nuclei. However, when the endonuclease is not enriched in the cytosolic fraction (like in SK-N-AS), cells are defective in the generation of DNA laddering (Iglesias-Guimarais *et al.*, 2012). More recently, we have described the absence of oligonucleosomal DNA hydrolysis as a common trait in human glioblastoma cells due to the low expression levels of the endonuclease (Sanchez-Osuna *et al.*, 2016).

3.4.2. Other nucleases and factors for DNA cleavage

As previously reported by Dr. Wyllie, upon cell death, nuclear DNA can be cleaved into multiples of 180-200 base pairs (bp) (Wyllie, 1980). This DNA degradation, also referred to as low molecular weight (LMW) cleavage or DNA ladder, is considered an apoptotic hallmark and occurs in the latest stages of cell death.

Early in the apoptotic execution, DNA fragmentation occurs into high molecular weight (HMW) fragments between 50-300 kb and in single-stranded cleavages (ssDNA). While the LMW is a specific hallmark of apoptosis, HMW and ssDNA breaks are sometimes observed in the absence of apoptosis (Solov'yan *et al.*, 1997). Different nucleases have been involved in the destruction of the DNA upon cell death. Apart from the nucleases, cofactors such as AIF (Susin *et al.*, 1999) and enzymes such as topoisomerase II (Li *et al.*, 1999) are also implicated in the higher-order DNA cleavage reaction.

In general terms, two main categories have been defined to include the different nucleases: cell-autonomous nucleases and waste-management nucleases (Samejima and Earnshaw, 2005).

3.4.2.1. Cell-autonomous nucleases

This group of nucleases cleaves the DNA within the dying cell thanks to its direct access to the nucleoplasm. Cell-autonomous nucleases are not essential for apoptotic cell death or the life of the organism but, as an intrinsic part of the apoptotic program, might affect the efficiency of cell death. Among cell-autonomous nucleases, we find DFF40/CAD, extensively reviewed above and one of the most important apoptotic nucleases, and other nucleases such as endonuclease G or DNaseγ.

Endonuclease G

Endonuclease G (endoG) is an evolutionarily conserved nuclease that has been reported to act as an apoptotic nuclease in the settings where the DFF40/CAD system does not function (Li *et al.*, 2001). As the DNA laddering observed in DFF40-knock out cells is not completely recapitulated by endoG, different candidates including exonuclease III and Dnase I have been suggested to help endoG to generate dsDNA cleavage products. EndoG localizes in the mitochondrial intermembrane space in normal cells and translocates from the mitochondria to the nucleus upon apoptosis. Once it is in the nucleus, it hydrolyzes the chromatin into

fragments of 50 kDa. Endo G can also induce inter- and intranucleosomal DNA cleavages resulting in oligonucleosomal DNA fragments (190 bp) with internal single-strand nicks (10 bp periodicity). Although in general, the activation of caspases is not required (Li *et al.*, 2001), in some circumstances, caspase activation may be required to allow the release of endoG from mitochondria (Arnoult *et al.*, 2003). The preferred substrate of this nuclease is ssDNA or RNA over dsDNA, and other requirements include Mg^{2+} or Mn^{2+}, but not Ca^{2+} (Ruiz-Carrillo and Renaud, 1987). EndoG can be inhibited at physiological [K^{+}] and by the presence of Fe^{2+} or Zn^{2+} (Widlak *et al.*, 2001). Further information of this nuclease is addressed in the following references (Widlak and Garrard, 2005) (Prats *et al.*, 1997) (Schafer *et al.*, 2004) (Samejima and Earnshaw, 2005).

DNase γ/DNASE1L3

This nuclease is a DNase I-related protein that functions as a cell-autonomous nuclease during apoptosis in some differentiated cells. The N-terminal sequence of this nuclease presents high homology with the DNase I. In healthy cells, DNase γ is stored in the nuclear envelope lumen; following the induction of apoptosis, this nuclease is released into the nucleus (Yakovlev *et al.*, 2000) (Shiokawa *et al.*, 1997b) (Shiokawa and Tanuma, 1998) (Shiokawa and Tanuma, 2001) (Shiokawa *et al.*, 2003). Depending on the differentiation state of neuronal cells, DNase γ may replace CAD and may act as the main nuclease responsible for LMW DNA fragmentation (Shiokawa and Tanuma, 2004). DNase γ generates 3'-OH/5'P fragments and requires Ca^{2+} and Mg^{2+}, Ca^{2+} and $Mn^{2+,}$ or Mn^{2+} only for its activity as a nuclease. This activity can be inhibited by Zn^{2+} or by DR396, which has been described as an inhibitor of DNase γ (Sunaga *et al.*, 2004). Moreover, according to the work performed by Ryushin Mizuta *et al.,* DNase γ is a single-stranded DNA nickase with high activity at low ionic strength (Mizuta *et al.*, 2006), it is also the effector endonuclease for necrosis-associated DNA fragmentation (Mizuta *et al.*, 2013) and it acts as a backup endonuclease for DFF40/CAD in the secondary necrosis phase (Koyama *et al.*, 2016). More recently, the group of Ryushin Mizuta has reported the role of DNase γ in the generation of cell-free DNA in blood circulation (Watanabe *et al.*, 2019) and in the karyolysis of necrotic cells (Takada *et al.*, 2020).

3.4.2.2. Waste-management nucleases

The waste-management nucleases are essential nucleases for the life of the organisms and are crucial elements in the destruction of the DNA engulfed by phagocytic cells. This DNA, coming from different sources, is mainly destroyed in the lysosomes. Lysosomal nucleases are

responsible for "cleaning up" the corpses of apoptotic cells, necrotic cells, or microorganisms such as bacteria that have been killed by the immune system. Apart from been compartmentalized in lysosomes, after its synthesis in the endoplasmic reticulum (ER), waste-management nucleases can be secreted to the extracellular space. The secreted nucleases "mop up" the DNA that have been released in the blood or the digestive system as a result of cell or bacterial lysis.

DNase I

DNase I is primarily a secreted protein released into the digestive system and bloodstream that requires Ca^{2+} and Mg^{2+} to generate DNA breaks (3'-OH free). DNase I-deficient mice evidenced the importance of this nuclease in the removal of DNA released by dead cells and the potential risk of incomplete clearance of this DNA (Napirei *et al.*, 2000). Although it generally functions as a waste-management nuclease responsible for the degradation of extracellular DNA, in some cells undergoing drug-induced apoptosis, DNase I can work as a cell-autonomous nuclease and mediates internucleosomals DNA degradation (Oliveri *et al.*, 2001). Indeed, different DNase I-like proteins including DNase γ participate in apoptosis (Liu *et al.*, 1999a).

DNase II

This nuclease is a ubiquitous lysosomal endonuclease independent of cations that requires an acidic environment to cleave DNA (Evans and Aguilera, 2003). This intracellular acidification generally occurs during apoptosis. Once activated, DNase II generates dsDNA and ssDNA breaks with 3'P ends (Evans and Aguilera, 2003). The laboratory of Eastman was the first reporting the implication of DNase II in DNA fragmentation during apoptosis and suggested the secretion of DNase II from lysosomes to cleave nuclear DNA (Barry *et al.*, 1993). NUC-1 was identified as the DNase II homolog in *C. elegans*. NUC-1 and functions as a cell-autonomous nuclease degrading the extremes 3'-OH free and generating 5'-OH and 3'-P groups (Wu *et al.*, 2000). Thanks to studies in Drosophila, DNasae II has been suggested as the nuclease responsible for degrading the LMW fragments generated by CAD to oligo-mono-nucleotides. DNase II knockout mice die at birth due to multiple developmental defects (Kawane *et al.*, 2001) (Krieser *et al.*, 2002). Different tissues from these mice have an accumulation of DNA containing bodies that result from engulfed but undigested cell corpses. These observations confirmed DNase II as an essential nuclease in the waste management of the cell.

From a theoretical point of view, it is easy to separate the nucleases in cell-autonomous and waste-management enzymes. However, the observation that under certain circumstances the nucleases safely sequestered in the lysosomes can be released into the cytoplasm and may function in a cell-autonomous manner complicates the classification of the nucleases into two exclusive groups (Samejima and Earnshaw, 2005). Moreover, although cell death can occur without significant DNA degradation, cell-autonomous DNA breakdown of tumor, or virally-infected cells is important to prepare the resulting apoptotic corpses for engulfment by phagocytes. This mechanism is key to prevent the transforming potential of any hazardous oncogenes. The incomplete DNA clearance may promote pathological consequences, including tumorigenesis or autoimmune diseases (Napirei *et al.*, 2000).

Nuclease	Optimal pH	Cofactor	Substrate preference	Cleavage products
DFF40/CAD	Neutral	Mg^{2+}	dsDNA	3'-OH 5'-P
Endonuclease G	Neutral; Basic	Mg^{2+}, Mn^{2+}	ssDNA, RNA	3'-OH 5'-P
DNase γ/DNAS1L3	Neutral	Ca^{2+}, Mg^{2+}	ssDNA, dsDNA	3'-OH 5'-P
DNase I	Neutral	Ca^{2+}, Mg^{2+}	ssDNA, dsDNA	3'-OH 5'-P
DNase II	Acidic	None	ssDNA, dsDNA	3'-P 5'-OH

TABLE I5. Nucleases involved in apoptotic DNA degradation. ds, double-stranded; ss, single-stranded. The biochemical properties of DNase family members are reviewed in Samejima and Earnshway, 2005 and Keyel, 2017.

3.4.2.3. Apoptosis inducing factor (AIF)

Apoptosis inducing factor (AIF) is a flavoprotein ubiquitously expressed in mammals (Susin *et al.*, 1999). After its synthesis in the cytosol, AIF is recruited to the mitochondria by its mitochondrial localization sequences (MLS). Inside the mitochondria, AIF folds into its functional configuration and binds to a prosthetic group of flavine adenine dinucleotide (FAD). Like many mitochondrial proteins, AIF plays a dual role in life and death; it supports a pro-survival role as a FAD-dependent oxidoreductase involved in mitochondrial respiration (Vahsen *et al.*, 2004) (Churbanova and Sevrioukova, 2008), and it can also exert a lethal role through caspase-independent apoptosis. More specifically, calpain- or cathepsin-mediated cleavage of AIF allows its removal from the IMM during mitochondrial permeabilization (Yuste *et al.*, 2005a) (Polster *et al.*, 2005) (Moubarak *et al.*, 2007). Once released to the cytosol, the truncated form of AIF (tAIF) translocates to the nucleus. PARP-1 together with cyclophilin A (CypA) are described as positive regulators of tAIF translocation to the nucleus

(Zhu *et al.*, 2007) and HSP70, as an inhibitor (Gurbuxani *et al.*, 2003). Inside the nucleus, AIF triggers a ring-shaped chromatin condensation (best known as stage I apoptotic morphology) and HMW DNA fragmentation (Susin *et al.*, 1999) (Ye *et al.*, 2002) (Cande *et al.*, 2004). Although frequently associated with an apoptotic caspase-independent pathway, chromatinolysis induced by AIF has also been observed during necrosis (now referred to as parthanathos) upon DNA damage induced by the alkylating agent MNNG (Moubarak *et al.*, 2007) (see *6. Other types of cell death and non-lethal processes*). In both cases, in apoptosis and necrosis, the phosphorylated form at Ser139 of H2AX (γH2AX or phospho-H2AX) exerts a regulatory role over the AIF-induced chromatolysis and cell death (Lu *et al.*, 2006a) (Artus *et al.*, 2010) (Baritaud *et al.*, 2010) (Baritaud *et al.*, 2012).

3.4.3. Nuclear morphology upon cell death

The interest in the nuclear morphology of death cells comes from the development of the first microscopes. The morphology of a cell, and especially of its nucleus, constitutes a reflection of some of the intracellular processes that take place inside the cell. In 1938, Spear and Glücksmann reported different degrees of degeneration performing experiments with x-irradiation (**Figure I28**).

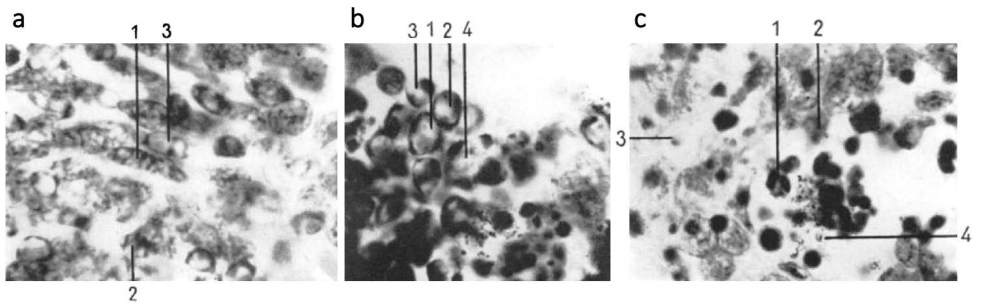

FIGURE I28. Three main stages in nuclear degeneration observed by Spear and Glücksmann. **a**, chromatopycnosis. **b**, hyperchromatosis. **c**, chromatolysis. The numbers indicate the sequence of the degenerate process in each stage. Modified from Spear and Glücksmann, 1938.

Like Spear and Glücksmann, many authors have invested great efforts to analyze and to understand how the nuclear phenotype varies upon cell death depending on factors such as the cell death stimuli or the cellular context. Some of the most relevant contributions are detailed hereafter.

In the late 1990s, three different pathways were described involved in apoptotic chromatin condensation: the group of Xiadong Wang reported a caspase-3 dependent pathway mediated by DFF40/CAD (Liu *et al.*, 1998); the group of Guido Kroemer described a caspase-3

independent pathway triggered by mitochondrial AIF (Susin *et al.*, 1999); and the group of Yoshihide Tsujimoto reported a caspase-3 dependent pathway triggered by the protein Acinus, a caspase-activated factor cleaved by caspase-3 and involved in apoptotic chromatin condensation but not in DNA fragmentation (Sahara *et al.*, 1999). Likewise, in 2000, Susin and co-workers revealed two redundant parallel pathways leading to different chromatin processing during apoptosis (Susin *et al.*, 2000). One of these pathways coincided with an initial and peripheral chromatin condensation (referred to as stage I) with large-scale DNA fragmentation and AIF involvement; the other corresponded to an advanced pattern of chromatin condensation (referred to as stage II) and coincided with oligonucleosomal DNA fragmentation. While stage I was reported as caspase-independent, the pathway leading to stage II involved Apaf-1, caspases, and DFF40/CAD. Similarly, Leist and Jäättela used the state of chromatin condensation to distinguish between apoptosis –"the chromatin condenses to compact and apparently simple geometric (globular, crescent-shaped) figures"– and apoptosis-like PCD –"chromatin condensation is less compact/complete than in apoptosis (geometrically more complex and lumpier shapes)"– (Leist and Jaattela, 2001) (**Figure I29**). The generation of the nuclear apoptotic morphology resulting from different stages of chromatin condensation and fragmentation was also addressed by Samejima and Earnshaw in 2005.

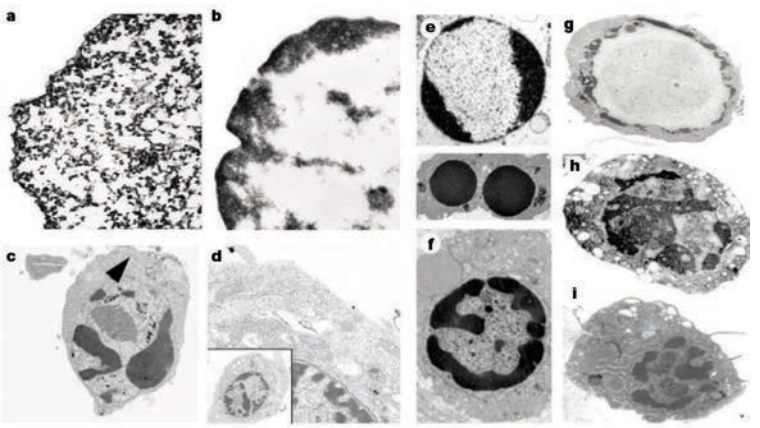

FIGURE I29. Nuclear alterations in different forms of cell death. a, control chromatin; **b**, caspase-independent chromatin margination triggered by AIF; **c**, caspase-dependent strong chromatin compaction; **d**, caspase-independent, AIF-driven lumpy chromatin condensation; **e**, caspase-dependent chromatin compaction to crescent-shaped masses at the nuclear periphery and chromatin fragmentation to two compact spheres; **f**, caspase-independent lumpy chromatin condensation without nuclear fragmentation in colchicine-induced neuronal cell death. **g**, **h**, **i**, incomplete, lumpy chromatin condensation in caspase-independent apoptosis-like PCD. Figure from Leist and Jaatela, 2001.

Another relevant contribution in the field comes from the group of William T. Garrard. In 2002, they described that chromatin condensation is accompanied by the release of nuclear

actin and that this phenomenon can be inhibited by agents that inhibit the depolymerization of actin (Widlak *et al.*, 2002). Moreover, the authors reported that agents targeting the minor groove of DNA, pretreatment with Ca^{2+}, Cu^{2+}, diamide, or low pH also inhibit chromatin condensation.

Furthermore, it was suggested that large clumps of condensed chromatin require disassembly of internal nuclear structures. This last statement was supported by Ruchaud *et al.,*. The group of William C. Earnshaw found that chromatin condensation and nuclear breakdown requires the cleavage of caspase-6-mediated nuclear proteins (such as lamin A) during apoptosis (Ruchaud *et al.*, 2002). Hence, attributed to caspases the role of releasing the chromatin from sites of tethering at the nuclear lamina. Using time-lapse imaging, biochemical and electron microscopy analysis of cell-free apoptosis, the group of William C. Earnshaw described three distinct stages of apoptotic nuclear condensation and characterized the dynamic changes in the chromatin upon apoptosis (Tone *et al.*, 2007) (**Figure I30**). Note that stage 3 coincides refers to the complete shrinkage of the nucleus and separation into individual fragments to form the apoptotic bodies.

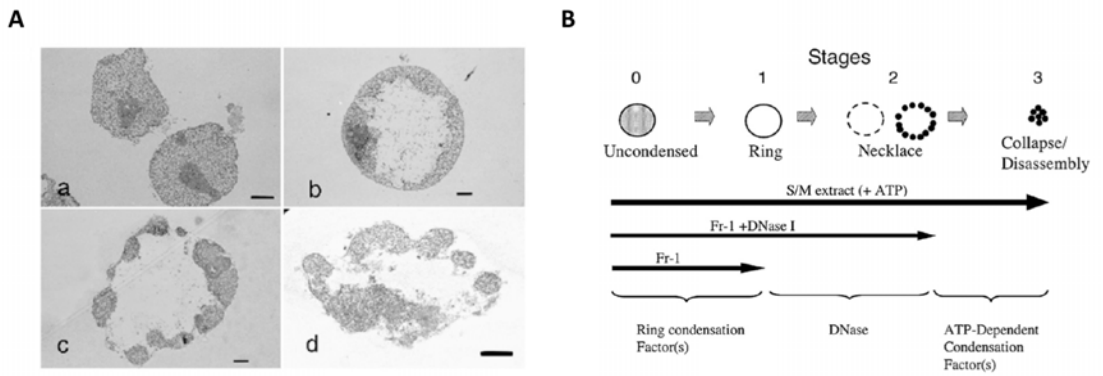

FIGURE I30. Stages of nuclear condensation proposed by Tone *et al.*. A, Transmission electron microscopy analysis of HeLa S3 nuclei incubated in the presence of ATP for 0 min (a), 15 min (b), 30 min (c) or 60 min (d). **B**, schematic illustration of the stages in nuclear condensation in cell-free apoptosis: stage 0, uncondensed; stage 1, ring condensation; stage 2, necklace condensation; stage 3, nuclear collapse/disassembly. The factors acting in each step are also included in the illustration (Tone *et al.*, 2007).

The same authors reported a non-required DNase activity for stage 1, but essential for the transition from stage 1 to stage 2. Moreover, hydrolyzable ATP was described to be required for chromatin compaction and nuclear collapse/disassembly during apoptotic execution.

It is worth noting that stage 3 (Tone *et al.*, 2007) should not be confused with the type III nuclear morphology (Yuste *et al.*, 2005b). Yuste *et al.* observed that D117E ICAD-overexpressing cells transfected with dsRNA against AIF (either R1 or R2) did not display

any of the classic nuclear morphologies related to apoptosis. Nuclei shrank and remained rounded with a highly compacted chromatin (**Figure I31B**). The authors referred to this nuclear outcome as type III. Additionally, cells overexpressing the single mutant D224E of ICAD and treated with STP displayed high chromatin condensation and fragmentation in rounded masses akin to the previously described stage II. By contrast, the overexpression of the single mutant D117E of ICAD prevented stage II nuclear morphology and coincided with homogeneously condensed chromatin (**Figure I31A**).

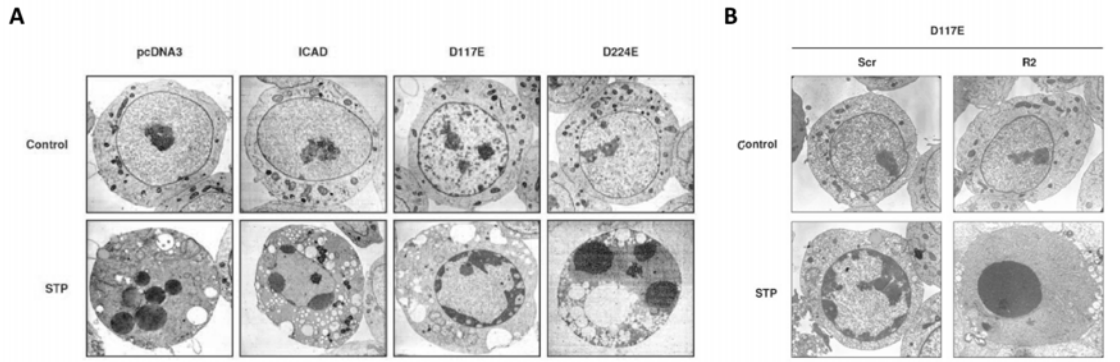

FIGURE I31. Different stages of DNA condensation upon staurosporine treatment. A, SH-SY5Y cells transfected with empty vector (pcDNA3), wild type (ICAD), or single mutant form D224E ICAD show high chromatin condensation and fragmentation in rounded masses (stage II) after staurosporine (STP) treatment. This nuclear morphology is prevented in single mutant D117E ICAD SH-SY5Y cells, which show chromatin marginalization in the periphery of the nucleus (stage I) after treatment with staurosporine. **B**, nuclear morphology observed in D117E hICAD-expressing cells transiently transfected with the dsRNA against AIF (R2) treated with staurosporine show highly compacted chromatin (a nuclear morphology referred to as type III) (Yuste *et al.*, 2005b).

The type III nuclear morphology with chromatin condensation without signs of fragmentations was also reported in human glioblastoma-derived LN-18 cells (**Figure I32**). More specifically, the analysis of the nuclear morphology of human glioblastoma-derived LN-18 cells after treatment with a broad panel of cytotoxic insults evidenced: type III nuclear morphologies upon vinblastine, rotenone or TRAIL; type I nuclear morphologies upon cisplatin, curcumin, ergocalciferol or MG132; and a mixture of type I and type III nuclear morphologies upon treatment with ceramide-8 (Sanchez-Osuna *et al.*, 2014). None of the challenges employed in the study revealed apoptotic type II nuclear morphology like those observed in apoptotic proficient SH-SY5Y cells after an apoptotic stimuli (**Figure I32**). The study of this particular apoptotic behavior depicted by LN-18 cells upon cell death constitutes an essential part of this Doctoral thesis.

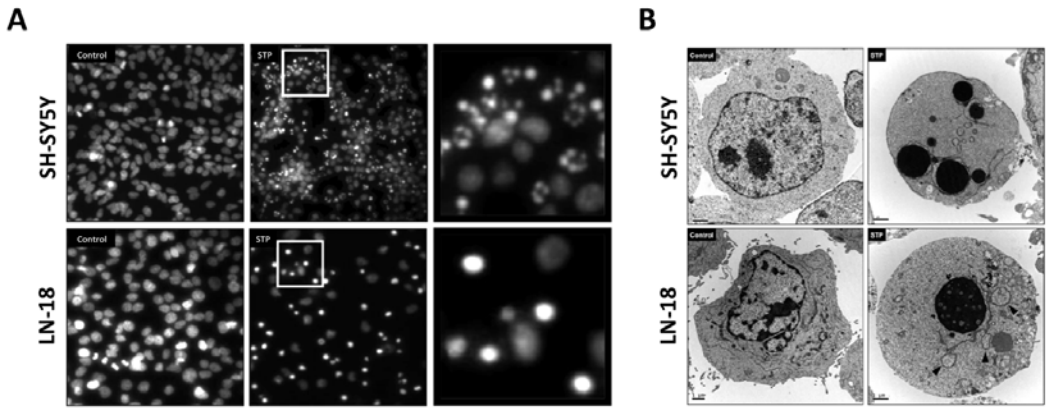

FIGURE I32. Type III nuclear morphology observed in LN-18 cells after apoptotic stimuli. A, representative micrographs of UV-light microscopy (nuclei stained with Hoechst 33258) (**A**) and representative images of transmission electron microscopy (**B**) from untreated (*Control*) or treated (*STP*, staurosporine) neuroblastoma-derived SHSY5Y cells and glioblastoma-derived LN-18 cells. The images show classical type II (nuclear collapse and disassembly) apoptotic nuclear morphology in SH-SY5Y-treated cells and type III (highly compacted chromatin without signs of karyorrhexis) nuclear morphology in LN-18-treated cells. Modified from Sanchez-Osuna *et al.*, 2014.

3.4.3.1. Nuclear envelope breakdown and cytoskeleton rearrangement

One of the principal consequences of apoptosis is the rearrangement of different cellular components leading to cellular retraction, nuclear condensation, and fragmentation into smaller pieces together with the breakdown of the nuclear envelope (see **BOX 3**). This demolition phase of apoptosis is mainly, but not exclusively, orchestrated by caspases (**Figure I34**). Indeed, due to the release of different molecules to attract phagocytes, the degradation of the cellular content initiated in apoptotic cells will be generally completed within engulfed cells.

The cleavage of the nuclear lamins constitutes one of the principal hallmarks of the nuclear envelope breakdown. Lamin cleavage disassembles the lamin complex and weakens the nuclear envelope. Lamins A and C were among the first reported caspase substrates (Orth *et al.*, 1996)(Rao *et al.*, 1996), being caspase-6 the caspase responsible for their cleavage (Slee *et al.*, 2001) (Ruchaud *et al.*, 2002). The proteolytic cleavage of lamin A/C occurs in a highly conserved region at position 230 (VEID[230]N) and leads into 47- and 37-kD fragments, respectively. Caspase-6 cleavage has been described as a late event occurring after caspase-3 and caspase-7 cleavage (Inoue *et al.*, 2009). Lamin B1 is also cleaved by caspases; however, it occurs at a different sequence and position (VEVD[231]S).

BOX 3. Nuclear envelope

The nuclear envelope (NE) represents the boundary between the nucleus and the cytoplasm of eukaryotic cells. The communication between both compartments is allowed through a large complex of proteins referred to as nuclear pore complexes (NPCs). Many nuclear pores perforate the NE connecting the two phospholipid bilayer membranes that compose the NE: the inner nuclear membrane (INM), and the outer nuclear membrane (ONM), both separated by a space called the perinuclear space (PNS). The NE is continuous with the endoplasmic reticulum (ER) membrane and is generally dotted with ribosomes. Nesprin proteins at the ONM connect the nucleoskeleton and the cytoskeleton, which includes cytoplasmic structures such as microtubules, intermediate filaments, and actin filaments (Dobrzynska *et al.*, 2016). The INM is covered by the nuclear lamina, which is a net of intermediate filament proteins that give support to the structure of the nuclear envelope.

More than a hundred proteins have been described as INM proteins and are referred to as NETs (nuclear envelope transmembrane proteins). Among them, lamin B receptor (LBR), lamin-associated polypeptide-2 (LAP2), emerin and MAN1 are some of the best characterized (Hetzer, 2010) (Koch and Holaska, 2014) (Stewart *et al.*, 2007). These proteins interact with barrier-to-autointegration factor (BAF) and heterochromatin protein 1 (HP1), function as DNA-bridging proteins and play a key role in chromatin organization. BAF and HP1 have been described to interact with different proteins including histones H1 and H3 (Nielsen *et al.*, 2001) (Montes de Oca *et al.*, 2005). Although most of the specific functions of NETs are not yet elucidated, a tissue-specific expression controlling genomic organization, cell cycle and regulation of cytoskeletal organization is generally accepted (Wilkie *et al.*, 2011) (Zuleger *et al.*, 2013). Further knowledge is needed to better comprehend the functions of the NE proteins and specially, their contribution to the inner organization of the nucleus and to the nuclear morphology.

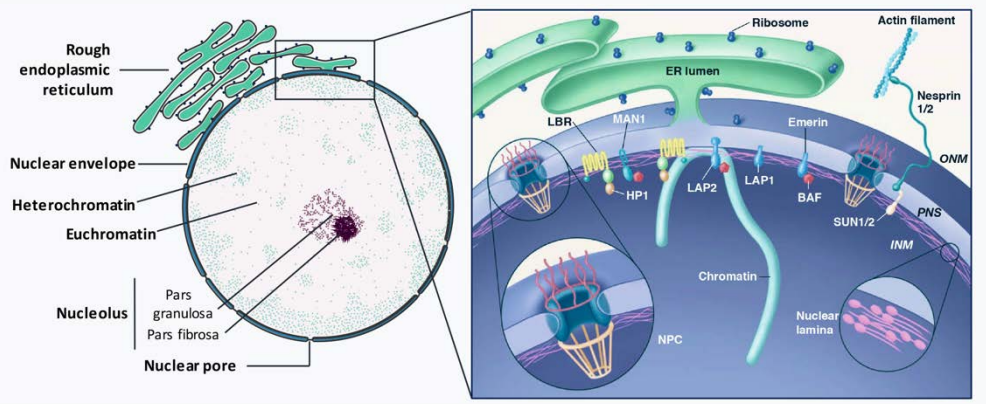

FIGURE I33. Organization of the nuclear envelope. On the left, schematic representation of the different parts of the nucleus and the continuity of the nuclear envelope with the endoplasmic reticulum (ER). On the right, some selected INM and ONM proteins and its association with cytoskeleton proteins and the chromatin. Modified from Stewart *et al.*, 2007.

Together with lamins cleavage, the cytoskeleton rearrangement and the cleavage and activation of the serine/threonine Rho-associated protein kinase (ROCK1) are key for the nuclear envelope breakdown (Taylor *et al.*, 2008). While nuclear disintegration during mitosis requires microtubule-based forces and lamin phosphorylation and depolymerization, apoptotic cells require actin-myosin contractile force and lamin proteolysis (Croft *et al.*, 2005). In this sense, ROCK1 kinase exerts a crucial role in modifying actin cytoskeletal structures, which is degraded at the final stages of apoptosis (Coleman and Olson, 2002). Because of the attachment between the nuclear envelope and actin cytoskeleton, the ROCK1-induced reorganization of the actin-myosin system tears the nucleus apart during apoptosis (Croft *et al.*, 2005). The cytoskeleton rearrangement induced upon cleavage of ROCK1 also participates in the initiation of the membrane blebbing (Coleman *et al.*, 2001). Additionally, myosin light chain (MLC) phosphorylation and MLC ATPase activity are also relevant for the breakdown of nuclear structure and apoptotic membrane blebbing (Sebbagh *et al.*, 2001) (Mills *et al.*, 1998). However, a recent publication describes that the generation of thin apoptotic membrane protrusions, called apoptopodia, and subsequent apoptotic body formation can occur in the absence of actin polymerization and microtubule assembly (Caruso *et al.*, 2019).

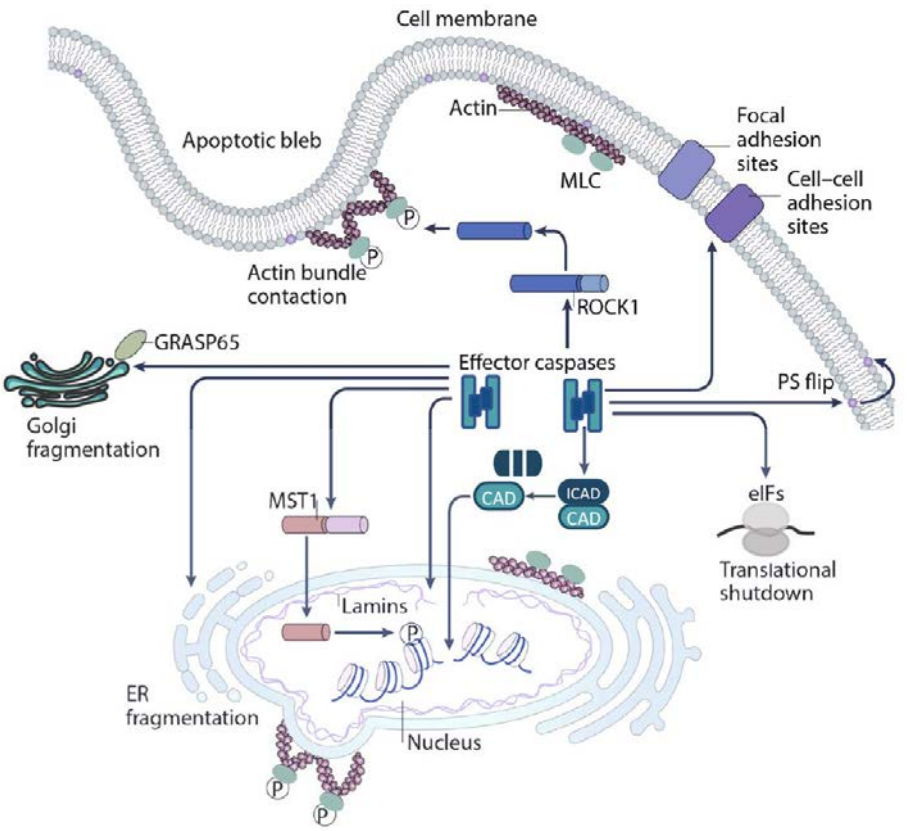

FIGURE I34. Dismantling of key cellular structures and organelles by caspases. Different proteolytic events orchestrated by effector caspases are here illustrated. The cleavage of ICAD leads to the release of CAD,

which then catalyse internucleosomal DNA cleavage. Caspase-mediated cleavage of nuclear lamins weakens the nuclear lamina, allowing nuclear fragmentation. Proteolysis of proteins at focal adhesion sites and cell–cell adhesion sites allows cell detachment and retraction. Proteolysis of the Rho effector ROCK1 leads to contraction of the actin cytoskeleton and plasma membrane blebbing as well as nuclear fragmentation. Proteolysis of the mammalian sterile-20 kinase MST1 results in translocation of a catalytically active fragment of this kinase to the nucleus where it phosphorylates histone H2B to provoke chromatin condensation. Caspases also cleave the Golgi-stacking protein GRASP65 and other Golgi proteins, causing fragmentation of the Golgi apparatus. Caspases are required for the exposure of phosphatidylserine (PS) and other phagocytic signals on the cell surface. Additionally, relevant cellular functions such as translation are disrupted through caspase-mediated proteolysis of multiple translation initiation factors (eIFs). ER, endoplasmic reticulum; MLC, myosin light chain. Modified from Taylor *et al.*, 2008.

Furthermore, actin-associated proteins such as myosin, fodrin (Martin *et al.*, 1995), gelsolin (Kothakota *et al.*, 1997), or filamin (Browne *et al.*, 2000) are major constituents of the cell cytoskeleton that become cleaved by caspases upon apoptosis. Moreover, microtubular proteins such as tubulins are also caspase substrates, and other intermediate filament proteins such as vimentin or keratins are also targeted (Morishima, 1999) (Ku *et al.*, 1997). Specifically, caspase-3 and caspase-7 can cleave vimentin at Asp85, and caspase-6 can cleave vimentin at Asp259. The proteolytical processing of vimentin during apoptosis disrupts the cytoplasmic network and has been reported to coincide with nuclear fragmentation. Indeed, the pro-apoptotic amino-terminal fragment generated from the cleavage of vimentin at Asp85 plays a role in apoptosis by amplifying the cell death signal (Byun *et al.*, 2001). Additional caspase substrates associated with apoptotic morphology are referred in (Earnshaw *et al.*, 1999) (Saraste and Pulkki, 2000).

Moreover, non-chromatin nuclear proteins such as the nuclear mitotic apparatus protein (NuMA) have also been described to play a role in chromatin condensation and apoptotic nuclear breakdown (Taimen and Kallajoki, 2003) (Lin *et al.*, 2007). Reorganization of NuMA is dependent on caspase activation – NuMA can be cleaved by caspases such as caspase-6 or caspase-3– but also on the proper processing of the endonuclease DFF40/CAD (Dieker *et al.*, 2012). Colocalization of the endonuclease with NuMA confirmed the tethering of DFF40/CAD to the nuclear matrix (Lechardeur *et al.*, 2004). Nucleolytic action of DFF40/CAD has been suggested to occur in matrix attachment regions (MARs) with the purpose to switch off the genome function and to promote complete condensation of the chromatin in apoptotic cells (Dieker *et al.*, 2012). The function of these short nucleotide sequences referred to as matrix attachment regions (MARs) or scaffold attachment regions (SARs) is to anchor the chromatin loops to the nuclear matrix proteins such as NuMA, lamin B, histone H1 or SATB1 and to play a role in fundamental nuclear processes including organization of the chromatin within the nucleus and regulation of gene expression. Mapping

of scaffold/matrix attachment regions in the human genome has recently been published (Narwade *et al.*, 2019). The web interface MARome contains the data from this study.

Together, the cellular architecture perturbations that cells suffer upon cell death contribute to the relocation of chromatin into plasma membrane blebs. This process, which requires both actin and microtubules, constitutes an "eat me" signal for phagocytic cells and contributes to the complete DNA degradation (Lane *et al.*, 2005). A controlled demolition is essential to prepare apoptotic cells for its removal by phagocytes.

After more than 80 years of studying how the nuclear shape and the chromatin changes upon cell death, the specific mechanism behind the generation of the different nuclear morphologies has not precisely been clarified yet. Thanks to the study of particular cellular models such as the human glioblastoma-derived LN-18 cells, described to be resistant to display apoptotic nuclear morphologies (Sanchez-Osuna *et al.*, 2014), this Doctoral thesis sheds light and suggests some key points governing the morphology of the nuclei upon cell death.

4. Necrosis

The concept of necrosis was initially coined to describe an accidental uncontrolled form of cell death characterized by the absence of morphological traits of apoptosis or autophagy (Kroemer *et al.*, 2009) (Galluzzi *et al.*, 2007).

Morphologically, necrosis is characterized by oncosis (gain in cell volume), swelling of organelles, plasma membrane rupture, and loss of intracellular contents.

Biochemically, this mode of cell death is associated with a reduction of ATP levels (which drop to almost zero) and failure of ATP-dependent ion channels and pumps. This failure leads to a massive cell volume increase through Na^+ influx (Barros *et al.*, 2001), activation of the Na^+/K^+-ATPase, and a further decrease of ATP levels. ATP depletion prompts the opening of non-selective Ca^{2+} channels and leads to the activation of Ca^{2+}-ATPase and mitochondrial depolarization. The general ionic homeostasis failure leads to further Na^+ and water influx and, therefore, swelling and collapse of the cells (Barros *et al.*, 2001) (Padanilam, 2003) (**Figure I35**). Osmotic shock, mechanical stress, and heat or freeze-thawing are some of the physicochemical stresses described as responsible for this morphological and biochemical outcomes.

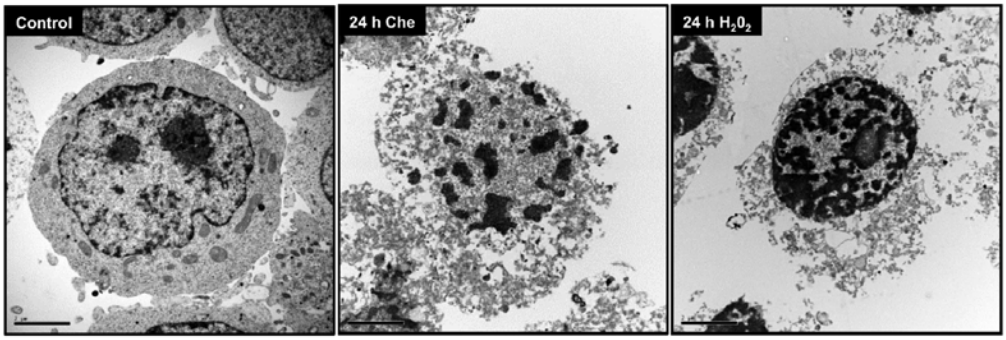

FIGURE I35. Ultrastructural morphology of necrotic cells. Transmission electron microscopy images of SH-SH-SY5Y cells left untreated (*Control*) or treated with chelerythrine (*Che*) or hydrogen peroxide (H_2O_2). Both treatments show cellular changes described for necrotic cell death, including cell swelling, loss of plasma membrane integrity, cell rupture, and irregular chromatin destruction. Images from Garcia-Belinchon *et al.*, 2015.

4.1. Necroptosis

Thanks to the effort of many laboratories, we know that necrosis can also be a regulated mode of cell death and is manifested with a necrotic morphotype (**Figure I35**). The observation of RIPK1 activation and its suppression, either genetically or pharmacologically by RIPK1inhibitors (including necrostatin-1) led to the introduction of necroptosis or necroptotic cell death concepts (Degterev *et al.*, 2005); Hanson, 2016). However, as RIPK3 (a homolog of RIPK1) has been implicated in instances of regulated necrosis with the independence of RIPK1 and insensitive to necrostatins, particular care is needed when referring to this type of cell death (Wang *et al.*, 2019a) (Degterev *et al.*, 2008). In this sense, regulated necrosis should be further characterized and named with regard to its dependence on specific signaling modules (Galluzzi *et al.*, 2018) (**Figure I9**). According to the latest report of NCCD, necroptosis is defined as "a modality of RCD triggered by perturbations of extracellular or intracellular homeostasis that critically depends on MLKL (mixed lineage kinase domain like pseudokinase), RIPK3, and (at least in some settings) on the kinase activity of RIPK1" (Galluzzi *et al.*, 2018).

In general terms, extracellular or intracellular perturbations are detected by specific death receptors, such as FAS and TNFR1; or pathogen recognition receptors (PRRs), including Toll-like receptors 3 or 4 (TLR3 or TLR4) and Z-DNA binding protein 1 (ZBP1) or DNA-dependent activator of interferon regulatory factors (DAI), which is a sensor of cytosolic DNA (Maelfait *et al.*, 2017) (Lin *et al.*, 2016) (Newton *et al.*, 2016). RIPK1 through TNFR1 signaling; TRIF upon TLR3 or TLR4 activation and; ZBP1 activated by type I interferon (IFN-I) response, are required for the sequential activation of RIPK3 and MLKL (**Figure I36**). Necroptosis through TNFR1 involves the catalytic activity of RIPK1 and leads to the

formation of RIPK1-containing and RIPK3-containing amyloid-like signaling complex, referred to as necrosome or "Complex IIb" (Vandenabeele *et al.*, 2010) (Cho *et al.*, 2009). This complex signals MLKL recruitment through trans-phosphorylation or auto-phosphorylation events (Li *et al.*, 2012). Phosphorylated MLKL results in its oligomer formation and its translocation to the plasma membrane, where it triggers permeabilization (Galluzzi *et al.*, 2014). Some of the specific effects that MLKL oligomerization promotes include Ca^{2+} influx and phosphatidylserine (PS) exposure (Gong *et al.*, 2017). At the plasma membrane, MLKL can also activate cell-surface proteases to promote shedding of plasma membrane-associated proteins or formation of Mg^{2+} permeant channels (Xia *et al.*, 2016).

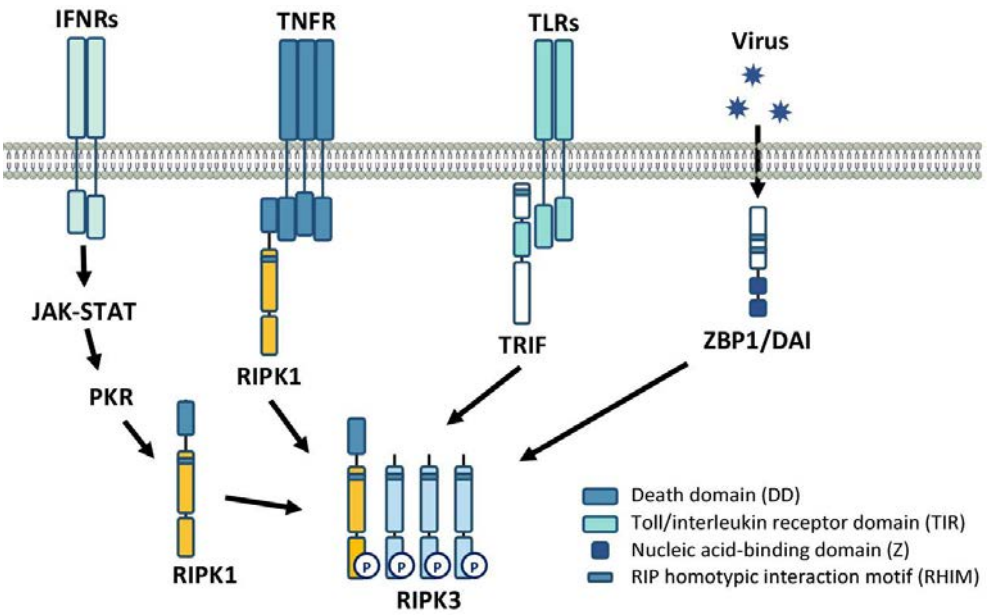

FIGURE I36. Activation of receptor-interacting kinase 3 (RIPK3). Various upstream stimuli activate RIPK3 via pro-necrotic RHIM (RIP homotypic interaction motif)-containing proteins. TNF receptor (TNFR) recruits RIPK1 and associates with RIPK3 via RHIM domains. Other RIP3-activating stimuli include TIR-domain-containing adapter-inducing interferon-β (TRIF) or the RHIM-containing cellular protein Z-DNA binding protein 1 or DNA-dependent activator of interferon regulatory factors (ZBP1/DAI). TRIF interacts with Toll-like receptors (TLRs) through its TIR domain and with RIPK3 through its RHIM domain. ZBP1 sense cytosolic DNA. Alternatively, type I or II IFNs induce RNA-responsive protein kinase PKR activation through the Janus kinase (JAK)-signal transducer and the activator of transcription (STAT) pathway. Once activated, PKR interacts with RIPK1 and subsequently initiates RIPK1/RIPK3-dependent necrosis. Modified from Sun and Wang, 2014.

The laboratory of Dr. Xiaodong Wang reported pharmacological inhibition of MLKL by using necrosulfonamide (NSA) (Sun *et al.*, 2012). Additionally, pharmacological or genetic inactivation of caspase-8 (Kaiser *et al.*, 2011) (Oberst *et al.*, 2011) and RIPK1 deubiquitination-dependent phosphorylation (favored by SMAC mimetics) have been described in the

necrosome formation upon TNFR1 stimulation. The ubiquitin carboxyl-terminal hydrolase (CYLD), a proteolytic target of caspase-8, is described as a deubiquitinating protein of RIPK1 at the "complex I" level (O'Donnell *et al.*, 2011). Deubiquitination of RIPK1 favors its release from "complex I" and its association with FADD and caspase-8 in the cytosol to form "complex II" and to drive extrinsic apoptosis (Hitomi *et al.*, 2008). The ubiquitination of RIPK1 by c-IAPs has been described as an inhibitory mechanism of necroptosis. At the same time, cIAP1 and cIAP2 can inhibit caspase-8 thus favoring necroptosis (Tenev *et al.*, 2011) (Feoktistova *et al.*, 2011) (Sun and Wang, 2014) (**Figure I9**).

Although previous results described the recruitment of PGAM5 and phosphorylation by RIPK3 at the necrosome, as well as the implication of the dynamin related protein 1 (DRP1) in the mitochondrial fragmentation upon necroptosis (Wang *et al.*, 2012), recent studies point to a dispensable role of mitochondria and, specifically, of those mitochondrial proteins in necroptotic cell death (Lu *et al.*, 2016) (Moriwaki *et al.*, 2016) (Moujalled *et al.*, 2014) (Tait *et al.*, 2013) (Alvarez-Diaz *et al.*, 2016). However, at least in some cells, mitochondrial ROS promote RIPK1 activation by autophosphorylation and, therefore, enhance necrosome formation (Schenk and Fulda, 2015) (Zhang *et al.*, 2017). Besides phosphorylation of MLKL, RIPK3 enhances necrosome assembly via the generation of ROS by activating the pyruvate dehydrogenase (PDH) complex (Yang *et al.*, 2018) (**Figure I12**). Hence, progressive mitochondrial dysfunction may increase the likelihood of cells to undergo apoptosis (Bock and Tait, 2020).

Apart from the role of RIPK1 in necroptosis, this protein has a pro-survival role and can inhibit RIPK3-dependent necroptosis and/or caspase-8-dependent extrinsic apoptosis (Orozco *et al.*, 2014).

5. Autophagy

Autophagy is a key biological process for cell survival that can also elicit cell death (Bialik *et al.*, 2018) (Galluzzi *et al.*, 2017). The concept of autophagy-dependent cell death (ADCD) or type 2 cell death (*see 2.1. Cell death classification*) is described by the NCCD (Galluzzi *et al.*, 2018) as "a form of RCD that mechanistically depends on the autophagic machinery (or components thereof)". Hence, to comprehend this mode of cell death results indispensable to know what the concept of autophagy refers to, and the mechanism behind it.

The term autophagy, from the Ancient Greek αὐτόφαγος for "self-eating" was coined in 1963 by Christian de Duve at the Ciba Foundation symposium on lysosomes (Yang and Klionsky,

2010). He coined out these term to describe the presence of single- or double-membrane vesicles that contain parts of cytoplasm and organelles in various states of disintegration (De Duve *et al.*, 1955) (De Duve and Wattiaux, 1966) (**Figure I37**).

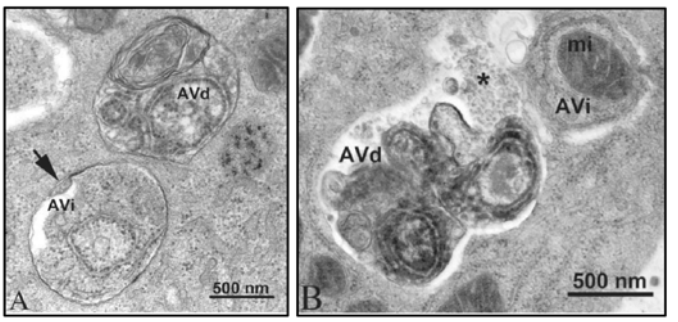

FIGURE I37. TEM images of autophagic vacuoles. On the left, the autophagosome or early initial autophagic vacuoles (AVi) can be identified by its contents (morphologically intact cytoplasm, including ribosomes, and rough ER), and the limiting membrane that is partially visible as two bilayers separated by a narrow electron-lucent cleft, i.e., as a double membrane (arrow). The degradative autophagic vacuole (AVd) can be identified by its contents, partially degraded, electron-dense rough ER. On the right, the AVi contains rough ER and a mitochondrion (mi), and the AVd contains partially degraded rough ER. The AVd contains a region filled by small internal vesicles (asterisk), indicating that the AVd has fused with a multivesicular endosome. Images from Klionsky *et al.*, 2016.

This cellular process is a highly evolutionarily conserved mechanism by which eukaryotic cells degrade intracellular components in the lysosomal compartment. Autophagy allows removal of long-lived, aggregated and misfolded proteins or clearance of damaged organelles. Despite this function, autophagy is also involved in other biological functions such as regulation of growth, development, cellular differentiation, defense against pathogens, or nutritional starvation.

Generally, autophagy is subdivided into three different types: macroautophagy, microautophagy, and chaperone-mediated autophagy. **Macroautophagy** is characterized by the formation of double-membrane vesicles called autophagosomes. This autophagosomes sequester cytoplasmic material and then fuse with lysosomes, thereby forming autolysosomes for degradation. Moreover, autophagosomes come from the phagophore and can be derived from different membranes, including endoplasmic reticulum (ER) membranes (Axe *et al.*, 2008), the outer membrane of mitochondria (Hailey *et al.*, 2010), or the trans-Golgi network (Young *et al.*, 2006). By contrast, **microautophagy** and chaperone-mediated autophagy do not require autophagosomes formations, they directly deliver cytoplasmic components to the lysosomal compartment. Microautophagy involves the direct engulfment of cytoplasm at the lysosome surface. Vesicles trapping cytoplasm content are formed as a result of lysosomal

membrane invagination (Kunz *et al.*, 2004). **Chaperone-mediated autophagy**, a specific mechanism observed in higher eukaryotes, comprises the selective degradation of proteins containing the motive KFERQ. Those proteins are identified in the cytosol by a chaperone complex, transferred to the lysosomal membrane, and then gain access to the lumen thanks to the translocation complex formed by the receptor protein LAMP2A (lysosomal-associated membrane protein A2) for its degradation (Orenstein and Cuervo, 2010) (Cuervo and Wong, 2014).

Macroautophagy and microautophagy can be nonselective processes or can specifically target damaged or superfluous organelles. The specific degradation of damaged organelles is referred to as mitophagy (mitochondria), reticulophagy (endoplasmic reticulum), pexophagy (peroxisomes), lipophagy (lipid droplets) nucleophagy (nucleus), agregophagy (protein aggregates), ferritinophagy (ferritin) or proteophagy (proteasomes) (Parzych and Klionsky, 2014) (Galluzzi *et al.*, 2017). Here, the term autophagy will be used as synonymous of macroautophagy.

5.1. The process of autophagy: molecular mechanisms

As in apoptosis, initial studies of autophagy (from the 1950s to 1980s) were based on morphological observations. Later, and thanks to the studies of Yoshinori Ohsumi performed in yeast (Tsukada and Ohsumi, 1993), the first autophagy-related gene (ATG1) was identified (Matsuura *et al.*, 1997). Now, around 15 ATGs are described and involved in different stages of autophagy (Mizushima *et al.*, 2011).

The process of autophagy is divided into distinct stages: **initiation**, which is triggered upon activation of the proteins involved in the early stages; **vesicle nucleation**, which occurs when part of the cytoplasm containing long-lived proteins or damaged organelles are surrounded by a cisternal membrane called phagophore; **vesicle elongation**, the process by which the phagophore expands to form a double-membrane vacuole to form autophagosomes; **vesicle fusion** with lysosomes to form autolysosomes; and **cargo degradation or recycling** with the involvement of active acid hydrolases such as cathepsin B and D (Ohsawa *et al.*, 1998). Some of the resulting products are re-used in the cytosol for effective use by the cell, like to synthesize essential cellular components to survive starvation conditions.

The principal molecular machinery governing the distinct stages of autophagy is hereafter mentioned.

The **initiation** step is controlled by the Unc-51-like kinase (ULK) complex that consists of ULK1/2, ATG13, ATG101, and FIP200 (focal adhesion kinase family kinase-interacting protein 200 kDa) (Mercer *et al.*, 2009) (Ganley *et al.*, 2009). When nutrients are available, mTORC1 (mammalian target of rapamycin complex 1) is active and it inactivates ULK1 complex formation through phosphorylation of ULK and ATG13 (Hosokawa *et al.*, 2009). In conditions of starvation, mTORC1 is inhibited and, consequently, ULK can interact with ATG13 and FIP200, and can trigger the activation of the initiator complex of autophagy (**Figure I38**).

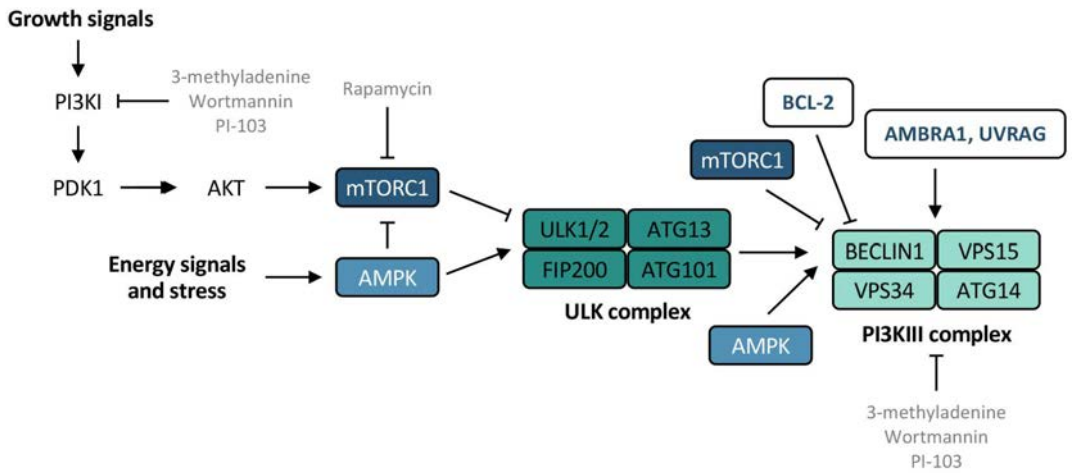

FIGURE I38. The process of macroautophagy: initiation and vesicle nucleation. Activators such as AMPK and inhibitors such as mTORC1 of the ULK and the PI3KIII complexes are here illustrated. The PI3KIII complex can be positively regulated by AMBRA1 and negatively regulated by BCL2 binding to BECLIN1 and preventing association with the complex. Autophagy modulator compounds are indicated in gray. Adapted from Meng et al., 2019 and Mizushima *et al.*, 2010.

The **vesicle nucleation** stage depends on the BECLIN1-PtdINs3KC3 (phosphatidylinositol 3-kinase class III)-ATG14L complex (**Figure I38**). ATG14-PI3KCIII complex generates the phosphatidylinositol 3-phosphate (PI3P) required for the nucleation process of autophagosomes. ULK1 phosphorylates the BH3 domain-only protein BECLIN1 (BCL-2 interacting myosin/moesin-like coiled-coil protein 1), which acts in concert with ATG14 and p150 (vps15 in yeast) to engage PtdINs3KC3. In mammals, the PtdINs3KC3 refers to the PI3KCIII or the vacuolar protein sorting 34 (VPS34) (Herman and Emr, 1990). Apart from ULK, mTOR complex and/or AMPK (AMP-activated protein kinase) directly phosphorylate components of the PI3KCIII complex and trigger VPS34 activity (Kim *et al.*, 2013) (Yuan *et al.*, 2013). BECLIN1 can interact with BIF-1 protein through UVRAG (UV radiation resistance-associated gene) and with WIPI1 and WIPI2 (WD repeat domain phosphoinositide-interacting) proteins. The first interaction is involved in the curvature of

autophagosome membrane (Takahashi *et al.*, 2007), and the second interaction seems to allow membrane rearrangements to occur for the formation of autophagosomes (Mauthe *et al.*, 2011).

The **elongation** of the growing double membrane is mediated by two ubiquitin-like conjugation systems (**Figure I39**). One system involves the conjugation of phosphatidylethanolamine (PE) to gamma-aminobutyric acid receptor-associated protein (GABARAP) or to cytoplasmic LC3-I to generate the lipidated form LC3-II for its incorporation into the growing membrane (Dikic and Elazar, 2018). In this ubiquitin-like conjugation system participates the protease ATG4B, which cleaves LC3 and generates the cytosolic ubiquitin-like protein, LC3-I; the E1-like enzyme ATG7; and the E2-like enzyme ATG3. The other ubiquitin-like conjugation system is mediated by the same E1-like enzyme ATG7, and the E2-like enzyme ATG10 and results in an ATG12-ATG5 conjugate. ATG16L1 is then associated with ATG5 to form the ATG12-ATG5-ATG16L1 complex, and also binds to other ATG16L1-ATG5-ATG12 trimers to form multimeric structures, that bind to the membrane of phagophore until the complete formation of the autophagosome. Once generated, the transport of autophagosomes to lysosomes is mediated by microtubules (Nakamura and Yoshimori, 2017).

In mammals, the autophagosome **fusion** with lysosomes is mediated by LAMP2, the GTPase RAB7, and SNARE proteins (Jager *et al.*, 2004) (Fader *et al.*, 2009). The resulting autolysosomes, characterized by low pH conditions and the presence of active acid hydrolases such as cysteine-cathepsin (B, C, H, K, L) and aspartil-cathepsins (D, E), are responsible for the **cargo degradation** (Ohsawa *et al.*, 1998).

Although under debate, there is some evidence supporting that the formation of functional autophagosomes can bypass some of the detailed steps described above. The variation of the canonical pathway, best known as non-canonical autophagy, includes characteristics such as the non-hierarchical intervention of ATG proteins for the formation of the double-membrane autophagosome, initiation of autophagy bypassing ULK1, nucleation bypassing BECLIN1 and elongation and closure bypassing ATG7, ATG5, and LC3. Variations between canonical and non-canonical autophagy are deeply addressed in (Codogno *et al.*, 2011).

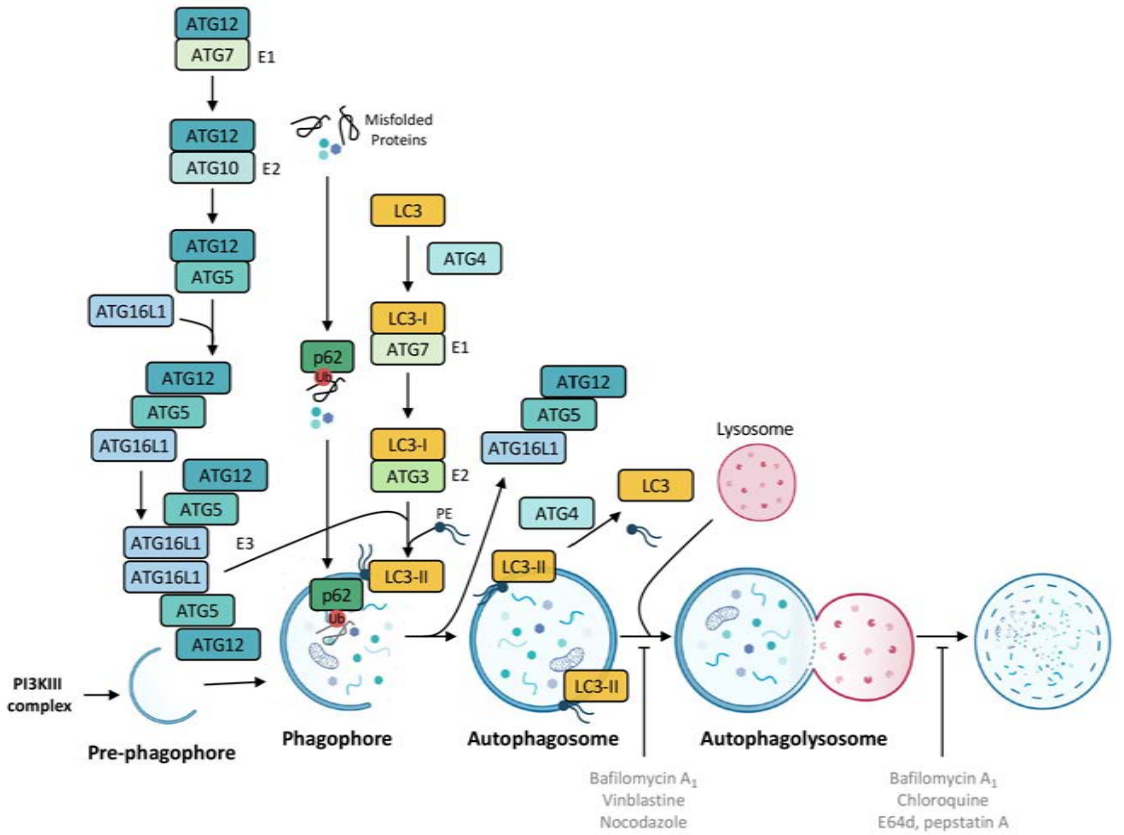

FIGURE I39. The process of macroautophagy: elongation, fusion and cargo degradation. The ubiquitin-like conjugation systems that participate in the elongation are here illustrated. The ATG12-ATG5-ATG16L1 complex participates as an E3 ligase in the conjugation of PE (phosphatidylethanolamine) to LC3-I to create LC3-II, which associates with the phagophore. LC3-II can subsequently be cleaved by ATG4 to release LC3 (deconjugation). Misfolded ubiquitinated proteins are detected by the adaptor protein p62/SQSTM1, which binds to LC3-II and localize ubiquitinated proteins into autophagic compartments for its degradation through autophagy. The fusion of autophagosome with the lysosome and the subsequent cargo degradation can be inhibited by different autophagy modulator compounds (indicated in gray). Adapted from Mizushima *et al.*, 2010; Parzych and Klionsky, 2014; and Pedroza *et al.*, 2020.

5.2. Regulation of autophagy

The principal regulator of autophagy is the mTORC1 complex. This complex, which functions as a sensor of different signaling pathways activated under various stimuli, coordinates cellular anabolism and catabolism (Saxton and Sabatini, 2017). mTORC1 consists of mTOR (mammalian target of rapamycin), RAPTOR (regulatory-associated protein of mTOR) and mLST8 (mammalian lethal with SEC13 protein 8), and two inhibitory subunits: PRAS40 and DEPTOR (DEP domain containing mTOR interacting protein). Once active,

mTORC1 inhibits autophagy. Consequently, mTORC1 inhibition leads to autophagy activation. Regulators of mTORC1 include the PI3K-AKT-mTORC1 pathway and AMPK.

The PI3K-AKT-mTORC1 pathway controls basic cellular processes such as growth, proliferation, survival, metabolism, motility, or angiogenesis (Guertin and Sabatini, 2007), and is one of the most common altered signaling pathways in tumor cells. The consequences of overactivation of this pathway include resistance to cell death or uncontrolled proliferation. Once activated, AKT phosphorylates a huge amount of proteins (Manning and Toker, 2017) involved in different signaling pathways that became positively or negatively regulated. Among them, the best-characterized substrates included GSK3 (glycogen synthase kinase 3), the first reported AKT substrate that becomes inhibited upon phosphorylation by AKT (Cross *et al.*, 1995); FoxO (Forkhead Box O) transcription factors, which control apoptosis, cell cycle arrest and cell catabolism and translocates outside of the nuclei upon AKT phosphorylation; and TSC2 (Tuberous Sclerosis Complex 2) complex, a regulator element of the AKT/mTORC1 pathway that upon AKT phosphorylation allows mTORC1 activation (Manning *et al.*, 2002) (Inoki *et al.*, 2002). As mentioned above, activated mTORC1 regulates anabolic processes such as the synthesis of proteins, lipids or nucleotides, and inhibits catabolic processes like autophagy (Saxton and Sabatini, 2017).

The AMPK is the master sensor of cellular bioenergetics (Shaw *et al.*, 2004). AMPK is activated through LKB1 kinase by a decreased ATP/AMP ratio, and also via Ca^{2+}/calmodulin-dependent kinase kinaseβ (CaMKKβ) by an increase in the cytosolic free Ca^{2+}. Regarding autophagy, phosphorylation and activation of the TSC1/TSC2 complex by AMPK indirectly lead to autophagy activation by mTORC1 inhibition, and RAPTOR is also inhibited by AMPK. Alternatively, AMPK can directly activate autophagy via ULK activation (Egan *et al.*, 2011). Autophagy can also be triggered through the unfolded protein response (UPR) via PERK (PKR-like ER kinase) inhibition of AKT/mTORC1, and activation via TRIB3 (Ord and Ord, 2017), or via CaMKKβ (Hoyer-Hansen and Jaattela, 2007). Among the different cascades that can be involved in the restorage of the homeostasis when cells are exposed to stress, stimulation of protein degradation by UPR via autophagy constitute an important cellular response. Nonetheless, proteins involved in the restorage of the homeostasis can also induce cell death by mitochondrial apoptosis or necroptosis. The involvement of UPR and the core autophagy machinery and cell death induced by endoplasmic reticulum stress has been extensively reviewed (Song *et al.*, 2018) (Iurlaro and Munoz-Pinedo, 2016) (**Figure I40**).

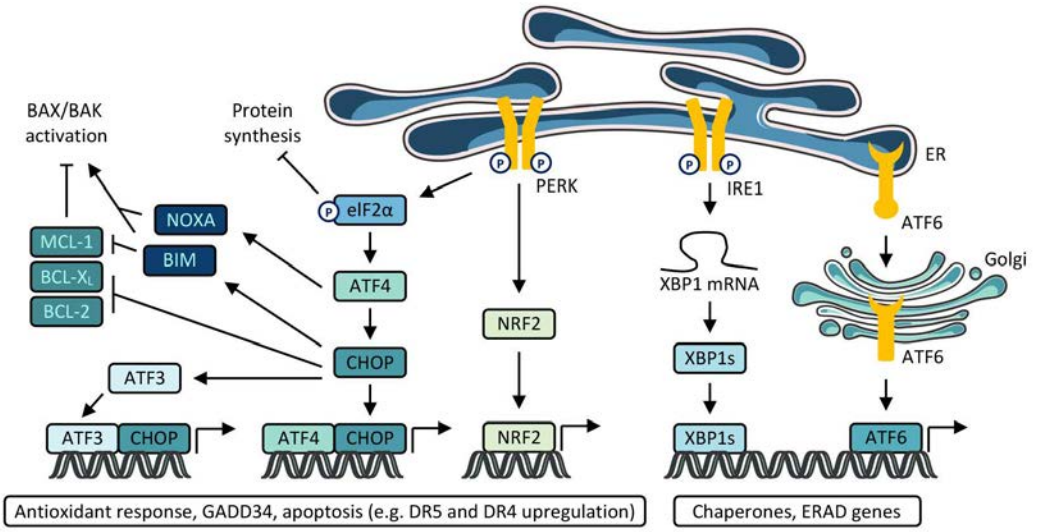

FIGURE I40. The unfolded protein response and ER stress-induced cell death. The three main sensors of the UPR are PERK, IRE1 and ATF6. PERK phosphorylates eIF2α attenuating mRNA translation and induces the transcription factors ATF4 and CHOP, which regulate the expression of genes involved in the restoration of the homeostasis and GADD34, an inhibitor of eIF2α, attenuating the response. PERK also activates the transcription factor NRF2, which induces antioxidant responses. Under ER stress, ATF4 induces the activation of NOXA. CHOP, which can also be induced by ATF6 (not indicated), induces BIM and inhibits BCL-2 anti-apoptotic proteins. Additionally, CHOP induces the expression of ATF3. CHOP and ATF3 have been shown to bind to the promoter of DR5 and DR4 genes and upregulate their expression thus promoting caspase-8 activation and cell death. IRE1 is a kinase and an endonuclease that regulates the splicing of the transcription factor XBP1, resulting in the transcription of genes involved in restoring the ER folding capacity. ATF6 is translocated into the Golgi where it is cleaved to release the transcription factor that regulates chaperones expression and ER-associated degradation genes. Modified from Iurlaro and Muñoz-Pinedo, 2016.

BCL-2 family proteins are additional regulators of autophagy. Beside its role in cell death (see *3.2.1. BCL-2 family proteins*), this family of proteins may function as inhibitors or as inducers of autophagy. The BCL-2 and BCL-X_L proteins interact with BECLIN1 at the BH3 domain to impair its interaction with VPS34 and, hence, to inhibit its pro-autophagic activity (Liang *et al.*, 1999) (Liang *et al.*, 2008). By contrast, AMBRA1 (activating molecule in BECLIN1 regulated autophagy protein 1) binds to BECLIN1 to prevent association with BCL-2 and, therefore, positively regulates vesicle nucleation and stabilize the PI3KCIII complex (Fimia *et al.*, 2007) (**Figure I38**). The link between apoptosis and autophagy is further addressed below.

5.3. Methods for monitoring and measuring autophagy

The different methods for monitoring autophagy have been extensively reviewed (Mizushima *et al.*, 2010) (Klionsky *et al.*, 2016) (Yoshii and Mizushima, 2017). Briefly, hereafter are

described the principal approaches employed for direct observation of autophagy-related structures and determination of autophagic flux, which refers to the amount of autophagy-/lysosome-dependent degradation of proteins and organelles.

Regarding the identification of autophagic structures, electron microscopy provides evidences for autophagosomes and autolysosomes; the first contain cytoplasmic components enclosed in double-membraned vesicles; the second are single-membraned structures that contain degraded cytoplasmic components (**Figure I37**). Since the morphology of autophagic structures can differ depending on the conditions and/or fixatives used, the identification of those structures through electron microscopy can be challenge. Alternatively, markers including ULK1, ATG5, and LC3 are commonly employed to identify autophagosomes and LysoTracker or LAMP1/2 as markers for lysosomes. Among them, LC3 detection is the most extended approach to identify autophagic structures and to measure autophagic flux.

Nascent LC3 or pro-LC3 is immediately processed after C-terminal glycine by ATG4 family proteins into LC3-I and, subsequently, conjugated to phosphatidylethanolamine (PE) to generate LC3-II. As mentioned above, this conjugation with PE requires the autophagy conjugation systems ATG12 and LC3/GABARAB systems. After Western blotting, two bands of LC3 can be detected: one corresponding to LC3-I and the other one to LC3-II. Although the molecular weight of LC3-II is larger than that of LC3-I, the extreme hydrophobicity of LC3-II results in a faster migration of LC3-II and thus, in a smaller apparent molecular weight: 14kDa for LC3-II compared to the 16 kDa for LC3-I. The presence of LC3-II on isolation membranes and autophagosomes (on both inner and outer membranes) makes to correlate this LC3 conversion (LC3-I to LC3-II) with the number of autophagosomes and, therefore, to autophagy (Mizushima and Yoshimori, 2007) (Kabeya *et al.*, 2000) (Kabeya *et al.*, 2004).

Nonetheless, although LC3 detection is a widely used tool to monitor autophagy and a good indicator of autophagosome formation (Kabeya *et al.*, 2000) (Kabeya *et al.*, 2004), it is necessary to emphasize that LC3-II can be itself degraded by autophagy; hence, special care is needed to avoid misinterpretation (Mizushima and Yoshimori, 2007). Degradation of LC3-II can be partially inhibited by using lysosomal protease inhibitors such as E64d and pepstatin A or bafilomycin A1, a V-ATPase inhibitor that impedes autophagosome-lysosome fusion (Yamamoto *et al.*, 1998) (**Figure I39**). The level of autophagic flux is represented by differences in the levels of LC3-II between samples with and without these lysosome inhibitors. Autophagic flux can also be measured by p62 degradation, which binds to LC3 and is selectively degrades by autophagy (Bjorkoy *et al.*, 2005). However, as the expression level of

p62 can change independent of autophagy, presentation of p62 data only may lead to inappropriate interpretation.

Besides Western blotting, visualization of LC3 puncta formation through fluorescence microscopy may be an additional powerful tool to assess autophagosome formation. Moreover, LC3 modification can occur during autophagy-unrelated processes (Schaaf *et al.*, 2016). Hence, it is necessary to compile multiple evidence from different methodologies to prove the involvement of autophagy in each experimental conditions. In this sense, GFP-LC3 degradation determined by flow cytometry or the GFP-LC3-RFP-LC3ΔG are alternative methods to prove the involvement of autophagy in any experimental condition. This last, correspond to a fusion protein of GFP-LC3 and RFP-LC3 that is cleaved by the endogenous ATG4 proteins at the C-terminal glycine of the first LC3. As a result, the same number of GFP-LC3 and RFP-LC3ΔG are generated in the cytosol. While GFP-LC3 can be conjugated to PE and localize to autophagosomes, RFP- LC3ΔG cannot because the C-terminal glycine of LC3 is delated. As a result, the GFP/RFP ratio quantifies the cumulative GFP-LC3 degradation by autophagy. Autophagy induction results in a reduction in the GFP/RFP ratio due to an increase in GFP-LC3 degradation. Extensive and specific experimental information regarding these methods is detailed in (Zhang *et al.*, 2016) (Singh and Bhaskar, 2019).

5.4. The link between autophagy and cell death

Eukaryotic cells often activate autophagy to overcome stressful situations. The activation of this cellular process provides nutrients and helps for the removal of damaged macromolecules and organelles. Hence, activation of autophagy exerts a cytoprotective role and favors the re-establishment of the cellular homeostasis and survival. However, as introduced in this section, autophagy has also been associated with cell death. When cells are faced to excessive stress, autophagy may be used as a suicide mechanism (type II cell death). Nevertheless, it is controversial if autophagy triggers cell death itself or if it is a mediator of the cellular program that finally executes cell death (Denton *et al.*, 2012) (Aredia *et al.*, 2012).

Regarding apoptosis, different effectors of this mode of cell death have been found to exert a regulating role in autophagy. Indeed, under basal conditions, both cellular processes cross-regulate each other at multiple points. Regulators of the extrinsic and intrinsic apoptotic pathways converge with autophagy pathway at multiple points through protein-protein interactions, post-translational modifications, protein cleavage and/or protein degradation (Fairlie *et al.*, 2020). The BCL-2 family protein and caspases are clear examples of this

connection. More specifically, when BECLIN-1 dissociates from BCL-2, it triggers autophagy and, consequently, increases the amount of free BCL-2 that may interact with pro-apoptotic proteins such as BAX (Shimizu *et al.*, 2004) (Gump and Thorburn, 2011). In the case of caspases, these proteases can be cleared from the cytosolic environment upon autophagy activation (Hou *et al.*, 2010) or can cleave themselves many ATG proteins and non-ATG proteins (Norman *et al.*, 2010) (Djavaheri-Mergny *et al.*, 2010) (Zhu *et al.*, 2010) (**Figure I41**). The interplay between ATGs and caspases is addressed in depth in the following reference (Tsapras and Nezis, 2017).

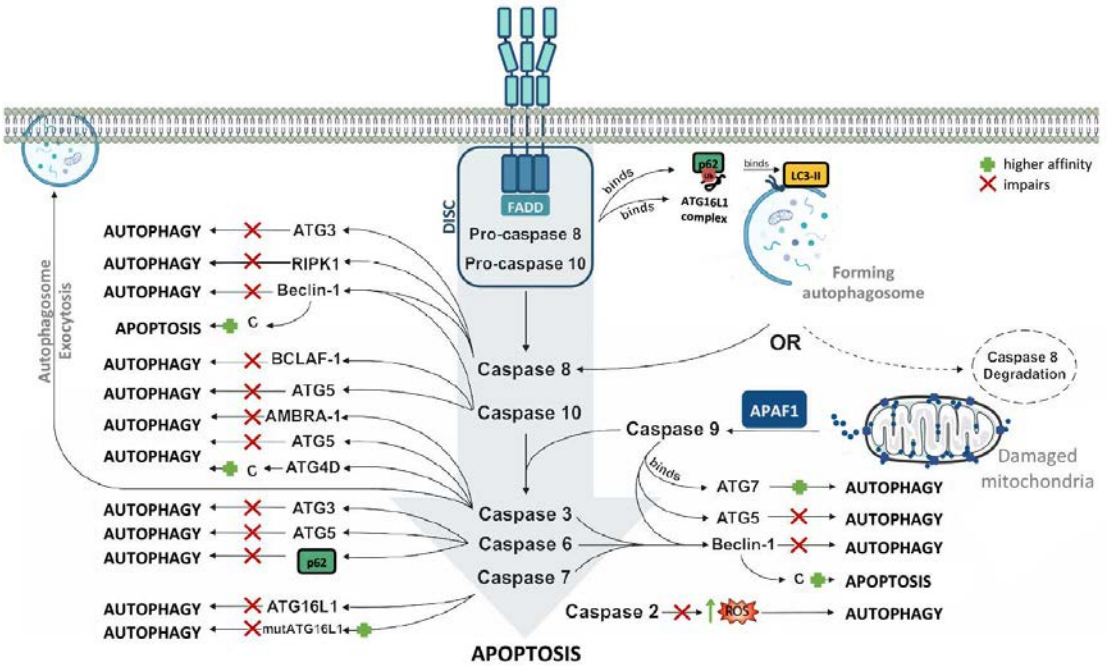

FIGURE I41. Schematic representation of reported effects of caspases in autophagy-related effectors. The central blue arrow depicts the activation of caspases during the apoptotic cascade. Upon death ligation, pro-caspase-8 is converted to caspase-8 via DISC formation; or in ways which can also involve the ATG16L1 complex, and targeting of pro-caspase-8 oligomers to the autophagosomal surface by p62. Sequestration of pro-caspase-8 to the autophagosome can lead to caspase-8 activation, or degradation by lysosomal hydrolases upon autolysosome formation. The side arrows on each caspase depict its known interactions with ATG targets and other autophagy-related proteins. The resulting outcome on autophagy is shown with an 'X' over, or a '+' behind the arrows that indicate the otherwise physiological effect of the autophagic protein on the pathway. C corresponds to c-terminal fragments, blue dots released from the mitochondrion correspond to cytochrome *c* and ↑ means increase of reactive oxygen species (ROS). Modified from Tsapras and Nezis, 2017.

The NCCD recommends to avoid the term "autophagy-dependent cell death" in the absence of strong experimental data mechanistically linking RCD to components of the autophagy machinery, as well as when pharmacological or genetic manipulations of the molecular machinery for autophagy impact on other RCD subroutines. Bialik *et al.,* reviewed where, how,

and why autophagy-dependent cell death occurs (Bialik *et al.*, 2018). This review also refers to autosis, a type of ADCD morphologically characterized "by the accumulation of autophagosomes and autolysosomes, nuclear convolution with moderate chromatin condensation, as well as abnormal mitochondria structures and ER fragmentation and dilatation" (Bialik *et al.*, 2018). According to Liu *et al.*, inhibition of lysosome fusion does not block autosis or cell death. This type of ADCD is associated with a secondary necrosis-like phenotype that may involve changes in osmolarity mediated by Na^+/K^+-ATPase pumps and ion transport (Liu *et al.*, 2013) (Bialik *et al.*, 2018).

6. Other types of cell death and non-lethal processes

Intracellular and extracellular microenvironments are continuously exposed to different perturbations. If those perturbations are unrecoverable, cells can activate one of many signal transduction cascades that will ultimately lead to their death. This section lists some of the principal cell death modes described until now and their definition according to the NCCD (Galluzzi *et al.*, 2018) (**Figure I**).

Ferroptosis

"A form of RCD initiated by oxidative perturbations of the intracellular microenvironment that is under constitutive control by the reduced glutathione (GSH)-dependent enzyme glutathione peroxidase 4 (GPX4) and can be inhibited by iron chelators and lipophilic antioxidants". This mode of cell death generally occurs independently of caspases and manifests with a necrotic morphotype. ROS generation and iron availability are among the predominant perturbations of the intracellular microenvironment. Different molecular compounds have been developed to induce ferroptosis (i.e., erastin, liproxstatins) (Dolma *et al.*, 2003). Other agents such as ferrostatin-1 (Fer-1), liproxstatin-1 (Lip-1), vitamin E or coenzyme Q_{10} have been proven to prevent this RCD by limiting lipid peroxidation and operating as ROS scavengers (Skouta *et al.*, 2014) (Friedmann Angeli *et al.*, 2014). Moreover, sorafenib (tyrosine kinase inhibitor) and altretamine (alkylating agent), both approved by the FDA, can trigger ferroptosis in distinct cellular models. This type of RCD is extensively reviewed in (Qiu *et al.*, 2020) (Li *et al.*, 2020).

Pyroptosis

"A type of RCD that critically depends on the formation of plasma membrane pores by members of the gasdermin (GSDM) protein family, often (but not always) as a consequence

of inflammatory caspase activation". Pyroptosis has a key role in innate immunity against intracellular pathogens (Villunger *et al.*, 2003), and induced by lipopolysaccharide (LPS), is involved in pathological conditions, including lethal septic shock. Type I IFN and IFN gamma contribute to pyroptosis. Often, this type of RCD is associated with IL-1β and IL18 secretion, which mediates a robust pro-inflammatory effect. The term pyroptosis was initially used to define a type of RCD resembling apoptosis but dependent on inflammatory caspase-1. Further studies have pointed to other caspases such as caspase-3, caspases-4, and caspase-5, which oligomerize and can be activated as a result of its interaction with LPS through its CARD domain. Once activated, catalyze the proteolytic cleavage of GSDMD. Upon release of the pyroptotic inducer GSDMD-N, it oligomerizes and generates a pore that is responsible for rapid plasma membrane permeabilization (Ding *et al.*, 2016) (Liu *et al.*, 2016) (Chen *et al.*, 2016) (Sborgi *et al.*, 2016). GSDME/DFNA5, as well as other gasdermin family proteins, resemble GSDMD and display pore-forming and pyroptotic activity upon multiple challenges such as TNF, DNA damaging chemotherapeutic agents and/or infections (Rogers *et al.*, 2017) (Wang *et al.*, 2017). *In vitro*, in cells undergoing caspase-3 driven apoptosis in the absence of proficient phagocytosis, DFNA5 has also been involved in the acquisition of necrotic phenotypes.

Parthanatos

"A modality of RCD initiated by PARP1 hyperactivation and precipitated by the consequent bioenergetic catastrophe coupled to AIF-dependent and MIF-dependent DNA degradation". The hyperactivation of this specific factor of the DNA damage response (DDR) machinery occurs as a consequence of severe/prolonged alkylating DNA damage in response to hypoxia, oxidative stress, hypoglycemia, or inflammatory cues (Fatokun *et al.*, 2014) (Virag *et al.*, 2013) (David *et al.*, 2009). The bioenergetic catastrophe caused as a result of PARP1 hyperactivation consists of NAD+ and ATP depletion. It occurs coupled with the accumulation of poly(ADP-ribose polymers), which, in turns, binds to AIF and promotes its release into the cytosol and translocation to the nucleus. Cytosolic AIF also promotes the translocation of MIF (macrophage migration inhibitory factor) into the nucleus where it catalyzes DNA cleavage.

Entotic cell death

"A type of RCD that originates from actomyosin-dependent cell-in-cell internalization (entosis) and is executed by lysosomes". Some authors have referred to this type of cell death as a form of cell cannibalism that occurs by engulfment of viable cells by non-phagocytic cells. This internalization of cells occurs through cell invasion rather than by phagocytosis and can

end (often, but not always) with the demise of internalized cells, also referred to as "entotic cells". This elimination relies on a specific RCD subroutine implicating the LC3-associated phagocytosis (LAP), and leading to lysosome fusion, degradation and generation of nutrients that are recovered by engulfing cells.

NETotic cell death

"A ROS-dependent modality of RCD restricted to cells of hematopoietic derivation and associated with NET extrusion". The term NET refers to neutrophil extracellular traps. The particular molecular mechanisms of this RCD are not fully elucidated; however, the activity of NDPH oxidases and the consequent ROS generation have been described.

Lysosome-dependent cell death (LDCD)

"A type of RCD demarcated by primary lysosomal membrane permeabilization (LMP) and precipitated by cathepsins, with optional involvement of MOMP and caspases". Perturbations of intracellular homeostasis involving ROS and activation of lysosomal Ca^{2+} channels lead to the permeabilization of lysosomal membranes and release of lysosomal contents such as the cathepsin family to the cytoplasm. In some settings the LMP takes place before mitochondria in other downstream of MOMP (Serrano-Puebla and Boya, 2016) (Boya *et al.*, 2003a) (Boya *et al.*, 2003b). Thus, LDCD does not necessarily involve MOMP or caspases.

Immunogenic cell death (ICD)

"A form of RCD that is sufficient to activate an adaptive immune response in immunocompetent hosts". Different stimuli have been pointed as initiators of ICD, among them: viral infection, FDA-approved chemotherapeutics (anthracyclines or bortezomib), or specific forms of radiation therapy. These agents stimulate the release of a series of damage-associated molecular patterns (DAMPs) involving calreticulin, HMGB1, type I IFN, cancer cell-derived nucleic acids, and annexin A1. The immunogenicity of RCD can be suppressed by some caspases such as caspase-8 or -3; thus, specific caspase-inhibitors may boost this immunogenicity.

Two non-lethal processes, mistakenly considered cell death processes in some publications, are also listed in the 2018 NCCD classification.

Cellular senescence

"Irreversible loss of proliferative potential associated with specific morphological and biochemical features, including the senescence-associated secretory phenotype (SASP). Cellular senescence does not constitute a form of RCD". This is in part, because senescent cells remain viable and metabolically active (Campisi, 2013) (Sharpless and Sherr, 2015) (van Deursen, 2014). Morphologically, those cells exhibit intracellular vacuolization, flattening shapes with cellular and nuclear enlargement and altered chromatin. From a biochemical perspective, increased galactosidase beta 1 (GLB1) activity, inhibition of cyclin-dependent kinases (CDKs), absence of proliferation markers, activation of the DNA-damage response (DDR) machinery, and presence of senescence-associated heterochromatic foci (SAHF) are characteristics of senescent cells.

Mitotic catastrophe

"Oncosuppressive mechanism for the control of mitosis-incompetent cells by RCD or cellular senescence. Per se, mitotic catastrophe does not constitute a form or RCD". Extensive DNA damage, problems with the mitotic machinery, and/or failure of mitotic checkpoints can lead to mitotic catastrophe (Castedo *et al.*, 2004) (Vitale *et al.*, 2011). Morphologically, those cells exhibit multi- and micronucleation as a consequence of chromosomal missegregation, and micronucleation. Although not always resulting in RCD, mitotic catastrophe can drive RCD processes such as cellular senescence.

This section evidences the high degree of interconnectivity existing between different types of RCD. The study of this cross-talk and of the signals that are released after the different modes of cell death will be of particular interest to better comprehend the different consequences that may be derived from those different released signals (Boada-Romero *et al.*, 2020) (**Figure I42**).

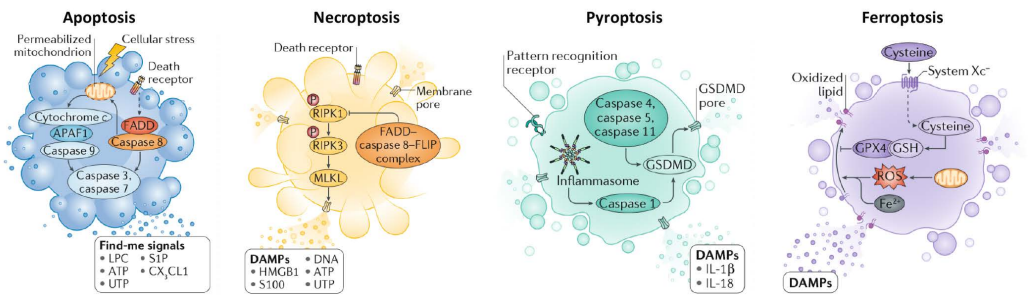

FIGURE I42. Presented signals from different modes of cell death. Cells present different signaling moieties depending on the mode of cell death that have undergone. These signals lead to efferocytosis and to a variety of distinct physiological outcomes (Boada-Romero *et al.*, 2020).

7. Cross-talk between cell death subroutines

In line with the above described, an increasing number of non-apoptotic forms of regulated cell death (RCD) has been identified. The existence of distinct subroutines of cell death with different intracellular pathways provides cells a wide range of possibilities to respond to persisting perturbations (Tang *et al.*, 2019). The activation of RCD generally constitutes the last effort of stressed cells to preserve the integrity of the whole organism (Fuchs and Steller, 2011). Indeed, in most cases, and with the final purpose of preserving the organism, the effect of the RCD is not only addressed to the elimination of damaged cells. Stressed cells will emit different molecules (locally or systemically) to alert surrounding cells of the state of danger (Galluzzi *et al.*, 2016). Moreover, although generally referred to as a mere suicide process, most of the members involved in the execution of RCD also participate in adaptive responses to stress. This connection between the systems that attempt to recover homeostasis and the machinery that controls cell death shows the complexity of stress responses. The activation of autophagy clearly exemplifies this connection. Autophagy is a key component of the integrated stress response that can be activated by different stress stimuli (nutrient and energy stress, ER stress, hypoxia, mitochondrial damage…). Once activated, it can integrate other cellular stress responses (including cell cycle and growth, intermediary metabolism, or cellular death programs) (Kroemer *et al.*, 2010).

Increasing evidence support the existence of an interplay between different cell death signaling pathways (Marino *et al.*, 2014). In this sense, apoptotic activation of caspases its described to regulate autophagy through cleavage of essential pro-autophagic proteins. Indeed, resulting fragments of essential autophagy proteins may have additional roles in pro-apoptotic signaling. Autophagy-independent functions of the autophagy machinery are extensively reviewed in (Galluzzi and Green, 2019), and caspase involvement in autophagy is deeply addressed in (Tsapras and Nezis, 2017). Alternatively, caspases have also been described to be involved in other cellular functions such as differentiation, proliferation, or migration (Connolly *et al.*, 2014). Moreover, other apoptosis-regulatory proteins, such as ligand-bound death receptors, may trigger regulated necrosis. The activation of NF-κB by death receptors such as TNFR1 may lead to the transactivation of genes with anti-apoptotic functions or may drive the production of pro-inflammatory mediators and inflammation responses involving caspases (caspases-1 and -5) (Galluzzi *et al.*, 2012a). Overall, this data suggests that lots of proteins classically characterized in the context of a single cellular process may participate in different processes. So, the specific inhibition of any intracellular component may have an impact on different processes.

From a general perspective, this cellular plasticity to undergo different modes of cell death implies higher adaptability of cells to deal with adverse situations. However, in certain pathological situations such as cancer, tumor cells may take profit of this adaptability to integrate different responses and escape from perturbing situations. Consequently, the activation of different stress responses constitutes a benefit for tumor cells, but may hamper the proper elimination of those cells when faced to different stresses such as those induced by radio-chemotherapy. More research is needed to better comprehend the cross-talk between different forms of RCD, as well as with non-cell death processes activated upon stress. Moreover, how the interplay that occurs between different cellular processes is affected in a context-dependent manner will also be important for the future research.

8. Cell death in the tumor context

The exposure of cells to different stresses prompts the activation of various systems to restore cellular homeostasis. However, although the general purpose is to preserve the organismal homeostasis, if adaptive stress responses fail to repair the damage, and activation of RCD fails to eliminate damaged cells, those cells containing unrepaired DNA will be prone to accumulate somatic mutations as they divide. The dysregulation of RCD may lead to detrimental consequences such as cancer. The presence of pre-malignant cells will constitute a threat to the entire organism (Hanahan and Weinberg, 2011) (Galluzzi *et al.*, 2016). In this sense, activation of cellular responses, including autophagy, may impair transformation. However, several genetic and epigenetic changes that drive malignant transformation affect key autophagy regulators (Galluzzi *et al.*, 2015b) and may be required to enable malignant transformation (Rybstein *et al.*, 2018). Indeed, autophagy constitutes an essential mechanism not only for cancer initiation but also for progression and response to therapy (Rybstein *et al.*, 2018). Inhibition of autophagy is generally considered an oncogenic event, and the elimination of oncogenic protein substrates may function as a tumor suppressive mechanism (Marino *et al.*, 2014). Nonetheless, in some cancers (such as pancreatic cancer or lung cancer), autophagic defects or autophagy inhibition may promote, rather than inhibit, tumor progression (Guo *et al.*, 2013). In those cancers, defective autophagy may support genomic instability and metabolic reprogramming while preserving adaptation to stress. Consequently, the pro-survival effects of autophagy may also lead to cancer progression (Amaravadi *et al.*, 2016).

In this sense, it is necessary to stress that the activation of other intracellular pathways described as responsible for certain cell death types does not always end with the death of the cells. Regarding apoptosis, although it is generally considered a tumor suppressor mechanism,

it can also function as an oncogenic mechanism (Cao and Tait, 2018) (Ichim and Tait, 2016). Among the different regulators involved in the apoptotic signaling, caspase-3, as well as the mitochondrial nuclease EndoG, have been described to promote oncogenic transformation (Cartwright *et al.*, 2017) (Liu *et al.*, 2015) (Liu *et al.*, 2017). The implication of executioner caspases in mutagenesis has been described in cells treated with TRAIL or vincristine (Lovric and Hawkins, 2010) (Miles and Hawkins, 2017). Indeed, the same authors involved DFF40/CAD, the principal apoptotic nuclease, in the mutagenesis activated upon treatment with those chemotherapeutic drugs. Sublethal apoptotic signals leading to DFF40/CAD activation and DNA breaks constitutes a stress to genome stability. If this stress is not sufficient to cause the death of the cell, surviving cells may incorporate oncogenic mutations (Ichim *et al.*, 2015). The oncogenic potential of failed apoptosis may be explained by the potential mutagenic repair of the DNA breaks generated by the apoptotic nucleases (Larsen and Sorensen, 2017). Indeed, CAD-dependent DNA breaks within the mixed lineage leukemia (MLL) gene have been involved in the rearrangement of this gene as the result of erroneous DNA repair processes (Hars *et al.*, 2006) (Gole and Wiesmuller, 2015). Besides the potential role of DFF40/CAD leading to oncogenic mutations and cellular transformation, it is necessary to emphasize that DNA fragmentation triggered by this endonuclease also constitutes a barrier to tumorigenesis (Yan *et al.*, 2006a) (Larsen and Sorensen, 2017). Certainly, although the murine loss of function models for DFF40/CAD display normal development, increased susceptibility to tumor formation is observed when challenged with carcinogenic stimuli (Zhang *et al.*, 1998) (Yan *et al.*, 2009). Loss of DFF40/CAD-dependent DNA fragmentation may delay the removal of highly mutated cells and, consequently, provide cells of more time to adapt to genome instability (Yan *et al.*, 2006b). Genomic instability will provide tumor cells with higher genomic plasticity, which is necessary to acquire pro-tumor capacities and to introduce different mutations and epigenetic modifications to survive.

In this sense, although extensive somatic mutations in DFF40/CAD have not been documented in cancer cells, our group has recently described low expression levels of the endonuclease as a common trait in human glioblastoma cells (Sanchez-Osuna *et al.*, 2016). This intrinsic deficiency of DFF40/CAD impairs DNA fragmentation during caspase-dependent cell death (Sanchez-Osuna *et al.*, 2016). Moreover, as mentioned above, cells from this tumor are particularly refractory to die showing apoptotic nuclear morphologies when faced with different insults. In this line, results from our laboratory, together with the aggressiveness of this tumor and its resistance to most of the therapeutic approaches, make glioblastoma an exciting and attractive model of study.

8.1. Glioblastoma (GB)

The World Health Organization (WHO) presented in 2016 the last update of the Classification of Tumors of the Central Nervous System (CNS). The 2016 CNS WHO broke with the century-old principle of diagnosis, based entirely on microscopy, and incorporated molecular parameters to histology features into the classification of CNS tumor entities. This conceptual and practical advance over its 2007 predecessor implied major restructuring of CNS tumors, including diffuse gliomas (Louis *et al.*, 2007) (Louis *et al.*, 2016).

Although molecular genetic features mean an improvement in the diagnosis of CNS tumors, phenotype remains essential. Indeed, the WHO grade determinations, which consist of four different WHO grades (I-IV) –from lower to higher malignancy– are still based on histological criteria.

However, according the latest recommendations from cIMPAC-NOW (the Consortium to Inform Molecular and Practical Approaches to CNS Tumor Taxonomy) "histologic grade II and III IDH-wildtype diffuse astrocytic gliomas, which contain high-level EGFR amplification, the combination of whole chromosome 7 gain and whole chromosome 10 loss (+ 7/− 10), or TERT promoter mutations, correspond to WHO grade IV and should be referred to as *diffuse astrocytic glioma, IDH-wildtype, with molecular features of glioblastoma, WHO grade IV*"(Brat *et al.*, 2018). This observation highlights the necessity to combine phenotypic and genotypic features for the classification of CNS tumors.

Glioblastoma, considered as the most common primary brain malignancy, accounts for over 50% of all high-grade gliomas. In the 2016 CNS WHO, glioblastomas are divided into (**Table I6**):

- **Glioblastoma, IDH-wildtype:** corresponds to the 90% of glioblastoma cases and associates frequently with the clinically defined primary or *de novo* glioblastoma. This entity predominates in patients over 55 years of age. The morphological variants of epithelioid glioblastoma, giant cell glioblastoma, and gliosarcoma have been included as new variants under the umbrella of IDH-wildype glioblastoma.
- **Glioblastoma, IDH-mutant:** counts for about 10% of the cases and corresponds narrowly to secondary glioblastoma with a history of prior lower grade diffuse glioma. Secondary glioblastomas, which preferentially arise in younger patients, have a lesser degree of necrosis, are preferentially located in the frontal lobe, and carry a significantly better prognosis. Histologically, primary and secondary glioblastomas are very similar; however, they differ in their genetic and epigenetic profiles being IDH1 mutations one of

the most decisive genetic signposts of secondary glioblastomas (Ohgaki and Kleihues, 2013).

- **Glioblastoma, NOS:** refers to a diagnosis in which the full IDH evaluation cannot be performed.

	IDH-wildtype glioblastoma	IDH-mutant glioblastoma
Synonym	Primary glioblastoma, IDH-wildtype	Secondary glioblastoma, IDH-mutant
Precursor lesion	Not identifiable; develops de novo	Diffuse astrocytoma Anaplastic astrocytoma
Proportion of glioblastomas	~90%	~10%
Median age at diagnosis	~62 years	~44 years
Male-to-female ratio	1.42:1	1.05:1
Mean length of clinical history	4 months	15 months
Median overall survival **Surgery + radiotherapy** **Surgery + radiotherapy + chemotherapy**	 9.9 months 15 months	 24 months 31 months
Necrosis	Extensive	Limited
***TERT* promoter mutations**	72%	26%
***TP53* mutations**	27%	81%
***ATRX* mutations**	Exceptional	71%
***EGFR* amplification**	35%	Exceptional
***PTEN* mutations**	24%	Exceptional

TABLE I6. Characteristics of IDH-wildtype and IDH-mutant glioblastomas. Modified from Louis *et al.*, 2016.

The above-mentioned nomenclature referring to IDH comes from mutations in isocitrate dehydrogenase genes. In mammalian cells, three different genes encode for three enzymes: IDH1 (cytosolic, $NADP^+$-dependent), IDH2 (mitochondrial, $NADP^+$-dependent), and the multi-subunit enzyme IDH3 (mitochondrial, NAD^+-dependent). Especially IDH1 mutations constitute a molecular marker of secondary glioblastomas.

8.1.1. Detection, diagnosis, and therapeutic approach of glioblastoma

According to the European Association for Neuro-Oncology (EANO) publication from 2017, around 6 cases per 100,000 individuals worldwide are diagnosed with a glioma, including

glioblastoma, and a slight predominance is registered in males (Weller *et al.*, 2017). In Spain, 4,000 new malignant gliomas are diagnosed each year from which more than one-third are glioblastomas. The mean age at diagnosis is 62 years (Galceran *et al.*, 2017).

Detection and diagnosis

The brain MRI (magnetic resonance imaging) is the gold standard for imaging gliomas with the regular protocols including fluid-attenuated inversion recovery (FLAIR), contrast (gadolinium or Gd)-enhanced T1-weighted (T1Gd) and relative cerebral blood volume (rCBV) imaging sequences (Ellingson *et al.*, 2015). An example is shown in **Figure I43**.

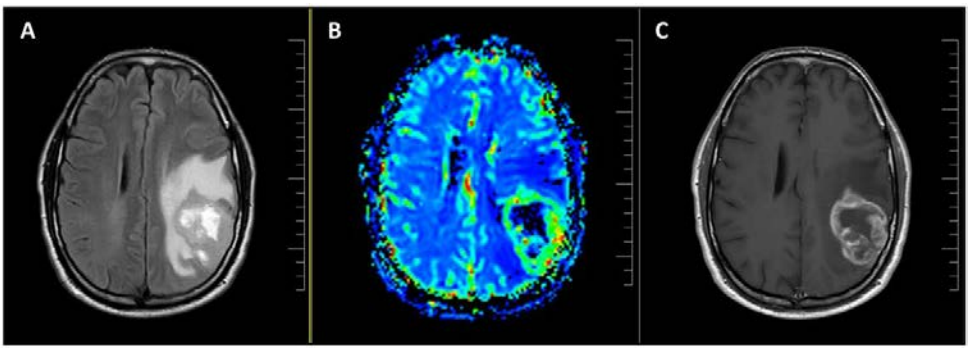

FIGURE I43. MRI sequences for glioblastoma detection. A, axial MRI FLAIR sequence demonstrates an extensive diffuse and infiltrative mass located in the left temporoparietal lobe. **B**, rCBV map shows an elevated rCBV in the periphery of the tumor (in green). C, axial MRI T1Gd sequence shows a heterogeneous irregular peripheral enhancement associated with the left temporoparietal lobe mass with non-enhancing central areas, formed by necrosis and hemorrhagic components. These images are from the Unit of Neuro-Oncology (Hospital Universitari de Bellvitge-ICO Duran I Reynals, Barcelona, Spain).

Additionally, magnetic resonance spectroscopy (MRS) can substantially improve the categorization/grade of gliomas providing metabolic information. Metabolites which can be identified include lipids, N-acetyl-aspartate (NAA), choline (Cho), creatine (Cr), myo-inositol (MI) and glutamine compounds (Glu-n). In the setting of glioblastoma, lipid and Cho raised peaks with a NAA depressed peak are typical MRS findings (Guo *et al.*, 2012).

Glioblastomas, IDH-wildtype are preferentially located at the temporal lobe, and glioblastomas, IDH-mutant at the frontal lobe; however, they can be detected at any part of the central nervous system.

Unfortunately, prevention strategies are not available (Rice *et al.*, 2016) unless screenings limited to individuals with genetic risk syndromes. Among the diseases considered as a risk of developing gliomas, there are neurofibromatosis type I, Turcot syndrome and Li Fraumeni

syndrome. Of note, exogenous risk factors, including exposure to radiation, should be considered in the patient history. Furthermore, some viral infections, such as the induced by human Cytomegalovirus (HCMV), have been associated with glioma formation (McFaline-Figueroa and Wen, 2017), but its role remains uncertain.

In most of the cases, the manifestation of these tumors will be through new onset epilepsy, focal deficits, and indicators of intracranial hypertension (vomiting, headache, and altered consciousness).

Once clinicians suspect of brain tumor, multidisciplinary discussion in a brain tumor board review (including neuroradiologists, neuropathologists, neurosurgeons, radiation oncologists, and neurooncologists), is key to decide the best management of the patient. As most treatment decisions depend on tissue diagnosis, and now also on molecular markers, biopsy or resection are almost always performed with diagnostic and therapeutic objectives. Only when the prognosis is likely to be unfavorable (even with treatment), or the risk of the biopsy is considered too high, clinicians may initiate palliative care without a histological diagnosis.

A biopsy needle, which is performed through a stereotactic procedure, or tumor resection allow obtaining serial samples from the tumor mass. Indeed, part of the samples obtained during the surgical process can be assessed intraoperatively. This procedure helps to safeguard that enough tissue is obtained to establish a diagnosis. The diagnosis will be based on the conventional histological staining from formalin-fixed and embedded tumor tissue in paraffin (including hematoxylin-eosin staining); immunochemical; and molecular analyses. According to 2016 WHO CNS, histological tumor typing grades tumors in four different WHO grades (I-IV) coinciding with different biological behavior, prognosis, and outcome.

Concerning tissue-based molecular biomarkers, the screening of isocitrate dehydrogenase 1 (IDH1) codon 132 or IDH2 codon 172 missense mutations is a major diagnostic tool. In addition to IDH mutation, three other molecular biomarkers are crucial for the diagnosis and treatment of gliomas: 1p/19q codeletion, histone H3 K27M or H3 G34 mutation, and methylation at the O^6-methylguanine DNA methyltransferase (MGMT) promoter. Moreover, telomerase reverse transcriptase (TERT) promoter mutations are also assessed. Further recommended parameters are epidermal growth factor receptor (EGFR) amplification, losses of chromosome 10, and gains of chromosome 7 (Yeaney and Brat, 2019).

Therapeutic approaches

Three different antitumoral therapeutic strategies are currently available: surgery, radiation, and chemotherapy (**Figure I44**).

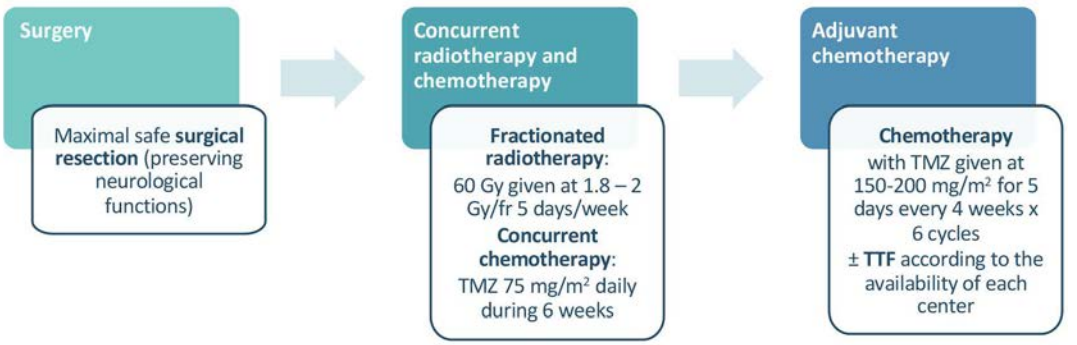

FIGURE I44. Therapeutic approach scheme for glioblastomas. Gy, grays; fr, fraction; TMZ, temozolomide; TTF, tumor treating fields.

Surgical approaches are generally performed to obtain a histological diagnosis. Beyond this goal, **surgery** is performed to remove as much of the tumor as possible. However, it is especially complicated due to the infiltrating behavior of glioblastoma cells. Approaches such as navigation systems with functional MRI datasets and the fluorescent dye 5-aminolevulinic acid are employed to visualize better the tumor tissue (Stummer *et al.*, 2006). These approaches help to increase the extent of resection as safely possible to preserve and/or improve the neurological functions of glioblastoma patients. However, glioblastomas are generally surrounded by a zone of migrating, infiltrating tumor cells, which invade nearby tissues and make it impossible to remove the tumor entirely (Jackson *et al.*, 2001). The result of surgery is assessed by early MRI.

Due to the surgical incurability of these tumors, radiotherapy and chemotherapy are of key importance to eliminate remaining tumor cells that have infiltrated the surrounding non-tumor brain tissue. Of note, as gliomas are not cured by surgery, prevention of new, permanent neurological deficits is even more critical than the extent of resection. The quality of life is a high priority. Nonetheless, two retrospective studies from the early 1990s (Simpson *et al.*, 1993) (Curran *et al.*, 1993), and subsequent multiple retrospective studies identified surgery with respect to biopsy as an independent variable associated with higher survival (Bruna and Alemany, 2020). Indeed, unless contraindicated, IDH-wildtype glioblastomas are treated with surgery with gross total resection (Weller *et al.*, 2017).

Since the 1980s, **radiotherapy** has been the standard of care for glioblastoma. The use of gamma irradiation roughly doubled survival in glioblastoma patients (Laperriere *et al.*, 2002) (Walker *et al.*, 1978). Now, approaches such as focused radiotherapy, including intensity-modulated or image-guided radiotherapy, are among the improvements developed to target radiotherapy's target delivery while better protecting surrounding tissue (Mann *et al.*, 2017). Under the purpose of improving local control at a reasonable risk benefit ratio, the standard treatment consist in focal radiotherapy with an ionizing radiation dose of 60 Gy, given in 1.8-2 Gy fractions (Gy/day, 5 days/week). In the case of individuals with poor prognostic factors (defined by age or Karnofsky score), hypofractionated radiotherapy (e.g., 40 Gy in 15 fractions) is recommended. In children or adults with deeply localized tumors, interstitial brachytherapy and proton or heavy ion radiotherapy may be used as an alternative. Note that hypofractionated regimens, brachytherapy, radiosurgery, and stereotactic radiotherapy improvements (the most standard) confer no survival advantage compared with regular regiments (Niyazi *et al.*, 2016).

Glioblastoma **chemotherapy** was initially based on nitrosourea addition but it had little success (Stewart, 2002). Nitrosoureas, including lomustine, carmustine, nimustine, and fotemustine, cause prolonged leukopenia, thrombocytopenia, and pulmonary fibrosis (in the case of carmustine). This toxicity, together with the increased survival induced by temozolomide (Stupp *et al.*, 2005), moved nitrosoureas from the first-line treatment to a second choice after temozolomide in most European countries.

Stupp *et al.* described an extend in median survival from 12 to 15 months and an increase of 2-years survival to 27% when giving temozolomide concomitantly with radiation and continued after that. From 2005, temozolomide, a DNA alkylating agent, is used as the first-line of treatment for glioblastoma (Stupp *et al.*, 2005). After surgery, oral temozolomide is given concomitantly at 75 mg/m^2/day for 7 days/week during the 6 weeks of radiotherapy. Temozolomide is continued thereafter at 150-200 mg/m^2 for 6 cycles of 5 days every 28 days. This is the standard of care for newly diagnosed adult patients (aged up to 70 years) in good neurological and general conditions (Stupp *et al.*, 2009) (Hart *et al.*, 2013).

The good blood-barrier penetration and the favorable safety profile made temozolomide a promising option for glioblastoma patients. Temozolomide has low toxic effects, but it can cause myelosuppression or thrombocytopenia in some cases. So, regular hepatic, renal, and hematological laboratory tests are performed during cytotoxic chemotherapy. Blood counts should also be monitored during treatment.

The MGMT promoter's methylation status is the strongest predictor for the outcome and benefits from temozolomide chemotherapy (Stupp *et al.*, 2009). MGMT is a DNA repair enzyme that removes alkyl groups from the O^6-position of guanines and protects DNA from the damage induced by temozolomide. Consequently, patients with MGMT promoter-methylated glioblastoma (loss/low levels of functional MGMT protein) present most obvious effect (Perry *et al.*, 2017) **(Hegi *et al.*, 2005)** (**Table I7**). The MGMT promoter methylation status is assessed by immunocytochemistry or molecular genetic tests, including methylation-specific PCR or pyrosequencing of bisulfite-modified tumor DNA(Weller *et al.*, 2013).

	MGMT methylated	MGMT unmethylated
Surgery + radiotherapy	15.3	11.8
Surgery + radiotherapy + temozolomide	23.4	12.6

TABLE I7. Median overall survival of glioblastoma patients by MGMT status and type of treatment. The overall survival is indicated in months. MGMT, O^6-methylguanine methyltransferase. Data from Stupp *et al.*, 2009.

Unfortunately, combined treatment with temozolomide is unlikely to be curative for many patients. In this sense, a huge number of compounds have been proposed for the treatment of glioblastomas. Among the different clinical trials developed in glioma patients, bevacizumab, an antibody to vascular endothelial growth factor, is the only anti-angiogenic drug approved for recurrent glioblastoma in the USA. However, due to no single biomarker showing predictive benefit or resistance to bevacizumab in independent datasets, and the non-described effect on overall survival (OS), used as first-line treatment, the European Union has not approved this drug for newly diagnosed glioblastoma. Different immunological therapies have been developed for glioma therapy; however, most of them are still of unknown efficacy or have not demonstrated the expected efficacy.

A novel treatment modality is the tumor-treating fields (TTFields). This modality consists of low-intensity, intermediate-frequency (200 kHz) alternating electric fields that are delivered locoregionally via transducer arrays. The principle of mechanism of this technology is to impede the correct formation of mitotic fuse and, therefore, to impair cellular division by using an electric field (Delgado-Lopez and Corrales-Garcia, 2016) (Kirson *et al.*, 2007). When added to standard maintenance temozolomide, this approach showed longer progression-free survival (PFS) and overall survival (almost five month higher) than standard maintenance of temozolomide alone (Stupp *et al.*, 2017). Despite the controversy and skepticism surrounding this method (Wick, 2016), it is necessary to stress that it is the unique phase III clinical study with positive results after more than ten years of research in glioblastoma.

More recently, it has been suggested that lomustine-temozolomide chemotherapy might improve survival compared with temozolomide standard therapy in patients with newly diagnosed glioblastoma with methylated MGMT promoter. However, the findings need to be interpreted with caution due to the small size of the trial (Herrlinger *et al.*, 2019).

Moreover, while the treatment for newly diagnosed glioblastomas is well defined, this is not the case for the standards of care for patients with recurrent glioblastoma. The clinical decision is made considering age, Karnofsky performance score, previous treatment and patterns of progression, and several clinical factors. The main systemic treatment options at progression include nitrosoureas (lomustine is increasingly considered standard treatment), temozolomide rechallenge, and bevacizumab.

8.1.2. The aggressiveness of glioblastoma: from a histological, biochemical and molecular perspective

As mentioned above, histological diagnosis is an essential part of the management of glioblastomas. Histological traits include necrosis and microvascular proliferation with hyperplastic blood vessels, both used as pathologic definition of glioblastomas. Areas of necrotizing tissue are generally surrounded by anaplastic cells or pseudopalisading cells. Pseudopalisades refer to the hypercellular zone containing pyknotic nuclei surrounding necrotic tissue (Brat and Mapstone, 2003) (Plate *et al.*, 1992).

Behind the clinical outcome and the histological aspect of glioblastomas, different genomic abnormalities influence glioblastoma aggressiveness. In parallel with histological observations, the study of the molecular and biochemical characteristics have been crucial to comprehend gliomagenesis. The growth factor receptor tyrosine kinase (RTK)-triggered pathways, including the Ras sarcoma (Ras) pathway and the phosphatidylinositol 3-kinase (PI3K)/phosphatase and tensin homolog (PTEN)/AKT; the retinoblastoma (RB)/cyclin-dependent kinase (CDK) N2A-p16$^{INK4\alpha}$; and the TP53/mouse double minute 2 (MDM2)/MDM 4/CDKN2A-p14^{ARF} are major signaling pathways altered in glioblastomas resulting in brain tumor growth and progression (**Figure I45**). The different alterations have been extensively reviewed (Furnari *et al.*, 2007) (Cancer Genome Atlas Research, 2008) (Dunn *et al.*, 2012) (Crespo *et al.*, 2015) (Pearson and Regad, 2017). Below are briefly described some of the most well-characterized and recurrent genomic abnormalities leading to uncontrolled cellular proliferation, diffuse infiltration, a tendency for necrosis, tumor angiogenesis,

widespread genomic aberrations, and resistance to apoptosis (Meyer, 2008) (Furnari *et al.*, 2007).

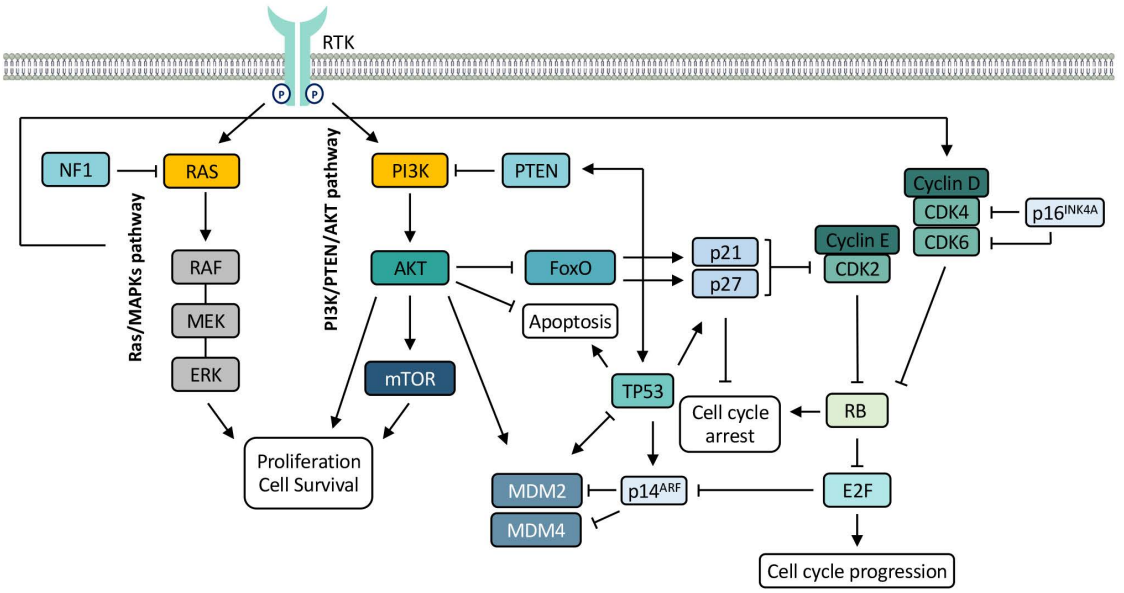

FIGURE I45. Schematic representation of the major signaling pathways altered in glioblastomas. In the phosphatidylinositol 3-kinase (PI3K)/phosphatase and tensin homolog (PTEN)/AKT signaling pathway, the growth factor receptor becomes activated and recruits PI3K to the cell membrane, converting phosphatidylinositol-4,5-bisphosphate to the PIP3 second messenger molecule. Downstream effector molecules, such as AKT and the mammalian target of rapamycin (mTOR), are then activated, which help to induce cell proliferation and block apoptosis. Inactivation of PTEN, which terminates the phosphatidylinositol 3,4,5-trisphosphate (PIP3) signal, leads to increased availability of PI3K. PI3K activates AKT, which, in turn, leads to an increased proliferative activity and survival. Activated AKT phosphorylates and excludes the transcription factor FoxO from the nucleus, a positive regulator of p21 and p27 expression. In the TP53 pathway, TP53 mutation or increased degradation of TP53 because of increased mouse double minute (MDM) 2 activity interrupts the normal cell cycle arrest and apoptosis after DNA damage. p53 protein, which increase after DNA damage can enhance PTEN transcription leading to a positive feedback loop that protects p53 from degradation. In the retinoblastoma protein (RB) pathway, cyclin-dependent kinase (CDK) 4 and CDK6 form complexes with members of the cyclin D family and phosphorylate the RB, which releases the E2F transcription factor, inducing cell proliferation by transcription of genes that promote DNA synthesis. Loss of RB leads to elevated levels of E2F and, therefore, cell proliferation. The mitogen-activated protein kinase (MAPK) pathway also contributes to cell proliferation by inducing the expression of cyclin D1. RTK, receptor tyrosine kinase (include EGFR, epidermal growth factor receptor, and PDGFR, platelet-derived growth factor receptor); NF1, neurofibromatosis type I; P, phosphorylation. Modified from Crespo *et al.*, 2015.

Mutations and/or amplifications in cell cycle regulators such as RB or TP53 lead to uncontrolled cellular proliferation. Mutations, deletions, or promoter methylations of RB locus, as well as alterations on RB regulators, impair the RB pathway in glioblastoma (Patil *et*

al., 2013) (Crespo *et al.*, 2015). Active RB (when hypophosphorylated) prevents cell cycle progression by binding to E2F and preventing transcription of essential genes for cell cycle and proliferation. When RB is inactive, mainly due to phosphorylation by cyclin-dependent kinases (CDK)-cyclin complexes, E2F is released, and transcriptional activation of growth-promoting genes is allowed. In the case of TP53, since it regulates the promoter of p21 (which in turn blocks cell cycle progression), mutations or loss of TP53 directly contribute to reduced p21 expression and, therefore, to cell cycle progression. Moreover, TP53 exerts a key function in the cellular responses to DNA damage facilitating DNA repair or prompting cells to die when the damage is too high. Other alterations in that pathway include overexpression of MDM2 and/or loss of expression of CDKN2A-p14^{ARF} (Zawlik *et al.*, 2009). Indeed, TP53 and RB pathway can be simultaneously inactivated when the genetic locus of CDKN2A, which produces CDKN2A-p14^{ARF} –that inactivates MDM2– and CDKN2A-p16$^{INK4\alpha}$ –that prevents phosphorylation of RB by negatively regulating CDKs– is altered.

Constitutive activation of the MAPK (mitogen-activated protein kinase) pathway induces the expression of cyclin D1, which activates CDK4/6. These CDK proteins are among the most important positive cell cycle regulators (Malumbres and Barbacid, 2009). Regarding PI3K, its recruitment to the cell membrane activates AKT and leads to cell proliferation, increased survival, and blocking of apoptosis (Furnari *et al.*, 2007). PI3K is negatively regulated by PTEN, but PTEN activity is frequently lost in glioblastomas due to gene mutations or loss of heterozygosity (LOH). Therefore, constitutive activation of the PI3K pathway and higher levels of activate AKT are detected in glioma cells. Activated AKT deregulates cell growth, plays an anti-apoptotic activity by impairing pro-apoptotic proteins such as BAD and caspase-9, and contributes to tumor invasion.

Overexpression of platelet-derived growth factor (PDGF) and epidermal growth factor (EGF) receptors in glioblastoma suggest RTK-signaling pathways as critical targets regulating proliferation, differentiation, and survival. Indeed, EGFR signaling can be activated in a ligand dependent or independent manner, not only via overexpression of the receptor and ligands (leading to an autocrine loop), but also by mutation of the receptor (leading to constitutive activation in the absence of ligand) and/or amplification of EGFR (Huang *et al.*, 2009). More specifically, an EGFR variant 3 (EGFRvIII) is frequently altered in glioblastoma and is reported to enhance tumorigenicity through increased cellular proliferation and reduced apoptosis (Hatanpaa *et al.*, 2010). Downstream signal transduction pathways triggered by ligand-activated EGF receptors include: the Ras/rapidly accelerated fibrosarcoma (Raf)/MAPK pathway, the PI3K/AKT pathway, the STAT pathway, and the protein kinase C pathway. Together these pathways impact on cell proliferation, migration, invasion,

resistance to apoptosis, and tumor neovascularization of glioblastomas (Patil *et al.*, 2013). In the case of the Ras pathway, RAS activity has been highly observed in glioblastoma (Rajasekhar *et al.*, 2003); but RAS mutation is rarely detected. This is in line with the above-mentioned implication of upstream factors such as RTK activation, including EGFR or PDGFR. Moreover, it also points to the involvement of downstream effectors, such as Raf-kinase/MAPK and PI3K. Furthermore, a negative regulator of Ras, neurofibromatosis type I (NF1), is also reported to be altered in glioblastoma, specifically loss-of-function mutations of the NF1 gene are described (Patil *et al.*, 2013).

Concerning the robust microvascular proliferation and angiogenesis, pathways involving hypoxic inducible factors (HIF) and non-HIF-dependent downstream effectors can be altered in glioblastomas. Positive regulators or glioblastoma 93ngiogenesis are PDGF or VEGF – which promotes endothelial cell proliferation in malignant gliomas– and negative regulators are interferons (Nyberg *et al.*, 2005). The upregulation of VEGF-A in malignant gliomas leads to the development of humanized monoclonal antibodies like Bevacizumab, which has gained approval in different countries and is mainly used as a second line therapeutic approach like fotemustine or lomustine. Regarding HIF-1, it plays a key role in hypoxic conditions by activating the transcription of genes encoding glucose transporters and glycolytic enzymes take up glucose and convert it to lactate. Alternatively, IDH1 has also been reported to regulate hypoxic cellular responses. In hypoxic cells, IDH1 wildtype cells drive lipogenesis by converting glutamine to α-ketoglutarate (α-KG) (Metallo *et al.*, 2011).

Regarding microvasculature proliferation, although it provides oxygen support and nutrients to hypoxic zones, it may also contribute to more hypoxia and, thereafter, to the tendency of glioblastomas to necrosis. Proteins such as the BCL-2L12 are responsible proteins of necrotic areas in glioblastomas. This BCL-2 family protein is found overexpressed in primary glioblastoma and has been detected to inhibit post-mitochondrial apoptosis (Stegh *et al.*, 2007) while favoring the activation of regulated necrosis (Stegh *et al.*, 2008a). In more detail, when located at the cytoplasm, BCL-2L12 has the potential to inhibit executioner caspases such as caspase-3 and -7 (Stegh *et al.*, 2008b). When located at the nucleus, BCL-2L12 reduces p53 stability and impairs the expression of tumor suppressor genes such as p21, DR5, NOXA, or PUMA (Stegh and DePinho, 2011) (Stegh *et al.*, 2010).

The intense resistance to apoptosis can be explained by the alterations of the above mentioned pathways (RTKs and PI3K/PTEN/AKT), and by alterations of members of the cell death pathway. As an example, the BCL-2 family proteins are among the preferential deregulated apoptotic proteins responsible for the resistance to apoptosis. In the case of glioblastomas,

BCL-2, BCL-X_L, and MCL-1 can be found upregulated (Karpel-Massler *et al.*, 2015). Indeed, BCL-X_L is up-regulated by overexpression of EGFRvIII (Nagane *et al.*, 1998). Resistance to apoptosis can also be due to low expression of death receptors or high expression of proteins such as cFLIP or RIPK1 (Furnari *et al.*, 2007) (Bellail *et al.*, 2010). Inhibitor of apoptosis proteins (IAPs), widely expressed in glioma cell lines, have been reported to have an influence in the resistance of gliomas to apoptosis induced by radio- and chemotherapy (Wagenknecht *et al.*, 1999). Furthermore, our laboratory has described a common trait in glioblastomas, consisting of deficient DFF40/CAD levels (Sanchez-Osuna *et al.*, 2016), which may also contribute to incomplete apoptosis, genomic instability, and widespread genomic aberrations.

According to telomere length, which can be maintained in tumors either via re-activation of telomerase or through telomerase-independent mechanisms so-called alternative lengthening of telomeres (ALT), TERT promoter mutations and the α thalassemia/mental retardation syndrome X-linked (ATRX) are relevant for glioma formation and development. TERT mutations lead to increased telomerase activity while ATRX mutations correlate with ALT pathway activation (Liu *et al.*, 2019) (Pekmezci *et al.*, 2017). Both mutations are associated with prognosis and, especially, TERT promoter mutation is becoming more important as molecular criteria of histologically WHO grade II or III neoplasm that would follow an aggressive clinical course resembling glioblastomas, IDH-wildtype (Brat *et al.*, 2018).

Overall, the above genetic and molecular alterations contribute to the development and maintenance of the malignant phenotype of these aggressive malignant tumors either detected as primary or secondary glioblastomas when originated from low-grade astrocytomas. Defects in cell death mechanisms facilitate tumorigenesis and promote resistance to current anticancer therapies.

BOX 4. Origin and history of gossypol

Gossypol is a naturally occurring compound extracted from the cotton plant (genus Gossypium, family Malvaceae). Gossypol is mainly embedded in the pigment glands of the cottonseed kernel; however, other parts of the cotton plant, including leaves, flowers, roots, stem, or the seeds of the cotton plant, may also contain gossypol. The levels of gossypol vary depending on the species, variety of cotton plant, or external conditions such as water supply, fertilizers, or soil conditions (Stansbury *et al.*, 1954).

FIGURE I46. The cotton plant: the source of gossypol. Own image.

Historically, gossypol was first discovered and isolated in 1886 by Longmore as a crude pigment from the cottonseed oil foot (Longmore, 1886). In 1899, Marchlewski purified the chemical via precipitation from an ether solution using acetic acid. Once isolated, this yellowish pigment received the name of gossypol (Marchlewski, 1899). In 1927, Clark established the chemical formula of gossypol ($C_{30}H_{30}O_8$) (Clark, 1927), further data of the chemical structure of gossypol was reported by Adams and Edwards (Adams *et al.*, 1960) who elucidated the complete structure of gossypol [1,1',6,6'7,7'-hexahydroxy-5,5'-di-isopropyl-3,3'-dimethyl-(2,2'-binaphthalene)-8,8'-dicarboxaldehyde].

In cotton plants, gossypol constitutes a natural toxin that slows down the reproduction of the insects that try to eat cotton bolls and seeds. Since its isolation from cotton plants, gossypol has revealed a wide range of biological properties. One of the first attempts to get profit from this compound was to use it as a dye; however, at that time, gossypol was found to be unstable when exposed to light. Later, gossypol use as crude cottonseed oil for cooking revealed that families consuming this oil showed lower birth rates than the average of Chinese families. The study of this observation revealed an antifertility effect of gossypol, and during the 1970s, gossypol constituted a male contraceptive in China. Unfortunately, the contraceptive effect appeared to be associated with toxic effects (Keshmiri-Neghab and Goliaei, 2014). Additional properties, including antioxidant, anticancer, antivirus, or antimicrobial activity, as well as an effect lowering plasma cholesterol levels, have been attributed to gossypol (see *8.2. Mechanism of action*).

The complex and challenging chemistry behind this polyphenolic compound has been the object of the study of many researchers from different fields and it is still the object of unanswered questions.

9. Gossypol

9.1. Structure and derivatives of gossypol

Gossypol is produced in the cotton plant by dimerization of two molecules of hemigossypol and exists in two optically active forms: (-) or I-gossypol (M-form) and (+)- or (S)-gossypol (P-form) enantiomer. The two enantiomers of this chiral compound are the result of the restricted rotation bound around the C2-C2' internaphthyl bound. Gossypol can be equally found as a racemate in high concentrations in the pigment glands of the cotton plant (Gossypium); however, excess of one of the enantiomeric forms over the other has been reported in different Gossypium species (Cass *et al.*, 1991) (Zhou and Lin, 1988). The separation, preparation, and study of single isomers of gossypol demonstrated that generally, (-)-gossypol exhibits better biological activities than (+)-gossypol and racemic gossypol (Zhang *et al.*, 2009) (Lin *et al.*, 1989) (Shelley *et al.*, 1999).

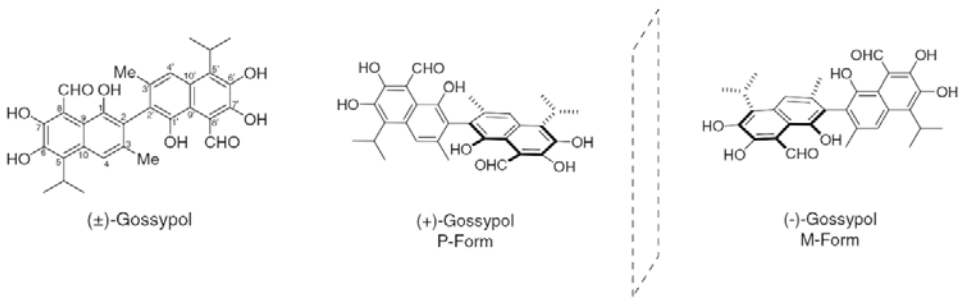

FIGURE I47. Enantiomeric forms of gossypol. Modified from Lu *et al.*, 2017.

Gossypol is an amphipathic molecule and lipid-soluble polyphenolic compound in which the polar domains are the carbonyl and the hydroxyl groups, and the non-polar moiety resides in the naphthalene rings and the iso-propyl group. This property leads to the gossypol interaction with phospholipids in biological membranes through its hydrophobic rings, and this interaction may increase the microviscosity of phospholipid membranes (Wu *et al.*, 1989) (Tanphaichitr *et al.*, 1995). While the presence of polar groups makes gossypol soluble in most organic solvents, the presence of dialkylnapthalene groups makes gossypol insoluble in water.

In more detail, the structure of this polyphenolic dialdehyde compound consists of two naphthalene rings linked by a single internaphtyl bond, three hydroxyl groups in each napththyl scaffold (six hydroxyl groups in total), and two reactive aldehyde groups making this compound chemically reactive. Aldehyde groups play a key role in tautomeric forms of gossypol and provide the modification sites in the development of novel gossypol derivatives.

In 1960, Adams *et al.* detected aldehyde, ketone (quinoid), and lactol (hemiacetal) tautomeric forms in different solvents (Adams *et al.*, 1960). Further studies revealed that in basic solvent systems, ketol is the predominant form; in inert solvents and acidic conditions, the aldehyde is the main form; and in polar solvents, such as dimethyl sulfoxide (DMSO) with alkali conditions, dynamic equilibrium is found among the different forms (Stipanovic *et al.*, 1973) (Abdullaev *et al.*, 1990). As DMSO is the principal solvent used to dissolve gossypol, several tautomeric forms must be contributing to gossypol-dependent biological activities when using a stock solution of gossypol in DMSO. Although subjected to modifications, the three principal tautomeric forms of gossypol are aldehyde-aldehyde, ketone-ketone, and lactol-lactol forms (**Figure I48**). The stability of gossypol under different storage conditions is deeply addressed in (Wang *et al.*, 2019b).

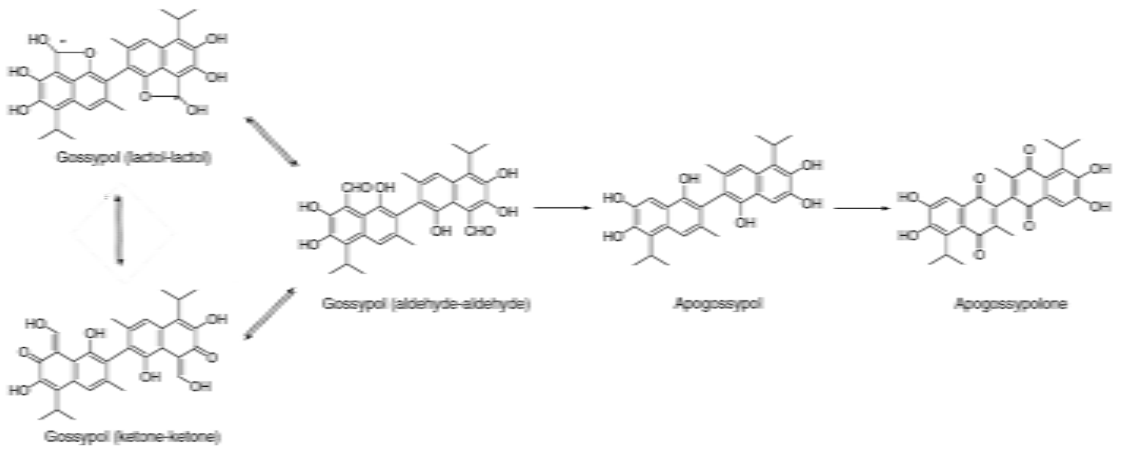

FIGURE I48. Tautomeric forms of gossypol and scaffolds based on gossypol. Common scaffolds derived from gossypol are apogossypol, which do not contain the aldehyde group, and apogossypolone, the oxidation product of apogossypol. Modified from Lu *et al.*, 2017.

Apart from its contribution in tautomeric forms, the two aldehyde groups can interact with basic amino acids (including glutamine, lysine, or phenylalanine) and form Schiff's bases. This condensation between the aldehyde groups of gossypol and amino groups of proteins leads to gossypol interaction with proteins and allows gossypol to inhibit the activity of plenty of enzymes (Levinsky *et al.*, 1991) (Shelley *et al.*, 2000). Interestingly, the rate of reaction of gossypol with amino acids increases with an increase of pH value (5.7-7.5). The formation of a Schiff base constitute a relatively labile bond, readily reversible by hydrolysis in aqueous solution, that can be enhanced at alkaline pH values and can be chemically stabilized by reduction (Wang *et al.*, 2009). Although the majority of gossypol exists as Schiff bases, it can form other complexes via chelating with metal ions such as iron (Muzaffaruddin and Saxena, 1966) (**Figure I49**), forming gossypol polymers or being oxidized (Scheiffele and Shirley,

1964). Indeed, gossypol is unstable and can be easily oxidized (usually in alkaline solutions) into different products with structural differences (sometimes giving an orange color). By contrast, derivatives such as gossypol ethers are much more stable.

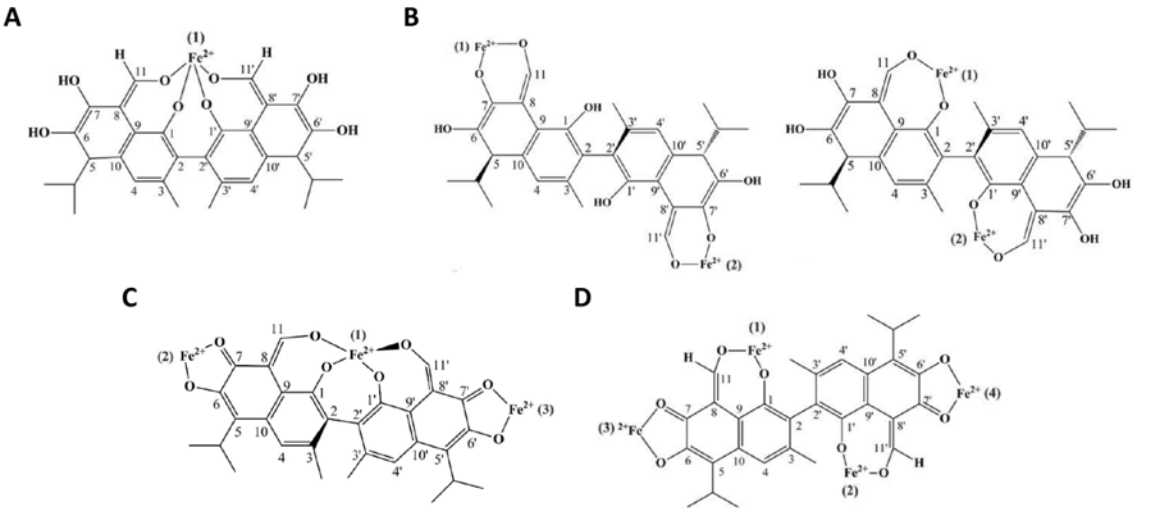

FIGURE I49. Chemical structure of the complexes of gossypol with iron at different molar ratios. 1: 1 complex (**A**), 1: 2 complexes (**B**), 1: 3 complex (**C**), 1: 4 complex (**D**) of gossypol with ferric iron. Modified from Zhang *et al.*, 2019b.

Among gossypol derivatives, apogossypol is of special interest as a dialdehyde product of gossypol. In 1985, Meltzer *et al.* obtained apogossypol from the reaction between gossypol and 40% aqueous sodium hydroxide at 85ºC under a nitrogen atmosphere for 1.75 hours (Meltzer *et al.*, 1985). This derivative of gossypol may change from a yellow color to brown within a short time when exposed to the air. Apogossypol, synthesized without the aldehyde group and without affecting hydroxyl groups of phenol, lead to apogossypolone through oxidation (**Figure I48**). In general, gossypol derivatives such as apogossypol exhibit less cytotoxicity than gossypol because of aldehyde group absence. However, only one aldehyde seems to be important in cytotoxicity irrespective of the stereoconfiguration (Shelley *et al.*, 2000). The chemical and biological developments of gossypol and its analogs from around 1990 to 2016 are recapitulated in detail in (Lu *et al.*, 2017).

9.2. Mechanism of action of gossypol

Clark *et al.*, reported the relevance of the aldehyde group in gossypol pharmacological actions (Clark, 1927). The two aldehydes can lead to changes in the metabolism and to the production of toxic chemicals. However, although the toxicity of gossypol lies in the aldehyde groups,

phenolic hydroxyl groups and the bulky binaphtalene structure may also contribute to the chemical reactivity of gossypol. Depending on the number and position of phenolic hydroxyl groups, phenolic compounds such as gossypol may induce DNA breakage. At the same time, modifications of phenolic hydroxyl groups can decrease the chemical antioxidant properties of gossypol (Wang *et al.*, 2008b). According to (Li *et al.*, 2000a), in relation to a more reactive species, gossypol exerts an antioxidant and DNA-protecting activity; while in relation to a less reactive species, phenolic compounds show a prooxidant and DNA-breaking activity.

The interesting structure of gossypol has been reported to account for diverse pharmacological properties. Although initially gossypol was reported as a potent anti-fertility agent (Qian and Wang, 1984), gossypol has also shown anti-viral (Radloff *et al.*, 1986), anti-parasitic (Montamat *et al.*, 1982), anti-inflammatory (Benhaim *et al.*, 1994) and cytotoxic effects in cancer cells. The biological properties of gossypol are deeply reviewed in (Wang *et al.*, 2009).

Briefly, some of the principal properties that have been reported and make gossypol a potential antineoplastic agent are listed hereafter. Regarding DNA replication, it is reported a role of gossypol blocking the G_1/S checkpoint and inhibiting key nuclear enzymes responsible for DNA synthesis and repair such as DNA polymerase α (Rosenberg *et al.*, 1986) and topoisomerase II (Senarisoy *et al.*, 2013). Moreover, gossypol may regulate cell cycles by modulating cell-cycle regulators such as Rb and cyclin D1 (Ligueros *et al.*, 1997). In this line, induction of the cell proliferation inhibitor TGF-β1 (which regulates the expression of cyclin D1) is also reported in cancer cells treated with gossypol (Jiang *et al.*, 2004). Furthermore, gossypol may suppress telomerase activity by transcriptional downregulation of hTERT, causing inactivation of c-Myc and posttranslational modifications of TERT inducing inactivation of AKT (c-Myc and AKT, both described as regulators of BCL-2 family proteins) (Moon *et al.*, 2008a).

Concerning apoptotic pathways, DNA fragmentation and PARP cleavage, induction of Bid protein truncation, loss of mitochondrial membrane potential, the release of cytochrome *c* from mitochondria into the cytosol, and activation of caspases such as caspase-3, -8, and -9 are associated to gossypol (Hou *et al.*, 2004). Moreover, gossypol induces Fas/Fas ligand-mediated apoptosis, and treatment with gossypol may also downregulate the expression of NF-κB-regulated gene products such as IAP-1, IAP-2, or XIAP (Moon *et al.*, 2008b). Indeed, gossypol is described as a BH3 mimetic due to its binding to the BH3-binding domain of proapoptotic proteins of the BCL-2 family and the consequent displacement of proapoptotic partners, therefore leading to apoptosis (Balakrishnan *et al.*, 2008). Furthermore, inhibition of BCL-XL has been reported upon gossypol treatment accompanied by an increase of

proapoptotic proteins NOXA and PUMA (Meng *et al.*, 2008). Additionally, gossypol interferes with cytoplasmic and mitochondrial enzymes implicated in energy production, uncouples oxidative phosphorylation, and depletes cells of cellular adenosine triphosphate (ATP) (Zhai *et al.*, 2006) (Ueno *et al.*, 1988). In this sense, recent reports link the role of gossypol as a pan ALDH inhibitor with a role in the reduction of ATP levels (Park *et al.*, 2018). Blockade of ALDH3A1 by gossypol has been described to impair cancer cell metabolism due to the requirement of ALDH3A1 for fatty acid oxidation (Lee *et al.*, 2019).

Interestingly, most of the described antineoplastic properties of gossypol refer to targets that have been described altered in glioblastomas. Indeed, different studies have been performed using gossypol as a potential clinical therapy in glioblastoma. Among them, gossypol has been suggested to enhance ionizing radiation effect, to increase the accumulation of acidic vesicular organelle (Keshmiri-Neghab *et al.*, 2014), to inhibit tumor-associated angiogenesis, invasion, and proliferation in combination with temozolomide (Jarzabek *et al.*, 2014), to have a role inhibiting tumor bioenergetics (Park *et al.*, 2018), and to have a role in the mitochondrial permeability transition pore, on oxidative stress (Warnsmann *et al.*, 2018). Moreover, a phase II clinical trial (NCT00540722) using gossypol in patients with progressive or recurrent glioblastoma has also been designed but conclusive results have not been published yet.

The improvement of the therapeutic approach of glioblastoma and the deeper knowledge of the mechanism behind the antitumoral action of gossypol are both a challenge for researchers and clinicians.

OBJECTIVES

The analysis of the cellular morphology of dead cells and, especially, of their nuclear alterations, was fundamental to define different types of cell death. Later, biochemical and molecular studies provided knowledge of the principal cellular components that regulate those different types of death. However, it is becoming evident that these cellular components, characterized mostly in the context of a specific mode of cell death, cross-talk to decide the fate of a cell in response to cytotoxic stimuli. In this sense, our group evidenced the crucial role of caspases and the endonuclease DFF40/CAD in the interplay between different subroutines of cell death. We established that the rate and the level of caspase activation dictate whether cells die displaying apoptotic or necrotic features (Garcia-Belinchon *et al.*, 2015). Alternatively, the study of human glioblastoma cells evidenced the low expression of DFF40/CAD as a common trait in glioblastomas, and as the principal molecular feature impairing complete apoptotic cell death (Sanchez-Osuna *et al.*, 2016). Nonetheless, the study of the nuclear alterations of glioblastoma cells challenged with γ-irradiation and the alkylating agent temozolomide, the first-line treatment for glioblastoma, evidenced nuclear features coinciding with nuclear fragmentation and condensation. Interestingly, those nuclear features were also observed when treating human glioblastoma-derived LN-18 cells with gossypol. Hence, the general objective of this work was to characterize the nuclear morphological alterations induced by gossypol. We asked whether caspases and DFF40/CAD, the main molecular events involved in apoptotic nuclear morphologies, were driving the nuclear morphologies observed upon gossypol treatment in human glioblastoma cells.

The specific objectives of this work were:

1. To analyze the nuclear alterations triggered by gossypol over time and depending on the concentration in LN-18 cells.
2. To ultrastructurally analyze the nuclear morphological changes induced upon gossypol treatment in LN-18 cells.
3. To analyze the nuclear morphological changes induced by gossypol in different commercial human glioblastoma-derived cell lines and in non-commercial (primary or relapse)-derived glioblastoma cells.
4. To assess the implication of caspases in the nuclear morphologies observed upon gossypol treatment in LN-18 cells.
5. To determine the implication of the ICAD·CAD system in the formation of the nuclear morphologies observed in LN-18 cells treated with gossypol.
6. To study potential inhibitors or modulators of the nuclear morphologies observed upon gossypol treatment in LN-18 cells.

MATERIALS AND METHODS

1. Cell cultures

1.1. Cell lines

The different cell lines employed along this work are detailed below:

A172 cells: (ATCC® CRL-1620™) human adherent brain cells with epithelial morphology obtained from a male glioblastoma patient of 53 years.

IMR-5 cells: human adherent cells with fibroblast/neuroblast morphology. Parental cells of IMR-5 cells are IMR-32 cells (ATCC® CCL-127™): human cells obtained from the brain tissue (derived from metastatic site: abdominal mass) of a male neuroblastoma patient of 13 months (Reed *et al.*, 1991). IMR-5 cells were kindly provided by Dr. Dionisio Martín Zanca (Salamanca, Spain).

LN-18 cells: (ATCC® CRL-2610™) human adherent cells with epithelial morphology obtained from the right temporal lobe of a female glioblastoma patient of 60 years.

LN-229 cells: (ATCC® CRL-2611™) human adherent cells with epithelial morphology obtained from the right frontal parieto-occipital cortex of a male glioblastoma patient of 65 years.

MCF-7 cells: (ATCC® HTB-22™) human adherent cells with epithelial morphology derived from a breast adenocarcinoma of a Caucasian female patient of 69 years.

MEFs: SV40 immortalize mouse embryonic fibroblasts (MEFs) generated either from wild-type (wt) mice or from *Bax/Bak* double-knockout (DKO) mice. *Bax/Bak* wild-type and *Bax/Bak* DKO MEFs were generous gifts from Dr. Stanley J. Korsmeyer (Wei *et al.*, 2001) (Lindsten *et al.*, 2000). *Atg5*$^{+/+}$and *Atg5*$^{-/-}$ T-large antigen MEFs were generous gifts from the Protein kinases in Cancer Group, led by Dr. José Miguel Lizcano (Universitat Autònoma de Barcelona, Barcelona, Spain) who received these cells from Dr. Guillermo Velasco (Universidad Complutense, Madrid, Spain) (Salazar *et al.*, 2009).

SH-SY5Y cells: (ATCC® CRL-2266™) human mixed, adherent, and suspension cells with epithelial morphology obtained from the bone marrow of a female neuroblastoma patient of 5 years. SH-SY5Y cells transfected with the hICAD$_L$-D117E mutant were previously generated by Dr. Victor Yuste Mateos (Yuste *et al.*, 2005b).

U251MG cells: (ECACC 09063001) human adherent pleomorphic/astrocytoid cells obtained from a human glioblastoma (those cells were formerly known as U-373 MG cells).

1.2.Patient-derived glioblastoma cell cultures

Patient-derived non-commercial glioblastoma **#04 cells** (from a primary glioblastoma resection) and **#12 cells** (from a glioblastoma relapse) were obtained as indicated in (Sanchez-Osuna *et al.*, 2016). Tumor samples from Hospital Universitari de Bellvitge - ICO Duran i Reynals were rinsed with Phosphate-Buffered saline (PBS), mechanically dissociated into pieces, and incubated with trypsin (0.025% trypsin and 0.01% EDTA) (Life Technologies) for 3 minutes at 37ºC. The resulting cellular suspension was carefully recovered without disturbing non-dissociated aggregates and mixed with Dulbecco's modified Eagle's medium (DMEM) supplemented with penicillin/streptomycin (100 U/mL and 100 µg/mL, respectively) and 10% of heat-inactivated fetal bovine serum (FBS) (Invitrogen S.A., Barcelona, Spain). The trypsinization process was repeated four times with the remaining pellets. Cellular suspensions were centrifuged at 200 x g for 5 minutes and incubated in Red Blood Lysis Buffer (155 mM NH4Cl, 12mM NaHCO3, 0.1 mM EDTA) for 10 minutes. After centrifugation, the cells were resuspended and plated in a 25 cm^2 flask (BD Falcon, Madrid, Spain).

1.3.Glioblastoma-derived spheres

Generation of glioblastoma-derived spheres

Human glioblastoma-derived LN-229 cells were seeded onto Petri dishes with a non-treated surface (Thermo Scientific 123-17) and left to grow. Cells were kept in complete medium in order to maintain the same culture conditions used for the 2D or adherent cell experiments. After about three months, sufficient gliospheres were collected. After about three months, enough glioblastoma (GB)-derived spheres were generated to proceed with the experimental approach. Then, spheres were divided onto different 60 mm Petri dishes with non-treated surfaces (Thermo Scientific 123-17) and were left untreated or treated with the indicated treatments. After 18 hours of treatment, we collected the spheres and proceeded as described below. Due to the strong adhesion of LN-18 cells to even non-treated surfaces, the procedure to obtain GB-derived spheres from this line is still under evaluation.

Processing of the spheres after treatment

After treatment, spheres were collected in 15 ml tubs and fixed with 4% paraformaldehyde (PFA) (v/v) for 3 hours at 4ºC in a tube roller. Fixed spheres were washed with Sorenson's Sodium Phosphate Buffer (PB) (0.1M pH 7.2-7.4), once for 20 minutes and twice for 15 minutes, to remove the remains of PFA as much as possible. After the last wash, spheres were transferred to 30% sucrose solution prepared in PB (0.1M pH 7.2-7.4) and maintained for 15 days. Note that washes and maintenance in sucrose were performed at 4ºC and continuous agitation in a tube roller. Then, samples were transferred to optimal cutting temperature (O.C.T. Compound (Tissue tek), Sakura, 4583), a viscous, transparent solution at room temperature that turns white, opaque, and hard when frozen. O.C.T. Compound was used to embed tissue samples on cryomolds (Tissue-Tek® Cryomold®; Sakura Finetek, 62534-25) before frozen sectioning on a Leica cryostat (Leica CM3050S). This step onward was performed with technical support at the histology core facility from the Institut de Neurociències (INc). Resulting sections (between 20 – 10 μm) were placed onto adherent slides (Thermo Scientific Menzel®, SuperFrost Plus™) and left to dry at least for 20 minutes on a heated plate (37ºC) to increase the adherence. Resulting slides were kept at 4ºC for short periods or at -20ºC for long periods.

Hematoxylin staining of the spheres

Slides were rinsed with PBS and stained with Hematoxylin solution, Mayer's (Sigma-Aldrich, MHS16) for 2 minutes. Then, after rinsing in water, slides were passed through several alcohol changes to remove all traces of water: 3 minutes (x1) at 70% ethanol, 3 minutes (x2) at 95% ethanol and, 3 minutes (x3) at 100% ethanol. Then, slides were rinsed for 6 minutes in 3 baths of xylene. A thin layer of DPX Mountant for histology (Sigma-Aldrich, 06522) was applied, followed by a glass coverslip and left to dry. Corresponding images were obtained with a Nikon ECLIPSE 90i microscope equipped with a Nikon DXM1200F photographic camera and ACT-1 software.

1.4.Cell culture procedures

All cells used were routinely grown in 100-mm culture dishes (BD Falcon) containing 10 ml of Dulbecco's modified Eagle's medium (DMEM) supplemented with penicillin/streptomycin (100 U/mL and 100 μg/mL, respectively) and 10% of heat-inactivated fetal bovine serum (FBS) (Invitrogen S.A.). Alternatively, we refer to this culture medium as a complete medium. The medium was routinely changed every 3 days. Once at 80-

90% of confluence, cells were rinsed with Phosphate-Buffered Saline (PBS) (100 mM pH 7.4) and incubated at 37ºC for 3 minutes with 0.05% trypsin-EDTA (Sigma-Aldrich) until their dissociation. Trypsin was neutralized by adding DMEM with 10% FBS, and the resulting cell suspension was centrifuged at 200 x g for 5 minutes. Finally, cell pellets were resuspended in complete medium. Note that cells were maintained at 37ºC in a saturating humidity atmosphere containing 95% air and 5% CO_2.

The storage of cell lines was performed via cryopreservation. Pre-confluent cultures and with no signs of microbial contamination were detached as described before. Pelleted cells were resuspended in 90% FBS (Invitrogen S.A.) and 10% dimethyl sulfoxide (DMSO) (Sigma-Aldrich). Cryovials containing the cells were placed in Nalgene Mr. Frosty Freezing Container. These containers, which allow slow freezing by decreasing the temperature of approximately 1ºC per minute, were kept at -80ºC for 24 hours. Then cryovials were transferred to liquid phase nitrogen.

Note that all procedures were performed in a laminar flow cell culture hood using sterile techniques. Cells were routinely tested for contamination by the Servei de Cultius Cel·lulars from Institut de Neurociències - UAB.

1.5.Cell treatments and reagents

For the different experiments, cells were grown at the adequate cell densities in culture dishes or multiwell plates (BD Falcon) using the same culture conditions as described above.

The specific **seeding densities** were: 0.8 x 10^6 cells for 60 mm dishes; 0.3 x 10^6 cells for 35 mm dishes; 0.06 x 10^6 cells for 24-well; 0.01 x 10^6 cells for 96-well and 0.03 x 10^6 cells for 8-well Lab-Tek chamber slides.

Once at 80-90% of confluence (generally after 40-48 hours post-seeding), the culture medium was removed, and fresh media was added in the absence (referred to as "untreated" condition) or in the presence of the indicated treatments. The corresponding percentage of DMSO was always tested in parallel for each condition.

Alternatively (when indicated), cells were treated with DMEM in the absence of FBS or with Krebs-Henseleit (KH) buffer without glucose (116 mM NaCl, 4.7 mM KCl, 25mM $NaHCO_3$, 1.2 mM $MgSO_4$, 1.2 mM KH_2PO_4, 1.3 mM $CaCl_2$, pH 7.4).

The different compounds used in this work are detailed in **Table M1**. The corresponding range of concentrations tested, catalog numbers (Cat. No.), and suppliers are also indicated.

Compound	Concentrations	Cat. No.	Supplier
3-Methyladenine (3-MA)	2.5 – 10 mM	S2767	Selleckchem
ABT-737	50 µM	S1002	Selleckchem
Apogossypol (ApoG)	25 – 400 µM	B4902	APExBIO
Apogossypolone (ApoG)	25 – 400 µM	sc-480059	ChemCruz
Astemizole	2.5 – 320 µM	A2861-10MG	Sigma-Aldrich
AT-101	25 – 400 µM	S2812	Selleckchem
Bafilomycin A_1	100 nM	11038	Cayman Chemical
Brefeldin A	1 – 100 µM	B7651	Sigma-Aldrich
Chelerytrine chloride	20 µM	C2932	Sigma-Aldrich
Cobalt (II) chloride hexahydrate ($CoCl_2 \cdot 6H_2O$)	6.25 – 800 µM	C8661	Sigma-Aldrich
Copper (II) chloride dihydrate ($CuCl_2 \cdot 2H_2O$)	0.25 – 2 mM	C3279	Sigma-Aldrich
Copper (II) sulfate hydrate ($CuSO_4 \cdot xH_2O$)	0.25 – 2 mM	209201	Sigma-Aldrich
EM20-25	50 µM	SML0183	Sigma-Aldrich
Gossypol	25 – 400 µM	S2303	Selleckchem
HA14-1	100 µM	H8787	Sigma-Aldrich
Iron (III) sulfate hydrate ($Fe_2(SO_4)_3 \cdot xH_2O$)	0.25 – 1 mM	307718	Sigma-Aldrich
Ivermectin	2.5 – 320 µM	I8898	Sigma-Aldrich
Nordihydroguaiaretic acid (NDGA)	200 – 800 µM	S3984	Selleckchem
Obatoclax (Gx15-070)	100 µM	S1057	Selleckchem
PI-103	0.1 – 20 µM	528100	Calbiochem
Q-VD-OPh	20 – 50 µM	A8165	APExBIO
Rapamycin	1 – 20 µM	553210	Calbiochem
Staurosporine	1 µM	569397	Sigma-Aldrich
Temozolomide	100 µM – 5 mM	T2577	Sigma-Aldrich
Terfenadine	2.5 – 320 µM	T9652	Sigma-Aldrich

Thapsigargin	100 μM	586005	Calbiochem
TRAIL Protein, Recombinant human	100 – 200 ng/ml	GF092	Sigma-Aldrich
TW-37	50 – 800 μM	S1121	Selleckchem
Wortmannin	25 – 400 μM	S2758	Selleckchem

TABLE M1. Compounds used in this Doctoral thesis. Note that all compounds were resuspended in DMSO except cobalt (II) chloride hexahydrate, copper (II) chloride dihydrate, copper (II) sulfate hydrate, and iron (III) sulfate hydrate, which were resuspended in water; and TRAIL Protein, which was resuspended in water containing 0,1% bovine serum albumin (BSA). Cat. No. corresponds to Catalog number of each compound.

1.6.Cell irradiation

The irradiation of cells was performed at the Unitat Tècnica de Protecció Radiològica at Universitat Autònoma de Barcelona by using the IBL 437 C (Cis bio international), a self-shielded irradiator containing up to 189 TB1 (5100 curies) of cesium 137. Cell culture-plates were placed into a 3.8-liter canister and installed into the irradiation unit. When the IBL 437 C is activated from the control panel, the drum rotates on 180º for exposure to radiation sources. Simultaneously, the sample canister began its rotation at 18 rpm to provide a homogeneous dosage of the samples. Here cells were irradiated with 10 grays (Gy) of gamma irradiation.

1.7.Clonogenic assay and crystal violet staining

3.5 x 10^5 cells were seeded in a 60-mm culture dish, left to attach, and treated for 4 days as indicated in the corresponding figure legend. After 4 days, cells were harvested and seeded in a 24-well plate at 300 cells/well in 1 mL/well of DMEM with 10% FBS plus 1 mL/well of conditioned medium. The conditioned medium consists of DMEM with 10% FBS from routinely growing cells and contains nutrients required for the cells to grow at low density. After the indicated days, culture media was removed, cells were rinsed with PBS, and fixed with pure ice-cold methanol for 10 minutes at -20ºC. Methanol was removed and cells were stained with crystal violet (DC Panreac) (0.5 g crystal violet diluted in deionized water). Note that crystal violet stain cells by binding to ribose type molecules such as DNA. After 10 minutes of incubation at room temperature, crystal violet solution was removed, and serial washings were performed by immersing the plates in deionized water until no more distaining was observed. Plates were left to dry and images were obtained by scanning. Crystal violet was dissolved in 15% acetic acid (Scharlau) in PBS and shaking for 10 min to obtain a quantitative

value. Optical absorbance at 595 nm was measured in triplicates in a 96-well plate with a Power Wave XS spectrophotometer (BioTek).

2. Cell viability assays

MTT reduction assay

MTT (3-(4,5-Dimethylthiazol-2-yl)-2,5-di-phenyltetrazolium bromide) is a water-soluble tetrazolium salt that can be reduced only by metabolically viable cells. The result is a colored water-insoluble formazan salt that, through its measurements, allows to extrapolate cell viability upon different cultures or treatment conditions. After treatment, 0.5 mg/mL of MTT (diluted in DMEM) was added to the culture medium of cells growing in 96-well plates. Plates were incubated at 37ºC for 30 minutes, and the MTT-containing medium was replaced with 100 µL DMSO plus 0.05% Triton X-100. In order to dissolve formazan salts in DMSO, plates were shaken for 10 minutes at room temperature. Finally, the assay was quantified by BIO-TEK Power Wave XS. Final values were the result of subtracting 620 nm from 590 nm lectures. Results are represented as the means of the percentage of viability ± *SD*. This protocol was adapted from Boix *et al.*, 1997.

Direct staining of nuclei with propidium iodide (PI)

Propidium iodide (PI) is a red fluorescence dye that can bind to DNA and RNA. PI can cross disrupted cell membranes of dead cells, whereas membranes of living cells are more selective and can reject it. To assess cytotoxicity by PI staining, cells were seeded at the corresponding densities according to the plates used, and treated for the indicated times and concentrations. After treatment, and without aspirating the medium, PBS containing propidium iodide (Sigma-Aldrich) at a final concentration of 2 µg/mL was added and incubated 10 minutes at 4ºC. Alternatively, nuclei were stained simultaneously with 1 µg/mL Hoechst bisbenzimide 33342 (cell-permeable) and 2 µg/mL PI (cell impermeable). Microphotographs were taken under a UV light (for Hoechst 33342), 500 nM excitation (for PI) or phase contrast with a Nikon ECLIPSE TE2000-E microscope equipped with a Hamamatsu ORCA-ER camera. Cell death was expressed as the percentage of PI-stained cells (PI+) over the total number of cells. Alternatively, results were presented as percentage of PI-positive (+) cells and PI-negative (-) cells. All experimental conditions were repeated at least three times.

Trypan blue exclusion assay

For trypan blue staining, cells were seeded and treated with the appropriate drugs for the indicated times. Then, cells were gently dissociated with a blue tip in their culture medium (or if needed with 1/3 diluted trypsin/EDTA), and a sample was taken and mixed with trypan blue solution (0.4%) (Sigma-Aldrich). 10 µl of the resulting cell suspension were counted with a hemocytometer. This assay is based on the principle that living cells possess intact cell membranes that exclude certain dyes, such as trypan blue, whereas dead cells do not. Therefore, cell death was expressed as percentages of trypan blue-stained cells over the total number of cells. All experimental conditions were repeated at least three times.

Calcein-AM assay

An acetoxymethyl (AM) ester form of calcein (Calcein-AM) is a cell-permeable and non-fluorescent compound that is widely used for determining cell viability. In living cells, the non-fluorescent Calcein-AM is hydrolyzed by intracellular esterases into the strongly green fluorescent anion calcein. The fluorescent calcein is well-retained in the cytoplasm in living cells, and it is a measure of viability. This technique was carried out in 96-multiwell plates. After different cell treatments, the medium was aspirated, and 100 µl Calcein-AM solution (0.5 µM Calcein-AM diluted in PBS) (Sigma-Aldrich) were added in each well. After 30 minutes of incubation at 37ºC, the reaction was aspirated and 100 µl of PBS were added to each well. Fluorescence was quantified on BIO-TEK Power Wave XS at 494/517 nm and expressed as arbitrary units of fluorescence *(A.U.F.)*. All experimental conditions were repeated at least three times to obtain the corresponding percentages shown in the Results section.

3. DEVD-directed caspase activity

Caspase activity was evaluated using the caspase fluorogenic substrate Ac-DEVD-afc (Calbiochem). Fluorescence is emitted when the molecule afc is released from the DEVD peptide after its cleavage. Quantitative DEVD-like activities in cell lysates were performed as previously described in (Sanchez-Osuna *et al.*, 2014). This assay was performed in 96-multiwell plates, by using 9 µg of protein Igepal extracts (final volume: 50 µl) in each well. Then, 50 µl of 2X assay buffer 100 mM Tris-HCl pH 7.4, 4 mM EDTA, 4 mM EGTA, 10 mM DTT, 20% sucrose, 2 mM PMSF, 40µM Ac-DEVD-afc) were added to the samples.

Alternatively, caspase activity was assessed directly on cells. Cells were seeded on 96-multiwell plates and treated (final volume: 50 µl). After treatment, 50 µl of 2X Caspase Activity Buffer (40mM HEPES-NaOH, pH 7.2, 300mM NaCl, 20mM dithiothreitol, 10mM EDTA, 2% Igepal CA-630, 0.2% CHAPS and 20% sucrose, 50 µM Ac-DEVD-afc) were added to each well.

In both cases, the 96-multiwell plate was incubated at 35ºC for 12 -24 hours in a BIO-TEK Synergy HT fluorimeter under an excitation filter of 360 nm (40 nm bandwidth) and an emission filter of 530 nm (25 nm bandwidth). Results are expressed as the means of arbitrary units of fluorescence (*A.U.F.)*. Alternatively, data were obtained by using Thermo Scientific Varioskan™ LUX multimode microplate reader under an excitation filter of 360 nm and an emission filter of 530 nm.

4. Hematoxylin and Eosin staining

Tumor samples from different patients from the Unit of Neuro-Oncology (Hospital Universitari de Bellvitge-I.C.O Duran i Reynals, Barcelona, Spain) were fixed with formalin and embedded in paraffin blocks immediately after surgery. Next, slices of 5-mm thick were sectioned and conventionally staining with hematoxylin and eosin was performed at the Neuropathology Institute of the same hospital according to the standard protocols. Clinical data from all participants are summarized in **Table M2**.

	Patient #B14-24722	Patient #B09-02962	Patient #B11-02000	Patient #B12-14343	Patient #B09-06103	Patient #B08-00689
Age/Sex	66/M	57/M	68/M	36/	54/M	50/M
Location	Frontal	Frontal	Temporal	Temporal	Frontal	Frontal
Surgery	Partial resection	Total resection	Total resection	Total resection	Total resection	Total resection
KPS	90	100	80	90	70	80
Complementary treatment	RDT + TMZ	RDT + TMZ	RDT + TMZ	RDT + TMZ	RDT + TMZ	RDT + TMZ
MGMT status	Unmeth.	Unknown	Unknown	Unknown	Unknown	Meth
PFS (months)	3.02	9.13	8.02	-	54.80	38.11
OS (months)	5.59	11.66	11.73	60.09	55.36	58.81

TABLE M2. Clinical data from glioblastoma patients corresponding to hematoxylin & eosin histological sections. M, male; KPS, Karnofsky Performance Status; RDT, focal radiotherapy (total dose 60

Gy); RDT+TMZ, concurrent and adjuvant temozolomide; MGMT, O6-methylguanine methyltransferase; un/meth., un/methylated; PFS, progression free survival; OS, overall survival.

5. Immunofluorescence

Cells were seeded onto 8-wells Lab-Tek chamber slides (Nalge Nunc International Corp., Rochester, NY) and treated as indicated in the respective figure legends. After treatment, cells were fixed with 1% paraformaldehyde (v/v) (overnight at 4ºC), washed once with PBS, and washed twice with PBS containing 0.1% Triton X-100 (v/v). After preincubation during 30 minutes at 25ºC with a blocking solution (3% bovine serum albumin (BSA) and 0.1% Triton X-100 in PBS), cells were incubated with the specific antibodies (overnight at 4ºC). After incubating primary antibodies, cells were washed three times with PBS containing 0.1% Triton X-100. Then, appropriate secondary antibodies were incubated for 45 minutes at 25ºC in the presence of 0.5 μg/ml of Hoechst 33258 and Alexa Fluor^{647}-phalloidin (when indicated) in blocking solution (3% BSA and 0.1% Triton X-100 in PBS). Finally, chambers were removed, and slides were mounted with an aqueous mounting medium (FluorSave^{TM} reagent, Calbiochem). Slides were examined using a laser confocal microscope (Zeiss LSM 700, Carl Zeiss) and the specific confocal software (ZEN, Carl Zeiss). Alternatively, images were obtained with a Nikon ECLIPSE 90i microscope equipped with epifluorescence optics, a Nikon DXM1200F photographic camera and ACT-1 software. Images were analyzed with Fiji - ImageJ or Imaris 8.3.4. (Bitplane) software. Three dimensional (3D) isosurface rendered z-stack confocal images were generated using Imaris 8.3.4. (Bitplane) software. The RGB profile plots were obtained by using the RGB profiler plugging. First, the corresponding images were transformed to RGB color image (*Image* > *Type* > *RGB color*). Then, different lines were drawn and, finally, the RGB profiler plugging was used to obtain the red and blue profile plot (on the same plot) for each line selection (*Plugins* > *RGB profiler*).

Fiji – Image J software was also used to quantify the phospho-H2AX positive staining. For this specific purpose, images were transformed to 8-bit type images (*Image* > *Type* > *8-bit*). Then, we followed the following steps: *Image* > *Adjust* > *Threshold (35/255)* > *Apply*. *Analyze* > *Analyze particles*. The analyze particles command was used to count the number of phospho-H2AX positive cells detected above the threshold value (35/255) and with a size (area) ranging between 100 and 'Infinity' (*Pixel Units*). Corresponding values are represented as indicated in **Figure R31B**.

All antibodies employed in this Doctoral thesis are indicated in **Table M4**.

6. Low Molecular Weight (LMW) or oligonucleosomal DNA degradation analysis

Cells treated or not, growing in 35-mm plates, were collected and centrifuged at 500 x*g* for 5 minutes. Cell pellets were resuspended in 250 µl of bi-distillate miliQ water containing 400 µg/ml proteinase K and 20 µg/ml RNase. Then, 250 µl of SET buffer 2X (20 mM Tris-HCl, pH 6.8, 300 mM NaCl, 2 mM EDTA, and 2% SDS) were added carefully, without resuspending. Subsequently, the extracts were heated at 50°C for 30-60 minutes and resuspended every 20 minutes. Then, 400 µl phenol: chloroform: isoamyl alcohol (Sigma-Aldrich) were added. After mixing vigorously, suspensions were centrifuged at 13.400 rpm for 15 minutes at RT. After centrifugation, two phases and a lipid interphase appeared in the sample: the upper aqueous phase, where the DNA was present, and the organic phase. Hence, the aqueous phases were slowly and very carefully recollected and the DNA was precipitated by adding 800 µl of ethanol 100% and 200 µl of ammonium acetate 7.5 M for at least 1 hour at -20°C. DNA extracts were centrifuged at 4°C for 10 minutes at 14.800 rpm and the supernatant was discarded by decanting. The pellets containing DNA were washed with 500 µl of 70% ethanol and centrifuged at 4°C for 5 minutes at 14.800 rpm again. The DNA pellets were left to dry at RT or 37°C until the pellet was transparent. Subsequently, 20 µl of TE (10 mM Tris-HCl pH 8.8, 1 mM EDTA) supplemented with RNase 10 µg/mL was added and heated at 50°C for 30 minutes.

An agarose gel electrophoresis was performed to identify the LMW DNA degradation. Before loading into a 1.8% agarose gel, 10% of glycerol was added and samples. The run was carried out at 90 V in TAE buffer (40 mM Tris acetate, pH 7.5, 1mM EDTA). The gel was dyed with 0.5 µg/mL of ethidium bromide for 10 minutes and washed twice with distilled water. Extracted DNA was visualized using a Syngene Gene Genius UV transilluminator equipped with a photographic camera. This procedure was previously described in (Boix *et al.*, 1997).

7. Morphology analysis by Scanning Electron Microscopy (SEM) following a cryo-fracture or freeze-fracture method with critical point drying

LN-18 cells were seeded at 0.06 x 10^6 cells/well onto glass cover slides, previously placed on a 24-well plate. Once attached, cells were left untreated or treated with the indicated treatments for 14 hours. Then, cells were fixed with phosphate buffer (PB) (100 mM, pH 7.4) containing 2.5% (v/v) glutaraldehyde and 2% (v/v) paraformaldehyde (EM grade, Merck) at

4ºC for 1-2 h. The procedure from the primary fixation until visualization of the samples was performed at the Servei de Microscopia from Universitat Autònoma de Barcelona (UAB) by Dr. Alejandro Sánchez-Chardi. This cryo-fracture method, in conjunction with critical point drying, is still under evaluation. Dr. Alejandro Sánchez-Chardi is performing a series of trials regarding the times and the order of the steps to optimize the procedure. The specific steps followed before the analysis of the samples presented in this work are described hereafter. Following primary fixation, samples were postfixed in PB containing 1% (w/v) osmium tetroxide (TAAB Laboratories, Berkshire, UK) and freeze-fractured in liquid nitrogen. Alternatively, samples were freeze-fractured before post-fixation. Note that all samples were cryopreserved in 2.3 M sucrose before freezing. Finally, samples were dehydrated in ethanol and critical point drying (with CO_2) was applied before examination in the Scanning Electron Microscope (SEM). The evaluation of the samples with field emission scanning electron microscope (MERLIN FE-SEM) was done at the same service (Servei de Microscopia - UAB).

8. Morphological analysis by Transmission Electron Microscopy (TEM)

Transmission electron microscopy was used to examine the nuclear morphology of different glioblastoma cells untreated or treated with the indicated compounds and times. Untreated or treated cells were collected and processed as previously described (Sanchez-Osuna *et al.*, 2014). Specifically, after treatments, cells were detached, rinsed twice with PBS (100 mM, pH 7.4) and fixed with phosphate buffer (100 mM, pH 7.4) containing 2.5% (v/v) glutaraldehyde and 2% (v/v) paraformaldehyde (EM grade, Merck) at 4ºC for 2 h. Fixed cells were rinsed four times with phosphate buffer and post-fixed in 1% (w/v) osmium tetroxide (TAAB Laboratories, Berkshire, UK) containing 0.8% (w/v) potassium hexacyanoferrate (III) (Sigma-Aldrich) at 4ºC for 2 h. After four washes with deionized water, pellets were sequentially dehydrated in acetone. Finally, samples were then embedded in Eponate 12™ resin (EPON resin) (Ted Pella Inc., Redding, CA) and polymerized for 48 h at 60ºC. Ultrathin (70 nm thick) sections were obtained and placed on noncoated copper grids (200 meshes), contrasted with uranyl acetate and lead citrate. Sections were evaluated with a transmission electron microscope (Jeol JEM-1400) equipped with a CCD GATAN ES1000W Erlangshen camera at the Servei de Microscopia - *UAB*.

9. Nuclear morphology analysis by chromatin staining with a non-cell permeable bisbenzimide (Hoechst 33258)

For apoptotic nuclear morphology assessment, cells were seeded in 96-multiwell plate at 0.01 x 10^6 cells/well. Alternatively, for the γ-irradiation experiments, cells were seeded onto 8 chamber polystyrene vessel tissue culture treated glass slide (Falcon) (0.03 x 10^6 cells for 8-well Lab-Tek chamber slide). After treatment, cells were fixed with 2% paraformaldehyde (v/v) (Electron microscopy sciences, Hatfield, PA), permeabilized with 0.01% Triton (v/v), and stained with 1 μg/ml Hoechst 33258 for 10 minutes at 4°C as previously established (Boix *et al.*, 1997). Nuclei were visualized under UV illumination with a Nikon ECLIPSE TE2000-E microscope equipped with epifluorescence optics and a Hamamatsu ORCA-ER photographic camera. Stained nuclei were scored as at type I (partial chromatin condensation in a ring-like shape in the absence of karyorrhexis), type II (nuclear pyknosis and karyorrhexis), or type III (nuclei shrinkage and highly compacted chromatin in the absence of karyorrhexis) nuclear morphology (Yuste *et al.*, 2005b). More than 300 nuclei from each experimental condition from at least three independent experiments were scored.

10. Protein extractions and quantification

After treatments, cells were detached from 35-mm or 60-mm culture dish, pelleted at 500 x g for 5 min, and washed once with PBS. Then cells were lysed on ice for 15 minutes with 50 μl of Igepal buffer (50mM Tris-HCl, pH 6.8, 1 mM EDTA, 150 mM NaCl, 1% Igepal CA-630 X-100, 1 x protease inhibitor cocktail (Roche Applied Science). The supernatants, representing the soluble fraction containing cytosol and mitochondria, were clarified by centrifugation at 21,000 x g for 10 minutes at 4 °C. Protein concentration at the supernatants was quantified by a modified Lowry assay (DC protein assay, Bio-Rad).

Lowry assay (DC protein assay, Bio-Rad) was performed in 96 multi-well plates. First, Reagen A and Reagen S were mixed in a ratio 50:1 at added at a volume of 25 μL/well. Second, 1 μL/well of standards or protein samples (triplicates) were added and, finally, mixed with 200 μL/well of Reagen B. Microplates were incubated at room temperature for a minimum of 15 min. Absorbance at 750 nm was measured with a Power Wave XS spectrophotometer (BioTek).

Additionally, cytosolic extracts were performed as previously described in (Casanelles *et al.*, 2013). Cells were collected and centrifuged at 200 x g for 5 min, rinsed in ice-cold PBS (pH

7.2), resuspended in 5 volumes of cytosolic extraction buffer (70 mM Sucrose, 220 mM Mannitol, 5 mM HEPES-KOH pH7.2, 10 mM KCl, 2 mM MgCl2, 5 mM EDTA, 5 mM EGTA, 0.025% Digitonine, 1 mM PMSF, 1 mM DTT), shortly vortexed and kept at 4 °C for 5 min. The lysates were centrifuged for 5 minutes at 600 x g in a bench microcentrifuge at 4 °C and the supernatants were collected and quantified by the Bio-Rad protein assay Lowry based method.

Total extracts were obtained by using lysing the cells with SET buffer (10 mM Tris-HCl, pH 6.8, 150 mM NaCl, 1 mM EDTA, 1% SDS) and heating the samples at 95 °C for 10 min. The protein concentration in the supernatants was quantified by the modified Lowry assay (DC protein assay; Bio-Rad) described above. This procedure was previously detailed in (Sanchez-Osuna *et al.*, 2014).

11. Transfection of siRNA

siRNA transfection was performed by using DharmaFECT™ siRNA Transfection Reagent according to the manufacturer's instructions. 150.000 cells were seeded onto 35-mm culture dishes in complete media. After 24 hours and in separate tubes, we diluted 4,8 µL volume of the siRNA (non-relevant (NR) or DFF40/CAD (hCAD)) (tube 1) and 4,8 µL DharmaFECT™ transfection reagent (tube 2) with serum-free medium (DMEM) up to 200 µL (values for each transfection). Gently we mixed the contents of each tube and incubated the tubes for 5 minutes at room temperature. After the indicated time, we mixed the contents of tube 1 and tube 2 by pipetting carefully up and down and incubated the mix for 20 minutes at room temperature. In the meantime, we removed the culture medium from the 35-mm culture dishes, rinsed the cells with PBS and added 1400 µL of DMEM. After the 20 minutes of incubation, the 400 µL of transfection mix were added drop by drop to the 35-mm culture dish. Cells were incubated at 37ºC in 5% CO_2 for 6 hours and then supplemented with penicillin/streptomycin (100 U/mL and 100 µg/mL, respectively) and a final concentration of 10% FBS. Three days after transfection, cells were detached and seeded in the corresponding plates for the desired experiment.

To evaluate the down-regulation of protein expression Western blots of total protein extracts were performed at the initial time of treatment.

The sequences employed for each siRNA are detailed in **Table M3**.

siRNA	Sequence
DFF40/CAD	5'-GGAACAAGAUGGAAGAGAA-3'
Non-relevant (NR)	5'- AUAUGCGAUCGAGAUAUCG-3'

TABLE M3. SiRNA sequences. The specific sequences employed for CAD and non-relevant (NR) siRNA are here detailed. The stock solution of each siRNA was at 50 mM.

12. Transfection of DFF40/CAD

LN-18 cells were transfected with the eukaryotic expression vector pcDNA3 (Invitrogen) containing or not the full-length open reading frame cDNA sequence of human DFF40/CAD (GenBank™ accession number NM_004402) by Dr. María Sánchez Osuna as described in Sanchez-Osuna *et al.,* 2014. 0.3 x 10^6 cells were seeded onto 35-mm culture dishes in complete media and transfected after 24 hours. For each transfection sample we prepared the complexes of DNA (non-relevant (NR) or DFF40/CAD (hCAD)) and Lipofectamine™ 2000 Reagent according to manufacturer's instructions. In separate tubes, we diluted 4 μg of DNA in 250 μL of serum-free medium (DMEM) (tube 1) and 10 μL of Lipofectamine™ 2000 Reagent in 250 μL of serum-free medium (DMEM) (tube 2). Gently we mixed the contents of each tube and incubated the tubes for 5 minutes at room temperature. After the indicated time, we added the content of tube 1 to tube 2, mixed by pipetting carefully up and down and incubated the mix for 20 minutes at room temperature. In the meantime, we removed the culture medium from the 35-mm culture dishes, rinsed the cells with PBS and added 2000 μL of complete media without antibiotics. After 20 minutes of incubation, the mixture was added drop by drop to the 35-mm culture dish. Cells were incubated at 37ºC in 5% CO_2 for 6 hours and then the medium was removed and replaced for fresh complete media. 24 hours after transfection, cells were grown in selective medium containing 1 mg/ml G-418 (Geneticin) (Invitrogen) for 25–30 days (until non-transfected cells died in selective medium) and were used as a pool. DFF40/CAD overexpression was assessed by Western blot.

13. TUNEL Assay

SH-SY5Y and LN-18 cells were seeded onto 8-wells Lab-Tek chamber slides (Nalge Nunc International Corp., Rochester, NY) and treated with gossypol or staurosporine as indicated in the respective figure legends. Detection of DNA fragments carrying 3'-OH groups was carried out as described in (Iglesias-Guimarais *et al.*, 2013). After treatment, cells were fixed in freshly prepared 2% paraformaldehyde for 30 minutes at 4 °C and, after washing with PBS,

fixed cells were permeabilized with 0.1% Triton X-100 and 0.1% sodium citrate for 30/90 minutes at 4 °C. Then, cells were rinsed with PBS containing 0.1% Triton X-100 and incubated with 100 µl of a reaction mixture containing 0.025 nmol fluorescein-12-dUTP, 0.25 nmol dATP, 2.5 mM $CoCl_2$, 40 units of recombinant terminal deoxynucleotidyl transferase and 1X terminal deoxynucleotidyl transferase reaction buffer (Roche Applied Science) for 1 h at 37 °C. The reaction was ended by adding 20 mM EGTA. Cells were washed twice with PBS, counterstained with 0.05 µg/ml Hoechst 33258 in 20 mM EGTA, and microphotographs were taken under fluorescein-isothiocyanate or UV filters in an epifluorescence microscope (Nikon ECLIPSE TE2000-E) coupled to a Hamamatsu ORCA-ER camera.

14. Western blotting

Among 20–35 µg of protein, previously quantified by a modified Lowry assay (DC protein assay, Bio-Rad), were loaded in SDS-polyacrylamide gels. Protein samples were electrophoresed and electrotransferred onto nitrocellulose membranes (*Protran Nitrocellulose Transfer membrane*, GE Healthcare). After blocking with Tris-buffered saline (TBS), 0.1% Tween-20 (referred to as TBS-T) containing 5% nonfat dry milk, the membranes were probed with the appropriate specific primary antibodies for 1h at room temperature (RT) or overnight at 4ºC. Note that primary antibodies were prepared in TBS-T. Then, membranes were washed 3 times with TBS 0.1% Tween-20 and incubated with the adequate secondary antibodies conjugated with peroxidase for 1 hour at RT. Finally, immunoblots were developed with the Clarity™ Western ECL Blotting Substrate kit (Bio-Rad).

After the specific antibodies were blotted, membranes were stained for 5 minutes in a 10% methanol, 2% acetic acid solution containing 0.1% Naphthol blue. Then, membranes were destained in the 10% methanol and 2% acetic acid solution for 10 minutes, allowed to dry, scanned, and used as a loading control.

All antibodies employed in this Doctoral thesis are indicated in **Table M4**.

Fiji – Image J software was used to quantify the ratio of LC3-II/naphthol blue ratio (**Figure R46A**). For this specific purpose, images were transformed to 8-bit type images (*Image* > *Type* > *8-bit*). Then, we drew a rectangle around the first lane using the rectangular sections tool from the Fiji – Image J toolbar and set the rectangle in place with the option: *Analyze* > *Gels* > *Select First Lane*. For each subsequent lanes, we dragged the rectangle to the next lane and selected *Analyze* > *Gels* > *Select Next Lane*. After setting the rectangles in place for all the lanes,

we draw a profile plot of each line with the option *Analyze* > *Gels* > *Plot Lanes*. By using the Straight Line selection tool, we drew the corresponding lines to subtract the background signal. Finally, we selected each peak with the Wand tool and obtained the corresponding values.

15. Statistical analysis

The significance of the differences between two experimental conditions was determined by using the Student's *t*-test. Multiple comparisons between groups were performed using one-way ANOVA and the Tukey's post-hoc test using the statistical package Prism - GraphPad. Statistical significance was represented by asterisks (* means $p < 0.05$; ** means $p < 0.01$; *** means $p < 0.005$ and **** means $p < 0.001$).

16. Study Approval

All participants included in this study provided informed consent in accordance with the Hospital Universitari de Bellvitge Ethics Committee prior to their participation. Paraffin tissues were obtained from the archives of the Institute of Neurophatology, Hospital Universitari de Bellvitge, according to the tissue bank regulations of the same center and were used after approval by the local regulatory authorities.

Antibody	Source	Dilution	Cat. No.	Supplier
Alexa Fluor^{488} goat anti-rabbit IgG	Goat	IF: 1:250	A11034	Thermo Fisher Scientific
Alexa Fluor^{555} goat anti-mouse IgG	Goat	IF: 1:250	A21424	Thermo Fisher Scientific
Alexa Fluor^{647} goat anti-rat IgG	Goat	IF: 1:250	ab150159	Abcam
Alexa Fluor^{647}-phalloidin	_	IF: 1:40	A22287	Thermo Fisher Scientific
BAK	Rabbit	WB: 1:1,000	06-536	Sigma-Aldrich
BAX	Rabbit	WB: 1:200	2772	Cell Signaling Technology
CAD (F11)	Mouse	IF: 1:40	sc-374067	Santa Cruz Biotechnology
Calnexin	Rabbit	IF: 1:200	SPA-865	Assay Designs

Caspase-3	Rabbit	WB: 1:2,000	9662	Cell Signaling Technology
Caspase-6 (clone 3E8)	Mouse	WB: 1:2,000	M070-3	MBL
Caspase-7	Rabbit	WB: 1:2,000	9492	Cell Signaling Technology
Caspase-8	Mouse	WB: 1:1,000	551242	BD Biosciences
Caspase-9	Mouse	WB: 1:1,000	9508	Cell Signaling Technology
CD44	Rat	IF: 1:200	ab119863	Abcam
Cleaved caspase-3 (Asp175)	Rabbit	IF: 1:200	9661	Cell Signaling Technology
Cytochrome *c*	Mouse	WB: 1:1,000	556433	BD Pharmingen
DFF40	Rabbit	WB: 1:500	AB16926	Millipore Iberica S.A.U
DFF45/ICAD (clone 6B8)	Mouse	WB: 1: 5,000	M037-3	MBL
Emerin (FL-254)	Rabbit	IF: 1: 200	sc-15378	Santa Cruz Biotechnology
HRP-conjugated anti-mouse IgG	Rabbit	WB: 1:20,000	A9044	Sigma-Aldrich-
HRP-conjugated anti-rabbit IgG	Goat	WB: 1:20,000	A0545	Sigma-Aldrich-
Id1 (C-20)	Rabbit	IF: 1:50	sc-488	Santa Cruz Biotechnology
Lamin A/C (clone JOL2)	Mouse	WB: 1:2,000	ab40567	Abcam
LC3B	Mouse	WB: 1:5,000	ab48394	Abcam
MGMT	Rabbit	WB: 1:1,000	2739	Cell Signaling Technology
p23 antibody (clone JJ3)	Mouse	WB: 1:10,000	NB300-576	Novus Biological Europe, Inc
Phospho-histone H2A.X (Ser 139) (clone JBW301)	Mouse	IF: 1:2,000	05-636	Millipore Iberica S.A.U
Spectrin α-chain (clone AA6)	Mouse	WB: 1:20,000	MAB1622	Millipore Iberica S.A.U

TABLE M4. Antibodies used in this Doctoral thesis. The name of the antibody, dilution, catalog number (Cat. No.), and supplier of each antibody is here indicated. Nota that spectrin α-chain (clone AA6) antibody is referred to as α-fodrin in this text. WB, Western blot; IF, immunofluorescence

RESULTS

1. Precedents

Before presenting the results obtained during this Doctoral thesis, it is necessary to introduce some of the results obtained during my Final Master Thesis Work; a work presented at the Universitat de Barcelona as part of the Master's Degree in Biomedicine and performed under the supervision of Dr. María Sanchez Osuna and Dr. Victor Jose Yuste Mateos. These precedent results are directly related to the field of the present work and may help to understand the rationale of this Doctoral thesis.

Among the possibilities that could explain the resistance of glioblastoma to most of the drugs used in the clinic, our group pointed out the impossibility of glioblastoma (GB)-derived cells to undergo a complete apoptotic cell death (Sanchez-Osuna *et al.*, 2014). It is worth mentioning that the study of the standard treatment, which includes the combination of γ-irradiation and the alkylating agent temozolomide, was no yet addressed at this level. Thus, whether the standard treatment combination could be able or not to induce a complete canonical apoptotic cell death in GB-derived cells remained unelucidated. To achieve a better knowledge of GB aggressiveness and to find possible reasons explaining the refractoriness of this tumor to undergo cell death, we went deeper into the underlying cell death pathways activated after γ-irradiation and temozolomide insults in GB-derived cells.

1.1. Temozolomide triggers a cytostatic effect, rather than a cytotoxic effect, in human glioblastoma-derived cells

Temozolomide, the first-line chemotherapeutic treatment for glioblastoma patients, is generally considered as a cytotoxic compound. However, we observed no signs of cell death either by trypan blue exclusion assay (**Figure PR1A**) or by Calcein AM viability assay (**Figure PR1B**) after treating GB-derived LN-18 cells with temozolomide. The broad kinase inhibitor and well-known apoptotic inductor, staurosporine, was used as a positive control of cell death in both experiments (**Figure PR1C**). We also analyzed the morphological changes generated by temozolomide in LN-18 cells by fixing the cells and staining the chromatin with Hoechst 33258. Contrary to that observed in staurosporine-treated cells with nuclear pyknosis without karyorrhexis (a nuclear morphology previously described as type III nuclear morphology) (Yuste *et al.*, 2005b) (Sanchez-Osuna *et al.*, 2014), no signs of nuclear compaction were observed upon temozolomide treatment in LN-18 cells (**Figure PR1A**). Similar results to those described above were observed up to 5 mM temozolomide, the concentration at which the cytotoxicity observed was due to dimethyl sulfoxide (DMSO), the solvent used to dissolve

temozolomide. The median of temozolomide concentration in serum of patients treated at 75 mg/m^2 in the clinical setting, roughly corresponds to 123,5 μM *in vitro* (Reagan-Shaw *et al.*, 2008).

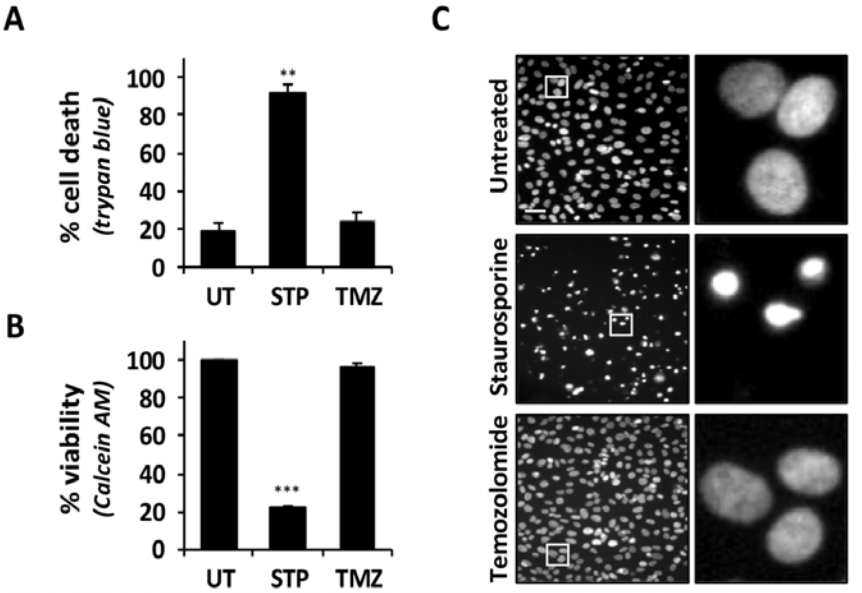

FIGURE PR1. Temozolomide does not induce cell death in LN-18 cells. LN-18 cells were left untreated (UT) or treated with 1 μM staurosporine (STP) or 100 μM temozolomide (TMZ) for 48 hours. **A**, cell death was assessed by trypan blue exclusion assay. **B**, cell viability was measured by Calcein AM assay. Values are expressed as means ± *SD*. The Student's *t*-test was used to determine the statistical significance (** means $p < 0.01$) (*** means $p < 0.005$). **C**, after treatment, cells were fixed with paraformaldehyde and nuclear morphology was analyzed by staining the nuclei with Hoechst 33258. Images were obtained with a Nikon ECLIPSE TE2000-E microscope equipped with UV-light epifluorescence and a Hamamatsu ORCA-ER photographic camera. Representative microphotographs of each condition are shown. The *right panels* are higher magnification of the cells framed in the *left panels*. Scale bar = 40 μm. This is a modified figure from Figure 4 from my Final Master thesis Work.

As an alkylating agent, temozolomide effectiveness has been associated with the status of a DNA repair enzyme known as *MGMT* (*O*^{6}-methylguanine DNA methyltransferase). This enzyme removes alkyl groups from the O^6-position of guanines, thus protecting DNA from damage. Variable levels of MGMT are reported in different GB-derived cell lines (Schafer *et al.*, 2012) (Fukai *et al.*, 2014). As an example, LN-18 cells, one of the most resistant cell lines, have high MGMT protein levels and activity. By contrast, the human GB-derived LN-229 cell line is reported negative for MGMT expression (Schafer *et al.*, 2012) (Kim *et al.*, 2014). Western blotting against MGMT was performed to assess the expression of MGMT in both cell lines. As shown in **Figure PR2A**, LN-18 cells showed expression of the DNA repair enzyme, whereas LN-229 cells did not. Hereafter, LN-18 cells will also be referred to as MGMT-positive cells and LN-229 to as MGMT-negative cells. This nomenclature may not be

confused with the clinical nomenclature of MGMT unmethylated or MGMT methylated as MGMT methylated glioblastomas coincide with loss or low levels of functional MGMT protein.

In order to evaluate if the lack of cytotoxicity observed upon temozolomide treatment in LN-18 cells was due to its MGMT levels, we decided to test the effect of this alkylating agent in LN-229 cells (MGMT-negative). Both cell lines were treated in parallel with temozolomide, and cell death was assessed by propidium iodide (PI) staining. Cytotoxicity was not observed in either MGMT-positive cells or MGMT-negative cells after 3 days of treatment (**Figure PR2B**). Similar results were obtained up to 5 days of treatment and by trypan blue exclusion assay. Additionally, nuclear morphologies were also analyzed by fixing the cells and staining the chromatin with Hoechst. As previously reported for LN-18 cells, nuclear morphologies were not altered upon temozolomide treatment in either of the cell lines employed (**Figure PR2C**). Thus, concluding that, regardless of MGMT status, temozolomide does not induce cytotoxicity in GB-derived cells.

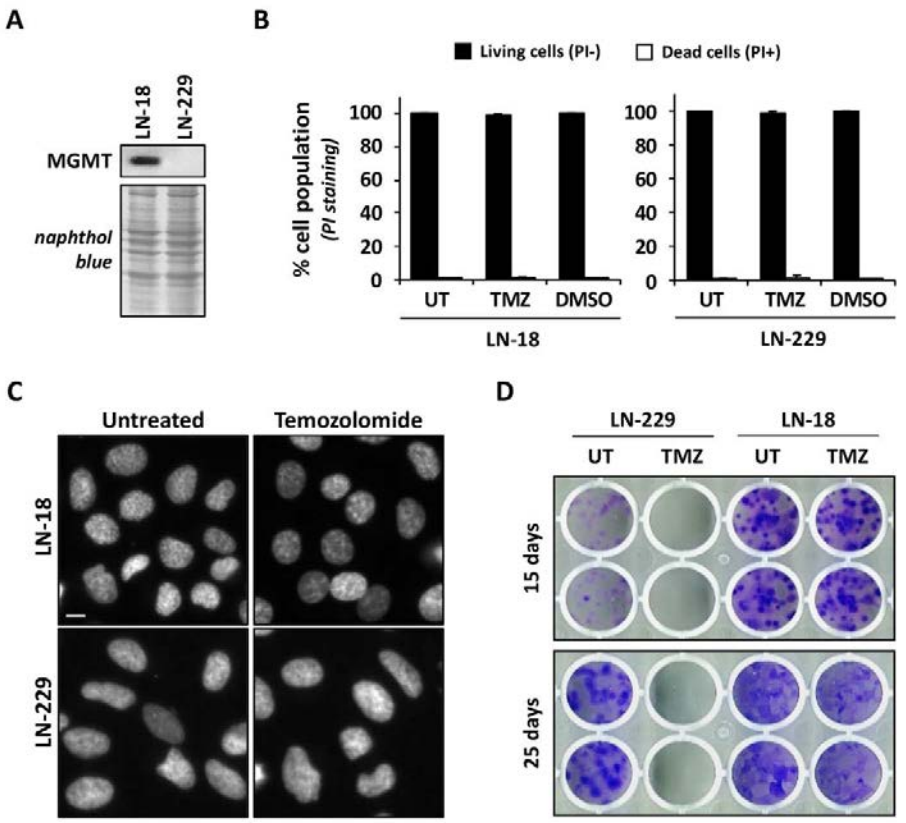

FIGURE PR2. Temozolomide triggers cytostaticity, rather than cytotoxicity, in MGMT-negative glioblastoma-derived cells. A, LN-18 and LN-229 cells were harvested and total protein extracts were obtained. Protein levels of MGMT were analyzed by Western blot. Naphthol blue staining served as a protein

loading control. **B**, LN-18 and LN-229 cells were left untreated (UT), treated with 150 μM temozolomide (TMZ) or treated with 0.0015% dimethyl sulfoxide (DMSO). Cell death was assessed by propidium iodide (PI) staining after 3 days of treatment. The graph represents the percentage of PI positive (+) death cells (*white bars*) and PI negative (-) living cells (*black bars*) ± *SD* (*error bars*). **C**, LN-18 and LN-229 cells were fixed after the indicated treatments. Nuclear morphology was analyzed by staining the nuclei with Hoechst 33258. Images were obtained with a Nikon ECLIPSE TE2000-E microscope equipped with UV-light epifluorescence and a Hamamatsu ORCA-ER photographic camera. Representative microphotographs of each condition are shown. Scale bar = 20 μm. **D**, after 4 days of treatment with 150 μM temozolomide or left untreated, LN-18 and LN-229 cells were harvested and seeded in a 24-well plate at 300 cells/well. Colony formation was evaluated by crystal violet staining after 15 and 25 days. Representative images of the plates are shown.

Besides the cytotoxicity analysis described above, we performed a colony formation assay with GB-derived cells treated with temozolomide up to 4 days. After treatment, cells were harvested, reseeded at 300 cells/well in a 24-well plate, and kept for up to 25 days. After 15 and 25 days of growth, colonies were formed and further stained with crystal violet. As shown in **Figure PR2D**, no colony formation was observed either after 15 days or 25 days in MGMT-negative LN-229 cells previously treated with temozolomide. By contrast, MGMT-positive LN-18 cells, left untreated or treated with temozolomide, proliferated, and formed colonies. Thus, suggesting that proliferation of MGMT-positive cells is not affected by temozolomide, whereas proliferation of MGMT-negative cells is impaired when facing those cells to the alkylating agent.

Part of the results presented in **Figure PR2** were obtained by Elena Garcia Borja, a master student that I supervised during this Doctoral thesis. Elena Garcia Borja performed its Final Master Thesis Work in our laboratory as part of the Master in Neuroscience offered by the Institut de Neurociències - Universitat Autònoma de Barcelona.

1.2. γ-irradiation induces apoptotic nuclear features in human glioblastoma-derived cells

Once demonstrated that temozolomide does not provoke cell death in human GB-derived cells, we were interested in knowing whether or not γ-irradiation triggered cytotoxicity. Since γ-irradiation is given concomitantly with temozolomide in the clinics, we also challenged glioblastoma cells with such double insult. By trypan blue exclusion assay, we determined that, contrary to temozolomide, γ-irradiation (alone, or in combination with temozolomide) was inducing cell death in GB-derived cells (**Figure PR3A**). Indeed, LN-18 cells were irradiated in the presence or absence of the pan-caspase inhibitor, q-VD-OPh, and as shown in **Figure PR3A**, the membrane permeability induced by γ-irradiation was significantly reduced in the presence of the caspase inhibitor. The cell death induced by the double treatment of γ-

irradiation plus temozolomide was also lowered by q-VD-OPh. Thus, these results pointed to a caspase-dependent triggered cell death upon γ-irradiation in GB-derived cells.

To analyze the nuclear outcome of LN-18 cells exposed to γ-irradiation alone or in combination with temozolomide, we fixed the cells and stained the chromatin with Hoechst 333258. Staurosporine was included as a representative compound of the previously depicted type III nuclear morphology, observed as the principal nuclear outcome when challenging GB-derived cells with different insults (Sanchez-Osuna *et al.*, 2014). Accordingly, as shown in **Figure PR3B** and as represented in **Figure PR3C**, type III was the principal nuclear type observed in LN-18 cells treated with staurosporine. Interestingly, this nuclear phenotype was changed upon γ-irradiation. After 3 days of irradiation, canonical apoptotic nuclear morphologies were observed in γ-irradiated cells (25.66 ± 8.80%) and γ-irradiated cells plus temozolomide (22.97 ± 8.33%) (**Figure PR3B**). Apoptotic nuclear morphologies were completely prevented in the presence of the pan-caspase inhibitor, q-VD-OPh (**Figure PR3B**). Remarkably, aberrant nuclei were observed in a caspase inhibition context (**Figure PR3B**). As shown in **Figure PR3C**, γ-irradiation triggered a pleiotropically phenotype, including a morphology resembling the previously described type III nuclear morphology, and a chromatin condensed and fragmented morphology. This last, akin to apoptotic type II nuclear morphology and not previously reported in GB-derived cells. In the presence of q-VD-OPh, both types of nuclear morphologies were inhibited. Of note, staurosporine was used for 6 hours to trigger a similar percentage of altered nuclei than the observed after 3 days of irradiation with or without temozolomide (**Figure PR3B**, **C**).

After demonstrating the implication of caspases in cell death and the nuclear morphologies induced by γ-irradiation, we performed Western blot analysis of caspases. As shown in **Figure PR3D**, we observed the processing of the initiator caspase-9 to its active fragments p37 and p35, and the caspase-3-mediated cleavage of α-fodrin to its p120 fragment after irradiation with or without temozolomide. The presence of the q-VD-OPh completely avoided these cleavages (**Figure PR3D**). Additionally, DEVD-directed caspase-like activity assay confirmed that the q-VD-OPh was able to inhibit caspase activity triggered by γ-irradiation (**Figure PR3E**). Similar results were obtained when irradiating the cells in combination with temozolomide. Indeed, higher caspase-processing and activity were observed in the double treatment compared to the single treatment (γ-irradiation alone). In the presence of q-VD-OPh, this activity was completely inhibited (**Figure PR3E**).

Given that DFF40/CAD activity is the primary molecular event driving the apoptotic (type II) nuclear morphology, the observation of this nuclear outcome upon γ-irradiation alone or

in combination with temozolomide raised the possibility that this endonuclease could be efficiently activated in glioblastoma cells.

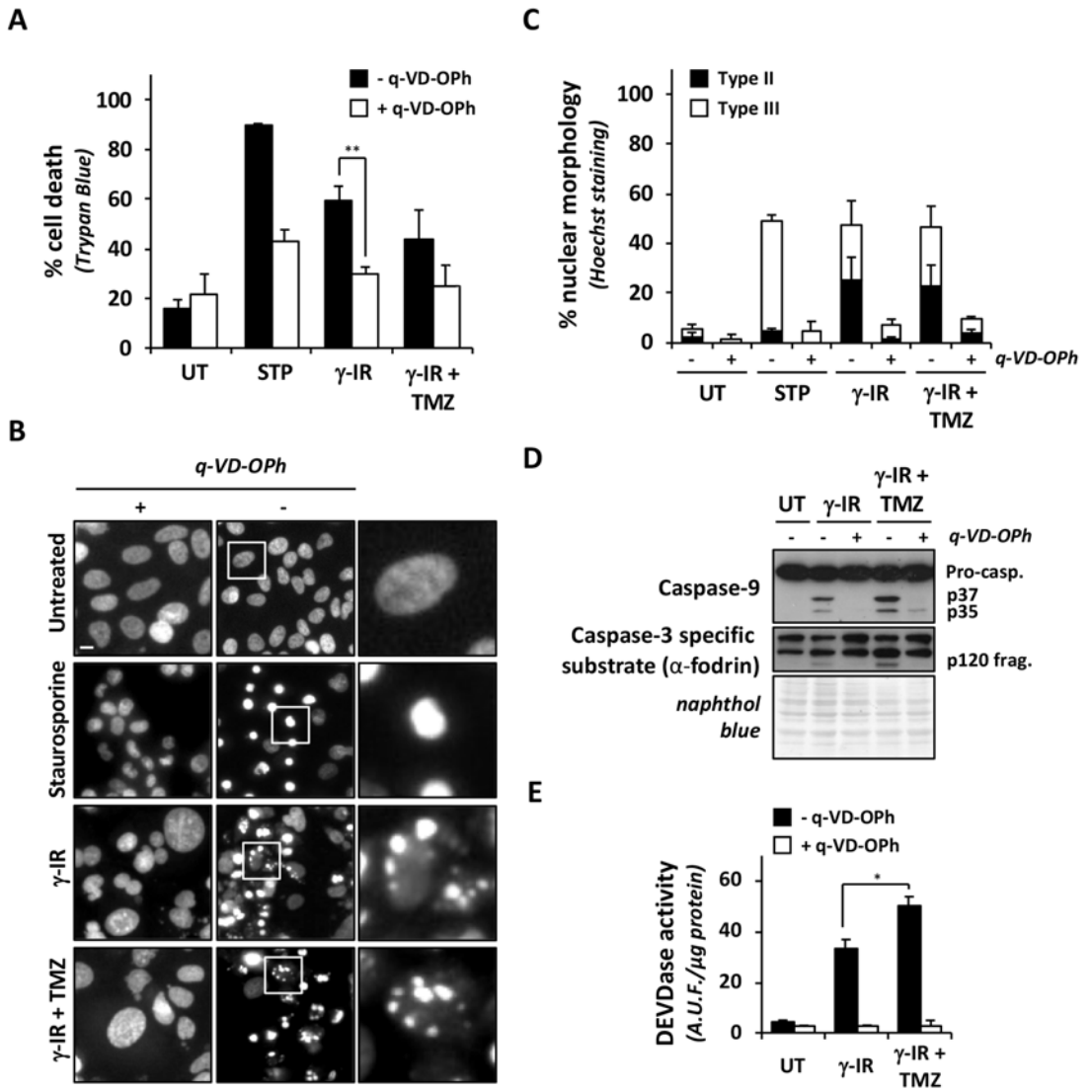

FIGURE PR3. LN-18 cells display caspase-dependent apoptotic nuclear morphologies upon γ-irradiation. LN-18 cells were left untreated (UT), treated with 1 μM staurosporine (STP) for 24 hours, irradiated with 10 Gy (γ-IR) for 3 days, or irradiated with concomitant temozolomide (TMZ) (100 μM) for 3 days. **A**, each condition was performed in the presence (*white bars*) or absence (*black bars*) of the pan-caspase inhibitor q-VD-OPh (20 μM), and, cell death was measured by Trypan Blue exclusion assay. The means ± *SEM* from three independent experiments are shown. The Student's *t*-test was used to determine the statistical significance (** means $p < 0.01$). **B**, after 3 days of treatment (except for staurosporine, 6 hours), cells were fixed with paraformaldehyde and nuclear morphology was analyzed by staining the nuclei with Hoechst 33258. Images were obtained with a Nikon ECLIPSE TE2000-E microscope equipped with UV-light epifluorescence and a Hamamatsu ORCA-ER photographic camera. Representative microphotographs of each condition are shown. The *right panels* are higher magnification of the cells framed in the *middle panels*. Scale bar: 40 μm. **C**, stained nuclei were scored as type II (nuclear pyknosis and karyorrhexis) or type III (nuclei shrinkage and highly compacted

chromatin). **D**, Western blot against initiator caspase-9 or α-fodrin (caspase-3 specific substrate). Naphthol blue staining served as a protein loading control. **E**, DEVD-directed caspase-like activity was measured and graphed. One-way ANOVA determined statistical significance between groups [$F(2,3) = 147.3$, $p < 0.001$]. Tukey's post hoc test determined significance between irradiated cells and irradiated cells plus temozolomide (* means $p < 0.05$). This is a modified figure from Figure 8 and Figure 10 from my Final Master thesis Work.

1.3. Histological sections from glioblastoma patients reveal nuclear condensation and fragmentation

As previously mentioned, human glioblastoma-derived cells are particularly refractory to display canonical apoptotic nuclear features when challenged with different cytotoxic compounds (Sanchez-Osuna *et al.*, 2014). In this sense, we reported an inherent defect in the expression of DFF40/CAD endonuclease as a common trait in human glioblastoma cells (Sanchez-Osuna *et al.*, 2016). This defect correlates with the refractoriness of these cancer cells to undergo complete apoptotic cell death. Indeed, the innate behavior of glioblastoma cells when challenged with different chemical insults is to show a nuclear morphology characterized by a unique mass of compacted chromatin in the absence of nuclear fragmentation (Sanchez-Osuna *et al.*, 2014). However, with the results obtained when challenging GB-derived cells with γ-irradiation, we have demonstrated that these tumor cells own the machinery necessary to complete an apoptotic cell death process.

Thanks to the collaboration with the Unit of Neuro-Oncology from the Hospital Universitari de Bellvitge-I.C.O. Duran i Reynals (Barcelona, Spain), we could analyze histological samples obtained from six different GB patients. The processing of the samples was performed at the Neuropathology Institute from the same hospital. As shown in **Figure PR4,** hematoxylin & eosin (H&E)-stained histological sections from GB-affected patients revealed few malignant cells displaying spontaneous condensation and fragmentation of the nucleus (*filled arrows*). Likewise, pyknotic nuclei, which represents the main altered nuclear morphology described in LN-18 cells (Sanchez-Osuna *et al.*, 2014), were also observed in H&E-stained histological sections. Specific data from each patient is detailed in **Table M2**.

Results from H&E-stained histological sections and, especially, results obtained from γ-irradiation experiments indicate that glioblastoma cells can display spontaneously- and therapeutically-triggered apoptotic nuclear morphologies. In this sense, it is necessary to stress that, although glioblastoma cells have been characterized as DFF40/CAD deficient cells, they express the endonuclease (Sanchez-Osuna *et al.*, 2016). Hence, it seems to indicate that the key to triggering complete apoptotic cell death may rely on the use of an adequate stimulus

and its ability to properly activate the intrinsic machinery and, particularly, DFF40/CAD, the endonuclease implicated in this cellular outcome.

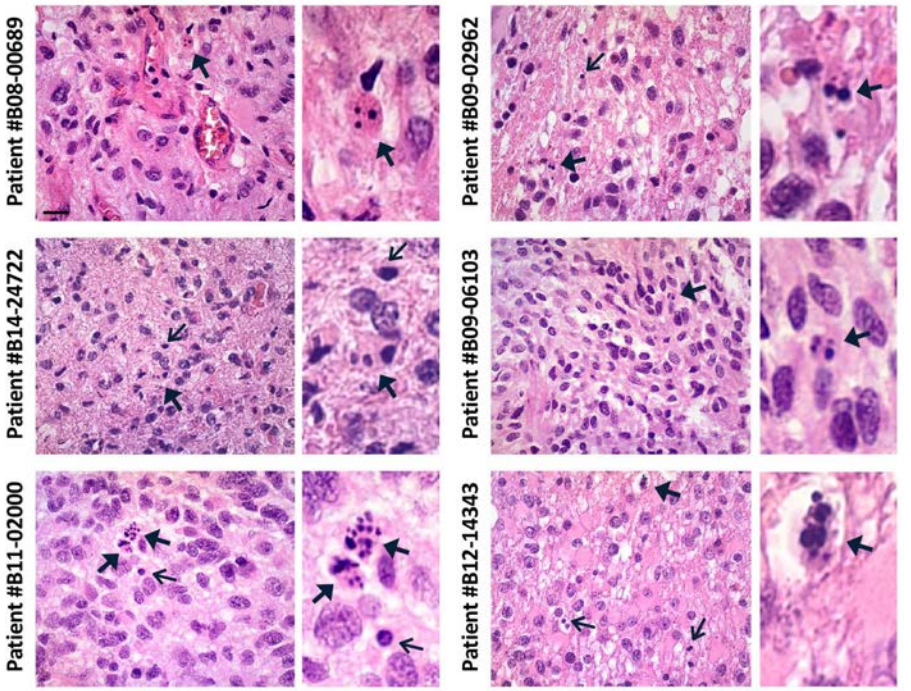

FIGURE PR4. Histological sections from glioblastoma patients reveal spontaneous apoptotic-like nuclear morphologies. Histological sections from six different GBM-affected patients were stained with hematoxylin & eosin (H&E) as described in *Material and Methods*. Representative images are shown. In each patient sample, the *right panels* are higher magnifications of *left panels*. *Filled arrows* indicate nuclear features with condensation and fragmentation and *open arrows* indicate pyknotic nuclei. Scale bar: 40 μm. Clinical data from all patients are summarized in **Table M2**.

1.4. The combination of gossypol and TRAIL induces nuclear fragmentation in human glioblastoma-derived cells

In parallel with the results mentioned above, LN-18 cells were faced to a broad panel of intrinsic compounds combined with extrinsic apoptotic ligands. The intrinsic compounds used were targeting therapies of the BCL-2 family members or BH3-mimetic compounds, including ABT-737, chelerythrine, EM20-25, gossypol, HA14-1, and obatoclax. As shown in **Figure PR5A**, the predominant morphology triggered by these BH3-mimetic compounds combined with TRAIL was the previously described type III nuclear morphology (Sanchez-Osuna *et al*., 2014), consisting of a pyknotic nucleus without signs of nuclear fragmentation. However, we found that gossypol plus TRAIL induced type II nuclear morphologies. Although here not presented, other extrinsic apoptotic inductors such as TNF or CH11

displayed a similar phenotype combined with gossypol. This result was part of the Doctoral thesis of María Sánchez Osuna. Further quantification of the different nuclear morphologies induced by each combination (not included in Dr. Sánchez Osuna's thesis) was performed, and the corresponding percentages were represented in bar graphs. As shown in **Figure PR5B,** LN-18 cells display a significant percentage of type II nuclear morphology after gossypol and TRAIL cotreatment, a nuclear phenotype previously observed after γ-irradiation (**Figure PR3**).

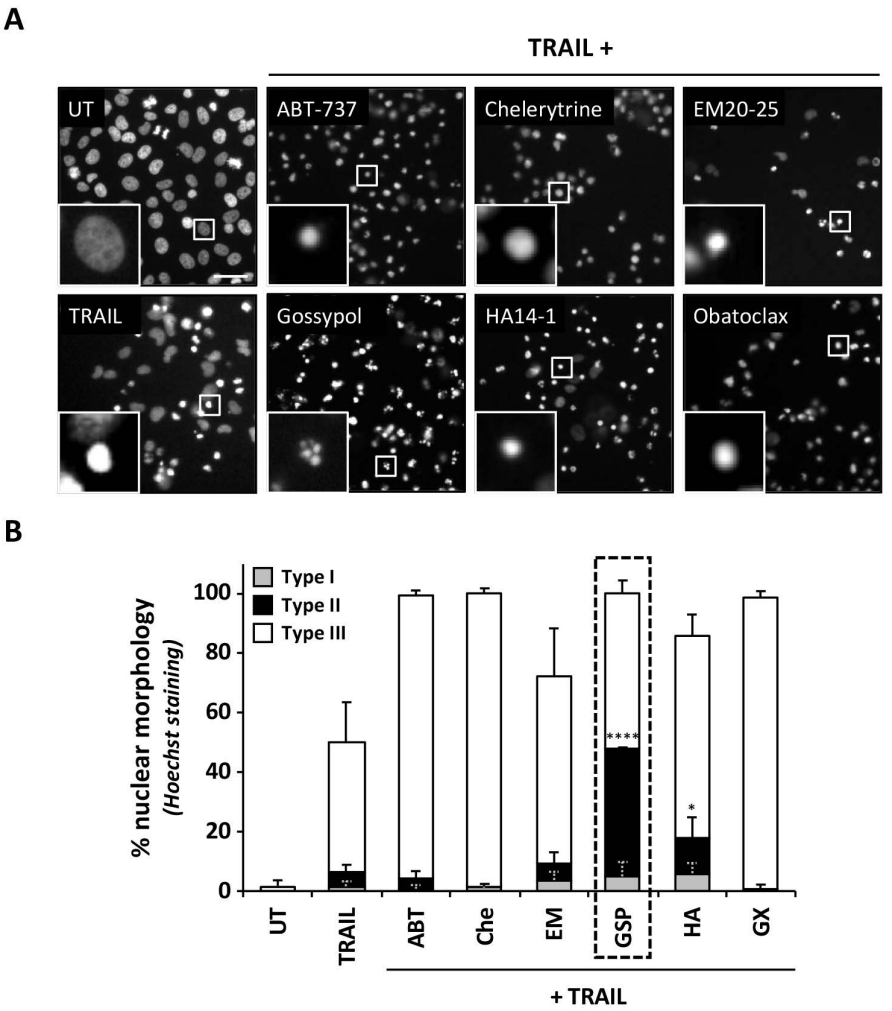

FIGURE PR5. Type II nuclear morphologies are observed upon treatment with gossypol and the death ligand TRAIL in LN-18 cells. A, LN-18 cells were left untreated or treated with 100 ng/ml TRAIL combined with 50 μM ABT-737 (ABT), 20 μM chelerythrine (Che), 50 μM EM20-25 (EM), 100 μM gossypol (GSP), 100 μM HA14-1 (HA) or 100 μM obatoclax (GX). After 24 hours, cells were fixed, and nuclear morphology was analyzed by staining the nuclei with Hoechst 33258. Images were obtained with a Nikon ECLIPSE TE2000-E microscope equipped with UV-light epifluorescence and a Hamamatsu ORCA-ER photographic camera. Representative microphotographs of each condition are shown. Magnifications show representative morphologies in each condition. Scale bar = 40 μm. Part of this data was presented in the Doctoral thesis of Dr.

María Sanchez Osuna. **B**, Quantification of different nuclear morphologies as type I (partial chromatin condensation in a ring-like shape), type II (nuclear pyknosis and karyorrhexis), or type III (nuclear pyknosis without karyorrhexis). The percentage of each nuclear morphology is represented by bar graphs ± *SEM* (*error bars*). One-way ANOVA test was used to determine the statistical significance between groups regarding type II [$F(7,9) = 45.73$, $p < 0.0001$]. The significance of the type II value of each treatment versus untreated was determined by the post hoc Tukey's test (* means $p < 0.05$)(**** means $p < 0.001$).

Γ-irradiation, coupled with surgical resection, has been reported as the therapeutic approach in glioblastomas with better results. In this sense, the combinatorial approach of gossypol plus TRAIL, which triggers a similar nuclear outcome than γ-irradiation, seemed to be an adequate stimulus to study. According to our results, this cotreatment had a particular interest since, except γ-irradiation, any of the different apoptotic insults employed before triggered a significant percentage of apoptotic nuclear morphologies in human GB-derived cells (Sanchez-Osuna *et al.*, 2014). To better comprehend the mechanisms whereby TRAIL-treated cells display a significant percentage of type II nuclear morphology when combined with gossypol, we started this work.

2. Gossypol induces type II nuclear morphologies in LN-18 cells

Before proceeding with the combinatorial approach (gossypol plus TRAIL), we decided to pay particular attention to the nuclear features displayed upon each treatment individually. For this, we treated LN-18 cells with gossypol or TRAIL, and we also included the treatment with the classical apoptotic inductor staurosporine. As mentioned above, staurosporine was previously reported to trigger a nuclear morphology characterized by nuclei shrinkage and highly compacted chromatin in the absence of karyorrhexis in LN-18 cells (Sanchez-Osuna *et al.*, 2014). This type of nuclear morphology is referred to as type III in this text. As shown in **Figure R1** (*filled arrows*), the treatment with the classical apoptotic inductor staurosporine confirmed the before described type III nuclear morphology in LN-18 cells (Sanchez-Osuna *et al.*, 2014). Although in a lower percentage, this morphology was also the primary altered nuclear morphology displayed by cells treated with TRAIL (*filled arrows*).

The treatment of LN-18 cells with gossypol changed this trend. Gossypol treatment, without its combination with TRAIL, significantly induced chromatin condensation and nuclear fragmentation (26.02 ± 2.69%) (**Figure R1**, *arrowheads*), a nuclear morphology previously referred to as type II. In the case of TRAIL- and staurosporine-treated cells, below 5% of the nuclei presented this type II nuclear morphology. Hence, although pleiotropically with other morphologies, including type III and type I morphologies (*open arrows*), gossypol was the only compound of the panel displaying a significant percentage of type II nuclear morphology.

It is necessary to stress that gossypol-induced type II nuclear morphologies were previously presented in the Doctoral thesis of Dr. María Sanchez Osuna. However, according to her results, a much lower percentage (6.71± 2.07%) of type II nuclear morphology was induced upon gossypol treatment in LN-18 cells. In this sense, considering that results from **Figure R1** were obtained from using the same cell line (LN-18 cells), same concentration (100 μM of gossypol) and after the same hours of treatment (24 hours), we wondered whether differences in the cellular confluence could explain different results regarding the formation of the nuclear morphologies. For this, we seeded LN-18 cells at different densities, as indicated in **Figure R2**, and treated the cells for 24 hours with 100 μM gossypol.

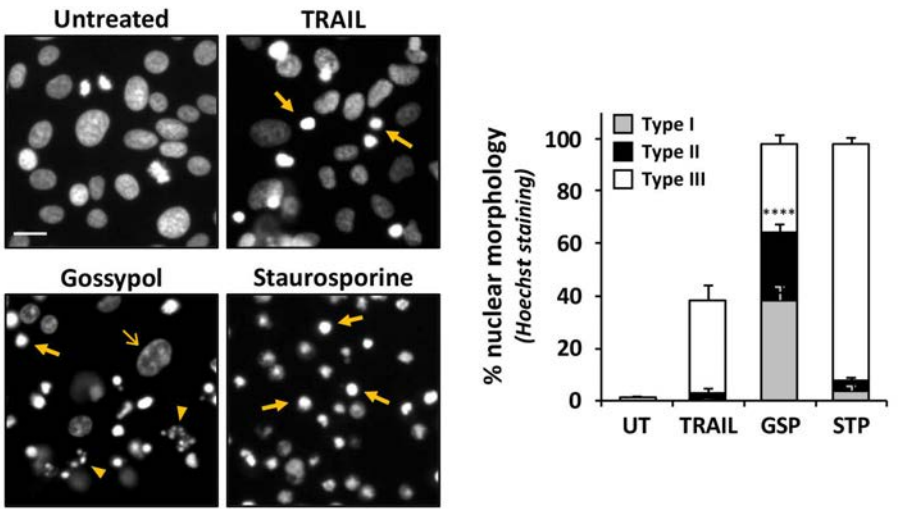

FIGURE R1. LN-18 cells display an increase in the percentage of type II nuclear morphologies upon gossypol treatment. LN-18 cells were treated with 100 ng/ml TRAIL, 100 μM gossypol (GSP), 1 μM staurosporine (STP), or left untreated (UT). After 24 hours of treatment, cells were fixed and nuclear morphology was analyzed by staining the nuclei with Hoechst 33258. Images were obtained with a Nikon ECLIPSE TE2000-E microscope equipped with UV-light epifluorescence and a Hamamatsu ORCA-ER photographic camera. Representative microphotographs of each condition are shown. Scale bar = 20 μm. Nuclei of each condition were scored either as type I (*open arrow*), type II (*arrowhead*), or type III (*filled arrow*). The corresponding percentages are represented by bar graphs ± *SEM* (*error bars*). One-way ANOVA test was used to determine the statistical significance between groups regarding type II [$F(3,11) = 53.73$, $p < 0.0001$]. The significance of the type II value of each treatment versus untreated was determined by the post hoc Tukey's test (**** means $p < 0.001$).

The analysis of nuclear morphology by staining the nuclei with Hoechst 33258 revealed that nuclear morphologies induced by gossypol in LN-18 cells are affected by the cellular density. Indeed, the type II nuclear morphology correlated with higher cellular densities. Hence suggesting that the addition of gossypol once LN-18 cells are confluent (80-90% of cellular confluence) facilitates the formation of apoptotic nuclear morphologies.

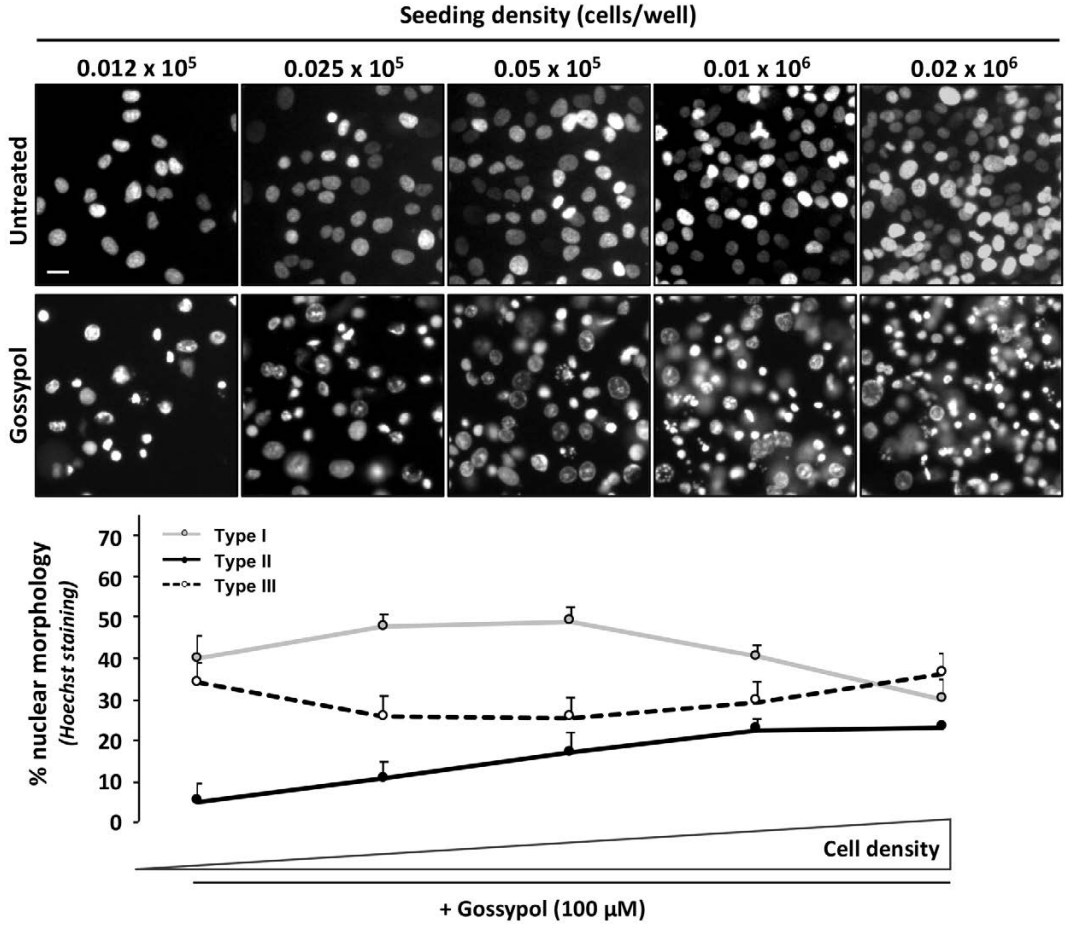

FIGURE R2. The cell density modifies the percentages of the nuclear morphologies observed after gossypol treatment in LN-18 cells. LN-18 cells were seeded at different densities, as indicated. Values refer to the seeding density per well of a 96-multiwell plate (cells/well). 48 hours after seeded, cells were treated with 100 µM gossypol or left untreated. After 24 hours of treatment, cells were fixed and nuclear morphology was analyzed by staining the nuclei with Hoechst 33258. Images were obtained with a Nikon ECLIPSE TE2000-E microscope equipped with UV-light epifluorescence and a Hamamatsu ORCA-ER photographic camera. Representative microphotographs of each condition are shown. Scale bar = 20 µm. Nuclei were scored either as type I, type II, or type III, and the corresponding percentages are represented by line charts ± *SEM* (*error bars*). Chart values correspond to the indicated seeding densities in the upper panels from gossypol-treated cells (increasing seeding densities from left to right).

In parallel, we decided to generate glioblastoma-derived spheres and to challenge them with the same compound. For this, LN-18 cells were seeded onto Petri dishes with non-treated surfaces and left to grow. Cells were kept in complete medium to maintain the same culture conditions used for the 2D or adherent cells. Unfortunately, due to the strong adhesion of LN-18 cells to even non-treated surfaces, we could not obtain enough LN-18-derived spheres to proceed with the experimental approach. Alternatively, we used LN-229 cells, another human glioblastoma-derived cell line, and proceeded as described before. After about three months, enough spheres were collected (**Figure R3**). Then, spheres were divided onto three

different 60 mm Petri dishes (with non-treated surfaces) and were left untreated or treated with gossypol or staurosporine. After 18 hours of treatment, we collected the spheres and proceeded as described in *Material and Methods*. As shown in **Figure R3**, a cellular decrease was observed inside the spheres treated with gossypol, indicating the permeability of gossypol when used in 3D cellular cultures. Cavities empty of cells are indicated in the same figure with an asterisk. Among the different nuclear morphologies, we observed a high degree of condensed nuclei –some of them also fragmented–, but the main trait upon gossypol treatment was a translucent appearance of glioblastoma cells. In the case of staurosporine, less loss of cellular content was observed, but pyknotic nuclei and fragmented nuclei were also evident. The optimization of the procedure to obtain GB-derived spheres, especially from LN-18 cells (the best characterized human GB-derived cell line in our laboratory), is under evaluation.

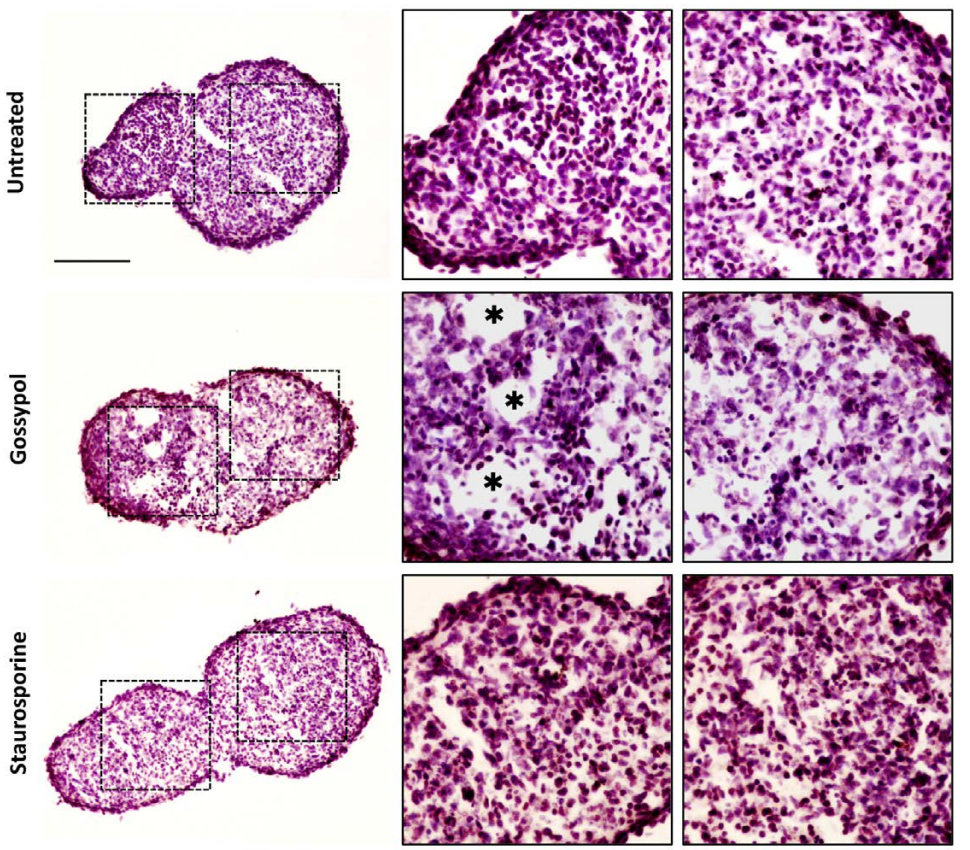

FIGURE R3. Glioblastoma-derived spheres challenged with gossypol or staurosporine. LN-229-derived gliospheres were left untreated or treated with 100 μM gossypol or 1 μM staurosporine. After 18 hours, spheres were fixed, processed, and stained with hematoxylin according to *Material and Methods*. Images were obtained with a Nikon ECLIPSE 90i microscope equipped with epifluorescence optics, a Nikon DXM1200F photographic camera and ACT-1 software. The middle and right panels are higher magnifications of the cells framed in the left panels. Scale bar = 100 μm. Asterisks (✱) indicate cavities inside gossypol-treated glioblastoma-derived spheres.

3. Gossypol induces a similar nuclear phenotype in three cellular models with dissimilar responses after staurosporine treatment

The interest of our group in the molecular and biochemical mechanisms that govern the final steps during cell death has led to describe three different cellular responses to apoptotic insults such as staurosporine.

By analyzing the nuclear outcomes of different tumor-derived cells, we reported that human neuroblastoma-derived SH-SY5Y cells responded to the alkaloid by inducing canonical apoptotic type II nuclear morphology. However, when adding staurosporine to the culture medium of IMR-5 cells, another human neuroblastoma-derived cell line, they did not display type II nuclear morphology (Boix *et al.*, 1997). The absence of type II nuclear morphology, when treating with staurosporine, was also reported in LN-18 cells (Sanchez-Osuna *et al.*, 2014).

Thus, we wondered how gossypol affected the nuclear outcomes in those previously described neuroblastoma models. As a control, we also treated the cells with staurosporine. As previously described, IMR-5 cells did not display type II nuclear morphology after staurosporine treatment. This neuroblastoma-derived cell line exhibited a partial chromatin condensation in a ring-like shape, previously referred to as type I nuclear morphology. Contrary, but as expected, SH-SY5Y cells underwent type II nuclear morphologies with nuclei shrinkage and karyorrhexis. Glioblastoma-derived LN-18 cells depicted a type III nuclear morphology characterized by compaction of the nuclear content into a single highly condensed mass of chromatin (**Figure R4**, *middle panel*).

When adding gossypol to the culture medium of either IMR-5, SH-SY5Y, or LN-18 cells, all cell lines displayed type II nuclear morphologies. Thus, indicating that gossypol was able to homogenize the nuclear phenotype induced in three different cellular models, previously described to show different nuclear aspects upon treatment with staurosporine (**Figure R4**, *right panel*). The ability of gossypol to trigger a similar nuclear outcome in different cellular models encouraged the study of this compound.

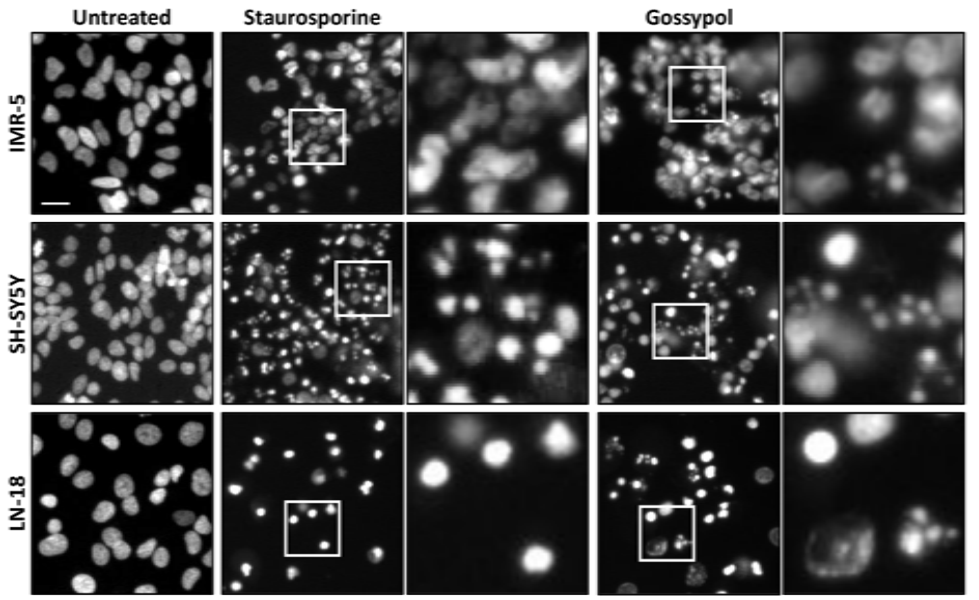

FIGURE R4. Gossypol-induced type II nuclear morphologies are observed throughout three different cellular models. IMR-5, SH-SY5Y, and LN-18 cells were treated with 1 μM staurosporine, 100 μM gossypol, or left untreated. After 24 hours of treatment, nuclear morphology was analyzed by fixing the cells and staining the nuclei with Hoechst 33258. Images were obtained with a Nikon ECLIPSE TE2000-E microscope equipped with UV-light epifluorescence and a Hamamatsu ORCA-ER photographic camera. Representative microphotographs of each condition are shown. The bottom panels are higher magnifications of the cells framed in the staurosporine or gossypol-treated conditions. Scale bar = 20 μm.

4. Type II nuclear morphology triggered by gossypol is dose- and time-dependent

The nuclear outcome observed upon gossypol treatment in LN-18 cells was further analyzed in a dose-dependent and time-dependent approach. LN-18 cells were treated with different concentrations of gossypol ranging from 25 μM to 400 μM. As shown in **Figure R5**, 50 μM of gossypol was the minimal concentration provoking 50% altered nuclear morphologies. More specifically, the percentage of type III nuclear morphology was maintained from 50 μM up to 200 μM (around 30%). By contrast, the percentage of type II varied from concentration to concentration and reached its maximum at 100 μM (24.12 ± 0.96%). This percentage decreased at higher concentrations. Regarding the type I nuclear morphology, this was especially evident at 100 and 200 μM. Those altered nuclei that did not fit among the nuclear types above described (I, II, or III) are here referred to as other altered nuclei (**Figure R5**). These morphologies were especially evident at 400 μM gossypol.

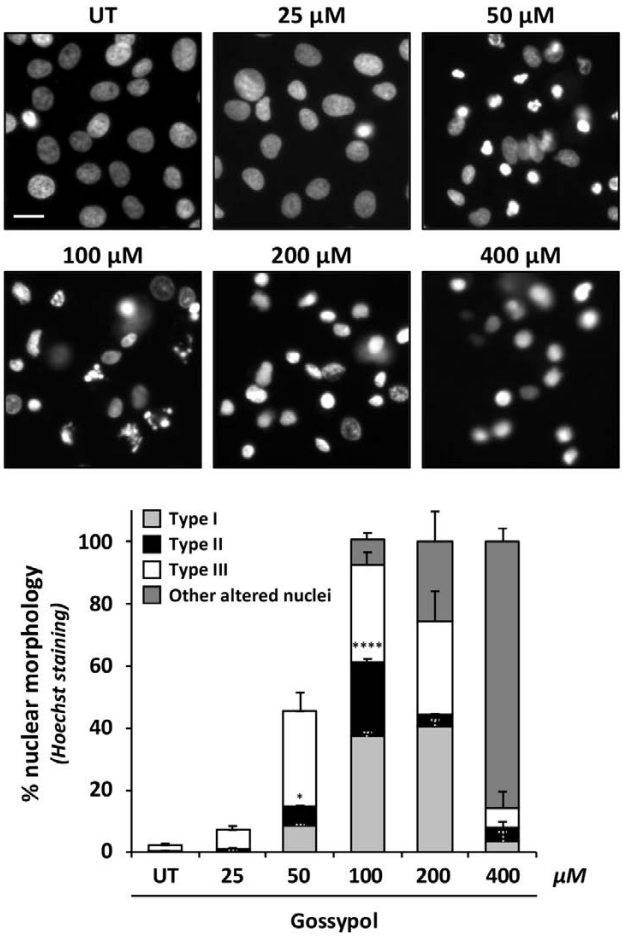

FIGURE R5. Gossypol-induced type II nuclear morphologies are observed in a dose-dependent manner. LN-18 cells were treated with different concentrations of gossypol, ranging from 25 to 400 µM, or left untreated (UT). After 24 hours of treatment, nuclear morphology was assessed by fixing cells and by staining the nuclei with Hoechst 33258. Images were obtained with a Nikon ECLIPSE TE2000-E microscope equipped with UV-light epifluorescence and a Hamamatsu ORCA-ER photographic camera. Representative microphotographs of each condition are shown. Scale bar = 20 µm. Nuclei were scored either as type I, II, III, or other altered nuclei. Percentages of each nuclear morphology are represented by bar graphs ± *SEM* (*error bars*). One-way ANOVA test was used to determine the statistical significance between groups regarding type II [$F(5,12) = 76.67$, $p < 0.05$]. The significance of the type II value of each treatment versus untreated was determined by the post hoc Tukey's test (* means $p < 0.05$) (**** means $p < 0.001$).

The nuclear phenotype displayed upon gossypol treatment in LN-18 cells was also affected in a time-dependent manner. Nuclear morphologies were analyzed from 6 hours up to 4 days (96 hours) by fixing the cells and staining the chromatin with bisbenzimide. As represented in **Figure R6,** type II nuclear morphologies were significantly detected from 12 hours of treatment for up to 96 hours. More specifically, type II gossypol-induced nuclear morphologies after 12 hours were 16.52 ± 2.65% and increased to 23.83 ± 1.31% after 24 hours. Indeed, while a similar percentage of type II morphologies was maintained from 12

hours and upward, the percentage of type I and type III morphologies varied with the different time points and was more stable for up to 48 hours. The type III nuclear morphology reached its maxim percentage after 48 hours and was maintained for up to 96 hours. The type I nuclear morphology reached its maximum percentage after 24 hours, and then it was decreased. Line charts alternatively represented these results (**Figure R6B**).

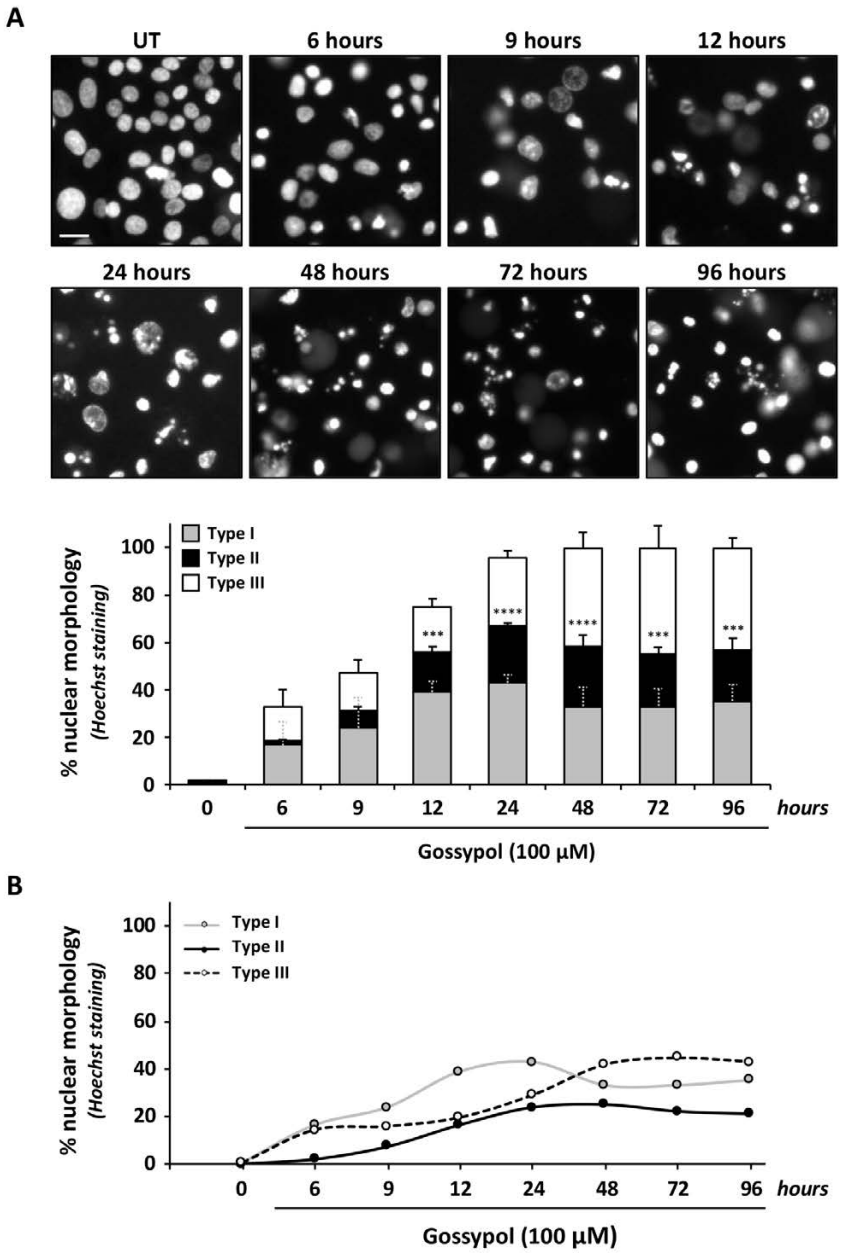

FIGURE R6. Gossypol-induced type II nuclear morphologies are observed in a time-dependent manner. LN-18 cells were treated with 100 µM of gossypol or left untreated. After 6, 9, 12, 24, 48, 72, and 96 hours (h), cells were fixed and nuclear morphology was analyzed by staining the nuclei with Hoechst 33258. Images were obtained with a Nikon ECLIPSE TE2000-E microscope equipped with UV-light epifluorescence

and a Hamamatsu ORCA-ER photographic camera. **A**, representative microphotographs of each condition are shown. Scale bar = 20 μm. Nuclei of each condition were scored either as type I, II, or III. Percentages of each nuclear morphology are represented by bar graphs ± *SEM* (*error bars*). One-way ANOVA test was used to determine the statistical significance between groups regarding type II [$F(7,18) = 21.66$, $p < 0.0001$]. The significance of the type II value of each treatment versus untreated was determined by the post hoc Tukey's test (*** means $p < 0.005$) (**** means $p < 0.001$). **B**, the percentages of each nuclear morphology are alternatively represented by line charts.

A time-course analysis of the nuclear morphologies observed in LN-18 cells treated with staurosporine was previously performed. As reported in (Sanchez-Osuna *et al.*, 2014), the type III nuclear morphology triggered by staurosporine in LN-18 cells was detected at around 20% after 4 hours of treatment, it reached a 60% after 10 hours, and it was detected almost at a 100% after 24 hours. By contrast, type II nuclear morphologies were observed below 5% at any time during treatment with the alkaloid.

Due to the differences observed when looking at the nuclear phenotype after gossypol or staurosporine treatment, we wondered if differences regarding cytotoxicity were also detected between both compounds. We measured cell death through two different assays, trypan blue exclusion assay, and propidium iodide staining. The measure of cell death by trypan blue exclusion assay evidenced higher percentages of cell death at earlier times upon gossypol treatment (**Figure R7A**). Contrarily, no differences were detected by propidium iodide staining comparing both treatments at different times (**Figure R7B**). Alternatively, we measured cell viability by MTT assay. As shown in **Figure R7C,** cell viability loss occurred earlier when treating LN-18 cells with staurosporine. However, after 24 hours of staurosporine or gossypol treatment, a similar cytotoxicity level (almost 100%) was detected regardless of the cell viability assay employed.

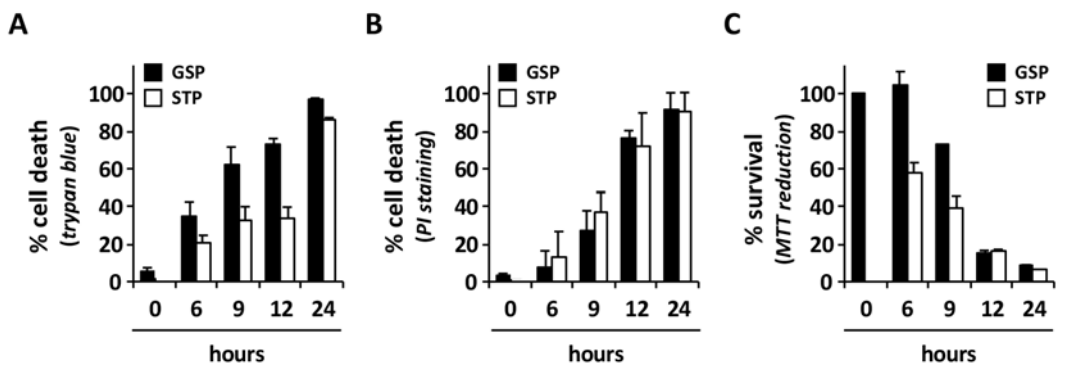

FIGURE R7. Cell death profile upon gossypol and staurosporine treatment in LN-18 cells. LN-18 cells were left untreated or treated with 100 μM gossypol (GSP) *(black bars)* or 1 μM staurosporine (STP) (*white bars*) for 24 hours. Cell death was assessed by trypan blue exclusion assay (**A**) or propidium iodide (PI) staining (**B**), and cell viability was measured by MTT assay (**C**). Values are expressed as means ± *SEM* (*error bars*).

5. Transmission electron microscopy images confirm type II apoptotic nuclear morphology after gossypol treatment in LN-18 cells

To gain further information about the ultrastructural changes, we examined gossypol-treated LN-18 cells through electron microscopy. Staurosporine was also included in the panel. As reported in (Sanchez-Osuna *et al.*, 2014), staurosporine-treated LN-18 cells displayed a unique mass of condensed chromatin (type III nuclear morphology) as the principal nuclear outcome (**Figure R8**, *right upper image*). Gossypol-treated LN-18 cells displayed type III nuclear morphologies (**Figure R8**, *right lower image*), but also morphologies with nuclear fragmentation. As shown in **Figure R8**, *left lower image*, these morphologies coincided with smaller pieces of highly-packed round masses of condensed chromatin surrounded by the nuclear envelope (**Figure R8**). Hence, electron microscopy analysis confirmed gossypol as a proficient stimulus to trigger the classical type II apoptotic nuclear morphology in LN-18 cells.

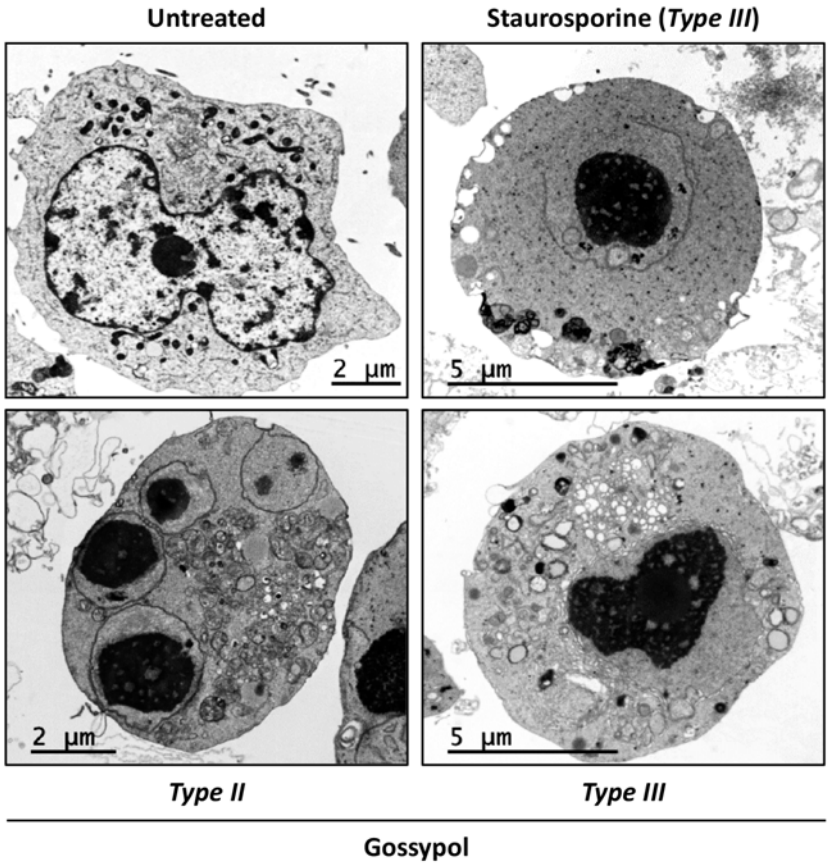

FIGURE R8. Electron microscopy confirms type II apoptotic nuclear morphology upon gossypol treatment. LN-18 cells were treated with 1 µM of staurosporine for 10 hours, 100 µM of gossypol for 17 hours, or left untreated. Representative images of transmission electron microscopy are shown.

Interestingly, electron microscopy images also revealed a prominent alteration of cellular membranes and an intense vacuolization process in LN-18 cells treated with gossypol. Additional electron microscopy images are presented in **Figure R38 and R48**.

6. Gossypol-triggered nuclear phenotype is shared among commercial and non-commercial glioblastoma cells

Before addressing the mechanism behind the type II nuclear morphology observed upon gossypol in LN-18 cells, we decided to extend the data to other glioblastoma cells. Hence, we performed an analysis of the nuclear outcome of commercial GB-derived cell lines (A172, LN-229, or U251-MG) and non-commercial GB-derived cells, including samples from a GB primary tumor (#04) and a GB relapse (#12) after gossypol treatment. Additionally, we also treated the cells with staurosporine.

By staining the chromatin with Hoechst, we observed that gossypol was triggering a similar nuclear outcome among the different glioblastoma cells employed (**Figure R9A**). As described for the LN-18 cell line, this coincided with a pleiotropically nuclear phenotype with an average percentage of around 20-25% of type II nuclear morphologies (**Figure R9B**). By contrast, dissimilar nuclear alterations were observed between glioblastoma cells after staurosporine treated. Indeed, this alkaloid, previously reported in LN-18 cells to deficiently trigger the type II nuclear morphology, induced an average percentage of 40% of type II nuclear morphologies in cells such as A172 and LN-229 (**Figure R9C**).

Note that, although not graphically represented, values obtained in non-treated cells were lower than 0,76% for the type II nuclear morphology and lower than 2% for the scored type III nuclear morphology.

7. Type II-like nuclear morphologies are triggered upon staurosporine treatment in glioblastoma cells

To better characterize the nuclear morphologies observed in some glioblastoma cells when challenged with staurosporine, we decide to perform an ultrastructural analysis.

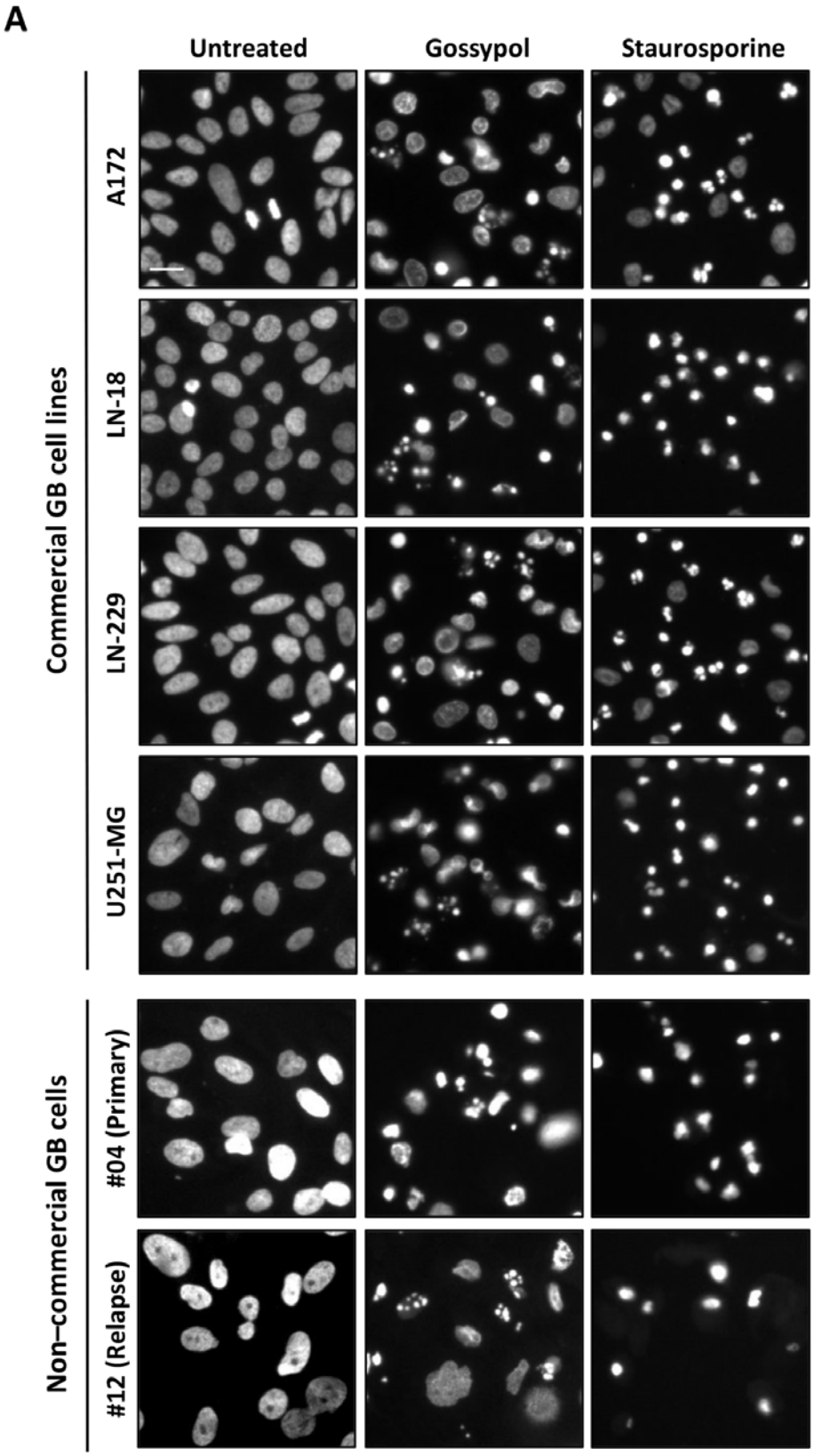

FIGURE R9. For figure legend, see next page.

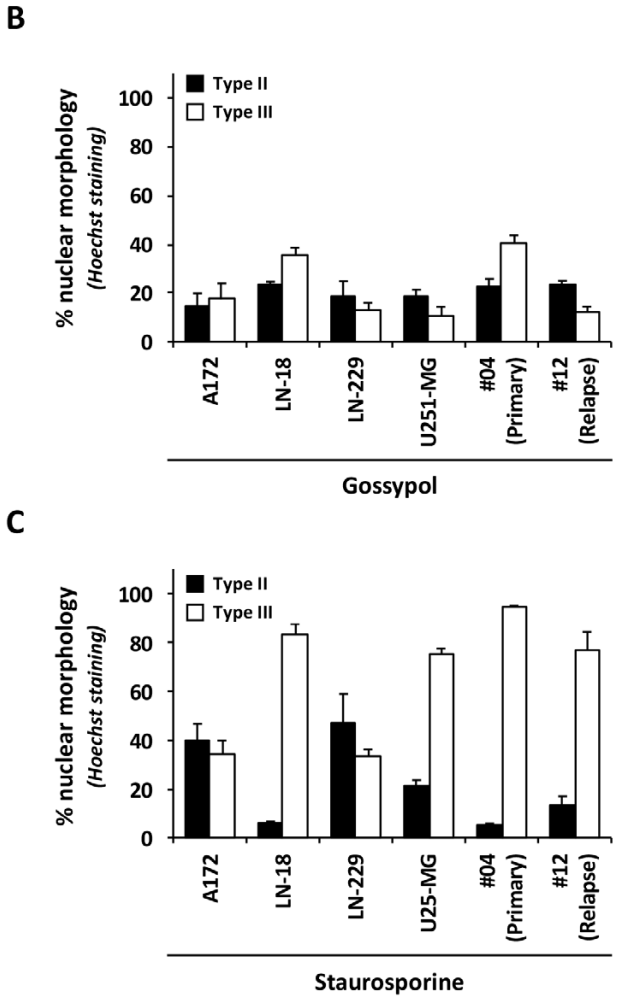

FIGURE R9. Commercial and non-commercial (primary or relapse)-derived glioblastoma cells display nuclear fragmentation upon gossypol treatment. Commercial and non-commercial glioblastoma (GB) cells were treated with 1 μM staurosporine, 100 μM gossypol, or left untreated for 24 hours. After 24 hours, cells were fixed and nuclear morphology was analyzed by staining the nuclei with Hoechst 33258. Images were obtained with a Nikon ECLIPSE TE2000-E microscope equipped with UV-light epifluorescence and a Hamamatsu ORCA-ER photographic camera. **A**, representative microphotographs of each condition are shown. Scale bar = 20 μm. **B**, **C**, Nuclei of each condition were scored either as type II *(black bars)* or type III (*white bars*). Percentages of each nuclear morphology are represented by bar graphs ± *SEM* (*error bars*).

The analysis of these morphologies through electron microscopy revealed that A172 and LN-229 cells display chromatin condensation and fragmentation without fragmentation of the nuclear envelope. This observation was in sharp contrast with the nuclear morphology observed upon gossypol treatment (**Figure R8**). As shown in **Figure R8,** *left lower image*, several small-size masses of compacted chromatin were observed after gossypol treatment due to both chromatin compaction and nuclear fragmentation in LN-18 cells. As shown in **Figure R10**, the same compartment, delimited by the nuclear envelope, surround the

chromatin condensed masses triggered upon staurosporine treatment in A172 and LN-229 cells. We referred to this nuclear morphology as type II-like nuclear morphology.

The classical type II nuclear morphology is shown in **Figure R10** (*lower panel*). This image corresponds to apoptotic-proficient SH-SY5Y cells challenged with staurosporine and was presented in the Doctoral thesis of María Sánchez Osuna. Further images showing classical apoptotic type II nuclear morphologies are shown in **Figure R48**.

In line with the results presented in the Doctoral thesis of María Sánchez Osuna, we conclude that none of the nuclear morphologies found in staurosporine-treated glioblastoma-derived cells completely recapitulate the classical apoptotic nuclear alteration. This lead to the conclusion that gossypol- and none staurosporine-treated glioblastoma cells display apoptotic type II nuclear morphologies.

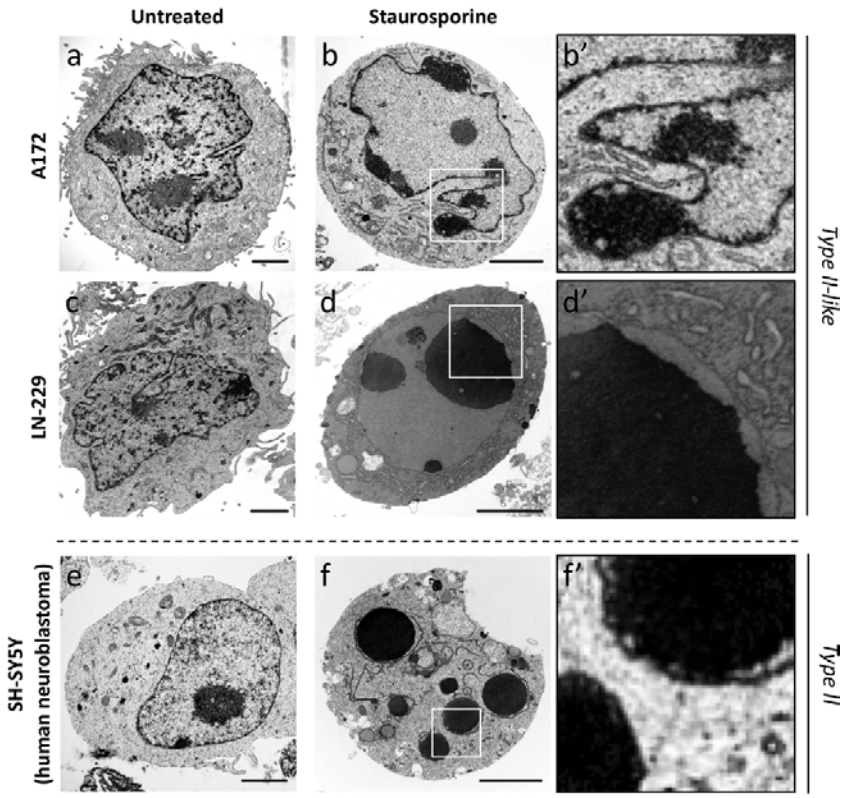

FIGURE R10. Electron microscopy images show type II-like nuclear morphology without nuclear envelope breakage after staurosporine treatment. A172 and LN-229 cells were treated with 1 μM of staurosporine for 10 hours or left untreated. Representative images of transmission electron microscopy are shown. *Right panels* are higher magnifications of staurosporine-treated cells *(middle panels)* Scale bar = 2 μm. Images from SH-SY5Y cells treated with 1 μM of staurosporine for 10 hours are here used as positive controls to show classical type II nuclear morphologies.

8. Reorganization of structural proteins upon gossypol treatment in LN-18 cells

The cleavage of different cellular proteins upon cell death, mainly driven by caspases, is required for cytoskeleton reorganization, nuclear condensation, and DNA fragmentation. To study the nuclear breakdown and the reorganization of the cytoskeleton, we proceeded with the immunofluorescent staining of some well-characterized proteins that participate in these processes.

Emerin is a serine-rich integral inner nuclear membrane (INM) protein of the nuclear envelope, anchored to lamins, and implicated in the nuclear structure and the chromatin architecture regulation. The binding of emerin to lamins is required for the proper localization of emerin at the nuclear envelope (Koch and Holaska, 2014).

As shown in **Figure R11,** untreated cells displayed perinuclear staining of emerin with some spicular structures inside the nucleus of LN-18 cells. By contrast, when looking at gossypol-induced type II nuclear morphology, emerin staining appeared disorganized surrounding small-size masses of compacted chromatin or was no longer detected in some fragmented nuclei. Indeed, dotted staining of emerin seemed to be emerin remnants detected before the complete dismantling of emerin (**Figure R11**, *middle panel corresponding to gossypol images)*. In the case of type III nuclear morphologies, emerin seemed to be less disorganized and to preserve better the perinuclear staining of emerin around the chromatin masses. Morphologies not coinciding with type II or type III nuclear morphologies presented longer spicular projections crossing the nucleus. By contrast, both type II and type III nuclear morphologies, either from gossypol or staurosporine treatment, showed excluded emerin from the nuclei. This result suggest that nuclear exclusion of emerin may be required for chromatin condensation, either as type III or as type II (**Figure R11**).

Because actin microfilaments are tightly regulated upon cell death, we wondered whether a different organization of actin was triggered after gossypol and staurosporine treatment, paying particular attention to type II and type III nuclear morphologies. Thanks to the development of fluorescently-labeled phalloidin consisting of a bicyclic peptide (which binds F-actin) coupled with Alexa Fluor 647 (which provides far-red fluorescence) actin cytoskeletal structures can be easily followed.

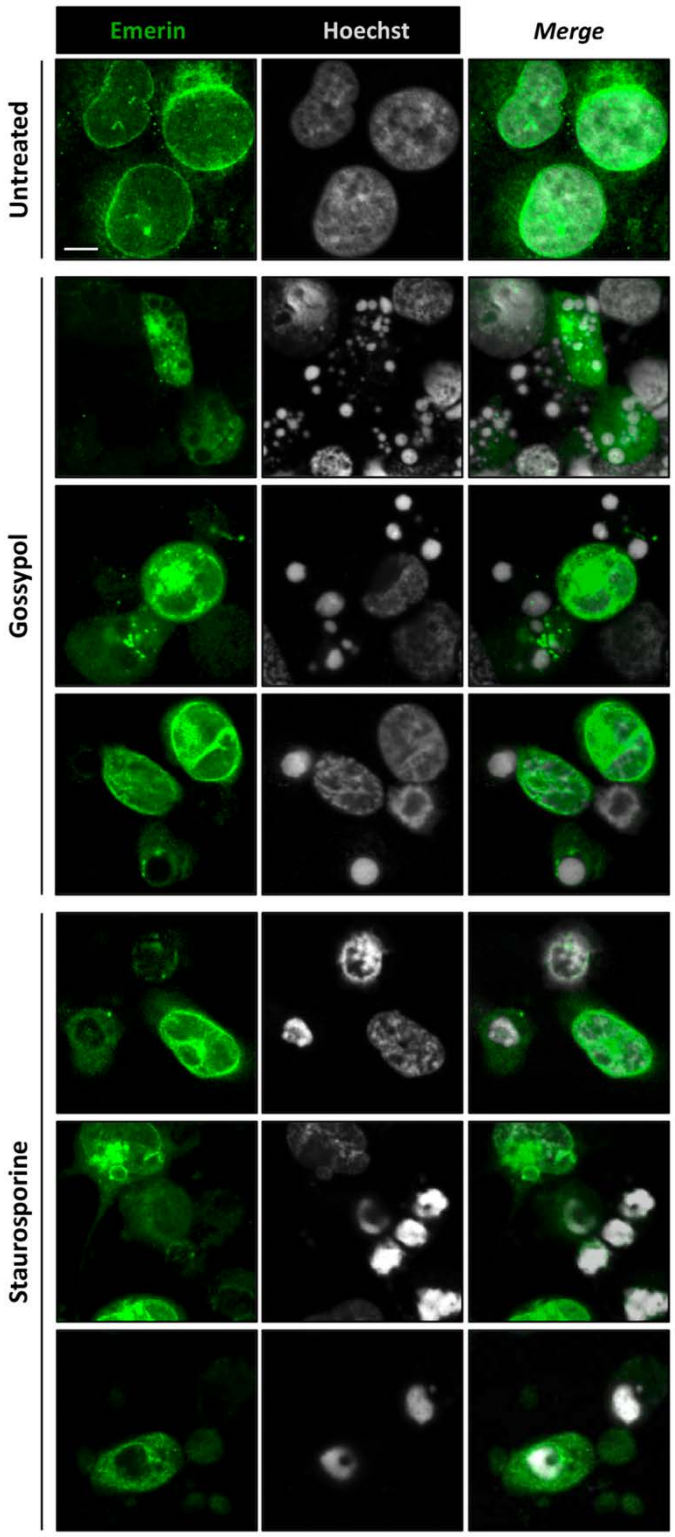

FIGURE R11. Structural changes of emerin upon gossypol or staurosporine treatments in LN-18 cells. LN-18 cells were treated with 100 μM of gossypol, 1 μM of staurosporine, or left untreated for 12 hours. After treatment, cells were fixed and immunostained with a specific antibody against emerin (green) (*left panel*) according to *Material and Methods*. Nuclei (gray) were stained with Hoechst 33258 (*middle panel*). Images were obtained with a laser confocal microscope (Zeiss LSM 700, Carl Zeiss) and the specific confocal software (ZEN, Carl Zeiss). Detailed microphotographs of each condition are shown. Scale bar = 10 μm.

As shown in **Figure R12**, staurosporine seemed to induce a more prominent disassembly and depolymerization of actin filaments than gossypol. However, this general conclusion was no longer fully reflective of what observed when looking at type II nuclear morphologies. Nuclear morphologies showing chromatin condensation and fragmentation coincided with absence or depolymerized actin filament. Moreover, phalloidin staining also suggested a sarcophagus shape structure adopted by type III-triggered morphology upon staurosporine treatment.

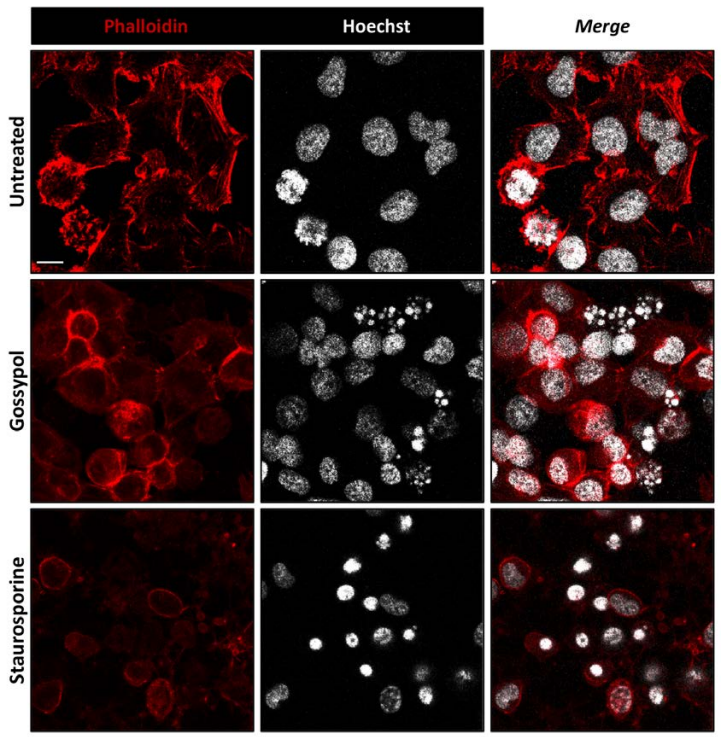

FIGURE R12. Effect of gossypol or staurosporine treatments on actin organization in LN-18 cells. LN-18 cells were treated with 100 µM of gossypol, 1 µM of staurosporine, or left untreated for 6 hours. After treatment, cells were fixed and stained with Alexa Fluor^{647}-phalloidin (red) (*left panel*) according to *Material and Methods*. Nuclei (gray) were stained with Hoechst 33258 (*middle panel*). Images were obtained with a laser confocal microscope (Zeiss LSM 700, Carl Zeiss) and the specific confocal software (ZEN, Carl Zeiss). Representative microphotographs of each condition are shown. Scale bar = 20 µm.

Moreover, we also analyzed CD44 and Id1. CD44 is a cell surface marker that plays a role in cell-cell interactions, adhesion, and migration. The cytoplasmic domain of CD44 has been involved in the coordination of signaling pathways that promote actin-mediated cytoskeleton reorganization (Bourguignon *et al.*, 2004). Id1 (inhibitor of DNA-binding protein) is a transcription factor with no DNA binding activity that negatively regulates the DNA-binding and transcriptional activation capacity of basic helix-loop-helix proteins. CD44 and Id1 have been described as markers of glioma-initiating cells (also called glioma stem cells) and to confer poor prognosis in glioblastoma patients (Anido *et al.*, 2010).

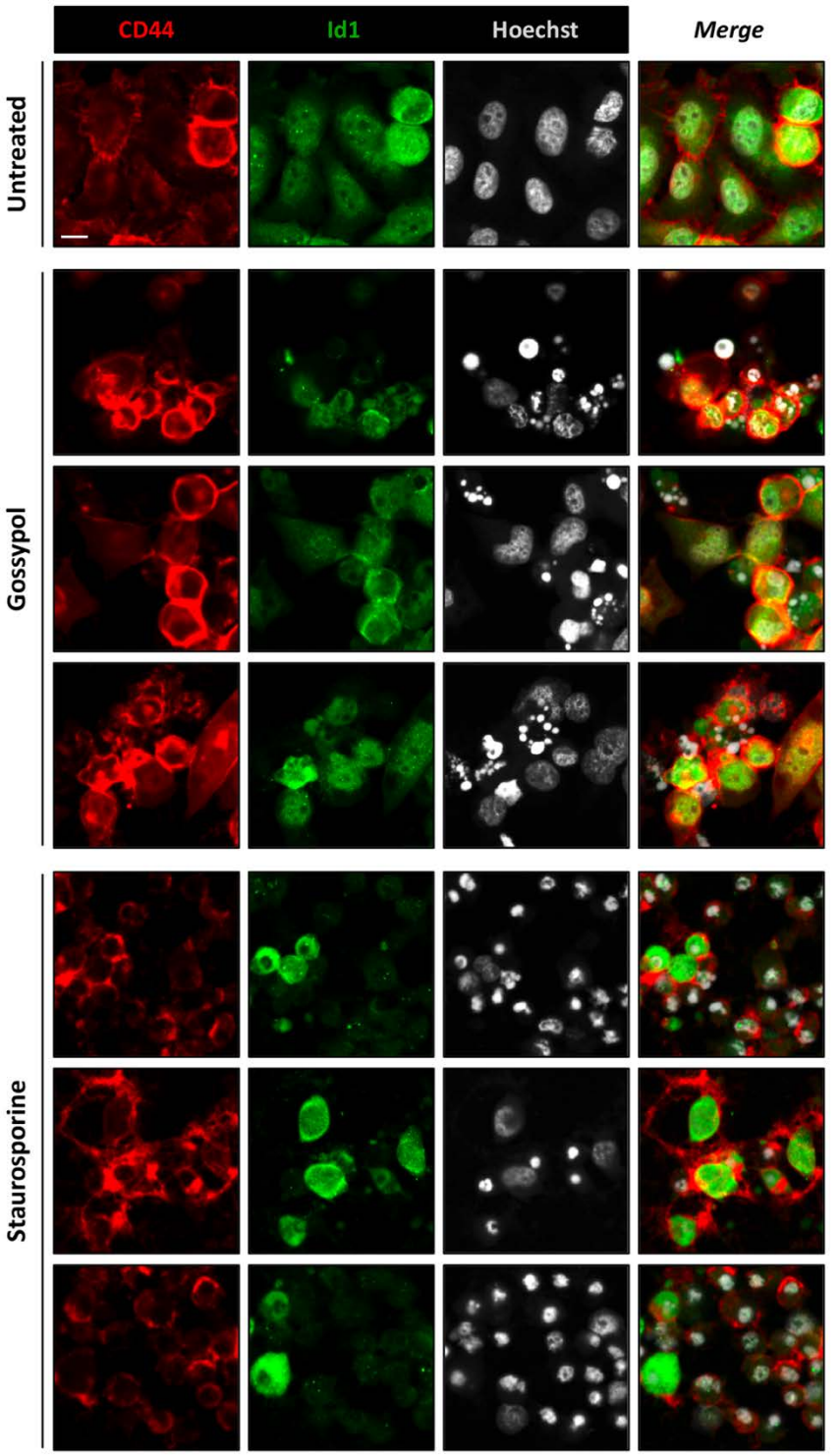

FIGURE R13. Effect of gossypol or staurosporine treatments on CD44 and Id1 cellular distribution in LN-18 cells. LN-18 cells were left untreated or treated with 100 µM of gossypol or 1 µM of staurosporine for 12 hours. After treatment, cells were fixed and immunostained with a specific antibody against CD44 (red) or Id1 (green) according to *Material and Methods*. Nuclei (gray) were stained with Hoechst 33258. Images were obtained with a laser confocal microscope (Zeiss LSM 700, Carl Zeiss) and the specific confocal software (ZEN, Carl Zeiss). Detailed microphotographs of each condition are shown. Scale bar = 20 µm.

In **Figure R13,** the general view of CD44 staining coincides, like in **Figure R12** (phalloidin staining), with higher disorganization in staurosporine-treated cells than gossypol-treated cells. More specifically, the long and relaxed projections of CD44 connecting different untreated LN-18 cells appeared as concentric and geometric layers in gossypol-treated LN-18 cells (**Figure R13**), and as dilated and enlarged structures surrounding the nucleus in staurosporine-treated cells. Regarding Id1, untreated cells showed nuclear staining, whereas Id1 was excluded from the nuclei or even completely dismantled in type II and type III nuclear morphologies (**Figure R13**).

Although interesting observations can be discussed from these results, to extrapolate a direct causal connection strictly differing between type II and type III nuclear morphologies, by only looking at structural proteins, results challenging. To find additional clues to understand the mechanism behind this nuclear outcome, we performed a biochemical analysis of the apoptotic pathway triggered upon gossypol treatment.

9. Gossypol induces a caspase-dependent nuclear fragmentation

To address whether caspases were implicated in the formation of gossypol-induced type II nuclear morphology, we took advantage of the pan-caspase inhibitor q-VD-OPh.

As shown in **Figure R14**, the type II nuclear morphology induced by gossypol was inhibited by q-VD-OPh. Likewise, gossypol-induced type III nuclear morphology was also inhibited in the presence of q-VD-OPh. The inhibition of type III nuclear morphology induced by staurosporine in LN-18 cells was previously described by our group (Sanchez-Osuna *et al.*, 2014). Thus, we concluded that type II and type III nuclear morphologies induced either by gossypol or staurosporine (here used as positive control) in LN-18 cells depend on caspase activation.

Although slightly different between gossypol and staurosporine-treated cells, the principal nuclear morphology observed after challenging LN-18 cells with these stimuli in the presence of q-VD-OPh coincided with peripheral compaction of the chromatin below the nuclear envelope. These caspase-independent nuclear morphologies were not further studied in detail. Hereafter, we focused our interest in the caspase-dependent type II and type III nuclear morphologies.

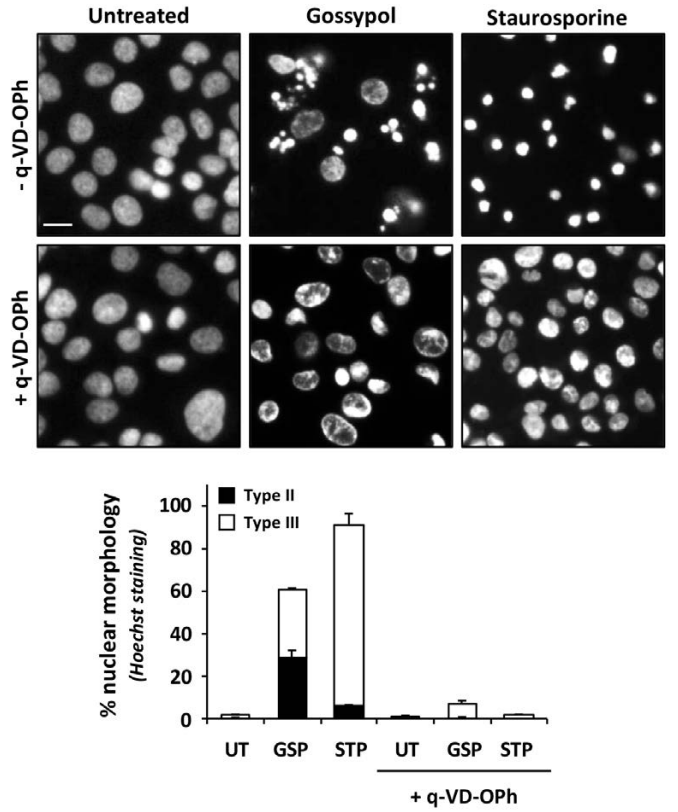

FIGURE R14. Gossypol-induced type II nuclear morphology is caspase-dependent. LN-18 cells were treated with 1 μM staurosporine (STP) or 100 μM gossypol (GSP) in the presence (+) or absence of the pan-caspase inhibitor q-VD-OPh (q-VD) (20 μM). After 24 hours of treatment, cells were fixed and nuclear morphology was analyzed by staining the nuclei with Hoechst 33258. Images were obtained with a Nikon ECLIPSE TE2000-E microscope equipped with UV-light epifluorescence and a Hamamatsu ORCA-ER photographic camera. Representative microphotographs of each condition are shown. Scale bar = 20 μm. Nuclei of each condition were scored either as type II *(black bars)* or III (*white bars*). Percentages of each nuclear morphology are represented by bar graphs ± *SEM* (*error bars*).

10. DFF40/CAD endonuclease is necessary for the type II apoptotic nuclear morphology induced by gossypol in LN-18 cells

Once confirmed that gossypol-induced nuclear morphologies are caspase-dependent, and because of DFF40/CAD is described as responsible for the apoptotic nuclear morphology, we wondered whether DFF40/CAD was involved in these morphological alterations. To address that question, we proceed with the RNA silencing of the endonuclease in LN-18 cells. Levels of DFF40/CAD were assessed by Western blot (**Figure R15A**). Then, we analyzed the apoptotic nuclear changes and scored the percentage of type II and type III nuclear morphologies induced by gossypol in NR siRNA-transfected and CAD siRNA-transfected LN-18 cells.

As shown in **Figure R15A**, type II, but not type III, nuclear morphologies were affected by the knockdown of the endonuclease. Therefore, we conclude that this type III nuclear phenotype observed in gossypol-treated LN-18 cells does not depend on the action of the DFF40/CAD. These results go along with the idea that DFF40/CAD is implicated in type II nuclear morphology but not in type III (Yuste *et al.*, 2005b) (Sanchez-Osuna *et al.*, 2014).

Furthermore, we took advantage of SH-SY5Y wild-type and stably-transfected cells with the empty vector (pcDNA3) or single mutant form $hICAD_L$-D117E to determine the relevance of ICAD in the nuclear apoptotic changes triggered by gossypol. Forced expression of $hICAD_L$-D117E single mutant prevented type II nuclear morphology from gossypol and (as previously presented in (Yuste *et al.*, 2005b)) from staurosporine-treated cells. As shown in **Figure R15B**, the type II apoptotic nuclear morphologies were allowed upon gossypol and staurosporine in both wild-type and stably-transfected cells with the empty vector (pcDNA3) SH-SY5Y cells. Protein extracts were obtained from untreated and treated cells, and levels of ICAD were assessed by Western blot. The overexpression of single mutant $hICAD_L$-D117E is evident by looking at $ICAD_L$ expression levels of untreated (UT) SH-SY5Y $hICAD_L$ D117E cells, higher than in SH-SY5Y pcDNA3 cells (**Figure R15B**).

Altogether, these results demonstrated that the type II nuclear morphology observed in glioblastoma cells after gossypol treatment is entirely dependent on the caspase-triggered ICAD cleavage and DFF40/CAD activation. More importantly, we concluded that limited amounts of DFF40/CAD in human glioblastoma-derived cells are sufficient to trigger canonical type II nuclear morphology when dying cells are adequately primed.

We have previously reported that the overexpression of DFF40/CAD did not change the type III nuclear outcome of LN-18 cells after staurosporine treatment (Sanchez-Osuna *et al.*, 2014). Indeed, the gain function experiment was insufficient to enable LN-18 cells to display type II apoptotic nuclear morphologies upon staurosporine treatment. However, we asked whether DFF40/CAD-dependent type II nuclear morphologies, triggered by gossypol in human DFF40/CAD deficient GB-derived cells, could be affected by the overexpression of the endonuclease. Therefore, we stably transfected LN-18 cells with the eukaryotic expression plasmid (pcDNA3) carrying the ORF of human CAD (hCAD) or with the empty vector (mock). Expression levels of DFF40/CAD were assessed by Western blot (**Figure R16A**). After 24 hours of gossypol treatment, levels of karyorrhexis were assessed by fixing the cells and staining the nuclei with Hoechst 333258. CAD-overexpressing LN-18 cells presented a slightly higher percentage of type II nuclear morphologies than mock-transfected cells.

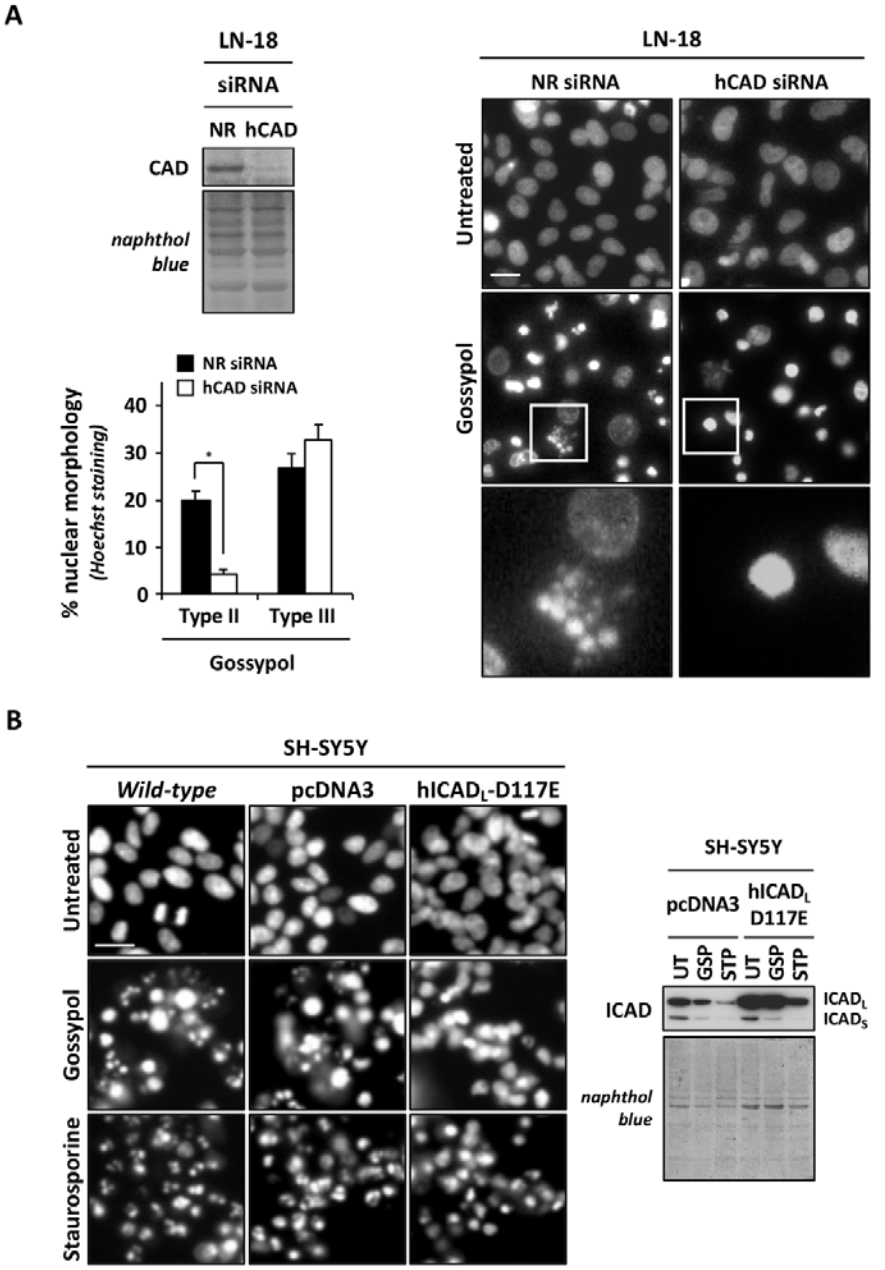

FIGURE R15. Gossypol triggers DFF40/CAD-dependent type II nuclear morphologies. A, LN-18 cells were transfected with non-relevant (NR) siRNA or DFF40/CAD (hCAD) siRNA (see *Materials and Methods*). Total protein extracts from untreated cells were analyzed by Western blot to confirm the down-regulation of DFF40/CAD. Then, cells were untreated or treated with 100 μM gossypol and fixed after 24 hours of treatment. Nuclear morphology was analyzed by staining the nuclei with Hoechst 33258. Type II and type III nuclear morphologies were scored and the corresponding percentage was represented in a bar graph (means ± *SD*) (*error bars*)). Images were obtained with a Nikon ECLIPSE TE2000-E microscope equipped with UV-light epifluorescence and a Hamamatsu ORCA-ER photographic camera. Representative microphotographs of each condition are shown. The bottom panels are higher magnifications of the cells framed in the middle panel. Scale bar = 20 μm. The Student's *t*-test was used to determine the statistical significance (* means $p < 0.05$). **B**, SH-SY5Y wild-type cells, transfected with empty vector (pcDNA3) or with the caspase non-degradable hICAD$_L$-

D117E single mutant were treated with 100 μM gossypol (GSP), 1 μM staurosporine (STP) or left untreated (UT). After 24 hours of treatment, nuclear morphology was analyzed by staining the nuclei with Hoechst 33258. Images were obtained with a Nikon ECLIPSE TE2000-E microscope equipped with UV-light epifluorescence and a Hamamatsu ORCA-ER photographic camera. Representative microphotographs of each condition are shown. Scale bar = 20 μm. Igepal CA-630-soluble protein extracts were obtained after 9 hours of treatment and Western blotting against ICAD was performed to corroborate its overexpression. Naphthol blue staining served as a protein loading control (**A**, **B**).

Besides this observation, gossypol was still inducing a limited percentage of type II nuclear morphologies pleiotropically with other nuclear outcomes such as the type III nuclear morphology (**Figure R16B**). Thus, indicating that although the typical apoptotic nuclear morphology is a manifestation of the activity of DFF40/CAD, the endonuclease is not the only limiting requirement impairing the induction of a homogenous type II nuclear phenotype. Therefore, it seems to suggest that additional molecular factors may be governing apoptotic type II nuclear morphology in glioblastoma cells.

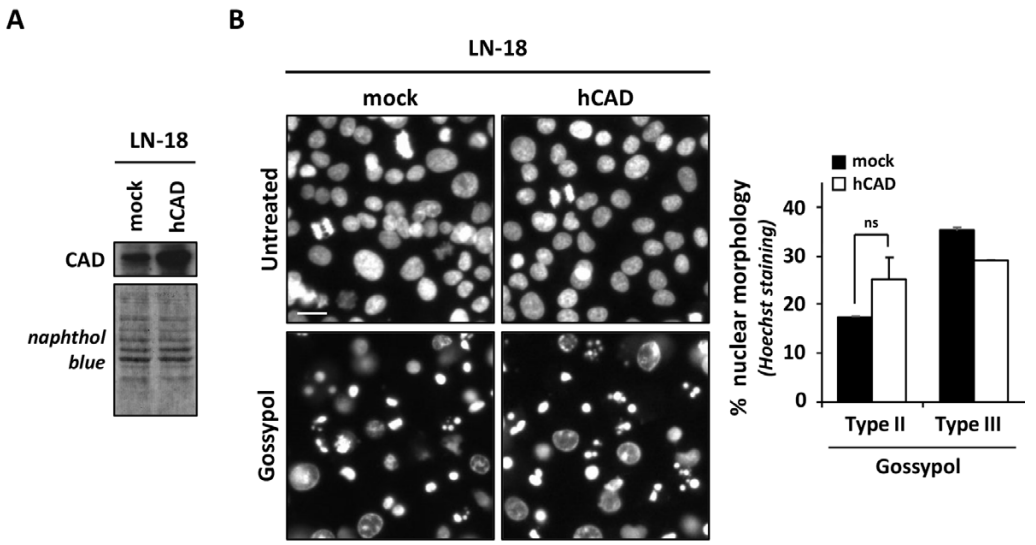

FIGURE R16. DFF40/CAD overexpression does not significantly modify gossypol-induced type II nuclear morphology. LN-18 cells were stably transfected with the human ORF of DFF40/CAD (hCAD) (NM_004402) or with the empty vector (mock). **A**, protein was extracted from untreated cells, and Western blotting against CAD was performed to corroborate the overexpression of the endonuclease. Naphthol blue staining served as a protein loading control. **B**, cells were treated with 100 μM gossypol or left untreated and fixed after 24 hours. Nuclear morphology was analyzed by staining the nuclei with Hoechst 33258. The percentage of type II or type III nuclear morphology was calculated and the graph represents the means ± *SD* (*error bars*). The Student's *t*-test was used to determine the statistical significance (ns means not significant). Images were obtained with a Nikon ECLIPSE TE2000-E microscope equipped with UV-light epifluorescence and a Hamamatsu ORCA-ER photographic camera. Representative microphotographs of each condition are shown. Scale bar = 20 μm.

11. Caspase-3 is required for type II-gossypol induced nuclear morphology

Since gossypol induces caspase-dependent type II and type III nuclear morphologies (**Figure R14**), we decided to explore the biochemical effects of gossypol in more detail. First, we took advantage of MCF-7 cells, a cellular model null for caspase-3. As shown in **Figure R17A**, type II nuclear morphology was impaired when treating MCF-7 cells with gossypol. Hence, indicating that caspase-3 is strictly necessary to induce type II nuclear morphology upon gossypol treatment. The slight percentage of type II nuclear morphology induced by staurosporine in LN-18 cells was also impaired in MCF-7 staurosporine-treated cells.

The absence of caspase-3 in MCF-7 cells was corroborated by Western blot. As shown in **Figure R17B** (*first panel*), no caspase-3 was detected in any of the MCF-7 loaded samples. As a positive control of caspase-3 expression and processing into its active p17 fragment, we used protein extracts from LN-18 cells treated with staurosporine. Our group did previously report that upon treatment with this potent cytotoxic insult, ICAD is efficiently degraded in LN-18 cells (Sanchez-Osuna *et al.*, 2014). This degradation of the inhibitor of CAD and its cleavage generating the p11 fragment was not observed either after gossypol or staurosporine treatment in MCF-7 (**Figure R17B**, *second panel*). Regarding DFF40/CAD, the endonuclease protein levels were lower in LN-18 cells compared to MCF-7 cells (**Figure R17B**, *third panel*).

Furthermore, while the addition of staurosporine to the culture medium of LN-18 cells induced an increase in DEVD-directed caspase-activity, here used as a positive control of the technique, no signs of DEVDase activity were detected in any of the conditions of the MCF-7 cells (**Figure R17B**).

The use of q-VD-OPh and MCF-7 cells evidenced a key role of caspase-3 in executing the nuclear outcome induced upon gossypol treatment. Since the caspase-3/ICAD/CAD axis constitutes the minimal system regulating the final steps of apoptosis, we asked whether a different caspase-3 processing or ICAD degradation was induced upon gossypol or staurosporine treatment in LN-18 cells. As shown in **Figure R18**, gossypol and staurosporine treatment resulted in the generation of the p19 and p17 fragment. This last, corresponding to the fully mature caspase-3. Moreover, the processing of procaspase-3 into the p19 and p17 fragments was inhibited in the presence of the pan-caspase inhibitor, q-VD-OPh. Only the p20 subunit corresponding to residual procaspase-3 processing was found in LN-18 cells treated with gossypol or staurosporine in the presence of q-VD-OPh (**Figure R18**, *first panel*). Regarding ICAD degradation, we detected the p11 fragment, which corresponds to the C-terminal fragment of $ICAD_L$, after both treatments (**Figure R18**, *second panel*).

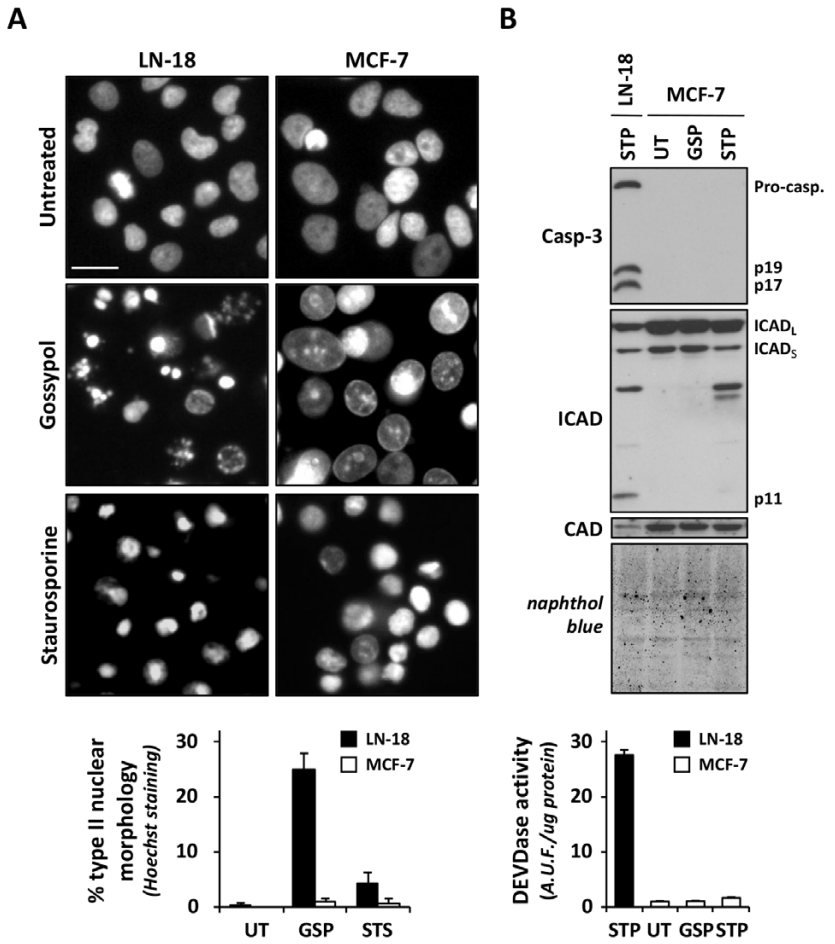

FIGURE R17. Caspase-3 is required for the type II nuclear morphology induced by gossypol. LN-18 and MCF-7 cells were left untreated (UT) or treated with 1 μM staurosporine (STP) or 100 μM gossypol (GSP). **A**, after 24 hours of treatment, cells were fixed and nuclear morphology was analyzed by staining the nuclei with Hoechst 33258. Images were obtained with a Nikon ECLIPSE TE2000-E microscope equipped with UV-light epifluorescence and a Hamamatsu ORCA-ER photographic camera. Representative microphotographs of each condition are shown. Scale bar = 20 μm. The percentage of type II nuclear morphology is represented by mean ± *SD* (*error bars*). **B**, after 9 hours of treatment, cells were detached and Igepal CA-630-soluble protein extracts were obtained. Protein levels of caspase-3, ICAD, and CAD were analyzed through Western blot. Naphthol blue staining served as a protein loading control. The same protein extracts were used to perform a DEVDase activity assay. *A.U.F.* corresponds to arbitrary units of fluorescence. Graphs represent the fold induction when compared to lysates from untreated cells (UT) ± *SD* (*error bars*). LN-18 cells treated with STP were used as a positive control.

Moreover, no significant differences in the levels of DFF40/CAD and no signs of degradation were observed between both treatments (**Figure R18**, *third panel*). In parallel, DEVDase activity was performed. Igepal CA-630-soluble protein extracts were obtained from LN-18 cells untreated or treated with gossypol, or staurosporine in the presence or absence of q-VD. As shown in **Figure R18**, a substantial increase in DEDVase-directed caspase activity was detected upon 9 hours of staurosporine or gossypol treatment. Note that higher values of

arbitrary units of fluorescence (A.U.F.) per microgram of protein were obtained in staurosporine-treated samples.

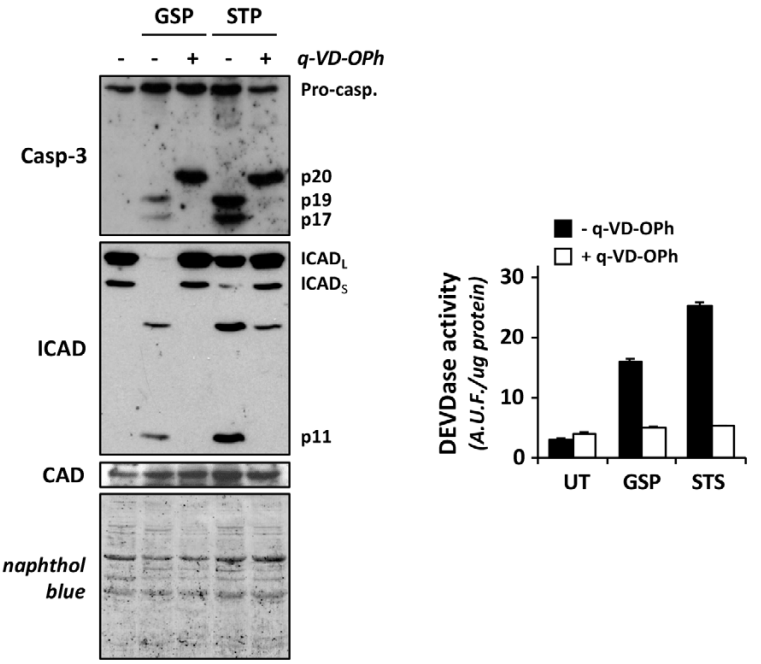

FIGURE R18. The Caspase-3/ICAD/CAD axis is correctly activated upon gossypol treatment in LN-18 cells. LN-18 cells were treated with 100 μM gossypol (GSP), 1 μM staurosporine (STP) or left untreated ± q-VD-OPh (20 μM) for 12 hours. After treatment, cells were detached and Igepal CA-630-soluble protein extracts were obtained. Western blotting against caspase-3, ICAD, and CAD were performed. Naphthol blue staining served as a protein loading control. DEVDase activity was measured and graphed by arbitrary units of fluorescence (A.U.F.) when compared to lysates from untreated cells.

12. Initiator and executioner caspases become activated after gossypol treatment

To complete the analysis of caspases, we looked at the processing of the initiator caspase-9 and the executioner caspase-7 and -6 after gossypol treatment in the presence or absence of q-VD-OPh. By Western blot, we observed that gossypol induced the processing of caspase-9 to its active fragments p37 and p35. In the presence of q-VD-OPh caspase-3-cleavage p37 fragment was inhibited. However, we still observed the p35 fragment from caspase-9. Thus, indicating a less powerful inhibitory effect of q-VD-OPh over initiator caspases (**Figure R19**, *left upper panel*). Concerning executioner caspases, caspase-7 processing to its active fragment p20 was detected upon both treatments after 12 hours (**Figure R19**, *right upper panel*). Likewise, the processing of caspase-6 to its p18 activation fragment was also detected (**Figure R19**, *right upper panel*). The presence of q-VD-OPh avoided this caspase-mediated cleavage.

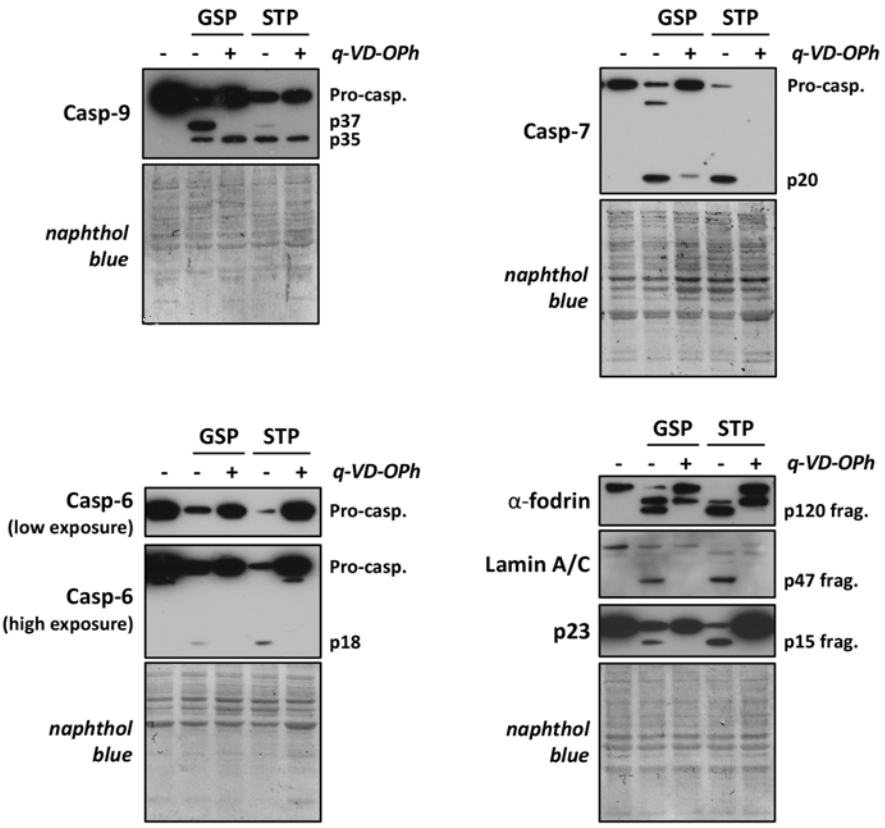

FIGURE R19. Initiator and executioner caspases are activated upon gossypol treatment in LN-18 cells. LN-18 cells were left untreated or treated 12 hours with 100 μM gossypol (GSP) or 1 μM staurosporine (STP) ± the pan-caspase inhibitor q-VD-OPh (20 μM). After treatment, cells were detached and Igepal CA-630-soluble protein extracts were obtained. Western blotting against the initiator caspase-9, and the executioner caspases-7 and -6 were performed. The activation of caspase-3, -6, or -7 was corroborated by the detection of p120 (α-fodrin), p47 (lamin A/C), and p15 (p23) proteolytic fragments, respectively. α-fodrin, lamina A/C and p23 co-chaperon are specific substrates of the executioner caspases -3, -6, and -7, respectively. Naphthol blue staining served as a protein loading control.

Additionally, the caspase specific cleavage of different substrates was also assessed by Western blot (**Figure R19**, *right lower panels*). The caspase-3-mediated p120 fragment of α-fodrin confirmed the activation of this executioner caspase after gossypol or staurosporine treatment. The p47 fragment indicated cleavage of lamins by caspase-6. The processing of p23 co-chaperone to a p15 fragment, a specific event mediated by active caspase-7 (Walsh *et al.*, 2008), corroborated the correct activation of this protease. The addition of q-VD-OPh avoided the caspase-mediated cleavage of those substrates observed upon gossypol or staurosporine treatment in LN-18 cells.

Although we have reported cleavage of executioner and initiator caspases in either gossypol or staurosporine-treated LN-18 cells, the global view of **Figure R18** and **Figure R19**,

suggested a higher intensity cleavage of caspases upon staurosporine treatment than upon gossypol treatment. Because those Western blots were only a reflection of 12 hours of treatment, we decided to perform a time-course and assess the processing of initiator and executioner caspases after 3, 6, and 9 hours of treatment. Western blots against the initiator caspase-9 and executioner caspases (caspase-7 and caspase-6) are shown in **Figure R20**. Staurosporine-induced caspase-9 cleavage to its p35 and p37 fragments, as well as caspase-7 processing to its p20 fragment were detected from 3 hours of treatment. The pro-form of caspase-6 was highly processed from 6 hours and above. By contrast, we barely detect caspase processing before 9 hours of gossypol treatment. Thus, results from **Figure R20** exclude an earlier cleavage of caspases upon gossypol treatment compared to staurosporine-treated LN-18 cells.

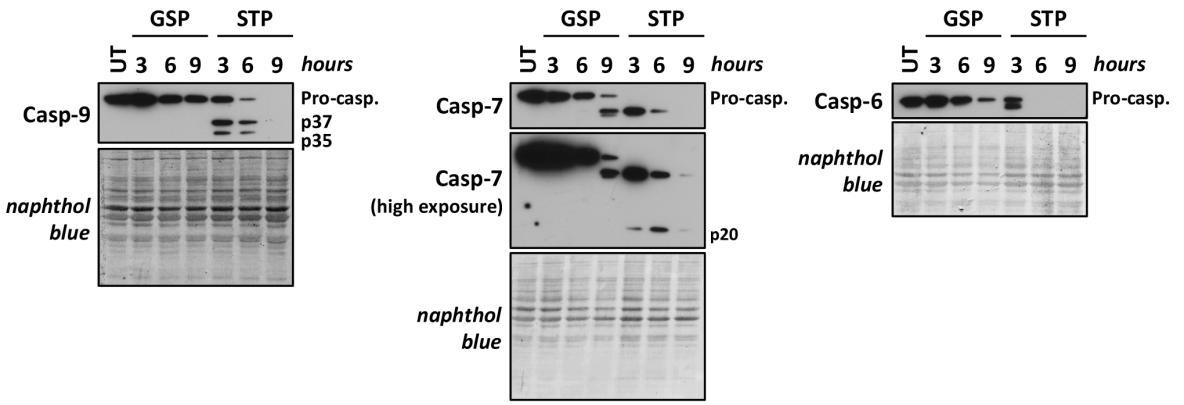

FIGURE R20. Caspase cleavage is detected at earlier times after staurosporine than gossypol treatment in LN-18 cells. LN-18 cells were left untreated or treated with 100 μM gossypol (GSP) or 1 μM staurosporine (STP) for 3, 6, or 9 hours (h). After treatment, cells were detached and Igepal CA-630-soluble protein extracts were obtained. Western blotting against the initiator caspase-9 (Casp-9), and the executioner caspase-7 (Casp-7), and -6 (Casp-6) were performed. Naphthol blue staining served as a protein loading control.

To experimentally answer if a higher and earlier caspase processing was related with type III nuclear morphologies, we decided to analyze the processing of caspases, and ICAD after the treatment with the combination of gossypol and TRAIL. As shown in **Figure R21**, type II nuclear morphology is detected at a higher percentage after this combinatorial approach than after its use as single agents. The processing of caspases was analyzed by Western blot after 6 hours of treatment. Staurosporine-treated LN-18 cells were used as positive controls of proper caspase and ICAD cleavage. As shown in **Figure R22A**, cleavage of caspase-9 to its active p37 and p35 fragments was evident upon TRAIL and staurosporine treatment. In the case of gossypol plus TRAIL (G + T), although active fragments were slightly detected, the pro-caspase form was totally processed. This higher processing of the pro-form was also observed when blotting against caspase-8 and ICAD. The cleavage of caspase-8 to its p43 and

p41 fragments was observed after TRAIL, staurosporine, and after gossypol and TRAIL cotreatment (**Figure R22A**).

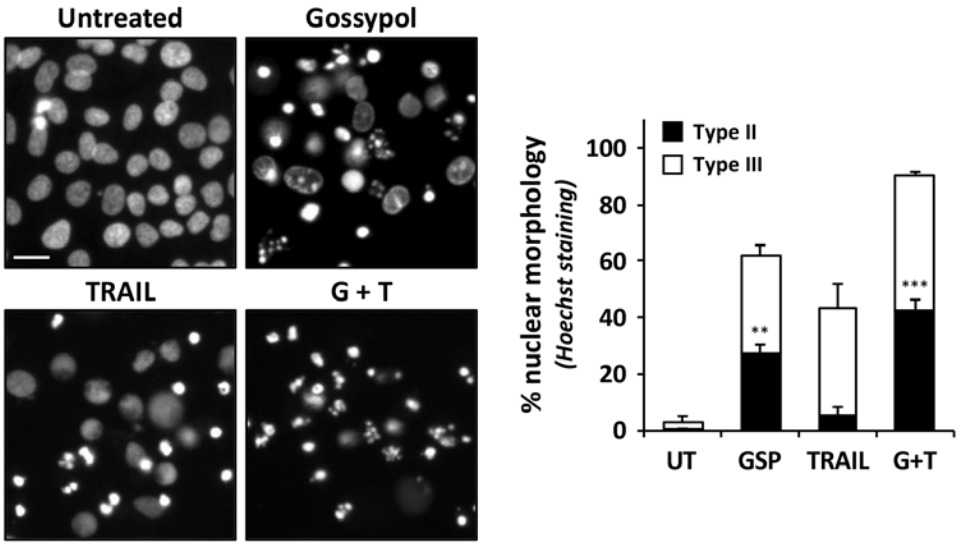

FIGURE R21. The combination of gossypol and TRAIL increases the percentage of both type II and type III nuclear morphologies in LN-18 cells. LN-18 cells were treated with 100 μM gossypol (GSP), 200 ng/ml TRAIL, with the combination of gossypol plus TRAIL (G+T) or left untreated (UT). After 24 hours of treatment, cells were fixed and nuclear morphology was analyzed by staining the nuclei with Hoechst 33258. Images were obtained with a Nikon ECLIPSE TE2000-E microscope equipped with UV-light epifluorescence and a Hamamatsu ORCA-ER photographic camera. Representative microphotographs of each condition are shown. Scale bar = 20 μm. The percentage of type II *(black bars)* and type III (*white bars*) nuclear morphology was calculated. The graph represents the mean ± *SEM* (*error bars*). One-way ANOVA test was used to determine the statistical significance between groups regarding type II [$F(3,9) = 32.53, p < 0.0001$]. The significance of the type II value of each treatment versus untreated was determined by the post hoc Tukey's test (** means $p < 0.01$) (*** means $p < 0.005$).

Moreover, the analysis of executioner caspases evidenced slight processing of caspase-3-mediated cleavage of α-fodrin to its p120 fragment and cleavage of $ICAD_L$ to its p24 fragment after gossypol treatment. By contrast, cleavage of α-fodrin to the p120 fragment and the processing of ICAD to its p11 were strongly detected after staurosporine treatment. As shown in **Figure R22B**, although a slightly p11 fragment was observed upon G+T, almost no non-processed ICAD was detected. Overall, these results indicate a prominent degradation of the inhibitor of DFF40/CAD after gossypol plus TRAIL cotreatment, and points to this combinatorial approach (G+T) as the most effective treatment to trigger caspase activation in LN-18 cells, as well as, type II nuclear morphology.

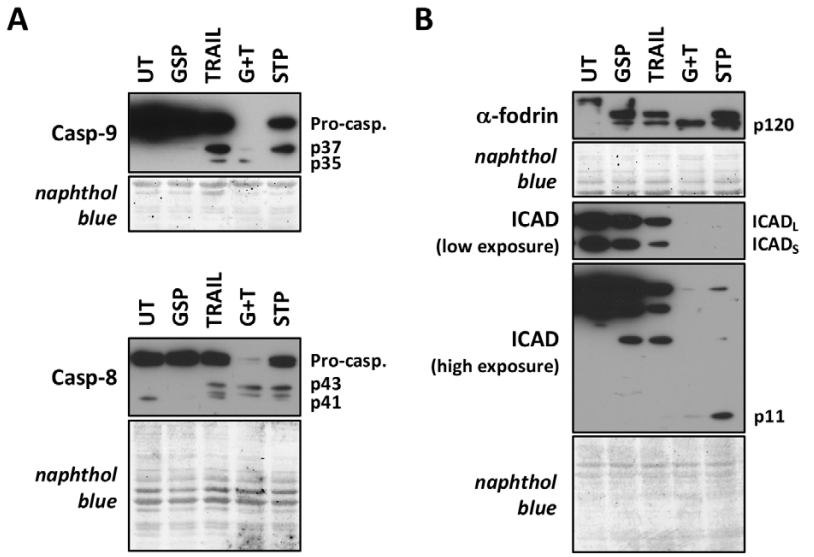

FIGURE R22. The combination of gossypol and TRAIL potentiates the processing of caspases and ICAD cleavage in LN-18 cells. LN-18 cells were treated with 100 μM gossypol (GSP), 200 ng/ml TRAIL, with the combination of gossypol plus TRAIL (G+T) or left untreated (UT). After 6 hours of treatment, cells were detached and Igepal CA-630-soluble protein extracts were obtained. Staurosporine (STP) (1 μM) was included as a positive control of caspases and ICAD cleavage. Western blotting against caspase-9 (Casp-9), caspase-8 (Casp-8) were performed (**A**). The specific caspase-3 substrate (α-fodrin) and ICAD were also analyzed (**B**). Naphthol blue staining served as a protein loading control (**A**,**B**).

Due to the low detection of the pro-forms or the active fragments of either caspase-9, -8 or ICAD, after 6 hours of treatment with gossypol plus TRAIL (**Figure R22**), we decide to analyze the caspase processing induced by this combinatorial approach at earlier times. Additionally, as cytochrome *c* is a crucial regulatory apoptotic factor triggering the activation of caspases, we asked whether a differential release of cytochrome *c* was detected over timer. We proceeded with digitonin-soluble protein extracts obtained from untreated or treated LN-18 cells with either gossypol, TRAIL, gossypol plus TRAIL, or staurosporine, after the indicated times (1, 3, or 6 hours). The last lane corresponds to Igepal CA-630-soluble protein extracts from 6 hours staurosporine-treated LN-18 cells and was here used as a positive control. The release of cytochrome *c* was evident after 3 and 6 hours of G+T and staurosporine treatment. Moreover, we analyzed caspase-9 and caspase-7 were analyzed as representatives initiator and executioner caspases, respectively. Both caspases were cleaved from 3 hours of treatment with TRAIL, gossypol plus TRAIL, and staurosporine treatment to its active fragments p37 and p35, and its p20 active fragment, respectively (**Figure R23**).

Overall, we concluded that each treatment's potency to activate caspases does not correlates with the nuclear changes observed. While a more higher processing of caspases is triggered by staurosporine compared to gossypol, staurosporine is less efficient at inducing nuclear

fragmentation than gossypol. On the contrary, the combinatorial treatment of gossypol plus TRAIL, which induces similar or even more processing of caspases and ICAD than staurosporine, it does trigger type II nuclear morphologies more efficiently than the alkaloid. Hence, a higher caspase processing does not seem to correlate with the presence or absence of type II nuclear morphologies in LN-18 cells.

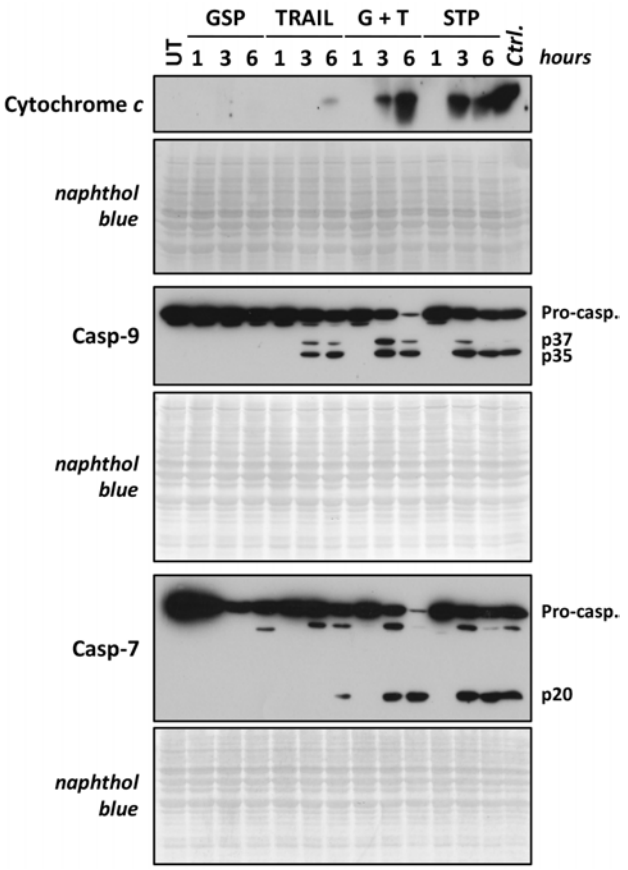

FIGURE R23. Cytochrome *c* release and caspase-9 and -7 processing are similar between staurosporine and the cotreatment of gossypol and TRAIL. LN-18 cells were treated with 100 μM gossypol (GSP), 200 ng/ml TRAIL, with the combination of gossypol plus TRAIL (G+T), 1 μM staurosporine (STP) or left untreated for the indicated times. After treatment, cells were detached and digitonin-soluble protein extracts were obtained according to *Material and Methods*. Igepal CA-630-soluble protein extract, obtained from LN-18 cells treated with staurosporine for 6 hours, was used as a positive control *(Ctrl.)*. Western blotting against cytochrome *c*, caspase-9 (Casp-9), and caspase-7 (Casp-7) were performed. Naphthol blue staining served as a protein loading control.

13. Gossypol-induced caspase-dependent nuclear morphologies are observed in *Bax*/*Bak* double-knockout cells

The activation of caspases upon staurosporine treatment, as well as the final steps of apoptosis triggered by the alkaloid, has been described to rely on the activation of BAX and BAK, two

pore-former proteins from the BCL-2 family proteins. More specifically, double-deficient cells for *Bax* and *Bak* were reported to be resistant to multiple apoptotic stimuli, including staurosporine, which acts through disruption of mitochondrial function (Lindsten *et al.*, 2000) (Wei *et al.*, 2001). Thus, we asked whether the same mechanism was necessary for gossypol to trigger type II nuclear morphologies in LN-18 cells. With this aim, we challenged wild-type (wt) and *Bax*/*Bak* double-knockout (DKO) mouse embryonic fibroblasts (MEFs) with gossypol or staurosporine in the presence or absence of the pan-caspase inhibitor, q-VD-OPh (q-VD). Then, by fixing the cells and staining the nuclei with Hoechst, we assessed the nuclear outcome after 24 hours of treatment.

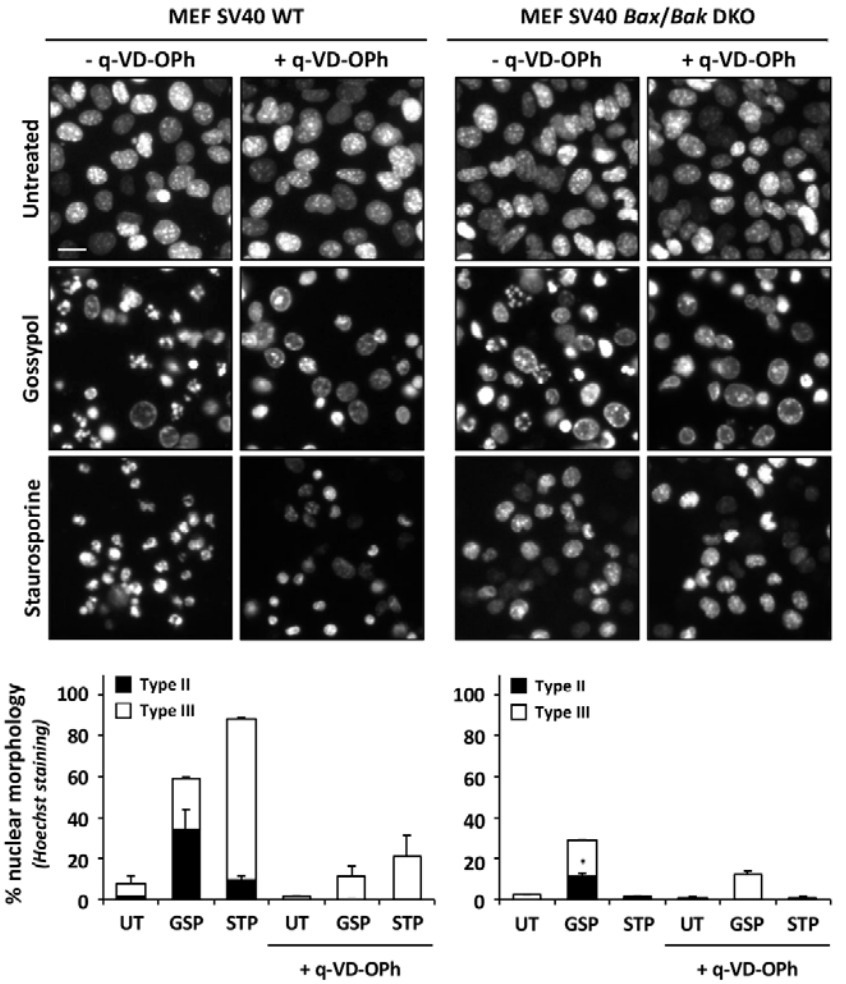

FIGURE R24. Type II and type III nuclear morphologies are partially rescued in gossypol-treated Bax/Bak DKO MEFs. Wild-type (wt) and Bax/Bak double-knockout (DKO) SV40 immortalized mouse embryonic fibroblasts (MEFs) were left untreated (UT) or treated with 100 μM gossypol (GSP) or 1 μM staurosporine (STP). Treatments were performed in the presence (+) or absence of the pan-caspase inhibitor q-VD-OPh (q-VD) (20 μM). After 24 hours of treatment, cells were fixed and nuclear morphology was analyzed by staining the nuclei with Hoechst 33258. Images were obtained with a Nikon ECLIPSE TE2000-E microscope equipped with UV-light epifluorescence and a Hamamatsu ORCA-ER photographic camera. Representative

microphotographs of each condition are shown. Scale bar = 20 μm. Nuclei of each condition were scored either as type II *(black bars)* or III (*white bars*). Percentages of each nuclear morphology are represented by bar graphs ± *SEM* (*error bars*). The Student's *t*-test was used to determine the statistical significance (* means $p < 0.05$).

As shown in **Figure R24**, the nuclear morphologies observed after staurosporine treatment in wt MEFs were inhibited in DKO *Bax/Bak* cells treated with the same alkaloid. After treating wt MEFs with gossypol, type II nuclear morphologies were observed pleiotropically with other nuclear phenotypes including type III nuclear morphology. The addition of q-VD-OPh inhibited both type II and type III nuclear morphologies triggered either by gossypol or staurosporine in wt MEFs. More interestingly, when treating *Bax/Bak* DKO MEFs with gossypol, type II and type III caspase-dependent morphologies were observed, despite with a lower frequency. Therefore, with the result from **Figure R24**, we confirmed that type II nuclear morphology triggered by gossypol is caspase-dependent but may occur independently of BAX and BAK. Up to this point, we have identified caspase-dependent, DFF40/CAD-dependent, and BAX/BAK-independent but caspase-dependent type II apoptotic nuclear morphologies upon gossypol treatment.

As shown in **Figure R25A**, the knockdown of *Bax* and *Bak* in double-knockout (DKO) SV40 immortalized mouse embryonic fibroblasts (MEFs) was corroborated by Western blotting. Furthermore, we obtained Igepal CA-630-soluble protein extracts from wt and *Bax/Bak* DKO MEFs, treated with gossypol or staurosporine in the presence or absence of q-VD-OPh, and performed a Western blot against α-fodrin.

Figure R25B indicates that the cleavage of α-fodrin to its p120 fragment was detected after staurosporine treatment in wt MEFs and was avoided when using the same alkaloid in *Bax/Bak* DKO MEFs. By contrast, the p120 fragment observed in wt MEFs after gossypol treatment was not avoided in *Bax/Bak* DKO MEFs. As expected, this caspase-mediated cleavage of α-fodrin detected after 10 hours of treatment was avoided in the presence of q-VD-OPh in any of the cells and treatments employed (**Figure R25B**).

We also assessed DEVDase activity on cells. As shown in **Figure R25C**, the addition of gossypol to the culture medium of wt MEFs induced an slight increase in the DEVDase activity (compared with untreated wt MEFs). DEVDase activity was higher after staurosporine treatment. By contrast, we barely detected DEVDase activity after staurosporine treatment in *Bax/Bak* DKO MEFs, but we observed an increase in the DEVDase activity after treating these cells with gossypol. As expected, either gossypol- or staurosporine-triggered DEVDase activity was rescued in the presence of q-VD-OPh (**Figure R25C**). Thus, by looking at p120 fragment, which is an indicator of caspase-3 processing,

together with results obtained with the DEVDase activity assay, we can conclude that caspase-3 can be activated upon gossypol treatment in a BAX/BAK-independent manner.

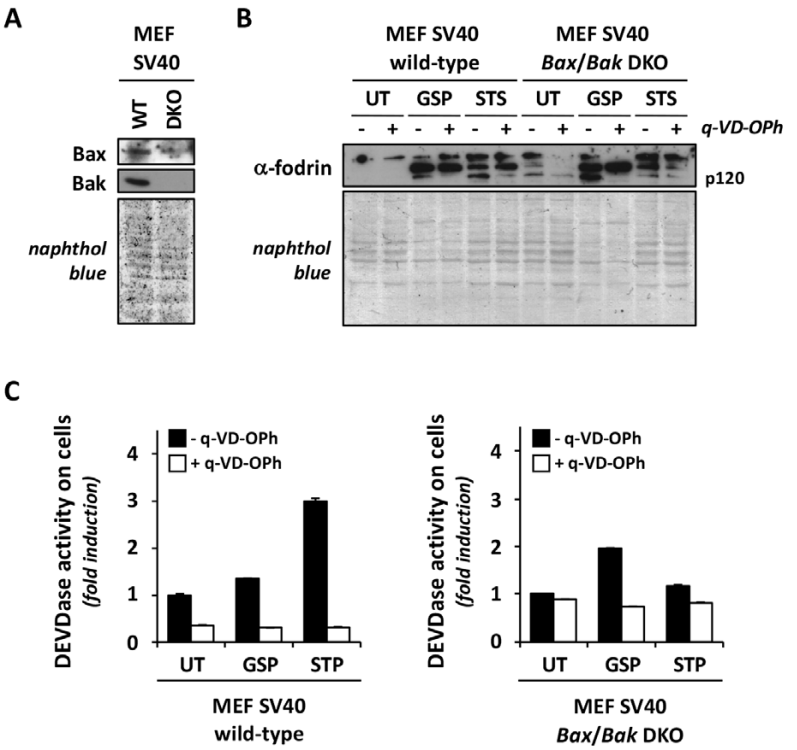

FIGURE R25. Caspase-3 is also activated upon gossypol treatment in *Bax/Bak* double-knockout (DKO) mouse embryonic fibroblasts (MEFs). A, total protein extracts were obtained from untreated cells and Western blotting against Bax and Bak was performed to corroborate the absence of Bax and Bak in DKO SV40 MEFs. **B**, **C**, wild-type (WT) and Bax/Bak DKO SV40 MEFs were left untreated (UT) or treated with 100 μM gossypol (GSP) or 1 μM staurosporine (STP). Treatments were performed in the presence (+) or absence (-) of the pan-caspase inhibitor q-VD-OPh (q-VD) (20 μM). **B**, Igepal CA-630-soluble protein extracts were obtained after 10 hours of treatment. Western blot was performed against α-fodrin (specific caspase-3 substrate). Naphthol blue staining served as a protein loading control (**A**, **B**). **C**, DEVDase activity was performed directly on cells after 10 hours of treatment. Graphs represent the fold induction from the untreated cells (UT) ± *SD* (*error bars*).

14. Differential processing of the minimal system regulating the final steps of apoptosis

In line with the differential processing of caspase-9, -7 and -6 observed over time upon gossypol or staurosporine treatment, we decided to analyze the minimal system regulating the final steps of apoptosis at different time points. Hence, LN-18 cells were treated with gossypol for 6, 9, and 12 hours and caspase-3/ICAD/CAD axis was analyzed by Western blot. LN-18 cells treated with staurosporine for 6 hours were used as positive controls.

As shown in **Figure R26A** (*upper panel*), after 12 hours of treatment, caspase 3 was activated, leading to the emergence of its active p17 fragment. The p19 fragment, which was also observed after 12 hours of gossypol, corresponds to the large subunit of the pro-caspase-3 together with a partial processed pro-domain. It is worth mentioning that despite treating LN-18 cells with gossypol for longer times, caspase-3 processing was always lower than the cleavage observed upon staurosporine treatment. In this line, similar results were observed with the time course analysis of ICAD processing upon gossypol treatment. The p11 fragment, corresponding to the c-terminal of $ICAD_L$ was detected from 9 hours of treatment (**Figure R26A**, *middle panel*). As mentioned above, the detection of this fragment, which results from the specific caspase-3 cleavage of ICAD at the Asp^{224} site, confirmed the correct hydrolysis of ICAD upon gossypol treatment. Although gossypol was more efficient at processing the pro-forms of $ICAD_{L/S}$, this did not correlate with higher detection of p11 fragment. DFF40/CAD, the last element of the axis, responsible for the DNA degradation in eukaryotic cells, was also analyzed by Western blot. As shown in **Figure R26A** (*lower panel*), no evident differences were observed upon treatment with gossypol when analyzing the expression of the endonuclease DFF40/CAD in LN-18 cells.

In parallel with the caspase-3/ICAD/CAD axis analysis through Western blot, we analyzed the activation of caspases using the fluorogenic substrate Ac-DEVD-afc. Extracts from staurosporine-treated LN-18 cells were included as a positive control (**Figure R26B**). Gossypol treatment induced a time-dependent increase in DEVD-directed activity; however, the maximal activity detected was lower than the DEVDase activity induced by staurosporine treatment in the same cell line.

In addition to caspase-3, ICAD, and CAD, lamins have been described as critical elements in the nuclear envelope breakdown. This specific substrate of activated caspase-6 constitutes and essential molecules influencing apoptotic nuclear packaging. The Western blot, presented in **Figure R26C**, was performed with digitonin-soluble protein extracts from LN-18 cells treated with gossypol for 6, 9, or 12 hours, or LN-18 cells treated with staurosporine for 6 hours. Western blot against Lamin A/C showed a p37 band upon staurosporine treatment that corresponds to the caspase-6 specific cleavage of Lamin C. A less intense band corresponding to the p37 fragment was detected upon 9 hours of treatment with gossypol. This earlier detection of lamin-released fragments suggested an earlier nuclear envelope breakdown due to an earlier and potent activation of caspases, specifically of caspase-6, upon treatment with staurosporine.

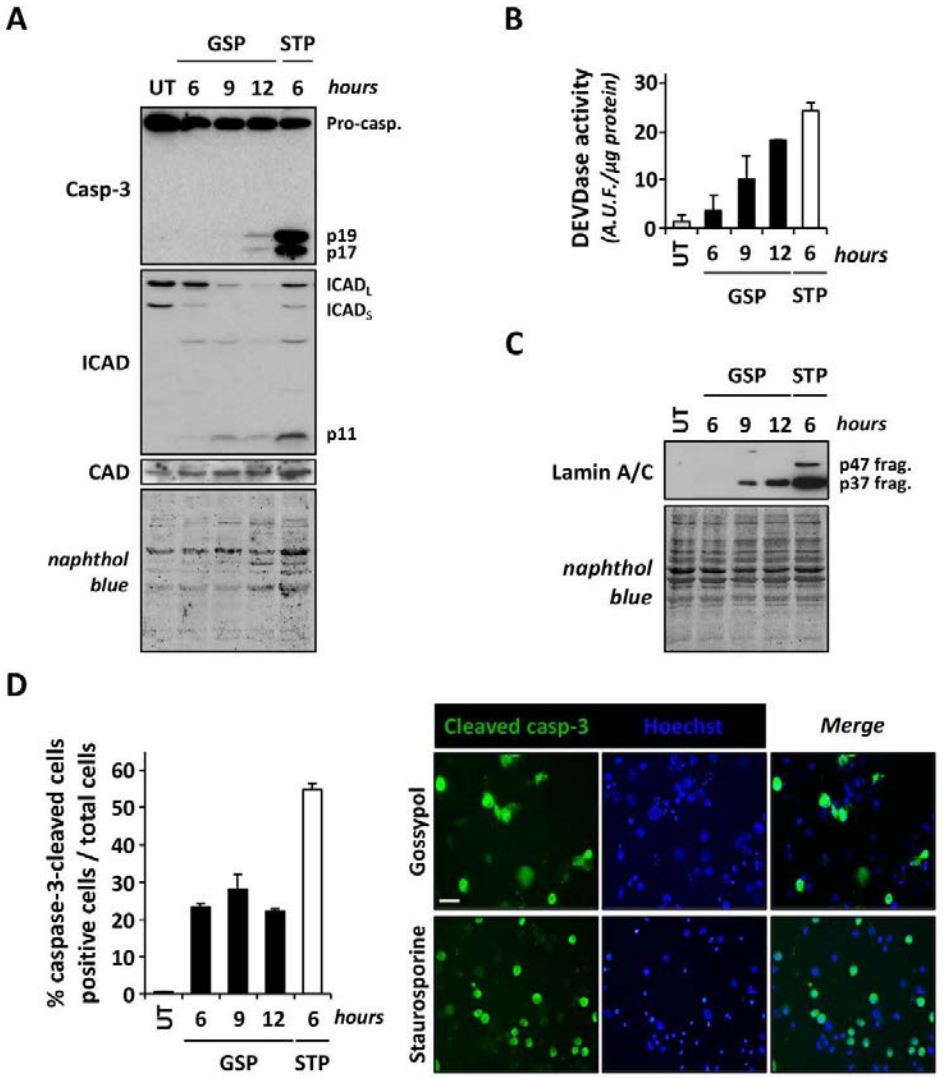

FIGURE R26. The percentage of caspase-3-cleaved positive cells is lower in gossypol-treated than in staurosporine-treated LN-18 cells. LN-18 cells were left untreated (UT) or treated with 100 µM gossypol (GSP) for 6, 9, or 12 hours. LN-18 cells treated for 6 hours with 1 µM staurosporine (STP) were used as a positive control (**A**-**C**). **A**, Igepal CA-630-soluble protein extracts were obtained after the indicated treatments, and Western blotting against caspase-3, ICAD, and CAD were performed. **B**, alternatively, protein extracts were used to perform a DEVDase activity assay. *A.U.F.* corresponds to arbitrary units of fluorescence. Graphs represent the fold induction compared to lysates from untreated cells (UT) ± *SD* (*error bars*). **C**, after treatment, cells were detached and digitonin-soluble protein extracts were obtained according to *Material and Methods*. Western blotting against Lamin A/C was performed. Naphthol blue staining served as a protein loading control (**A**, **C**). **D**, LN-18 cells were treated with gossypol (100 µM) for 6, 9, and 12 hours or with staurosporine (1 µM) for 6 hours. After treatment, cells were fixed and immunostained with a specific antibody against cleaved caspase-3 (Asp175) (green) (*left panel*) according to *Material and Methods*. Nuclei (blue) were stained with Hoechst 33258 (*middle panel*). Images were obtained with a Nikon ECLIPSE 90i microscope equipped with epifluorescence optics, a Nikon DXM1200F photographic camera and ACT-1 software. Positive cells for cleaved caspase-3 (green) were scored. Results are represented as the percentage of caspase-3-cleaved positive cells per total number of cells (blue). Percentages are represented by bar graphs ± *SD* (*error bars*). Representative images after 12 hours of gossypol and 6 hours of staurosporine are shown. Scale bar = 40 µm.

As referred along this section, the analysis of caspases by Western blot showed lower intensity bands in gossypol samples compared to staurosporine samples. With the objective of dismiss a possible influence of the membrane permeability resulting in fragment loss and, consequently, impairing caspase fragment detection upon gossypol treatment, we proceeded with immunofluorescence. As shown in **Figure R7**, experimental procedures that require cell detachment may show different results than those that do not require detachment and proceed by fixing the cells after treatment. Hence, LN-18 cells were treated with gossypol or staurosporine, fixed, and immunostained against cleaved-caspase-3. **Figure R26D**, shows the percentage of caspase-3-cleaved positive cells after 6, 9, or 12 hours of treatment with gossypol. LN-18 cells treated with gossypol at different time points were compared with LN-18 cells treated with staurosporine for 6 hours, the time point of maximal caspase-3 positive cell detection in LN-18 cells. Although not included, 12 hours of treatment with staurosporine in LN-18 cells induced around 42% of caspase-3-cleaved positive cells. This percentage was lower than the 54% detected after 6 hours of staurosporine treatment but higher than the percentage detected after 6, 9, or 12 hours of gossypol (around 25%). Therefore, gossypol either for 6, 9, or 12 hours of treatment is a less potent insult than staurosporine to trigger caspase-3 cleavage. However, despite gossypol is less potent at inducing caspase activation, it is necessary to stress that it is more effective at inducing apoptotic type II nuclear morphologies (**Figure R1**).

Overall, we concluded that the biochemical analysis of caspases itself did not explain the different nuclear outcomes triggered by staurosporine, gossypol, or the treatment of gossypol plus TRAIL. Nevertheless, the activation of DFF40/CAD was confirmed as a bottleneck of type II nuclear morphologies (**Figure R15**). Hence, against this backdrop, we decided to perform an in-depth study of the endonuclease that allows cells to proceed with the final steps of apoptosis.

15. DFF40/CAD distribution is affected upon cell death in LN-18 cells

The cellular subfraction analysis of DFF40/CAD in human glioblastoma-derived cells revealed that this endonuclease mainly accumulates at the nucleoplasmic subcellular compartment in these cells (Sanchez-Osuna *et al.*, 2016). Here, we took advantage of the immunofluorescence of DFF40/CAD to provide an image of the intracellular distribution of the endonuclease in glioblastoma-derived cells. Hence, human glioblastoma-derived LN-18 cells and the proficient apoptotic SH-SY5Y cells were seeded onto 8-wells Lab-Tek chamber slides and immunostained against DFF40/CAD. As shown in **Figure R27**, higher

DFF40/CAD immunoreactivity, presented in red, was detected in SH-SY5Y cells compared to LN-18 cells. This result was consistent with the different total protein levels of DFF40/CAD observed previously by Western blot comparing both cell lines (Sanchez-Osuna *et al.*, 2014). To better determine the distribution of the endonuclease, we took advantage of the RGB profile tool of Image J software to draw the DFF40/CAD (red) and Hoechst (blue) profile plot of confocal images from **Figure R27A. Figure R27B** shows that red profile (DFF40/CAD) coincide within and without the blue profile (Hoechst) in SH-SY5Y, but is mainly detected under the blue profile in LN-18 cells. Thus, concluding that the immunostaining of the endonuclease may be detected in both cytoplasm and nuclei compartment in untreated SH-SY5Y cells, whereas it is confined to the nuclear or perinuclear region in LN-18 cells.

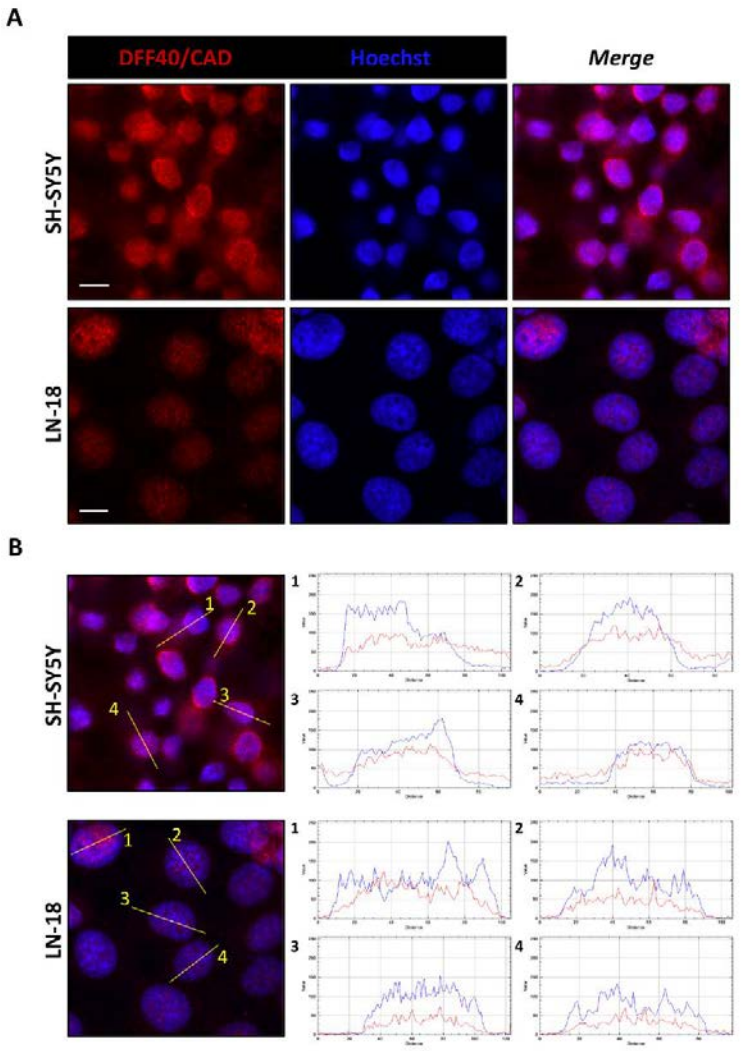

FIGURE R27. DFF40/CAD endonuclease is differentially expressed and distributed between SH-SY5Y and LN-18 cells. SH-SY5Y and LN-18 cells were seeded, fixed and immunostained with a specific

antibody against DFF40/CAD (red) (*left panel*) according to *Material and Methods*. Nuclei (blue) were stained with Hoechst 33258 (*middle panel*). Images were obtained with a Zeiss LSM 700 laser confocal microscope and the specific confocal software (ZEN, Carl Zeiss). Detailed representative confocal scanning images of each condition are shown. Scale bar = 10 μm. **A**, representative microphotographs of each condition are shown. Scale bar = 10 μm. **B**, distribution of DFF40/CAD in different nuclei (*yellow lines*) analyzed by using the RGB profile tool from the Image J software. DFF40/CAD profile is shown in red and Hoechst 33258 staining profile is represented in blue. Microphotographs in **B** corresponds to the same *merge* microphotographs shown in **A** *(right panel)*. The X-axis represents distance along the line and the Y-axis is the pixel intensity. The specific position of the number next to the *yellow lines* indicates the beginning (left side) of the corresponding profile plot indicated with the same number.

According to our interest in the nuclear morphologies displayed in LN-18 cells after treatment, we decided to analyze the intracellular migration of DFF40/CAD endonuclease during apoptosis. Thus, we treated cells with staurosporine and gossypol for 12 hours and proceeded with the immunofluorescence protocol.

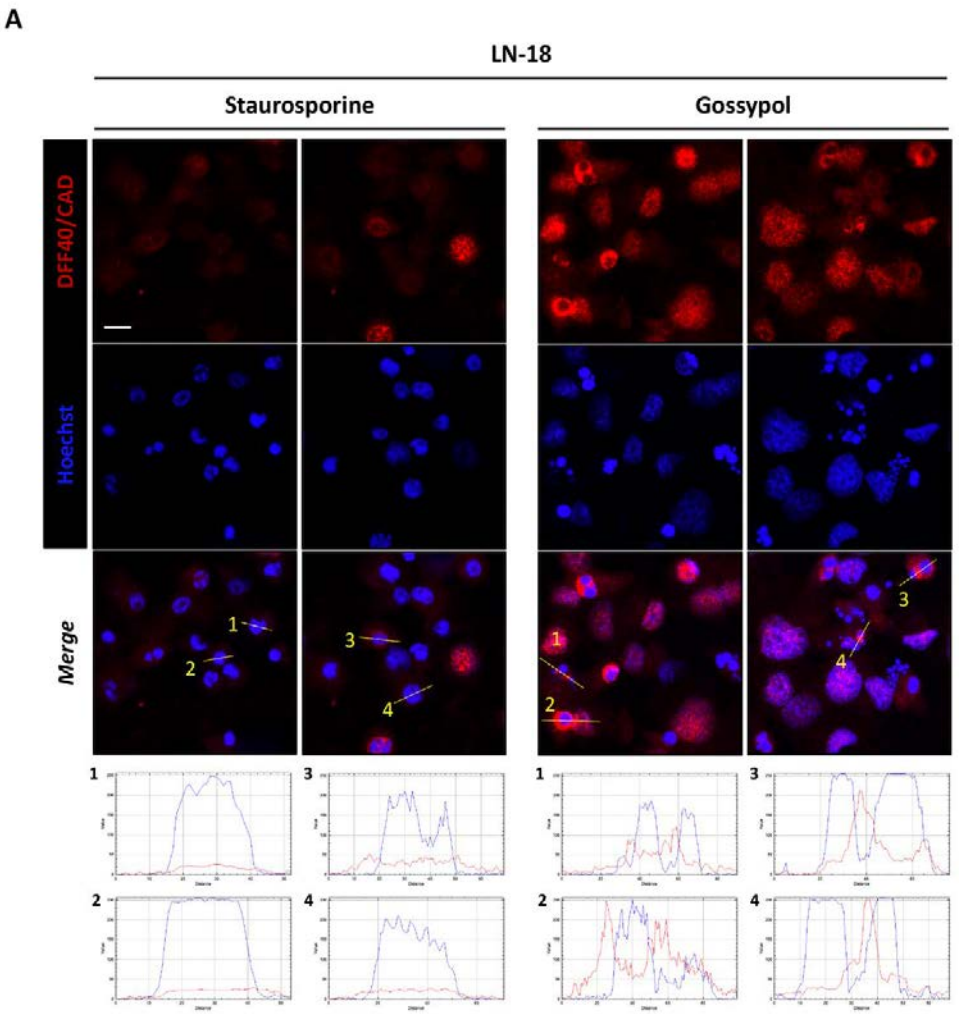

FIGURE R28. For figure legend, see next page.

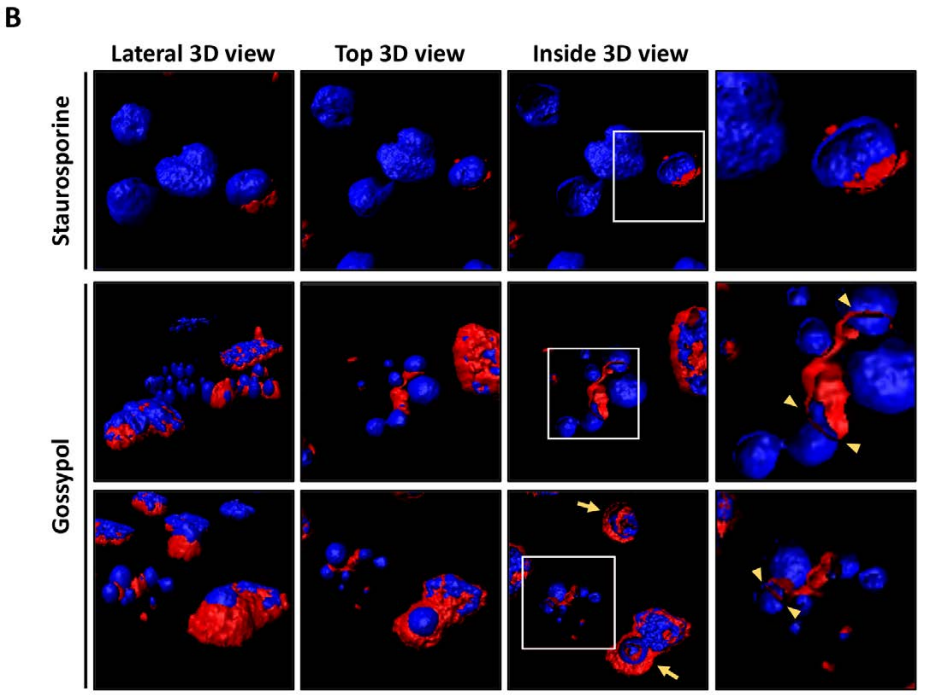

FIGURE R28. Representation of the DFF40/CAD immunoreactivity in LN-18 cells treated with gossypol or staurosporine. LN-18 cells were treated with 100 μM gossypol or 1 μM staurosporine for 12 hours. After treatment, cells were fixed and immunostained with a specific antibody against DFF40/CAD (red) (*left panel*) according to *Material and Methods*. Nuclei (blue) were stained with Hoechst 33258 (*middle panel*). **A**, representative microphotographs of each condition are shown. Scale bar = 10 μm. Distribution of DFF40/CAD in different nuclei (*yellow lines*) were analyzed by using the RGB profile tool from the Image J software. DFF40/CAD profile is shown in red and Hoechst 33258 staining profile is represented in blue. The specific position of the number next to the *yellow lines* indicates the beginning (left side) of the corresponding profile plot indicated with the same number. **B**, Images obtained with a confocal microscope were analyzed with 3D rendering software of Imaris 8.3.4. (Bitplane). Three-dimensional isosurface rendered z-stack confocal images are shown. Inside 3D view (*right panel*) was obtained using the clipping plane tool from the same software. The images next to *right panels* are higher magnification of the cells framed in the *inside 3D view image*. *Filled arrows* point to type III nuclei. *Arrowheads* point to type II nuclei and indicate DFF40/CAD distribution (red) across some masses of DNA (in blue).

As shown in **Figure R28**, low or even no labeling for DFF40/CAD was detected in staurosporine-treated cells. By contrast, gossypol-treated cells displayed higher DFF40/CAD immunostaining. Indeed, RGB profile plots showed that the endonuclease is excluded from type III nuclear morphologies displayed by staurosporine-treated LN-18 cells. DFF40/CAD seems to be also excluded from the nuclei in gossypol-treated cells; however, red peaks beside blue profiles, suggest that DFF40/CAD may be surrounding smaller pieces of highly packed round masses of condensed chromatin. Indeed, type II and type III nuclear morphologies triggered by gossypol seems to maintain the expression of DFF40/CAD, which is in sharp

contrast with the results obtained with staurosporine. Thus, suggesting that different cytotoxic treatments may affect CAD distribution differently.

Stacked, deconvoluted confocal images were next reconstructed using rendering software (Imaris 8.3.4. Bitplane) to generate 3 dimensional (3D) reconstructions of individual cells from **Figure R28A**. 3D isosurface rendered z-stack confocal images evidenced a major loss of DFF40/CAD upon staurosporine treatment compared to gossypol-treated cells (**Figure R28B)**. Moreover, confocal images analyzed with 3D rendering software revealed an attachment of DFF40/CAD to some parts of the DNA (*top 3D view*). The clipping plane tool allowed insight into the inside of the nuclei and evidenced part of DFF40/CAD crossing different small-sized masses of DNA (*inside 3D view*). Alternatively, DFF40/CAD showed a layered structure with the DNA in those nuclei coinciding with a type III nuclear morphology (**Figure R28B**). Overall, suggesting the dissimilar distribution of the endonuclease among the different altered nuclei.

16. Nuclear fragmentation does not correlate with TUNEL positivity either with DNA ladder in LN-18 cells

A classical readout of the endonuclease activity of DFF40/CAD is based on its generation of free 3'-OH group DNA ends (Widlak *et al.*, 2000). It can be detected by labeling with modified nucleotides e.g., FITC-dUTP (see *Material and Methods*). By taking advantage of this experimental approach, best known as TUNEL assay, we wanted to study whether the apoptotic nuclear morphology observed after gossypol treatment in LN-18 cells correlated with the generation of 3'-OH DNA ends. As a positive control, we included SH-SY5Y cells, which are reported to be TUNEL-positive after staurosporine treatment (Iglesias-Guimarais *et al.*, 2013). As shown in **Figure R29A** (*left panel*), TUNEL reactivity was detected in SH-SY5Y cells treated with staurosporine for 9 hours.

When challenging SH-SY5Y cells with gossypol, the percentage of TUNEL-positive cells was lower than after staurosporine treatment (**Figure R29B**). This observation directly correlated with the number of cells displaying type II and type III nuclear morphologies (**Figure R29B**, *left panel*). These results evidenced that both gossypol and staurosporine treatments induces endonuclease activity in SH-SY5Y cells evidenced by the generation of free 3-OH DNA ends.

By contrast, when treating LN-18 cells with gossypol or staurosporine, we barely observed TUNEL positivity (**Figure R29A**). Moreover, we did not detect a correlation between the percentage of TUNEL-positive nuclei and the percentage of nuclear changes indicative of

apoptosis (here visualized by Hoechst staining) observed in gossypol- or staurosporine-treated LN-18 cells (**Figure R29B**, *right panel*).

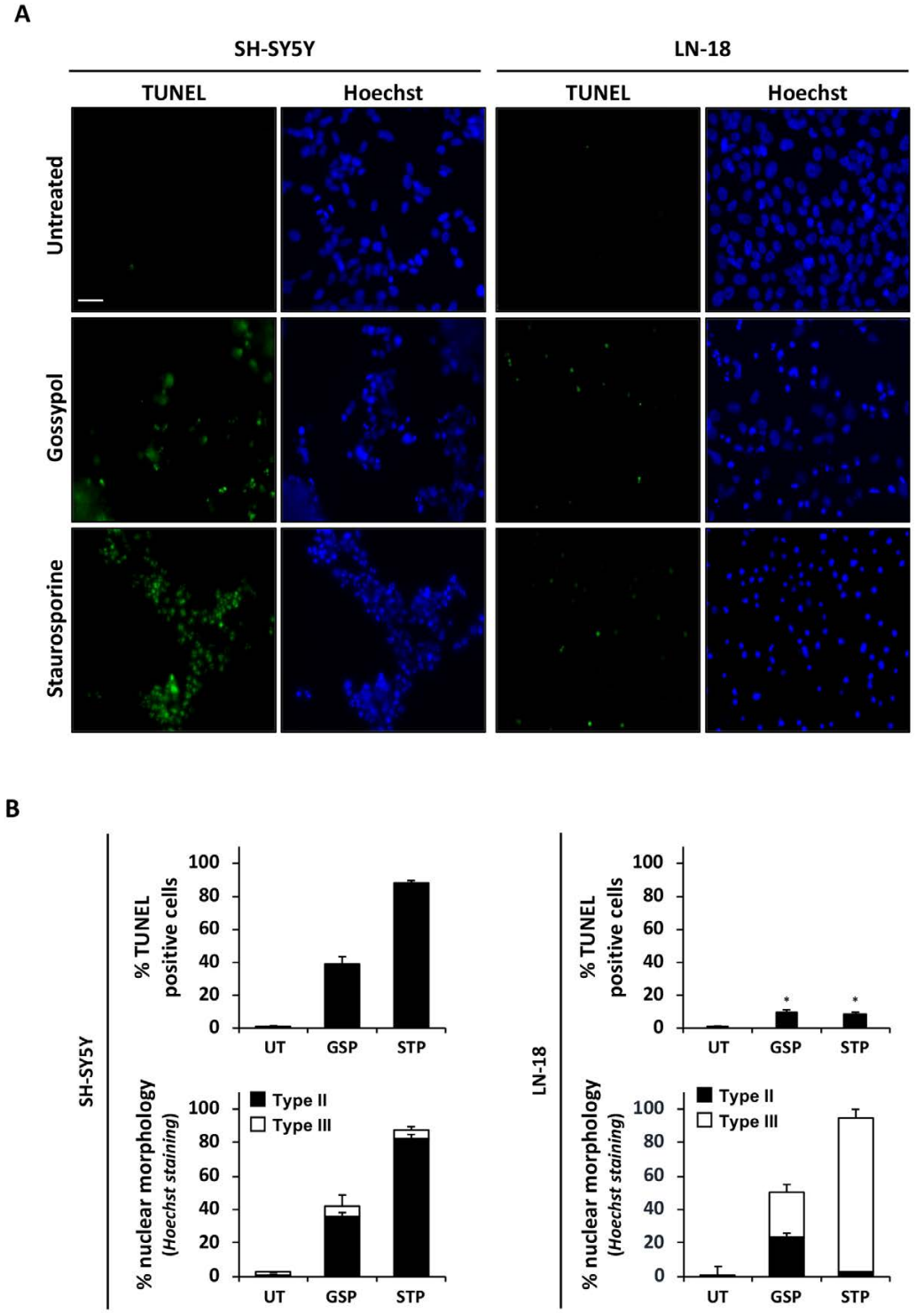

FIGURE R29. For figure legend, see next page.

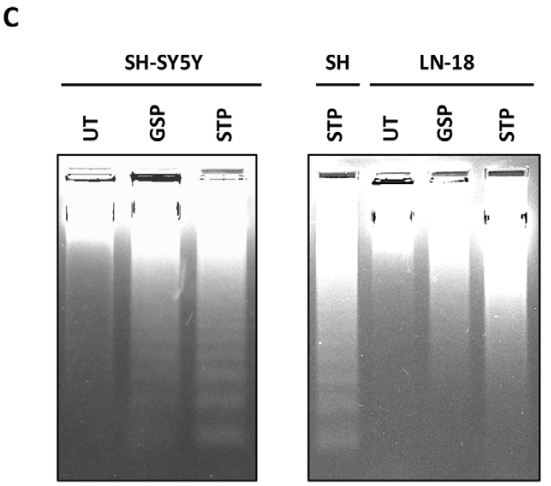

FIGURE R29. Type II nuclear morphology induced after gossypol in LN-18 cells does not correlate with either TUNEL positivity or DNA ladder. A, SH-SY5Y (SH) and LN-18 cells were left untreated (UT) or treated with 100 μM gossypol (GSP) or 1 μM staurosporine (STP) for 9 hours. TUNEL reactivity and nuclear staining with Hoechst 33258 were performed as detailed in *Material and Methods*. Representative images are shown. Scale bar = 40 μm. **B**, quantification of the data showed in A representing TUNEL-positive nuclei (upper panel) and apoptotic nuclei (lower panel) in SH-SY5Y and LN-18 cells upon GSP or STP treatment, is presented by means ± *SD* (*error bars*). The Student's *t*-test was used to determine the statistical significance (* means $p < 0.05$). **C**, cells were left untreated or treated with 100 μM gossypol (GSP) or 1 μM staurosporine (STP) for 6 hours (SH-SY5Y (SH) cells), or 12 hours (LN-18 cells). Genomic DNA was extracted and analyzed by conventional agarose gel electrophoresis and subsequent ethidium bromide staining.

Additionally, we wanted to determine whether DNA damage occurs in both cell lines challenged with gossypol or staurosporine by analyzing the DNA degradation. Genomic DNA was extracted from untreated or treated cells and analyzed by conventional agarose gel electrophoresis and subsequent ethidium bromide staining. As shown in **Figure R29C**, and as previously reported (Boix *et al.*, 1997), staurosporine was able to induce oligonucleosomal DNA degradation in SH-SY5Y cells (**Figure 29C**, *left panel*). Indeed, SH-SY5Y cells treated with staurosporine for 6 hours were used as a positive control in **Figure R29C** (*right panel*). The treatment of SH-SY5Y with gossypol induced less efficient DNA ladder compared with staurosporine. The different intensity between both treatments may correlate with the lower percentage of apoptotic nuclei displayed upon gossypol treatment in SH-SY5Y cells compared with staurosporine. Thus, it correlates with type II nuclear morphologies and the percentage of TUNEL-positive nuclei.

LN-18 cells were previously reported to be defective in generating oligonucleosomal DNA degradation and apoptotic nuclear morphologies after different cytotoxic insults (Sanchez-Osuna *et al.*, 2014). Here, we challenged LN-18 cells with staurosporine and gossypol. SH-SY5Y cells treated with STP were used as a positive control. Like previously reported, no

DNA ladder was detected upon staurosporine treatment in LN-18 cells. This absence of DNA ladder upon treatment with the alkaloid coincided with an impairment in the generation of type II apoptotic nuclear morphologies.

Regarding gossypol treatment in LN-18 cells, although it was able to induce a significant percentage of type II nuclear morphologies, oligonucleosomal DNA degradation was not observed. Only a smear of DNA was detected after gossypol or staurosporine treatment, indicating degradation of the genomic content. This cellular response, with the presence of type II nuclear morphology but the absence of oligonucleosomal DNA degradation was previously reported in my Final Master Thesis Work. LN-18 cells displayed type II apoptotic morphologies in the absence of DNA ladder after γ-irradiation in the presence or absence of temozolomide. Other cellular models, such as the neuroblastoma cell line SK-N-AS (treated with staurosporine), have also been reported to display apoptotic nuclear morphology in the absence of DNA ladder (Iglesias-Guimarais *et al.*, 2012). The in-depth study of this model, revealed that apoptotic nuclear morphology can occur independently of DFF40/CAD-mediated DNA fragmentation and that both 3'OH DNA breaks and type II nuclear morphology rely on DNA SSB generation rather than on DSB oligonucleosomal DNA fragmentation. However, the results presented in **Figure R29** indicate that type II nuclear morphology correlates with neither TUNEL positivity nor with oligonucleosomal DNA degradation in LN-18 cells.

17. Different phospho-H2AX intensity levels are detected upon gossypol or staurosporine treatment

Since the levels of 3'-OH ends and oligonucleosomal DNA degradation induced after treatment could be below the detection threshold of the techniques employed, we took advantage of an alternative readout of DNA damage, and specifically of the DFF40/CAD activity (Rogakou *et al.*, 2000) –a phosphospecific antibody that recognizes the phosphorylated serine (S)-139 residue of H2AX–. This member of the H2A histone family becomes phosphorylated after the induction of DNA breaks (Rogakou *et al.*, 1998).

As shown in **Figure R30**, we treated LN-18 cells with gossypol and staurosporine in the presence or absence of q-VD-OPh. After 9 hours of treatment, we fixed the cells and used a phospho-histone H2AX (Ser 139 clone) antibody to analyze the extent of DNA damage (**Figure R30**).

Cells stained positive against phospho-H2AX (here in red) were quantified over the total number of cells stained with Hoechst 33258 (here in blue). The resulting percentage was represented in bar graphs (**Figure R30A**). The percentage of phospho-H2AX positive cells was higher in staurosporine-treated cells (73.85 ± 2.64%) than in gossypol-treated cells (53.84 ± 6.08%).

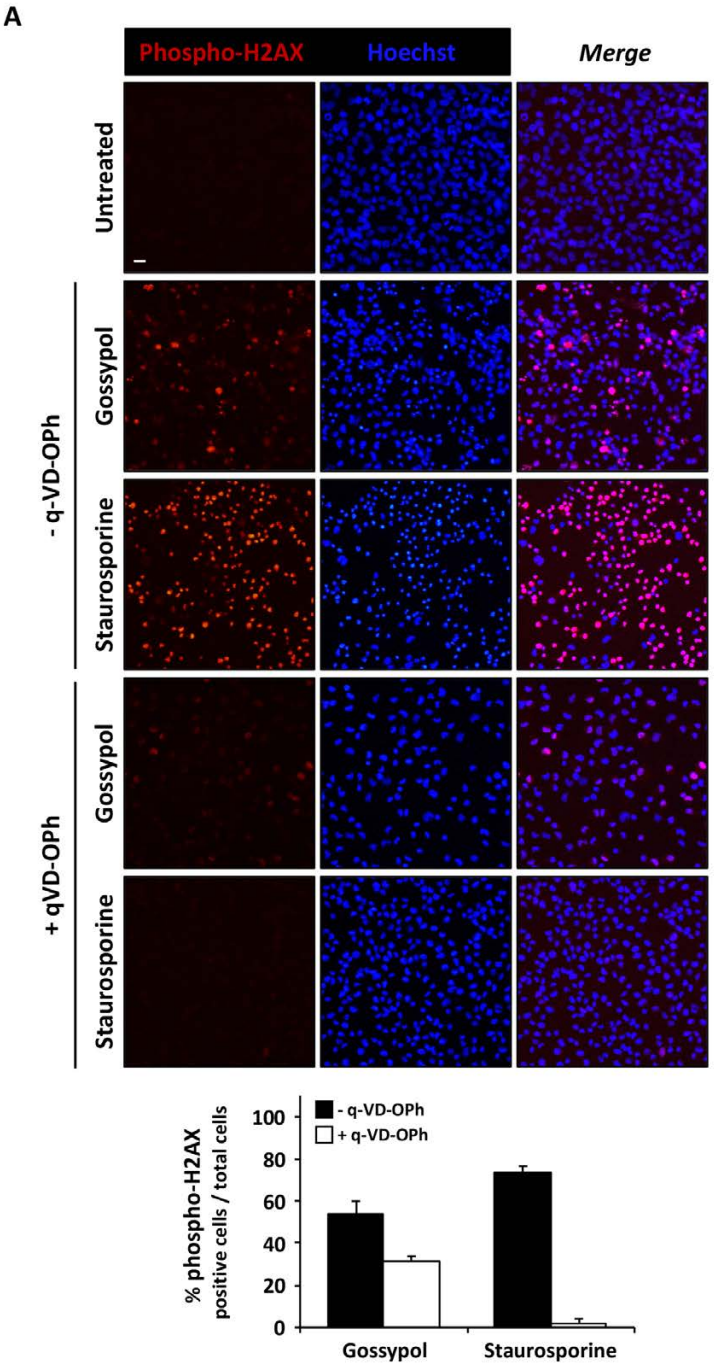

FIGURE R30. For figure legend, see next page.

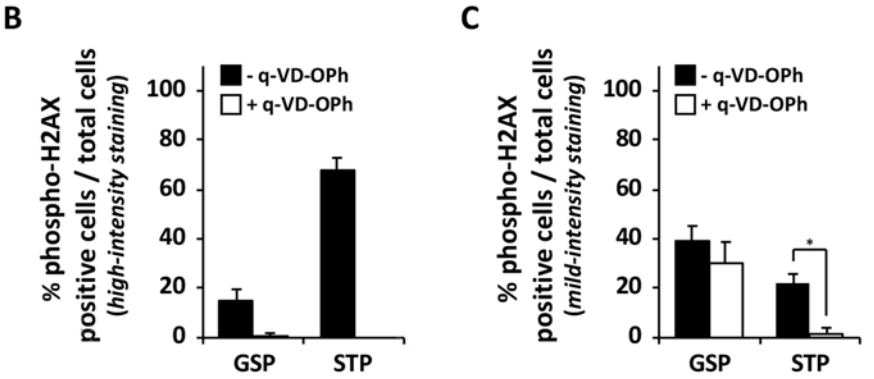

FIGURE R30. Caspase-independent DNA damage is induced upon gossypol in LN-18 cells. LN-18 cells were left untreated or treated with 100 μM gossypol (GSP) or 1 μM staurosporine (STP) for 9 hours. Then, cells were fixed and immunostained with a specific antibody against phospho-H2AX (Ser 139 clone) (red) (*left panel*) according to *Material and Methods*. Nuclei (blue) were stained with Hoechst 33258 (*middle panel*). **A**, representative images of each condition are shown. Scale bar = 20 μm. Manual counting of phospho-H2AX positive cells (red) over the total number of cells (blue) was performed without establishing any threshold. The corresponding percentages were represented in bar graphs ± *SD* (*error bars*). **B**, a threshold value was established to determine the positivity of phospho-H2AX induced by each condition (*see Material and Methods*). The percentage of cells with high-intensity phospho-H2AX staining (red) over the total number of cells (blue) is represented in bar graphs ± *SD* (*error bars*). **C**, mild-intensity staining of phospho-H2AX was determined by subtracting the number of cells with high-intensity staining determined after setting up a high threshold value (represented in **B**) to the total phospho-H2AX positive cells determined without establishing a limiting threshold (represented in **A**). The percentage of cells with mild-intensity phospho-H2AX staining over the total number of cells is represented in bar graphs ± *SD* (*error bars*). The Student's *t*-test was used to determine the statistical significance (* means $p < 0.05$).

Nevertheless, the visual impression of the representative images shown in **Figure R30A** suggested a higher difference between both conditions. To address this inconsistency concerning the quantification (graph A) and the images (**Figure R30A**), we decided to establish a specific threshold value to quantify the percentage of phospho-H2AX positive cells upon each treatment. The set-up of a high threshold value (see *Material and Methods*) evidenced a higher difference regarding phospho-H2AX staining between treatments. While 68.09 ± 4.78% of staurosporine-treated LN-18 cells showed positivity against phospho-H2AX, only 14.65 ± 4.96% of cells were phospho-H2AX positive upon gossypol treatment (**Figure R30B**). It indicated that the number of positive cells above the high threshold value established and, therefore, that coincide with high-intensity staining, is higher upon staurosporine treatment than after gossypol treatment. By contrast, the percentage of cells with a mild-intensity staining of phospho-H2AX was higher upon gossypol (39.19 ± 6.07%) than staurosporine treatment (21.7 ± 4.11%) (**Figure R30C**).

As detailed in the figure legend, mild-intensity staining of phospho-H2AX was determined by subtracting the number of cells with high-intensity staining (graph B) to the total phospho-H2AX positive cells determined without establishing a limiting threshold value (graph A). Interestingly, graphs from **Figure R30A** and **R30C** showed that the percentage of phospho-H2AX induced by gossypol was not rescued in the presence of q-VD-OPh. Therefore, results from **Figure R30** suggest that a lower, but caspase-independent, DNA damage response is triggered upon gossypol treatment in LN-18 cells.

18. Gossypol derivatives are less effective at inducing type II nuclear morphologies in LN-18 cells

As concluded above, caspase-independent DNA damage is induced when using gossypol in LN-18 cells. In this line, articles from the late 20th century proposed a DNA degradation or DNA-breaking activity linked to gossypol structure. Here, we decided to employ different gossypol derivatives and to analyze the nuclear morphology triggered by each compound in LN-18 cells. **Figure R31A** shows the structure of gossypol (aldehyde-aldehyde form); apogossypol (ApoG), which derives from the removal of the two aldehyde groups (-CHO) from gossypol; and apogossypolone (ApoG2) that derives from the oxidation of apogossypol.

As shown in **Figure R31A**, the color of stock solutions (100 mM, in DMSO) changed from a more dark-brown color in apogossypol to a more yellowish color in gossypol and AT-101. Note that AT-101 corresponds to the R-(-) enantiomer of gossypol. To assess the nuclear morphologies induced by each compound in LN-18 cells, we fixed the cells and stained the chromatin with bisbenzimide Hoechst.

Figure R31B shows representative images of each condition and the corresponding percentage of type II and type III nuclear morphologies detected after 24 hours of treatment. Apogossypol, apogossypolone or AT-101 (employed at a final concentration of 100 μM) induced a percentage of type II nuclear morphology below 10%. By contrast, type III nuclear morphologies were similarly induced by the different derivatives employed. As gossypol-induced type II nuclear morphologies are triggered in a dose-dependent manner (**Figure R6**), we tested different concentrations of each gossypol derivative and the R-(-) enantiomer of gossypol.

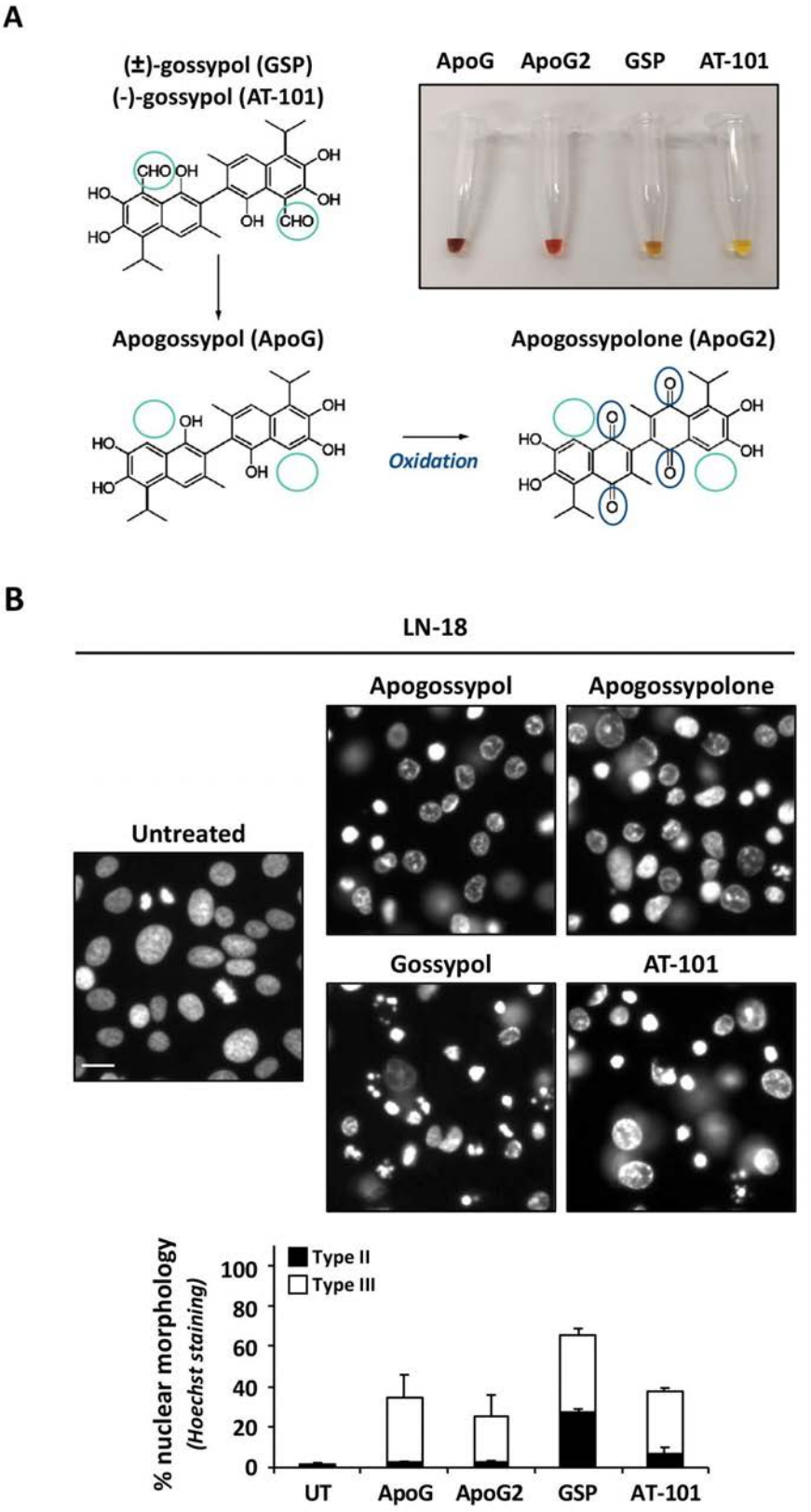

FIGURE R31. For figure legend, see page 181.

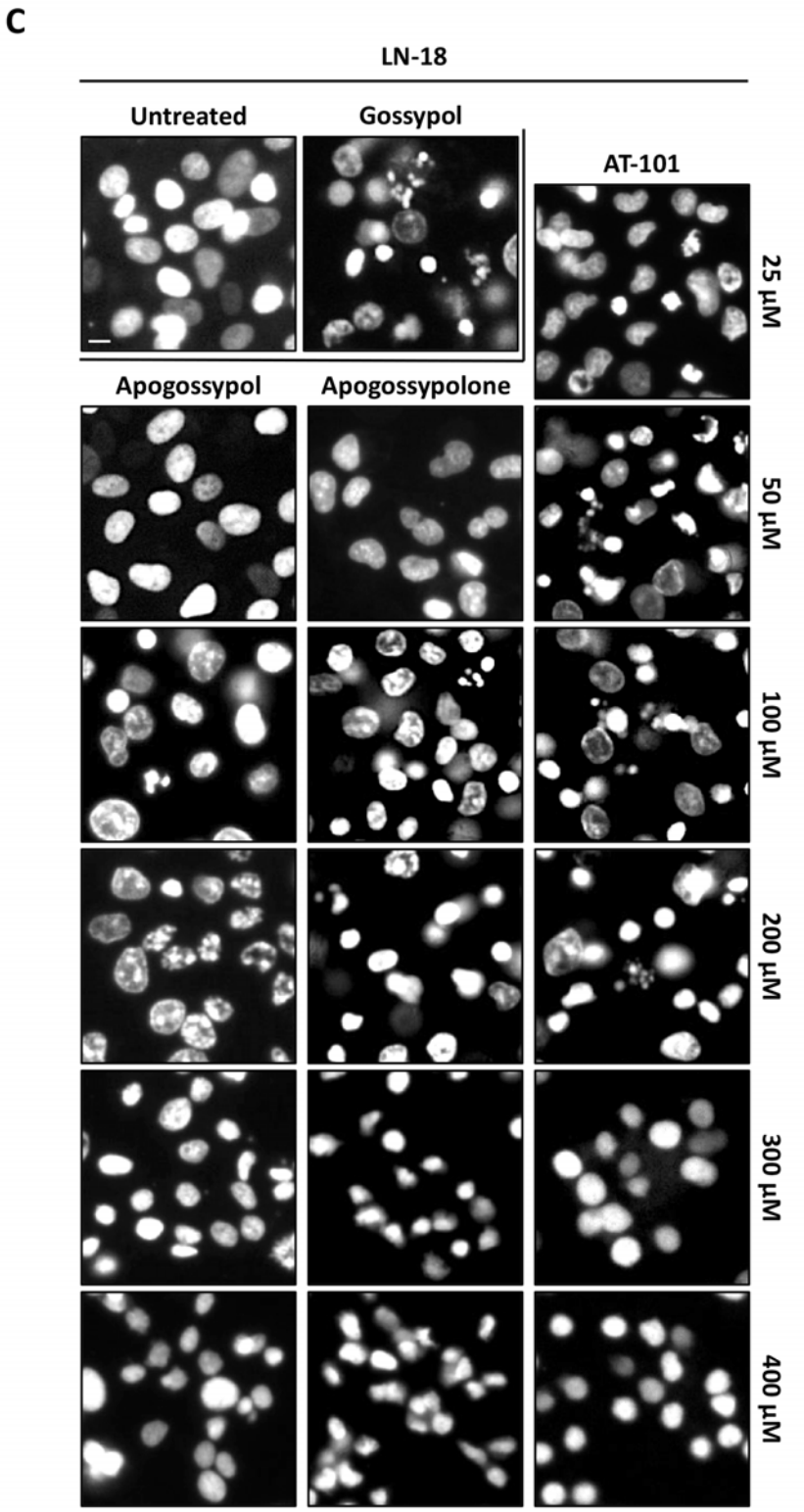

FIGURE R31. For figure legend, see next page.

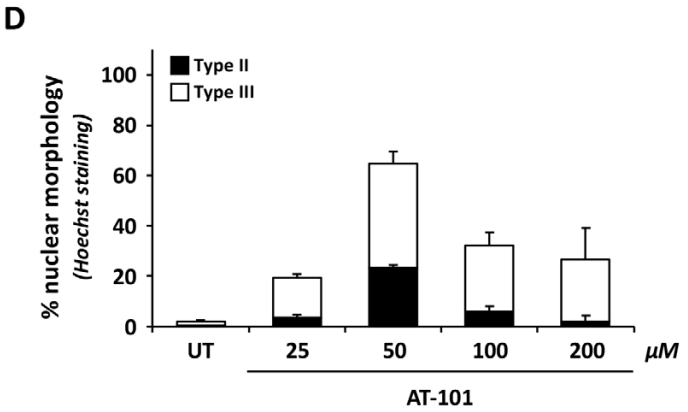

FIGURE R31. Type II nuclear morphologies are impaired upon treatment with gossypol derivatives. **A**, the chemical structure of gossypol –the racemic (±)-gossypol (GSP) and the R-(-) enantiomer of gossypol (AT-101)–, apogossypol (ApoG) and apogossypolone (ApoG2); and the aspect of stock aliquots is shown. **B**, LN-18 cells were left untreated or treated with 100 μM apogossypol, 100 μM apogossypolone, 100 μM gossypol or 100 μM AT-101. **C**, same compounds were used at the indicated concentrations. ApoG and ApoG2 from 50 μM to 400 μM, and AT-101 from 25 μM to 400 μM. Untreated cells and gossypol (100 μM) were used as controls. After 24 hours of treatment, cells were fixed and nuclear morphology was analyzed by staining the nuclei with Hoechst 33258. Images were obtained with a Nikon ECLIPSE TE2000-E microscope equipped with UV-light epifluorescence and a Hamamatsu ORCA-ER photographic camera. Representative microphotographs of each condition are shown (**B**, **C**). Scale bar = 20 μm. The percentage of type II *(black bars)* and type III (*white bars*) nuclear morphology was calculated (**A**, **D**). The graph represents the means ± *SD* (*error bars*) (**A**, **D**).

Figure R31C evidences a similar nuclear outcome between AT-101 and gossypol. **Figure R31D**, which corresponds to the quantification of the nuclear morphologies induced by different concentrations of AT-101, shows that 50 μM of AT-101 triggers a percentage of type II nuclear morphology (23.50 ± 0.95%) comparable to the percentage induced by 100 μM gossypol (**Figure R5).** Thus, it suggested that less amount of the R-(-) enantiomer of gossypol, than the racemic (±)-gossypol form is needed to display type II nuclear morphologies. Like with gossypol, AT-101 displayed a nuclear phenotype including type II nuclear morphology and type III nuclear morphologies (**Figure R31C**). In the case of apogossypol and apogossypolone, concentrations lower and above than 100 μM were even less efficient at inducing type II nuclear morphologies than 100 μM (**Figure R31B, C**).

Overall, results from **Figure R31** pointed to a dissimilar effect over the nuclear morphology upon treatment with different gossypol derivatives in LN-18 cells.

In order to correlate the absence of aldehyde groups (-CHO) with a general impairment in the formation of apoptotic nuclear morphologies, we decided to test gossypol derivatives in apoptotic-proficient cells such as the human neuroblastoma-derived SH-SY5Y cells. As previously reported, SH-SY5Y cells challenged with staurosporine displayed classical type II nuclear morphologies (**Figure R32**). SH-SY5Y cells treated with apogossypol,

apogossypolone, gossypol, or AT-101 displayed a similar nuclear phenotype and evidenced type II nuclear morphologies regardless of the compound (**Figure R32**).

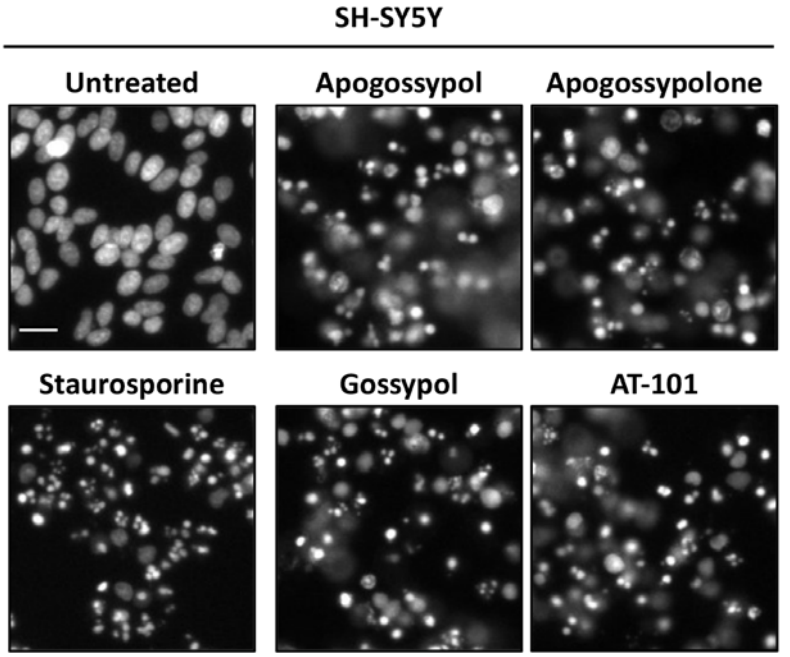

FIGURE R32. Gossypol derivatives can induce the type II nuclear morphology in SH-SY5Y cells. SH-SY5Y cells were left untreated or treated with 1 μM staurosporine, 100 μM apogossypol, 100 μM apogossypolone, 100 μM gossypol or 50 μM AT-101. After 24 hours, cells were fixed and nuclear morphology was analyzed by staining the nuclei with Hoechst 33258. Images were obtained with a Nikon ECLIPSE TE2000-E microscope equipped with UV-light epifluorescence and a Hamamatsu ORCA-ER photographic camera. Representative microphotographs of each condition are shown. Scale bar = 20 μm.

19. The combination of apogossypolone, but not of apogossypol, with TRAIL induces type II nuclear morphology in LN-18 cells

As shown in **Figure R21**, the combination of gossypol and TRAIL increases the percentage of the gossypol-induced type II nuclear morphology in LN-18 cells. Thus, we wondered whether LN-18 cells were sensitized to display type II nuclear morphologies when co-treated with gossypol derivatives and TRAIL.

LN-18 cells were left untreated or treated with TRAIL in the presence or absence of apogossypol, apogossypolone, gossypol, or AT-101 for 24 hours and then, nuclei were stained with Hoechst (**Figure R33**). As expected, the treatment with TRAIL induced type III nuclear morphologies, and its combination with gossypol increased the type II apoptotic nuclear morphology. The combination of AT-101 with TRAIL triggered a similar nuclear outcome

than gossypol. Regarding gossypol derivatives, the combination of TRAIL plus apogossypolone increased the percentage of type II nuclear morphologies from 2.55 ± 0.83% (ApoG2, **Figure R31B**) to 34.97 ± 9.50% (ApoG2 + TRAIL, **Figure R33**). In the case of apogossypol, the percentage of type II nuclear morphology changed from 2.82 ± 0.17% (ApoG, **Figure R31B**) to 10.03 ± 2.78% (ApoG + TRAIL, **Figure R33**). The principal nuclear outcome observe upon TRAIL plus apogossypol was a peripheral chromatin condensation with slightly fragmented masses of chromatin –also observed when using apogossypol alone (**Figure R31B**)–, and an increase in the type III nuclear morphology.

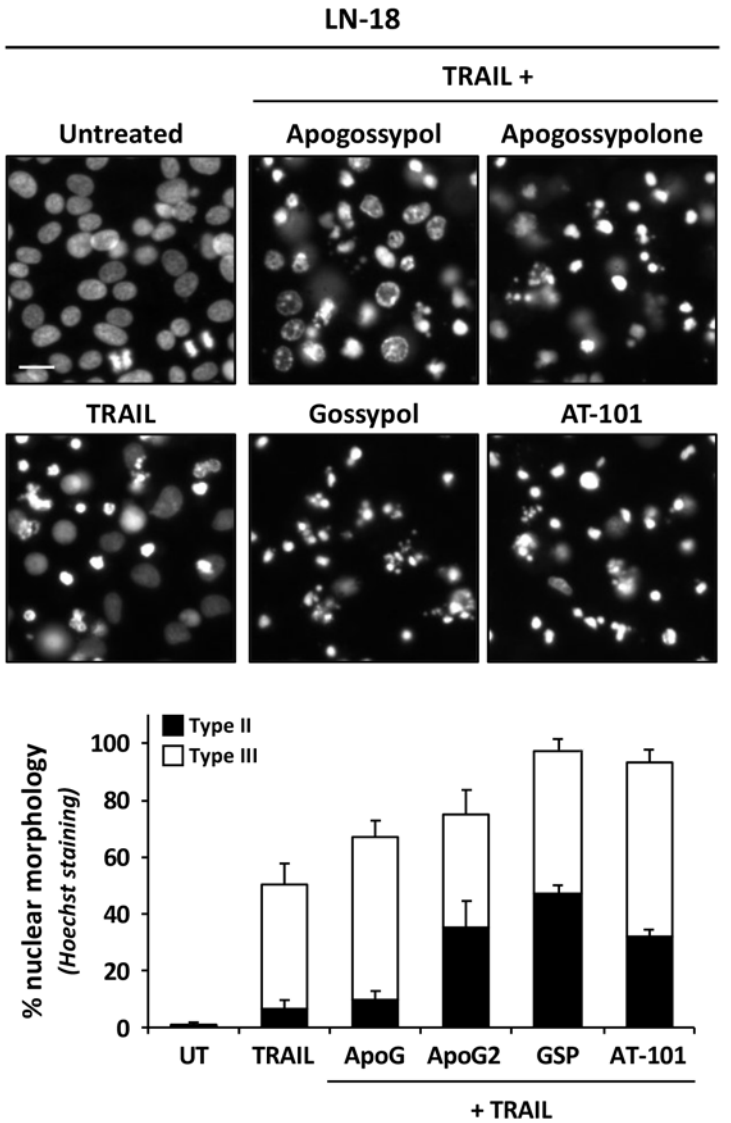

FIGURE R33. LN-18 cells are sensitized to display type II nuclear morphologies when treated with TRAIL and gossypol derivatives except for apogossypol. LN-18 cells were left untreated or treated with 200 ng/ml TRAIL alone or in combination with 100 μM apogossypol, 100 μM apogossypolone, 100 μM

gossypol or 50 μM AT-101. **A**, After 24 hours, cells were fixed and nuclear morphology was analyzed by staining the nuclei with Hoechst 33258. Images were obtained with a Nikon ECLIPSE TE2000-E microscope equipped with UV-light epifluorescence and a Hamamatsu ORCA-ER photographic camera. Representative microphotographs of each condition are shown. Scale bar = 20 μm. The percentage of type II *(black bars)* and type III (*white bars*) nuclear morphology was calculated. The graph represents the means ± *SD* (*error bars*).

Because gossypol structure seems to be relevant in the outcome of nuclear morphologies, we decided to modify the structure of gossypol via pH modification. It has been previously described that the addition of sodium hydroxide (NaOH) to gossypol leads to apogossypol and, therefore, to the elimination of the two carbonyl groups from gossypol. Moreover, this gossypol transformation was described to take place in parallel with a color reaction (Clark, 1928).

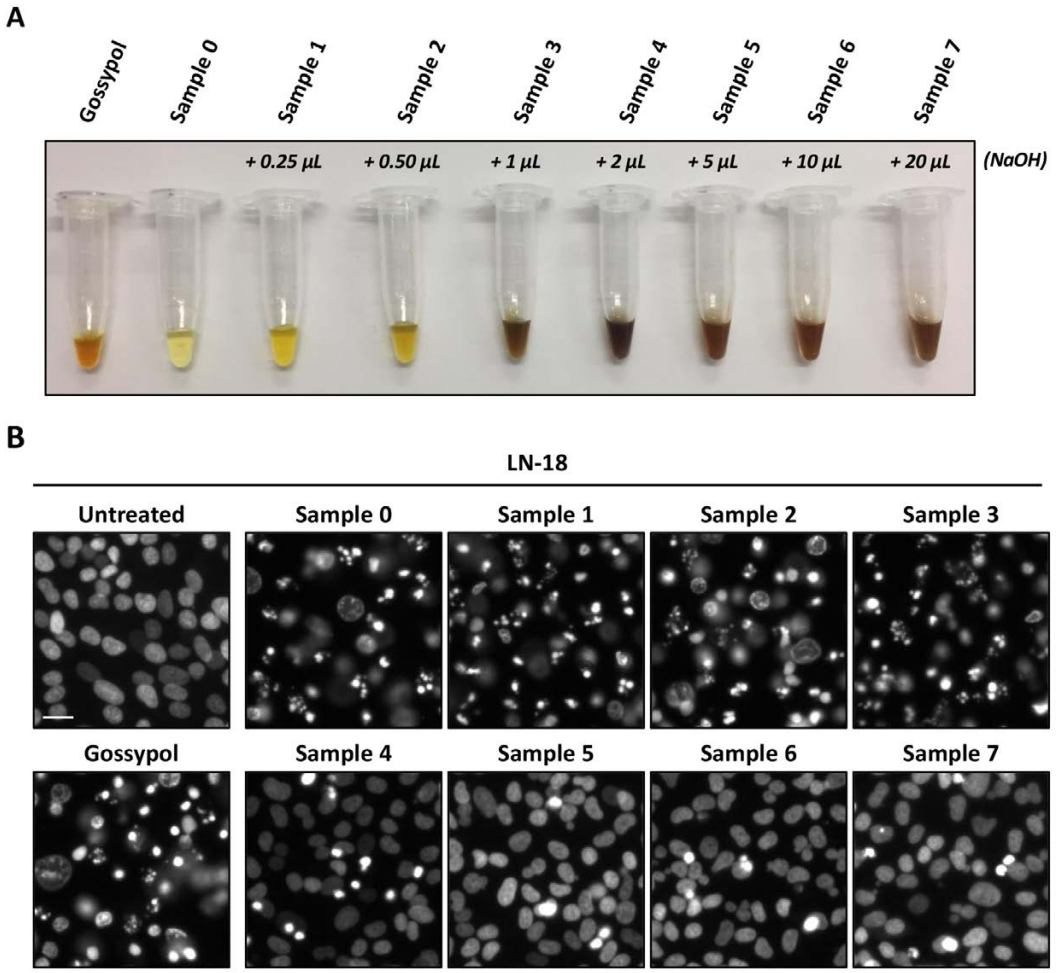

FIGURE R34. Chemical modification of gossypol by NaOH impairs the nuclear alterations induced by the alkaloid. A, a stock aliquot of gossypol prepared with DMSO at 100 mM was diluted with DMSO to 5 mM (*sample 0*) and equal volumes (20 μL/Eppendorf) were distributed in seven different Eppendorfs. Then, increasing volumes of NaOH (1 M) were added as indicated (*sample 1 – sample 7*). The reaction was maintained at room temperature for 1 hour and then 20 μL of DMSO were added to each tube (*sample 0 – sample 7).* The

color of each sample after the reaction is shown in **A**. **B**, LN-18 cells were left untreated, treated with 100 μM of gossypol, or treated with 100 μM of *sample 1* – *sample 7*. After 24 hours, cells were fixed and nuclear morphology was analyzed by staining the nuclei with Hoechst 33258. Images were obtained with a Nikon ECLIPSE TE2000-E microscope equipped with UV-light epifluorescence and a Hamamatsu ORCA-ER photographic camera. Representative microphotographs of each condition are shown. Scale bar = 20 μm.

As shown in **Figure R34A**, the orange color of the stock aliquot changed to a yellowish appearance when diluted in DMSO and to dark orange color when adding increasing volumes of NaOH. After one hour at room temperature, no changes in the color aspect were appreciated (**Figure R34A**). The corresponding volumes were diluted in complete medium to treat LN-18 cells with the different gossypol transformed forms at a final concentration of 100 μM.

As shown in **Figure R34B**, Sample 0 to Sample 3 displayed a similar nuclear outcome than gossypol, including type I, type II, and type III nuclear morphologies. However, the effect was lost from Sample 4 and above. The maximal concentration of NaOH (equal to sample 7) was also tested in LN-18 cells, and no evident affected nuclear morphologies were observed. Altogether, results from **Figure R34** suggested that certain levels of NaOH (samples 4 - 7) may modify gossypol structure and, consequently, impair the nuclear effect of gossypol in LN-18 cells.

Moreover, results from **Figure R31** and **R32** suggested that the color of stock aliquots (**Figure R31A**) could be related with the potency of each compound to induce type II nuclear morphology, being AT-101 and gossypol with a yellowish appearance more effective than apogossypol or apogossypolone with a dark orange/brown color. Nonetheless, Sample 3, with a dark brown appearance, induced a similar nuclear phenotype than gossypol. Hence, results from **Figure R34** evidence that the color of the aliquots does not seem to be an indicator of the effectiveness to induce apoptotic nuclear morphology.

20. Different metal ions alter the nuclear morphologies induced by gossypol in LN-18 cells

Regarding gossypol structure, it has been described that gossypol can form metal complexes via chelating with metal ions (Muzaffaruddin and Saxena, 1966). Hence, in line with our study of the influence of gossypol structure over the nuclear morphologies, we decided to challenge LN-18 cells with gossypol in the presence or absence of different metal ions. For this, LN-18 cells were left untreated or treated with gossypol in the presence or absence of Cu^{2+}, Co^{2+}, or Fe^{3+}.

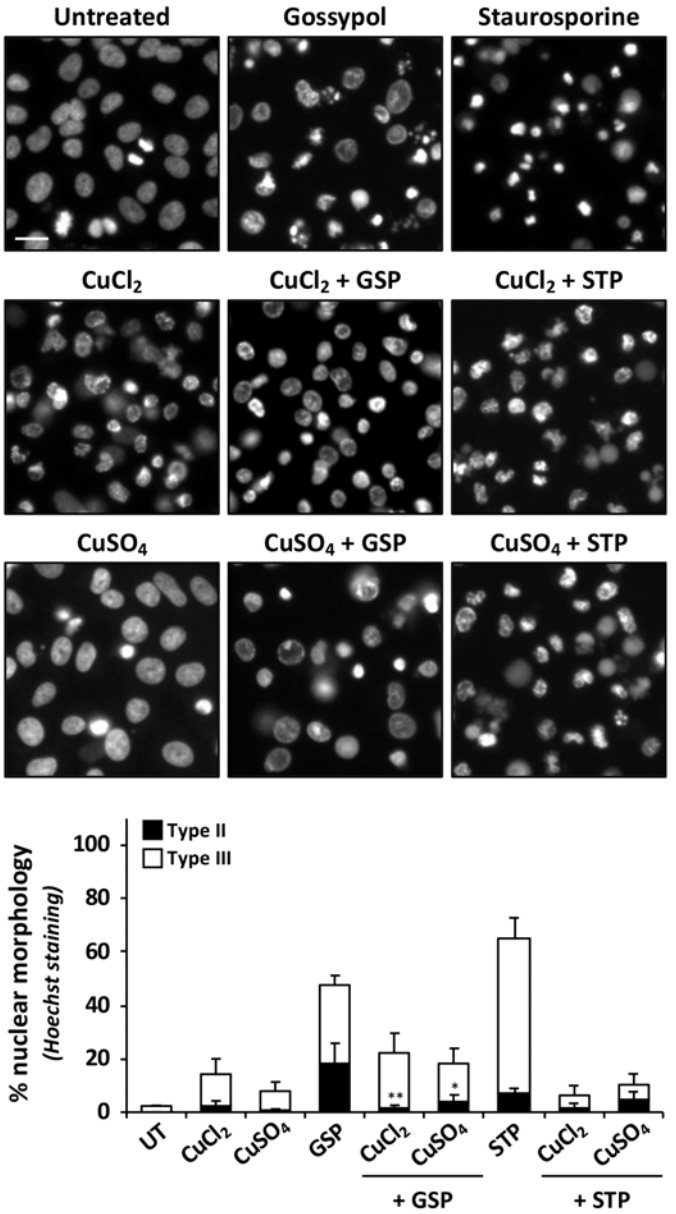

FIGURE R35. $CuCl_2$ or $CuSO_4$ alters the structure of the chromatin in LN-18 cells and modifies gossypol and staurosporine effect. LN-18 cells were treated with 2 mM $CuCl_2 \cdot 2H_2O$ or 2 mM $CuSO_4 \cdot xH_2O$ for 30 minutes. Then, both metal ions were kept at 1 mM in combination or not with 100 μM gossypol (GSP) or 1 μM staurosporine (STP). After 24 hours, cells were fixed and nuclear morphology was analyzed by staining the nuclei with Hoechst 33258. Images were obtained with a Nikon ECLIPSE TE2000-E microscope equipped with UV-light epifluorescence and a Hamamatsu ORCA-ER photographic camera. Representative microphotographs of each condition are shown. Scale bar = 20 μm. The percentage of type II *(black bars)* and type III (*white bars*) nuclear morphology was calculated. The graph represents the means ± *SD* (*error bars*). One-way ANOVA test was used to determine the statistical significance between groups regarding type II [$F(8,9) = 7.22$, $p < 0.01$]. The significance of the type II value of each combinatorial treatment versus the single treatment (gossypol or staurosporine) was determined by the post hoc Tukey's test (* means $p < 0.05$) (** means $p < 0.01$).

As shown in **Figure R35**, the addition of copper to the culture media impaired the type II nuclear morphology triggered by gossypol. Indeed, the nuclear phenotype induced by staurosporine was also changed in the presence of this metal ion. Chromatin staining with Hoechst 33258 revealed that LN-18 cells exposed to $CuCl_2$ display nuclear morphologies with chromatin marginalization and points of breakage, a nuclear morphology slightly different from the type I nuclear morphology observed so far. This effect triggered by $CuCl_2$ seemed to be potentiated in combination with staurosporine and was also observed when treating LN-18 cells with $CuSO_4$ plus staurosporine. In the case of gossypol, while type II nuclear morphologies were impaired in the presence of either $CuCl_2$ or $CuSO_4$, type I and type III nuclear morphology seemed to be better preserved.

The effect of cobaltous, in combination or not with gossypol or staurosporine, was also analyzed.

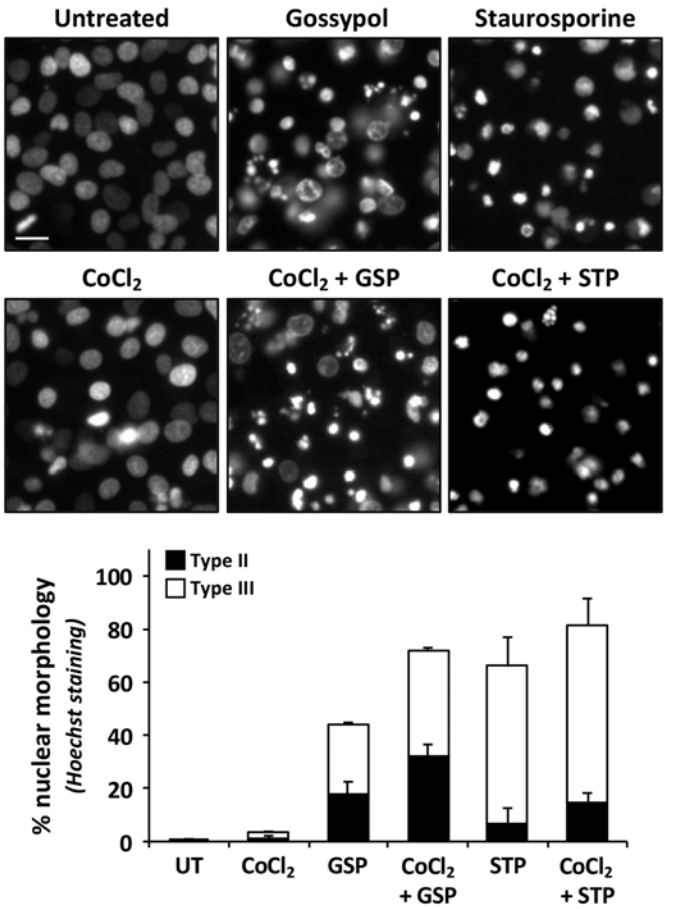

FIGURE R36. The combination of $CoCl_2$ plus gossypol increases the percentage of type II and type III nuclear morphologies in LN-18 cells. LN-18 cells were pre-treated with 800 μM $CoCl_2 \cdot 6H_2O$ for 30 minutes. Then $CoCl_2 \cdot 6H_2O$ was kept at 400 μM in combination or not with 100 μM gossypol (GSP) or 1 μM

staurosporine (STP) for 24 hours. In parallel, LN-18 cells were left untreated (UT) or treated with 100 μM GSP or 1 μM STP for 24 hours. **A**, after treatment, cells were fixed and nuclear morphology was analyzed by staining the nuclei with Hoechst 33258. Images were obtained with a Nikon ECLIPSE TE2000-E microscope equipped with UV-light epifluorescence and a Hamamatsu ORCA-ER photographic camera. Representative microphotographs of each condition are shown. Scale bar = 20 μm. The percentage of type II *(black bars)* and type III (*white bars*) nuclear morphology was calculated. The graph represents the means ± *SD* (*error bars*). One-way ANOVA test was used to determine the statistical significance between groups regarding type II [$F(5,6) = 19.94$, $p < 0.01$]. The post hoc Tukey's test determined no significance of the type II value of the combinatorial treatment versus the value from the corresponding single treatment (gossypol or staurosporine).

As shown in **Figure R36**, the presence of $CoCl_2$ in the culture medium of LN-18 cells did not induce apparent differences compared to untreated cells. Although not statistically significant, the combination of this metal ion with gossypol or staurosporine seemed to increase the percentage of type II nuclear morphology. The percentage type III nuclear morphology induced either by gossypol or staurosporine was also increased in the presence of cobaltous.

In the case of Fe^{3+}, we challenged LN-18 cells as previously performed with Cu^{2+}, Co^{2+}, but no effect over the nuclear morphology was observed when combining this metal ion (Fe^{3+}) with gossypol. To address a possible influence of extracellular Fe^{3+} impeding gossypol to trigger any effect over the nuclear morphology, we proceeded with a more complex experimental approach.

As schematically represented in **Figure R37A**, LN-18 cells were maintained in complete media in the absence (*conditions a*) or presence of $Fe_2(SO_4)_3$ (*conditions b* and *c*) for 24 hours. Then, cells were washed twice with PBS to remove as much as possible the excess of this metal ion in the culture medium. To proceed equally, cells maintained in culture media without $Fe_2(SO_4)_3$ (*condition a*) were also washed twice with PBS. Subsequently, cells from *conditions a* and *b* were left untreated (UT) (complete fresh media was added) or treated with gossypol (GSP) or staurosporine (STP). Alternatively, cells from *condition c* were left untreated or treated with gossypol or staurosporine in the presence of $Fe_2(SO_4)_3$. After 24 hours, cells were fixed, chromatin was stained with Hoechst 33258, and images were obtained under a UV-light microscope.

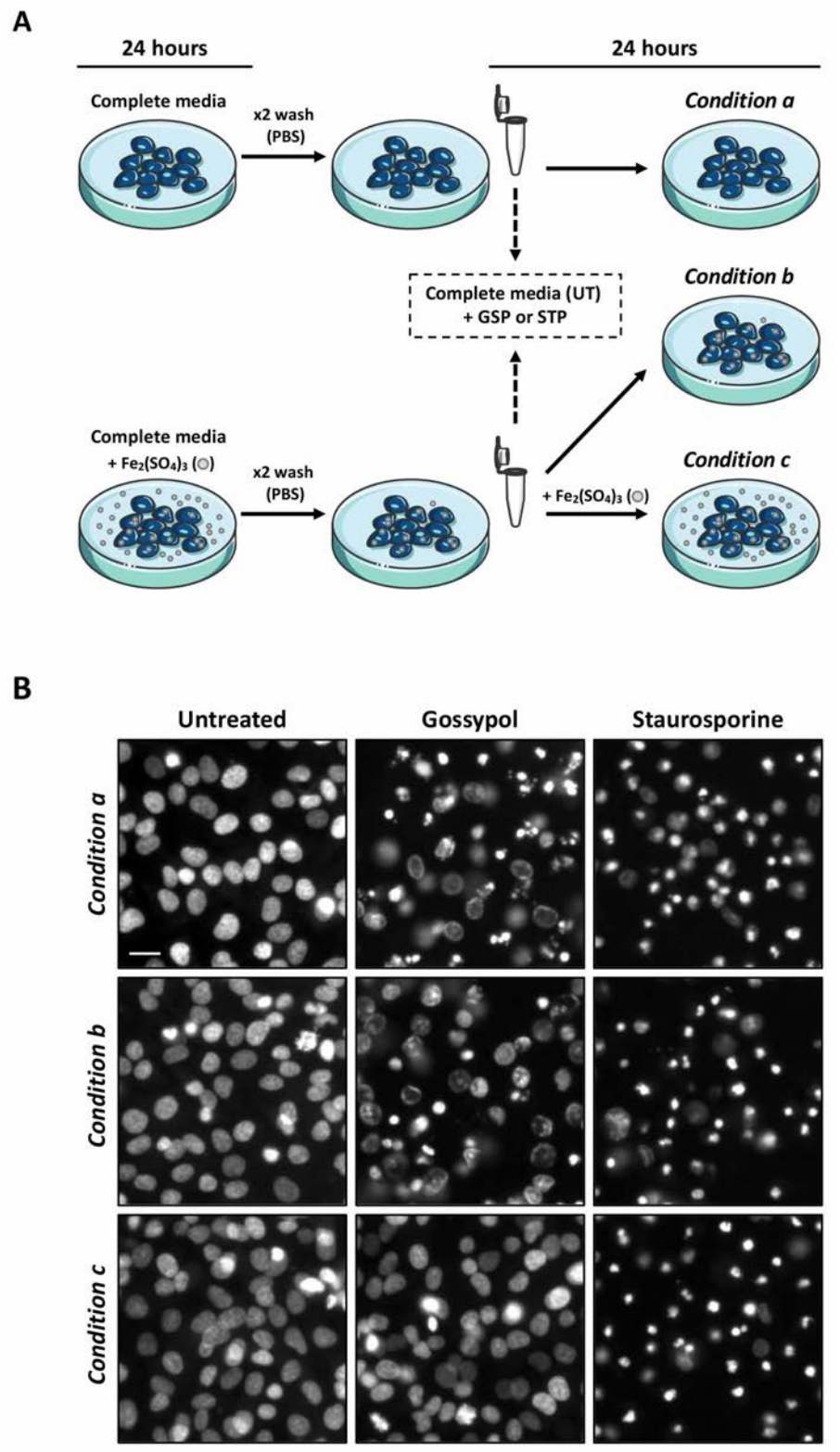

FIGURE R37. For figure legend, see next page.

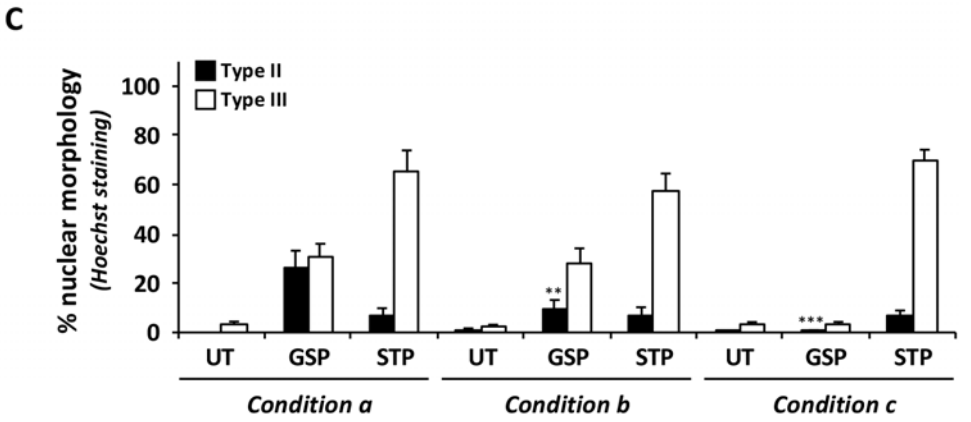

FIGURE R37. The presence of $Fe_2(SO_4)_3$ interferes in the nuclear effect triggered upon gossypol treatment in LN-18 cells. LN-18 cells were maintained in complete media (*see material and methods*) or 1 mM $Fe_2(SO_4)_3 \cdot xH_2O$. After 24 hours, cells were washed twice with phosphate-buffered saline (PBS). Then, cells previously maintained in complete media were treated with 100 μM gossypol (GSP), 1 μM staurosporine (STP), or left untreated (UT) for 24 hours (*condition a*). Cells previously maintained in 1 mM $Fe_2(SO_4)_3 \cdot xH_2O$ were treated as in condition a (*condition b*) or, treated as in condition a, in the presence (+) of 1 mM $Fe_2(SO_4)_3 \cdot xH_2O$ (*condition c*). **A**, schematic representation of the experimental procedure. **B**, after 24 hours of treatment, cells were fixed and nuclear morphology was analyzed by staining the nuclei with Hoechst 33258. Images were obtained with a Nikon ECLIPSE TE2000-E microscope equipped with UV-light epifluorescence and a Hamamatsu ORCA-ER photographic camera. Representative microphotographs of each condition are shown. Scale bar = 20 μm. **C**, the percentage of type II *(black bars)* and type III (*white bars*) nuclear morphology were calculated. The graph represents the means ± *SD* (*error bars*). One-way ANOVA test was used to determine the statistical significance between groups regarding type II [$F(8,9) = 14.92$, $p < 0.005$]. The significance of the type II value of each combinatorial treatment versus the corresponding single treatment (gossypol or staurosporine) was determined by the post hoc Tukey's test (** means $p < 0.01$) (*** means $p < 0.005$).

Overall, results from **Figure R35, R36,** and **R37** suggest that metal ions may influence the nuclear morphologies induced by different compounds such as gossypol or staurosporine.

21. Gossypol triggers an intense vacuolization process together with a general alteration of internal cellular membranes

In addition to the formation of complexes with metal ions, the two aldehyde groups of gossypol can interact with amino groups leading to gossypol interaction with proteins and promoting protein aggregates. To detect possible ultrastructural changes induced upon gossypol treatment and electrodense structures akin to aggregates, we took advantage of electron microscopy.

We observed that although LN-18 cells treated with gossypol displayed different nuclear morphologies, structural changes characterized by a general alteration of cellular membranes

and an intense vacuolization process is shared among gossypol-treated cells (**Figure R38**). This observation was previously perceived in **Figure R8**. **Figure R38**, confirms the induction of ultrastructural alterations coinciding with extensive dilatation of the endoplasmic reticulum (ER) and Golgi apparatus (GA), structures derived from nuclear envelope breakdown, swelling and alteration of mitochondria, accumulation, and precipitation of proteins and pseudo autophagic vacuoles. Protein build-up structures were also evident in LN-18 cells upon gossypol.

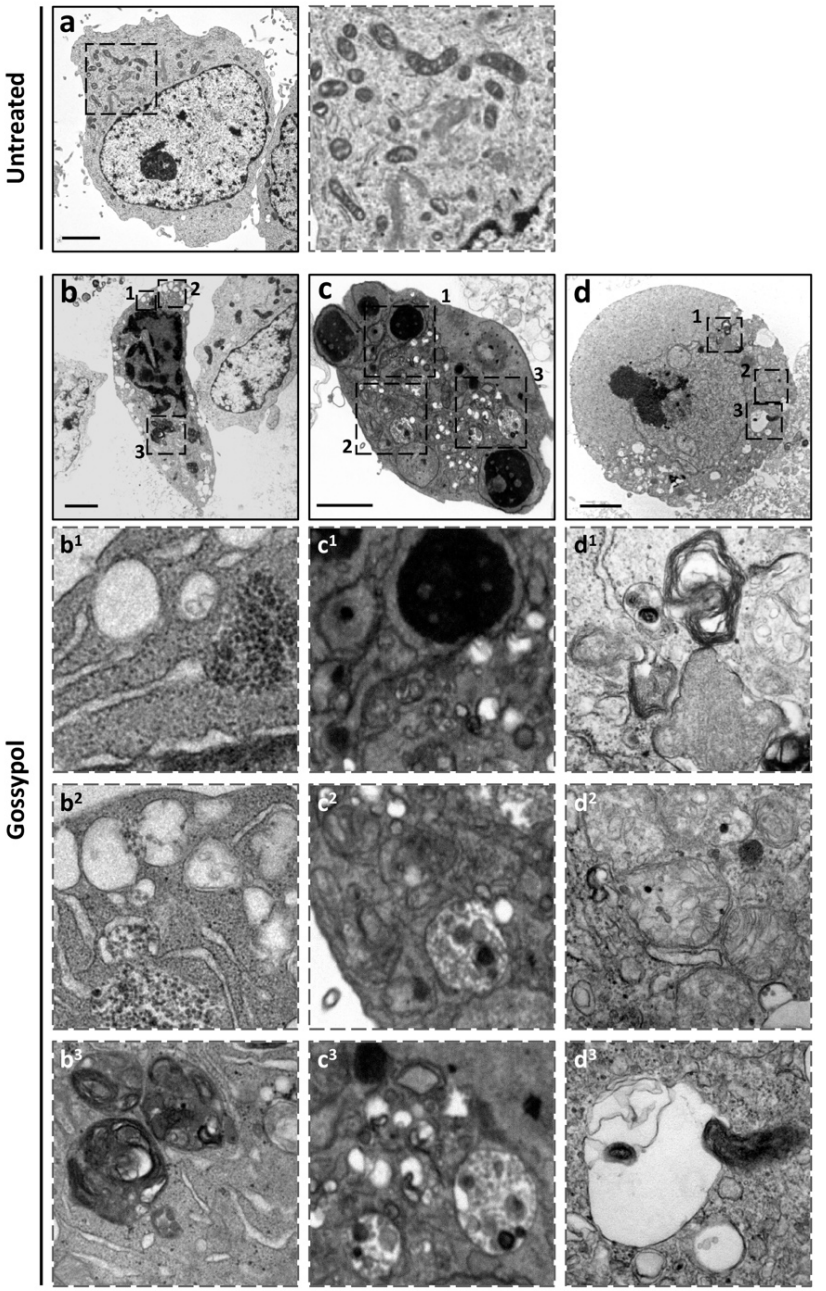

FIGURE R38. Different ultrastructural changes upon gossypol treatment in LN-18 cells. LN-18 cells were treated with 100 μM of gossypol for 14 hours or left untreated. Representative images of transmission electron microscopy are shown. Scale bar = 2 μm. Right panel (untreated) and lower panels (gossypol) are higher magnifications of the frames (numbers indicate the corresponding frame).

Overall, internal cellular membranes, including ER, GA, nuclear envelope, or mitochondria, appeared disrupted and dilatated (**Figure R38, b**[1,2]). Indeed, massive mitochondrial swelling was the principal ultrastructural feature observed after gossypol treatment. While mitochondria from untreated cells coincided with a well-defined transverse cristae (**Figure R38, a**), mitochondria from gossypol-treated cells were rounded and distended; with outer mitochondrial membrane discontinuities (**Figure R38, d**[2]); loss of cristae; and multi-laminated phospholipid whorls or concentric layers of phospholipids, probably originated from cristae membranes (**Figure R38, d**[1]). Additional electron microscopy images are presented in **Figure R48**.

As concluded above, the biochemical analysis of caspases was not sufficient to determine the particularity of gossypol versus other insults (such as staurosporine) to induce a higher percentage of apoptotic nuclear morphologies in GB-derived cells. This conclusion raised the possibility that additional biological processes could be involved. In this sense, results obtained from TEM images (**Figure R38**) suggested that a cellular process consistent with degradation and membrane reorganization may be behind the gossypol mechanism of action, being ER stress and/or an autophagic process possible candidates. Indeed, the bibliography supports gossypol both as an inducer of autophagy in glioma cells (Voss *et al.*, 2010) (Keshmiri-Neghab *et al.*, 2014), and as ER stress-inducing compound (Soderquist *et al.*, 2014).

As an easy readout to prove a gossypol-induced ER stress process in LN-18 cells, we used calnexin staining, a Ca^{2+}-binding chaperone lectin induced upon ER stress (Ni and Lee, 2007). We also took advantage of the pan-caspase inhibitor q-VD-OPh to report whether caspases were implicated or not in this process. Accordingly, LN-18 cells were left untreated or treated with gossypol in the presence or absence of q-VD-OPh. After 9 hours of treatment, cells were fixed and immunofluorescently stained for calnexin (green). The nuclei were counterstained with Hoechst 33258 (blue).

As shown in **Figure R39**, calnexin exhibited aggregation of the ER membrane proteins upon gossypol treatment regardless of caspase activation. Hence, indicating a caspase-independent induction of ER aggregates formation triggered by gossypol.

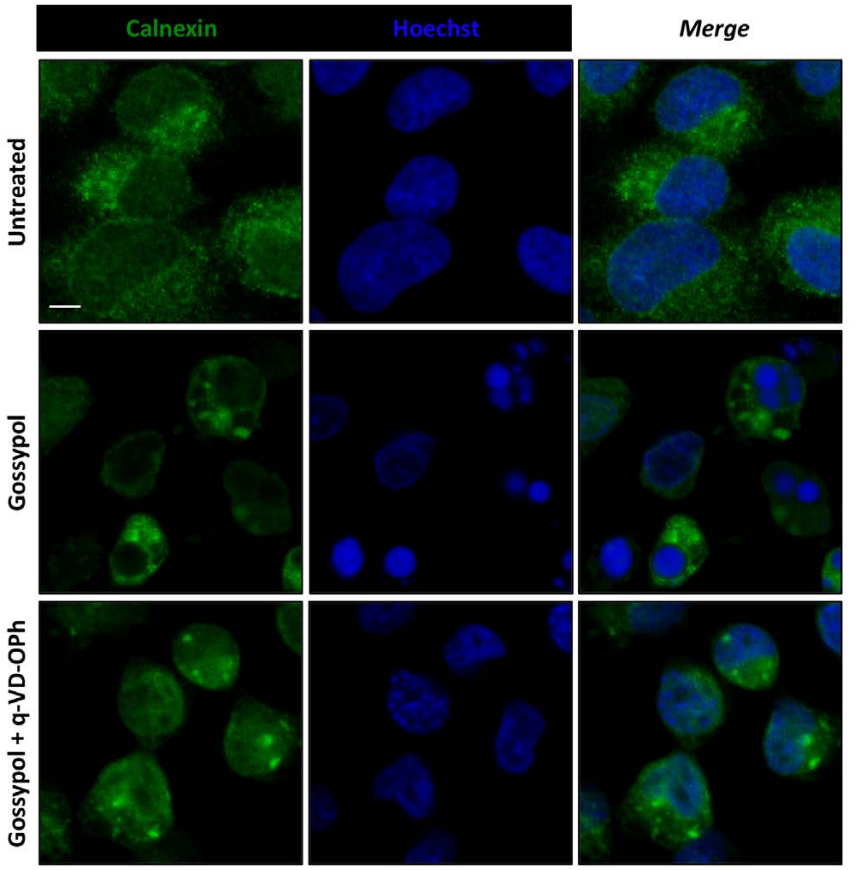

FIGURE R39. Caspase-independent aggregates of calnexin are detected upon gossypol treatment in LN-18 cells. LN-18 cells were treated with 100 μM of gossypol or left untreated in the presence (+) or absence of the pan-caspase inhibitor q-VD-OPh (q-VD) (20 μM). After 12 hours of treatment, cells were fixed and immunostained with a specific antibody against calnexin (green) (*left panel*) according to *Material and Methods*. Nuclei (gray) were stained with Hoechst 33258 (*middle panel*). Detailed representative confocal scanning images of each condition are shown. Arrows indicate calnexin aggregates. Scale bar = 5 μm.

Before performing a deeply biochemical study of the potential ER stress-induced upon gossypol treatment, we decided to challenge LN-18 cells to different ER stressed-described compounds (Varadarajan *et al.*, 2012). After 24 hours of treatment, cells were fixed, and nuclei were stained with bisbenzimide Hoechst.

As shown in **Figure R40**, dissimilar effects were observed when comparing the nuclear morphologies displayed upon each compound in LN-18 cells. Among them, two compounds (ivermectin and TW-37) depicted similar nuclear phenotype than gossypol. They induced the appearance of nuclear morphologies with chromatin compaction and fragmentation akin to type II apoptotic morphologies. However, the rest of the ER stressed-described compounds were not efficient at inducing those morphologies. Thus, suggesting that ER stress does not

seem to be the main mechanism of action responsible for the appearance of apoptotic nuclear morphologies in glioblastoma cells.

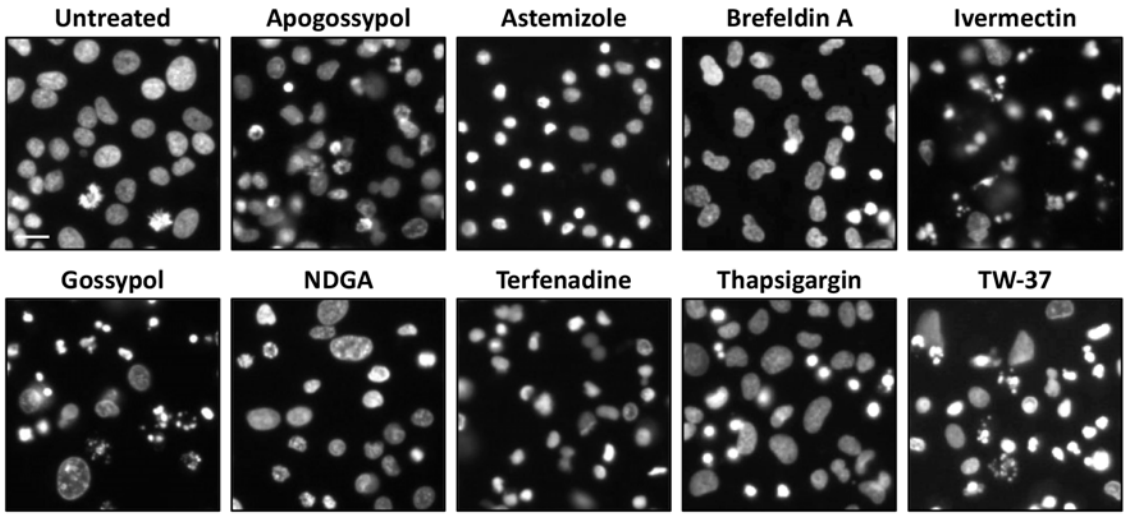

FIGURE R40. ER-stressor compounds trigger different nuclear outcomes in LN-18 cells. LN-18 cells were left untreated or treated with gossypol (100 μM), apogossypol (100 μM), astemizole (20 μM), brefeldin A (100 μM), ivermectin (100 μM), NDGA (400 μM), terfenadine (20 μM), thapsigargin (100 μM) and TW-37 (200 μM) for 24 hours. Then, cells were fixed and nuclear morphology was analyzed by staining the nuclei with Hoechst 33258. Images were obtained with a Nikon ECLIPSE TE2000-E microscope equipped with UV-light epifluorescence and a Hamamatsu ORCA-ER photographic camera. Representative microphotographs of each condition are shown. Scale bar = 20 μm.

22. Gossypol modulates autophagy in LN-18 cells

To address a possible involvement of autophagy over the nuclear morphologies observed in LN-18 cells upon gossypol treatment, we decided to challenge these cells with gossypol under serum-starved conditions. The different morphologies observed after 100 μM gossypol in complete media were impaired when using the same gossypol concentration in the absence of fetal bovine serum (FBS). Cells displayed an undefined nuclear aspect different from untreated cells but also different from type I, type II, or type III nuclear morphologies. Hence, lower concentrations of gossypol were used to determine the dose-effect profile of gossypol in the absence of FBS over the nuclear morphologies in LN-18 cells.

As shown in **Figure R41**, type II and type III nuclear morphologies were observed at lower concentrations of gossypol in the absence of FBS.

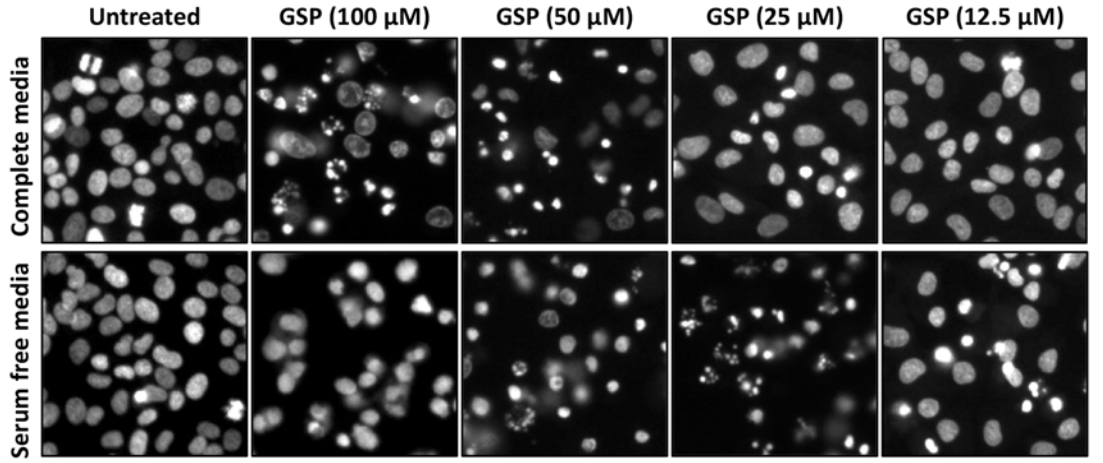

FIGURE R41. Gossypol induces dose-dependent apoptotic nuclear morphologies in the absence of fetal bovine serum in LN-18 cells. LN-18 cells were left untreated or treated with different concentrations of gossypol (GSP) in complete media or serum free media (DMEM). After 24 hours, cells were fixed and nuclear morphology was analyzed by staining the nuclei with Hoechst 33258. Images were obtained with a Nikon ECLIPSE TE2000-E microscope equipped with UV-light epifluorescence and a Hamamatsu ORCA-ER photographic camera. Representative microphotographs of each condition are shown. Scale bar = 20 μm.

As unfavorable cellular environments, such as nutrient deprivation, trigger pro-survival cellular processes such as autophagy, we wondered if this biological process may be behind the mechanism of gossypol. Since the location of LC3-II at the growing autophagosomes has rendered this lipidated form of LC3-I as an indicator of autophagy, we performed Western blot analysis of LC3 after gossypol treatment. Staurosporine, used in this project as a classical apoptotic inductor, was also included in the panel. Likewise, the pan-caspase inhibitor q-VD-OPh was also included in combination or not with gossypol or staurosporine. LN-18 cells were left untreated or treated with gossypol or staurosporine for 9 hours in complete media (which constitute the experimental culture condition employed in this work) in the presence or absence of q-VD-OPh. Then, we obtained protein extracts and proceeded with the Western blot.

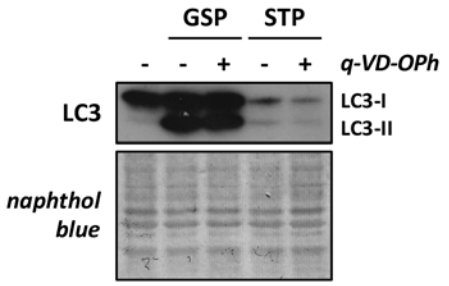

FIGURE R42. LC3- II accumulates in a caspase-independent manner upon treatment with gossypol in LN-18 cells. LN-18 cells were left untreated or treated for 9 hours with 100 μM gossypol (GSP) or 1 μM staurosporine (STP) in the presence (+) or absence (-) of the pan-caspase inhibitor q-VD-OPh (20 μM). After

treatment, cells were detached and Igepal CA-630-soluble protein extracts were obtained. Western blotting against LC3B was performed. Naphthol blue staining served as a protein loading control.

Figure R42 shows that LC3-I conversion to LC3-II occurs in LN-18 cells treated with gossypol in the presence or absence of q-VD-OPh. The differences between gossypol and staurosporine or untreated samples were apparent.

Due to these results, we decided to analyze the nuclear morphology triggered by gossypol in LN-18 cells combined with different compounds described as modulators of the autophagic process. For this, we used 3-methyladenine (3-MA), wortmannin, and PI-103, which inhibits autophagy by blocking autophagosome formation via the inhibition of type III Phosphatidylinositol 3-kinases (PI-3K), and rapamycin, which acts as an activator through inhibition of mTOR (Klionsky *et al.*, 2016). LN-18 cells were pre-incubated for 30 minutes with each compound and then treated in combination or not with gossypol. After 24 hours, cells were fixed and stained with Hoechst.

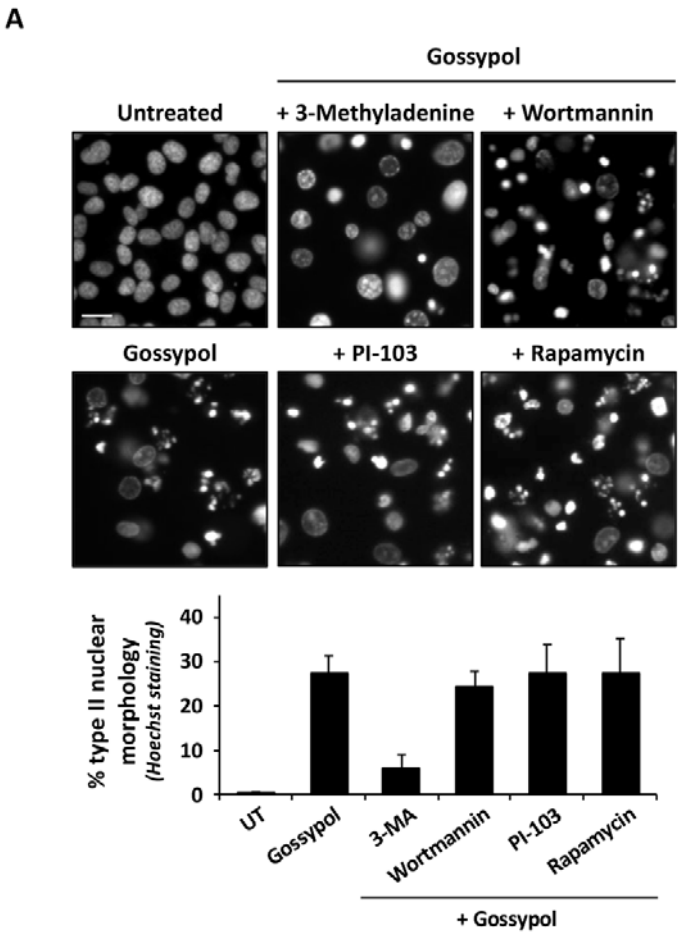

FIGURE R43. Gossypol-induced type II nuclear morphology is deferentially affected by different autophagy modulators. LN-18 cells were left untreated (UT) or treated with 3-methyladenine (3-MA) (10 mM),

wortmannin (200 μM), PI-103 (20 μM) or rapamycin (10 μM) for 30 minutes. Then, cells were left untreated (UT) or treated with gossypol (GSP) (100 μM) in the presence (+) or absence of 3-MA (5 mM), wortmannin (100 μM), PI-103 (10 μM), or rapamycin (5 μM) for 24 hours. After 24 hours, cells were fixed, and nuclear morphology was analyzed by staining the nuclei with Hoechst 33258. Images were obtained with a Nikon ECLIPSE TE2000-E microscope equipped with UV-light epifluorescence and a Hamamatsu ORCA-ER photographic camera. Representative microphotographs of each condition are shown. Scale bar = 20 μm. The percentage of type II *(black bars)* nuclear morphology was calculated. The graph represents the mean ± *SEM* (*error bars*).

As shown in **Figure R43**, only 3-MA impaired the type II nuclear morphologies observed upon gossypol treatment, decreasing the percentage of type II gossypol-induced morphologies from 27.14 ± 4.12 (gossypol) to 5.81 ± 3.19 (3-MA + gossypol). Therefore, we decided to proceed with this compound and to perform a more detailed study of the nuclear phenotype observed in the presence of 3-MA. Comparative analysis of gossypol and staurosporine, both in the presence or absence of 3-MA, was addressed.

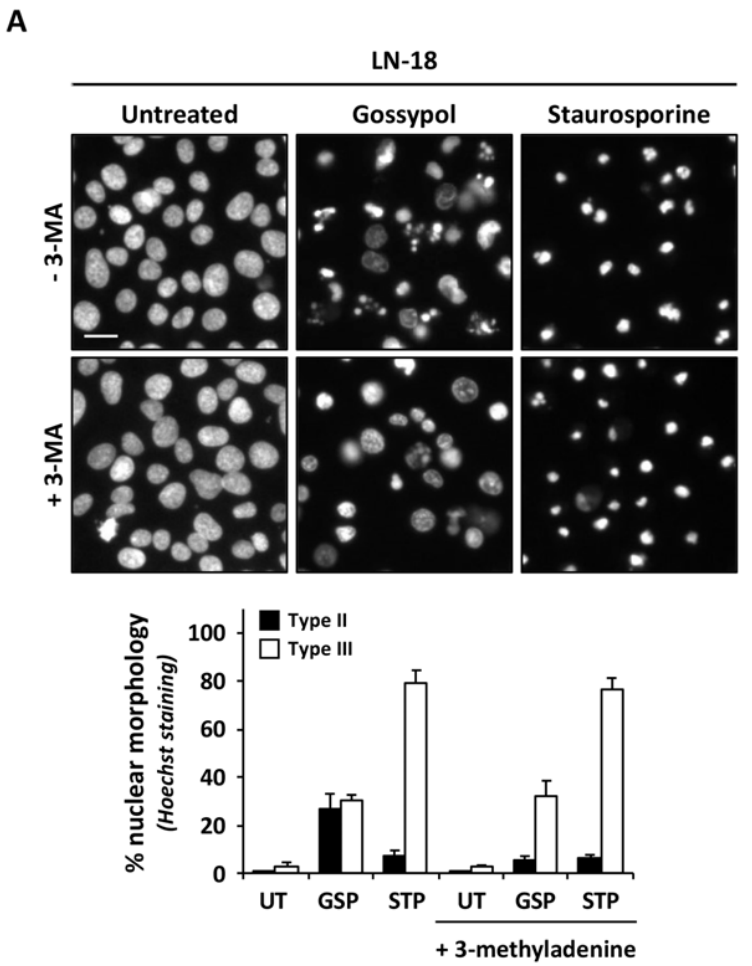

FIGURE R44. For figure legend, see next page.

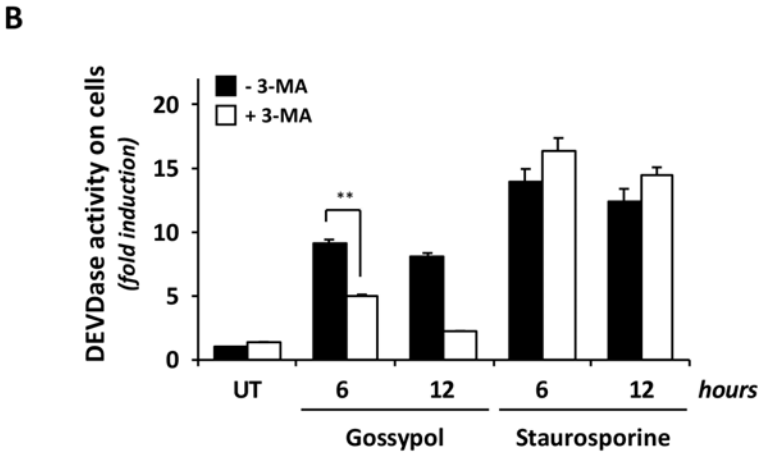

FIGURE R44. 3-methyladenine inhibits gossypol-triggered type II nuclear morphology and DEVDase activity in LN-18 cells. LN-18 cells were left untreated or treated with 3-methyladenine (3-MA) (10 mM) for 30 minutes. Then, cells were left untreated (UT) or treated with gossypol (GSP) (100 μM) or staurosporine (STP) (1 μM) in the presence (+) or absence (-) of 3-methyladenine (3-MA) (5 mM) for 24 hours (**A**) and 6 or 12 hours (**B**). **A,** after 24 hours of treatment, cells were fixed and nuclear morphology was analyzed by staining the nuclei with Hoechst 33258. Images were obtained with a Nikon ECLIPSE TE2000-E microscope equipped with UV-light epifluorescence and a Hamamatsu ORCA-ER photographic camera. Representative microphotographs of each condition are shown. Scale bar = 20 μm. The percentage of type II *(black bars)* and type III (*white bars*) nuclear morphology was calculated. The graph represents the mean ± *SEM* (*error bars*). **B**, DEVDase activity directly on cells was performed after the indicated times of treatments. Graphs represent the fold induction when compared to lysates from untreated cells (UT) from WT or DKO cells ± *SD* (*error bars*). The Student's *t*-test was used to determine the statistical significance (** means $p < 0.01$).

As previously shown in **Figure R43**, type II apoptotic nuclear morphologies induced by gossypol after 24 hours in LN-18 cells were impaired in the presence of 3-MA, whereas 3-MA did not affect type III nuclear morphologies induced either by gossypol or staurosporine (**Figure R44A**).

Regarding the involvement of caspases in both type II and type III nuclear morphology, we performed a DEVDase activity assay after 6 and 12 hours of treatment (**Figure R44B**).As shown in **Figure R44B**, DEVDase activity was impaired in gossypol-treated cells in the presence of 3-MA, whereas no differences were observed when using staurosporine in the presence or the absence of 3-MA. Thus, indicating that DEVDase activity induced by gossypol or staurosporine is differently affected by the addition of 3-MA.

Furthermore, we performed Western blotting to analyze the caspase-3 specific substrate α-fodrin upon gossypol treatment over time in the presence or absence of 3-MA. Unexpectedly, the p150 fragment and, to a lesser extent, the p120 fragment were detected from 1 hour of treatment with gossypol in the presence of 3-MA. However, these proteolytic fragments were

not detected before 6 hours of treatment with gossypol (**Figure R45A**). This result indicated that in the presence of 3-MA, the proteolysis of substrates such as α-fodrin is detected at earlier times.

The same protein extracts were used to analyze LC3-I conversion into LC3-II. As shown in **Figure R45B**, the conversion of LC3-I to LC3-II was detected from 1 hour of treatment with 3-MA in combination with gossypol in LN-18 cells. By contrast, we did not observe LC3-II before 3 hours of treatment when using gossypol alone. Levels of LC3-II were observed in a time-dependent manner when treating LN-18 cells with gossypol in the absence of 3-MA.

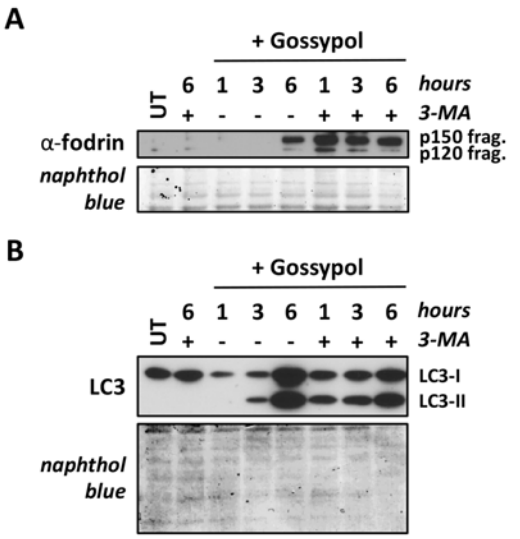

FIGURE R45. Gossypol-induced LC3-II lipidation and processing of α-fodrin are altered in the presence of 3-methyladenine. LN-18 cells were left untreated or treated with 3-methyladenine (3-MA) (10 mM) for 30 minutes. Then, cells were left untreated (UT) or treated with gossypol (100 μM) in the presence (+) or absence (-) of 3-methyladenine (3-MA) (5 mM) for 1, 3 and 6 hours. After the indicated times, cells were detached and Igepal CA-630-soluble protein extracts were obtained. Western blotting against LC3B (**A**) and α-fodrin (specific caspase-3 substrate) (**B**) were performed. Naphthol blue staining served as a protein loading control.

Because results showing LC3-II at a particular time point may not accurately reflect autophagic activity, the autophagic flux into the lysosomal compartment was investigated by analyzing LC3-II in the presence of a specific inhibitor of vacuolar-type H-ATPase. We treated LN-18 cells with gossypol in the presence or absence of the vacuolar ATPase inhibitor bafilomycin A_1 (Baf A_1). In parallel, and as a positive control, we used Krebs buffer (KH) (starvation medium), to induce the build-up of autophagosomes and autophagic flux. Levels of lipidated and non-lipidated LC3 proteins were analyzed through Western blot. According

to the latest recommendations (Klionsky *et al.*, 2016), the levels of LC3-II were compared to the loading control.

As shown in **Figure R46A**, cells cultured in KH showed increased levels of LC3-II in the presence of Baf A_1. Thus, suggesting that the autophagic flux triggered during starvation was appropriately inhibited in LN-18 cells in the presence of Baf A_1. Interestingly, the sole addition of Baf A_1 in LN-18 cells cultured in complete media reflected a basal autophagic flux in this cell line. Upon gossypol, LC3-II levels were detected after 3 hours and increased after 6 hours of treatment. In the presence of Baf A_1 treatment, the levels of LC3-II detected upon gossypol treatment were only increased after 3 hours (**Figure R46A**). Thus, suggesting a possible decrease of the autophagic flux, especially after 6 hours of gossypol treatment.

Regarding the nuclear morphologies induced by gossypol in the presence or absence of Baf A_1, we did not observe any difference either in the percentage of type II or type III nuclear morphologies (**Figure R46B**).

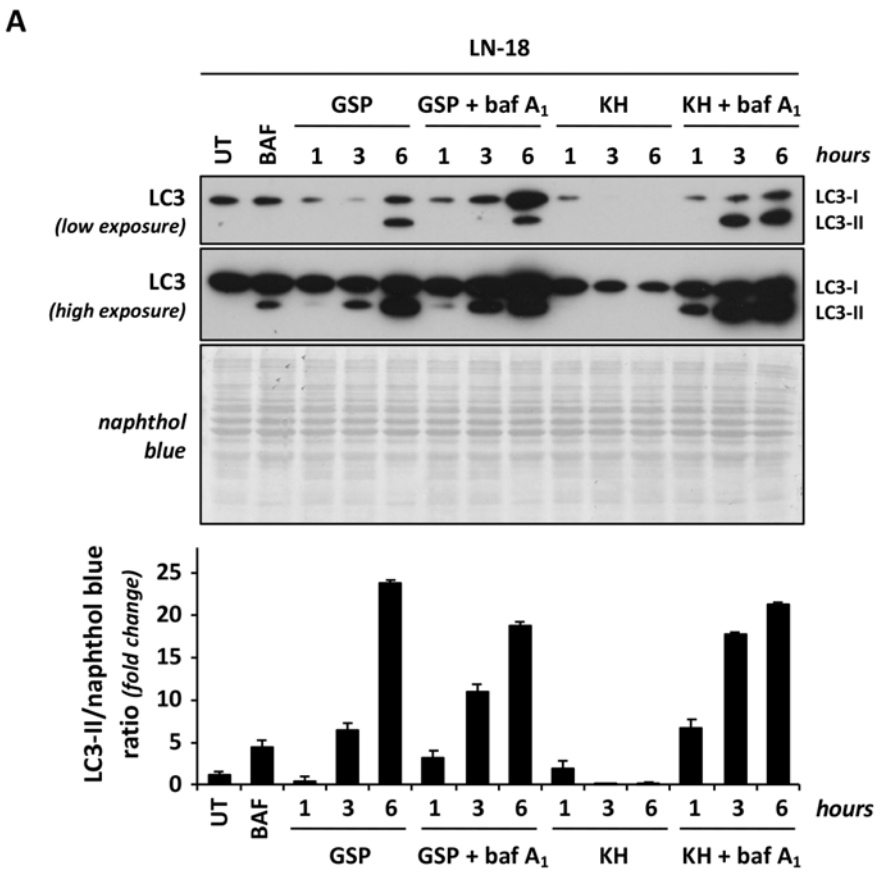

FIGURE R46. For figure legend, see next page.

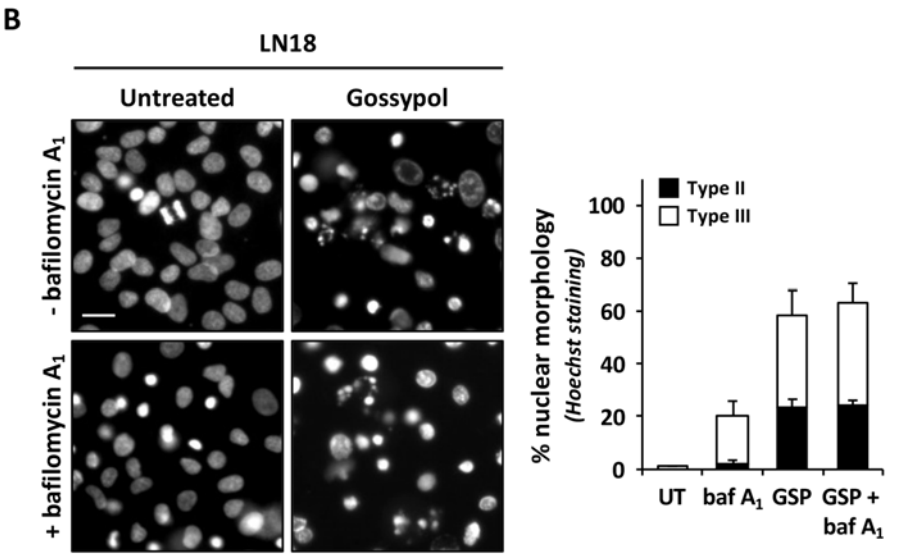

FIGURE R46. The autophagic flux is modulated upon gossypol treatment in LN-18 cells. LN-18 cells were left untreated (UT) or treated with bafilomycin A_1 (baf A_1) (200 nM) for 30 minutes. Then, cells were left untreated (UT) or treated with gossypol (100 μM) in the presence (+) or absence (-) of baf A_1 (100 nM). In parallel, cells were maintained in Krebs buffer (KH) in the presence (+) or absence of baf A_1 (100 nM). **A**, after 1, 3, and 6 hours, cells were detached and Igepal CA-630-soluble protein extracts were obtained. Western blotting against LC3B was performed. Naphthol blue staining served as a protein loading control. The ratio of LC3-II to naphthol blue was calculated based on densitometry analysis by using Fiji – ImageJ. Bars are shown as fold-change relative to untreated cells (UT) ± *SD* (*error bars*). **B**, after 24 hours, cells were fixed and nuclear morphology was analyzed by staining the nuclei with Hoechst 33258. Images were obtained with a Nikon ECLIPSE TE2000-E microscope equipped with UV-light epifluorescence and a Hamamatsu ORCA-ER photographic camera. Representative microphotographs of each condition are shown. Scale bar = 20 μm. The percentage of type II *(black bars)* and type III (*white bars*) nuclear morphology was calculated. The graph represents the means ± *SD* (*error bars*).

Considering the potential role of autophagy behind the gossypol mechanism of action and, especially, over the nuclear morphology, we blocked autophagy more specifically by depleting ATG5, a broadly accepted regulator of autophagy. We took advantage of $Atg5^{+/+}$ and $Atg5^{-/-}$ T-large antigen mouse embryonic fibroblasts (MEFs) (Salazar *et al.*, 2009).

As shown in **Figure R47**, the knockout of Atg5 ($Atg5^{-/-}$) allowed gossypol-treated cells to display condensation and fragmentation of the nucleus. Indeed, quantification of the nuclear morphologies showed that a higher percentage of type II nuclear morphologies were scored from $Atg5^{-/-}$ MEFs than from $Atg5^{+/+}$ MEFs. Overall, our results indicate that type II apoptotic nuclear morphologies triggered by gossypol are promoted in the absence of a key autophagy component such as ATG5.

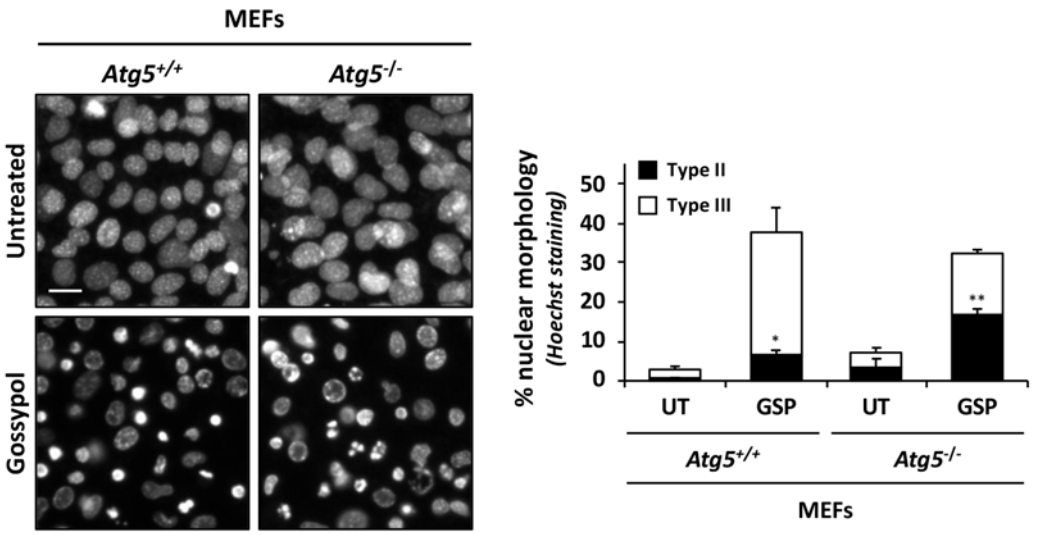

FIGURE R47. The percentage of type II nuclear morphology induced by gossypol increase in *Atg5*$^{-/-}$ MEFs. Atg5$^{+/+}$ and Atg5$^{-/-}$ mouse embryonic fibroblasts (MEFs) were left untreated (UT) or treated with 100 μM gossypol (GSP). After 24 hours of treatment, cells were fixed and nuclear morphology was analyzed by staining the nuclei with Hoechst 33258. Images were obtained with a Nikon ECLIPSE TE2000-E microscope equipped with UV-light epifluorescence and a Hamamatsu ORCA-ER photographic camera. Representative microphotographs of each condition are shown. Scale bar = 20 μm. Nuclei of each condition were scored either as type II *(black bars)* or III (*white bars*). Percentages of each nuclear morphology are represented by bar graphs ± *SEM* (*error bars*). The Student's *t*-test was used to determine the statistical significance of type II nuclear morphologies comparing treated (GSP) versus untreated (UT) conditions in each cell line (* means $p < 0.05$) (** means $p < 0.01$).

23. Electron microscopy images revel different ultrastructural changes between treatments in LN-18 cells

The nuclear morphology analysis by staining the nuclei with Hoechst 33258 and its visualization through a UV-light microscope has constituted a fundamental approach in this work. It has been essential to draw different conclusions related to the signaling pathways activated upon exposure of human glioblastoma-derived cells to different insults.

Alternatively, we took advantage of other microscope techniques, such as transmission electron microscopy (TEM) and scanning electron microscopy (SEM), to analyze ultrastructural changes in human glioblastoma-derived cells prompted to die. Additionally to the micrographs presented in **Figure R8** and **Figure R38**, **Figure R48** gathers further pieces of evidence to the morphological features displayed by human glioblastoma-derived LN-18 cells left untreated or treated with staurosporine, gossypol, TRAIL or the combination of gossypol and TRAIL.

Ultrastructural analysis of untreated LN-18 cells revealed different morphologies in size and shape with a large nucleus containing euchromatin and heterochromatin distributed throughout the nuclear compartment (**Figure R48A**). The analysis of different ultrathin sections evidenced an electro dense granular material compatible with the nucleoli and distribution of different organelles throughout the cytoplasm of LN-18 cells. As shown in **Figure R48B**, the integrity of the organelles was impaired in the presence of staurosporine. At the nuclear level, the main characteristics of cells challenged with this alkaloid coincided with a unique mass of highly condensed chromatin delimited by the nuclear envelope. The integrity of this nuclear membrane was affected in different staurosporine-treated cells. Due to the presence of discontinuities in the nuclear envelope, almost no differences were detected between nuclear and cytoplasm content. Moreover, points of attachment of the chromatin to the nuclear envelope were hardly identified.

However, we observed some cells showing chromatin compaction, fragmentation, and/or attachments to the nuclear membrane trying to display typical apoptotic images. Nonetheless, proper fragmentation of the nuclear envelope enclosing masses of compacted chromatin was not detected in staurosporine-treated cells. We only detected loop structures of the nuclear envelope, some of them closed and some others still open, free of chromatin, resembling empty apoptotic nuclear bodies (**Figure R48B**). Most of those characteristics coincided with the previously described in Sanchez-Osuna et al., 2014, and differed in texture, shape and pattern distribution with typical apoptotic images.

In the case of gossypol, the principal features observed at the cytoplasmic compartment included the presence of several vacuoles and vesicles, massive organelles disruption and disturbance, and dilatation of internal cellular membranes. Some cells also presented multiple breaks at the plasma membrane. At the nuclear level, electron microscopy analysis confirmed the pleiotropic nuclear phenotype of gossypol-damaged cells. Among the different nuclear morphologies displayed in LN-18 cells after treatment with gossypol, we observed cells with marginal condensation of the chromatin, forming irregular and interconnected masses of chromatin and a round compact nucleolus; cells displaying irregular non-interconnected chromatin masses dispersed throughout the nucleus; and morphologies resembling the nuclear phenotype of staurosporine-treated cells, showing a highly condensed electrodense mass detached from the nuclear envelope (and disrupted in some cells). Moreover, the ultrastructural morphology of gossypol-treated cells coincided with condensed and fragmented nuclei. Pieces of highly packed round masses of condensed chromatin surrounded by nuclear envelope were detected by electron microscopy in LN-18 cells treated with gossypol (**Figure R48C**).

Ultrastructural morphological analysis of TRAIL-treated cells revealed cells with an ultrastructural morphology akin to untreated LN-18 cells and cells with different degrees of chromatin condensation. We observed cells with chromatin migration to the edge of the nuclear envelope showing marginal condensation and with the presence of the nucleoli. Moreover, we observed cells with a compact chromatin margination towards a nuclear pole forming a cap-shaped mass beneath the nuclear envelope, and cells with nuclear shrinkage and abnormal chromatin condensation into a central nuclear clump containing small electron-lucent areas. In some cells, we could event detect two masses of highly condensed chromatin enclosed by the nuclear envelope. At the cytoplasmic level, disruption of the intracellular structural organization was observed in TRAIL-treated cells (**Figure R48D**).

As shown in **Figure R48E**, cells cotreated with gossypol and TRAIL presented a heavily damaged cytoplasm with alteration of cellular membranes, intracellular vesicle swelling and/or loss of mitochondrial ultrastructure. We observed cytosolic compartments with non-identifiable organelles and with long projections of membranous structures. The ultrastructural morphological appearance of the nuclei coincided with different chromatin clumps around the inner nuclear membrane and preserved attachment points. Multiple small rounded masses of condensed chromatin enclosed by continuous nuclear envelope were also detected.

Alternatively, in some LN-18 cells treated with gossypol and TRAIL, chromatin appeared condensed into a single highly condensed mass surrounded by a nuclear membrane, disrupted in some cells. Electro-lucent areas were observed inside the masses of condensed chromatin. Regarding this observation, it is necessary to stress that these small electron-lucent areas observed inside the highly condensed masses may coincide with parts of the nucleoli, such as the fibrillar center, which is a less dense material surrounded by the pars fibrosa or the nucleolus, or the nuclear lacunae. Hence, the high grade of compaction of different nuclear structures is complicated to discriminate between chromatin or nucleolar mass structures. Our results suggest condensation and fragmentation of the chromatin but also nucleoli breakage with segregation of the pars fibrosa and the pars granulosa.

Furthermore, electron microscopy revealed the invagination of the nuclear envelope and two double-membrane structures that appeared in close contact with one another with different attachment points (**Figure R48E**).

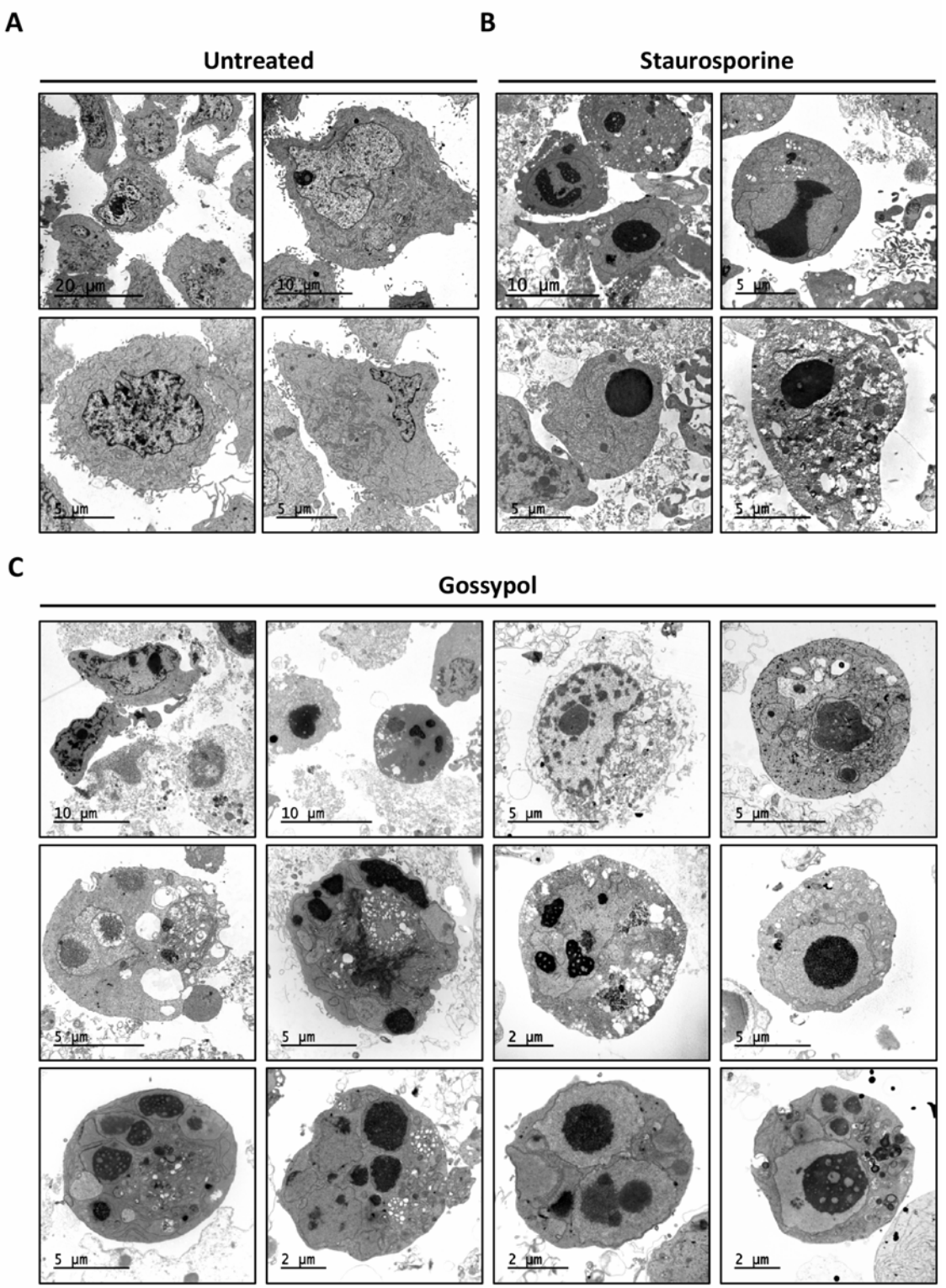

FIGURE R48. For figure legend, see next page.

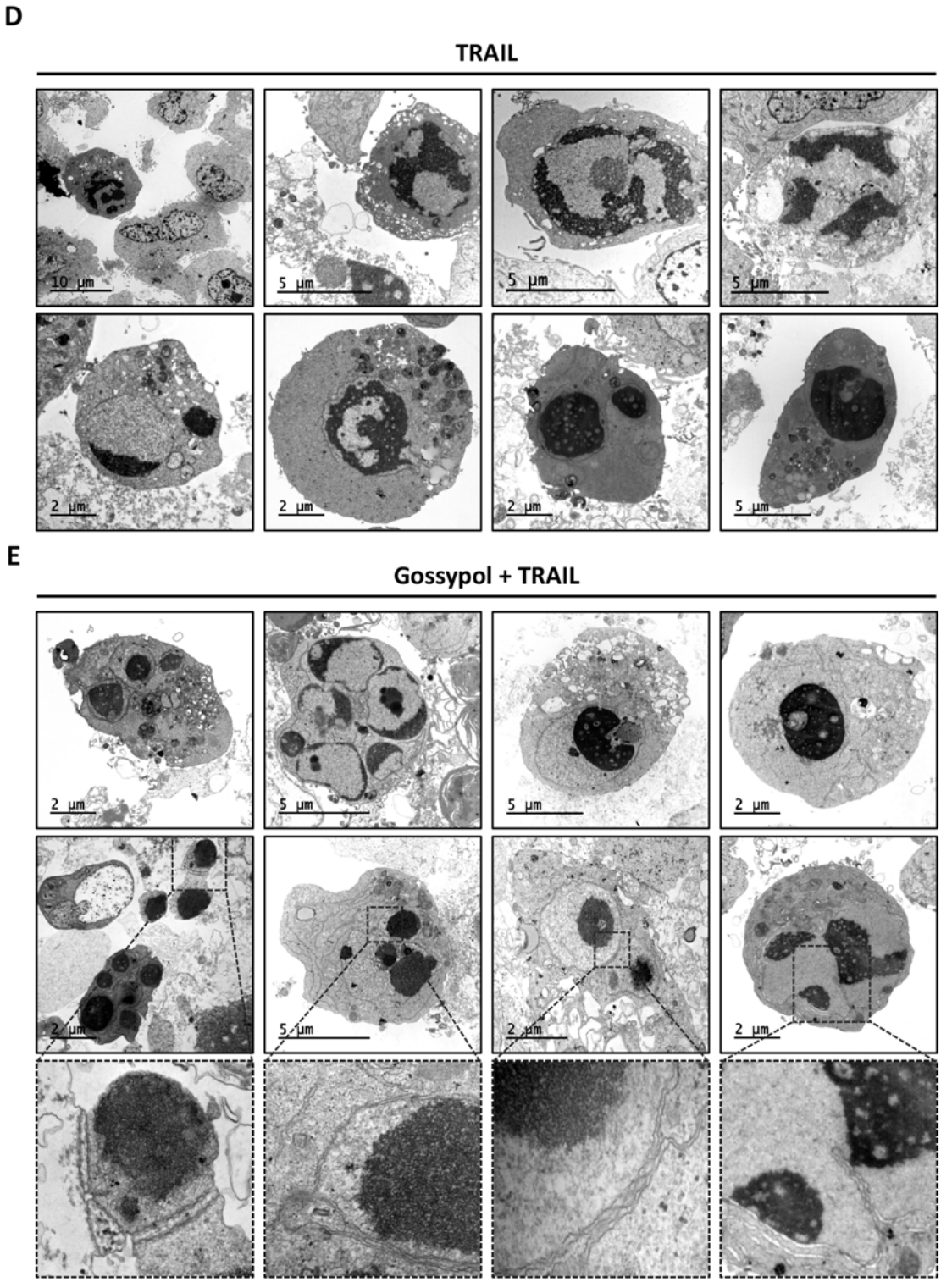

FIGURE R48. Transmission electron micrographs of LN-18 cells. LN-18 cells were left untreated (**A**) or treated with 1 µM staurosporine (**B**), 100 µM gossypol (**C**), 200 ng/ml TRAIL (**D**), or treated with the combination of gossypol plus TRAIL (**E**). After 14 hours, cells were detached and processed as described in *Material and Methods*. Representative general and detailed electron micrographs are shown. The frames indicate the area detailed in the bottom panels.

As mentioned above, we also performed morphological analysis of LN-18 cells by scanning electron microscopy (SEM) following a freeze-fracture method. The principal purpose of this technique was to study hidden internal structures, including the clustering of nuclear pores in LN-18 cells when faced to different insults. However, the breakage of frozen specimens did not always allow the observation of internal structures. As shown in **Figure R49A**, different untreated cells (upper panels) preserved the cellular plasma membrane; hence, hiding intracellular compartments. Indeed, when the cell was uncovered from its cellular membrane, we still observed conservation of the nuclear envelope. Fracture surfaces shown in the left bottom panel may be compatible with the inside face of the cellular membrane and the external face of the nuclear membrane. Cracked cells showing the inside of untreated cells are shown in the middle and right lower panels of **Figure R49A**. Concerning the principal features observed through TEM in staurosporine-treated cells, most of the structures presented in **Figure R49B** may reflect nuclei with a highly compacted chromatin mass limited by the nuclear envelope.

We also observed structures with holes that may coincide with the small electron-lucent areas evidenced by TEM and detected inside the unique mass of highly condensed chromatin or nucleolar structure in staurosporine-treated cells. As proper nuclear envelope fragmentation and formation of chromatin irregular masses of chromatin clumping was barely detected, the membrane structures observed close to the nuclear structure may coincide with empty apoptotic nuclear bodies. It is necessary to stress that chromatin-free closed-loop structures of the nuclear envelope were previously evidenced by TEM. Furthermore, we also treated LN-18 cells with the combination of gossypol and TRAIL to maximize the percentage of apoptotic nuclear morphologies.

As shown in **Figure R49C,** several blebs were present in LN-18 cells treated with this combinatorial approach. The blebs formed on the surface of different cells presented different textures and shapes. While some of them seemed to content dense structures inside, compatible with chromatin clumps, some others were empty. Chain-shaped structures were also visible, connecting different structures, which may be compatible with arrangements of membranes that presumably arose from the nuclear envelope or the endoplasmic reticulum. Morphologies akin to type I or type III nuclear morphologies were identified by SEM (upper panels **Figure R49C**).

The procedure followed to obtain scanning electron micrographs is under evaluation. The optimization of this method will help define the different structures identified and, therefore,

to understand better the different nuclear morphologies displayed upon cell death in human glioblastoma-derived cells.

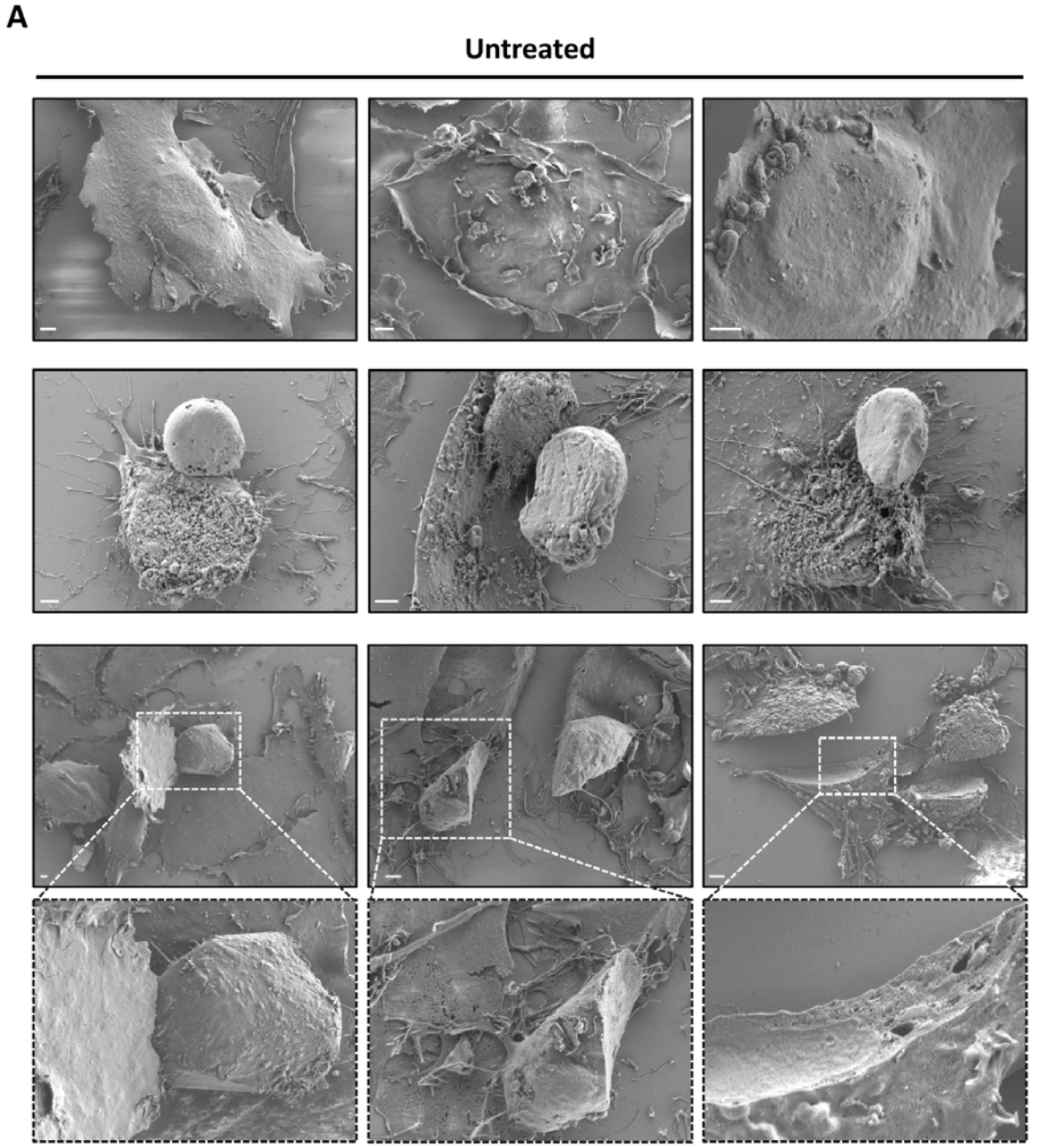

FIGURE R49. For figure legend, see page 210.

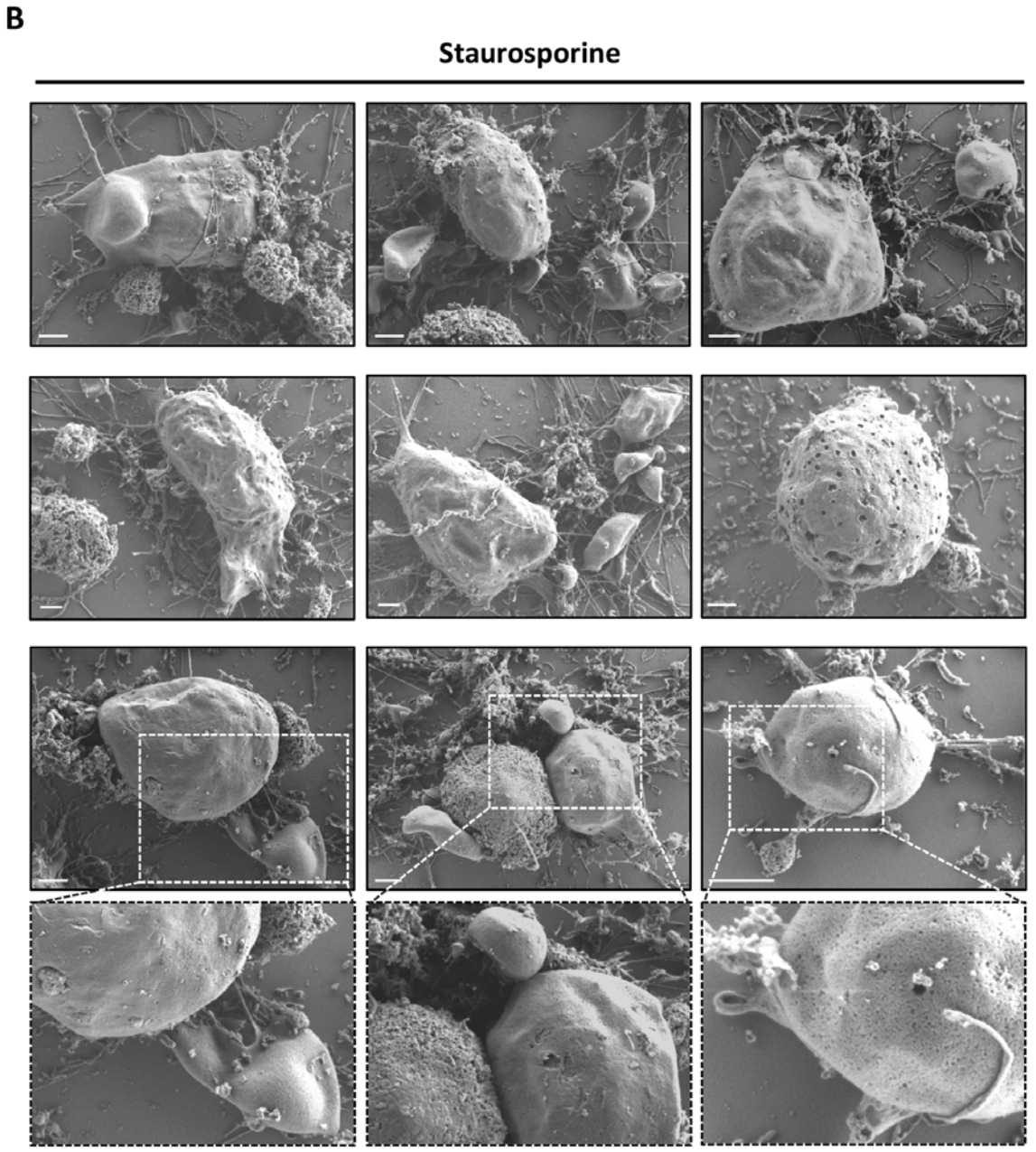

FIGURE R49. For figure legend, see next page.

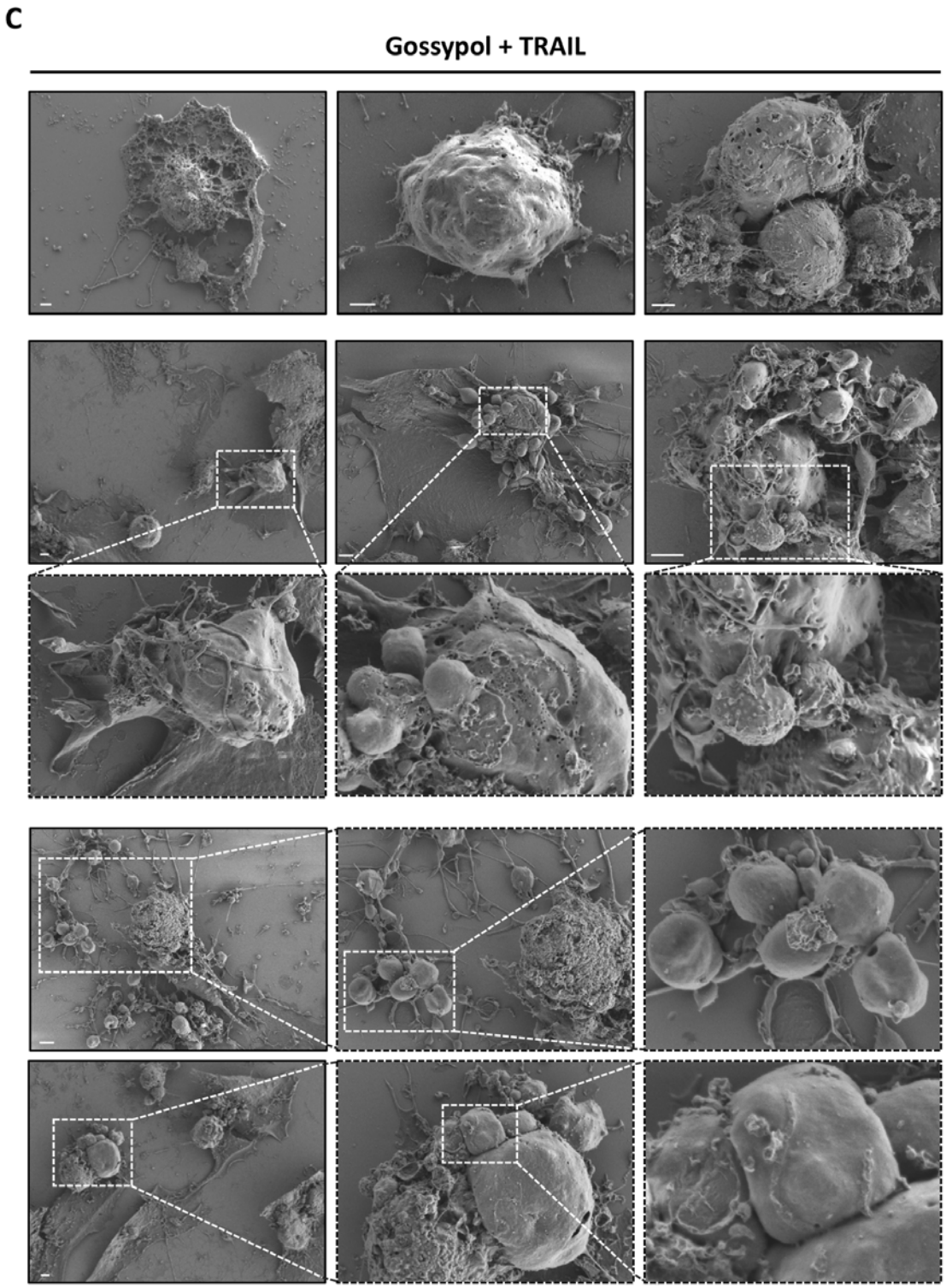

FIGURE R49. Scanning electron micrographs of LN-18 cells. LN-18 cells were left untreated (**A**) or treated with 1 μM staurosporine (**B**) or treated with the combination of 100 μM gossypol plus 200 ng/ml TRAIL (**C**). After 14 hours, cells were fixed and processed as described in *Material and Methods*. Representative general and detailed electron micrographs are shown. The frames indicate the area detailed in the bottom or right panels. Scale bar = 2 μm.

DISCUSSION

1. The nuclear morphology as a readout of intracellular differences in dying tumor cells

The cell is the basic unit of structure and organization in organisms. All cells from an organism will keep alive until its death. These simple affirmations hide more complex questions like *What pushes a cell to end with its life? What are the consequences (if there are any) for the neighboring cells? Do these consequences vary depending on the mechanism/s that this cell has employed to die?* These questions and many others have been on the focus of many researchers for more than two hundred years and still are. Only by understanding how these biological processes work, we will be able to have control over them and to fight against pathological situations such as cancer.

In the context of a tumor, strategies such as radiotherapy or chemotherapy have been developed to prompt tumor cells to die. However, defects on the machinery responsible for dismantling the cell are frequently detected and hamper the elimination of tumor cells (Hanahan and Weinberg, 2011). Glioblastoma, a highly aggressive brain tumor, clearly exemplifies the complexity to fully eliminate malignant cells not only due to the high resistance to cell death processes, such as apoptosis, but also because of its infiltrative behavior in the brain parenchyma. From our group, considerable efforts have been focused on the elucidation of potential mechanisms underlying the refractoriness of this cancer to therapeutically-induced cell death.

Although the actual trend is to define major cell death modalities based on genetic, biochemical, pharmacological, and functional parameters, it is necessary to stress the significance of the direct observation of cellular morphological changes during cell death. Many groups have invested substantial efforts to comprehend how cells and, especially, the nucleus change during the process of cell death (Clarke, 1990) (Tone *et al.*, 2007). Indeed, the detailed study of the cellular morphology was crucial to determine different types of cell death (Kerr *et al.*, 1972) (Leist and Jaattela, 2001).

In apoptosis, the condensation and fragmentation of the nucleus into smaller pieces is a particular morphological aspect linked to this type of cell death (a nuclear morphology referred to as type II in this text). However, alternative morphological outcomes have been identified in different cell types challenged with apoptotic-described insults. Upon staurosporine treatment, neuroblastoma-derived SH-SY5Y cells undergo apoptosis with type II nuclear morphology, whereas IMR-5 and IMR-32 cells, different human neuroblastoma-derived cell lines, display peripheral chromatin condensation with marginal and irregular masses of heterochromatin (a nuclear morphology referred to as type I) (Boix *et al.*, 1997).

The addition of staurosporine to the culture media of IMR-5 cells prompts an adequate activation of the principal machinery involved in apoptosis but does not trigger type II nuclear morphology. Therefore, it evidences that staurosporine, although described as a well-known inductor of apoptosis in many cell types (Bertrand *et al.*, 1994) (Jacobson *et al.*, 1994), may not be able to trigger typical apoptotic images of chromatin condensation and fragmentation in some cells. Another example of an alternative morphological phenotype induced upon staurosporine treatment was described by our group in human glioblastoma derived LN-18 cells (Sanchez-Osuna *et al.*, 2014). The analysis of the nuclear morphology after treatment with a broad panel of cytotoxic insults, including staurosporine, revealed a prominent nuclear pyknosis in the absence of karyorrhexis as the principal nuclear outcome displayed in these cells (a nuclear morphology here referred to as type III). Some treatments induced type I or a mixture of type I and type III nuclear morphologies, but classical apoptotic nuclear features were not identified after the different challenges (Sanchez-Osuna *et al.*, 2014). Together, results obtained from human neuroblastoma- and glioblastoma-derived cells evidence that different cells may show different morphological aspects when challenged with the same compound, and the same cell line may display different nuclear outcomes when faced to different compounds.

The stimuli employed but also the intracellular machinery from each cell type will determine the final morphological aspect. In this line, the analysis of the nuclear morphology may give us clues to better understand different intracellular signaling pathways governing cell death.

This work evidences that human glioblastoma-derived cells, previously defined as apoptotic-defective cells (Sanchez-Osuna *et al.*, 2014), holds the intracellular machinery required to display apoptotic nuclear morphologies. Commercial glioblastoma cell lines (A172, LN-229, LN-18 or U251-MG) and non-commercial glioblastoma cells (#04, #12) display type II nuclear morphologies upon treatment with gossypol. It indicates that the nuclear morphology displayed by these cells can be manipulated by using the adequate stimuli. Moreover, the electron microscopy analysis of gossypol-treated cells reveals cells with classical apoptotic nuclear morphologies with condensation, fragmentation, and packaging of the genomic content. By contrast, electron microscopy images from staurosporine-treated LN-18 cells evidence nuclei with condensed chromatin without proper enclosure by the nuclear envelope and without segregation of the chromatin into smaller masses. Considering that the nuclear outcome induced by staurosporine is shared among most of the cytotoxic insults employed (Sanchez-Osuna *et al.*, 2014), we may hypothesize that glioblastoma cells tend to do not safely package the chromatin content upon cell death. How does gossypol alter this tendency and

prompts human-glioblastoma cells to safeguard the genomic content into small rounded bodies delimited by nuclear envelope?

A family of cysteine proteases called caspases, and the endonuclease DFF40/CAD have been extensively reported as principal drivers of this apoptotic nuclear outcome. Hence, the observation of type II nuclear morphology upon gossypol treatment suggests that this compound may trigger an adequate activation of caspases and DFF40/CAD in human glioblastoma-derived cells.

2. The intracellular machinery behind the nuclear morphologies induced upon gossypol treatment

Activated caspases are principal regulators of the proteolytic cleavage of different cellular substrates (Talanian *et al.*, 1997) (Stroh and Schulze-Osthoff, 1998) (Taylor *et al.*, 2008). The culture of LN-18 cells in the presence of a pan-caspase inhibitor (q-VD-OPh) impedes classical apoptotic type II nuclear morphologies induced by gossypol. A nuclear outcome also impaired in gossypol-treated breast carcinoma MCF-7 cells, a cell line reported to lose caspase-3 due to a base pair deletion impeding translation of the CASP-3 mRNA (Janicke *et al.*, 1998b). The authors of this publication revealed the absence of DNA fragmentation and of the typical apoptotic morphological changes regardless of the sensitivity of these cells to TNF- (tumor necrosis factor) or staurosporine-induced apoptosis (Janicke *et al.*, 1998b). From our results, it is necessary to stress that type III nuclear morphologies induced by gossypol are also impeded in the presence of a caspase inhibitor and in cells null for caspase-3 such as MCF-7 cells. Hence, our results sustain the key role of caspases in the regulation of the nuclear changes observed upon cell death and, specifically, point caspase-3 activation as the bottleneck for both type II and type III nuclear morphologies induced by gossypol. As previously reported by our group, the addition of q-VD-OPh to the culture media of staurosporine-treated LN-18 cells impairs type III nuclear morphologies (Sanchez-Osuna *et al.*, 2014). Therefore, regardless of the stimuli, either gossypol or staurosporine, type II and type III nuclear morphologies require from the activation of caspases.

Regarding the nuclear morphologies observed in the context of caspases inhibition, Johnson *et al.* claim that the nuclear aspect of Jurkat T cells cultured in the presence of staurosporine and caspase inhibitors correspond to a pre-apoptotic nuclear morphology preceding chromatin condensation (Johnson *et al.*, 2000). The principal characteristics reported by the authors included convoluted nuclei with cavitations and patches of localized partially-condensed chromatin abutted along the inner part of the nuclear membrane. The idea of a

key morphological change of the nuclei preceding DNA degradation was previously referred to in (Cohen *et al.*, 1992). Cohen *et al.* observed a partial chromatin condensation in thymocytes treated with dexamethasone in the presence of Zn^{2+}. Note that DFF40/CAD was not discovered at that time yet. Conversely, other authors described that the nuclear morphology of Rat-1/c-MycER^{TM} cells undergoing apoptosis in the presence of caspase inhibitors coincided with a dramatic cytoplasmic blebbing in the absence of chromatin condensation (McCarthy *et al.*, 1997). However, according to the experience acquired by doing this Thesis, a detailed analysis of the images provided by the authors suggests higher peripheral chromatin condensation and an electrodense mass inside the nucleus of these cells.

Regarding our results, the analysis of the nuclear morphology by Hoechst 33258 staining indicates that the aspect of the chromatin of LN-18 cells treated with gossypol in the presence of q-VD-OPh is clearly different to that of untreated cells. The nuclear morphology observed in these cells coincides with a peripheral chromatin condensation that resembles the nuclear morphology (referred to as type I) induced by gossypol. The observation of this caspase-independent nuclear morphology in LN-18 cells treated with gossypol, in the absence of a caspase inhibitor, and also in MCF-7 cells challenged with gossypol indicate that caspases, and caspase-3 in particular, are not involved in the generation of type I nuclear morphology induced upon gossypol treatment (a nuclear aspect not observed in staurosporine-treated LN-18 cells, and slightly different from the caspase-independent nuclear morphology observed in cells cultured with staurosporine and q-VD-OPh or in staurosporine-treated MCF-7 cells). In this sense, our results suggest that different caspase-independent nuclear morphologies may be displayed upon cell death. Considering this possibility, we may hypothesize that different intracellular processes may be governing caspase-independent nuclear morphologies induced either by staurosporine or gossypol. In this sense, electron microscopy analysis may help to determine possible differences between caspase-independent morphologies observed after gossypol or staurosporine treatment.

Besides the study of caspases and their implication in the dismantling of damaged cells, the discovery of DFF40/CAD (Liu *et al.*, 1997) (Enari *et al.*, 1998) (Halenbeck *et al.*, 1998), the endonuclease responsible of the DNA degradation during apoptosis, meant significant progress in the comprehension of this type of cell death. Works from the group of Dr. Xiaodong Wang revealed that DFF40 is sufficient to trigger both DNA fragmentation and chromatin condensation during apoptosis (Liu *et al.*, 1998). In cells proficient at displaying apoptotic morphologies, the knockdown of DFF40/CAD reveals type I nuclear morphologies and impairs apoptotic nuclear morphologies (Iglesias-Guimarais *et al.*, 2013). Likewise, the silencing of DFF40/CAD in LN-18 cells impairs gossypol-induced chromatin

condensation and fragmentation. Type II nuclear morphologies induced by gossypol are also impeded in the hICAD$_L$-D117E mutant. Thus, either by knockdown of the endonuclease in LN-18 cells or through experiments with a non-functional ICAD·CAD system (like SH-SY5Y hICAD$_L$ D117E cells), we confirm that DFF40/CAD endonuclease is necessary for the type II nuclear morphology observed upon gossypol treatment. Nonetheless, as demonstrated in previous work performed in CAD-deficient chicken DT40 cells (Samejima *et al.*, 2001), DFF40/CAD is dispensable for the formation of type I nuclear morphologies. Moreover, our results also determine that DFF40/CAD does not participate in the formation of type III nuclear morphologies induced by gossypol in LN-18 cells, which is in line with unpublished results from our laboratory showing that the specific knockdown of the endonuclease does not affect this nuclear morphology in staurosporine-treated LN-18 cells. In this sense, results from our group suggest that LN-18 cells may be equipped with molecular cues that hamper the completion of apoptosis in these cells (Sanchez-Osuna *et al.*, 2014). Therefore, this intrinsic obstacle for the formation of type II nuclear morphologies may prompt glioblastoma cells to display type III nuclear morphologies upon caspases activation.

Considering that the overexpression of DFF40/CAD was enough to restore apoptotic nuclear features in defective cells such as IMR-5 (Yuste *et al.*, 2001), we could assume that overexpression of the endonuclease in DFF40/CAD-deficient human glioblastoma-derived cells would be sufficient to prompt cells to display type II nuclear morphologies. Nonetheless, the percentage of type III nuclear morphologies induced upon staurosporine treatment in DFF40/CAD-overexpressing LN-18 cells is similar to that observed in mock-transfected LN-18 cells, and the overexpression of the endonuclease is not sufficient to observe type II nuclear morphologies in LN-18 cells treated with staurosporine (Sanchez-Osuna *et al.*, 2014).

We may argue that staurosporine is a non-adequate stimulus to trigger this nuclear outcome in human glioblastoma-derived cells. However, the number of DFF40/CAD-dependent nuclear morphologies observed upon gossypol treatment is not significantly affected by the overexpression of the endonuclease.

The fact that the overexpression of DFF40/CAD does not increase significantly gossypol-induced type II nuclear morphologies leads to the conclusion that the levels of the endonuclease *per se* are not the only limiting factor impairing the formation of this nuclear outcome in glioblastoma cells. In this sense, different intracellular proteins have been described to regulate DFF40/CAD (Hanus *et al.*, 2008). Therefore, an intracellular excess of negative regulators or limited presence of positive regulators of the endonuclease will impair the proper condensation and fragmentation of the chromatin in these cells upon cytotoxicity.

Overall, our results suggest that an unfavorable intracellular context impedes the proper function of DFF40/CAD as an endonuclease.

The observation of type III nuclear morphologies as the principal nuclear outcome displayed by glioblastoma after treatment with different insults gives more weight to this hypothesis. Regardless of the stimuli and the levels of the endonuclease, human glioblastoma-derived cells own an intrinsic mechanism limiting the number of cells that die inducing chromatin condensation, fragmentation, and enclosure of its genomic content into different apoptotic nuclear bodies. Results obtained from cell-free *in vitro* assays performed in our laboratory determined that the refractoriness of LN-18 cells to undergo apoptotic nuclear morphology relies on both nuclear and cytoplasmic impairments (Sanchez-Osuna *et al.*, 2014). In this sense, it seems feasible to hypothesize that gossypol, either directly or indirectly, facilitates the proper activation of the endonuclease and, therefore, prompts human glioblastoma-derived cells to display type II nuclear morphologies.

Since both type III (DFF40/CAD-independent) and type II (DFF40/CAD-dependent) are here confirmed as caspase-dependent nuclear morphologies, differences regarding caspase activation and/or ICAD cleavage, the principal regulator of DFF40/CAD, may explain differences between staurosporine- and gossypol-induced nuclear morphologies. In this line, we present that gossypol induces the generation of the p17 fragment of caspase-3 and the generation of the p11 fragment of ICAD. In the case of caspase-3, p17 fragment corresponds to the fully mature form of caspase-3 (Han *et al.*, 1997). In the case of ICAD, the generation of p11 fragment is described to be necessary for the complete release of the endonuclease (Tang and Kidd, 1998). Thus, our results show adequate caspase-3 activation, as well as proper ICAD processing upon gossypol treatment. As this result was previously described upon staurosporine treatment in glioblastoma cells (Sanchez-Osuna *et al.*, 2016), we conclude that caspase-3 cleavage and processing of ICAD can be detected regardless of the final nuclear outcome and, therefore, are not an accurate reflection of complete apoptotic cell death with chromatin condensation and fragmentation. The same is concluded regarding the processing of other caspases such as the initiator caspase-9 and executioner caspases-7 and -6.

Nevertheless, although initiator and executioner caspases become correctly processed to its active fragments after gossypol or staurosporine treatments, we do observe differences regarding the intensity of those fragments. Here, we present that the comparison of the same time points of treatment mirror higher intensity cleavage of caspases upon staurosporine treatment than upon gossypol treatment. Indeed, we show that cleavage of initiator and effector caspases occurs at earlier times after staurosporine than after gossypol treatment. The

fact that staurosporine is inducing higher and earlier caspase processing than gossypol may suggest that an early and potent activation of caspases would be facilitating and promoting type III nuclear morphologies with chromatin condensation without signs of fragmentation in glioblastoma cells. In this sense, published results from our group show that early and robust activation of caspases impedes the formation of apoptotic nuclear morphologies in SH-SY5Y cells treated with chelerythrine. Moreover, we described that a delay in the activation of caspase-3 allows chelerythrine-treated SH-SY5Y cells to display apoptotic-like nuclear alterations (Garcia-Belinchon *et al.*, 2015). In the case of LN-18 cells, a delay in the activation of caspases, like observed upon gossypol treatment, may contribute to a better formation of type II nuclear morphologies. However, it is necessary to stress that the nuclear morphology observed in SH-SY5Y cells as a result of early and prominent activation of caspases concedes with the nuclear morphology of necrotic cells. This nuclear morphology differs from the type III nuclear morphology induced by staurosporine in LN-18 cells.

Moreover, the hypothesis that early and high levels of caspase activation could be detrimental for the formation of type II nuclear morphologies is here rejected by the results obtained from the combination of gossypol and TRAIL. This combinatorial approach, which triggers the processing of caspases and ICAD cleavage similar to staurosporine, allows the formation of type II nuclear morphologies. Indeed, compared to gossypol treatment, the percentage of both type II and type III nuclear morphologies are higher after the cotreatment of gossypol and TRAIL. Thus, our results suggest a dissimilar model from that described in chelerythrine-treated SH-SY5Y cells (Garcia-Belinchon *et al.*, 2015). Early and robust activation of caspases does not impede the formation of apoptotic nuclear morphologies in LN-18 cells treated with gossypol in combination with TRAIL. The differential activation of caspases seems to be determined by the relative potency of each treatment.

Since the cytoplasmic release of cytochrome *c* from the mitochondria constitutes an upstream signal in the activation of caspases (Ow *et al.*, 2008), differences in the induction of its release may explain the differences observed in the activation of caspases. In this line, the release of cytochrome *c* to the cytoplasm is detected from 3 hours of either staurosporine or gossypol plus TRAIL treatments. In contrast, it is not detected over 6 hours of treatment with gossypol in LN-18 cells. This delay in the activation of caspases upon gossypol treatment was also observed in chronic lymphocytic leukemia (CLL) cells. A comparative study of different BH3-mimetic compounds in CLL cells determined that cytochrome *c* release and the activation of caspases are detected at later times upon gossypol treatment than upon treatment with ABT-737 or chelerythrine (Vogler *et al.*, 2009). Hence, our results suggest that the delay in caspase

activation upon gossypol treatment may be due to late permeabilization of the mitochondria compared to staurosporine or gossypol and TRAIL treatments.

According to the literature, most intrinsic cytotoxic insults require from the formation of BAX/BAK pores at the mitochondrial membrane for mitochondrial other membrane permeabilization (MOMP), the release of cytochrome *c* and activation of caspases (Wei *et al.*, 2001). In this sense, we may presume that the same mechanism may be required to trigger apoptosis upon gossypol treatment. However, our results show that type II and type III nuclear morphologies induced by gossypol in *wild-type* (*wt*) mouse embryonic fibroblasts (MEFs) are only partially rescued in *Bax/Bak* double-knockout (DKO) MEFs. This result is in sharp contrast with the nuclear response observed after staurosporine treatment in the same cells. Staurosporine-induced type III and type II nuclear morphologies in *wt* MEFs are completely prevented in *Bax/Bak* DKO MEFs. It is necessary to stress that the observation of type III nuclear morphologies as the principal nuclear outcome induced by staurosporine in *wt* MEFs suggests these cells as a similar model to LN-18 cells. Hence, these results indicate that type III nuclear morphologies induced upon staurosporine treatment depend on the mitochondrial or intrinsic pathway that involves BAX and BAK. By contrast, a different pathway seems to be triggered upon gossypol treatment. The lower percentage of type III and type II nuclear morphologies induced by gossypol in *Bax/Bak* DKO MEFs suggests that two different mechanisms may be behind the formation of these morphologies in *wt* cells: a BAX/BAK-dependent and a BAX/BAK-independent mechanism. Similarly, Vogler *et al.* stated that gossypol-induced cell death in *wt* MEFs is clearly more potent that in DKO MEFs, which suggests that BAX and/or BAK are involved in cell death induction upon gossypol treatment. Moreover, our results indicate that both mechanisms require the activation of caspases to induce these nuclear morphologies. The activation of executioner caspases such as caspase-3 and the formation of type II and type III nuclear morphologies in *wt* or DKO MEFs are impaired in the presence of q-VD-OPh. In this sense, it gives further confirmation of caspases as the bottleneck for these nuclear morphologies regardless of the cellular model.

The activation of caspases and the induction of apoptotic morphologies in the absence of BAX/BAK is supported by different studies. The group of Y. Tsujimoto reported a BAX/BAK-independent mechanism of cytochrome *c* release after the exposure to the combination of calcium ionophore A23187 and arachidonic acid. Besides cytochrome *c* release, *Bax/Bak* DKO MEFs faced to these agents show activation of caspases and nuclear pyknosis with signs of fragmentation (Mizuta *et al.*, 2007). Moreover, the authors stated that this mechanism of cytochrome *c* release is regulated by serine protease(s) but neither by the BCL-2 family proteins nor cyclophilin D (CypD), which is involved in Ca^{2+}-dependent

cyclosporin A (CsA)-sensitive increase of mitochondrial permeability transition (MPT). Similarly, Zamorano *et al.* described a BAX/BAK and CypD-independent intrinsic apoptosis pathway under combined stimulation of ER stress and mild serum withdrawal (Zamorano *et al.*, 2012). Together, both articles suggest the existence of an alternative mitochondrial regulatory mechanism in which the release of cytochrome *c* and the activation of caspases occur in the absence of BAX and BAK and CypD.

More recently, Heimer *et al.* have described that BAX/BAK and BOK are dispensable for the activation of caspases upon Raptinal treatment (Heimer *et al.*, 2019). The particularity of this newly developed compound is that it rapidly triggers cytochrome *c* release and subsequent caspase-9-dependent propagation of the death signal (Palchaudhuri *et al.*, 2015) (Heimer *et al.*, 2019). However, since the release of cytochrome *c* and caspase activation triggered by gossypol does not occur as quickly, the speed of activation of the intrinsic apoptotic pathway does not seem to be an essential factor for the activation of apoptosis.

Some factors that could be involved in BAX/BAK-independent cytochrome *c* release include: the cleavage of serine protease substrates in the mitochondria leading to conformation changes allowing the release of cytochrome *c* (Mizuta *et al.*, 2007); the existence of a specific signal emerging from the ER (Zamorano *et al.*, 2012); the involvement of specific lipids such as ceramides (Colombini, 2017); or the participation of Ca^{2+}-regulated proteins (Mizuta *et al.*, 2007).

In this sense, like calcium ionophore A23187 and arachidonic acid, gossypol treatment has also been described to induce a rise in cytoplasmic Ca^{2+} levels (Soderquist *et al.*, 2014). More specifically, gossypol treatment leads to a rapid increase in the activity of phospholipase A2 (PLA2) that causes a rise in cytoplasmic Ca^{2+} that activates endoplasmic reticulum stress, and that leads to increased expression of BH3-only proteins such as NOXA (Soderquist *et al.*, 2014). The authors of this publication demonstrated that products of PLA2 such as arachidonic acid mimic treatment with gossypol leading to an increase in calcium and NOXA. Hence, this observation, together with the study of Mizuta *et al.*, gives further weight to the activation of a BAX/BAK-independent mechanism of intrinsic apoptotic pathway upon gossypol treatment. A mechanism that, according to our results, may prompt the activation of caspases and may trigger the formation of apoptotic nuclear morphologies.

However, the specific mechanism of this alternative activation of the intrinsic pathway has not been elucidated yet. Moreover, although above-presented studies (Mizuta *et al.*, 2007) (Zamorano *et al.*, 2012) suggest that this mechanism seems to the independent of

mitochondrial permeability transition pore (MPTP) formation, we cannot rule out this possibility. Mitochondrial swelling and cristae remodeling are detected by electron microscopy in LN-18 cells treated with gossypol, both features also described in gossypol-treated CLL cells (Vogler *et al.*, 2009). Indeed, the authors of this publication conclude that the cell death induced by gossypol is mainly the result of a non-specific severe mitochondrial damage that requires neither BAX/BAK nor caspase-9. In this sense, the damage induced upon gossypol treatment over mitochondria may be part of the gossypol-induced cell death mechanism (Warnsmann *et al.*, 2018).

Nonetheless, our results indicate that the mechanism triggered upon gossypol treatment in the absence of BAX and BAK does not differentially influence type II and type III caspase-dependent nuclear morphologies. Likewise, as concluded before, the activation of caspases *per se* does not help to discriminate between these two different types of nuclear morphologies. The relative potency of each treatment inducing differential activation of caspases does not explain the differences regarding the nuclear morphologies induced in LN-18 cells. Indeed, despite gossypol induce activation of caspases in fewer cells (evidenced by immunofluorescence of cleaved caspase-3), it induces a higher percentage of type II nuclear morphology than staurosporine. Therefore, not the levels of caspase activation, but how DFF40/CAD becomes properly activate will determine the formation of type II nuclear morphology in LN-18 cells.

3. Subcellular location and activation of DFF40/CAD in human glioblastoma-derived cells

The biochemical analysis of caspases is not sufficient to discriminate between type II and type III nuclear morphologies. However, these nuclear outcomes are differently affected by the downregulation of DFF40/CAD. Hence, since DFF40/CAD is the key molecular bottleneck allowing cells to display complete apoptotic nuclear morphologies, how is the endonuclease distributed intracellularly may be determinant to allow cells to display apoptotic hallmarks after the proteolytic action of caspases.

The subcellular localization of DFF40/CAD has been an object of controversy since its discovery. In the context of glioblastoma, histological slices from glioblastoma patients revealed less cytosolic DFF40/CAD immunoreactivity than non-tumoral samples (Sanchez-Osuna *et al.*, 2016). Here, through immunofluorescence analysis of DFF40/CAD, we show low cytosolic immunoreactivity for the endonuclease in LN-18 cells compared to proficient apoptotic cells such as SH-SY5Y. Nonetheless, results presented in this Doctoral thesis

evidence that despite its levels, the endonuclease can be activated and, therefore, DFF40/CAD-dependent nuclear morphologies can be observed in glioblastoma cells. Our results showing apoptotic nuclear morphologies in LN-18 cells after gossypol treatment exclude the hypothesis that low levels of DFF40/CAD, preferentially at a nuclear or perinuclear location, impede the formation of type II nuclear morphologies in human glioblastoma-derived cells. This observation is in agreement with previously published results from our laboratory showing apoptotic nuclear morphologies in cells where the endonuclease is poorly expressed in the cytosolic fraction (Iglesias-Guimarais *et al.*, 2012).

Nonetheless, it is remarkable to mention that in glioblastoma cells, only an adequate stimulus, such as gossypol, can prompt these cells to properly activate the endonuclease and, consequently, to display this specific nuclear outcome. Changes on the distribution of DFF40/CAD and on its accessibility to DNA in the presence of different cytotoxic insults may be key determinants of the proper action of the endonuclease and, subsequently, the detection of type II nuclear morphologies.

In this sense, the immunofluorescence analysis of DFF40/CAD after staurosporine or gossypol treatment evidences different immunoreactivity against the endonuclease in LN-18 cells. DFF40/CAD seems to be less preserved in staurosporine-treated LN-18 cells. We could conclude that the endonuclease becomes degraded upon staurosporine treatment, but this hypothesis seems unlikely since similar levels of DFF40/CAD are detected through Western blot after both treatments. The different levels of immunoreactivity against the endonuclease between gossypol- and staurosporine-treated cells seem to be the result of differential concentration or aggregation of the endonuclease around DNA upon each treatment. In this sense, RGB profiles from confocal scanning images show a major concentration of DFF40/CAD between masses of condensed chromatin in type II apoptotic nuclear morphologies induced by gossypol. Likewise, three dimensional (3D) isosurface rendered z-stack confocal images of gossypol-treated cells reveal attachment of DFF40/CAD to some parts of the DNA connecting different small-sized masses of DNA. These results suggest different distribution of the endonuclease after gossypol or staurosporine treatments.

Gossypol seems to be a better insult to promote the accumulation of DFF40/CAD at what appears to be chromatin breakage sites. According to recent studies, CIDE domains of DFF40/CAD tends to form helical structures by head-to-tail polymerization (Choi *et al.*, 2017). These higher-order helical oligomers serving as scaffolding components have been described to be critical for DNA fragmentation. In this line, it seems feasible that this major concentration of DFF40/CAD observed in the presence of gossypol may be relevant for the

formation of apoptotic nuclear morphologies. In this sense, we could hypothesize that gossypol-triggered apoptotic nuclear morphologies may be the result of a major concentration of DFF40/CAD.

Alternatively, we may also hypothesize that the structure of chromatin adopted in the presence of gossypol favors the accumulation and accessibility of the endonuclease to its substrate. Indeed, it has been described that differences in the chromatin structure might result in different functions of the endonuclease (Kuribayashi *et al.*, 1996).

Furthermore, conformational and/or compositional changes of DFF40/CAD binding partners may be critical for nuclear entrapment of DFF40/CAD (Lechardeur *et al.*, 2004). Lechardeur *et al.* described that the movement of the endonuclease is gradually restricted during apoptosis due to its association with the nuclear matrix. In this sense, how staurosporine or gossypol affects the components of the nuclear matrix may also determine the accumulation of the endonuclease and its proper function in human glioblastoma cells.

Altogether, either directly or indirectly, our results evidence that different cytotoxic treatments may differentially influence DFF40/CAD distribution and, consequently, may lead to different final nuclear outcomes. In this line, previous results from our laboratory evidence that the cell-specific pattern of DFF40/CAD distribution governs chromatin condensation and fragmentation. We have described that differences in the distribution of the endonuclease coincide with dissimilar cell death outcomes during apoptosis (Iglesias-Guimarais *et al.*, 2012) (Sanchez-Osuna *et al.*, 2014) (Sanchez-Osuna *et al.*, 2016). The specific study of SK-N-AS cells determined that the DNA degradation into oligonucleosomal fragments, but not apoptotic nuclear morphologies, relies on a cytosolic pool of DFF40/CAD (Iglesias-Guimarais *et al.*, 2012). Regarding apoptotic nuclear morphologies, Iglesias-Guimarais *et al.* reported for the first time that chromatin compaction relies on DFF40/CAD mediated DNA damage by generating 3'-OH ends in single-strand (SSB) rather than double-strand DNA breaks (DSB) (Iglesias-Guimarais *et al.*, 2013).

Detection of 3'-OH ends constitutes a reflection of the activity of the endonuclease. Approaches like the TUNEL assay, which detects 3'-OH groups, enable the determination of the actual fraction of cells undergoing cell death (Gavrieli *et al.*, 1992). As evidenced by our results, the percentage of TUNEL-positive SH-SY5Y cells detected after treatment with staurosporine coincides with the percentage of apoptotic nuclear morphologies induced by this alkaloid in these cells. By contrast, in the case of LN-18 cells, the use of the same alkaloid is not effective to induce neither type II nuclear morphologies nor TUNEL positivity. We

could assume that the absence of 3'-OH ends upon staurosporine treatment is because the absence of DFF40/CAD activity, which at the same corroborates that DFF40/CAD is involved in type III nuclear morphologies. In the case of gossypol, like with staurosporine-treated cells, the percentage of apoptotic nuclear morphologies correlates with TUNEL positivity in SH-SY5Y cells. Differences in the percentage of TUNEL positivity and in the percentage of apoptotic nuclear morphologies may rely on the potency of each treatment to activate the endonuclease. In this sense, results obtained from SH-SY5Y cells indicate that gossypol compound is less effective at inducing apoptotic nuclear morphologies than staurosporine in SH-SY5Y cells. However, regardless of stimuli, our results corroborate that TUNEL positivity in apoptotic proficient cells, such as SH-SY5Y cells, constitutes an accurate expression of the percentage of nuclei showing condensation and fragmentation. Surprisingly, this is not the case in LN-18 cells. Despite the fact that above 20% of cells display apoptotic nuclear morphologies upon gossypol treatment in LN-18 cells, less than 10% of TUNEL positivity is detected. Hence, our results indicate that TUNEL positivity does not correlate with the percentage of type II nuclear morphologies in LN-18 cells treated with gossypol.

Assuming that 3'-OH endonucleolytic activity is required for apoptotic nuclear collapse, we may conclude that the absence of TUNEL staining detection in LN-18 cells could reflect a lower, below the detection limit, DFF40/CAD activity.

Alternatively, we may also consider that cells challenged with gossypol may repair 3'-OH ends or that, other endonucleases are triggering DNA breaks with the absence of 3'-OH ends. Among the different endonucleases described, DNase II, generally present in lysosomes of phagocytizing cells, have the ability to generate DNase II-type breaks (3'-PO_4/5'-OH). Indeed, this type of break may be introduced after DNase I-type (3'-OH/5'-PO_4) breaks previously generated by self-autonomous nucleases such as DFF40/CAD (Didenko, 2011) (Weir, 1993). It is necessary to stress that while 3'-OH and 5'-PO_4 termini can be recognized by TdT and labeled by using the TUNEL assay, DNA breaks with 3'- PO_4/5'-OH ends are undetectable by the same assay (Lecoeur, 2002). In this sense, it will be interesting to address if DNase II-like endonucleases are hidden in acidic compartments such as the lysosomes of human-glioblastoma cells and, if so, to employ fluorescent probes to label molecular fingerprint of this endonuclease such as the blunt-ended 5'-OH DNA breaks (Minchew and Didenko, 2011).

Nonetheless, regardless of the above-mentioned possibilities, since the percentage of apoptotic nuclear morphologies induced by gossypol in SH-SY5Y and LN-18 cells is similar,

we may concluded that less number of 3'-OH ends are needed to show a similar percentage of type II nuclear morphologies in LN-18 cells compared to SH-SY5Y cells.

According to our results, massive DNA breakage does not seem to be required to display apoptotic nuclear morphologies. In this sense, the above-described accumulation of DFF40/CAD upon gossypol treatment may help to induce a better and targeted activation of the endonuclease.

From a biochemical point of view, DNA degradation into oligonucleosomal-sized fragments is another considerate distinctive event of apoptotic cell death (Bortner *et al.*, 1995) (Lecoeur, 2002). Here, we show apoptotic nuclear morphologies in the absence of DNA degradation when challenging LN-18 cells with gossypol. Cells displaying nuclear apoptotic morphology in absence of internucleosomal DNA degradation have been extensively reported in the literature, even before DFF40/CAD discovery (Falcieri *et al.*, 1993) (Oberhammer *et al.*, 1993b) (Oberhammer *et al.*, 1993a) (Kuribayashi *et al.*, 1996). Some cells, such as IMR-5 cells, can enter apoptosis without displaying apoptotic features like the DNA degradation in a ladder pattern (Boix *et al.*, 1997). Additional models showing cell death in absence of DNA ladder include MCF-7 cells (Janicke *et al.*, 1998b), the human neuronal-like cell NT2 (Walker *et al.*, 1999) or the human androgen-independent prostatic cancer cell DU-145 (Oberhammer *et al.*, 1993b).

Oberhammer *et al.* suggested that changes in the integrity of DNA, indicative of the release of chromatin loop domains, occur before the cleavage at internucleosomal sites is initiated. They described that the latter is not an essential step in the apoptotic process (Oberhammer *et al.*, 1993b). Similarly, studies performed in MOLT-4 cells (Falcieri *et al.*, 1993) revealed that DNA degradation is not concomitant to chromatin condensation. As mentioned above, our group reported that type II nuclear morphologies observed in the absence of the DNA ladder in SK-N-AS coincide with the presence of single-strand DNA breaks (Iglesias-Guimarais *et al.*, 2013). More recently, Sanchez-Osuna *et al.,* also reported that disassembling of the nucleus and chromatin packaging are two processes that can be molecularly dissociated (Sanchez-Osuna *et al.*, 2014). In this sense, our results from LN-18 cells challenged with gossypol show additional evidence to defy the dogma that the apoptotic nuclear morphology depends on DNA fragmentation. Indeed, the absence of oligonucleosomal DNA fragmentation during caspase-dependent cell death in human glioblastoma cells has been strictly correlated with an intrinsic deficiency of the endonuclease and its predominant location at the nucleoplasmic subcellular compartment (Sanchez-Osuna *et al.*, 2016). According to a previous publication from our group, oligonucleosomal DNA degradation is directly correlated with adequate

DFF40/CAD cytosolic levels (Iglesias-Guimarais *et al.*, 2012). DNA laddering in human-glioblastoma cells is only rescued upon overexpression of the endonuclease (Sanchez-Osuna *et al.*, 2014).

Until now, any of the stimuli previously employed in human glioblastoma-derived cells was described to activate DFF40/CAD properly and to induce apoptotic nuclear morphologies. Here, we demonstrate that LN-18 cells can display this nuclear outcome. From one side, we may assume that DNA degradation upon gossypol treatment in LN-18 cells is not visualized on a conventional agarose gel due to the limited representation of type II nuclear morphologies induced by gossypol. However, a similar percentage of apoptotic nuclear morphologies induced by gossypol in SH-SY5Y cells correlates with a slight oligonucleosomal DNA degradation.

These results support the conclusion that less number of breaks are required in LN-18 cells to display a similar percentage of apoptotic nuclear morphologies than in SH-SY5Y cells. The levels of DFF40/CAD in LN-18 cells are sufficient to display apoptotic nuclear morphologies but not to show oligonucleosomal DNA breakdown. Limiting levels of the endonuclease are the principal obstacle impairing visualization of the DNA ladder in human glioblastoma-derived cells.

Together, our results evidence that in some cellular models such as the LN-18 cells, approaches like the TUNEL assay or the oligonucleosomal DNA degradation analysis are not an accurate reflection of the actual fraction of cells that show nuclear condensation and fragmentation.

In this sense, approaches such as the detection of a phosphoserine motive at the position 139 of human H2AX (referred to as phospho-H2AX or γ-H2AX) may be an alternative tool for the analysis of the DNA fragmentation. This technique is generally used as an indicator of DNA double-stranded breaks (Rogakou *et al.*, 1998) (Kuo and Yang, 2008), but single-stranded breaks can also be detected (Stiff *et al.*, 2006). This is of special interest since chromatin collapse and formation of apoptotic nuclear morphologies rely on DFF40/CAD-mediated 3'-OH single-strand DNA Breaks (Iglesias-Guimarais *et al.*, 2013).

According to our results, the percentage γH2AX positive cells better correlates with the percentage of altered nuclear morphologies induced either by staurosporine or by gossypol in LN-18 cells. The use of a γH2AX antibody is here suggested as a better approach to estimate the amount of DNA damage in LN-18 cells than TUNEL assay or DNA ladder analysis.

More specifically, the phosphorylation of H2AX appears as a diffuse pattern, referred to as pan-nuclear staining (Bonner *et al.*, 2008) in LN-18 cells faced to either gossypol or staurosporine. A staining pattern also described after exposure to insults such as ultraviolet C irradiation (Stiff *et al.*, 2006) or after TRAIL treatment (Solier *et al.*, 2009). In more detail, Solier *et al.* described three different γH2AX staining patterns after TRAIL treatment: a peripheral or ring nuclear staining, observed at earlier times of treatment; a pan-staining, observed in nuclei without alterations of its overall shape or size; and a fully and brightly staining, observed in apoptotic nuclear bodies (Solier *et al.*, 2009). Regarding our results, although apoptotic bodies are barely detected after staurosporine treatment, the unique mass of condensed chromatin observed in LN-18 cells (type III nuclear morphologies) treated with this alkaloid are fully stained with γH2AX. Hence, this staining pattern does not seem exclusive of cells showing apoptotic nuclear morphologies. Indeed, brighter staining is detected in staurosporine-treated LN-18 cells.

Considering that each DNA DSB yields a visible γ-H2AX focus (Sedelnikova *et al.*, 2002), our results indicate that staurosporine triggers a higher number of DNA breaks. The quantification of the intensity of γH2AX staining evidenced that higher DNA damage is induced upon staurosporine than upon gossypol treatment in LN-18 cells. While above 60% of staurosporine-treated LN-18 cells display high-intensity staining for phospho-H2AX, only about 14% of gossypol-treated cells show similar staining.

Considering that type III nuclear morphology induced by staurosporine are DFF40/CAD-independent, it seems feasible to assume that DFF40/CAD does not trigger this massive damage. Indeed, according to our results from the TUNEL assay, this massive DNA damage does not coincide with the detection of 3'-OH groups.

While DFF40/CAD does not seem to participate in these breaks, we do know from our results that this damage is driven by caspases. In the presence of a pan-caspase inhibitor, phosphorylation of H2AX is completely prevented. Similar results were observed upon TRAIL (Solier *et al.*, 2009). Solier *et al.,* reported that apoptosis triggered by TRAIL is induced by direct DNA damage and that TRAIL-induced DNA damage response is inhibited in the presence of caspase inhibitors or in the absence of BAX.

Concerning the involvement of caspases in DNA damage, we may conclude that the higher immunoreactivity for γH2AX observed upon staurosporine treatment is the result of higher activation of caspases compared to gossypol treatment. However, this higher activation of caspases, leading to massive DNA damage after staurosporine treatment, does not seem to be

effectively geared to activate DFF40/CAD and to induce type II nuclear morphologies in LN-18 cells.

According to our results, although the packaging of fragmented DNA into apoptotic bodies may be facilitated by γH2AX (Rogakou *et al.*, 2000), the level and the intensity of the damage detected by γH2AX antibody is not indicative of apoptotic nuclear morphologies. Likewise, although H2AX phosphorylation by JNK has been described to regulate DNA fragmentation mediated by DFF40/CAD after caspase-3 activation (Lu *et al.*, 2006a), our results show that staining for γH2AX neither correlates with the ability of cells to degrade its DNA into oligonucleosomal fragments.

In this sense, our results evidence that lower levels of phospho-H2AX induced after gossypol treatment are sufficient to trigger the formation of apoptotic nuclear morphologies in LN-18 cells. This lower immunoreactivity for γH2AX may be the reflex of less activation of caspases upon gossypol than staurosporine treatment.

Alternatively, we may hypothesize that lower levels of γH2AX upon gossypol treatment may be because the breaks induced by gossypol are concealed by chromatin proteins and, so, less γH2AX is induced (Bonner *et al.*, 2008) or because a higher frequency of DNA repair is triggered upon gossypol treatment. In this sense, protein phosphatase 2A (PP2A) has been described to facilitate DNA double-strand break repair and, consequently, to induce removal of γH2AX (Chowdhury *et al.*, 2005). However, the expression of the catalytic subunit of PP2A was described to be downregulated in gossypol-treated cells (Sahin *et al.*, 2010). Thus, although we cannot rule out this possibility from our results, it seems unlikely that the lower immunoreactivity for γH2AX upon gossypol treatment is explained by increased activity of PP2A.

Moreover, the detailed analysis of the intensity of γH2AX staining evidences that gossypol preferentially triggers mild DNA damage rather than massive DNA damage. Results obtained from the analysis of γH2AX lead again to the conclusion that high levels of DNA damage are not required to trigger apoptotic nuclear morphologies in LN-18 cells.

The ability of each cytotoxic stimulus to properly activate DFF40/CAD will make the difference between adequate stimuli and non-adequate stimuli, able or not, respectively, to promote the formation of type II nuclear morphologies in human glioblastoma-derived cells.

Interestingly, the mild damage induced by gossypol in LN-18 cells is not inhibited in the presence of caspase inhibitors. Hence, gossypol is able to induce DNA damage in a caspase-independent manner. This alternative pathway of damage could participate in the formation of type II nuclear morphologies.

Potential factors that can induce this DNA damage in the presence of gossypol include: the activation of caspase-independent nucleases, the involvement of topoisomerases, the production of reactive oxygen species (ROS), or the chemical damage induced by the direct interaction of gossypol with DNA.

First, since it is caspase-independent, we may assume that DFF40/CAD is not the nucleases involved in this DNA damage. Nevertheless, according to the literature, nucleases such as endonuclease G can cleave chromatin DNA into nucleosomal fragments independently of caspases (Li *et al.*, 2001). Besides endoG, the mitochondrial protein AIF can act as an endonuclease without the requirement of an active caspase system. AIF can induce chromatinolysis and cell death via its association with histone H2AX in the nucleus and its interaction with cyclophilin A (CypA), a latent endonuclease (Artus *et al.*, 2010). In this sense, the release of AIF from mitochondria to cytosol was observed in PC-3 cells treated with gossypol (Zhang *et al.*, 2007), and the blockage of AIF translocation leads to a decreased apoptosis in CLL lymphocytes exposed to gossypol (Balakrishnan *et al.*, 2008). Therefore, we cannot rule out the involvement of such nucleases in the caspase-independent DNA damage induced by gossypol in LN-18 cells.

Second, since topoisomerases are involved in the generation of transient breaks in DNA double-helix, we may consider the participation of topoisomerases in the DNA damage induced by gossypol. Indeed, in the context of cell death, topoisomerases can nick DNA around specific DNA attachment sites (scaffold-attachment regions (SARs)) (Adachi *et al.*, 1989) and can interact with DFF40/CAD to promote chromatin condensation during apoptotic execution (Durrieu *et al.*, 2000). Durrieu *et al.* suggested that DFF40/CAD cleavage might initiate at or near topoisomerase IIα-binding sites. According to the literature, gossypol has been described as a potential class II inhibitor of topoisomerases that interferes with the catalytic function of topoisomerases but without generating strand breaks (Senarisoy *et al.*, 2013). Besides inhibition of topoisomerases, gossypol has been described to inhibit key nuclear enzymes responsible for DNA synthesis and repair such as DNA polymerase α (Rosenberg *et al.*, 1986). In this sense, the impairment of the inhibitory effect of gossypol over enzymes responsible for the DNA damage repair response may lead to the accumulation of DNA damage detected by γH2AX antibody.

Third, ROS are well-recognized mediators of DNA damage (Srinivas *et al.*, 2019). Clusters of ROS close to DNA are responsible for multiple single- or double-stranded lesions per cell (Klaunig and Kamendulis, 2004). In this line, since ROS production by gossypol has been extensively reported in the literature (Arinbasarova *et al.*, 2012) (He *et al.*, 2017) (Ko *et al.*, 2007), it seems likely to consider, at least to some extent, that phosphorylation of H2AX may be due to ROS-dependent DNA damage. Besides the chemical damage induced by the generation of ROS, some authors have pointed to direct chemical activity of gossypol over the DNA (Nordenskjold and Lambert, 1984) (Zaidi and Hadi, 1992b) (Srivastava and Padmanaban, 1987). Zaidi *et al.* suggested a possible binding of gossypol to DNA, causing a change in the configuration of the sugar-phosphate backbone (Zaidi and Hadi, 1992b). In this sense, we may hypothesize that this change induced by gossypol over the DNA structure could facilitate the assembly of the scissor-like structure of DFF40/CAD and the accommodation of double-stranded DNA (dsDNA). Hence, it seems plausible to consider that the chemical structure of gossypol may be of key relevance in the mechanism of action of gossypol.

4. The relevance of the chemical structure of gossypol in the nuclear morphology

Here, we present that the chemical structure of gossypol strongly determines its effect over the nuclear morphology in LN-18 cells. Our results show that gossypol aldehyde group removed derivatives such as apogossypol or apogossypolone are less effective than gossypol to trigger apoptotic nuclear morphologies in LN-18 cells. Even when used at higher concentrations than gossypol, type II apoptotic nuclear morphologies are almost not detected.

A different picture is observed when using apogossypol and apogossypolone in proficient apoptotic cells such as SH-SY5Y. In that case, gossypol derivatives trigger a similar nuclear phenotype than gossypol. Type II nuclear morphologies are not impaired in SH-SY5Y cells faced to these gossypol derivatives. These results indicate that proficient apoptotic cells such as SH-SY5Y do not require a specific structure of gossypol to display type II nuclear morphologies.

By contrast, deficient apoptotic cells such as LN-18 cells do require from this specific structure of gossypol. From one side, as SH-SY5Y cells express higher levels of DFF40/CAD than LN-18 cells (Sanchez-Osuna *et al.*, 2014), we may conclude that changes in the chemical structure of gossypol will interfere with the final nuclear outcome display in cells with low levels of DFF40/CAD. However, as mentioned above, the intracellular levels of the

endonuclease do not explain the LN-18 cells' impairment to display apoptotic type II nuclear morphologies when challenged with different cytotoxic insults. Hence, intracellular differences between SH-SY5Y and LN-18 cells beyond the endonuclease levels may dictate a differential requirement of the gossypol structure in the formation of apoptotic type II nuclear morphologies.

The chemical structure of gossypol and, especially, the aldehyde groups are essential to activate the endonuclease properly and, therefore, to induce DFF40/CAD-dependent apoptotic nuclear morphologies in LN-18 cells.

He *et al.* described that the aldehyde group of gossypol is required to induce mitochondrial apoptosis (He *et al.*, 2017). However, our results show that the absence of the aldehyde group in apogossypolone structure and its impairment to induce type II nuclear morphologies is rescued when used in combination with TRAIL. In this sense, we may assume that the increase in the activation of caspases by the addition of TRAIL may facilitate the formation of type II nuclear morphologies. Nevertheless, the combination of TRAIL with apogossypol does not induce the same effect in LN-18 cells. Despite the addition of TRAIL, apogossypol is not an adequate stimulus to induce type II nuclear morphology in LN-18 cells, which suggests a different mechanism of action of apogossypol.

In this sense, Vogler *et al.* described different morphological changes implying significant differences in the biochemical pathways in CLL cells treated with apogossypol (Vogler *et al.*, 2009). More specifically, the authors reported endoplasmic reticulum localized in clusters as the principal ultrastructural alteration. Further research revealed that due to ER membrane reorganization, activation of BAX, cytochrome *c* release, and phosphatidylserine externalization are inhibited upon apogossypol treatment. The same authors described that ER membrane reorganization induced by apogossypol antagonize mitochondrial fission (Yedida *et al.*, 2019). In this sense, the impairment of mitochondrial fusion-fission dynamics and the intrinsic apoptotic pathway may directly impair the proper formation of apoptotic nuclear morphologies.

Moreover, considering the hypothesis that gossypol structure could facilitate the formation of DFF40/CAD complexes in LN-18 cells and, consequently, type II nuclear morphologies, the impairment of this morphology upon apogossypol treatment suggest that the structure of this compound is not triggering a similar effect.

Likewise, in the absence of gossypol or apogossypolone, TRAIL is not efficient at inducing type II nuclear morphologies in LN-18 cells, which give further weight to the particularity of these molecules to induce this effect in LN-18 cells. More specifically, this hypothesized mechanism by which gossypol (or apoggosypolone) could facilitate the formation of type II nuclear morphologies in LN-18 cells may be first, due to the induction of a direct change of the structure of the DNA by these compounds (Zaidi and Hadi, 1992b); or second, due to the interaction of gossypol with elements that may alter the structure of the DNA or the formation of DFF40/CAD complexes. In this line, the capacity of gossypol or apogossypolone to interact with those elements would dictate the final nuclear outcome upon cytotoxicity in human glioblastoma-derived cells.

Potential candidates that could interact with gossypol or interfere with the activity of the endonuclease are metal ions. This work evidences that the gossypol-induced nuclear morphologies described in LN-18 cells are modulated by different metal ions.

According to the literature, aldehydic oxygens and the two acidic hydroxyl groups of gossypol can interact with various metal cations and form gossypol metal complexes (Ramaswamy and O'Connor, 1968) (Ramaswamy and O'Connor, 1969) (Kenar, 2006). These metal complexes are coordination complexes that in chemistry consist of a central metal atom and a surrounding array of bound molecules or ions.

Different works support the potential of gossypol metal complexes to act in a catalytic fashion. Srivastava *et al.* reported gossypol as a mediator of DNA degradation in the presence of Fe^{3+} and Co^{2+} and prevention of this gossypol mediated DNA damage in the presence of Ca^{2+} and Mg^{2+}(Srivastava and Padmanaban, 1987). The same authors also described that gossypol in the presence of Cu^{2+} ions converts supercoiled pBR322 DNA to open circular form. However, results controlling the effect of Cu^{2+} and the different metal ions employed in the absence of gossypol were not presented. In this sense, preliminary results from our group suggest that gossypol but also metal ions (such as Cu^{2+} or Fe^{3+}) by themselves can both affect DNA topology of plasmid DNA.

Here, we show that the nuclear morphology of LN-18 cells is altered by adding these ions to the culture media. More specifically, the nuclear morphologies induced upon $CuCl_2$ suggest a potential chromatin breakage role of cooper. However, the combination of cooper with staurosporine or gossypol was not efficient at inducing type II nuclear morphologies. This result may be explained due to the inhibitory effect of Cu^{2+} over DFF40/CAD. It has been reported that the endonuclese becomes inactivated in the presence of Cu^{2+} (Widlak, 2000)

(Widlak and Garrard, 2001). Despite this, gossypol metal complexes have been involved in different reactions such as DNA cleavage (Zaidi and Hadi, 1992c) (Zaidi and Hadi, 1992a) (Zubair *et al.*, 2012). In this sense, we may hypothesize that cooper induces a DFF40/CAD-independent mechanism consistent with major points of DNA breakage but in the absence of proper nuclear condensation and packaging in LN-18 cells.

A different nuclear outcome is observed in the presence of cobaltous. Type II and type III nuclear morphologies are slightly promoted in the presence of Cl_2Co. In this sense, since cobalt has a potential in the oxidative esterification of aldehydes and may lead to aldehyde dimerization (Jiang *et al.*, 2019), we may hypothesize that the alteration of gossypol aldehydes by cobaltous may positively influence the mechanism of gossypol to trigger apoptotic nuclear morphologies. As mentioned above, gossypol aldehydes are essential for the formation of apoptotic nuclear morphologies. Moreover, besides the physiological role of cobalt (in the form of cobalamin or vitamin B12) in essential biological processes (Hunger *et al.*, 2014), it may also play key roles in cell death (Mahey *et al.*, 2016). In this sense, a concentration range of 0.2 – 0.8 mM $CoCl_2$ is described to cause toxic effects on primary cultures of mouse astrocytes (Karovic *et al.*, 2007). Moreover, other authors have reported DNA fragmentation and activation of caspases in PC12 cells in the presence of cobalt chloride (Zou *et al.*, 2001) (Zou *et al.*, 2002). Since the concentrations employed in this work are above the physiological amounts detected in the human body (Czarnek *et al.*, 2015), it seems feasible to conclude that the effects observed in LN-18 cells are due to a cytotoxic effect of cobaltous. Interestingly, this cytotoxic effect does not negatively interfere with the ability of gossypol to induce apoptotic nuclear morphologies. Hence, further research may give additional clues of the mechanism behind cobalt-induced cytotoxicity and, especially, in apoptotic nuclear morphology.

A completely different scenario is described in the presence of iron. From our results, the presence of intracellular iron allows gossypol to trigger type I and type III nuclear morphologies but impedes the type II nuclear morphology. In the case of staurosporine, iron neither impedes type III nuclear morphologies and, indeed, higher DNA condensation is detected. Moreover, the presence of extracellular iron in the culture media impedes gossypol to trigger any effect over the nuclear morphology. Mutual sequestering between iron and gossypol may explain the absence of gossypol effect in LN-18 cells. In this line, ferric sulfate binding with reactive groups from gossypol forming a conjugate has been described (Li *et al.*, 2000a). The identification of gossypol as the toxic principle in cottonseed (Withers and Carruth, 1916) led to the research of mechanisms for gossypol inactivation to prevent gossypol toxicity. In this sense, the inclusion of soluble iron salts in cottonseed was the more

successful approach since the formation of iron-gossypol complexes prevents gossypol absorption (Withers and Carruth, 1917).

Further research in this context addressed the molar ration of iron: gossypol necessary for gossypol inactivation. Muzaffaruddin and Saxena reported that one mole of ferric ion combines with one mole of gossypol to form the iron gossypol complex (Muzaffaruddin and Saxena, 1966), and Shieh *et al.* indicated a ratio of 2: 1 (iron:gossypol) and no changes in absorption spectrum upon an increase of ferrous ions. More recently, the spectra analysis of structures of complexes of gossypol has revealed that aromatic aldehyde groups in gossypol molecules are entirely involved in the coordination with Fe^{2+} (Zhang *et al.*, 2019b). The same authors reported that in 1: 3 and 1: 4 complexes of gossypol with ferrous cations, all aldehyde groups and the hydroxyl groups participate in the coordination with ferrous cations. This data, together with our results, supports the relevance of gossypol aldehyde groups in the apoptotic nuclear morphologies.

Since high intracellular and extracellular levels of iron impede type II nuclear morphologies in LN-18 cells, we may hypothesize that the chelation of iron by gossypol may be part of the mechanism to allow this nuclear morphology.

According to the above-mentioned hypothesis, we may conclude that the interaction of gossypol with iron may favor a proper DNA structure for DFF40/CAD complexes and, consequently, for its activation and formation of DFF40/CAD-dependent nuclear morphologies. This hypothesis implies that iron interacts with the DNA and that this interaction can alter the structure of the DNA.

This assumption is supported by different studies that demonstrate interaction of iron with DNA (Netto *et al.*, 1991) (Ouameur *et al.*, 2005) (Yiu *et al.*, 2013). Specifically, Ouameur *et al.* studied the iron cation binding sites, the binding constants, helix stability, and DNA secondary structure. Through capillary electrophoresis and spectroscopy methods, the authors determined that iron cations can bind DNA via guanine N-7 (major groove) and the backbone phosphate group. Moreover, no DNA conformational changes were described upon iron cation complex formation, but helix destabilization and DNA condensation were reported in the presence of high cation concentration of Fe(II) and Fe(III), respectively (Ouameur *et al.*, 2005). Since Fe(III) may be transformed into Fe(II) inside the cells, we may consider both effects in our experiments. Interestingly, type III nuclear morphologies with a major degree of chromatin condensation are detected in LN-18 cells faced to either staurosporine or gossypol treatment.

Moreover, preliminary results from our laboratory reveal that iron may alter the topology of plasmid DNA by inducing different points of breakage. This is in line with previous studies showing that there is a strong correlation between the iron cation binding sites and the cleavage sites in DNA (Ouameur *et al.*, 2005). Excess of iron may trigger toxic effects through the generation of reactive oxygen species, DNA damage, irreversibly modification of proteins, and further stimulation of iron release (Stohs and Bagchi, 1995) (Jomova and Valko, 2011) (Papanikolaou and Pantopoulos, 2005) (Torti and Torti, 2020).

Altogether, we may conclude that the type III nuclear morphology observed in human glioblastoma cells may be the consequence of massive DNA breakage and DNA condensation due to high intracellular levels of iron cations. Moreover, considering that the active site motif of DFF40/CAD faces the DNA minor groove (Reh *et al.*, 2005), the minor helix destabilization caused at high cation concentration may impair the proper binding and assembly of the scissor-like structure of the endonuclease with the DNA. This impairment to properly activate the endonuclease in the presence of certain levels of cations would contribute to the formation of DFF40/CAD-independent type III nuclear morphology and would prevent DFF40/CAD-dependent type II nuclear morphologies.

According to the literature, iron accumulation in the brain has been linked to increased blood-brain-barrier permeability with aging (Farrall and Wardlaw, 2009) and to cognitive severity in Parkinson's disease (Thomas *et al.*, 2020) (Ward *et al.*, 2014). In the case of glioblastoma, the iron oxidation state has been related to the malignancy grade of brain tumors (Wandzilak *et al.*, 2013). Moreover, iron metabolism has been involved in the maintenance of glioblastoma stem-like cells (Schonberg *et al.*, 2015), in glioblastoma development and in treatment resistance (Legendre and Garcion, 2015). The requirement of iron in different biological processes such as DNA synthesis made cancer cells, including glioblastoma cells, to increase iron assimilation to sustain proliferation and, subsequently, to modulate the expression of proteins involved in iron uptake like transferrin receptor protein 1 (TfR1) (Recht *et al.*, 1990). In this sense, according to our results, an iron increase may be an adaptive process undergone in glioblastoma cells impairing apoptotic nuclear morphologies.

5. Non-apoptotic mechanisms governing apoptotic nuclear morphologies induced by gossypol

Besides the binding to nucleic acids and their nucleobases, iron has a strong affinity towards complexation with other cell components, including lipids or proteins. Alterations in lipids including cholesterol or sphingolipids are frequently caused by high levels of iron, and these

iron-mediated alterations are involved in the progression of diseases, including neurodegenerative disorders (Rockfield *et al.*, 2018). Elevated ferric iron concentrations have been described to trigger aggregation of proteins involved in different neurodegenerative disorders (Yamamoto *et al.*, 2002) (Joppe *et al.*, 2019). Moreover, free iron has been reported to induce the formation of protein aggregates as a cellular response to oxidative stress (Vasconcellos *et al.*, 2016) (Travassos *et al.*, 2017).

Alternatively, protein aggregates may be generated as a result of the covalent binding of aldehyde groups from gossypol with amino acids of proteins (Gadelha *et al.*, 2014). Hence, since gossypol can interact with both proteins and iron, it is foreseeable that protein aggregates together with metal complexes may be formed upon gossypol treatment. According to the literature, the accumulation of these complexes with protein aggregates could cause endoplasmic reticulum stress (Liu and Connor, 2012) (Almanza *et al.*, 2019). Indeed, different studies describe gossypol as an ER stress-inducing compound (Soderquist *et al.*, 2014) (Zhang *et al.*, 2019a).

From our results, electron microscopy images of gossypol-treated LN-18 cells evidence a general alteration of cellular membranes with extensive dilatation of the endoplasmic reticulum (ER) and the Golgi apparatus (GA). Moreover, we show aggregation of ER membrane proteins such as calnexin in LN-18 cells treated with gossypol. Since the aggregation of calnexin upon gossypol treatment is not inhibited in the presence of a caspase inhibitor, we conclude that gossypol-induced ER stress occurs through a caspase-independent mechanism. In line with the emerging role of ER as a central organelle regulating the core mitochondrial apoptotic pathway (Pihan *et al.*, 2017), we may consider the induction of ER stress as an essential mechanism for the formation of apoptotic nuclear morphologies in human glioblastoma cells.

However, our results facing LN-18 cells to different ER stressor compounds (Varadarajan *et al.*, 2012) show dissimilar nuclear outcomes. Thus, ER stress induction in human glioblastoma cells does not correlate with type II nuclear morphology, at least considering the experimental conditions used in this studied. Nonetheless, since different ER stress responses may be triggered by different ER stressor compounds, we cannot exclude that gossypol-induced ER stress may be important for the final nuclear outcome observed in LN-18 cells. Indeed, as mentioned above, increased intracellular levels of calcium and induction of ER stress by gossypol may lead to BAX/BAK-independent intrinsic apoptosis and to caspase activation (Mizuta *et al.*, 2007) (Zamorano *et al.*, 2012).

Moreover, cellular responses like ER stress have been related to the activation of autophagy (Song *et al.*, 2018). In this line, electron microscopy images from LN-18 cells treated with gossypol reveal accumulation and precipitation of proteins, an intense vacuolization process, and ultrastructural changes compatible with an autophagic process. Hence, ER stress-mediated autophagy characterized by the formation of autophagosomes may occur in cells exposed to gossypol with the purpose to eliminate protein aggregates and damaged organelles. This possibility suggests autophagy as an additional mechanism that may be triggered upon gossypol treatment to overcome the cellular stress-induced and to maintain cellular homeostasis.

Here, we show that starvation-driven autophagy does not impede gossypol-induced type II nuclear morphologies. Indeed, in the absence of serum, less concentration of gossypol is needed to trigger a similar effect to that observed in the presence of serum. From one side, we may conclude that the difference between both conditions may be due to the sequestration of gossypol by serum proteins. Certainly, previous studies indicate that the genotoxic effect of gossypol is reduced by binding to serum proteins (Nordenskjold and Lambert, 1984). However, beyond this, we could conclude that gossypol may take profit of the inhibition of survival pathways and of autophagy activation in a context of growth factor withdrawal to induce caspase-dependent nuclear morphologies. This is supported by different articles demonstrating that serum starvation triggers caspase activation and sensitizes cells to its death (Goyeneche *et al.*, 2006) (Mattiolo *et al.*, 2015) (Ponder and Boise, 2019).

Although autophagy is generally considered as a mechanism to promote cell survival, it can also be the mechanism responsible for cell demise (Mattiolo *et al.*, 2015). Mattiolo *et al.* stated that the time frame is the variable determining the final outcome of autophagy. More specifically, the authors reported that at long times of starvation, pro-survival autophagic effects are promoted, whereas autophagy induced at short times of starvation sensitizes cells to MOMP and caspase activation. According to the literature, different articles support gossypol and its enantiomer AT-101 as inducers of autophagy in different cellular models (Lian *et al.*, 2011) (Mani *et al.*, 2015) (Antonietti *et al.*, 2016) (Benvenuto *et al.*, 2017) (Zhang *et al.*, 2019a) including glioma cells (Voss *et al.*, 2010) (Keshmiri-Neghab *et al.*, 2014) (Meyer *et al.*, 2018). However, it is not as clear whether gossypol-induced autophagy is cytoprotective (Mani *et al.*, 2015) (Antonietti *et al.*, 2016) (Zhang *et al.*, 2019a) or if it is required for the cell death mechanism (Voss *et al.*, 2010) (Keshmiri-Neghab *et al.*, 2014).

From our results, the induction of autophagy upon gossypol treatment in LN-18 cells is suggested by the observation of ultrastructural changes compatible with an autophagic process

through electron microscopy analysis and detection of LC3-I conversion to LC3-II through Western blot. Conversely, LC3-II is observed neither in untreated nor in staurosporine-treated LN-18 cells. Hence, since LC3-II is generally accepted as an excellent marker for autophagic structures (Kabeya *et al.*, 2000), we may conclude that gossypol prompts the formation of such structures.

However, LC3-II levels on their own do not address issues of autophagic flux (Klionsky *et al.*, 2016). In the case of staurosporine-treated cells, the low detection of LC3-I and LC3-II may be because of the high conversion of LC3-I to LC3-II and a high autophagic flux degrading autophagosomes. In this line, different authors support staurosporine as an inducer of autophagy (Kaizuka *et al.*, 2016) (Ding *et al.*, 2017). However, besides autophagy can be activated by staurosporine treatment, we cannot rule out the possibility that in our model and at the time point analyzed, low detection of both LC3-I and LC3-II may be because of a general degradative process triggered by this alkaloid. In the case of gossypol, higher detection of LC3-II in gossypol-treated cells compared to untreated or staurosporine-treated cells does not necessarily associate with more induction of autophagy. It may be because of the increased autophagic activity or the result of a blockage in the trafficking of autophagosomes to lysosomes without a concomitant change in autophagosome biogenesis. In any case, our results evidence that autophagy may participate somehow in the mechanism of action of gossypol in LN-18 cells.

Nevertheless, this data is not sufficient to determine if caspases activation and, consequently, caspase-dependent nuclear morphologies induced by gossypol require or not from the activation of autophagy.

To better determine the potential role of autophagy in our model and, especially, over the nuclear morphology, we faced LN-18 cells to gossypol in the presence or absence of different pharmacological autophagic modulators, including 3-methyladenine (3-MA), wortmannin, PI-103, and rapamycin (Tavakol *et al.*, 2019). The analysis of the nuclear morphology reveals that only the combination of gossypol plus 3-MA diminishes the percentage of apoptotic nuclear morphologies observed in LN-18 cells.

Different facts have to be considerated in the interpretation of this results. Although 3-MA and wortmannin have been generally employed to abrogate autophagy, this inhibitory effect of autophagy may be highly determined by the culture conditions and the time of exposure. Indeed, according to the latest guidelines for the use and interpretation of assays for monitoring autophagy, although accepted as sequestration inhibitors, none of these can be

considered as specific autophagy inhibitors. The authors state that 3-MA is "a phosphatidylinositol 3-kinase (PtdIns3K) inhibitor that effectively blocks an early stage of autophagy by inhibiting the class III PtdIns3K, it can also inhibit the class I phosphoinositide 3-kinases (PI3K) and can thus, at suboptimal concentrations in long-term experiments, promote autophagy in some systems, as well as affect cell survival through AKT and other kinases" (Klionsky *et al.*, 2016). Wu *et al.* reported 3-MA to promote autophagy in nutrient-rich conditions and to inhibit autophagy in nutrient-poor conditions due to different kinetics of class I and III PtdIns3K inhibition (Wu *et al.*, 2010). Thanks to the development of a novel autophagic flux probe (GFP-LC3-RFP-LC3ΔG), Kaizuka *et al.* reevaluated different reported autophagy-modulating compounds (Kaizuka *et al.*, 2016). Specifically, the authors distinguished between the effects of different drugs when used in HeLa cells cultured in regular medium (10% serum and 1x amino acids) or in starvation medium (1% serum and 0.1x amino acids) after 6, 12 and 24 hours. Their results confirmed 3-MA as a potential activator of autophagy when used in the presence of serum, and as an inhibitor when used under starvation. In the case of wortmannin, it is described in the guidelines as "an inhibitor of PI3K and PtdIns3K that blocks autophagy". The measurement of autophagic flux by using the autophagic flux probe evidenced wortmannin as an inhibitor in a regular medium at any of the times studied. Under starvation, wortmannin was described as: an efficient inhibitor after 6 hours, a less efficient inhibitor after 12 hours, and an inducer of autophagy after 24 hours (Kaizuka *et al.*, 2016). Rapamycin, an mTOR inhibitor, was confirmed as an activator of autophagy at any of the times studied either when used in regular medium or in starvation medium with the exception of 6 hours in starvation medium. Rapamycin was reported as a potential autophagy inhibitor at short times of starvation (Kaizuka *et al.*, 2016). Moreover, autophagy modulators such as 3-MA may induce autophagy-independent effects. As an example, treatment with 3-MA induces caspase-3 activation and cell viability decrease in a time- and dose-dependent manner in HeLa cells (Hou *et al.*, 2012). Indeed, cell death induced by 3-MA is described to be independent of its ability to inhibit autophagy, as neither knockdown of *BECLIN1* in HeLa cells nor deletion of *Atg5* in MEFs affects the cell death induced by 3-MA (Hou *et al.*, 2012).

Overall, it leads to the conclusion that special care is needed to draw conclusions when using autophagy-modulator compounds such as 3-MA, not only because of its side effects but also because of the cell culture conditions and the time of exposure to this compound may significantly affect the final result. In this sense, from our results, we conclude that in LN-18 cells, 3-MA is the only autophagic modulator (among those tested) able to significantly impair gossypol-induced type II nuclear morphologies while preserving type I and type III.

The inhibition of type II nuclear morphology correlates with a decrease in the activation of caspases, evidenced by a decrease in the DEVDase activity. Moreover, considering that type III nuclear morphology requires caspase activation, the DEVDase activity detected upon gossypol treatment in the presence of 3-MA should correspond to this type of nuclear morphology, not altered in the presence of 3-MA. Similarly, type III nuclear morphology induced by staurosporine is not impaired by the addition of 3-MA, which correlates with similar DEVDase activity in staurosporine-treated cells in the presence or not of 3-MA. Thus, we may conclude that 3-MA impairs DEVDase activity required for type II nuclear morphologies but not the DEVDase activity driving type III nuclear morphologies. Considering that our results show that both type II and type III nuclear morphologies require from the activation of caspases, and especially of caspase-3, the impairment of type II but not of type III by 3-MA suggests that specific signaling may be behind the activation of caspases in each case. In this line, we may hypothesize the existence of different pools of caspases, the differential activation of which will determine the final nuclear outcome displayed by LN-18 cells upon cell death.

Unexpectedly, the treatment of LN-18 cells with gossypol in the presence of 3-MA revealed advanced processing of α-fodrin especially to its p150 fragment. Among different proteases (Vanags *et al.*, 1996), calpains have been described as responsible for this p150 fragment (Waterhouse *et al.*, 1998). Since calpains are calcium-regulated cytosolic cysteine proteases, increased cytoplasmic Ca^{2+} levels caused by gossypol (Soderquist *et al.*, 2014) might activate such proteases.

The role of calpains in the context of autophagy is controversial. Some authors state that calpains are required for macroautophagy (Demarchi *et al.*, 2006) (Marcassa *et al.*, 2017) whereas others state that calpains negatively regulate autophagy (Menzies *et al.*, 2015) (Ong *et al.*, 2019). In cell death, calpains are essential cofactors upstream or downstream of caspases (Waterhouse *et al.*, 1998) and, as mentioned above, can cleave caspase substrates such as the specific substrate of caspase-3 α-fodrin (Janicke *et al.*, 1998) (Vanags *et al.*, 1996). Our results show that, although less intense, the specific cleavage of α-fodrin by caspase-3 generating the p120 fragment is also detected in advance in the presence of 3-MA. Hence, proteolytic processes, including the processing of proteins such as α-fodrin, may occur in advance due to the combination of gossypol and 3-MA when used in culture-reach conditions. According to previous studies from our group, this advance in the activation of the proteolytic machinery, including calpains and caspases, could explain the impairment of apoptotic nuclear morphologies (Garcia-Belinchon *et al.*, 2015). According to our results, besides the analysis of

α-fodrin, lipidation of LC3-I to LC3-II is also detected earlier and with a higher intensity when combining gossypol with 3-MA.

Regarding the different profiles of LC3-II in gossypol-treated cells in the presence or not of 3-MA, and according to the previously reported role of 3-MA as an autophagic inducer in the presence of nutrient-rich conditions (Kaizuka *et al.*, 2016), we could conclude that increased lipidation of LC3-II may be indicative of increased autophagic flux. Nonetheless, we cannot rule out that the increase in LC3-II after 1 hour of treatment of gossypol and 3-MA is due to a blockage of the autophagic flux. In this sense, assuming the role of 3-MA as an activator, gossypol would be functioning as an inhibitor of the autophagic flux.

Whether the time-dependent increase of LC3-II upon gossypol treatment is the result of inducing autophagy over time or gossypol itself is inhibiting autophagy cannot be concluded from these results. Results showing transient accumulation of LC3-II at static time points do not accurately reflect the autophagic activity. Thus, according to the latest guidelines, bafilomycin A_1 –which is described as "a vacuolar H(+)-adenosine triphosphatase ATPase (V-ATPase) inhibitor that causes an increase in lysosomal/vacuolar pH, and, ultimately, blocks fusion of autophagosomes with the vacuole"– constitutes a useful tool to measure autophagic flux correlating with the number of autophagosomes that are degraded by fusion with lysosomes (Mizushima *et al.*, 2010) (Klionsky *et al.*, 2016). Here, we show that the simple addition of bafilomycin A_1 evidences the accumulation of LC3-II in LN-18 cells cultured under nutrient-rich conditions. This increase appears since the turnover of LC3-II by basal autophagy is blocked.

As previously observed in other cellular models (Musiwaro *et al.*, 2013), basal autophagy may be detected in cells grown in medium containing amino acids and serum. This basal autophagy, which constitutes a physiologically significant pathway in most tissues, has also been described to support malignant growth in a context-dependent manner. As an example, the silencing of *ATG5* or inhibition of autophagy by chloroquine induces tumor regression in a mouse model of ductal adenocarcinoma of the pancreas (PDAC) (Yang *et al.*, 2011). The activation of autophagy during exposure to stress conditions exerts a positive role for cancer cell maintenance (Levy *et al.*, 2017) (Levine and Kroemer, 2019) (Pedroza *et al.*, 2020). Accordingly, increased basal levels of autophagy can be detected in many cancer cells, which correlate to their higher survival during stress conditions compared to non-cancer cells. In the case of glioblastoma, significant levels of basal autophagy have been detected in U87MG and T98G (Ivanov *et al.*, 2020). Conversely, other authors have reported very low basal activity of autophagy in glioblastomas and support the activation of autophagy as a potential therapeutic

approach (Jiang *et al.*, 2009) (Arcella *et al.*, 2013) (Zhuang *et al.*, 2011). In this line, the progression of astrocytic tumors has been related to a decrease in autophagic capacity due to the loss of LC3B-II and BECLIN1 expression (Huang *et al.*, 2010), and glioblastoma growth can be inhibited by autophagy activators such as rapamycin (Arcella *et al.*, 2013).

From our results, we cannot define if the level of LC3-II detected in LN-18 cells cultured in complete media in the presence of bafilomycin A_1 correspond to higher or lower levels of autophagy. However, we can conclude that a certain level of autophagic flux is already present when facing this human glioblastoma-derived cell line to different forms of stress, such as nutrient depletion or cytotoxic compounds.

As we show here, the basal rate of autophagy is further increased when culturing LN-18 cells with an starvation medium. Incubation with Krebs-Henseleit buffer induces stimulation of the autophagic flux from 1 hour and is sustained over time. In the case of gossypol, the autophagic flux is increased at earlier times but is blocked after 6 hours of treatment. More specifically, while the accumulation of LC3-II after 3 hours is enhanced by the presence of bafilomycin A_1, similar levels are detected after 6 hours regardless of the addition of bafilomycin A_1. In this sense, the accumulation of autophagosomes induced in the presence of gossypol may be the result of defects at downstream steps impairing autophagosome-lysosome fusion or perturbation of the transport machinery (Fass *et al.*, 2006).

Alternatively, decreased flux may also be the consequence of an inefficient degradation of the cargo after fusion (Kovacs *et al.*, 1982). Furthermore, it is necessary to stress that we cannot rule out the possibility that gossypol-induced LC3 lipidation after 6 hours of treatment is the result of noncanonical autophagy. Gao *et al.* suggested that the Golgi complex may serve as a membrane platform for the noncanonical lipidation of LC3. According to their proposed mechanism of noncanonical autophagy, the V-ATPase is required to activate the LC3 conjugation system (Gao *et al.*, 2016). In this context, the use of inhibitors such as bafilomycin A_1 may coincide with a decrease of LC3-II due to suppression of Golgi signaling. In this sense, gossypol has been reported to induce noncanonical autophagy in HeLa cells, but an enhanced accumulation of LC3-II was observed in the presence of bafilomycin A_1 (Gao *et al.*, 2010). This difference may be explained because, in the first case (Gao *et al.*, 2016), noncanonical autophagy coincides with a ULK-1- and BECLIN1-independent mechanism, whereas in the second case (Gao *et al.*, 2010), it coincides with a BECLIN-1-independent but VPS34-dependent mechanism. Moreover, canonical autophagy has also been described in MCF-7 treated with gossypol. Further research is needed to determine whether the time-dependent

induction of autophagy observed in LN-18 cells upon gossypol treatment comes from a canonical and/or noncanonical activation of autophagy.

Regarding the increase of LC3-I upon gossypol treatment, especially in the presence of bafilomycin A_1 and after 6 hours, we may hypothesize that it is the result of increased proteolytic cleavage of pro-LC3 by ATG4 or the result of less conversion of LC3-I to LC3-II. This second option may be due to increased delipidation of LC3-II by ATG4 or due to an effect over the ubiquitin-like conjugation systems Atg12-Atg5 and/or LC3-PE, both required for the formation of autophagosomes. In this sense, and in line with the strong recommendations of the guidelines to use multiple assays to monitor autophagy, we here present results from the genetic inhibition of the autophagy essential gene *ATG5*. Specifically, we show that the knockout of *Atg5* sensitizes MEFs to display a higher percentage of apoptotic nuclear morphologies upon treatment with gossypol. Although the inhibition of autophagy leading to a more apoptotic outcome has been extensively reported in the literature, we specifically show that the absence of ATG5 may help to the condensation and fragmentation of the nuclei of dying cells.

Regarding the nuclear functions of this autophagy-related protein (Simon and Friis, 2014), low levels of DNA damage were linked to an upregulation of autophagy and to the recruitment of ATG5 to the nucleus. At the nucleus, ATG5 is described to interfere with the correct assembly of the chromosome passenger complex. Consequently, massive genetic modifications and stable aneuploidy may be present in cells that have upregulated ATG5 and that have undergone mitotic catastrophe in response to DNA-damaging agents (Maskey *et al.*, 2013). The same authors suggested that pharmacological inhibition of autophagy shifts the balance to an early caspase-dependent cell death upon drug-induced DNA damage, but ATG5-dependent mitotic catastrophe is preserved. Consequently, a dual and different role of ATG5 is described: in the cytosol, it contributes to increased autophagic activity; and in the nucleus, it induces mitotic catastrophe independently of autophagy.

Besides its cytosolic role in the formation of autophagosomes (either via canonical or noncanonical autophagy), ATG5 has been described to modulate the immune system (Ye *et al.*, 2018) and to bind with FADD (Fas associated protein with death domain) contributing to IFN-γ-induced autophagic cell death (Pyo *et al.*, 2005). The role of ATG5 in cell death seems to be context-dependent. While Pyo *et al.* reported that ATG5 does not modulate cell death induced by staurosporine, etoposide or cisplatin (Pyo *et al.*, 2005), Yousefi *et al.* reported a protective effect of Atg5-knockdown in staurosporine-induced cell death and identified a truncated form of ATG5 as a cleavage product of calpains (Yousefi *et al.*, 2006). Calpain-

mediated cleavage of ATG5 switches autophagy to apoptosis. This switch occurs through translocation from the cytosol to mitochondria, association with the anti-apoptotic molecule BCL-xL and triggering of cytochrome *c* release and caspase activation (Yousefi *et al.*, 2006). In the absence of autophagy, the death-inducing activity of the truncated form of ATG5 is also observed (Yousefi *et al.*, 2006). Since ATG5 has been found to be implicated in the mitochondrial quality control (Mai *et al.*, 2012), the knockdown of this protein can directly interfere in this organelle and change the signaling pathways activated upon gossypol treatment. In this line, since most autophagic components are also involved in non-autophagic functions (Galluzzi and Green, 2019), precise characterization of the autophagic machinery that participates in the gossypol-induced signaling pathways needs to be further addressed.

Nonetheless, as far as we know, the direct link between genetic inhibition of an important autophagic regulator such as ATG5 and the formation of apoptotic nuclear morphologies has not been reported before. Moreover, since the inhibition of type II nuclear morphologies in the presence of 3-MA coincides with an alteration of the gossypol-induced autophagic flux and with an advanced activation of caspases, we may conclude that the temporality of these events strongly determines the final nuclear outcome of human glioblastoma cells treated with gossypol. Accordingly, we may conclude that the specific crosstalk between autophagy and apoptosis needs to occur at the adequate time. In part, this may be because, besides the activation of caspases, caspase-independent events, including gossypol binding to metal ions or DNA structural changes, seem to be required for the proper activation of DFF40/CAD and, consequently, for the formation of type II nuclear morphologies.

Overall, we may conclude that autophagy is a cytoprotective response triggered in the presence of gossypol and its inhibition at an adequate time point will allow the activation of caspases and, consequently, the formation of apoptotic nuclear morphologies. Similarly, Zhang *et al.* described a dual effect of gossypol on human hepatocellular carcinoma via ER stress and autophagy (Zhang *et al.*, 2019a). More specifically, the authors described that autophagy constitutes a feedback mechanism that protects cells from ER stress-related apoptosis. Gao *et al.* also suggested that gossypol-induced autophagy is cytoprotective (Gao *et al.*, 2010). Alternatively, other authors sustain that autophagy protects glioma cells against calcium mobilization (Vu *et al.*, 2018). In this sense, the activation of autophagy in LN-18 cells may be part of the mechanism of these cells to protect themselves from increased calcium levels induced by gossypol (Soderquist *et al.*, 2014), which, as mentioned above, may participate in the mechanism of activation of caspases and, consequently, in type II nuclear morphologies.

Better characterization of the autophagic machinery will be required to understand its crosstalk with the cell death machinery and, especially, with caspases and DFF40/CAD, both required for the condensation, fragmentation, and packaging of the genomic content of damaged cells.

6. General discussion: relevance of the results presented in this Doctoral Thesis and future directions

This work demonstrates that human glioblastoma-derived cells, previously characterized as apoptotic-defective cells (Sanchez-Osuna *et al.*, 2014), owns the machinery required to display apoptotic nuclear morphologies. These cells can display this cellular outcome when challenged under the appropriate conditions with the adequate stimuli. Here, we show gossypol as an adequate insult able to prompt human glioblastoma-derived cells to condense and fragment their genomic content. Likewise, gamma irradiation, which is already used as a first-line treatment of glioblastomas, may also be an adequate stimulus to induce such nuclear phenotype. Hence, without genetically modifying these cells, the tendency of human glioblastoma-derived cells from dying without properly fragmenting the nuclei can be changed by using the adequate stimulus.

From a biological point of view, apoptosis-associated chromatin condensation and fragmentation constitute a fundamental process to prevent the spreading of harmful genes, such as viral DNA or oncogenes (Susin *et al.*, 2000) (Widlak and Garrard, 2009). Therefore, although we could simplistically conclude that irrespective of the final nuclear outcome tumor cells die, reduced efficiency in the elimination of apoptotic cells with genome damage may contribute to tumorigenesis. Hence, considering the carcinogenic potential of a non-accurate packaging of the DNA, we may hypothesize that the human-glioblastoma cells' tendency to undergo incomplete apoptosis may be an advantageous adaptation mechanism contributing to the aggressiveness of this tumor. In this line, the presence of necrotic areas has been established not only as a histomorphologic criterion in the diagnosis of glioblastoma but also as a powerful predictor of poor patient prognosis. Abortive apoptotic processes, such as those described in LN-18 cells when treated with different cytotoxic agents (Sanchez-Osuna *et al.*, 2014), could be a potential cause driving glioblastoma cells necrosis. Interestingly, caspase-3 activity has been observed next to necrotic areas (Gdynia *et al.*, 2007). This observation, which strongly suggests the interconnection between apoptosis and necrosis, could indicate that cell death occurring in the context of necrotic areas may be the consequence of an initial apoptotic

process (Gdynia *et al.*, 2007). Cells that have undergone an apoptotic process may enter into a phase called secondary necrosis if they are not adequately scavenged (Rogers *et al.*, 2017).

The secretion and exposure of signals by dying cells constitute a critical homeostatic mechanism to attract phagocytes and, consequently, to favor the adequate clearance of dying cells. It has recently been reviewed that disruption of normal efferocytosis, which means the engulfment and clearance of dead and dying cells, may contribute to the development of a wide range of diseases, including glioblastoma (Boada-Romero *et al.*, 2020). Because different effects may be derived from different cell death modes, we may expect distinct consequences from the different nuclear morphologies observed in glioblastoma-derived-damaged cells. Hence, the intrinsic disability of glioblastoma cells to undergo complete apoptotic cell death may not only constitute a risk of incorporation of the DNA of dead cells into adjacent cells, but also lead to distinct effects on inflammation and the adaptive immune responses (Zitvogel *et al.*, 2004) (Boada-Romero *et al.*, 2020) and may contribute to tumorigenesis.

As clearly exemplified in DFF40/CAD-deficient cells, which are more prone to mutations and chromosomal instability (Yan *et al.*, 2006a), different outcomes may be expected from a cell death process with participation or not of the endonuclease. Cleavage of susceptible A/T rich matrix attachment regions (MARs) of chromatin by DFF40/CAD has been described as a fundamental mechanism not only for the complete condensation of the chromatin in apoptotic cells, but also for switching off the genome function (Dieker *et al.*, 2012). At the same time, it is necessary to stress that besides the role of the endonuclease maintaining genomic stability and promoting the removal of DNA-damaged cells, we cannot ignore that the DNA damage induced by the endonuclease can also lead to oncogenic transformation after sublethal activation of caspases (Cao and Tait, 2018) (Liu *et al.*, 2017).

Thanks to the results here presented, we do know different insults are able to trigger different levels of caspase activation and DFF40/CAD activation. Hence, given the critical role of DFF40/CAD on tumorigenesis, it would be interesting to determine the gene expression pattern induced as a result of a sublethal activation of caspases both in wild-type and in DFF40/CAD-overexpressing glioblastoma-derived cells (both commercial and non-commercial) untreated or treated with different insults. The study of the influence of the endonuclease in the gene expression in human glioblastoma cells would help us to understand the behavior of this tumor better.

According to our results, the activation of DFF40/CAD constitutes the molecular bottleneck to display classical apoptotic nuclear features in human glioblastoma-derived cells. However,

as mentioned above, the limitation of human glioblastoma cells to show this nuclear outcome is not completely reliant on the levels of the endonuclease. Neither the proper activation of caspases constitutes the limiting factor impairing nuclear fragmentation (Sanchez-Osuna *et al.*, 2014).

As reviewed in Ichim and Tait, 2016, the level of caspase activity required to trigger cell death does not seem to be very high. Rehm *et al.*, 2006 highlighted the requirement of an efficient effector caspase activation to elicit significant morphological changes and execution of apoptosis. Linked to this concept of efficiency, we add the concepts of 'quantity' and 'quality'. Here, we demonstrate that, although caspases are necessary for chromatin condensation and fragmentation, the 'quantity' or the intensity of activation by itself does not determine the final nuclear outcome of dying cells either as type II or type III. It is the 'quality' of the activation what determines the formation of apoptotic nuclear morphologies. Considering that contrary to gossypol, the challenge of LN-18 cells with TRAIL is not sufficient to display apoptotic nuclear morphologies, we conclude that the 'quality' of the activation of caspases is offered by gossypol. According to our results, alternative requirements besides the activation of caspases seem to be needed to trigger classical apoptotic nuclear alterations in glioblastoma cells. In this sense, the 'quality' of the activation of caspases but also of DFF40/CAD by gossypol relies on its ability to interfere with intracellular impairments that impede the formation of apoptotic nuclear morphologies in human glioblastoma cells. Here, we show that intracellular levels of metal ions are determinants of the final nuclear morphology displayed by glioblastoma cells when challenged with different cytotoxic stimuli. We propose that metal ions may directly inhibit DFF40/CAD catalytic activity or may indirectly affect the activity of DFF40 due to the alteration of DNA that is the substrate of the endonuclease. Thanks to its structure, gossypol can interact with such ions and, consequently, allows an adequate activation of caspases and DFF40/CAD to prompt condensation and fragmentation of the nuclei. Further research in this field will help to comprehend the formation of classical apoptotic nuclear morphologies precisely.

Moreover, the study of binding partners required for the nuclear entrapment of DFF40/CAD may also be fundamental. Among them, histones are key signaling platforms controlling nuclear apoptotic events: H2B phosphorylation is relevant for apoptotic chromatin condensation (Cheung *et al.*, 2003), and histone H1 interacts with DFF40/CAD and tethers the endonuclease to the chromatin (Zhang and Xu, 2002). Recently, Kijima *et al.,* have described that the efficiency of chromatin condensation both in apoptotic and live cells is determined by histone H1 quantity (Kijima and Mizuta, 2019) (Kijima *et al.*, 2019). The authors describe that cells with lower levels of histone H1 coincided with more open chromatin and

high accessibility of DNases. Previously, Ryushin Mizuta *et al.* described that the presence of linker histone H1 enhances the activity of other endonucleases such as the DNase γ (Mizuta *et al.*, 2006), which may function as a backup endonuclease of DFF40/CAD after apoptosis in the secondary necrosis phase (Koyama *et al.*, 2016). The study of other endonucleases, including DNase γ, and how histones, especially the linker histone H1, participate in the formation of apoptotic nuclear morphologies in human glioblastoma cells constitutes another interesting future approach.

Furthermore, besides TRAIL, the combination of high levels of cobaltous with gossypol also leads to an increase in the percentage of gossypol-induced type II nuclear morphologies. Hence, we may hypothesize that both stimuli may share a similar mechanism. In this sense, different articles describe the activation of the mitochondrial and death receptor-dependent pathway by $CoCl_2$ (Zou *et al.*, 2001) (Zou *et al.*, 2002) (Jung and Kim, 2004) (Lee *et al.*, 2013). More specifically, in the presence of $CoCl_2$, an upregulation of Fas and Fas-ligand has been detected in PC12 cells (Jung and Kim, 2004) and in mouse embryonic stem cells (Lee *et al.*, 2013). Elevated levels of TNFα were detected upon treatment with cobalt oxide nanoparticles in human leukemia cells (Chattopadhyay *et al.*, 2015). In this line, we may consider that the activation of the extrinsic apoptotic pathway may play a key role in the mechanism of action of gossypol. It has been described that MOMP induces TNF synthesis under caspase-deficient conditions (Giampazolias *et al.*, 2017). Accordingly, we may hypothesize that the limited MOMP and caspases activation triggered by gossypol could induce an increase in TNF secretion and activation of the extrinsic pathway. Besides this, the induction of TRAIL receptors and activation of caspase-8 through ER stress is extensively reported in the literature (Iurlaro and Munoz-Pinedo, 2016) (Munoz-Pinedo and Lopez-Rivas, 2018). In this line, CHOP has been reported as a key factor leading to the apoptotic cell death induced by gossypol (Zhang *et al.*, 2019a).

Regarding the mechanism of activation of TRAIL receptors, Sullivan *et al.* have recently described ER stress responses leading to ligand-independent activation of TRAIL receptors resulting in a FADD/caspase-8/RIPK1 (FADDosome)-dependent NF-κB activation and inflammatory cytokine production (Sullivan *et al.*, 2020). This ligand-independent activation may occur after reaching a receptor density resulting in receptor interactions and spontaneous signaling, due to entrapment in an ER-Golgi compartment promoting autoactivation, or because of binding of misfolded proteins (Roca Portoles and Tait, 2020). Lam *et al.* reported that misfolded proteins might activate DR5 intracellularly by acting as ligands. Activated DR5 can assemble pro-apoptotic caspase-8 at the ER-Golgi intermediate compartment to promote

apoptosis (Lam *et al.*, 2020). Alternatively, Yedida *et al.* reported that ER membrane reorganization at the level of ER tubules upon apogossypol treatment impairs the activation of the intrinsic apoptotic pathway (Yedida *et al.*, 2019). Electron microscopy images revealed swelling of the nuclear envelope and continuity of the ER membrane aggregates with the outer nuclear membrane (Varadarajan *et al.*, 2012). Our results show that this gossypol derivative allows LN-18 cells to display some type III nuclear morphologies but is inefficient at inducing type II nuclear morphologies. The close contact with the nuclear envelope and its connection with the cytoskeleton points to this organelle as an important regulator of the process of packaging and formation of apoptotic nuclear bodies. From our results, we may hypothesize that protein aggregates induced by gossypol could activate DR5 and lead to the activation of caspase-8. Considering that caspase-3 may be activated in the absence of BAX and BAK upon gossypol treatment, we may consider that some human glioblastoma cells may respond as type I cells and directly activate executioner caspases by caspase-8 in a mitochondrion-independent manner. This different mechanism of caspase activation could activate the pool of caspases required for the formation of type II nuclear morphologies. However, the induction of ER stress *per se* does not explain the formation of apoptotic nuclear morphologies in human glioblastoma-derived cells, because different ER stressor compounds induce different nuclear outcomes in LN-18 cells.

The latest results of this work support the role of gossypol as an autophagy modulating compound. Our results suggest that the blockage of this protective mechanism in a time-dependent manner may be essential to promote apoptotic nuclear morphologies in human glioblastoma cells. ATG5, which is well accepted as an important regulator of autophagy, is here presented as a potential key regulator of the final nuclear outcome of dying cells. Alternative pharmacological and genetic approaches will be needed to gain insight into the biochemical of this gossypol-related autophagic process and on its possible regulatory role over chromatin compaction, fragmentation, and packaging of the genomic content. The study of the crosstalk of autophagy with apoptosis and with ER stress will help to better comprehend the cell death mechanism behind the gossypol-induced formation of apoptotic nuclear morphologies.

This study will be of particular interest because the biological consequences of the therapeutically-induced cell death will be strongly determined by the different modes of cell death activated in the targeted cells. To know and understand which biological consequences may be derived from the treatments that we use, it is essential to know the signaling pathways that become activated or switched off when we face the cells to these treatments.

In line with the recommendation of NCCD (Galluzzi *et al.*, 2012b) (Galluzzi *et al.*, 2018), this work evidences the necessity of analyzing different biochemical features to achieve this purpose. By only analyzing cytochrome *c* release, activation of caspases, or MTT reduction, we may be ignoring the complexity behind the cell death triggered upon any treatment. Although the NCCD recommends abandoning morphological criteria, we encourage researchers to combine the biochemical criteria with the study of the nuclear morphology. As we present here, this powerful and straightforward experimental approach may help to puzzle out the crosstalk between different intracellular modes of cell death and to comprehend better the complex process of dying.

CONCLUSIONS

First: human glioblastoma-derived LN-18 cells display nuclei with partial chromatin condensation in a ring-like shape (type I), nuclei with chromatin condensation and fragmentation (type II), and pyknotic nuclei without karyorrhexis (type III) after treatment with gossypol.

Second: the percentage of the different nuclear morphologies induced by gossypol varies depending on the concentration of gossypol, the time of exposure, or the cellular density.

Third: transmission electron microscopy images corroborate gossypol as an adequate stimulus to induce classical apoptotic nuclear morphology characterized by different masses of condensed chromatin wholly closed and separated by nuclear envelope in LN-18 cells.

Forth: different commercial human glioblastoma-derived cell lines and non-commercial (primary or relapse)-derived glioblastoma cells display a similar nuclear phenotype after gossypol treatment.

Fifth: gossypol induces the activation of caspases and the processing of ICAD.

Sixth: the activation of caspases, especially of caspase-3, is required for type II and type III nuclear morphologies, but not for the type I nuclear morphology induced upon gossypol treatment.

Seventh: the combination of gossypol with TRAIL enhances the activation of caspases, the processing of ICAD, and, consequently, the percentage of caspase-dependent nuclear morphologies (type II and type III) induced by gossypol.

Eight: gossypol can induce the activation of caspase-3 and the subsequent formation of caspase-dependent nuclear morphologies (type II and type III) in the absence of BAX and BAK.

Ninth: the specific silencing of the endonuclease DFF40/CAD impedes the formation of the apoptotic type II nuclear morphology, but not of type III nuclear morphology.

Tenth: the overexpression of the endonuclease DFF40/CAD does not significantly increase the number of apoptotic nuclear morphologies induced by gossypol in LN-18 cells.

Eleventh: gossypol induces higher concentration or aggregation of the endonuclease DFF40/CAD around DNA.

Twelfth: the percentage of apoptotic nuclear morphologies correlates with TUNEL positivity and DNA ladder in apoptotic proficient SH-SY5Y cells but not in human glioblastoma-derived LN-18 cells.

Thirteen: phosphorylation of H2AX at Ser139 is induced by gossypol regardless of caspase activation in LN-18 cells.

Fourteenth: gossypol derivatives induce type II nuclear morphologies in apoptotic proficient SH-SY5Y cells but not in human glioblastoma-derived LN-18 cells.

Fifteenth: the addition of metal ions to the culture medium of LN-18 cells modifies the percentage of cells showing apoptotic nuclear morphology; cooper or iron inhibit the formation of gossypol-induced type II nuclear morphology, whereas high levels of cobaltous increases this type of nuclear morphology.

Sixteenth: ER stress and autophagy are induced upon gossypol treatment in LN-18 cells regardless of caspase activation.

Seventeenth: the modulation of the autophagic flux has a direct impact on the formation of the apoptotic type II nuclear morphology induced by gossypol in LN-18 cells.

BIBLIOGRAPHY

Abdullaev, N.D., Tyshchenko, A.A., Nazarova, I.P., Ul'chenko, N.T., Yagudaev, M.R., and Glushenkova, A.I. (1990). 1H and13C NMR spectra of transformation products of gossypol in solutions. *Chemistry of Natural Compounds* 26, 129-138.

Adachi, Y., Kas, E., and Laemmli, U.K. (1989). Preferential, cooperative binding of DNA topoisomerase II to scaffold-associated regions. *EMBO J* 8, 3997-4006.

Adams, R., Geissman, T.A., and Edwards, J.D. (1960). Gossypol, a pigment of cottonseed. *Chem Rev* 60, 555-574.

Ahn, J.Y., Liu, X., Cheng, D., Peng, J., Chan, P.K., Wade, P.A., and Ye, K. (2005). Nucleophosmin/B23, a nuclear PI(3,4,5)P(3) receptor, mediates the antiapoptotic actions of NGF by inhibiting CAD. *Mol Cell* 18, 435-445.

Almanza, A., Carlesso, A., Chintha, C., Creedican, S., Doultsinos, D., Leuzzi, B., [. . .], Samali, A. (2019). Endoplasmic reticulum stress signalling - from basic mechanisms to clinical applications. *FEBS J* 286, 241-278.

Alnemri, E.S., Livingston, D.J., Nicholson, D.W., Salvesen, G., Thornberry, N.A., Wong, W.W., and Yuan, J. (1996). Human ICE/CED-3 protease nomenclature. *Cell* 87, 171.

Alvarez-Diaz, S., Dillon, C.P., Lalaoui, N., Tanzer, M.C., Rodriguez, D.A., Lin, A., [. . .], Strasser, A. (2016). The Pseudokinase MLKL and the Kinase RIPK3 Have Distinct Roles in Autoimmune Disease Caused by Loss of Death-Receptor-Induced Apoptosis. *Immunity* 45, 513-526.

Amaravadi, R., Kimmelman, A.C., and White, E. (2016). Recent insights into the function of autophagy in cancer. *Genes Dev* 30, 1913-1930.

Anido, J., Saez-Borderias, A., Gonzalez-Junca, A., Rodon, L., Folch, G., Carmona, M.A., [. . .], Seoane, J. (2010). TGF-beta Receptor Inhibitors Target the CD44(high)/Id1(high) Glioma-Initiating Cell Population in Human Glioblastoma. *Cancer Cell* 18, 655-668.

Antonietti, P., Gessler, F., Dussmann, H., Reimertz, C., Mittelbronn, M., Prehn, J.H., and Kogel, D. (2016). AT-101 simultaneously triggers apoptosis and a cytoprotective type of autophagy irrespective of expression levels and the subcellular localization of Bcl-xL and Bcl-2 in MCF7 cells. *Biochim Biophys Acta* 1863, 499-509.

Aranovich, A., Liu, Q., Collins, T., Geng, F., Dixit, S., Leber, B., and Andrews, D.W. (2012). Differences in the mechanisms of proapoptotic BH3 proteins binding to Bcl-XL and Bcl-2 quantified in live MCF-7 cells. *Mol Cell* 45, 754-763.

Arcella, A., Biagioni, F., Antonietta Oliva, M., Bucci, D., Frati, A., Esposito, V., [. . .], Fornai, F. (2013). Rapamycin inhibits the growth of glioblastoma. *Brain Res* 1495, 37-51.

Aredia, F., Guaman Ortiz, L.M., Giansanti, V., and Scovassi, A.I. (2012). Autophagy and cancer. *Cells* 1, 520-534.

Arinbasarova, A.Y., Medentsev, A.G., and Krupyanko, V.I. (2012). Gossypol Inhibits Electron Transport and Stimulates ROS Generation in Yarrowia lipolytica Mitochondria. *Open Biochem J* 6, 11-15.

Arnoult, D., Gaume, B., Karbowski, M., Sharpe, J.C., Cecconi, F., and Youle, R.J. (2003). Mitochondrial release of AIF and EndoG requires caspase activation downstream of Bax/Bak-mediated permeabilization. *EMBO J* 22, 4385-4399.

Artus, C., Boujrad, H., Bouharrour, A., Brunelle, M.N., Hoos, S., Yuste, V.J., [. . .], Susin, S.A. (2010). AIF promotes chromatinolysis and caspase-independent programmed necrosis by interacting with histone H2AX. *EMBO J* 29, 1585-1599.

Ashkenazi, A., and Dixit, V.M. (1998). Death receptors: signaling and modulation. *Science* 281, 1305-1308.

Axe, E.L., Walker, S.A., Manifava, M., Chandra, P., Roderick, H.L., Habermann, A., [. . .], Ktistakis, N.T. (2008). Autophagosome formation from membrane compartments enriched in phosphatidylinositol 3-phosphate and dynamically connected to the endoplasmic reticulum. *J Cell Biol* 182, 685-701.

Balakrishnan, K., Wierda, W.G., Keating, M.J., and Gandhi, V. (2008). Gossypol, a BH3 mimetic, induces apoptosis in chronic lymphocytic leukemia cells. *Blood* 112, 1971-1980.

Baritaud, M., Boujrad, H., Lorenzo, H.K., Krantic, S., and Susin, S.A. (2010). Histone H2AX: The missing link in AIF-mediated caspase-independent programmed necrosis. *Cell Cycle* 9, 3166-3173.

Baritaud, M., Cabon, L., Delavallee, L., Galan-Malo, P., Gilles, M.E., Brunelle-Navas, M.N., and Susin, S.A. (2012). AIF-mediated caspase-independent necroptosis requires ATM and DNA-PK-induced histone H2AX Ser139 phosphorylation. *Cell Death Dis* 3, e390.

Barnhart, B.C., Alappat, E.C., and Peter, M.E. (2003). The CD95 type I/type II model. *Semin Immunol* 15, 185-193.

Barros, L.F., Hermosilla, T., and Castro, J. (2001). Necrotic volume increase and the early physiology of necrosis. *Comp Biochem Physiol A Mol Integr Physiol* 130, 401-409.

Barry, M.A., and Eastman, A. (1993). Identification of deoxyribonuclease II as an endonuclease involved in apoptosis. *Arch Biochem Biophys* 300, 440-450.

Barry, M.A., Reynolds, J.E., and Eastman, A. (1993). Etoposide-induced apoptosis in human HL-60 cells is associated with intracellular acidification. *Cancer Res* 53, 2349-2357.

Beg, A.A., and Baltimore, D. (1996). An essential role for NF-kappaB in preventing TNF-alpha-induced cell death. *Science* 274, 782-784.

Bell, R.A.V., and Megeney, L.A. (2017). Evolution of caspase-mediated cell death and differentiation: twins separated at birth. *Cell Death Differ* 24, 1359-1368.

Bellail, A.C., Tse, M.C., Song, J.H., Phuphanich, S., Olson, J.J., Sun, S.Y., and Hao, C. (2010). DR5-mediated DISC controls caspase-8 cleavage and initiation of apoptosis in human glioblastomas. *J Cell Mol Med* 14, 1303-1317.

Benhaim, P., Mathes, S.J., Hunt, T.K., Scheuenstuhl, H., and Benz, C.C. (1994). Induction of neutrophil Mac-1 integrin expression and superoxide production by the medicinal plant extract gossypol. *Inflammation* 18, 443-458.

Benvenuto, M., Mattera, R., Masuelli, L., Taffera, G., Andracchio, O., Tresoldi, I., [. . .], Bei, R. (2017). (+/-)-Gossypol induces apoptosis and autophagy in head and neck carcinoma cell lines and inhibits the growth of transplanted salivary gland cancer cells in BALB/c mice. *Int J Food Sci Nutr* 68, 298-312.

Bertrand, R., Solary, E., O'Connor, P., Kohn, K.W., and Pommier, Y. (1994). Induction of a common pathway of apoptosis by staurosporine. *Exp Cell Res* 211, 314-321.

Bialik, S., Dasari, S.K., and Kimchi, A. (2018). Autophagy-dependent cell death - where, how and why a cell eats itself to death. *J Cell Sci* 131.

Billen, L.P., Shamas-Din, A., and Andrews, D.W. (2008). Bid: a Bax-like BH3 protein. *Oncogene* 27 Suppl 1, S93-104.

Bjorkoy, G., Lamark, T., Brech, A., Outzen, H., Perander, M., Overvatn, A., [. . .], Johansen, T. (2005). p62/SQSTM1 forms protein aggregates degraded by autophagy and has a protective effect on huntingtin-induced cell death. *J Cell Biol* 171, 603-614.

Bleicken, S., Hantusch, A., Das, K.K., Frickey, T., and Garcia-Saez, A.J. (2017). Quantitative interactome of a membrane Bcl-2 network identifies a hierarchy of complexes for apoptosis regulation. *Nat Commun* 8, 73.

Boada-Romero, E., Martinez, J., Heckmann, B.L., and Green, D.R. (2020). The clearance of dead cells by efferocytosis. *Nat Rev Mol Cell Biol*.

Bock, F.J., and Tait, S.W.G. (2020). Mitochondria as multifaceted regulators of cell death. *Nat Rev Mol Cell Biol* 21, 85-100.

Bodmer, J.L., Schneider, P., and Tschopp, J. (2002). The molecular architecture of the TNF superfamily. *Trends Biochem Sci* 27, 19-26.

Bogner, C., Leber, B., and Andrews, D.W. (2010). Apoptosis: embedded in membranes. *Curr Opin Cell Biol* 22, 845-851.

Boix, J., Llecha, N., Yuste, V.J., and Comella, J.X. (1997). Characterization of the cell death process induced by staurosporine in human neuroblastoma cell lines. *Neuropharmacology* 36, 811-821.

Boldin, M.P., Varfolomeev, E.E., Pancer, Z., Mett, I.L., Camonis, J.H., and Wallach, D. (1995). A novel protein that interacts with the death domain of Fas/APO1 contains a sequence motif related to the death domain. *J Biol Chem* 270, 7795-7798.

Bonner, W.M., Redon, C.E., Dickey, J.S., Nakamura, A.J., Sedelnikova, O.A., Solier, S., and Pommier, Y. (2008). GammaH2AX and cancer. *Nat Rev Cancer* 8, 957-967.

Bortner, C.D., Oldenburg, N.B., and Cidlowski, J.A. (1995). The role of DNA fragmentation in apoptosis. *Trends Cell Biol* 5, 21-26.

Bouchier-Hayes, L., and Green, D.R. (2012). Caspase-2: the orphan caspase. *Cell Death Differ* 19, 51-57.

Bourguignon, L.Y., Singleton, P.A., and Diedrich, F. (2004). Hyaluronan-CD44 interaction with Rac1-dependent protein kinase N-gamma promotes phospholipase Cgamma1 activation, Ca(2+) signaling, and cortactin-cytoskeleton function leading to keratinocyte adhesion and differentiation. *J Biol Chem* 279, 29654-29669.

Boya, P., Andreau, K., Poncet, D., Zamzami, N., Perfettini, J.L., Metivier, D., [. . .], Kroemer, G. (2003a). Lysosomal membrane permeabilization induces cell death in a mitochondrion-dependent fashion. *J Exp Med* 197, 1323-1334.

Boya, P., Gonzalez-Polo, R.A., Poncet, D., Andreau, K., Vieira, H.L., Roumier, T., [. . .], Kroemer, G. (2003b). Mitochondrial membrane permeabilization is a critical step of lysosome-initiated apoptosis induced by hydroxychloroquine. *Oncogene* 22, 3927-3936.

Boyer, P.D., Chance, B., Ernster, L., Mitchell, P., Racker, E., and Slater, E.C. (1977). Oxidative phosphorylation and photophosphorylation. *Annu Rev Biochem* 46, 955-966.

Brat, D.J., Aldape, K., Colman, H., Holland, E.C., Louis, D.N., Jenkins, R.B., [. . .], Weller, M. (2018). cIMPACT-NOW update 3: recommended diagnostic criteria for "Diffuse astrocytic glioma, IDH-wildtype, with molecular features of glioblastoma, WHO grade IV". *Acta Neuropathol* 136, 805-810.

Brat, D.J., and Mapstone, T.B. (2003). Malignant glioma physiology: cellular response to hypoxia and its role in tumor progression. *Ann Intern Med* 138, 659-668.

Bredesen, D.E. (2008). Programmed cell death mechanisms in neurological disease. *Curr Mol Med* 8, 173-186.

Browne, K.A., Johnstone, R.W., Jans, D.A., and Trapani, J.A. (2000). Filamin (280-kDa actin-binding protein) is a caspase substrate and is also cleaved directly by the cytotoxic T lymphocyte protease granzyme B during apoptosis. *J Biol Chem* 275, 39262-39266.

Brumatti, G., Salmanidis, M., and Ekert, P.G. (2010). Crossing paths: interactions between the cell death machinery and growth factor survival signals. *Cell Mol Life Sci* 67, 1619-1630.

Bruna, J., and Alemany, M. (2020). [Historical perspective of the studies with the greatest impact on the treatment of gliomas]. *Rev Neurol* 70, 220-230.

Byun, Y., Chen, F., Chang, R., Trivedi, M., Green, K.J., and Cryns, V.L. (2001). Caspase cleavage of vimentin disrupts intermediate filaments and promotes apoptosis. *Cell Death Differ* 8, 443-450.

Callus, B.A., and Vaux, D.L. (2007). Caspase inhibitors: viral, cellular and chemical. *Cell Death Differ* 14, 73-78.

Campisi, J. (2013). Aging, cellular senescence, and cancer. *Annu Rev Physiol* 75, 685-705.

Cancer Genome Atlas Research, N. (2008). Comprehensive genomic characterization defines human glioblastoma genes and core pathways. *Nature* 455, 1061-1068.

Cande, C., Vahsen, N., Kouranti, I., Schmitt, E., Daugas, E., Spahr, C., [. . .], Kroemer, G. (2004). AIF and cyclophilin A cooperate in apoptosis-associated chromatinolysis. *Oncogene* 23, 1514-1521.

Cao, K., and Tait, S.W.G. (2018). Apoptosis and Cancer: Force Awakens, Phantom Menace, or Both? *Int Rev Cell Mol Biol* 337, 135-152.

Cartwright, I.M., Liu, X., Zhou, M., Li, F., and Li, C.Y. (2017). Essential roles of Caspase-3 in facilitating Myc-induced genetic instability and carcinogenesis. *Elife* 6.

Caruso, S., Atkin-Smith, G.K., Baxter, A.A., Tixeira, R., Jiang, L., Ozkocak, D.C., [. . .], Poon, I.K.H. (2019). Defining the role of cytoskeletal components in the formation of apoptopodia and apoptotic bodies during apoptosis. *Apoptosis* 24, 862-877.

Casanelles, E., Gozzelino, R., Marques-Fernandez, F., Iglesias-Guimarais, V., Garcia-Belinchon, M., Sanchez-Osuna, M., [. . .], Yuste, V.J. (2013). NF-kappaB activation fails to protect cells to TNFalpha-induced apoptosis in the absence of Bcl-xL, but not Mcl-1, Bcl-2 or Bcl-w. *Biochim Biophys Acta* 1833, 1085-1095.

Caserta, T.M., Smith, A.N., Gultice, A.D., Reedy, M.A., and Brown, T.L. (2003). Q-VD-OPh, a broad spectrum caspase inhibitor with potent antiapoptotic properties. *Apoptosis* 8, 345-352.

Cass, Q.B., Tiritan, E., Matlin, S.A., and Freire, E.C. (1991). Gossypol enantiomer ratios in cotton seeds. *Phytochemistry* 30, 2655-2657.

Castedo, M., Perfettini, J.L., Roumier, T., Andreau, K., Medema, R., and Kroemer, G. (2004). Cell death by mitotic catastrophe: a molecular definition. *Oncogene* 23, 2825-2837.

Cerretti, D.P., Kozlosky, C.J., Mosley, B., Nelson, N., Van Ness, K., Greenstreet, T.A., [. . .], et al. (1992). Molecular cloning of the interleukin-1 beta converting enzyme. *Science* 256, 97-100.

Chai, J., Du, C., Wu, J.W., Kyin, S., Wang, X., and Shi, Y. (2000). Structural and biochemical basis of apoptotic activation by Smac/DIABLO. *Nature* 406, 855-862.

Chan, S.L., Lee, M.C., Tan, K.O., Yang, L.K., Lee, A.S., Flotow, H., [. . .], Yu, V.C. (2003). Identification of chelerythrine as an inhibitor of BclXL function. *J Biol Chem* 278, 20453-20456.

Chattopadhyay, S., Dash, S.K., Tripathy, S., Das, B., Kar Mahapatra, S., Pramanik, P., and Roy, S. (2015). Cobalt oxide nanoparticles induced oxidative stress linked to activation of TNF-alpha/caspase-8/p38-MAPK signaling in human leukemia cells. *J Appl Toxicol* 35, 603-613.

Chen, D., Stetler, R.A., Cao, G., Pei, W., O'Horo, C., Yin, X.M., and Chen, J. (2000). Characterization of the rat DNA fragmentation factor 35/Inhibitor of caspase-activated DNase (Short form). The endogenous inhibitor of caspase-dependent DNA fragmentation in neuronal apoptosis. *J Biol Chem* 275, 38508-38517.

Chen, H.C., Kanai, M., Inoue-Yamauchi, A., Tu, H.C., Huang, Y., Ren, D., [. . .], Cheng, E.H. (2015). An interconnected hierarchical model of cell death regulation by the BCL-2 family. *Nat Cell Biol* 17, 1270-1281.

Chen, X., He, W.T., Hu, L., Li, J., Fang, Y., Wang, X., [. . .], Han, J. (2016). Pyroptosis is driven by non-selective gasdermin-D pore and its morphology is different from MLKL channel-mediated necroptosis. *Cell Res* 26, 1007-1020.

Cheng, T.C., Hong, C., Akey, I.V., Yuan, S., and Akey, C.W. (2016). A near atomic structure of the active human apoptosome. *Elife* 5.

Cheung, W.L., Ajiro, K., Samejima, K., Kloc, M., Cheung, P., Mizzen, C.A., [. . .], Allis, C.D. (2003). Apoptotic phosphorylation of histone H2B is mediated by mammalian sterile twenty kinase. *Cell* 113, 507-517.

Chinnaiyan, A.M., O'Rourke, K., Tewari, M., and Dixit, V.M. (1995). FADD, a novel death domain-containing protein, interacts with the death domain of Fas and initiates apoptosis. *Cell* 81, 505-512.

Chipuk, J.E., Kuwana, T., Bouchier-Hayes, L., Droin, N.M., Newmeyer, D.D., Schuler, M., and Green, D.R. (2004). Direct activation of Bax by p53 mediates mitochondrial membrane permeabilization and apoptosis. *Science* 303, 1010-1014.

Cho, S.G., Kim, J.W., Lee, Y.H., Hwang, H.S., Kim, M.S., Ryoo, K., [. . .], Choi, E.J. (2003). Identification of a novel antiapoptotic protein that antagonizes ASK1 and CAD activities. *J Cell Biol* 163, 71-81.

Cho, Y.S., Challa, S., Moquin, D., Genga, R., Ray, T.D., Guildford, M., and Chan, F.K. (2009). Phosphorylation-driven assembly of the RIP1-RIP3 complex regulates programmed necrosis and virus-induced inflammation. *Cell* 137, 1112-1123.

Choi, J.Y., Qiao, Q., Hong, S.H., Kim, C.M., Jeong, J.H., Kim, Y.G., [. . .], Park, H.H. (2017). CIDE domains form functionally important higher-order assemblies for DNA fragmentation. *Proc Natl Acad Sci U S A* 114, 7361-7366.

Chowdhury, D., Keogh, M.C., Ishii, H., Peterson, C.L., Buratowski, S., and Lieberman, J. (2005). gamma-H2AX dephosphorylation by protein phosphatase 2A facilitates DNA double-strand break repair. *Mol Cell* 20, 801-809.

Chowdhury, I., Tharakan, B., and Bhat, G.K. (2008). Caspases - an update. *Comp Biochem Physiol B Biochem Mol Biol* 151, 10-27.

Churbanova, I.Y., and Sevrioukova, I.F. (2008). Redox-dependent changes in molecular properties of mitochondrial apoptosis-inducing factor. *J Biol Chem* 283, 5622-5631.

Clark, E. (1927). Studies on gossypol i. The preparation, purification, and some of the properties of gossypol, the toxic principle of cottonseed. *Journal of Biological Chemistry* 75, 725-739.

Clark, E. (1928). Studies on gossypol IV. Apogossypol. *Journal of Biological Chemistry* 78, 159-166.

Clarke, P.G. (1990). Developmental cell death: morphological diversity and multiple mechanisms. *Anat Embryol (Berl)* 181, 195-213.

Clarke, P.G., and Clarke, S. (1996). Nineteenth century research on naturally occurring cell death and related phenomena. *Anat Embryol (Berl)* 193, 81-99.

Codogno, P., Mehrpour, M., and Proikas-Cezanne, T. (2011). Canonical and non-canonical autophagy: variations on a common theme of self-eating? *Nat Rev Mol Cell Biol* 13, 7-12.

Cohen, G.M. (1997). Caspases: the executioners of apoptosis. *Biochem J* 326 (Pt 1), 1-16.

Cohen, G.M., Sun, X.M., Snowden, R.T., Dinsdale, D., and Skilleter, D.N. (1992). Key morphological features of apoptosis may occur in the absence of internucleosomal DNA fragmentation. *Biochem J* 286 (Pt 2), 331-334.

Coleman, M.L., and Olson, M.F. (2002). Rho GTPase signalling pathways in the morphological changes associated with apoptosis. *Cell Death Differ* 9, 493-504.

Coleman, M.L., Sahai, E.A., Yeo, M., Bosch, M., Dewar, A., and Olson, M.F. (2001). Membrane blebbing during apoptosis results from caspase-mediated activation of ROCK I. *Nat Cell Biol* 3, 339-345.

Colombini, M. (2017). Ceramide channels and mitochondrial outer membrane permeability. *J Bioenerg Biomembr* 49, 57-64.

Connolly, P.F., Jager, R., and Fearnhead, H.O. (2014). New roles for old enzymes: killer caspases as the engine of cell behavior changes. *Front Physiol* 5, 149.

Conradt, B., Wu, Y.C., and Xue, D. (2016). Programmed Cell Death During Caenorhabditis elegans Development. *Genetics* 203, 1533-1562.

Crawford, E.D., and Wells, J.A. (2011). Caspase substrates and cellular remodeling. *Annu Rev Biochem* 80, 1055-1087.

Crespo, I., Vital, A.L., Gonzalez-Tablas, M., Patino Mdel, C., Otero, A., Lopes, M.C., [. . .], Tabernero, M.D. (2015). Molecular and Genomic Alterations in Glioblastoma Multiforme. *Am J Pathol* 185, 1820-1833.

Croft, D.R., Coleman, M.L., Li, S., Robertson, D., Sullivan, T., Stewart, C.L., and Olson, M.F. (2005). Actin-myosin-based contraction is responsible for apoptotic nuclear disintegration. *J Cell Biol* 168, 245-255.

Cross, D.A., Alessi, D.R., Cohen, P., Andjelkovich, M., and Hemmings, B.A. (1995). Inhibition of glycogen synthase kinase-3 by insulin mediated by protein kinase B. *Nature* 378, 785-789.

Cuervo, A.M., and Wong, E. (2014). Chaperone-mediated autophagy: roles in disease and aging. *Cell Res* 24, 92-104.

Curran, W.J., Jr., Scott, C.B., Horton, J., Nelson, J.S., Weinstein, A.S., Fischbach, A.J., [. . .], et al. (1993). Recursive partitioning analysis of prognostic factors in three Radiation Therapy Oncology Group malignant glioma trials. *J Natl Cancer Inst* 85, 704-710.

Czabotar, P.E., Lee, E.F., Thompson, G.V., Wardak, A.Z., Fairlie, W.D., and Colman, P.M. (2011). Mutation to Bax beyond the BH3 domain disrupts interactions with pro-survival proteins and promotes apoptosis. *J Biol Chem* 286, 7123-7131.

Czabotar, P.E., Lessene, G., Strasser, A., and Adams, J.M. (2014). Control of apoptosis by the BCL-2 protein family: implications for physiology and therapy. *Nat Rev Mol Cell Biol* 15, 49-63.

Czarnek, K., Terpilowska, S., and Siwicki, A.K. (2015). Selected aspects of the action of cobalt ions in the human body. *Cent Eur J Immunol* 40, 236-242.

Dai, H., Smith, A., Meng, X.W., Schneider, P.A., Pang, Y.P., and Kaufmann, S.H. (2011). Transient binding of an activator BH3 domain to the Bak BH3-binding groove initiates Bak oligomerization. *J Cell Biol* 194, 39-48.

Danial, N.N., and Korsmeyer, S.J. (2004). Cell death: critical control points. *Cell* 116, 205-219.

David, K.K., Andrabi, S.A., Dawson, T.M., and Dawson, V.L. (2009). Parthanatos, a messenger of death. *Front Biosci (Landmark Ed)* 14, 1116-1128.

De Duve, C., Pressman, B.C., Gianetto, R., Wattiaux, R., and Appelmans, F. (1955). Tissue fractionation studies. 6. Intracellular distribution patterns of enzymes in rat-liver tissue. *Biochem J* 60, 604-617.

De Duve, C., and Wattiaux, R. (1966). Functions of lysosomes. *Annu Rev Physiol* 28, 435-492.

Degterev, A., Hitomi, J., Germscheid, M., Ch'en, I.L., Korkina, O., Teng, X., [. . .], Yuan, J. (2008). Identification of RIP1 kinase as a specific cellular target of necrostatins. *Nat Chem Biol* 4, 313-321.

Degterev, A., Huang, Z., Boyce, M., Li, Y., Jagtap, P., Mizushima, N., [. . .], Yuan, J. (2005). Chemical inhibitor of nonapoptotic cell death with therapeutic potential for ischemic brain injury. *Nat Chem Biol* 1, 112-119.

Delgado-Lopez, P.D., and Corrales-Garcia, E.M. (2016). Survival in glioblastoma: a review on the impact of treatment modalities. *Clin Transl Oncol* 18, 1062-1071.

Demarchi, F., Bertoli, C., Copetti, T., Tanida, I., Brancolini, C., Eskelinen, E.L., and Schneider, C. (2006). Calpain is required for macroautophagy in mammalian cells. *J Cell Biol* 175, 595-605.

Denecker, G., Hoste, E., Gilbert, B., Hochepied, T., Ovaere, P., Lippens, S., [. . .], Declercq, W. (2007). Caspase-14 protects against epidermal UVB photodamage and water loss. *Nat Cell Biol* 9, 666-674.

Denton, D., Nicolson, S., and Kumar, S. (2012). Cell death by autophagy: facts and apparent artefacts. *Cell Death Differ* 19, 87-95.

Dick, S.A., and Megeney, L.A. (2013). Cell death proteins: an evolutionary role in cellular adaptation before the advent of apoptosis. *Bioessays* 35, 974-983.

Dickens, L.S., Boyd, R.S., Jukes-Jones, R., Hughes, M.A., Robinson, G.L., Fairall, L., [. . .], Macfarlane, M. (2012a). A death effector domain chain DISC model reveals a crucial role for caspase-8 chain assembly in mediating apoptotic cell death. *Mol Cell* 47, 291-305.

Dickens, L.S., Powley, I.R., Hughes, M.A., and MacFarlane, M. (2012b). The 'complexities' of life and death: death receptor signalling platforms. *Exp Cell Res* 318, 1269-1277.

Didenko, V.V. (2011). 5'OH DNA breaks in apoptosis and their labeling by topoisomerase-based approach. *Methods Mol Biol* 682, 77-87.

Dieker, J., Iglesias-Guimarais, V., Decossas, M., Stevenin, J., van der Vlag, J., Yuste, V.J., and Muller, S. (2012). Early apoptotic reorganization of spliceosomal proteins involves caspases, CAD and rearrangement of NuMA. *Traffic* 13, 257-272.

Dikic, I., and Elazar, Z. (2018). Mechanism and medical implications of mammalian autophagy. *Nat Rev Mol Cell Biol* 19, 349-364.

Ding, J., Wang, K., Liu, W., She, Y., Sun, Q., Shi, J., [. . .], Shao, F. (2016). Pore-forming activity and structural autoinhibition of the gasdermin family. *Nature* 535, 111-116.

Ding, Y., Wang, B., Chen, X., Zhou, Y., and Ge, J. (2017). Staurosporine suppresses survival of HepG2 cancer cells through Omi/HtrA2-mediated inhibition of PI3K/Akt signaling pathway. *Tumour Biol* 39, 1010428317694317.

Dix, M.M., Simon, G.M., and Cravatt, B.F. (2008). Global mapping of the topography and magnitude of proteolytic events in apoptosis. *Cell* 134, 679-691.

Djavaheri-Mergny, M., Maiuri, M.C., and Kroemer, G. (2010). Cross talk between apoptosis and autophagy by caspase-mediated cleavage of Beclin 1. *Oncogene* 29, 1717-1719.

Dobrzynska, A., Gonzalo, S., Shanahan, C., and Askjaer, P. (2016). The nuclear lamina in health and disease. *Nucleus* 7, 233-248.

Dolma, S., Lessnick, S.L., Hahn, W.C., and Stockwell, B.R. (2003). Identification of genotype-selective antitumor agents using synthetic lethal chemical screening in engineered human tumor cells. *Cancer Cell* 3, 285-296.

Du, C., Fang, M., Li, Y., Li, L., and Wang, X. (2000). Smac, a mitochondrial protein that promotes cytochrome c-dependent caspase activation by eliminating IAP inhibition. *Cell* 102, 33-42.

Dugès, A. (1835). Recherches sur l'ostéologie et la myologie des Batracien à leurs diffŕents âges. Mémories de l'Acad. Royale. Sciences mathématiques et physiques. T. *VI Paris.*

Dumitru, R., Gama, V., Fagan, B.M., Bower, J.J., Swahari, V., Pevny, L.H., and Deshmukh, M. (2012). Human embryonic stem cells have constitutively active Bax at the Golgi and are primed to undergo rapid apoptosis. *Mol Cell* 46, 573-583.

Dunn, G.P., Rinne, M.L., Wykosky, J., Genovese, G., Quayle, S.N., Dunn, I.F., [. . .], Hahn, W.C. (2012). Emerging insights into the molecular and cellular basis of glioblastoma. *Genes Dev* 26, 756-784.

Durrieu, F., Samejima, K., Fortune, J.M., Kandels-Lewis, S., Osheroff, N., and Earnshaw, W.C. (2000). DNA topoisomerase IIalpha interacts with CAD nuclease and is involved in chromatin condensation during apoptotic execution. *Curr Biol* 10, 923-926.

Earnshaw, W.C., Martins, L.M., and Kaufmann, S.H. (1999). Mammalian caspases: structure, activation, substrates, and functions during apoptosis. *Annu Rev Biochem* 68, 383-424.

Eckelman, B.P., and Salvesen, G.S. (2006). The human anti-apoptotic proteins cIAP1 and cIAP2 bind but do not inhibit caspases. *J Biol Chem* 281, 3254-3260.

Eckelman, B.P., Salvesen, G.S., and Scott, F.L. (2006). Human inhibitor of apoptosis proteins: why XIAP is the black sheep of the family. *EMBO Rep* 7, 988-994.

Eckhart, L., Ballaun, C., Hermann, M., VandeBerg, J.L., Sipos, W., Uthman, A., [. . .], Tschachler, E. (2008). Identification of novel mammalian caspases reveals an important role of gene loss in shaping the human caspase repertoire. *Mol Biol Evol* 25, 831-841.

Edlich, F., Banerjee, S., Suzuki, M., Cleland, M.M., Arnoult, D., Wang, C., [. . .], Youle, R.J. (2011). Bcl-x(L) retrotranslocates Bax from the mitochondria into the cytosol. *Cell* 145, 104-116.

Egan, D., Kim, J., Shaw, R.J., and Guan, K.L. (2011). The autophagy initiating kinase ULK1 is regulated via opposing phosphorylation by AMPK and mTOR. *Autophagy* 7, 643-644.

Eisner, V., Picard, M., and Hajnoczky, G. (2018). Mitochondrial dynamics in adaptive and maladaptive cellular stress responses. *Nat Cell Biol* 20, 755-765.

Ellingson, B.M., Bendszus, M., Boxerman, J., Barboriak, D., Erickson, B.J., Smits, M., [. . .], Jumpstarting Brain Tumor Drug Development Coalition Imaging Standardization Steering, C. (2015). Consensus recommendations for a standardized Brain Tumor Imaging Protocol in clinical trials. *Neuro Oncol* 17, 1188-1198.

Ellis, H.M., and Horvitz, H.R. (1986). Genetic control of programmed cell death in the nematode C. elegans. *Cell* 44, 817-829.

Enari, M., Sakahira, H., Yokoyama, H., Okawa, K., Iwamatsu, A., and Nagata, S. (1998). A caspase-activated DNase that degrades DNA during apoptosis, and its inhibitor ICAD. *Nature* 391, 43-50.

Esposti, M.D. (1998). Apoptosis: who was first? *Cell Death & Differentiation* 5, 719-719.

Evans, C.J., and Aguilera, R.J. (2003). DNase II: genes, enzymes and function. *Gene* 322, 1-15.

Fader, C.M., Sanchez, D.G., Mestre, M.B., and Colombo, M.I. (2009). TI-VAMP/VAMP7 and VAMP3/cellubrevin: two v-SNARE proteins involved in specific steps of the autophagy/multivesicular body pathways. *Biochim Biophys Acta* 1793, 1901-1916.

Fairlie, W.D., Tran, S., and Lee, E.F. (2020). Crosstalk between apoptosis and autophagy signaling pathways. *Int Rev Cell Mol Biol* 352, 115-158.

Falcieri, E., Martelli, A.M., Bareggi, R., Cataldi, A., and Cocco, L. (1993). The protein kinase inhibitor staurosporine induces morphological changes typical of apoptosis in MOLT-4 cells without concomitant DNA fragmentation. *Biochem Biophys Res Commun* 193, 19-25.

Farrall, A.J., and Wardlaw, J.M. (2009). Blood-brain barrier: ageing and microvascular disease--systematic review and meta-analysis. *Neurobiol Aging* 30, 337-352.

Fass, E., Shvets, E., Degani, I., Hirschberg, K., and Elazar, Z. (2006). Microtubules support production of starvation-induced autophagosomes but not their targeting and fusion with lysosomes. *J Biol Chem* 281, 36303-36316.

Fatokun, A.A., Dawson, V.L., and Dawson, T.M. (2014). Parthanatos: mitochondrial-linked mechanisms and therapeutic opportunities. *Br J Pharmacol* 171, 2000-2016.

Feoktistova, M., Geserick, P., Kellert, B., Dimitrova, D.P., Langlais, C., Hupe, M., [. . .], Leverkus, M. (2011). cIAPs block Ripoptosome formation, a RIP1/caspase-8 containing intracellular cell death complex differentially regulated by cFLIP isoforms. *Mol Cell* 43, 449-463.

Fernando, P., and Megeney, L.A. (2007). Is caspase-dependent apoptosis only cell differentiation taken to the extreme? *FASEB J* 21, 8-17.

Fesik, S.W. (2000). Insights into programmed cell death through structural biology. *Cell* 103, 273-282.

Fimia, G.M., Stoykova, A., Romagnoli, A., Giunta, L., Di Bartolomeo, S., Nardacci, R., [. . .], Cecconi, F. (2007). Ambra1 regulates autophagy and development of the nervous system. *Nature* 447, 1121-1125.

Fischer, H., Koenig, U., Eckhart, L., and Tschachler, E. (2002). Human caspase 12 has acquired deleterious mutations. *Biochem Biophys Res Commun* 293, 722-726.

Flemming, W. (1885). Uber die bildung von richtungsfiguren in saugethiereiern beim untergang graaf'scher follikel. *Arch Anat EntGesch*, 221-244.

Fleten, K.G., Florenes, V.A., Prasmickaite, L., Hill, O., Sykora, J., Maelandsmo, G.M., and Engesaeter, B. (2016). hvTRA, a novel TRAIL receptor agonist, induces apoptosis and sustained growth retardation in melanoma. *Cell Death Discov* 2, 16081.

Fontana, A., de Laureto, P.P., Spolaore, B., Frare, E., Picotti, P., and Zambonin, M. (2004). Probing protein structure by limited proteolysis. *Acta Biochim Pol* 51, 299-321.

Fricker, N., Beaudouin, J., Richter, P., Eils, R., Krammer, P.H., and Lavrik, I.N. (2010). Model-based dissection of CD95 signaling dynamics reveals both a pro- and antiapoptotic role of c-FLIPL. *J Cell Biol* 190, 377-389.

Friedmann Angeli, J.P., Schneider, M., Proneth, B., Tyurina, Y.Y., Tyurin, V.A., Hammond, V.J., [. . .], Conrad, M. (2014). Inactivation of the ferroptosis regulator Gpx4 triggers acute renal failure in mice. *Nat Cell Biol* 16, 1180-1191.

Fuchs, Y., and Steller, H. (2011). Programmed cell death in animal development and disease. *Cell* 147, 742-758.

Fuentes-Prior, P., and Salvesen, G.S. (2004). The protein structures that shape caspase activity, specificity, activation and inhibition. *Biochem J* 384, 201-232.

Fukai, J., Koizumi, F., and Nakao, N. (2014). Enhanced anti-tumor effect of zoledronic acid combined with temozolomide against human malignant glioma cell expressing O6-methylguanine DNA methyltransferase. *PLoS One* 9, e104538.

Fukushima, K., Kikuchi, J., Koshiba, S., Kigawa, T., Kuroda, Y., and Yokoyama, S. (2002). Solution structure of the DFF-C domain of DFF45/ICAD. A structural basis for the regulation of apoptotic DNA fragmentation. *J Mol Biol* 321, 317-327.

Furnari, F.B., Fenton, T., Bachoo, R.M., Mukasa, A., Stommel, J.M., Stegh, A., [. . .], Cavenee, W.K. (2007). Malignant astrocytic glioma: genetics, biology, and paths to treatment. *Genes Dev* 21, 2683-2710.

Gadelha, I.C., Fonseca, N.B., Oloris, S.C., Melo, M.M., and Soto-Blanco, B. (2014). Gossypol toxicity from cottonseed products. *ScientificWorldJournal* 2014, 231635.

Gahl, R.F., Dwivedi, P., and Tjandra, N. (2016). Bcl-2 proteins bid and bax form a network to permeabilize the mitochondria at the onset of apoptosis. *Cell Death Dis* 7, e2424.

Galceran, J., Ameijide, A., Carulla, M., Mateos, A., Quiros, J.R., Rojas, D., [. . .], Group, R.W. (2017). Cancer incidence in Spain, 2015. *Clin Transl Oncol* 19, 799-825.

Galluzzi, L., Baehrecke, E.H., Ballabio, A., Boya, P., Bravo-San Pedro, J.M., Cecconi, F., [. . .], Kroemer, G. (2017). Molecular definitions of autophagy and related processes. *EMBO J* 36, 1811-1836.

Galluzzi, L., Bravo-San Pedro, J.M., Kepp, O., and Kroemer, G. (2016). Regulated cell death and adaptive stress responses. *Cell Mol Life Sci* 73, 2405-2410.

Galluzzi, L., Bravo-San Pedro, J.M., Vitale, I., Aaronson, S.A., Abrams, J.M., Adam, D., [. . .], Kroemer, G. (2015a). Essential versus accessory aspects of cell death: recommendations of the NCCD 2015. *Cell Death Differ* 22, 58-73.

Galluzzi, L., and Green, D.R. (2019). Autophagy-Independent Functions of the Autophagy Machinery. *Cell* 177, 1682-1699.

Galluzzi, L., Kepp, O., and Kroemer, G. (2014). MLKL regulates necrotic plasma membrane permeabilization. *Cell Res* 24, 139-140.

Galluzzi, L., Kepp, O., Trojel-Hansen, C., and Kroemer, G. (2012a). Non-apoptotic functions of apoptosis-regulatory proteins. *EMBO Rep* 13, 322-330.

Galluzzi, L., Pietrocola, F., Bravo-San Pedro, J.M., Amaravadi, R.K., Baehrecke, E.H., Cecconi, F., [. . .], Kroemer, G. (2015b). Autophagy in malignant transformation and cancer progression. *EMBO J* 34, 856-880.

Galluzzi, L., Vitale, I., Aaronson, S.A., Abrams, J.M., Adam, D., Agostinis, P., [. . .], Kroemer, G. (2018). Molecular mechanisms of cell death: recommendations of the Nomenclature Committee on Cell Death 2018. *Cell Death Differ* 25, 486-541.

Galluzzi, L., Vitale, I., Abrams, J.M., Alnemri, E.S., Baehrecke, E.H., Blagosklonny, M.V., [. . .], Kroemer, G. (2012b). Molecular definitions of cell death subroutines: recommendations of the Nomenclature Committee on Cell Death 2012. *Cell Death Differ* 19, 107-120.

Galluzzi, L., Zamzami, N., de La Motte Rouge, T., Lemaire, C., Brenner, C., and Kroemer, G. (2007). Methods for the assessment of mitochondrial membrane permeabilization in apoptosis. *Apoptosis* 12, 803-813.

Ganley, I.G., Lam du, H., Wang, J., Ding, X., Chen, S., and Jiang, X. (2009). ULK1.ATG13.FIP200 complex mediates mTOR signaling and is essential for autophagy. *J Biol Chem* 284, 12297-12305.

Gao, P., Bauvy, C., Souquere, S., Tonelli, G., Liu, L., Zhu, Y., [. . .], Mehrpour, M. (2010). The Bcl-2 homology domain 3 mimetic gossypol induces both Beclin 1-dependent and Beclin 1-independent cytoprotective autophagy in cancer cells. *J Biol Chem* 285, 25570-25581.

Gao, Y., Liu, Y., Hong, L., Yang, Z., Cai, X., Chen, X., [. . .], Li, M. (2016). Golgi-associated LC3 lipidation requires V-ATPase in noncanonical autophagy. *Cell Death Dis* 7, e2330.

Garcia-Belinchon, M., Sanchez-Osuna, M., Martinez-Escardo, L., Granados-Colomina, C., Pascual-Guiral, S., Iglesias-Guimarais, V., [. . .], Yuste, V.J. (2015). An Early and Robust Activation of Caspases Heads Cells for a Regulated Form of Necrotic-like Cell Death. *J Biol Chem* 290, 20841-20855.

Gardai, S.J., Hildeman, D.A., Frankel, S.K., Whitlock, B.B., Frasch, S.C., Borregaard, N., [. . .], Henson, P.M. (2004). Phosphorylation of Bax Ser184 by Akt regulates its activity and apoptosis in neutrophils. *J Biol Chem* 279, 21085-21095.

Gavrieli, Y., Sherman, Y., and Ben-Sasson, S.A. (1992). Identification of programmed cell death in situ via specific labeling of nuclear DNA fragmentation. *J Cell Biol* 119, 493-501.

Gdynia, G., Grund, K., Eckert, A., Bock, B.C., Funke, B., Macher-Goeppinger, S., [. . .], Roth, W. (2007). Basal caspase activity promotes migration and invasiveness in glioblastoma cells. *Mol Cancer Res* 5, 1232-1240.

Giampazolias, E., Zunino, B., Dhayade, S., Bock, F., Cloix, C., Cao, K., [. . .], Tait, S.W.G. (2017). Mitochondrial permeabilization engages NF-kappaB-dependent anti-tumour activity under caspase deficiency. *Nat Cell Biol* 19, 1116-1129.

Gibert, B., and Mehlen, P. (2015). Dependence Receptors and Cancer: Addiction to Trophic Ligands. *Cancer Res* 75, 5171-5175.

Goldschneider, D., and Mehlen, P. (2010). Dependence receptors: a new paradigm in cell signaling and cancer therapy. *Oncogene* 29, 1865-1882.

Gole, B., and Wiesmuller, L. (2015). Leukemogenic rearrangements at the mixed lineage leukemia gene (MLL)-multiple rather than a single mechanism. *Front Cell Dev Biol* 3, 41.

Gong, Y.N., Guy, C., Olauson, H., Becker, J.U., Yang, M., Fitzgerald, P., [. . .], Green, D.R. (2017). ESCRT-III Acts Downstream of MLKL to Regulate Necroptotic Cell Death and Its Consequences. *Cell* 169, 286-300 e216.

Goyeneche, A.A., Harmon, J.M., and Telleria, C.M. (2006). Cell death induced by serum deprivation in luteal cells involves the intrinsic pathway of apoptosis. *Reproduction* 131, 103-111.

Graper, L. (1914). Eine neue Anschauung uber physiologische Zellausschaltung. *Arch Zellforsch* 12, 373-394.

Green, D.R. (2016). A BH3 Mimetic for Killing Cancer Cells. *Cell* 165, 1560.

Green, D.R., and Kroemer, G. (2005). Pharmacological manipulation of cell death: clinical applications in sight? *J Clin Invest* 115, 2610-2617.

Gu, J., Dong, R.P., Zhang, C., McLaughlin, D.F., Wu, M.X., and Schlossman, S.F. (1999). Functional interaction of DFF35 and DFF45 with caspase-activated DNA fragmentation nuclease DFF40. *J Biol Chem* 274, 20759-20762.

Guertin, D.A., and Sabatini, D.M. (2007). Defining the role of mTOR in cancer. *Cancer Cell* 12, 9-22.

Gump, J.M., and Thorburn, A. (2011). Autophagy and apoptosis: what is the connection? *Trends Cell Biol* 21, 387-392.

Guo, J., Yao, C., Chen, H., Zhuang, D., Tang, W., Ren, G., [. . .], Zhou, L. (2012). The relationship between Cho/NAA and glioma metabolism: implementation for margin delineation of cerebral gliomas. *Acta Neurochir (Wien)* 154, 1361-1370; discussion 1370.

Guo, J.Y., Xia, B., and White, E. (2013). Autophagy-mediated tumor promotion. *Cell* 155, 1216-1219.

Gurbuxani, S., Schmitt, E., Cande, C., Parcellier, A., Hammann, A., Daugas, E., [. . .], Garrido, C. (2003). Heat shock protein 70 binding inhibits the nuclear import of apoptosis-inducing factor. *Oncogene* 22, 6669-6678.

Gyrd-Hansen, M., and Meier, P. (2010). IAPs: from caspase inhibitors to modulators of NF-kappaB, inflammation and cancer. *Nat Rev Cancer* 10, 561-574.

Hailey, D.W., Rambold, A.S., Satpute-Krishnan, P., Mitra, K., Sougrat, R., Kim, P.K., and Lippincott-Schwartz, J. (2010). Mitochondria supply membranes for autophagosome biogenesis during starvation. *Cell* 141, 656-667.

Halenbeck, R., MacDonald, H., Roulston, A., Chen, T.T., Conroy, L., and Williams, L.T. (1998). CPAN, a human nuclease regulated by the caspase-sensitive inhibitor DFF45. *Curr Biol* 8, 537-540.

Hamacher-Brady, A., and Brady, N.R. (2015). Bax/Bak-dependent, Drp1-independent Targeting of X-linked Inhibitor of Apoptosis Protein (XIAP) into Inner Mitochondrial Compartments Counteracts Smac/DIABLO-dependent Effector Caspase Activation. *J Biol Chem* 290, 22005-22018.

Han, Z., Hendrickson, E.A., Bremner, T.A., and Wyche, J.H. (1997). A sequential two-step mechanism for the production of the mature p17:p12 form of caspase-3 in vitro. *J Biol Chem* 272, 13432-13436.

Hanahan, D., and Weinberg, R.A. (2011). Hallmarks of cancer: the next generation. *Cell* 144, 646-674.

Hanson, B. (2016). Necroptosis: A new way of dying? *Cancer Biol Ther* 17, 899-910.

Hanus, J., Kalinowska-Herok, M., and Widlak, P. (2008). The major apoptotic endonuclease DFF40/CAD is a deoxyribose-specific and double-strand-specific enzyme. *Apoptosis* 13, 377-382.

Hars, E.S., Lyu, Y.L., Lin, C.P., and Liu, L.F. (2006). Role of apoptotic nuclease caspase-activated DNase in etoposide-induced treatment-related acute myelogenous leukemia. *Cancer Res* 66, 8975-8979.

Hart, M.G., Garside, R., Rogers, G., Stein, K., and Grant, R. (2013). Temozolomide for high grade glioma. *Cochrane Database Syst Rev*, CD007415.

Hatanpaa, K.J., Burma, S., Zhao, D., and Habib, A.A. (2010). Epidermal growth factor receptor in glioma: signal transduction, neuropathology, imaging, and radioresistance. *Neoplasia* 12, 675-684.

He, W.T., Wan, H., Hu, L., Chen, P., Wang, X., Huang, Z., [. . .], Han, J. (2015). Gasdermin D is an executor of pyroptosis and required for interleukin-1beta secretion. *Cell Res* 25, 1285-1298.

He, X., Wu, C., Cui, Y., Zhu, H., Gao, Z., Li, B., [. . .], Zhao, B. (2017). The aldehyde group of gossypol induces mitochondrial apoptosis via ROS-SIRT1-p53-PUMA pathway in male germline stem cell. *Oncotarget* 8, 100128-100140.

Hegi, M.E., Diserens, A.C., Gorlia, T., Hamou, M.F., de Tribolet, N., Weller, M., [. . .], Stupp, R. (2005). MGMT gene silencing and benefit from temozolomide in glioblastoma. *N Engl J Med* 352, 997-1003.

Heimer, S., Knoll, G., Schulze-Osthoff, K., and Ehrenschwender, M. (2019). Raptinal bypasses BAX, BAK, and BOK for mitochondrial outer membrane permeabilization and intrinsic apoptosis. *Cell Death Dis* 10, 556.

Hengartner, M.O., and Horvitz, H.R. (1994). C. elegans cell survival gene ced-9 encodes a functional homolog of the mammalian proto-oncogene bcl-2. *Cell* 76, 665-676.

Herman, P.K., and Emr, S.D. (1990). Characterization of VPS34, a gene required for vacuolar protein sorting and vacuole segregation in Saccharomyces cerevisiae. *Mol Cell Biol* 10, 6742-6754.

Herrlinger, U., Tzaridis, T., Mack, F., Steinbach, J.P., Schlegel, U., Sabel, M., [. . .], Neurooncology Working Group of the German Cancer, S. (2019). Lomustine-temozolomide combination therapy versus standard temozolomide therapy in patients with newly diagnosed glioblastoma with methylated MGMT promoter (CeTeG/NOA-09): a randomised, open-label, phase 3 trial. *Lancet* 393, 678-688.

Hetzer, M.W. (2010). The nuclear envelope. *Cold Spring Harb Perspect Biol* 2, a000539.

Hilton, B.A., Li, Z., Musich, P.R., Wang, H., Cartwright, B.M., Serrano, M., [. . .], Zou, Y. (2015). ATR Plays a Direct Antiapoptotic Role at Mitochondria, which Is Regulated by Prolyl Isomerase Pin1. *Mol Cell* 60, 35-46.

Hinds, M.G., Smits, C., Fredericks-Short, R., Risk, J.M., Bailey, M., Huang, D.C., and Day, C.L. (2007). Bim, Bad and Bmf: intrinsically unstructured BH3-only proteins that undergo a localized conformational change upon binding to prosurvival Bcl-2 targets. *Cell Death Differ* 14, 128-136.

Hitomi, J., Christofferson, D.E., Ng, A., Yao, J., Degterev, A., Xavier, R.J., and Yuan, J. (2008). Identification of a molecular signaling network that regulates a cellular necrotic cell death pathway. *Cell* 135, 1311-1323.

Hofmann, K. (1999). The modular nature of apoptotic signaling proteins. *Cell Mol Life Sci* 55, 1113-1128.

Hosokawa, N., Hara, T., Kaizuka, T., Kishi, C., Takamura, A., Miura, Y., [. . .], Mizushima, N. (2009). Nutrient-dependent mTORC1 association with the ULK1-Atg13-FIP200 complex required for autophagy. *Mol Biol Cell* 20, 1981-1991.

Hoste, E., Kemperman, P., Devos, M., Denecker, G., Kezic, S., Yau, N., [. . .], Declercq, W. (2011). Caspase-14 is required for filaggrin degradation to natural moisturizing factors in the skin. *J Invest Dermatol* 131, 2233-2241.

Hou, D.X., Uto, T., Tong, X., Takeshita, T., Tanigawa, S., Imamura, I., [. . .], Fujii, M. (2004). Involvement of reactive oxygen species-independent mitochondrial pathway in gossypol-induced apoptosis. *Arch Biochem Biophys* 428, 179-187.

Hou, H., Zhang, Y., Huang, Y., Yi, Q., Lv, L., Zhang, T., [. . .], Shi, Q. (2012). Inhibitors of phosphatidylinositol 3'-kinases promote mitotic cell death in HeLa cells. *PLoS One* 7, e35665.

Hou, W., Han, J., Lu, C., Goldstein, L.A., and Rabinowich, H. (2010). Autophagic degradation of active caspase-8: a crosstalk mechanism between autophagy and apoptosis. *Autophagy* 6, 891-900.

Hoyer-Hansen, M., and Jaattela, M. (2007). Connecting endoplasmic reticulum stress to autophagy by unfolded protein response and calcium. *Cell Death Differ* 14, 1576-1582.

Hu, S., and Yang, X. (2003). Cellular inhibitor of apoptosis 1 and 2 are ubiquitin ligases for the apoptosis inducer Smac/DIABLO. *J Biol Chem* 278, 10055-10060.

Huang, P.H., Xu, A.M., and White, F.M. (2009). Oncogenic EGFR signaling networks in glioma. *Sci Signal* 2, re6.

Huang, X., Bai, H.M., Chen, L., Li, B., and Lu, Y.C. (2010). Reduced expression of LC3B-II and Beclin 1 in glioblastoma multiforme indicates a down-regulated autophagic capacity that relates to the progression of astrocytic tumors. *J Clin Neurosci* 17, 1515-1519.

Hughes, M.A., Powley, I.R., Jukes-Jones, R., Horn, S., Feoktistova, M., Fairall, L., [. . .], MacFarlane, M. (2016). Co-operative and Hierarchical Binding of c-FLIP and Caspase-8: A Unified Model Defines How c-FLIP Isoforms Differentially Control Cell Fate. *Mol Cell* 61, 834-849.

Hunger, M., Mutti, E., Rieder, A., Enders, B., Nexo, E., and Krautler, B. (2014). Organometallic B12-DNA conjugate: synthesis, structure analysis, and studies of binding to human B12-transporter proteins. *Chemistry* 20, 13103-13107.

Ichim, G., Lopez, J., Ahmed, S.U., Muthalagu, N., Giampazolias, E., Delgado, M.E., [. . .], Tait, S.W.G. (2015). Limited mitochondrial permeabilization causes DNA damage and genomic instability in the absence of cell death. *Mol Cell* 57, 860-872.

Ichim, G., and Tait, S.W. (2016). A fate worse than death: apoptosis as an oncogenic process. *Nat Rev Cancer* 16, 539-548.

Iglesias-Guimarais, V., Gil-Guinon, E., Gabernet, G., Garcia-Belinchon, M., Sanchez-Osuna, M., Casanelles, E., [. . .], Yuste, V.J. (2012). Apoptotic DNA degradation into oligonucleosomal fragments, but not apoptotic nuclear morphology, relies on a cytosolic pool of DFF40/CAD endonuclease. *J Biol Chem* 287, 7766-7779.

Iglesias-Guimarais, V., Gil-Guinon, E., Sanchez-Osuna, M., Casanelles, E., Garcia-Belinchon, M., Comella, J.X., and Yuste, V.J. (2013). Chromatin collapse during caspase-dependent apoptotic cell death requires DNA fragmentation factor, 40-kDa subunit-/caspase-activated deoxyribonuclease-mediated 3'-OH single-strand DNA breaks. *J Biol Chem* 288, 9200-9215.

Inohara, N., Koseki, T., Chen, S., Wu, X., and Nunez, G. (1998). CIDE, a novel family of cell death activators with homology to the 45 kDa subunit of the DNA fragmentation factor. *EMBO J* 17, 2526-2533.

Inoki, K., Li, Y., Zhu, T., Wu, J., and Guan, K.L. (2002). TSC2 is phosphorylated and inhibited by Akt and suppresses mTOR signalling. *Nat Cell Biol* 4, 648-657.

Inoue, S., Browne, G., Melino, G., and Cohen, G.M. (2009). Ordering of caspases in cells undergoing apoptosis by the intrinsic pathway. *Cell Death Differ* 16, 1053-1061.

Iurlaro, R., and Munoz-Pinedo, C. (2016). Cell death induced by endoplasmic reticulum stress. *FEBS J* 283, 2640-2652.

Ivanov, V.N., Grabham, P.W., Wu, C.C., and Hei, T.K. (2020). Inhibition of autophagic flux differently modulates cannabidiol-induced death in 2D and 3D glioblastoma cell cultures. *Sci Rep* 10, 2687.

Jackson, R.J., Fuller, G.N., Abi-Said, D., Lang, F.F., Gokaslan, Z.L., Shi, W.M., [. . .], Sawaya, R. (2001). Limitations of stereotactic biopsy in the initial management of gliomas. *Neuro Oncol* 3, 193-200.

Jacobson, M.D., Burne, J.F., and Raff, M.C. (1994). Programmed cell death and Bcl-2 protection in the absence of a nucleus. *EMBO J* 13, 1899-1910.

Jager, S., Bucci, C., Tanida, I., Ueno, T., Kominami, E., Saftig, P., and Eskelinen, E.L. (2004). Role for Rab7 in maturation of late autophagic vacuoles. *J Cell Sci* 117, 4837-4848.

Janicke, R.U., Ng, P., Sprengart, M.L., and Porter, A.G. (1998a). Caspase-3 is required for alpha-fodrin cleavage but dispensable for cleavage of other death substrates in apoptosis. *J Biol Chem* 273, 15540-15545.

Janicke, R.U., Sprengart, M.L., Wati, M.R., and Porter, A.G. (1998b). Caspase-3 is required for DNA fragmentation and morphological changes associated with apoptosis. *J Biol Chem* 273, 9357-9360.

Jarzabek, M.A., Amberger-Murphy, V., Callanan, J.J., Gao, C., Zagozdzon, A.M., Shiels, L., [. . .], Byrne, A.T. (2014). Interrogation of gossypol therapy in glioblastoma implementing cell line and patient-derived tumour models. *Br J Cancer* 111, 2275-2286.

Jiang, B.-L., Lin, Y., Wang, M.-L., Liu, D.-S., Xu, B.-H., and Zhang, S.-J. (2019). Cobalt-catalyzed direct transformation of aldehydes to esters: the crucial role of an enone as a mediator. *Organic Chemistry Frontiers* 6, 801-807.

Jiang, H., White, E.J., Conrad, C., Gomez-Manzano, C., and Fueyo, J. (2009). Autophagy pathways in glioblastoma. *Methods Enzymol* 453, 273-286.

Jiang, J., Sugimoto, Y., Liu, S., Chang, H.L., Park, K.Y., Kulp, S.K., and Lin, Y.C. (2004). The inhibitory effects of gossypol on human prostate cancer cells-PC3 are associated with transforming growth factor beta1 (TGFbeta1) signal transduction pathway. *Anticancer Res* 24, 91-100.

Jimenez Fernandez, D., and Lamkanfi, M. (2015). Inflammatory caspases: key regulators of inflammation and cell death. *Biol Chem* 396, 193-203.

Johnson, V.L., Ko, S.C., Holmstrom, T.H., Eriksson, J.E., and Chow, S.C. (2000). Effector caspases are dispensable for the early nuclear morphological changes during chemical-induced apoptosis. *J Cell Sci* 113 (Pt 17), 2941-2953.

Jomova, K., and Valko, M. (2011). Importance of iron chelation in free radical-induced oxidative stress and human disease. *Curr Pharm Des* 17, 3460-3473.

Joppe, K., Roser, A.E., Maass, F., and Lingor, P. (2019). The Contribution of Iron to Protein Aggregation Disorders in the Central Nervous System. *Front Neurosci* 13, 15.

Julien, O., and Wells, J.A. (2017). Caspases and their substrates. *Cell Death Differ* 24, 1380-1389.

Jung, J.Y., and Kim, W.J. (2004). Involvement of mitochondrial- and Fas-mediated dual mechanism in CoCl2-induced apoptosis of rat PC12 cells. *Neurosci Lett* 371, 85-90.

Kabeya, Y., Mizushima, N., Ueno, T., Yamamoto, A., Kirisako, T., Noda, T., [. . .], Yoshimori, T. (2000). LC3, a mammalian homologue of yeast Apg8p, is localized in autophagosome membranes after processing. *EMBO J* 19, 5720-5728.

Kabeya, Y., Mizushima, N., Yamamoto, A., Oshitani-Okamoto, S., Ohsumi, Y., and Yoshimori, T. (2004). LC3, GABARAP and GATE16 localize to autophagosomal membrane depending on form-II formation. *J Cell Sci* 117, 2805-2812.

Kaiser, W.J., Upton, J.W., Long, A.B., Livingston-Rosanoff, D., Daley-Bauer, L.P., Hakem, R., [. . .], Mocarski, E.S. (2011). RIP3 mediates the embryonic lethality of caspase-8-deficient mice. *Nature* 471, 368-372.

Kaizuka, T., Morishita, H., Hama, Y., Tsukamoto, S., Matsui, T., Toyota, Y., [. . .], Mizushima, N. (2016). An Autophagic Flux Probe that Releases an Internal Control. *Mol Cell* 64, 835-849.

Kale, J., Osterlund, E.J., and Andrews, D.W. (2018). BCL-2 family proteins: changing partners in the dance towards death. *Cell Death Differ* 25, 65-80.

Kallenberger, S.M., Beaudouin, J., Claus, J., Fischer, C., Sorger, P.K., Legewie, S., and Eils, R. (2014). Intra- and interdimeric caspase-8 self-cleavage controls strength and timing of CD95-induced apoptosis. *Sci Signal* 7, ra23.

Kang, T.B., Oh, G.S., Scandella, E., Bolinger, B., Ludewig, B., Kovalenko, A., and Wallach, D. (2008). Mutation of a self-processing site in caspase-8 compromises its apoptotic but not its nonapoptotic functions in bacterial artificial chromosome-transgenic mice. *J Immunol* 181, 2522-2532.

Karin, M., and Lin, A. (2002). NF-kappaB at the crossroads of life and death. *Nat Immunol* 3, 221-227.

Karovic, O., Tonazzini, I., Rebola, N., Edstrom, E., Lovdahl, C., Fredholm, B.B., and Dare, E. (2007). Toxic effects of cobalt in primary cultures of mouse astrocytes. Similarities with hypoxia and role of HIF-1alpha. *Biochem Pharmacol* 73, 694-708.

Karpel-Massler, G., Shu, C., Chau, L., Banu, M., Halatsch, M.E., Westhoff, M.A., [. . .], Siegelin, M.D. (2015). Combined inhibition of Bcl-2/Bcl-xL and Usp9X/Bag3 overcomes apoptotic resistance in glioblastoma in vitro and in vivo. *Oncotarget* 6, 14507-14521.

Kataoka, T. (2005). The caspase-8 modulator c-FLIP. *Crit Rev Immunol* 25, 31-58.

Kawane, K., Fukuyama, H., Adachi, M., Sakahira, H., Copeland, N.G., Gilbert, D.J., [. . .], Nagata, S. (1999). Structure and promoter analysis of murine CAD and ICAD genes. *Cell Death Differ* 6, 745-752.

Kawane, K., Fukuyama, H., Kondoh, G., Takeda, J., Ohsawa, Y., Uchiyama, Y., and Nagata, S. (2001). Requirement of DNase II for definitive erythropoiesis in the mouse fetal liver. *Science* 292, 1546-1549.

Kenar, J.A. (2006). Reaction chemistry of gossypol and its derivatives. *Journal of the American Oil Chemists' Society* 83, 269-302.

Kerr, J.F. (1971). Shrinkage necrosis: a distinct mode of cellular death. *J Pathol* 105, 13-20.

Kerr, J.F., Wyllie, A.H., and Currie, A.R. (1972). Apoptosis: a basic biological phenomenon with wide-ranging implications in tissue kinetics. *Br J Cancer* 26, 239-257.

Keshmiri-Neghab, H., and Goliaei, B. (2014). Therapeutic potential of gossypol: an overview. *Pharm Biol* 52, 124-128.

Keshmiri-Neghab, H., Goliaei, B., and Nikoofar, A. (2014). Gossypol enhances radiation induced autophagy in glioblastoma multiforme. *Gen Physiol Biophys* 33, 433-442.

Keyel, P.A. (2017). Dnases in health and disease. *Dev Biol* 429, 1-11.

Kijima, M., and Mizuta, R. (2019). Histone H1 quantity determines the efficiencies of apoptotic DNA fragmentation and chromatin condensation. *Biomed Res* 40, 51-56.

Kijima, M., Yamagishi, H., Hara, Y., Kasai, M., Takami, Y., Takemura, H., [. . .], Mizuta, R. (2019). Histone H1 quantity determines the efficiency of chromatin condensation in both apoptotic and live cells. *Biochem Biophys Res Commun* 512, 202-207.

Kim, J., Kim, Y.C., Fang, C., Russell, R.C., Kim, J.H., Fan, W., [. . .], Guan, K.L. (2013). Differential regulation of distinct Vps34 complexes by AMPK in nutrient stress and autophagy. *Cell* 152, 290-303.

Kim, J.W., Kim, J.Y., Kim, J.E., Kim, S.K., Chung, H.T., and Park, C.K. (2014). HOXA10 is associated with temozolomide resistance through regulation of the homologous recombinant DNA repair pathway in glioblastoma cell lines. *Genes Cancer* 5, 165-174.

Kirson, E.D., Dbaly, V., Tovarys, F., Vymazal, J., Soustiel, J.F., Itzhaki, A., [. . .], Palti, Y. (2007). Alternating electric fields arrest cell proliferation in animal tumor models and human brain tumors. *Proc Natl Acad Sci U S A* 104, 10152-10157.

Kischkel, F.C., Lawrence, D.A., Chuntharapai, A., Schow, P., Kim, K.J., and Ashkenazi, A. (2000). Apo2L/TRAIL-dependent recruitment of endogenous FADD and caspase-8 to death receptors 4 and 5. *Immunity* 12, 611-620.

Kitada, S., Leone, M., Sareth, S., Zhai, D., Reed, J.C., and Pellecchia, M. (2003). Discovery, characterization, and structure-activity relationships studies of proapoptotic polyphenols targeting B-cell lymphocyte/leukemia-2 proteins. *J Med Chem* 46, 4259-4264.

Klaunig, J.E., and Kamendulis, L.M. (2004). The role of oxidative stress in carcinogenesis. *Annu Rev Pharmacol Toxicol* 44, 239-267.

Klionsky, D.J., Abdelmohsen, K., Abe, A., Abedin, M.J., Abeliovich, H., Acevedo Arozena, A., [. . .], Zughaier, S.M. (2016). Guidelines for the use and interpretation of assays for monitoring autophagy (3rd edition). *Autophagy* 12, 1-222.

Ko, C.H., Shen, S.C., Yang, L.Y., Lin, C.W., and Chen, Y.C. (2007). Gossypol reduction of tumor growth through ROS-dependent mitochondria pathway in human colorectal carcinoma cells. *Int J Cancer* 121, 1670-1679.

Koch, A.J., and Holaska, J.M. (2014). Emerin in health and disease. *Semin Cell Dev Biol* 29, 95-106.

Korn, C., Scholz, S.R., Gimadutdinow, O., Lurz, R., Pingoud, A., and Meiss, G. (2005). Interaction of DNA fragmentation factor (DFF) with DNA reveals an unprecedented mechanism for nuclease inhibition and suggests that DFF can be activated in a DNA-bound state. *J Biol Chem* 280, 6005-6015.

Korn, C., Scholz, S.R., Gimadutdinow, O., Pingoud, A., and Meiss, G. (2002). Involvement of conserved histidine, lysine and tyrosine residues in the mechanism of DNA cleavage by the caspase-3 activated DNase CAD. *Nucleic Acids Res* 30, 1325-1332.

Kothakota, S., Azuma, T., Reinhard, C., Klippel, A., Tang, J., Chu, K., [. . .], Williams, L.T. (1997). Caspase-3-generated fragment of gelsolin: effector of morphological change in apoptosis. *Science* 278, 294-298.

Kotschy, A., Szlavik, Z., Murray, J., Davidson, J., Maragno, A.L., Le Toumelin-Braizat, G., [. . .], Geneste, O. (2016). The MCL1 inhibitor S63845 is tolerable and effective in diverse cancer models. *Nature* 538, 477-482.

Kovacs, A.L., Reith, A., and Seglen, P.O. (1982). Accumulation of autophagosomes after inhibition of hepatocytic protein degradation by vinblastine, leupeptin or a lysosomotropic amine. *Exp Cell Res* 137, 191-201.

Koyama, R., Arai, T., Kijima, M., Sato, S., Miura, S., Yuasa, M., [. . .], Mizuta, R. (2016). DNase gamma, DNase I and caspase-activated DNase cooperate to degrade dead cells. *Genes Cells* 21, 1150-1163.

Krieser, R.J., MacLea, K.S., Longnecker, D.S., Fields, J.L., Fiering, S., and Eastman, A. (2002). Deoxyribonuclease IIalpha is required during the phagocytic phase of apoptosis and its loss causes perinatal lethality. *Cell Death Differ* 9, 956-962.

Kroemer, G., El-Deiry, W.S., Golstein, P., Peter, M.E., Vaux, D., Vandenabeele, P., [. . .], Nomenclature Committee on Cell, D. (2005). Classification of cell death: recommendations of the Nomenclature Committee on Cell Death. *Cell Death Differ* 12 Suppl 2, 1463-1467.

Kroemer, G., Galluzzi, L., and Brenner, C. (2007). Mitochondrial membrane permeabilization in cell death. *Physiol Rev* 87, 99-163.

Kroemer, G., Galluzzi, L., Vandenabeele, P., Abrams, J., Alnemri, E.S., Baehrecke, E.H., [. . .], Nomenclature Committee on Cell, D. (2009). Classification of cell death: recommendations of the Nomenclature Committee on Cell Death 2009. *Cell Death Differ* 16, 3-11.

Kroemer, G., Marino, G., and Levine, B. (2010). Autophagy and the integrated stress response. *Mol Cell* 40, 280-293.

Ku, N.O., Liao, J., and Omary, M.B. (1997). Apoptosis generates stable fragments of human type I keratins. *J Biol Chem* 272, 33197-33203.

Kudelova, J., Fleischmannova, J., Adamova, E., and Matalova, E. (2015). Pharmacological caspase inhibitors: research towards therapeutic perspectives. *J Physiol Pharmacol* 66, 473-482.

Kunz, J.B., Schwarz, H., and Mayer, A. (2004). Determination of four sequential stages during microautophagy in vitro. *J Biol Chem* 279, 9987-9996.

Kuo, L.J., and Yang, L.X. (2008). Gamma-H2AX - a novel biomarker for DNA double-strand breaks. *In Vivo* 22, 305-309.

Kuribayashi, N., Sakagami, H., Iida, M., and Takeda, M. (1996). Chromatin structure and endonuclease sensitivity in human leukemic cell lines. *Anticancer Res* 16, 1225-1230.

Kutscher, D., Pingoud, A., Jeltsch, A., and Meiss, G. (2012). Identification of ICAD-derived peptides capable of inhibiting caspase-activated DNase. *FEBS J* 279, 2917-2928.

Kuwana, T., Bouchier-Hayes, L., Chipuk, J.E., Bonzon, C., Sullivan, B.A., Green, D.R., and Newmeyer, D.D. (2005). BH3 domains of BH3-only proteins differentially regulate Bax-mediated mitochondrial membrane permeabilization both directly and indirectly. *Mol Cell* 17, 525-535.

Lam, M., Marsters, S.A., Ashkenazi, A., and Walter, P. (2020). Misfolded proteins bind and activate death receptor 5 to trigger apoptosis during unresolved endoplasmic reticulum stress. *Elife* 9.

Lane, J.D., Allan, V.J., and Woodman, P.G. (2005). Active relocation of chromatin and endoplasmic reticulum into blebs in late apoptotic cells. *J Cell Sci* 118, 4059-4071.

Laperriere, N., Zuraw, L., Cairncross, G., and Cancer Care Ontario Practice Guidelines Initiative Neuro-Oncology Disease Site, G. (2002). Radiotherapy for newly diagnosed malignant glioma in adults: a systematic review. *Radiother Oncol* 64, 259-273.

Larsen, B.D., and Sorensen, C.S. (2017). The caspase-activated DNase: apoptosis and beyond. *FEBS J* 284, 1160-1170.

Lavrik, I.N., Golks, A., and Krammer, P.H. (2005). Caspases: pharmacological manipulation of cell death. *J Clin Invest* 115, 2665-2672.

Leber, B., Geng, F., Kale, J., and Andrews, D.W. (2010). Drugs targeting Bcl-2 family members as an emerging strategy in cancer. *Expert Rev Mol Med* 12, e28.

Leber, B., Lin, J., and Andrews, D.W. (2007). Embedded together: the life and death consequences of interaction of the Bcl-2 family with membranes. *Apoptosis* 12, 897-911.

LeBlanc, A.C. (2003). Natural cellular inhibitors of caspases. *Prog Neuropsychopharmacol Biol Psychiatry* 27, 215-229.

Lechardeur, D., Drzymala, L., Sharma, M., Zylka, D., Kinach, R., Pacia, J., [. . .], Lukacs, G.L. (2000). Determinants of the nuclear localization of the heterodimeric DNA fragmentation factor (ICAD/CAD). *J Cell Biol* 150, 321-334.

Lechardeur, D., Xu, M., and Lukacs, G.L. (2004). Contrasting nuclear dynamics of the caspase-activated DNase (CAD) in dividing and apoptotic cells. *J Cell Biol* 167, 851-862.

Lecoeur, H. (2002). Nuclear apoptosis detection by flow cytometry: influence of endogenous endonucleases. *Exp Cell Res* 277, 1-14.

Lee, J.H., Choi, S.H., Baek, M.W., Kim, M.H., Kim, H.J., Kim, S.H., [. . .], Jung, J.Y. (2013). CoCl2 induces apoptosis through the mitochondria- and death receptor-mediated pathway in the mouse embryonic stem cells. *Mol Cell Biochem* 379, 133-140.

Lee, J.S., Kim, S.H., Lee, S., Kang, J.H., Lee, S.H., Cheong, J.H., and Kim, S.Y. (2019). Gastric cancer depends on aldehyde dehydrogenase 3A1 for fatty acid oxidation. *Sci Rep* 9, 16313.

Legendre, C., and Garcion, E. (2015). Iron metabolism: a double-edged sword in the resistance of glioblastoma to therapies. *Trends Endocrinol Metab* 26, 322-331.

Leist, M., and Jaattela, M. (2001). Four deaths and a funeral: from caspases to alternative mechanisms. *Nat Rev Mol Cell Biol* 2, 589-598.

Letai, A., Bassik, M.C., Walensky, L.D., Sorcinelli, M.D., Weiler, S., and Korsmeyer, S.J. (2002). Distinct BH3 domains either sensitize or activate mitochondrial apoptosis, serving as prototype cancer therapeutics. *Cancer Cell* 2, 183-192.

Levine, B., and Kroemer, G. (2019). Biological Functions of Autophagy Genes: A Disease Perspective. *Cell* 176, 11-42.

Levinsky, H., Singer, R., Sagiv, M., Lehrer, N., and Allalouf, D. (1991). Inhibition of sialyl transferase activity by gossypol acetic acid in human seminal plasma. *Andrologia* 23, 159-161.

Levy, J.M.M., Towers, C.G., and Thorburn, A. (2017). Targeting autophagy in cancer. *Nat Rev Cancer* 17, 528-542.

Li, A.S., Bandy, B., Tsang, S.S., and Davison, A.J. (2000a). DNA-breaking versus DNA-protecting activity of four phenolic compounds in vitro. *Free Radic Res* 33, 551-566.

Li, H., Kobayashi, M., Blonska, M., You, Y., and Lin, X. (2006). Ubiquitination of RIP is required for tumor necrosis factor alpha-induced NF-kappaB activation. *J Biol Chem* 281, 13636-13643.

Li, H., Zhu, H., Xu, C.J., and Yuan, J. (1998). Cleavage of BID by caspase 8 mediates the mitochondrial damage in the Fas pathway of apoptosis. *Cell* 94, 491-501.

Li, J., Cao, F., Yin, H.L., Huang, Z.J., Lin, Z.T., Mao, N., [. . .], Wang, G. (2020). Ferroptosis: past, present and future. *Cell Death Dis* 11, 88.

Li, J., McQuade, T., Siemer, A.B., Napetschnig, J., Moriwaki, K., Hsiao, Y.S., [. . .], Wu, H. (2012). The RIP1/RIP3 necrosome forms a functional amyloid signaling complex required for programmed necrosis. *Cell* 150, 339-350.

Li, K., Li, Y., Shelton, J.M., Richardson, J.A., Spencer, E., Chen, Z.J., [. . .], Williams, R.S. (2000b). Cytochrome c deficiency causes embryonic lethality and attenuates stress-induced apoptosis. *Cell* 101, 389-399.

Li, L.Y., Luo, X., and Wang, X. (2001). Endonuclease G is an apoptotic DNase when released from mitochondria. *Nature* 412, 95-99.

Li, M.X., Tan, I.K.L., Ma, S.B., Hockings, C., Kratina, T., Dengler, M.A., [. . .], Dewson, G. (2017). BAK alpha6 permits activation by BH3-only proteins and homooligomerization via the canonical hydrophobic groove. *Proc Natl Acad Sci U S A* 114, 7629-7634.

Li, P., Nijhawan, D., Budihardjo, I., Srinivasula, S.M., Ahmad, M., Alnemri, E.S., and Wang, X. (1997). Cytochrome c and dATP-dependent formation of Apaf-1/caspase-9 complex initiates an apoptotic protease cascade. *Cell* 91, 479-489.

Li, T.K., Chen, A.Y., Yu, C., Mao, Y., Wang, H., and Liu, L.F. (1999). Activation of topoisomerase II-mediated excision of chromosomal DNA loops during oxidative stress. *Genes Dev* 13, 1553-1560.

Lian, J., Wu, X., He, F., Karnak, D., Tang, W., Meng, Y., [. . .], Xu, L. (2011). A natural BH3 mimetic induces autophagy in apoptosis-resistant prostate cancer via modulating Bcl-2-Beclin1 interaction at endoplasmic reticulum. *Cell Death Differ* 18, 60-71.

Liang, C., Lee, J.S., Inn, K.S., Gack, M.U., Li, Q., Roberts, E.A., [. . .], Jung, J.U. (2008). Beclin1-binding UVRAG targets the class C Vps complex to coordinate autophagosome maturation and endocytic trafficking. *Nat Cell Biol* 10, 776-787.

Liang, X.H., Jackson, S., Seaman, M., Brown, K., Kempkes, B., Hibshoosh, H., and Levine, B. (1999). Induction of autophagy and inhibition of tumorigenesis by beclin 1. *Nature* 402, 672-676.

Ligueros, M., Jeoung, D., Tang, B., Hochhauser, D., Reidenberg, M.M., and Sonenberg, M. (1997). Gossypol inhibition of mitosis, cyclin D1 and Rb protein in human mammary cancer cells and cyclin-D1 transfected human fibrosarcoma cells. *Br J Cancer* 76, 21-28.

Lin, H.H., Hsu, H.L., and Yeh, N.H. (2007). Apoptotic cleavage of NuMA at the C-terminal end is related to nuclear disruption and death amplification. *J Biomed Sci* 14, 681-694.

Lin, J., Kumari, S., Kim, C., Van, T.M., Wachsmuth, L., Polykratis, A., and Pasparakis, M. (2016). RIPK1 counteracts ZBP1-mediated necroptosis to inhibit inflammation. *Nature* 540, 124-128.

Lin, T.S., Schinazi, R., Griffith, B.P., August, E.M., Eriksson, B.F., Zheng, D.K., [. . .], Prusoff, W.H. (1989). Selective inhibition of human immunodeficiency virus type 1 replication by the (-) but not the (+) enantiomer of gossypol. *Antimicrob Agents Chemother* 33, 2149-2151.

Lindsten, T., Ross, A.J., King, A., Zong, W.X., Rathmell, J.C., Shiels, H.A., [. . .], Thompson, C.B. (2000). The combined functions of proapoptotic Bcl-2 family members bak and bax are essential for normal development of multiple tissues. *Mol Cell* 6, 1389-1399.

Liu, J., Zhang, X., Yan, X., Sun, M., Fan, Y., and Huang, Y. (2019). Significance of TERT and ATRX mutations in glioma. *Oncol Lett* 17, 95-102.

Liu, Q.Y., Ribecco, M., Pandey, S., Walker, P.R., and Sikorska, M. (1999a). Apoptosis-related functional features of the DNaseI-like family of nucleases. *Ann N Y Acad Sci* 887, 60-76.

Liu, X., He, Y., Li, F., Huang, Q., Kato, T.A., Hall, R.P., and Li, C.Y. (2015). Caspase-3 promotes genetic instability and carcinogenesis. *Mol Cell* 58, 284-296.

Liu, X., Kim, C.N., Yang, J., Jemmerson, R., and Wang, X. (1996). Induction of apoptotic program in cell-free extracts: requirement for dATP and cytochrome c. *Cell* 86, 147-157.

Liu, X., Li, F., Huang, Q., Zhang, Z., Zhou, L., Deng, Y., [. . .], Li, C.Y. (2017). Self-inflicted DNA double-strand breaks sustain tumorigenicity and stemness of cancer cells. *Cell Res* 27, 764-783.

Liu, X., Li, P., Widlak, P., Zou, H., Luo, X., Garrard, W.T., and Wang, X. (1998). The 40-kDa subunit of DNA fragmentation factor induces DNA fragmentation and chromatin condensation during apoptosis. *Proc Natl Acad Sci U S A* 95, 8461-8466.

Liu, X., Zhang, Z., Ruan, J., Pan, Y., Magupalli, V.G., Wu, H., and Lieberman, J. (2016). Inflammasome-activated gasdermin D causes pyroptosis by forming membrane pores. *Nature* 535, 153-158.

Liu, X., Zou, H., Slaughter, C., and Wang, X. (1997). DFF, a heterodimeric protein that functions downstream of caspase-3 to trigger DNA fragmentation during apoptosis. *Cell* 89, 175-184.

Liu, X., Zou, H., Widlak, P., Garrard, W., and Wang, X. (1999b). Activation of the apoptotic endonuclease DFF40 (caspase-activated DNase or nuclease). Oligomerization and direct interaction with histone H1. *J Biol Chem* 274, 13836-13840.

Liu, Y., and Connor, J.R. (2012). Iron and ER stress in neurodegenerative disease. *Biometals* 25, 837-845.

Liu, Y., Shoji-Kawata, S., Sumpter, R.M., Jr., Wei, Y., Ginet, V., Zhang, L., [. . .], Levine, B. (2013). Autosis is a Na+,K+-ATPase-regulated form of cell death triggered by autophagy-inducing peptides, starvation, and hypoxia-ischemia. *Proc Natl Acad Sci U S A* 110, 20364-20371.

Llambi, F., Moldoveanu, T., Tait, S.W., Bouchier-Hayes, L., Temirov, J., McCormick, L.L., [. . .], Green, D.R. (2011). A unified model of mammalian BCL-2 protein family interactions at the mitochondria. *Mol Cell* 44, 517-531.

Lockshin, R.A., and Williams, C.M. (1965). Programmed cell death. IV. The influence of drugs on the breakdown of the intersegmental muscles of silkmoths. *J Insect Physiol* 11, 803-809.

Longmore, J. (1886). Cotton-seed oil: Its colouring matter and mucilage, and description of a new method of recovering the loss occurring in the refining process. *J Soc Chem Ind* 5, 200-206.

Louis, D.N., Ohgaki, H., Wiestler, O.D., Cavenee, W.K., Burger, P.C., Jouvet, A., [. . .], Kleihues, P. (2007). The 2007 WHO classification of tumours of the central nervous system. *Acta Neuropathol* 114, 97-109.

Louis, D.N., Perry, A., Reifenberger, G., von Deimling, A., Figarella-Branger, D., Cavenee, W.K., [. . .], Ellison, D.W. (2016). The 2016 World Health Organization Classification of Tumors of the Central Nervous System: a summary. *Acta Neuropathol* 131, 803-820.

Lovell, J.F., Billen, L.P., Bindner, S., Shamas-Din, A., Fradin, C., Leber, B., and Andrews, D.W. (2008). Membrane binding by tBid initiates an ordered series of events culminating in membrane permeabilization by Bax. *Cell* 135, 1074-1084.

Lovric, M.M., and Hawkins, C.J. (2010). TRAIL treatment provokes mutations in surviving cells. *Oncogene* 29, 5048-5060.

Low, I.C., Loh, T., Huang, Y., Virshup, D.M., and Pervaiz, S. (2014). Ser70 phosphorylation of Bcl-2 by selective tyrosine nitration of PP2A-B56delta stabilizes its antiapoptotic activity. *Blood* 124, 2223-2234.

Lu, C., Zhu, F., Cho, Y.Y., Tang, F., Zykova, T., Ma, W.Y., [. . .], Dong, Z. (2006a). Cell apoptosis: requirement of H2AX in DNA ladder formation, but not for the activation of caspase-3. *Mol Cell* 23, 121-132.

Lu, H., Hou, Q., Zhao, T., Zhang, H., Zhang, Q., Wu, L., and Fan, Z. (2006b). Granzyme M directly cleaves inhibitor of caspase-activated DNase (CAD) to unleash CAD leading to DNA fragmentation. *J Immunol* 177, 1171-1178.

Lu, W., Sun, J., Yoon, J.S., Zhang, Y., Zheng, L., Murphy, E., [. . .], Lenardo, M.J. (2016). Mitochondrial Protein PGAM5 Regulates Mitophagic Protection against Cell Necroptosis. *PLoS One* 11, e0147792.

Lu, Y., Li, J., Dong, C.E., Huang, J., Zhou, H.B., and Wang, W. (2017). Recent advances in gossypol derivatives and analogs: a chemistry and biology view. *Future Med Chem* 9, 1243-1275.

Lugovskoy, A.A., Zhou, P., Chou, J.J., McCarty, J.S., Li, P., and Wagner, G. (1999). Solution structure of the CIDE-N domain of CIDE-B and a model for CIDE-N/CIDE-N interactions in the DNA fragmentation pathway of apoptosis. *Cell* 99, 747-755.

Luo, X., Budihardjo, I., Zou, H., Slaughter, C., and Wang, X. (1998). Bid, a Bcl2 interacting protein, mediates cytochrome c release from mitochondria in response to activation of cell surface death receptors. *Cell* 94, 481-490.

Luthi, A.U., and Martin, S.J. (2007). The CASBAH: a searchable database of caspase substrates. *Cell Death Differ* 14, 641-650.

MacFarlane, M., Merrison, W., Bratton, S.B., and Cohen, G.M. (2002). Proteasome-mediated degradation of Smac during apoptosis: XIAP promotes Smac ubiquitination in vitro. *J Biol Chem* 277, 36611-36616.

Maelfait, J., Liverpool, L., Bridgeman, A., Ragan, K.B., Upton, J.W., and Rehwinkel, J. (2017). Sensing of viral and endogenous RNA by ZBP1/DAI induces necroptosis. *EMBO J* 36, 2529-2543.

Mahey, S., Kumar, R., Arora, R., Mahajan, J., Arora, S., Bhardwaj, R., and Thukral, A.K. (2016). Effect of cobalt(II) chloride hexahydrate on some human cancer cell lines. *Springerplus* 5, 930.

Mahrus, S., Trinidad, J.C., Barkan, D.T., Sali, A., Burlingame, A.L., and Wells, J.A. (2008). Global sequencing of proteolytic cleavage sites in apoptosis by specific labeling of protein N termini. *Cell* 134, 866-876.

Mai, S., Muster, B., Bereiter-Hahn, J., and Jendrach, M. (2012). Autophagy proteins LC3B, ATG5 and ATG12 participate in quality control after mitochondrial damage and influence lifespan. *Autophagy* 8, 47-62.

Malumbres, M., and Barbacid, M. (2009). Cell cycle, CDKs and cancer: a changing paradigm. *Nat Rev Cancer* 9, 153-166.

Mani, J., Vallo, S., Rakel, S., Antonietti, P., Gessler, F., Blaheta, R., [. . .], Kogel, D. (2015). Chemoresistance is associated with increased cytoprotective autophagy and diminished apoptosis in bladder cancer cells treated with the BH3 mimetic (-)-Gossypol (AT-101). *BMC Cancer* 15, 224.

Mann, J., Ramakrishna, R., Magge, R., and Wernicke, A.G. (2017). Advances in Radiotherapy for Glioblastoma. *Front Neurol* 8, 748.

Manning, B.D., Tee, A.R., Logsdon, M.N., Blenis, J., and Cantley, L.C. (2002). Identification of the tuberous sclerosis complex-2 tumor suppressor gene product tuberin as a target of the phosphoinositide 3-kinase/akt pathway. *Mol Cell* 10, 151-162.

Manning, B.D., and Toker, A. (2017). AKT/PKB Signaling: Navigating the Network. *Cell* 169, 381-405.

Marcassa, E., Raimondi, M., Anwar, T., Eskelinen, E.L., Myers, M.P., Triolo, G., [. . .], Demarchi, F. (2017). Calpain mobilizes Atg9/Bif-1 vesicles from Golgi stacks upon autophagy induction by thapsigargin. *Biol Open* 6, 551-562.

Marchlewski, L. (1899). Gossypol, ein bestandtheil der baumwollsamen. *Journal für Praktische Chemie* 60, 84-90.

Marino, G., Niso-Santano, M., Baehrecke, E.H., and Kroemer, G. (2014). Self-consumption: the interplay of autophagy and apoptosis. *Nat Rev Mol Cell Biol* 15, 81-94.

Marques-Fernandez, F., Planells-Ferrer, L., Gozzelino, R., Galenkamp, K.M., Reix, S., Llecha-Cano, N., [. . .], Comella, J.X. (2013). TNFalpha induces survival through the FLIP-L-dependent activation of the MAPK/ERK pathway. *Cell Death Dis* 4, e493.

Martin, S.J., and Green, D.R. (1995). Protease activation during apoptosis: death by a thousand cuts? *Cell* 82, 349-352.

Martin, S.J., O'Brien, G.A., Nishioka, W.K., McGahon, A.J., Mahboubi, A., Saido, T.C., and Green, D.R. (1995). Proteolysis of fodrin (non-erythroid spectrin) during apoptosis. *J Biol Chem* 270, 6425-6428.

Martinon, F., and Tschopp, J. (2007). Inflammatory caspases and inflammasomes: master switches of inflammation. *Cell Death Differ* 14, 10-22.

Maskey, D., Yousefi, S., Schmid, I., Zlobec, I., Perren, A., Friis, R., and Simon, H.U. (2013). ATG5 is induced by DNA-damaging agents and promotes mitotic catastrophe independent of autophagy. *Nat Commun* 4, 2130.

Matsuura, A., Tsukada, M., Wada, Y., and Ohsumi, Y. (1997). Apg1p, a novel protein kinase required for the autophagic process in Saccharomyces cerevisiae. *Gene* 192, 245-250.

Mattiolo, P., Yuste, V.J., Boix, J., and Ribas, J. (2015). Autophagy exacerbates caspase-dependent apoptotic cell death after short times of starvation. *Biochem Pharmacol* 98, 573-586.

Mauthe, M., Jacob, A., Freiberger, S., Hentschel, K., Stierhof, Y.D., Codogno, P., and Proikas-Cezanne, T. (2011). Resveratrol-mediated autophagy requires WIPI-1-regulated LC3 lipidation in the absence of induced phagophore formation. *Autophagy* 7, 1448-1461.

McCarthy, N.J., Whyte, M.K., Gilbert, C.S., and Evan, G.I. (1997). Inhibition of Ced-3/ICE-related proteases does not prevent cell death induced by oncogenes, DNA damage, or the Bcl-2 homologue Bak. *J Cell Biol* 136, 215-227.

McCarty, J.S., Toh, S.Y., and Li, P. (1999a). Multiple domains of DFF45 bind synergistically to DFF40: roles of caspase cleavage and sequestration of activator domain of DFF40. *Biochem Biophys Res Commun* 264, 181-185.

McCarty, J.S., Toh, S.Y., and Li, P. (1999b). Study of DFF45 in its role of chaperone and inhibitor: two independent inhibitory domains of DFF40 nuclease activity. *Biochem Biophys Res Commun* 264, 176-180.

McFaline-Figueroa, J.R., and Wen, P.Y. (2017). The Viral Connection to Glioblastoma. *Curr Infect Dis Rep* 19, 5.

McIlroy, D., Sakahira, H., Talanian, R.V., and Nagata, S. (1999). Involvement of caspase 3-activated DNase in internucleosomal DNA cleavage induced by diverse apoptotic stimuli. *Oncogene* 18, 4401-4408.

McIlwain, D.R., Berger, T., and Mak, T.W. (2013). Caspase functions in cell death and disease. *Cold Spring Harb Perspect Biol* 5, a008656.

McStay, G.P., Salvesen, G.S., and Green, D.R. (2008). Overlapping cleavage motif selectivity of caspases: implications for analysis of apoptotic pathways. *Cell Death Differ* 15, 322-331.

Meiss, G., Scholz, S.R., Korn, C., Gimadutdinow, O., and Pingoud, A. (2001). Identification of functionally relevant histidine residues in the apoptotic nuclease CAD. *Nucleic Acids Res* 29, 3901-3909.

Meltzer, P.C., Bickford, P.H., and Lambert, G. (1985). A regioselective route to gossypol analogs: the synthesis of gossypol and 5,5'-didesisopropyl-5,5'-diethyl gossypol. *The Journal of Organic Chemistry* 50, 3121-3124.

Meng, T., Lin, S., Zhuang, H., Huang, H., He, Z., Hu, Y., [. . .], Feng, D. (2019). Recent progress in the role of autophagy in neurological diseases. *Cell Stress* 3, 141-161.

Meng, Y., Tang, W., Dai, Y., Wu, X., Liu, M., Ji, Q., [. . .], Xu, L. (2008). Natural BH3 mimetic (-)-gossypol chemosensitizes human prostate cancer via Bcl-xL inhibition accompanied by increase of Puma and Noxa. *Mol Cancer Ther* 7, 2192-2202.

Menzies, F.M., Garcia-Arencibia, M., Imarisio, S., O'Sullivan, N.C., Ricketts, T., Kent, B.A., [. . .], Rubinsztein, D.C. (2015). Calpain inhibition mediates autophagy-dependent protection against polyglutamine toxicity. *Cell Death Differ* 22, 433-444.

Mercer, C.A., Kaliappan, A., and Dennis, P.B. (2009). A novel, human Atg13 binding protein, Atg101, interacts with ULK1 and is essential for macroautophagy. *Autophagy* 5, 649-662.

Metallo, C.M., Gameiro, P.A., Bell, E.L., Mattaini, K.R., Yang, J., Hiller, K., [. . .], Stephanopoulos, G. (2011). Reductive glutamine metabolism by IDH1 mediates lipogenesis under hypoxia. *Nature* 481, 380-384.

Meyer, M.A. (2008). Malignant gliomas in adults. *N Engl J Med* 359, 1850; author reply 1850.

Meyer, N., Zielke, S., Michaelis, J.B., Linder, B., Warnsmann, V., Rakel, S., [. . .], Kogel, D. (2018). AT 101 induces early mitochondrial dysfunction and HMOX1 (heme oxygenase 1) to trigger mitophagic cell death in glioma cells. *Autophagy* 14, 1693-1709.

Micheau, O., Thome, M., Schneider, P., Holler, N., Tschopp, J., Nicholson, D.W., [. . .], Grutter, M.G. (2002). The long form of FLIP is an activator of caspase-8 at the Fas death-inducing signaling complex. *J Biol Chem* 277, 45162-45171.

Milanesi, E., Costantini, P., Gambalunga, A., Colonna, R., Petronilli, V., Cabrelle, A., [. . .], Bernardi, P. (2006). The mitochondrial effects of small organic ligands of BCL-2: sensitization of BCL-2-

overexpressing cells to apoptosis by a pyrimidine-2,4,6-trione derivative. *J Biol Chem* 281, 10066-10072.

Miles, M.A., and Hawkins, C.J. (2017). Executioner caspases and CAD are essential for mutagenesis induced by TRAIL or vincristine. *Cell Death Dis* 8, e3062.

Miller, D.R., Cramer, S.D., and Thorburn, A. (2020). The interplay of autophagy and non-apoptotic cell death pathways. *Int Rev Cell Mol Biol* 352, 159-187.

Mills, J.C., Stone, N.L., Erhardt, J., and Pittman, R.N. (1998). Apoptotic membrane blebbing is regulated by myosin light chain phosphorylation. *J Cell Biol* 140, 627-636.

Minchew, C.L., and Didenko, V.V. (2011). Fluorescent probes detecting the phagocytic phase of apoptosis: enzyme-substrate complexes of topoisomerase and DNA. *Molecules* 16, 4599-4614.

Mizushima, N., and Yoshimori, T. (2007). How to interpret LC3 immunoblotting. *Autophagy* 3, 542-545.

Mizushima, N., Yoshimori, T., and Levine, B. (2010). Methods in mammalian autophagy research. *Cell* 140, 313-326.

Mizushima, N., Yoshimori, T., and Ohsumi, Y. (2011). The role of Atg proteins in autophagosome formation. *Annu Rev Cell Dev Biol* 27, 107-132.

Mizuta, R., Araki, S., Furukawa, M., Furukawa, Y., Ebara, S., Shiokawa, D., [. . .], Kitamura, D. (2013). DNase gamma is the effector endonuclease for internucleosomal DNA fragmentation in necrosis. *PLoS One* 8, e80223.

Mizuta, R., Mizuta, M., Araki, S., Shiokawa, D., Tanuma, S., and Kitamura, D. (2006). Action of apoptotic endonuclease DNase gamma on naked DNA and chromatin substrates. *Biochem Biophys Res Commun* 345, 560-567.

Mizuta, T., Shimizu, S., Matsuoka, Y., Nakagawa, T., and Tsujimoto, Y. (2007). A Bax/Bak-independent mechanism of cytochrome c release. *J Biol Chem* 282, 16623-16630.

Moldoveanu, T., Follis, A.V., Kriwacki, R.W., and Green, D.R. (2014). Many players in BCL-2 family affairs. *Trends Biochem Sci* 39, 101-111.

Montamat, E.E., Burgos, C., Gerez de Burgos, N.M., Rovai, L.E., Blanco, A., and Segura, E.L. (1982). Inhibitory action of gossypol on enzymes and growth of Trypanosoma cruzi. *Science* 218, 288-289.

Montes de Oca, R., Lee, K.K., and Wilson, K.L. (2005). Binding of barrier to autointegration factor (BAF) to histone H3 and selected linker histones including H1.1. *J Biol Chem* 280, 42252-42262.

Moon, D.O., Kim, M.O., Choi, Y.H., Lee, H.G., Kim, N.D., and Kim, G.Y. (2008a). Gossypol suppresses telomerase activity in human leukemia cells via regulating hTERT. *FEBS Lett* 582, 3367-3373.

Moon, D.O., Kim, M.O., Lee, J.D., and Kim, G.Y. (2008b). Gossypol suppresses NF-kappaB activity and NF-kappaB-related gene expression in human leukemia U937 cells. *Cancer Lett* 264, 192-200.

Morishima, N. (1999). Changes in nuclear morphology during apoptosis correlate with vimentin cleavage by different caspases located either upstream or downstream of Bcl-2 action. *Genes Cells* 4, 401-414.

Moriwaki, K., Farias Luz, N., Balaji, S., De Rosa, M.J., O'Donnell, C.L., Gough, P.J., [. . .], Chan, F.K. (2016). The Mitochondrial Phosphatase PGAM5 Is Dispensable for Necroptosis but Promotes Inflammasome Activation in Macrophages. *J Immunol* 196, 407-415.

Moubarak, R.S., Planells-Ferrer, L., Urresti, J., Reix, S., Segura, M.F., Carriba, P., [. . .], Comella, J.X. (2013). FAIM-L is an IAP-binding protein that inhibits XIAP ubiquitinylation and protects from Fas-induced apoptosis. *J Neurosci* 33, 19262-19275.

Moubarak, R.S., Yuste, V.J., Artus, C., Bouharrour, A., Greer, P.A., Menissier-de Murcia, J., and Susin, S.A. (2007). Sequential activation of poly(ADP-ribose) polymerase 1, calpains, and Bax is essential in apoptosis-inducing factor-mediated programmed necrosis. *Mol Cell Biol* 27, 4844-4862.

Moujalled, D.M., Cook, W.D., Murphy, J.M., and Vaux, D.L. (2014). Necroptosis induced by RIPK3 requires MLKL but not Drp1. *Cell Death Dis* 5, e1086.

Mukherjee, A., and Williams, D.W. (2017). More alive than dead: non-apoptotic roles for caspases in neuronal development, plasticity and disease. *Cell Death Differ* 24, 1411-1421.

Munoz, A.J., Wanichthanarak, K., Meza, E., and Petranovic, D. (2012). Systems biology of yeast cell death. *FEMS Yeast Res* 12, 249-265.

Munoz-Pinedo, C., and Lopez-Rivas, A. (2018). A role for caspase-8 and TRAIL-R2/DR5 in ER-stress-induced apoptosis. *Cell Death Differ* 25, 226.

Musiwaro, P., Smith, M., Manifava, M., Walker, S.A., and Ktistakis, N.T. (2013). Characteristics and requirements of basal autophagy in HEK 293 cells. *Autophagy* 9, 1407-1417.

Muzaffaruddin, M., and Saxena, E.R. (1966). Physicochemical studies on the composition and stability of metal-gossypol complexes. I. Fe+++ gossypol complex. *J Am Oil Chem Soc* 43, 429-430.

Nagane, M., Levitzki, A., Gazit, A., Cavenee, W.K., and Huang, H.J. (1998). Drug resistance of human glioblastoma cells conferred by a tumor-specific mutant epidermal growth factor receptor through modulation of Bcl-XL and caspase-3-like proteases. *Proc Natl Acad Sci U S A* 95, 5724-5729.

Nagata, T., Kishi, H., Liu, Q.L., Matsuda, T., Imanaka, T., Tsukada, K., [. . .], Muraguchi, A. (2002). The regulation of DNAse activities in subcellular compartments of activated thymocytes. *Immunology* 105, 399-406.

Nakajima, Y.I., and Kuranaga, E. (2017). Caspase-dependent non-apoptotic processes in development. *Cell Death Differ* 24, 1422-1430.

Nakamura, S., and Yoshimori, T. (2017). New insights into autophagosome-lysosome fusion. *J Cell Sci* 130, 1209-1216.

Napirei, M., Karsunky, H., Zevnik, B., Stephan, H., Mannherz, H.G., and Moroy, T. (2000). Features of systemic lupus erythematosus in Dnase1-deficient mice. *Nat Genet* 25, 177-181.

Narwade, N., Patel, S., Alam, A., Chattopadhyay, S., Mittal, S., and Kulkarni, A. (2019). Mapping of scaffold/matrix attachment regions in human genome: a data mining exercise. *Nucleic Acids Res* 47, 7247-7261.

Nechushtan, A., Smith, C.L., Hsu, Y.T., and Youle, R.J. (1999). Conformation of the Bax C-terminus regulates subcellular location and cell death. *EMBO J* 18, 2330-2341.

Neimanis, S., Albig, W., Doenecke, D., and Kahle, J. (2007). Sequence elements in both subunits of the DNA fragmentation factor are essential for its nuclear transport. *J Biol Chem* 282, 35821-35830.

Netto, L.E., Ferreira, A.M., and Augusto, O. (1991). Iron(III) binding in DNA solutions: complex formation and catalytic activity in the oxidation of hydrazine derivatives. *Chem Biol Interact* 79, 1-14.

Newton, K., Wickliffe, K.E., Maltzman, A., Dugger, D.L., Strasser, A., Pham, V.C., [. . .], Dixit, V.M. (2016). RIPK1 inhibits ZBP1-driven necroptosis during development. *Nature* 540, 129-133.

Nguyen, M., Marcellus, R.C., Roulston, A., Watson, M., Serfass, L., Murthy Madiraju, S.R., [. . .], Shore, G.C. (2007). Small molecule obatoclax (GX15-070) antagonizes MCL-1 and overcomes MCL-1-mediated resistance to apoptosis. *Proc Natl Acad Sci U S A* 104, 19512-19517.

Ni, M., and Lee, A.S. (2007). ER chaperones in mammalian development and human diseases. *FEBS Lett* 581, 3641-3651.

Nielsen, A.L., Oulad-Abdelghani, M., Ortiz, J.A., Remboutsika, E., Chambon, P., and Losson, R. (2001). Heterochromatin formation in mammalian cells: interaction between histones and HP1 proteins. *Mol Cell* 7, 729-739.

Niyazi, M., Brada, M., Chalmers, A.J., Combs, S.E., Erridge, S.C., Fiorentino, A., [. . .], Belka, C. (2016). ESTRO-ACROP guideline "target delineation of glioblastomas". *Radiother Oncol* 118, 35-42.

Nordenskjold, M., and Lambert, B. (1984). Gossypol induces DNA strand breaks in human fibroblasts and sister chromatid exchanges in human lymphocytes in vitro. *J Med Genet* 21, 129-132.

Norman, J.M., Cohen, G.M., and Bampton, E.T. (2010). The in vitro cleavage of the hAtg proteins by cell death proteases. *Autophagy* 6, 1042-1056.

Nyberg, P., Xie, L., and Kalluri, R. (2005). Endogenous inhibitors of angiogenesis. *Cancer Res* 65, 3967-3979.

O'Donnell, M.A., Perez-Jimenez, E., Oberst, A., Ng, A., Massoumi, R., Xavier, R., [. . .], Ting, A.T. (2011). Caspase 8 inhibits programmed necrosis by processing CYLD. *Nat Cell Biol* 13, 1437-1442.

O'Neill, K.L., Huang, K., Zhang, J., Chen, Y., and Luo, X. (2016). Inactivation of prosurvival Bcl-2 proteins activates Bax/Bak through the outer mitochondrial membrane. *Genes Dev* 30, 973-988.

Oberhammer, F., Fritsch, G., Schmied, M., Pavelka, M., Printz, D., Purchio, T., [. . .], Schulte-Hermann, R. (1993a). Condensation of the chromatin at the membrane of an apoptotic nucleus is not associated with activation of an endonuclease. *J Cell Sci* 104 (Pt 2), 317-326.

Oberhammer, F., Wilson, J.W., Dive, C., Morris, I.D., Hickman, J.A., Wakeling, A.E., [. . .], Sikorska, M. (1993b). Apoptotic death in epithelial cells: cleavage of DNA to 300 and/or 50 kb fragments prior to or in the absence of internucleosomal fragmentation. *EMBO J* 12, 3679-3684.

Oberst, A., Dillon, C.P., Weinlich, R., McCormick, L.L., Fitzgerald, P., Pop, C., [. . .], Green, D.R. (2011). Catalytic activity of the caspase-8-FLIP(L) complex inhibits RIPK3-dependent necrosis. *Nature* 471, 363-367.

Oberst, A., Pop, C., Tremblay, A.G., Blais, V., Denault, J.B., Salvesen, G.S., and Green, D.R. (2010). Inducible dimerization and inducible cleavage reveal a requirement for both processes in caspase-8 activation. *J Biol Chem* 285, 16632-16642.

Ohgaki, H., and Kleihues, P. (2013). The definition of primary and secondary glioblastoma. *Clin Cancer Res* 19, 764-772.

Ohsawa, Y., Isahara, K., Kanamori, S., Shibata, M., Kametaka, S., Gotow, T., [. . .], Uchiyama, Y. (1998). An ultrastructural and immunohistochemical study of PC12 cells during apoptosis induced by

serum deprivation with special reference to autophagy and lysosomal cathepsins. *Arch Histol Cytol* 61, 395-403.

Oliveri, M., Daga, A., Cantoni, C., Lunardi, C., Millo, R., and Puccetti, A. (2001). DNase I mediates internucleosomal DNA degradation in human cells undergoing drug-induced apoptosis. *Eur J Immunol* 31, 743-751.

Oltersdorf, T., Elmore, S.W., Shoemaker, A.R., Armstrong, R.C., Augeri, D.J., Belli, B.A., [. . .], Rosenberg, S.H. (2005). An inhibitor of Bcl-2 family proteins induces regression of solid tumours. *Nature* 435, 677-681.

Ong, S.B., Lee, W.H., Shao, N.Y., Ismail, N.I., Katwadi, K., Lim, M.M., [. . .], Ong, S.G. (2019). Calpain Inhibition Restores Autophagy and Prevents Mitochondrial Fragmentation in a Human iPSC Model of Diabetic Endotheliopathy. *Stem Cell Reports* 12, 597-610.

Ord, T., and Ord, T. (2017). Mammalian Pseudokinase TRIB3 in Normal Physiology and Disease: Charting the Progress in Old and New Avenues. *Curr Protein Pept Sci* 18, 819-842.

Orenstein, S.J., and Cuervo, A.M. (2010). Chaperone-mediated autophagy: molecular mechanisms and physiological relevance. *Semin Cell Dev Biol* 21, 719-726.

Orozco, S., Yatim, N., Werner, M.R., Tran, H., Gunja, S.Y., Tait, S.W., [. . .], Oberst, A. (2014). RIPK1 both positively and negatively regulates RIPK3 oligomerization and necroptosis. *Cell Death Differ* 21, 1511-1521.

Orth, K., Chinnaiyan, A.M., Garg, M., Froelich, C.J., and Dixit, V.M. (1996). The CED-3/ICE-like protease Mch2 is activated during apoptosis and cleaves the death substrate lamin A. *J Biol Chem* 271, 16443-16446.

Otomo, T., Sakahira, H., Uegaki, K., Nagata, S., and Yamazaki, T. (2000). Structure of the heterodimeric complex between CAD domains of CAD and ICAD. *Nat Struct Biol* 7, 658-662.

Ouameur, A.A., Arakawa, H., Ahmad, R., Naoui, M., and Tajmir-Riahi, H.A. (2005). A Comparative study of Fe(II) and Fe(III) interactions with DNA duplex: major and minor grooves bindings. *DNA Cell Biol* 24, 394-401.

Ow, Y.P., Green, D.R., Hao, Z., and Mak, T.W. (2008). Cytochrome c: functions beyond respiration. *Nat Rev Mol Cell Biol* 9, 532-542.

Padanilam, B.J. (2003). Cell death induced by acute renal injury: a perspective on the contributions of apoptosis and necrosis. *Am J Physiol Renal Physiol* 284, F608-627.

Palchaudhuri, R., Lambrecht, M.J., Botham, R.C., Partlow, K.C., van Ham, T.J., Putt, K.S., [. . .], Hergenrother, P.J. (2015). A Small Molecule that Induces Intrinsic Pathway Apoptosis with Unparalleled Speed. *Cell Rep* 13, 2027-2036.

Papanikolaou, G., and Pantopoulos, K. (2005). Iron metabolism and toxicity. *Toxicol Appl Pharmacol* 202, 199-211.

Park, J., Shim, J.K., Kang, J.H., Choi, J., Chang, J.H., Kim, S.Y., and Kang, S.G. (2018). Regulation of bioenergetics through dual inhibition of aldehyde dehydrogenase and mitochondrial complex I suppresses glioblastoma tumorspheres. *Neuro Oncol* 20, 954-965.

Parzych, K.R., and Klionsky, D.J. (2014). An overview of autophagy: morphology, mechanism, and regulation. *Antioxid Redox Signal* 20, 460-473.

Patil, C.G., Nuno, M., Elramsisy, A., Mukherjee, D., Carico, C., Dantis, J., [. . .], Bannykh, S.I. (2013). High levels of phosphorylated MAP kinase are associated with poor survival among patients with glioblastoma during the temozolomide era. *Neuro Oncol* 15, 104-111.

Pearson, J.R.D., and Regad, T. (2017). Targeting cellular pathways in glioblastoma multiforme. *Signal Transduct Target Ther* 2, 17040.

Pecot, J., Maillet, L., Le Pen, J., Vuillier, C., Trecesson, S.C., Fetiveau, A., [. . .], Juin, P.P. (2016). Tight Sequestration of BH3 Proteins by BCL-xL at Subcellular Membranes Contributes to Apoptotic Resistance. *Cell Rep* 17, 3347-3358.

Pedroza, D.A., Chandel, V., Kumar, D., Doddapattar, P., Biradar, M., Lakshmanaswamy, R., [. . .], Choudhari, R. (2020). Role of Autophagy in Cancer Cell Metabolism. In Cancer Cell Metabolism: A Potential Target for Cancer Therapy (Springer), pp. 65-87.

Pegoraro, L., Palumbo, A., Erikson, J., Falda, M., Giovanazzo, B., Emanuel, B.S., [. . .], Croce, C.M. (1984). A 14;18 and an 8;14 chromosome translocation in a cell line derived from an acute B-cell leukemia. *Proc Natl Acad Sci U S A* 81, 7166-7170.

Peitsch, M.C., Polzar, B., Stephan, H., Crompton, T., MacDonald, H.R., Mannherz, H.G., and Tschopp, J. (1993). Characterization of the endogenous deoxyribonuclease involved in nuclear DNA degradation during apoptosis (programmed cell death). *EMBO J* 12, 371-377.

Pekmezci, M., Rice, T., Molinaro, A.M., Walsh, K.M., Decker, P.A., Hansen, H., [. . .], Wrensch, M.R. (2017). Adult infiltrating gliomas with WHO 2016 integrated diagnosis: additional prognostic roles of ATRX and TERT. *Acta Neuropathol* 133, 1001-1016.

Perez-Galan, P., Roue, G., Villamor, N., Campo, E., and Colomer, D. (2007). The BH3-mimetic GX15-070 synergizes with bortezomib in mantle cell lymphoma by enhancing Noxa-mediated activation of Bak. *Blood* 109, 4441-4449.

Perry, J.R., Laperriere, N., O'Callaghan, C.J., Brandes, A.A., Menten, J., Phillips, C., [. . .], Trial, I. (2017). Short-Course Radiation plus Temozolomide in Elderly Patients with Glioblastoma. *N Engl J Med* 376, 1027-1037.

Pihan, P., Carreras-Sureda, A., and Hetz, C. (2017). BCL-2 family: integrating stress responses at the ER to control cell demise. *Cell Death Differ* 24, 1478-1487.

Plate, K.H., Breier, G., Weich, H.A., and Risau, W. (1992). Vascular endothelial growth factor is a potential tumour angiogenesis factor in human gliomas in vivo. *Nature* 359, 845-848.

Polster, B.M., Basanez, G., Etxebarria, A., Hardwick, J.M., and Nicholls, D.G. (2005). Calpain I induces cleavage and release of apoptosis-inducing factor from isolated mitochondria. *J Biol Chem* 280, 6447-6454.

Ponder, K.G., and Boise, L.H. (2019). The prodomain of caspase-3 regulates its own removal and caspase activation. *Cell Death Discov* 5, 56.

Pop, C., Fitzgerald, P., Green, D.R., and Salvesen, G.S. (2007). Role of proteolysis in caspase-8 activation and stabilization. *Biochemistry* 46, 4398-4407.

Pop, C., and Salvesen, G.S. (2009). Human caspases: activation, specificity, and regulation. *J Biol Chem* 284, 21777-21781.

Poreba, M., Strozyk, A., Salvesen, G.S., and Drag, M. (2013). Caspase substrates and inhibitors. *Cold Spring Harb Perspect Biol* 5, a008680.

Prats, E., Noel, M., Letourneau, J., Tiranti, V., Vaque, J., Debon, R., [. . .], Ruiz-Carrillo, A. (1997). Characterization and expression of the mouse endonuclease G gene. *DNA Cell Biol* 16, 1111-1122.

Puthalakath, H., Huang, D.C., O'Reilly, L.A., King, S.M., and Strasser, A. (1999). The proapoptotic activity of the Bcl-2 family member Bim is regulated by interaction with the dynein motor complex. *Mol Cell* 3, 287-296.

Pyo, J.O., Jang, M.H., Kwon, Y.K., Lee, H.J., Jun, J.I., Woo, H.N., [. . .], Jung, Y.K. (2005). Essential roles of Atg5 and FADD in autophagic cell death: dissection of autophagic cell death into vacuole formation and cell death. *J Biol Chem* 280, 20722-20729.

Qian, S.Z., and Wang, Z.G. (1984). Gossypol: a potential antifertility agent for males. *Annu Rev Pharmacol Toxicol* 24, 329-360.

Qiu, Y., Cao, Y., Cao, W., Jia, Y., and Lu, N. (2020). The Application of Ferroptosis in Diseases. *Pharmacol Res* 159, 104919.

Radloff, R.J., Deck, L.M., Royer, R.E., and Vander Jagt, D.L. (1986). Antiviral activities of gossypol and its derivatives against herpes simplex virus type II. *Pharmacol Res Commun* 18, 1063-1073.

Rajasekhar, V.K., Viale, A., Socci, N.D., Wiedmann, M., Hu, X., and Holland, E.C. (2003). Oncogenic Ras and Akt signaling contribute to glioblastoma formation by differential recruitment of existing mRNAs to polysomes. *Mol Cell* 12, 889-901.

Ramaswamy, H.N., and O'Connor, R.T. (1969). Metal complexes of gossypol. *Journal of Agricultural and Food Chemistry* 17, 1406-1408.

Ramaswamy, H.N., and O'Connor, R.T. (1968). Physical and chemical properties of selected metal complexes of gossypol. *Journal of the American Oil Chemists' Society* 45, 841-844.

Ramirez, M.L.G., and Salvesen, G.S. (2018). A primer on caspase mechanisms. *Semin Cell Dev Biol* 82, 79-85.

Rao, L., Perez, D., and White, E. (1996). Lamin proteolysis facilitates nuclear events during apoptosis. *J Cell Biol* 135, 1441-1455.

Rawlings, N.D., Barrett, A.J., and Bateman, A. (2010). MEROPS: the peptidase database. *Nucleic Acids Res* 38, D227-233.

Reagan-Shaw, S., Nihal, M., and Ahmad, N. (2008). Dose translation from animal to human studies revisited. *FASEB J* 22, 659-661.

Recht, L., Torres, C.O., Smith, T.W., Raso, V., and Griffin, T.W. (1990). Transferrin receptor in normal and neoplastic brain tissue: implications for brain-tumor immunotherapy. *J Neurosurg* 72, 941-945.

Reed, J.C., Meister, L., Tanaka, S., Cuddy, M., Yum, S., Geyer, C., and Pleasure, D. (1991). Differential expression of bcl2 protooncogene in neuroblastoma and other human tumor cell lines of neural origin. *Cancer Res* 51, 6529-6538.

Reh, S., Korn, C., Gimadutdinow, O., and Meiss, G. (2005). Structural basis for stable DNA complex formation by the caspase-activated DNase. *J Biol Chem* 280, 41707-41715.

Rehm, M., Huber, H.J., Dussmann, H., and Prehn, J.H. (2006). Systems analysis of effector caspase activation and its control by X-linked inhibitor of apoptosis protein. *EMBO J* 25, 4338-4349.

Ren, D., Tu, H.C., Kim, H., Wang, G.X., Bean, G.R., Takeuchi, O., [. . .], Cheng, E.H. (2010). BID, BIM, and PUMA are essential for activation of the BAX- and BAK-dependent cell death program. *Science* 330, 1390-1393.

Ribatti, D. (2018). An historical note on the cell theory. *Exp Cell Res* 364, 1-4.

Rice, T., Lachance, D.H., Molinaro, A.M., Eckel-Passow, J.E., Walsh, K.M., Barnholtz-Sloan, J., [. . .], Wrensch, M.R. (2016). Understanding inherited genetic risk of adult glioma - a review. *Neurooncol Pract* 3, 10-16.

Riedl, S.J., and Salvesen, G.S. (2007). The apoptosome: signalling platform of cell death. *Nat Rev Mol Cell Biol* 8, 405-413.

Riedl, S.J., and Shi, Y. (2004). Molecular mechanisms of caspase regulation during apoptosis. *Nat Rev Mol Cell Biol* 5, 897-907.

Roberts, A.W., Davids, M.S., Pagel, J.M., Kahl, B.S., Puvvada, S.D., Gerecitano, J.F., [. . .], Seymour, J.F. (2016). Targeting BCL2 with Venetoclax in Relapsed Chronic Lymphocytic Leukemia. *N Engl J Med* 374, 311-322.

Robin, A.Y., Krishna Kumar, K., Westphal, D., Wardak, A.Z., Thompson, G.V., Dewson, G., [. . .], Czabotar, P.E. (2015). Crystal structure of Bax bound to the BH3 peptide of Bim identifies important contacts for interaction. *Cell Death Dis* 6, e1809.

Roca Portoles, A., and Tait, S.W.G. (2020). ER Stress Leaves an Inflammatory TRAIL. *Dev Cell* 52, 678-680.

Rockfield, S., Chhabra, R., Robertson, M., Rehman, N., Bisht, R., and Nanjundan, M. (2018). Links Between Iron and Lipids: Implications in Some Major Human Diseases. *Pharmaceuticals (Basel)* 11.

Rogakou, E.P., Nieves-Neira, W., Boon, C., Pommier, Y., and Bonner, W.M. (2000). Initiation of DNA fragmentation during apoptosis induces phosphorylation of H2AX histone at serine 139. *J Biol Chem* 275, 9390-9395.

Rogakou, E.P., Pilch, D.R., Orr, A.H., Ivanova, V.S., and Bonner, W.M. (1998). DNA double-stranded breaks induce histone H2AX phosphorylation on serine 139. *J Biol Chem* 273, 5858-5868.

Rogers, C., Fernandes-Alnemri, T., Mayes, L., Alnemri, D., Cingolani, G., and Alnemri, E.S. (2017). Cleavage of DFNA5 by caspase-3 during apoptosis mediates progression to secondary necrotic/pyroptotic cell death. *Nat Commun* 8, 14128.

Roos, W.P., Thomas, A.D., and Kaina, B. (2016). DNA damage and the balance between survival and death in cancer biology. *Nat Rev Cancer* 16, 20-33.

Rosenberg, L.J., Adlakha, R.C., Desai, D.M., and Rao, P.N. (1986). Inhibition of DNA polymerase alpha by gossypol. *Biochim Biophys Acta* 866, 258-267.

Ruchaud, S., Korfali, N., Villa, P., Kottke, T.J., Dingwall, C., Kaufmann, S.H., and Earnshaw, W.C. (2002). Caspase-6 gene disruption reveals a requirement for lamin A cleavage in apoptotic chromatin condensation. *EMBO J* 21, 1967-1977.

Ruiz-Carrillo, A., and Renaud, J. (1987). Endonuclease G: a (dG)n X (dC)n-specific DNase from higher eukaryotes. *EMBO J* 6, 401-407.

Rybstein, M.D., Bravo-San Pedro, J.M., Kroemer, G., and Galluzzi, L. (2018). The autophagic network and cancer. *Nat Cell Biol* 20, 243-251.

Sabol, S.L., Li, R., Lee, T.Y., and Abdul-Khalek, R. (1998). Inhibition of apoptosis-associated DNA fragmentation activity in nonapoptotic cells: the role of DNA fragmentation factor-45 (DFF45/ICAD). *Biochem Biophys Res Commun* 253, 151-158.

Sahara, S., Aoto, M., Eguchi, Y., Imamoto, N., Yoneda, Y., and Tsujimoto, Y. (1999). Acinus is a caspase-3-activated protein required for apoptotic chromatin condensation. *Nature* 401, 168-173.

Sahin, F., Avci, C.B., Gunduz, C., Sezgin, C., Simsir, I.Y., and Saydam, G. (2010). Gossypol exerts its cytotoxic effect on HL-60 leukemic cell line via decreasing activity of protein phosphatase 2A and interacting with human telomerase reverse transcriptase activity. *Hematology* 15, 144-150.

Sakahira, H., Enari, M., and Nagata, S. (1998). Cleavage of CAD inhibitor in CAD activation and DNA degradation during apoptosis. *Nature* 391, 96-99.

Sakahira, H., Enari, M., and Nagata, S. (1999). Functional differences of two forms of the inhibitor of caspase-activated DNase, ICAD-L, and ICAD-S. *J Biol Chem* 274, 15740-15744.

Sakahira, H., Iwamatsu, A., and Nagata, S. (2000). Specific chaperone-like activity of inhibitor of caspase-activated DNase for caspase-activated DNase. *J Biol Chem* 275, 8091-8096.

Sakahira, H., and Nagata, S. (2002). Co-translational folding of caspase-activated DNase with Hsp70, Hsp40, and inhibitor of caspase-activated DNase. *J Biol Chem* 277, 3364-3370.

Sakahira, H., Takemura, Y., and Nagata, S. (2001). Enzymatic active site of caspase-activated DNase (CAD) and its inhibition by inhibitor of CAD. *Arch Biochem Biophys* 388, 91-99.

Salazar, M., Carracedo, A., Salanueva, I.J., Hernandez-Tiedra, S., Lorente, M., Egia, A., [. . .], Velasco, G. (2009). Cannabinoid action induces autophagy-mediated cell death through stimulation of ER stress in human glioma cells. *J Clin Invest* 119, 1359-1372.

Salvesen, G.S., and Ashkenazi, A. (2011). Snapshot: caspases. *Cell* 147, 476-476 e471.

Salvesen, G.S., and Dixit, V.M. (1997). Caspases: intracellular signaling by proteolysis. *Cell* 91, 443-446.

Salvesen, G.S., and Dixit, V.M. (1999). Caspase activation: the induced-proximity model. *Proc Natl Acad Sci U S A* 96, 10964-10967.

Salvesen, G.S., and Duckett, C.S. (2002). IAP proteins: blocking the road to death's door. *Nat Rev Mol Cell Biol* 3, 401-410.

Samejima, K., and Earnshaw, W.C. (1998). ICAD/DFF regulator of apoptotic nuclease is nuclear. *Exp Cell Res* 243, 453-459.

Samejima, K., and Earnshaw, W.C. (2000). Differential localization of ICAD-L and ICAD-S in cells due to removal of a C-terminal NLS from ICAD-L by alternative splicing. *Exp Cell Res* 255, 314-320.

Samejima, K., and Earnshaw, W.C. (2005). Trashing the genome: the role of nucleases during apoptosis. *Nat Rev Mol Cell Biol* 6, 677-688.

Samejima, K., Tone, S., and Earnshaw, W.C. (2001). CAD/DFF40 nuclease is dispensable for high molecular weight DNA cleavage and stage I chromatin condensation in apoptosis. *J Biol Chem* 276, 45427-45432.

Sanchez-Osuna, M., Garcia-Belinchon, M., Iglesias-Guimarais, V., Gil-Guinon, E., Casanelles, E., and Yuste, V.J. (2014). Caspase-activated DNase is necessary and sufficient for oligonucleosomal DNA

breakdown, but not for chromatin disassembly during caspase-dependent apoptosis of LN-18 glioblastoma cells. *J Biol Chem* 289, 18752-18769.

Sanchez-Osuna, M., Martinez-Escardo, L., Granados-Colomina, C., Martinez-Soler, F., Pascual-Guiral, S., Iglesias-Guimarais, V., [. . .], Yuste, V.J. (2016). An intrinsic DFF40/CAD endonuclease deficiency impairs oligonucleosomal DNA hydrolysis during caspase-dependent cell death: a common trait in human glioblastoma cells. *Neuro Oncol* 18, 950-961.

Saraste, A., and Pulkki, K. (2000). Morphologic and biochemical hallmarks of apoptosis. *Cardiovasc Res* 45, 528-537.

Saxton, R.A., and Sabatini, D.M. (2017). mTOR Signaling in Growth, Metabolism, and Disease. *Cell* 168, 960-976.

Sborgi, L., Ruhl, S., Mulvihill, E., Pipercevic, J., Heilig, R., Stahlberg, H., [. . .], Hiller, S. (2016). GSDMD membrane pore formation constitutes the mechanism of pyroptotic cell death. *EMBO J* 35, 1766-1778.

Scaffidi, C., Schmitz, I., Krammer, P.H., and Peter, M.E. (1999). The role of c-FLIP in modulation of CD95-induced apoptosis. *J Biol Chem* 274, 1541-1548.

Schaaf, M.B., Keulers, T.G., Vooijs, M.A., and Rouschop, K.M. (2016). LC3/GABARAP family proteins: autophagy-(un)related functions. *FASEB J* 30, 3961-3978.

Schafer, A., Teufel, J., Ringel, F., Bettstetter, M., Hoepner, I., Rasper, M., [. . .], Schlegel, J. (2012). Aldehyde dehydrogenase 1A1--a new mediator of resistance to temozolomide in glioblastoma. *Neuro Oncol* 14, 1452-1464.

Schafer, P., Scholz, S.R., Gimadutdinow, O., Cymerman, I.A., Bujnicki, J.M., Ruiz-Carrillo, A., [. . .], Meiss, G. (2004). Structural and functional characterization of mitochondrial EndoG, a sugar non-specific nuclease which plays an important role during apoptosis. *J Mol Biol* 338, 217-228.

Schechter, I., and Berger, A. (1967). On the size of the active site in proteases. I. Papain. *Biochem Biophys Res Commun* 27, 157-162.

Scheiffele, E.W., and Shirley, D.A. (1964). The Oxidation of Gossypol. I. Early Stages in the Reaction of Gossypol and Oxygen. *The Journal of Organic Chemistry* 29, 3617-3620.

Schenk, B., and Fulda, S. (2015). Reactive oxygen species regulate Smac mimetic/TNFalpha-induced necroptotic signaling and cell death. *Oncogene* 34, 5796-5806.

Schleich, K., Buchbinder, J.H., Pietkiewicz, S., Kahne, T., Warnken, U., Ozturk, S., [. . .], Lavrik, I.N. (2016). Molecular architecture of the DED chains at the DISC: regulation of procaspase-8 activation by short DED proteins c-FLIP and procaspase-8 prodomain. *Cell Death Differ* 23, 681-694.

Schneider-Brachert, W., Tchikov, V., Neumeyer, J., Jakob, M., Winoto-Morbach, S., Held-Feindt, J., [. . .], Schutze, S. (2004). Compartmentalization of TNF receptor 1 signaling: internalized TNF receptosomes as death signaling vesicles. *Immunity* 21, 415-428.

Schonberg, D.L., Miller, T.E., Wu, Q., Flavahan, W.A., Das, N.K., Hale, J.S., [. . .], Rich, J.N. (2015). Preferential Iron Trafficking Characterizes Glioblastoma Stem-like Cells. *Cancer Cell* 28, 441-455.

Schutze, S., Tchikov, V., and Schneider-Brachert, W. (2008). Regulation of TNFR1 and CD95 signalling by receptor compartmentalization. *Nat Rev Mol Cell Biol* 9, 655-662.

Schweichel, J.U., and Merker, H.J. (1973). The morphology of various types of cell death in prenatal tissues. *Teratology* 7, 253-266.

Seaman, J.E., Julien, O., Lee, P.S., Rettenmaier, T.J., Thomsen, N.D., and Wells, J.A. (2016). Cacidases: caspases can cleave after aspartate, glutamate and phosphoserine residues. *Cell Death Differ* 23, 1717-1726.

Sebbagh, M., Renvoize, C., Hamelin, J., Riche, N., Bertoglio, J., and Breard, J. (2001). Caspase-3-mediated cleavage of ROCK I induces MLC phosphorylation and apoptotic membrane blebbing. *Nat Cell Biol* 3, 346-352.

Sedelnikova, O.A., Rogakou, E.P., Panyutin, I.G., and Bonner, W.M. (2002). Quantitative detection of (125)IdU-induced DNA double-strand breaks with gamma-H2AX antibody. *Radiat Res* 158, 486-492.

Segura, M.F., Sole, C., Pascual, M., Moubarak, R.S., Perez-Garcia, M.J., Gozzelino, R., [. . .], Comella, J.X. (2007). The long form of Fas apoptotic inhibitory molecule is expressed specifically in neurons and protects them against death receptor-triggered apoptosis. *J Neurosci* 27, 11228-11241.

Senarisoy, M., Canturk, P., Zencir, S., Baran, Y., and Topcu, Z. (2013). Gossypol interferes with both type I and type II topoisomerase activities without generating strand breaks. *Cell Biochem Biophys* 66, 199-204.

Serrano-Puebla, A., and Boya, P. (2016). Lysosomal membrane permeabilization in cell death: new evidence and implications for health and disease. *Ann N Y Acad Sci* 1371, 30-44.

Shalini, S., Dorstyn, L., Dawar, S., and Kumar, S. (2015). Old, new and emerging functions of caspases. *Cell Death Differ* 22, 526-539.

Shamas-Din, A., Brahmbhatt, H., Leber, B., and Andrews, D.W. (2011). BH3-only proteins: Orchestrators of apoptosis. *Biochim Biophys Acta* 1813, 508-520.

Shamas-Din, A., Kale, J., Leber, B., and Andrews, D.W. (2013). Mechanisms of action of Bcl-2 family proteins. *Cold Spring Harb Perspect Biol* 5, a008714.

Sharif-Askari, E., Alam, A., Rheaume, E., Beresford, P.J., Scotto, C., Sharma, K., [. . .], Sekaly, R.P. (2001). Direct cleavage of the human DNA fragmentation factor-45 by granzyme B induces caspase-activated DNase release and DNA fragmentation. *EMBO J* 20, 3101-3113.

Sharpless, N.E., and Sherr, C.J. (2015). Forging a signature of in vivo senescence. *Nat Rev Cancer* 15, 397-408.

Shaw, R.J., Kosmatka, M., Bardeesy, N., Hurley, R.L., Witters, L.A., DePinho, R.A., and Cantley, L.C. (2004). The tumor suppressor LKB1 kinase directly activates AMP-activated kinase and regulates apoptosis in response to energy stress. *Proc Natl Acad Sci U S A* 101, 3329-3335.

Shelley, M.D., Hartley, L., Fish, R.G., Groundwater, P., Morgan, J.J., Mort, D., [. . .], Evans, A. (1999). Stereo-specific cytotoxic effects of gossypol enantiomers and gossypolone in tumour cell lines. *Cancer Lett* 135, 171-180.

Shelley, M.D., Hartley, L., Groundwater, P.W., and Fish, R.G. (2000). Structure-activity studies on gossypol in tumor cell lines. *Anticancer Drugs* 11, 209-216.

Shi, Y. (2002). Mechanisms of caspase activation and inhibition during apoptosis. *Mol Cell* 9, 459-470.

Shimizu, S., Kanaseki, T., Mizushima, N., Mizuta, T., Arakawa-Kobayashi, S., Thompson, C.B., and Tsujimoto, Y. (2004). Role of Bcl-2 family proteins in a non-apoptotic programmed cell death dependent on autophagy genes. *Nat Cell Biol* 6, 1221-1228.

Shiokawa, D., Iwamatsu, A., and Tanuma, S. (1997a). Purification, characterization, and amino acid sequencing of DNase gamma from rat spleen. *Arch Biochem Biophys* 346, 15-20.

Shiokawa, D., Ohyama, H., Yamada, T., and Tanuma, S. (1997b). Purification and properties of DNase gamma from apoptotic rat thymocytes. *Biochem J* 326 (Pt 3), 675-681.

Shiokawa, D., Shika, Y., and Tanuma, S. (2003). Identification of two functional nuclear localization signals in DNase gamma and their roles in its apoptotic DNase activity. *Biochem J* 376, 377-381.

Shiokawa, D., and Tanuma, S. (1998). Molecular cloning and expression of a cDNA encoding an apoptotic endonuclease DNase gamma. *Biochem J* 332 (Pt 3), 713-720.

Shiokawa, D., and Tanuma, S. (2001). Characterization of human DNase I family endonucleases and activation of DNase gamma during apoptosis. *Biochemistry* 40, 143-152.

Shiokawa, D., and Tanuma, S. (2004). Differential DNases are selectively used in neuronal apoptosis depending on the differentiation state. *Cell Death Differ* 11, 1112-1120.

Shlyakhtina, Y., Pavet, V., and Gronemeyer, H. (2017). Dual role of DR5 in death and survival signaling leads to TRAIL resistance in cancer cells. *Cell Death Dis* 8, e3025.

Siegmund, D., Lang, I., and Wajant, H. (2017). Cell death-independent activities of the death receptors CD95, TRAILR1, and TRAILR2. *FEBS J* 284, 1131-1159.

Silke, J., and Meier, P. (2013). Inhibitor of apoptosis (IAP) proteins-modulators of cell death and inflammation. *Cold Spring Harb Perspect Biol* 5.

Simon, H.U., and Friis, R. (2014). ATG5: a distinct role in the nucleus. *Autophagy* 10, 176-177.

Simpson, J.R., Horton, J., Scott, C., Curran, W.J., Rubin, P., Fischbach, J., [. . .], et al. (1993). Influence of location and extent of surgical resection on survival of patients with glioblastoma multiforme: results of three consecutive Radiation Therapy Oncology Group (RTOG) clinical trials. *Int J Radiat Oncol Biol Phys* 26, 239-244.

Singh, B., and Bhaskar, S. (2019). Methods for Detection of Autophagy in Mammalian Cells. *Methods Mol Biol* 2045, 245-258.

Singh, R., Letai, A., and Sarosiek, K. (2019). Regulation of apoptosis in health and disease: the balancing act of BCL-2 family proteins. *Nat Rev Mol Cell Biol* 20, 175-193.

Skalka, M., Matyasova, J., and Cejkova, M. (1976). Dna in chromatin of irradiated lymphoid tissues degrades in vivo into regular fragments. *FEBS Lett* 72, 271-274.

Skouta, R., Dixon, S.J., Wang, J., Dunn, D.E., Orman, M., Shimada, K., [. . .], Stockwell, B.R. (2014). Ferrostatins inhibit oxidative lipid damage and cell death in diverse disease models. *J Am Chem Soc* 136, 4551-4556.

Slee, E.A., Adrain, C., and Martin, S.J. (2001). Executioner caspase-3, -6, and -7 perform distinct, non-redundant roles during the demolition phase of apoptosis. *J Biol Chem* 276, 7320-7326.

Soderquist, R.S., Danilov, A.V., and Eastman, A. (2014). Gossypol increases expression of the pro-apoptotic BH3-only protein NOXA through a novel mechanism involving phospholipase A2, cytoplasmic calcium, and endoplasmic reticulum stress. *J Biol Chem* 289, 16190-16199.

Sole, C., Dolcet, X., Segura, M.F., Gutierrez, H., Diaz-Meco, M.T., Gozzelino, R., [. . .], Comella, J.X. (2004). The death receptor antagonist FAIM promotes neurite outgrowth by a mechanism that depends on ERK and NF-kapp B signaling. *J Cell Biol* 167, 479-492.

Solier, S., Sordet, O., Kohn, K.W., and Pommier, Y. (2009). Death receptor-induced activation of the Chk2- and histone H2AX-associated DNA damage response pathways. *Mol Cell Biol* 29, 68-82.

Solov'yan, V.T., Andreev, I.O., Kolotova, T.Y., Pogribniy, P.V., Tarnavsky, D.T., and Kunakh, V.A. (1997). The cleavage of nuclear DNA into high molecular weight DNA fragments occurs not only during apoptosis but also accompanies changes in functional activity of the nonapoptotic cells. *Exp Cell Res* 235, 130-137.

Song, S., Tan, J., Miao, Y., and Zhang, Q. (2018). Crosstalk of ER stress-mediated autophagy and ER-phagy: Involvement of UPR and the core autophagy machinery. *J Cell Physiol* 233, 3867-3874.

Souers, A.J., Leverson, J.D., Boghaert, E.R., Ackler, S.L., Catron, N.D., Chen, J., [. . .], Elmore, S.W. (2013). ABT-199, a potent and selective BCL-2 inhibitor, achieves antitumor activity while sparing platelets. *Nat Med* 19, 202-208.

Spear, F.G., and Glücksmann, A. (1938). The Effect of Gamma Radiation on Cells in vivo Single Exposures of the Normal Tadpole at Room Temperature. *The British Journal of Radiology* 11, 533-553.

Spinelli, J.B., and Haigis, M.C. (2018). The multifaceted contributions of mitochondria to cellular metabolism. *Nat Cell Biol* 20, 745-754.

Srinivas, U.S., Tan, B.W.Q., Vellayappan, B.A., and Jeyasekharan, A.D. (2019). ROS and the DNA damage response in cancer. *Redox Biol* 25, 101084.

Srinivasula, S.M., Hegde, R., Saleh, A., Datta, P., Shiozaki, E., Chai, J., [. . .], Alnemri, E.S. (2001). A conserved XIAP-interaction motif in caspase-9 and Smac/DIABLO regulates caspase activity and apoptosis. *Nature* 410, 112-116.

Srivastava, A.K., and Padmanaban, G. (1987). Gossypol mediated DNA degradation. *Biochem Biophys Res Commun* 146, 1515-1522.

Stansbury, M.F., Cucullu, A.F., and Den Hartog, G.T. (1954). Cottonseed Contents Variation, Influence of Variety and Environment On Oil Content of Cottonseed Kernels. *Journal of Agricultural and Food Chemistry* 2, 692-696.

Stegh, A.H., Brennan, C., Mahoney, J.A., Forloney, K.L., Jenq, H.T., Luciano, J.P., [. . .], Depinho, R.A. (2010). Glioma oncoprotein Bcl2L12 inhibits the p53 tumor suppressor. *Genes Dev* 24, 2194-2204.

Stegh, A.H., Chin, L., Louis, D.N., and DePinho, R.A. (2008a). What drives intense apoptosis resistance and propensity for necrosis in glioblastoma? A role for Bcl2L12 as a multifunctional cell death regulator. *Cell Cycle* 7, 2833-2839.

Stegh, A.H., and DePinho, R.A. (2011). Beyond effector caspase inhibition: Bcl2L12 neutralizes p53 signaling in glioblastoma. *Cell Cycle* 10, 33-38.

Stegh, A.H., Kesari, S., Mahoney, J.E., Jenq, H.T., Forloney, K.L., Protopopov, A., [. . .], DePinho, R.A. (2008b). Bcl2L12-mediated inhibition of effector caspase-3 and caspase-7 via distinct mechanisms in glioblastoma. *Proc Natl Acad Sci U S A* 105, 10703-10708.

Stegh, A.H., Kim, H., Bachoo, R.M., Forloney, K.L., Zhang, J., Schulze, H., [. . .], Chin, L. (2007). Bcl2L12 inhibits post-mitochondrial apoptosis signaling in glioblastoma. *Genes Dev* 21, 98-111.

Stewart, C.L., Roux, K.J., and Burke, B. (2007). Blurring the boundary: the nuclear envelope extends its reach. *Science* 318, 1408-1412.

Stewart, L.A. (2002). Chemotherapy in adult high-grade glioma: a systematic review and meta-analysis of individual patient data from 12 randomised trials. *Lancet* 359, 1011-1018.

Stiff, T., Walker, S.A., Cerosaletti, K., Goodarzi, A.A., Petermann, E., Concannon, P., [. . .], Jeggo, P.A. (2006). ATR-dependent phosphorylation and activation of ATM in response to UV treatment or replication fork stalling. *EMBO J* 25, 5775-5782.

Stipanovic, R.D., Bell, A.A., and Howell, C.R. (1973). Spectral identification of the ketol tautomer of gossypol. *Journal of the American Oil Chemists' Society* 50, 462-463.

Stohr, D., Jeltsch, A., and Rehm, M. (2020). TRAIL receptor signaling: From the basics of canonical signal transduction toward its entanglement with ER stress and the unfolded protein response. *Int Rev Cell Mol Biol* 351, 57-99.

Stohs, S.J., and Bagchi, D. (1995). Oxidative mechanisms in the toxicity of metal ions. *Free Radic Biol Med* 18, 321-336.

Strasser, A., and Vaux, D.L. (2018). Viewing BCL2 and cell death control from an evolutionary perspective. *Cell Death Differ* 25, 13-20.

Stroh, C., and Schulze-Osthoff, K. (1998). Death by a thousand cuts: an ever increasing list of caspase substrates. *Cell Death Differ* 5, 997-1000.

Stummer, W., Pichlmeier, U., Meinel, T., Wiestler, O.D., Zanella, F., Reulen, H.J., and Group, A.L.-G.S. (2006). Fluorescence-guided surgery with 5-aminolevulinic acid for resection of malignant glioma: a randomised controlled multicentre phase III trial. *Lancet Oncol* 7, 392-401.

Stupp, R., Hegi, M.E., Mason, W.P., van den Bent, M.J., Taphoorn, M.J., Janzer, R.C., [. . .], National Cancer Institute of Canada Clinical Trials, G. (2009). Effects of radiotherapy with concomitant and adjuvant temozolomide versus radiotherapy alone on survival in glioblastoma in a randomised phase III study: 5-year analysis of the EORTC-NCIC trial. *Lancet Oncol* 10, 459-466.

Stupp, R., Mason, W.P., van den Bent, M.J., Weller, M., Fisher, B., Taphoorn, M.J., [. . .], National Cancer Institute of Canada Clinical Trials, G. (2005). Radiotherapy plus concomitant and adjuvant temozolomide for glioblastoma. *N Engl J Med* 352, 987-996.

Stupp, R., Taillibert, S., Kanner, A., Read, W., Steinberg, D., Lhermitte, B., [. . .], Ram, Z. (2017). Effect of Tumor-Treating Fields Plus Maintenance Temozolomide vs Maintenance Temozolomide Alone on Survival in Patients With Glioblastoma: A Randomized Clinical Trial. *JAMA* 318, 2306-2316.

Subburaj, Y., Cosentino, K., Axmann, M., Pedrueza-Villalmanzo, E., Hermann, E., Bleicken, S., [. . .], Garcia-Saez, A.J. (2015). Bax monomers form dimer units in the membrane that further self-assemble into multiple oligomeric species. *Nat Commun* 6, 8042.

Sullivan, G.P., O'Connor, H., Henry, C.M., Davidovich, P., Clancy, D.M., Albert, M.L., [. . .], Martin, S.J. (2020). TRAIL Receptors Serve as Stress-Associated Molecular Patterns to Promote ER-Stress-Induced Inflammation. *Dev Cell* 52, 714-730 e715.

Sun, C., Cai, M., Gunasekera, A.H., Meadows, R.P., Wang, H., Chen, J., [. . .], Fesik, S.W. (1999). NMR structure and mutagenesis of the inhibitor-of-apoptosis protein XIAP. *Nature* 401, 818-822.

Sun, L., Wang, H., Wang, Z., He, S., Chen, S., Liao, D., [. . .], Wang, X. (2012). Mixed lineage kinase domain-like protein mediates necrosis signaling downstream of RIP3 kinase. *Cell* 148, 213-227.

Sun, L., and Wang, X. (2014). A new kind of cell suicide: mechanisms and functions of programmed necrosis. *Trends Biochem Sci* 39, 587-593.

Sunaga, S., Kobayashi, T., Yoshimori, A., Shiokawa, D., and Tanuma, S. (2004). A novel inhibitor that protects apoptotic DNA fragmentation catalyzed by DNase gamma. *Biochem Biophys Res Commun* 325, 1292-1297.

Susin, S.A., Daugas, E., Ravagnan, L., Samejima, K., Zamzami, N., Loeffler, M., [. . .], Kroemer, G. (2000). Two distinct pathways leading to nuclear apoptosis. *J Exp Med* 192, 571-580.

Susin, S.A., Lorenzo, H.K., Zamzami, N., Marzo, I., Snow, B.E., Brothers, G.M., [. . .], Kroemer, G. (1999). Molecular characterization of mitochondrial apoptosis-inducing factor. *Nature* 397, 441-446.

Suzuki, Y., Nakabayashi, Y., and Takahashi, R. (2001). Ubiquitin-protein ligase activity of X-linked inhibitor of apoptosis protein promotes proteasomal degradation of caspase-3 and enhances its anti-apoptotic effect in Fas-induced cell death. *Proc Natl Acad Sci U S A* 98, 8662-8667.

Taimen, P., and Kallajoki, M. (2003). NuMA and nuclear lamins behave differently in Fas-mediated apoptosis. *J Cell Sci* 116, 571-583.

Tait, S.W., and Green, D.R. (2012). Mitochondria and cell signalling. *J Cell Sci* 125, 807-815.

Tait, S.W., and Green, D.R. (2013). Mitochondrial regulation of cell death. *Cold Spring Harb Perspect Biol* 5.

Tait, S.W., Oberst, A., Quarato, G., Milasta, S., Haller, M., Wang, R., [. . .], Green, D.R. (2013). Widespread mitochondrial depletion via mitophagy does not compromise necroptosis. *Cell Rep* 5, 878-885.

Takada, S., Watanabe, T., and Mizuta, R. (2020). DNase gamma-dependent DNA fragmentation causes karyolysis in necrotic hepatocyte. *J Vet Med Sci* 82, 23-26.

Takahashi, Y., Coppola, D., Matsushita, N., Cualing, H.D., Sun, M., Sato, Y., [. . .], Wang, H.G. (2007). Bif-1 interacts with Beclin 1 through UVRAG and regulates autophagy and tumorigenesis. *Nat Cell Biol* 9, 1142-1151.

Talanian, R.V., Quinlan, C., Trautz, S., Hackett, M.C., Mankovich, J.A., Banach, D., [. . .], Wong, W.W. (1997). Substrate specificities of caspase family proteases. *J Biol Chem* 272, 9677-9682.

Tang, D., Kang, R., Berghe, T.V., Vandenabeele, P., and Kroemer, G. (2019). The molecular machinery of regulated cell death. *Cell Res* 29, 347-364.

Tang, D., and Kidd, V.J. (1998). Cleavage of DFF-45/ICAD by multiple caspases is essential for its function during apoptosis. *J Biol Chem* 273, 28549-28552.

Tanphaichitr, N., Namking, M., Tupper, S., Hansen, C., and Wong, P.T.T. (1995). Gossypol effects on the structure and dynamics of phospholipid bilayers: A FT-IR study. *Chemistry and Physics of Lipids* 75, 119-125.

Tavakol, S., Ashrafizadeh, M., Deng, S., Azarian, M., Abdoli, A., Motavaf, M., [. . .], Kumar, A.P. (2019). Autophagy Modulators: Mechanistic Aspects and Drug Delivery Systems. *Biomolecules* 9.

Taylor, R.C., Cullen, S.P., and Martin, S.J. (2008). Apoptosis: controlled demolition at the cellular level. *Nat Rev Mol Cell Biol* 9, 231-241.

Tenev, T., Bianchi, K., Darding, M., Broemer, M., Langlais, C., Wallberg, F., [. . .], Meier, P. (2011). The Ripoptosome, a signaling platform that assembles in response to genotoxic stress and loss of IAPs. *Mol Cell* 43, 432-448.

Thomas, G.E.C., Leyland, L.A., Schrag, A.E., Lees, A.J., Acosta-Cabronero, J., and Weil, R.S. (2020). Brain iron deposition is linked with cognitive severity in Parkinson's disease. *J Neurol Neurosurg Psychiatry* 91, 418-425.

Thornberry, N.A., Bull, H.G., Calaycay, J.R., Chapman, K.T., Howard, A.D., Kostura, M.J., [. . .], et al. (1992). A novel heterodimeric cysteine protease is required for interleukin-1 beta processing in monocytes. *Nature* 356, 768-774.

Tinel, A., Janssens, S., Lippens, S., Cuenin, S., Logette, E., Jaccard, B., [. . .], Tschopp, J. (2007). Autoproteolysis of PIDD marks the bifurcation between pro-death caspase-2 and pro-survival NF-kappaB pathway. *EMBO J* 26, 197-208.

Todt, F., Cakir, Z., Reichenbach, F., Emschermann, F., Lauterwasser, J., Kaiser, A., [. . .], Edlich, F. (2015). Differential retrotranslocation of mitochondrial Bax and Bak. *EMBO J* 34, 67-80.

Tone, S., Sugimoto, K., Tanda, K., Suda, T., Uehira, K., Kanouchi, H., [. . .], Earnshaw, W.C. (2007). Three distinct stages of apoptotic nuclear condensation revealed by time-lapse imaging, biochemical and electron microscopy analysis of cell-free apoptosis. *Exp Cell Res* 313, 3635-3644.

Torti, S.V., and Torti, F.M. (2020). Iron: The cancer connection. *Mol Aspects Med*, 100860.

Travassos, L.H., Vasconcellos, L.R., Bozza, M.T., and Carneiro, L.A. (2017). Heme and iron induce protein aggregation. *Autophagy* 13, 625-626.

Trudel, S., Li, Z.H., Rauw, J., Tiedemann, R.E., Wen, X.Y., and Stewart, A.K. (2007). Preclinical studies of the pan-Bcl inhibitor obatoclax (GX015-070) in multiple myeloma. *Blood* 109, 5430-5438.

Tsapras, P., and Nezis, I.P. (2017). Caspase involvement in autophagy. *Cell Death Differ* 24, 1369-1379.

Tse, C., Shoemaker, A.R., Adickes, J., Anderson, M.G., Chen, J., Jin, S., [. . .], Elmore, S.W. (2008). ABT-263: a potent and orally bioavailable Bcl-2 family inhibitor. *Cancer Res* 68, 3421-3428.

Tsujimoto, Y., Cossman, J., Jaffe, E., and Croce, C.M. (1985). Involvement of the bcl-2 gene in human follicular lymphoma. *Science* 228, 1440-1443.

Tsukada, M., and Ohsumi, Y. (1993). Isolation and characterization of autophagy-defective mutants of Saccharomyces cerevisiae. *FEBS Lett* 333, 169-174.

Tummers, B., and Green, D.R. (2017). Caspase-8: regulating life and death. *Immunol Rev* 277, 76-89.

Ueno, H., Sahni, M.K., Segal, S.J., and Koide, S.S. (1988). Interaction of gossypol with sperm macromolecules and enzymes. *Contraception* 37, 333-341.

Vahsen, N., Cande, C., Briere, J.J., Benit, P., Joza, N., Larochette, N., [. . .], Kroemer, G. (2004). AIF deficiency compromises oxidative phosphorylation. *EMBO J* 23, 4679-4689.

van Deursen, J.M. (2014). The role of senescent cells in ageing. *Nature* 509, 439-446.

Vanags, D.M., Porn-Ares, M.I., Coppola, S., Burgess, D.H., and Orrenius, S. (1996). Protease involvement in fodrin cleavage and phosphatidylserine exposure in apoptosis. *J Biol Chem* 271, 31075-31085.

Vandenabeele, P., Declercq, W., Van Herreweghe, F., and Vanden Berghe, T. (2010). The role of the kinases RIP1 and RIP3 in TNF-induced necrosis. *Sci Signal* 3, re4.

Varadarajan, S., Bampton, E.T., Smalley, J.L., Tanaka, K., Caves, R.E., Butterworth, M., [. . .], Cohen, G.M. (2012). A novel cellular stress response characterised by a rapid reorganisation of membranes of the endoplasmic reticulum. *Cell Death Differ* 19, 1896-1907.

Varfolomeev, E., Goncharov, T., Fedorova, A.V., Dynek, J.N., Zobel, K., Deshayes, K., [. . .], Vucic, D. (2008). c-IAP1 and c-IAP2 are critical mediators of tumor necrosis factor alpha (TNFalpha)-induced NF-kappaB activation. *J Biol Chem* 283, 24295-24299.

Vasconcellos, L.R., Dutra, F.F., Siqueira, M.S., Paula-Neto, H.A., Dahan, J., Kiarely, E., [. . .], Travassos, L.H. (2016). Protein aggregation as a cellular response to oxidative stress induced by heme and iron. *Proc Natl Acad Sci U S A* 113, E7474-E7482.

Vaseva, A.V., and Moll, U.M. (2009). The mitochondrial p53 pathway. *Biochim Biophys Acta* 1787, 414-420.

Verhagen, A.M., Ekert, P.G., Pakusch, M., Silke, J., Connolly, L.M., Reid, G.E., [. . .], Vaux, D.L. (2000). Identification of DIABLO, a mammalian protein that promotes apoptosis by binding to and antagonizing IAP proteins. *Cell* 102, 43-53.

Villunger, A., Michalak, E.M., Coultas, L., Mullauer, F., Bock, G., Ausserlechner, M.J., [. . .], Strasser, A. (2003). p53- and drug-induced apoptotic responses mediated by BH3-only proteins puma and noxa. *Science* 302, 1036-1038.

Virag, L., Robaszkiewicz, A., Rodriguez-Vargas, J.M., and Oliver, F.J. (2013). Poly(ADP-ribose) signaling in cell death. *Mol Aspects Med* 34, 1153-1167.

Vitale, I., Galluzzi, L., Castedo, M., and Kroemer, G. (2011). Mitotic catastrophe: a mechanism for avoiding genomic instability. *Nat Rev Mol Cell Biol* 12, 385-392.

Vogler, M., Weber, K., Dinsdale, D., Schmitz, I., Schulze-Osthoff, K., Dyer, M.J., and Cohen, G.M. (2009). Different forms of cell death induced by putative BCL2 inhibitors. *Cell Death Differ* 16, 1030-1039.

Vogt, K.C. (1842). Untersuchungen über die Entwicklungsgeschichte der Geburtshelferkröte (Alytes obstetricans) (Jent & Gassmann).

von Karstedt, S., Montinaro, A., and Walczak, H. (2017). Exploring the TRAILs less travelled: TRAIL in cancer biology and therapy. *Nat Rev Cancer* 17, 352-366.

Voss, V., Senft, C., Lang, V., Ronellenfitsch, M.W., Steinbach, J.P., Seifert, V., and Kogel, D. (2010). The pan-Bcl-2 inhibitor (-)-gossypol triggers autophagic cell death in malignant glioma. *Mol Cancer Res* 8, 1002-1016.

Vostinar, A.E., Goldsby, H.J., and Ofria, C. (2019). Suicidal selection: Programmed cell death can evolve in unicellular organisms due solely to kin selection. *Ecol Evol* 9, 9129-9136.

Vu, H.T., Kobayashi, M., Hegazy, A.M., Tadokoro, Y., Ueno, M., Kasahara, A., [. . .], Hirao, A. (2018). Autophagy inhibition synergizes with calcium mobilization to achieve efficient therapy of malignant gliomas. *Cancer Sci* 109, 2497-2508.

Wagenknecht, B., Glaser, T., Naumann, U., Kugler, S., Isenmann, S., Bahr, M., [. . .], Weller, M. (1999). Expression and biological activity of X-linked inhibitor of apoptosis (XIAP) in human malignant glioma. *Cell Death Differ* 6, 370-376.

Wajant, H. (2002). The Fas signaling pathway: more than a paradigm. *Science* 296, 1635-1636.

Walker, M.D., Alexander, E., Jr., Hunt, W.E., MacCarty, C.S., Mahaley, M.S., Jr., Mealey, J., Jr., [. . .], Strike, T.A. (1978). Evaluation of BCNU and/or radiotherapy in the treatment of anaplastic gliomas. A cooperative clinical trial. *J Neurosurg* 49, 333-343.

Walker, N.P., Talanian, R.V., Brady, K.D., Dang, L.C., Bump, N.J., Ferenz, C.R., [. . .], et al. (1994). Crystal structure of the cysteine protease interleukin-1 beta-converting enzyme: a (p20/p10)2 homodimer. *Cell* 78, 343-352.

Walker, P.R., Leblanc, J., Carson, C., Ribecco, M., and Sikorska, M. (1999). Neither caspase-3 nor DNA fragmentation factor is required for high molecular weight DNA degradation in apoptosis. *Ann N Y Acad Sci* 887, 48-59.

Walsh, J.G., Cullen, S.P., Sheridan, C., Luthi, A.U., Gerner, C., and Martin, S.J. (2008). Executioner caspase-3 and caspase-7 are functionally distinct proteases. *Proc Natl Acad Sci U S A* 105, 12815-12819.

Wandzilak, A., Czyzycki, M., Wrobel, P., Szczerbowska-Boruchowska, M., Radwanska, E., Adamek, D., and Lankosz, M. (2013). The oxidation states and chemical environments of iron and zinc as potential indicators of brain tumour malignancy grade - preliminary results. *Metallomics* 5, 1547-1553.

Wang, C.Y., Mayo, M.W., and Baldwin, A.S., Jr. (1996). TNF- and cancer therapy-induced apoptosis: potentiation by inhibition of NF-kappaB. *Science* 274, 784-787.

Wang, J.L., Liu, D., Zhang, Z.J., Shan, S., Han, X., Srinivasula, S.M., [. . .], Huang, Z. (2000). Structure-based discovery of an organic compound that binds Bcl-2 protein and induces apoptosis of tumor cells. *Proc Natl Acad Sci U S A* 97, 7124-7129.

Wang, L., Chang, X., Feng, J., Yu, J., and Chen, G. (2019a). TRADD Mediates RIPK1-Independent Necroptosis Induced by Tumor Necrosis Factor. *Front Cell Dev Biol* 7, 393.

Wang, L., Du, F., and Wang, X. (2008a). TNF-alpha induces two distinct caspase-8 activation pathways. *Cell* 133, 693-703.

Wang, L., Liu, Y., Zhang, Y., Yasin, A., and Zhang, L. (2019b). Investigating Stability and Tautomerization of Gossypol-A Spectroscopy Study. *Molecules* 24.

Wang, X., Beckham, T.H., Morris, J.C., Chen, F., and Gangemi, J.D. (2008b). Bioactivities of gossypol, 6-methoxygossypol, and 6,6'-dimethoxygossypol. *J Agric Food Chem* 56, 4393-4398.

Wang, X., Howell, C.P., Chen, F., Yin, J., and Jiang, Y. (2009). Gossypol--a polyphenolic compound from cotton plant. *Adv Food Nutr Res* 58, 215-263.

Wang, Y., Gao, W., Shi, X., Ding, J., Liu, W., He, H., [. . .], Shao, F. (2017). Chemotherapy drugs induce pyroptosis through caspase-3 cleavage of a gasdermin. *Nature* 547, 99-103.

Wang, Z., Jiang, H., Chen, S., Du, F., and Wang, X. (2012). The mitochondrial phosphatase PGAM5 functions at the convergence point of multiple necrotic death pathways. *Cell* 148, 228-243.

Ward, R.J., Zucca, F.A., Duyn, J.H., Crichton, R.R., and Zecca, L. (2014). The role of iron in brain ageing and neurodegenerative disorders. *Lancet Neurol* 13, 1045-1060.

Warnsmann, V., Meyer, N., Hamann, A., Kogel, D., and Osiewacz, H.D. (2018). A novel role of the mitochondrial permeability transition pore in (-)-gossypol-induced mitochondrial dysfunction. *Mech Ageing Dev* 170, 45-58.

Watanabe, T., Takada, S., and Mizuta, R. (2019). Cell-free DNA in blood circulation is generated by DNase1L3 and caspase-activated DNase. *Biochem Biophys Res Commun* 516, 790-795.

Waterhouse, N.J., Finucane, D.M., Green, D.R., Elce, J.S., Kumar, S., Alnemri, E.S., [. . .], Watters, D.J. (1998). Calpain activation is upstream of caspases in radiation-induced apoptosis. *Cell Death Differ* 5, 1051-1061.

Wei, M.C., Zong, W.X., Cheng, E.H., Lindsten, T., Panoutsakopoulou, V., Ross, A.J., [. . .], Korsmeyer, S.J. (2001). Proapoptotic BAX and BAK: a requisite gateway to mitochondrial dysfunction and death. *Science* 292, 727-730.

Weir, A.F. (1993). Deoxyribonuclease I (EC 3.1.21.1) and II (EC 3.1.22.1). *Methods Mol Biol* 16, 7-16.

Weller, M., Pfister, S.M., Wick, W., Hegi, M.E., Reifenberger, G., and Stupp, R. (2013). Molecular neuro-oncology in clinical practice: a new horizon. *Lancet Oncol* 14, e370-379.

Weller, M., van den Bent, M., Tonn, J.C., Stupp, R., Preusser, M., Cohen-Jonathan-Moyal, E., [. . .], European Association for Neuro-Oncology Task Force on, G. (2017). European Association for Neuro-Oncology (EANO) guideline on the diagnosis and treatment of adult astrocytic and oligodendroglial gliomas. *Lancet Oncol* 18, e315-e329.

Wick, W. (2016). TTFields: where does all the skepticism come from? *Neuro Oncol* 18, 303-305.

Widlak, P. (2000). The DFF40/CAD endonuclease and its role in apoptosis. *Acta Biochim Pol* 47, 1037-1044.

Widlak, P., and Garrard, W.T. (2001). Ionic and cofactor requirements for the activity of the apoptotic endonuclease DFF40/CAD. *Mol Cell Biochem* 218, 125-130.

Widlak, P., and Garrard, W.T. (2005). Discovery, regulation, and action of the major apoptotic nucleases DFF40/CAD and endonuclease G. *J Cell Biochem* 94, 1078-1087.

Widlak, P., and Garrard, W.T. (2006). The apoptotic endonuclease DFF40/CAD is inhibited by RNA, heparin and other polyanions. *Apoptosis* 11, 1331-1337.

Widlak, P., and Garrard, W.T. (2009). Roles of the major apoptotic nuclease-DNA fragmentation factor-in biology and disease. *Cell Mol Life Sci* 66, 263-274.

Widlak, P., Li, L.Y., Wang, X., and Garrard, W.T. (2001). Action of recombinant human apoptotic endonuclease G on naked DNA and chromatin substrates: cooperation with exonuclease and DNase I. *J Biol Chem* 276, 48404-48409.

Widlak, P., Li, P., Wang, X., and Garrard, W.T. (2000). Cleavage preferences of the apoptotic endonuclease DFF40 (caspase-activated DNase or nuclease) on naked DNA and chromatin substrates. *J Biol Chem* 275, 8226-8232.

Widlak, P., Palyvoda, O., Kumala, S., and Garrard, W.T. (2002). Modeling apoptotic chromatin condensation in normal cell nuclei. Requirement for intranuclear mobility and actin involvement. *J Biol Chem* 277, 21683-21690.

Wilkie, G.S., Korfali, N., Swanson, S.K., Malik, P., Srsen, V., Batrakou, D.G., [. . .], Schirmer, E.C. (2011). Several novel nuclear envelope transmembrane proteins identified in skeletal muscle have cytoskeletal associations. *Mol Cell Proteomics* 10, M110 003129.

Wilson, K.P., Black, J.A., Thomson, J.A., Kim, E.E., Griffith, J.P., Navia, M.A., [. . .], et al. (1994). Structure and mechanism of interleukin-1 beta converting enzyme. *Nature* 370, 270-275.

Withers, W., and Carruth, F.E. (1916). Gossypol, A Toxic Substance in the Cottonseed. *Journal of Association of Official Agricultural Chemists* 2, 35-35.

Withers, W., and Carruth, F.E. (1917). Iron as an antidote to cottonseed meal injury. *Journal of Biological Chemistry* 32, 245-257.

Woo, E.J., Kim, Y.G., Kim, M.S., Han, W.D., Shin, S., Robinson, H., [. . .], Oh, B.H. (2004). Structural mechanism for inactivation and activation of CAD/DFF40 in the apoptotic pathway. *Mol Cell* 14, 531-539.

Wu, Y.C., Stanfield, G.M., and Horvitz, H.R. (2000). NUC-1, a caenorhabditis elegans DNase II homolog, functions in an intermediate step of DNA degradation during apoptosis. *Genes Dev* 14, 536-548.

Wu, Y.T., Tan, H.L., Shui, G., Bauvy, C., Huang, Q., Wenk, M.R., [. . .], Shen, H.M. (2010). Dual role of 3-methyladenine in modulation of autophagy via different temporal patterns of inhibition on class I and III phosphoinositide 3-kinase. *J Biol Chem* 285, 10850-10861.

Wu, Y.W., Chik, C.L., and Knazek, R.A. (1989). An in vitro and in vivo study of antitumor effects of gossypol on human SW-13 adrenocortical carcinoma. *Cancer Res* 49, 3754-3758.

Wyllie, A.H. (1980). Glucocorticoid-induced thymocyte apoptosis is associated with endogenous endonuclease activation. *Nature* 284, 555-556.

Xia, B., Fang, S., Chen, X., Hu, H., Chen, P., Wang, H., and Gao, Z. (2016). MLKL forms cation channels. *Cell Res* 26, 517-528.

Yakovlev, A.G., Wang, G., Stoica, B.A., Boulares, H.A., Spoonde, A.Y., Yoshihara, K., and Smulson, M.E. (2000). A role of the Ca2+/Mg2+-dependent endonuclease in apoptosis and its inhibition by Poly(ADP-ribose) polymerase. *J Biol Chem* 275, 21302-21308.

Yamada, T., Ohyama, H., Kinjo, Y., and Watanabe, M. (1981). Evidence for the internucleosomal breakage of chromatin in rat thymocytes irradiated in vitro. *Radiat Res* 85, 544-553.

Yamamoto, A., Shin, R.W., Hasegawa, K., Naiki, H., Sato, H., Yoshimasu, F., and Kitamoto, T. (2002). Iron (III) induces aggregation of hyperphosphorylated tau and its reduction to iron (II) reverses the

aggregation: implications in the formation of neurofibrillary tangles of Alzheimer's disease. *J Neurochem* 82, 1137-1147.

Yamamoto, A., Tagawa, Y., Yoshimori, T., Moriyama, Y., Masaki, R., and Tashiro, Y. (1998). Bafilomycin A1 prevents maturation of autophagic vacuoles by inhibiting fusion between autophagosomes and lysosomes in rat hepatoma cell line, H-4-II-E cells. *Cell Struct Funct* 23, 33-42.

Yan, B., Wang, H., Peng, Y., Hu, Y., Wang, H., Zhang, X., [. . .], Li, C.Y. (2006a). A unique role of the DNA fragmentation factor in maintaining genomic stability. *Proc Natl Acad Sci U S A* 103, 1504-1509.

Yan, B., Wang, H., Wang, H., Zhuo, D., Li, F., Kon, T., [. . .], Li, C.Y. (2006b). Apoptotic DNA fragmentation factor maintains chromosome stability in a P53-independent manner. *Oncogene* 25, 5370-5376.

Yan, B., Wang, H., Xie, D., Wakamatsu, N., Anscher, M.S., Dewhirst, M.W., [. . .], Li, C.Y. (2009). Increased skin carcinogenesis in caspase-activated DNase knockout mice. *Carcinogenesis* 30, 1776-1780.

Yang, S., Wang, X., Contino, G., Liesa, M., Sahin, E., Ying, H., [. . .], Kimmelman, A.C. (2011). Pancreatic cancers require autophagy for tumor growth. *Genes Dev* 25, 717-729.

Yang, Y., Fang, S., Jensen, J.P., Weissman, A.M., and Ashwell, J.D. (2000). Ubiquitin protein ligase activity of IAPs and their degradation in proteasomes in response to apoptotic stimuli. *Science* 288, 874-877.

Yang, Z., and Klionsky, D.J. (2010). Eaten alive: a history of macroautophagy. *Nat Cell Biol* 12, 814-822.

Yang, Z., Wang, Y., Zhang, Y., He, X., Zhong, C.Q., Ni, H., [. . .], Han, J. (2018). RIP3 targets pyruvate dehydrogenase complex to increase aerobic respiration in TNF-induced necroptosis. *Nat Cell Biol* 20, 186-197.

Ye, H., Cande, C., Stephanou, N.C., Jiang, S., Gurbuxani, S., Larochette, N., [. . .], Wu, H. (2002). DNA binding is required for the apoptogenic action of apoptosis inducing factor. *Nat Struct Biol* 9, 680-684.

Ye, X., Zhou, X.J., and Zhang, H. (2018). Exploring the Role of Autophagy-Related Gene 5 (ATG5) Yields Important Insights Into Autophagy in Autoimmune/Autoinflammatory Diseases. *Front Immunol* 9, 2334.

Yeaney, G.A., and Brat, D.J. (2019). What Every Neuropathologist Needs to Know: Update on cIMPACT-NOW. *J Neuropathol Exp Neurol* 78, 294-296.

Yedida, G., Milani, M., Cohen, G.M., and Varadarajan, S. (2019). Apogossypol-mediated reorganisation of the endoplasmic reticulum antagonises mitochondrial fission and apoptosis. *Cell Death Dis* 10, 521.

Yeh, W.C., Itie, A., Elia, A.J., Ng, M., Shu, H.B., Wakeham, A., [. . .], Mak, T.W. (2000). Requirement for Casper (c-FLIP) in regulation of death receptor-induced apoptosis and embryonic development. *Immunity* 12, 633-642.

Yiu, H.H., Bouffier, L., Boldrin, P., Long, J., Claridge, J.B., and Rosseinsky, M.J. (2013). Comprehensive study of DNA binding on iron (II,III) oxide nanoparticles with a positively charged polyamine three-dimensional coating. *Langmuir* 29, 11354-11365.

Yoshii, S.R., and Mizushima, N. (2017). Monitoring and Measuring Autophagy. *Int J Mol Sci* 18.

Young, A.R., Chan, E.Y., Hu, X.W., Kochl, R., Crawshaw, S.G., High, S., [. . .], Tooze, S.A. (2006). Starvation and ULK1-dependent cycling of mammalian Atg9 between the TGN and endosomes. *J Cell Sci* 119, 3888-3900.

Young, M.M., Takahashi, Y., Khan, O., Park, S., Hori, T., Yun, J., [. . .], Wang, H.G. (2012). Autophagosomal membrane serves as platform for intracellular death-inducing signaling complex (iDISC)-mediated caspase-8 activation and apoptosis. *J Biol Chem* 287, 12455-12468.

Yousefi, S., Perozzo, R., Schmid, I., Ziemiecki, A., Schaffner, T., Scapozza, L., [. . .], Simon, H.U. (2006). Calpain-mediated cleavage of Atg5 switches autophagy to apoptosis. *Nat Cell Biol* 8, 1124-1132.

Yuan, H.X., Russell, R.C., and Guan, K.L. (2013). Regulation of PIK3C3/VPS34 complexes by MTOR in nutrient stress-induced autophagy. *Autophagy* 9, 1983-1995.

Yuan, J., Shaham, S., Ledoux, S., Ellis, H.M., and Horvitz, H.R. (1993). The C. elegans cell death gene ced-3 encodes a protein similar to mammalian interleukin-1 beta-converting enzyme. *Cell* 75, 641-652.

Yuste, V.J., Bayascas, J.R., Llecha, N., Sanchez-Lopez, I., Boix, J., and Comella, J.X. (2001). The absence of oligonucleosomal DNA fragmentation during apoptosis of IMR-5 neuroblastoma cells: disappearance of the caspase-activated DNase. *J Biol Chem* 276, 22323-22331.

Yuste, V.J., Moubarak, R.S., Delettre, C., Bras, M., Sancho, P., Robert, N., [. . .], Susin, S.A. (2005a). Cysteine protease inhibition prevents mitochondrial apoptosis-inducing factor (AIF) release. *Cell Death Differ* 12, 1445-1448.

Yuste, V.J., Sanchez-Lopez, I., Sole, C., Moubarak, R.S., Bayascas, J.R., Dolcet, X., [. . .], Comella, J.X. (2005b). The contribution of apoptosis-inducing factor, caspase-activated DNase, and inhibitor of caspase-activated DNase to the nuclear phenotype and DNA degradation during apoptosis. *J Biol Chem* 280, 35670-35683.

Zaidi, R., and Hadi, S.M. (1992a). Complexes involving gossypol, DNA and Cu(II). *Biochem Int* 28, 1135-1143.

Zaidi, R., and Hadi, S.M. (1992b). Interaction of gossypol with DNA. *Toxicol In Vitro* 6, 71-76.

Zaidi, R., and Hadi, S.M. (1992c). Strand scission in DNA by gossypol and Cu(II): role of Cu(I) and oxygen-free radicals. *J Biochem Toxicol* 7, 213-217.

Zamorano, S., Rojas-Rivera, D., Lisbona, F., Parra, V., Court, F.A., Villegas, R., [. . .], Hetz, C. (2012). A BAX/BAK and cyclophilin D-independent intrinsic apoptosis pathway. *PLoS One* 7, e37782.

Zamzami, N., Marchetti, P., Castedo, M., Decaudin, D., Macho, A., Hirsch, T., [. . .], Kroemer, G. (1995a). Sequential reduction of mitochondrial transmembrane potential and generation of reactive oxygen species in early programmed cell death. *J Exp Med* 182, 367-377.

Zamzami, N., Marchetti, P., Castedo, M., Zanin, C., Vayssiere, J.L., Petit, P.X., and Kroemer, G. (1995b). Reduction in mitochondrial potential constitutes an early irreversible step of programmed lymphocyte death in vivo. *J Exp Med* 181, 1661-1672.

Zawlik, I., Kita, D., Vaccarella, S., Mittelbronn, M., Franceschi, S., and Ohgaki, H. (2009). Common polymorphisms in the MDM2 and TP53 genes and the relationship between TP53 mutations and patient outcomes in glioblastomas. *Brain Pathol* 19, 188-194.

Zeitlin, B.D., Joo, E., Dong, Z., Warner, K., Wang, G., Nikolovska-Coleska, Z., [. . .], Nor, J.E. (2006). Antiangiogenic effect of TW37, a small-molecule inhibitor of Bcl-2. *Cancer Res* 66, 8698-8706.

Zhai, D., Jin, C., Satterthwait, A.C., and Reed, J.C. (2006). Comparison of chemical inhibitors of antiapoptotic Bcl-2-family proteins. *Cell Death Differ* 13, 1419-1421.

Zhang, G., Wang, Z., Chen, W., Cao, Y., Wu, J., Qiang, G., [. . .], Jiang, C. (2019a). Dual effects of gossypol on human hepatocellular carcinoma via endoplasmic reticulum stress and autophagy. *Int J Biochem Cell Biol* 113, 48-57.

Zhang, J., Liu, X., Scherer, D.C., van Kaer, L., Wang, X., and Xu, M. (1998). Resistance to DNA fragmentation and chromatin condensation in mice lacking the DNA fragmentation factor 45. *Proc Natl Acad Sci U S A* 95, 12480-12485.

Zhang, J., Ran, H., Xiong, W., Yang, T., Mei, Y., He, D., [. . .], Song, G. (2019b). Structures of Complexes of Gossypol with Ferrous Sulfate Based on High-Performance Liquid Chromatography Separation, Spectroscopic Analysis, and PM3 calculations. *ChemistrySelect* 4, 5484-5488.

Zhang, J., and Xu, M. (2002). Apoptotic DNA fragmentation and tissue homeostasis. *Trends Cell Biol* 12, 84-89.

Zhang, L., Jiang, H., Cao, X., Zhao, H., Wang, F., Cui, Y., and Jiang, B. (2009). Chiral gossypol derivatives: evaluation of their anticancer activity and molecular modeling. *Eur J Med Chem* 44, 3961-3972.

Zhang, M., Liu, H., Guo, R., Ling, Y., Wu, X., Li, B., [. . .], Yang, D. (2003). Molecular mechanism of gossypol-induced cell growth inhibition and cell death of HT-29 human colon carcinoma cells. *Biochem Pharmacol* 66, 93-103.

Zhang, M., Liu, H., Tian, Z., Griffith, B.N., Ji, M., and Li, Q.Q. (2007). Gossypol induces apoptosis in human PC-3 prostate cancer cells by modulating caspase-dependent and caspase-independent cell death pathways. *Life Sci* 80, 767-774.

Zhang, Y., Su, S.S., Zhao, S., Yang, Z., Zhong, C.Q., Chen, X., [. . .], Han, J. (2017). RIP1 autophosphorylation is promoted by mitochondrial ROS and is essential for RIP3 recruitment into necrosome. *Nat Commun* 8, 14329.

Zhang, Z., Singh, R., and Aschner, M. (2016). Methods for the Detection of Autophagy in Mammalian Cells. *Curr Protoc Toxicol* 69, 20 12 21-20 12 26.

Zhivotovsky, B.D., Zvonareva, N.B., and Hanson, K.P. (1981). Characteristics of rat thymus chromatin degradation products after whole-body x-irradiation. *Int J Radiat Biol Relat Stud Phys Chem Med* 39, 437-440.

Zhou, P., Lugovskoy, A.A., McCarty, J.S., Li, P., and Wagner, G. (2001). Solution structure of DFF40 and DFF45 N-terminal domain complex and mutual chaperone activity of DFF40 and DFF45. *Proc Natl Acad Sci U S A* 98, 6051-6055.

Zhou, Q., and Salvesen, G.S. (2000). Viral caspase inhibitors CrmA and p35. *Methods Enzymol* 322, 143-154.

Zhou, Q., Snipas, S., Orth, K., Muzio, M., Dixit, V.M., and Salvesen, G.S. (1997). Target protease specificity of the viral serpin CrmA. Analysis of five caspases. *J Biol Chem* 272, 7797-7800.

Zhou, R.H., and Lin, X.D. (1988). Isolation of (-)-gossypol from natural plant. *Contraception* 37, 239-245.

Zhu, C., Wang, X., Deinum, J., Huang, Z., Gao, J., Modjtahedi, N., [. . .], Blomgren, K. (2007). Cyclophilin A participates in the nuclear translocation of apoptosis-inducing factor in neurons after cerebral hypoxia-ischemia. *J Exp Med* 204, 1741-1748.

Zhu, Y., Zhao, L., Liu, L., Gao, P., Tian, W., Wang, X., [. . .], Chen, Q. (2010). Beclin 1 cleavage by caspase-3 inactivates autophagy and promotes apoptosis. *Protein Cell* 1, 468-477.

Zhuang, W., Li, B., Long, L., Chen, L., Huang, Q., and Liang, Z. (2011). Induction of autophagy promotes differentiation of glioma-initiating cells and their radiosensitivity. *Int J Cancer* 129, 2720-2731.

Zitvogel, L., Apetoh, L., Ghiringhelli, F., and Kroemer, G. (2008). Immunological aspects of cancer chemotherapy. *Nat Rev Immunol* 8, 59-73.

Zitvogel, L., Casares, N., Pequignot, M.O., Chaput, N., Albert, M.L., and Kroemer, G. (2004). Immune response against dying tumor cells. *Adv Immunol* 84, 131-179.

Zou, W., Yan, M., Xu, W., Huo, H., Sun, L., Zheng, Z., and Liu, X. (2001). Cobalt chloride induces PC12 cells apoptosis through reactive oxygen species and accompanied by AP-1 activation. *J Neurosci Res* 64, 646-653.

Zou, W., Zeng, J., Zhuo, M., Xu, W., Sun, L., Wang, J., and Liu, X. (2002). Involvement of caspase-3 and p38 mitogen-activated protein kinase in cobalt chloride-induced apoptosis in PC12 cells. *J Neurosci Res* 67, 837-843.

Zubair, H., Khan, H.Y., Ullah, M.F., Ahmad, A., Wu, D., and Hadi, S.M. (2012). Apogossypolone, derivative of gossypol, mobilizes endogenous copper in human peripheral lymphocytes leading to oxidative DNA breakage. *Eur J Pharm Sci* 47, 280-286.

Zuleger, N., Boyle, S., Kelly, D.A., de las Heras, J.I., Lazou, V., Korfali, N., [. . .], Schirmer, E.C. (2013). Specific nuclear envelope transmembrane proteins can promote the location of chromosomes to and from the nuclear periphery. *Genome Biol* 14, R14.

ANNEX: Ph.D. program activities

In this section are indicated some of the training activities performed during the training period of the Ph.D. program in Biochemistry, Molecular Biology and Biomedicine (academic years from 2015 to 2020).

1. Conference presentations

Authors: **Laura Martínez-Escardó**, María Sánchez-Osuna, Pilar Baldominos, Jordi Bruna and Victor J. Yuste
Title: "Temozolomide does not improve γ-irradiation-triggered caspase-dependent cell death in glioblastoma-derived human cells"
Participation: Oral and Poster (P01r-3)
Congress: *XXXIX Congreso SEBBM. Congreso anual de la Sociedad Española de Bioquímica y Biología Molecular*
Place: Salamanca, Spain
Date: 5th – 8th September 2016

Authors: Pilar Baldominos, **Laura Martínez-Escardó**, Victor J. Yuste
Title: "Characterization of the release of histones in glioblastoma-derived cells after cytotoxic insult and its relationship with the apoptotic endonuclease DFF40/CAD"
Participation: Poster (P01-10)
Congress: *XXXIX Congreso SEBBM. Congreso anual de la Sociedad Española de Bioquímica y Biología Molecular*
Place: Salamanca, Spain
Date: 5th – 8th September 2016

Authors: Lucía Villamañán, **Laura Martínez-Escardó**, Victor J. Yuste, Carles Arús, Ana Paula Candiota
Title: "Elucidating the mechanism of action of temozolomide in GL261 glioma cells"
Participation: Poster (P3-06)
Congress: *XIV Jornada Científica del Departament de Bioquímica i Biologia Molecular*
Place: Universitat Autònoma de Barcelona, Barcelona
Date: 6th June 2017

Authors: Pablo Subías; **Laura Martínez-Escardó,** Victor J. Yuste; Enrique Claro
Title: "Long chain acyl-CoA synthetases (ACSL) as antitumor targets. Their role in lipid droplet biogenesis and catabolism in glioma cells under stress"
Participation: Poster (P5-21)
Congress: *XIV Jornada Científica del Departament de Bioquímica i Biologia Molecular*
Place: *Universitat Autònoma de Barcelona, Barcelona*
Date: 6th June 2017

Authors: **Laura Martínez-Escardó,** María Sánchez-Osuna, Víctor J. Yuste
Title: "Gossypol promotes caspase-dependent chromatin disassembly in DFF40/CAD-deficient glioblastoma cells"
Participation: Oral
Congress: XIII National Congress on Cell Death. *XIII Aporeunión. Reunión biannual de la red Española de Apoptosis (ApoRed)*
Place: Parque de las Ciencias, Granada, Spain
Date: 10th – 12th November 2017

Authors: **Laura Martínez-Escardó**, Anna Koessinger, Stephen Tait
Title: "Bcl-2 family proteins and their role in maintaining glioblastoma stemness"
Participation: Poster
Congress: *21st Cancer Research UK Beatson International Cancer Conference "Talk to the Niche – Understanding the Biology of the Metastatic Niche"*
Place: Glasgow, Scotland
Date: 1st – 4th July 2018

Authors: **Laura Martínez-Escardó**, María Sánchez-Osuna, Sarah Besora, Jordi Bruna, Victor J. Yuste
Title: "DFF40/CAD-dependent chromatin disassembly in DFF40/CAD-deficient glioblastoma derived cells"
Participation: Poster (Panel-31)
Congress: *1st Oncobell International Symposium: Mechanisms of Cancer and New Therapeutic Strategies*
Place: IDIBELL – Hospital Duran i Reynals, Hospitalet, Spain
Date: 20th – 21st September 2018

Authors: Marc Danti, **Laura Martínez-Escardó**, Victor J. Yuste, Enrique Claro, Maria Antonia Baltrons
Title: "The relationship between HIF activation, lipid droplet formation and cell death following the stimulation of NO-cGMP mediated pathway in LN18 human glioblastoma-derived cells"

Participation: Poster (P2-10)
Congress: *XVI Jornada Científica del Departament de Bioquímica i Biologia Molecular*
Place: Universitat Autònoma de Barcelona, Barcelona, Spain
Date: 3rd June 2019

Authors: Elena Garcia-Borja, Brenda Martina, Victor J. Yuste, **Laura Martínez-Escardó**
Title: "Temozolomide therapeutic effect on glioblastoma-derived cells could be due to proliferation arrest rather than to the induction of cytotoxicity"
Participation: Poster (P2-09)
Congress: *XVI Jornada Científica del Departament de Bioquímica i Biologia Molecular*
Place: Universitat Autònoma de Barcelona, Barcelona, Spain
Date: 3rd June 2019

Authors: Brenda Martina, Elena Garcia-Borja, Victor J. Yuste, **Laura Martínez-Escardó**
Title: "Raptinal triggers apoptotic and non-apoptotic serial cell deaths in human neuroblastoma-derived cells"
Participation: Poster (P3-06)
Congress: *XVI Jornada Científica del Departament de Bioquímica i Biologia Molecular*
Place: Universitat Autònoma de Barcelona, Barcelona, Spain
Date: 3rd June 2019

Authors: Marc Danti, **Laura Martínez-Escardó**, Victor J. Yuste, Enrique Claro, María Antonia Baltrons
Title: "The relationship between HIF activation, lipid droplet formation and cell death following the stimulation of NO-cGMP mediated pathway in LN18 human glioblastoma-derived cells"
Participation: Poster (PS5-68) (P16)
Congress: *18th National meeting of the Spanish Society of Neuroscience (SENC)* and *X Reunión de la Red Glial Española*
Place: Santiago de Compostela, Galicia, Spain
Date: 3rd June 2019

---

2. Publications

Sánchez-Osuna M, **Martínez-Escardó L**, Granados-Colomina C, Martínez-Soler F, Pascual-Guiral S, Iglesias-Guimarais V, Velasco R, Plans G, Vidal N, Tortosa A, Barcia C, Bruna J and Yuste VJ. *An intrinsic DFF40/CAD endonuclease deficiency impairs oligonucleosomal DNA*

hydrolysis during caspase-dependent cell death: a common trait of human glioblastoma cells. *Neuro Oncol.* *2016 Jul;18(7):950-60.

*Cover caption Volume 18, Issue 7, July 2016: Modified image from Figure 5 from the article above mentioned.

3. Research stay

Centre: Cancer Research UK, Beatson Institute
Group: Mitochondria and Cell Death
Responsible: Prof. Stephen Tait
Project topic: "Mitochondria and cell death: BCL-2 family proteins and their role in maintaining glioblastoma stemness"
Place: Glasgow, United Kingdom
Date: 2nd April – 4th July 2018

Financial support for the stay:

- **Short Research stay fellowship for trainees**: provided by Universitat Autònoma de Barcelona (Apr. 2018 – Jul. 2018). Host Institution: Cancer Research UK, Beatson Institute under the supervision of Prof. Stephen Tait.

- **Erasmus + Traineeship**: fellowship provided by Erasmus + Program and Servei d'Ocupabilitat UAB (Apr. 2018 – Jun. 2018)- Short research stay at the Cancer Research UK, Beatson Institute (Glasgow, United Kingdom).

4. Teaching experience and student supervision

4.1. Master student supervision

Title: "Study of the apoptotic endonucleases DFF40/CAD in the release of nucleosomal histones during chemotherapy-induced cell death in human glioblastoma-derived cells"
Student: Pilar Baldominos Flores
Director/s: Laura Martínez Escardó and Victor J. Yuste Mateos
Type of work: Final Master Thesis Works from the M.Sc. in Advance Immunology
University: Universitat de Barcelona – Universitat Autònoma de Barcelona
Date: Jan. 2016 – Sept. 2016
Grade: Excellent (9,4/10)

Title: "Long chain acyl-CoA synthetases (ACSL) as antitumor targets. Their role in lipid droplet biogenesis and catabolism in glioblastoma cells"
Student: Pablo Subías Ginés
Director/s: Enrique Claro Izaguirre and Laura Martínez Escardó
Type of work: Final Master Thesis Works from the M.Sc. in Biochemistry, Molecular Biology and Biomedicine
University: Universitat Autònoma de Barcelona
Date: Jan. 2017 – Sept. 2017
Grade: Excellent (9,5/10)

Title: "YC-1, a HIF-1 alpha inhibitor, abrogates lipid droplets accumulation and increases NO donors-induced cell death in LN18 humangliobastoma-derived cells"
Student: Marc Danti Ramos
Director/s: María Antonia Baltrons and Laura Martínez Escardó
Type of work: Final Master Thesis Works from the M.Sc. in Biochemistry, Molecular Biology and Biomedicine
University: Universitat Autònoma de Barcelona
Academic course: 2018 – 2019
Grade: Excellent (9,2/10)

Title: "Raptinal media una muerte apoptótica y no apoptótica en serie en células derivadas de neuroblastoma humano"
Student: Brenda Martina
Director/s: Laura Martínez Escardó and Victor J. Yuste Mateos
Type of work: Final Master Thesis Works from the M.Sc. in Biochemistry, Molecular Biology and Biomedicine
University: Universitat Autònoma de Barcelona
Academic course: 2018 – 2019
Grade: Excellent (9,6/10)

Title: "Temozolomide triggers cytostaticity rather than cytotoxicity in human glioblastoma-derived cells"
Student: Elena Garcia Borja
Director/s: Laura Martínez Escardó and Victor J. Yuste Mateos
Type of work: Final Master Thesis Works from the M.Sc. in Neurociences
University: Universitat Autònoma de Barcelona
Academic course: 2018 – 2019
Grade: With honours (9,5/10)

4.2. Bachelor student supervision

Title: "Caracterización molecular de diferentes genes implicados en vías de muerte celular en líneas tumorales humanas"
Student: Tània Gavaldà Vives
Director/s: Laura Martínez Escardó and Victor J. Yuste Mateos
Type of work: Prácticas Académicas en Entidades programme included in the Bachelor's Degree in Biomedical Sciences
University: Universitat Autònoma de Barcelona
Academic years: 2019 – 2020
Grade: Excellent (9,7/10)

4.3. Teaching experience

Recognized practical teaching in *Structural Biochemistry and Molecular Biology* and *Metabolic Biochemistry*, subjects included in the first year of Bachelor's Degree in Medicine at the Universitat Autònoma de Barcelona (academic years 2015-2016, 2016-2017, 2017-2018).

Total teaching hours: 331.12 hours.

ACKNOWLEDGEMENTS

Ha arribat el moment d'escriure una de les parts més importants d'una tesi. I és que totes aquestes pàgines que precedeixen aquests agraïments no haurien estat possibles sense l'ajuda de moltíssima gent. Si ens hem creuat durant aquesta etapa i no trobeu el vostre nom entre les següents línies, disculpeu-me i, sobretot, doneu-vos per agraïts, segur que heu contribuït en certa manera al resultat final d'aquesta tesi.

Gràcies, Víctor, per donar-me l'oportunitat d'entrar al laboratori fa anys i poder quedar-m'hi a fer aquesta tesi. Gràcies per compartir la teva manera de pensar i de viure la ciència, i per apostar i tenir la voluntat de treure el millor de mi. M'emporto molt d'aprenentatge de tot el temps compartit.

Gràcies, membres del tribunal i suplents, per acceptar formar part del tribunal d'aquesta tesi. És d'agrair que accepteu un repte així en els temps de pandèmia que estem vivint i amb la incertesa que envolta els mesos que s'apropen.

Thank you, Stephen, for allowing me to join your group and be part of it for a few months. It was a great experience, and I learned a lot from you. Thank you, Anna, for sharing your project and taking so much care of me. It was a pleasure to work with you and learn from your way of thinking. I want to extend my thanks to the rest of the members of the lab. Cat, for your kindness and the sense of humour and the fun atmosphere you bring to the lab; Flo, Kai, Kirsteen, Esmée, Alba and Joel, for your help whenever I needed it. And also thanks to all the people from the Cancer Research UK Beatson Institute for their kind welcoming and their contribution to a very pleasant place of work.

Gracias, Cristina Muñoz, por tu recomendación y por el trabajo de mantenernos a todos informados de las publicaciones en el campo cada mes. Gràcies també a les responsables de les beques Erasmus+ pràctiques del Servei d'Ocupabilitat de la UAB; i a la coordinadora del programa de Doctorat, la doctora Anna Bassols, per l'accessibilitat i les facilitats ofertes a l'hora de fer tots els tràmits per a la realització de l'estada.

Sergi, Luís, Álvaro, Meri y Arantxa, gracias por dejarme entrar en esta familia tan especial que habéis construido en Glasgow. Sois una parte importante del buen recuerdo que guardo de los meses allí.

Des de l'hospital però amb els peus ben dins del laboratori, gràcies, Montse, per posar-hi mans, ulls i cap. Has estat una ajuda imprescindible en la recta final d'aquesta tesi. Gràcies, Jordi, per posar sempre facilitats i per les recomanacions i consells durant aquests anys. Gràcies també a la gent de l'Hospital Universitari de Bellvitge - I.C.O Duran i Reynals, i a la Sarah Besora per la seva col·laboració. Agrair també la col·laboració mantinguda amb el Grup d'Aplicacions Biomèdiques de la Ressonància Magnètica Nuclear de la UAB.

Gràcies a tots els alumnes que he tingut l'oportunitat de tutoritzar i de qui he tingut l'oportunitat d'aprendre, Pilar, Pablo, Brenda, Elena, Marc, Anna i Tània; gràcies també a les noves incorporacions, Mireia, Elena, Raquel, Anna i Laura, per portar un ambient agradable al laboratori; i gràcies molt especialment a la Maria i la Carla. No sabéis la de veces que he pensado en vosotras y como el tiempo me ha hecho entender tantas cosas. Si pude empezar un doctorado sin vosotras en el lab, es gracias a todo lo que me enseñasteis cuando estuvisteis. Gracias, María, por tu paciencia en los inicios y por aceptar en esta recta final ser una de las revisoras externas de este trabajo. Gracias por el esfuerzo de leerte esta tesis tan detenidamente. Un agraïment que vull compartir amb el Roger. Moltes gràcies als dos per l'esforç. Carla, habría sido genial poder seguir corriendo contigo a coger trenes, pero me quedo con saber que desde Valencia, Zurich, o desde cualquier parte del mundo, sigues siendo un gran apoyo.

Gràcies, Roser Masgrau, José Bayascas i José Lizcano per acceptar formar part de la comissió de seguiment des del primer moment i per l'ajuda rebuda durant tots aquests anys de doctorat. Una ajuda que vull fer extensiva a tota la gent que forma part del Departament de Bioquímica i de Biologia Molecular i de l'Institut de Neurociències. És una sort realitzar una tesi en un lloc on saps que pots trucar a la porta del costat, dues més enllà o pujar unes escales sabent que trobaràs algú disposat a ajudar.

Enrique Claro, ha sido una suerte tener cerca y compartir estos años con aquel profesor que entre goteras y proyectores rotos cogió tiza y empezó a dar una clase de lípidos en la pizarra, al poco de aterrizar en la universidad. Gràcies, Pepi Sabrià, per obrir-me les portes del dept. i per les estones compartides als Amics. Gracias, Fernando Picatoste, por el apoyo recibido estos años. Gràcies a la Marian Baltrons, l'Esther Dalfó i la Judit Ribas per engrescar-se a mirar nuclis i endinsar-se en les aventures del gossypol.

Vull transmetre un enorme agraïment a tots els serveis tècnics pels quals he passat i on sempre he rebut el suport i l'ajuda necessària. Sou peces fonamentals per a qualsevol tesi. Pràcticament cap dels resultats hauria estat possible sense comptar amb el Servei de Cultius. Cris, sabemos

que hay días en los que entrar a Cultivos puede llegar a ser una actividad de riesgo, pero vale la pena asumirlo cuando sabes que hay siempre la voluntad de ayudar y de trabajar para que cultivos funcione lo mejor posible. Una filosofía en la que Neus y Toni han encajado siempre a la perfección. Gràcies als tres per oferir sempre el millor de vosaltres i fer-nos la feina més fàcil. Gràcies al Servei de Microscopia. Núria, gràcies per l'ajuda, les facilitats i la paciència, tant des de l'INc com des de Biociències, per resoldre els dubtes especialment de la part de fluorescència. Part en la qual també agraeixo l'ajuda de la Saioa i la Meri, i les seves salvadores còpies de seguretat en moments de pànic. Paqui i Martí, la vostra feina i la vostra resposta, sempre ràpida, han estat clau per a la part de microscòpia electrònica. Àlex, gràcies per acceptar i animar els reptes pre-vacances i, especialment, per posar a punt les mostres per SEM i donar-me l'oportunitat d'incloure aquestes imatges (que no fotos) en aquesta tesi. Gràcies al Servei d'Histologia. Mar, treballar amb gent disposada a acceptar reptes nous i pensar estratègies per tirar endavant nous protocols ha estat una sort. Gràcies, Susana, per solucionar els diversos problemes tècnics que sovint ens persegueixen, i per les recomanacions culturals entre passadissos. Només una petició més, espera que marxi abans de fer volar pels aires la màquina de revelar. Elisabet, gràcies per l'ajuda rebuda durant les pràctiques. Mònica, Montse i Santi, gràcies per fer que els tràmits de paperassa burocràtica siguin més fàcils de gestionar.

Entre els becaris, Abel, Arantxa, Carmen, Sònia, Sergio, Guille, Judit, Dolo, Cris, Míriam, Laura, Carlos, Arnaldo, Anna, Lola, Elena i Paola. I als no tan becaris, Albert Quintana, Alfredo i Guillermo, gràcies per apostar per estones de SAF i desconnexió entre experiments. A tots, gràcies per fer i haver fet del dept. i l'INc un lloc agradable i generós on fer la tesi.

I un agraïment especial per al Lab Squad. Eli, creo que no hay persona más loca en ese dept., pero esa locura te hace especial. Gracias por cuidarnos tanto a base de comida buenísima, ibus de rescate y abrazos locos con salto a cuello que te alegran los pasillos. Nora (churrita), si algo tenéis en común tú y esta tesis es la montaña rusa de emociones por las que me habéis hecho pasar estos años. Ese carácter tuyo que me pone tan de los nervios, pero ese sud que le gusta a mi norte y sin el cual esto seguro no habría sido lo mismo. Creo que inconscientemente sabías desde el primer día que me clichaste que ibas a ser una de las personas más importantes de estos años. Pau, serà complicat trobar un company de ball, de sentit de l'humor, d'espontaneïtat i complicitat com tu, però... els escenaris ens estan esperant. Gràcies per tot el suport, l'optimisme i els ànims en els moments més complicats d'aquesta recta final. Quan tens a prop algú com tu, disposat sempre a donar un cop de mà, demanar ajuda resulta més fàcil. Gràcies per deixar que et coneguem una mica més.

Y a ti, Raquel, gracias por ser un apoyo vital durante el tiempo que coincidimos en el dept. y por seguir siéndolo después. Muchísimas gracias por la ayuda, el soporte y los ánimos de estos últimos meses.

No vull oblidar-me de la gent de biociències. Jordi, Samu, Jofre, Gisela, Valen i també a les noves generacions que tiren fort del carro! Gràcies per obrir-me les portes de biociències. Sou gent molt especial i trobar-vos sempre és una alegria.

I sortint de les parets del laboratori, tinc la sort de poder dir que sou molts els que heu estat en els moments més complicats, sense condicionants i sempre amb respecte i amb la millor de les voluntats. Sense ser-ne conscients, heu fet de dies difícils, moments de somriures i desconnexió, moments vitals per treure forces i poder seguir endavant.

Flavia, mi italiana preferida! Poco nos imaginábamos cuando llegaste al dept. que acabarías siendo "la chica de la habitación de al lado". Fue breve, pero muy intenso! Me quedo con muchas anécdotas, muchas charlas y muchos *buongiorno* cantados, pero sobretodo me quedo con alguien muy especial que espero conservar mucho más tiempo.

Pau, gràcies per fer que les coses semblin sempre tan fàcils. Perquè si al Pau li dius 'vens?', ve sense pensar-s'ho! Tinc un record molt especial de la teva visita a Glasgow i moltes ganes de sumar més aventures.

Gràcies, Elena, Iria, Inés, Maria, Roger, Aïda i Agus per donar-me tantes lliçons de vida i ser exemple de força, valentia i superació. Sou el millor d'haver fet Biomed.

Nenes, ens pot costar setmanes o fins i tot mesos veure'ns, però sé que sempre hi sou, que hi heu estat, i que hi sereu. Gràcies! Als Prouquehisomtots, gràcies! Judit, Juan, Alberto, Tianling i Suli, heu anat arribant de manera esglaonada i amb el vostre toc més personal heu fet d'aquest grup una mescla curiosa molt especial. Als més antics, Albert, Gemma i Anna, podríem omplir tantes pàgines com té aquesta tesi amb anècdotes compartides, però si amb alguna cosa em quedo, és que quan s'ha de fer un viatge exprés al rescat d'algú de nosaltres, es fa sense pensar-ho. Especialment, gràcies, Albert, per la teva entrega i dedicació en aquesta recta final. Ens separen força quilòmetres, però us hem sentit molt a prop tant a tu com al Juan (i al vostre Grammarly) aquests mesos de pandèmia. Francesc, gràcies per aguantar els efectes d'aquesta tesi en diversos moments, però, sobretot, per ser de manera inconscient part molt responsable de l'evolució i la maduresa adquirida al llarg d'aquests anys de tesi.

I a tu, Anna, ets de les persones que més ha patit aquesta tesi, saps com ha estat de complicat en molts moments i has fet sempre el possible perquè això seguís endavant. Moltíssimes gràcies per tanta paciència, per dedicar-hi tantes i tantes hores, pel teu suport i per tant de respecte. Tornar pot ser la millor part de l'aventura! Gràcies també a la teva família per cuidar-me tan bé i per l'ajuda en forma de *tuppers* i articles de contraban.

Família, als que hi sou i als que ja no hi sou, gràcies. Sempre m'heu ensenyat com l'esforç personal era un valor important per a un mateix. Probablement aquesta tesi n'és la millor definició. Aquest treball no hauria estat possible sense el vostre respecte, suport i la vostra comprensió en tot moment. Iaia, ens has de durar molts anys per poder recuperar tot el temps que la tesi (i el coronavirus) m'han tingut segrestada. Mama, papa i Arnau, sou la millor definició de l'exigència, la importància d'una bona canalització d'aquesta exigència i la complicitat. Gràcies per ser-hi sempre!

Diuen que davant dels reptes més complicats és quan t'adones de qui tens més prop. És ben cert. Si una cosa ha posat de manifest aquesta tesi, especialment la recta final, i escrivint aquestes línies en soc encara més conscient, és tota la gent que tinc la sort de tenir a prop i que heu estat disposats a donar un cop de mà en el que ha calgut. A tots, GRÀCIES!